

University of Nottingham
UK | CHINA | MALAYSIA

Characterisation of phenylethylamine analogues as calcium channel modulators focusing on transient receptor potential canonical (TRPC) channels

MAK YIN YING

Thesis submitted to the University of Nottingham for the degree of Doctor of Philosophy

July 2021

Abstract

Despite using three or more antihypertensive medications, patients with uncontrolled high blood pressure are diagnosed as having resistant hypertension. Persistent high blood pressure can lead to complications such as stroke, heart disease and kidney problems. Currently, this group of patients are not only taking more antihypertensive medicines but also at higher doses. Inevitably, this leads to a higher risk of adverse events. New molecules targeting different sites of action are the focus of new drug development for this condition. In previous work carried out in our research group, a novel phenylethylamine alkaloid, schwarzinicine A, was isolated from a locally grown fig tree, *Ficus schwarzii*. It has been shown to relax the rat aorta, porcine coronary and pulmonary arteries. One of its relaxation mechanisms was the inhibition of transient receptor potential canonical (TRPC) channels, particularly TRPC3, 4, 5, 6 channels. Theoretically, schwarzinicine A may possess a lower oral bioavailability as it violated Lipinski's and Veber's rules by having a molecular weight (MW) more than 500 Dalton (Da) and 15 rotatable bonds. Furthermore, the yield of schwarzinicine A from natural sources is very low. Hence, *N*-phenethyl-1,2,3,4-tetrahydronaphthalen-2-amine (FK244) and 1-(furan-2-yl)-*N*-phenethylpentan-3-amine (PM20), were synthesised based on the pharmacophore of schwarzinicine A. FK244 and PM20 obeyed all criteria outlined in Lipinski's and Veber's rules. This thesis investigated the vasorelaxation profile of FK244 and PM20 in rat isolated aorta and focused on characterising their roles in modulating calcium ion (Ca^{2+}) dynamics. To elucidate the underlying pharmacology of these two compounds, isometric tension recordings were performed on Sprague-Dawley (SD) rat isolated aorta using the organ bath technique. FK244 and PM20 displayed a higher drug selectivity in vascular smooth muscle (VSM) tissues. The findings from organ bath experiments have excluded the roles of FK244 and PM20 in regulating NO, cyclic nucleotides, adrenoceptors, and potassium ion (K^+) channels as their vasorelaxant mechanisms. The plausible vasorelaxation effects of FK244 and PM20 via an endothelium-dependent route have also been ruled out. FK244 and PM20 significantly suppressed the aortic contractile response to calcium chloride ($CaCl_2$) in a concentration-dependent manner. They also managed to reduce the vascular tone raised by phenylephrine, potassium chloride (KCl) and U46619. Pre-treatment with FK244 and PM20 attenuated phenylephrine-, KCl-, and serotonin-induced vasoconstriction but had no impact on U46619-induced vasoconstriction. However, in a Ca^{2+}-free

environment, they did not affect phenylephrine-, KCl- and U46619-induced contraction. These findings suggested that FK244 and PM20 mainly inhibit plasma membrane Ca^{2+} channels such as L-type voltage-gated Ca^{2+} channels (VGCCs) and TRPC channels. They do not influence the internal store Ca^{2+} release involved in smooth muscle contraction. Incubation with TRPC-selective inhibitors 2-aminoethoxydiphenyl borate (2-APB), Pyr3, Pyr6 and SKF-96365 reduced the efficacy of FK244 and PM20. However, the vascular effects of FK244 and PM20 were not affected by nifedipine and verapamil. These results point to a suggestion that FK244 and PM20 could be modulating TRPC channels in addition to L-type VGCCs. Exposure of FK244 and PM20 to *C. elegans* did not induce toxicity at low concentration but slightly reduced the nematodes' lifespan at high concentration. Assessment in disease models manifesting hypertension and diabetes have confirmed that the vascular effects of FK244 and PM20 were comparable to that in normotensive SD rats and non-diabetic rats. In addition, fluorometric intracellular Ca^{2+} recordings were carried out to measure the activity of FK244 and PM20 on TRPC3- and TRPC6-overexpressing human embryonic kidney (HEK) 293 cells. Intracellular Ca^{2+} measurements in HEK 293 cells have confirmed that FK244 and PM20 blocked extracellular Ca^{2+} influx via TRPC3 and TRPC6 channels. In summary, FK244 and PM20 displayed significant endothelium-independent vasorelaxation by inhibiting extracellular Ca^{2+} influx via plasmalemmal Ca^{2+} channels. One of the targeted Ca^{2+}-permeable channels is TRPC channels, particularly TRPC3 and TPRC6 subtypes. It highlighted TRPC channels as the possible new drug targets in hypertension. TRPC-targeting FK244 and PM20 which prevent vascular contraction, may be developed as antihypertensive agents for resistant hypertension.

Publications / Awards

Conference proceedings

1. **Mak, Y.Y.**, Lee F.K., Lim K.H., Kong C., Mbaki Y., Then S.M., Ting K.N. (2020). Investigating calcium channels modulation of a novel phenylethylamine compound in *Caenorhabditis elegans*. Abstracts of the 86th Annual Meeting of the German Society for Experimental and Clinical Pharmacology and Toxicology (DGPT) with contribution of the Arbeitsgemeinschaft für Angewandte Humanpharmakologie e. V. (AGAH). University of Leipzig. 2–5 March 2020, Leipzig, Germany. *Naunyn-Schmiedeberg's Arch Pharmacol*, 40, 393, 1-97. https://doi.org/10.1007/s00210-020-01828-y

2. **Mak, Y.Y.**, Lee F.K., Lim K.H., Kong C., Mbaki Y., Then S.M., Ting K.N. (2019). FK244 (*N*-phenethyl-1,2,3,4-tetrahydronaphthalen-2-amine), a newly discovered phenylethylamine as a calcium channel blocker. Selected Abstracts from Pharmacology 2018. Queen Elizabeth II Conference Centre. 18–20 December 2018, London, United Kingdom. *British Journal of Pharmacology*, P43, 176(16), 2977–3081. https://doi.org/10.1111/bph.14681

3. Lee F.K., **Mak, Y.Y.**, Lim K.H., Kong C., Mbaki Y., Then S.M., Ting K.N. (2019). Vasorelaxation effects of a newly discovered phenylethylamine (FK244) in hypertensive rat isolated aortae. Selected Abstracts from Pharmacology 2018. Queen Elizabeth II Conference Centre. 18–20 December 2018, London, United Kingdom. *British Journal of Pharmacology*, P48, 176(16), 2977–3081. https://doi.org/10.1111/bph.14681

Presentations

1. UNM Pharm/Biomed 6th Annual Postgraduate Research Symposium
   Characterisation of FK244 analogue as a calcium channel modulator focusing on Transient Receptor Potential Canonical (TRPC) channels

2. Faculty of Science and Engineering Postgraduate Research Showcase 2019
   Combat high blood pressure: Can fig do the trick?

3. UNM-Biomed/AAPS-NUS PharmSci @ Asia Symposium: Pharmaceutical & Biomedical Science in an Evolving Healthcare Landscape
   FK244 (N-phenethyl-1,2,3,4-tetrahydronaphthalen-2-amine), a newly discovered phenylethylamine as a calcium channel blocker

4. Three Minute Thesis competition (3MT®)
   Fighting high blood pressure using worms in soil

5. 4th Annual Biomedical Science Postgraduate Symposium 2018: Shaping life sciences from innovation to integration
   Take down high blood pressure - No more panic!

6. 2nd Faculty of Science Postgraduate Research Showcase 2018
   Natural Products to Drug Discovery: Could FK244 Be a New Treatment for High Blood Pressure?

Grant/Awards

1. Best Oral Presenter at UNM Pharm/Biomed 6th Annual Postgraduate Research Symposium

2. British Pharmacological Society (BPS) Schachter Award 2019

3. Grand prize at Faculty of Science and Engineering Postgraduate Research Showcase 2019

4. First runner-up at 2nd Faculty of Science Postgraduate Research Showcase 2018

5. Best Poster Award at 4th Annual Biomedical Science Postgraduate Symposium 2018

Acknowledgements

I would like to express my profound gratitude to my supervisor, Prof Ting Kang-Nee, who offered this postgraduate position to me. She always patiently clarifies the concepts and shedding light upon the research project with her extensive knowledge in pharmacology. I would like to convey my sincere gratitude to Prof Kuan-Hon Lim for his sentiments in the field of chemistry and for providing research compounds until the completion of this research. I am deeply thankful to Dr Alice Kong for her invaluable guidance in *C. elegans* work. Her vast knowledge and humble attitude have been a great inspiration to me.

I am extending my warmest thanks to our close collaborators, Dr Robin Bon, Dr Claudia Bauer, and Dr David Wright from the University of Leeds, who generously allowed me to work in their laboratory. Thank you for providing guidance on fluorometric intracellular calcium recording techniques and contributing your professional opinions and thoughts towards our publications.

I would like to acknowledge University Putra Malaysia for their kind cooperation in providing rat tissues for my research. To all the lab technicians, I wish to thank them for working tirelessly to provide various support in the laboratories, ensuring my lab work was able to finish on time. Credit also goes to all the staff in the Faculty of Science and Engineering, as well as Graduate School, who have always assisted me through all the administrative tasks and professional development.

I have been fortunate to be able to work with a few colleagues – Dr Mei-Kee Lee, Dr Kayatri Govindaraju, Dr Fong-Kai Lee and Boon-Hee. Many thanks to all of them for being welcoming when I first joined and offering help in my experiments. Thanks to Leanne, who kept me company in C1B07 always.

I would also like to express my immeasurable appreciation to the University of Nottingham Malaysia for offering scholarships for this PhD position, the Ministry of Higher Education Malaysia (FRGS/1/2017/SKK10/UNIM/01/1), British Heart Foundation (PG/19/2/34084) and BPS Schachter Award, for funding this research.

Finally, I wish to thank my beloved family and Hsin-Yuan for being considerate and supportive. This PhD would have been impossible without them.

Declaration

I declare that all experimental studies throughout this thesis were carried out by myself. This excludes:

1) Experimental work on the porcine pulmonary artery and bronchiole was carried out by Ms Yin-Ying Saw at the University of Nottingham, United Kingdom (UK). (**section 2.3.3.2** and **2.3.5.2**)
2) Blood pressure of spontaneously hypertensive rats (SHRs) was measured by Mr Boon-Hee Goh from Monash University, Malaysia campus. (**section 4.3.2**)
3) Induction of diabetes in Wistar rats was performed by Dr Fung Shin Yee and Mr Alvin Chee-Sum Yap, from the Department of Molecular Medicine, University of Malaya. (**section 4.3.4**)
4) The integrity of vascular endothelium in SHR was assessed by Dr Kayatri Govindaraju from the University of Nottingham Malaysia. (**section 4.3.7.1**)
5) Concentration-response curves (CRCs) of FK244 and PM20 in SHRs were constructed by Dr Fong-Kai Lee, from the University of Nottingham Malaysia. (**section 4.3.7.2**)

Abbreviations

$[Ca^{2+}]_i$	intracellular calcium concentration
2-APB	2-aminoethoxydiphenyl borate
3R	Reduce, Refine, Replace
4-AP	4-aminopyridine
5-HT	5-hydroxytryptamine
$Å^2$	square angstrom
AC	adenylyl cyclase
ACE	angiotensin-converting enzyme
ACh	acetylcholine
AcOH	acetic acid
ADME	absorption, distribution, metabolism, and excretion
ADP	adenosine 5'-diphosphate
AKT	protein kinase B
AM	acetoxymethyl
Ano1	anoctamin-1
ANOVA	analysis of variance
ANP	atrial natriuretic peptide
ARB	angiotensin-II receptor blocker
ARRIVE	Animal Research: Reporting of In Vivo Experiments
AT	angiotensin
ATP	adenosine 5'-triphosphate
AWERB	Animal Welfare and Ethics Review Body
$BaCl_2$	barium chloride
BASMC	basilar artery smooth muscle cells
BK_{Ca} channel	large-conductance Ca^{2+}-activated K^+ channel
BNP	brain natriuretic peptide
BPS	British Pharmacological Society
C. elegans	*Caenorhabditis elegans*
Ca^{2+}	calcium ion
CaCC	Ca^{2+}-activated chloride channel
$CaCl_2$	calcium chloride
CaM	calmodulin

cAMP	3’-5’-cyclic adenosine monophosphate
CGC	Caenorhabditis Genetics Centre
cGMP	3’-5’-cyclic guanosine monophosphate
CICR	Ca^{2+}-induced Ca^{2+} release
CKD	chronic kidney disease
Cl^-	chloride ion
$ClCH_2CH_2Cl$	1,2-dichloroethane
CNP	C-type natriuretic peptide
CO	carbon monoxide
CO_2	carbon dioxide
COX	cyclooxygenase
CRAC channel	Ca^{2+} release-activated Ca^{2+} channel
CRC	concentration-response curve
CRP	C-reactive protein
CVD	cardiovascular disease
Da	Dalton
DAG	1,2-diacyl-*sn*-glycerol
DBP	diastolic blood preesure
DHP	dihydropyridine
DMSO	dimethyl sulfoxide
E. coli	*Escherichia coli*
EC_{50}	half-maximal effective concentration
EDHF	endothelial-derived hyperpolarising factor
EET	epoxyeicosatrienoic acid
EGFR	epidermal growth factor receptor
E_{max}	maximum tissue response
eNOS	endothelial nitric oxide synthase
ERA	endothelin receptor antagonist
ET	endothelin
Et_2O	diethyl ether
EtOAc	ethyl acetate
GPCR	G-protein coupled receptor
GTP	guanosine-5'-triphosphate
H_2O_2	hydrogen peroxide

H_2S	hydrogen sulphide
HBA	hydrogen bond acceptor
HBD	hydrogen bond donor
HEK	human embryonic kidney
HPLC	high-performance liquid chromatography
HRESIMS	high resolution electrospray ionisation mass spectrometry
IACUC	Institutional Animal Care and Use Committee
IC_{50}	half-maximal inhibitory concentration
I_{CRAC}	Ca^{2+} release-activated channels current
IK_{Ca} channel	intermediate-conductance Ca^{2+}-activated K^+ channel
IP	intraperitoneal injection
IP_3	inositol-1,4,5-trisphosphate
IR	infrared spectroscopy
IUPHAR	International Union of Basic and Clinical Pharmacology
K^+	potassium ion
K_2HPO_4	dipotassium hydrogen phosphate
K_{ATP} channel	ATP-sensitive K^+ channel
K_{Ca} channel	Ca^{2+}-activated K^+ channel
KCl	potassium chloride
KH_2PO_4	potassium dihydrogen phosphate
K_{ir} channel	inwardly rectifying K^+ channel
K_v channel	voltage-gated K^+ channel
LB	Luria Bertani
LD_{50}	median lethal dose
logP	partition coefficient
$MgCl_2$	magnesium chloride
$MgSO_4$	magnesium sulphate
MLC	myosin light chain
MLCK	myosin light chain kinase
MLCP	myosin light chain phosphatase
MW	molecular weight
Na^+	sodium ion
Na_2HPO_4	disodium hydrogen phosphate
Na_2SO_4	sodium sulphate

$NaBH(OAc)_3$	sodium triacetoxyborohydride
NaCl	sodium chloride
$NaHCO_3$	sodium bicarbonate
NaOH	sodium hydroxide
NCX	Na^+-Ca^{2+} exchanger
NFAT	nuclear factor of activated T-cell
NGM	nematode growth media
NICE	National Institute for Health and Care Excellence
NMR	nuclear magnetic resonance
NO	nitric oxide
NSCC	non-selective cation channel
O_2	oxygen
OAG	1-oleoyl-2-acetyl-*sn*-glycerol
ORAI	Ca^{2+} release-activated Ca^{2+} channel modulator
PAH	pulmonary arterial hypertension
PASMC	pulmonary arterial smooth muscle cell
PDE	phosphodiesterase
PGI_2	prostacyclin / prostaglandin I_2
PI3K	phosphatidylinositol-3-kinase
PIP_2	phosphatidylinositol 4,5-bisphosphate
PKA	protein kinase A
PKC	protein kinase C
PKG	protein kinase G
PLC	phospholipase C
PMCA	plasma membrane Ca^{2+}-ATPase
RAAS	renin-angiotensin-aldosterone system
RDN	renal denervation
RhoA	Ras homolog family member A
ROCC	receptor-operated Ca^{2+} channel
ROCE	receptor-operated Ca^{2+} entry
ROCK	Rho-associated protein kinase
ROS	reactive oxygen species
RyR	ryanodine receptor
SAG	1-stearoyl-2-arachidonyl-*sn*-glycerol

SAR	structure-activity relationship
SBP	systolic blood pressure
SBS	standard buffer solution
SD	Sprague–Dawley
SEM	standard error of mean
SERCA	sarco/endoplasmic reticulum Ca^{2+}-ATPase
sGC	soluble guanylyl cyclase
SHR	spontaneous hypertensive rat
SK_{Ca} channel	small-conductance Ca^{2+}-activated K^+ channel
SNP	sodium nitroprusside
SOCC	store-operated Ca^{2+} channel
SOCE	store-operated Ca^{2+} entry
SR	sarcoplasmic reticulum
STIC	spontaneous transient inward current
STIM	stromal interaction molecule
STOC	spontaneous transient outward current
STZ	streptozotocin
TEA	tetraethylammonium chloride
TLC	thin-layer chromatography
TMEM16A	transmembrane member 16A
TP	thromboxane prostanoid
tPSA	topological polar surface area
TRP	transient receptor potential
TRPA	TRP ankyrin
TRPC	TRP canonical
TRPM	TRP melastatin
TRPML	TRP mucolipin
TRPP	TRP polycystin
TRPV	TRP vanilloid
TXA_2	thromboxane A_2
UK	United Kingdom
USA	United States of America
VGCC	voltage-gated Ca^{2+} channel
VSM	vascular smooth muscle

VSMC	vascular smooth muscle cell
WKY	Wistar Kyoto
Zn^{2+}	zinc ion

Figures and tables

Figures

Figure 1.1 Structures of the artery, consisting of the outermost layer called tunica adventitia, a middle section of tunica media, and an inner layer of tunica intima. Diagram adapted from Stanfield, (2005).....8

Figure 1.2 Summary of the treatment for hypertension (Malaysian Society of Hypertension, 2018; NICE, 2019).....10

Figure 1.3 Overview of Ca^{2+} signalling pathways entering or exiting VSMCs. Individual subcellular Ca^{2+} events are italicised. Solid pointed solid arrow denotes downstream effectors activation, blunt arrow denotes downstream effectors inhibition. Dotted arrows denote flow of ions. Abbreviations: BK_{Ca}, large-conductance Ca^{2+}-activated K^+ channel; Ca^{2+}, calcium ion; CaCC, Ca^{2+}-activated chloride channels; CICR, Ca^{2+}-induced Ca^{2+} release; Cl^-, chloride ion; DAG, diacylglycerol; IP_3, inositol-1,4,5-trisphosphate; IP_3R, IP_3 receptor; K^+, potassium ion; MCU, mitochondrial uniporter; NCX, Na^+-Ca^{2+} exchanger; ORAI, Ca^{2+} release-activated Ca^{2+} channel modulator; PIP_2, phosphatidylinositol 4,5-bisphosphate; PKC, protein kinase C; PLC; phospholipase C; PMCA, plasma membrane Ca^{2+}-ATPase; ROCE, receptor-operated Ca^{2+} entry; RyR, ryanodine receptor; SERCA, sarco/endoplasmic reticulum Ca^{2+}-ATPase; SOCE, store-operated Ca^{2+} entry; SR, sarcoplasmic reticulum; STIC, spontaneous transient inward current; STIM, stromal interaction molecule; STOC, spontaneous transient outward current; TRPC, transient receptor potential canonical; VGCC, voltage-gated Ca^{2+} channels.....16

Figure 1.4 Schematic diagram of Ca^{2+}-dependent (red box) and Ca^{2+}-independent (blue box) VSM contraction and relaxation mechanisms. These two pathways are interlinked to regulate smooth muscle tone. Pointed arrows denote downstream effectors activation; blunt arrows denote downstream effectors inhibition. Abbreviations: $[Ca^{2+}]_i$, intracellular Ca^{2+} concentration; AC, adenylyl cyclase; ATP, adenosine 5'-triphosphate, CaM, calmodulin; cAMP, 3'-5'-cyclic adenosine monophosphate; cGMP, 3'-5'-cyclic guanosine monophosphate; Ca^{2+}, calcium ion; GPCR: G-protein coupled receptor; GTP, guanosine-5'-triphosphate; MLC, myosin light chain; MLCK, MLC kinase; MLCP, MLC phosphatase; MLC-P, phosphorylated MLC; NO, nitric oxide; PKA, protein kinase A; PKG, protein kinase G; RhoA, Ras homolog family member A; ROCK, rho-associated protein kinase; sGC, soluble guanylyl cyclase. Diagram adapted from S. Ahmed & Warren (2018).19

Figure 1.5 Structural representation of TRPC3 and TRPC6 channels as Ca^{2+}-permeable plasmalemmal ion channels. Abbreviations: ANK, ankyrin; CBR, caveolin binding region; CIRB, calmodulin/IP_3 receptor binding region; COOH, carboxyl terminus; EC, extracellular; IC, intracellular; NH_2, amino terminus; P, pore; PM, plasma membrane; TM, transmembrane; TRP, transient receptor potential; TRPC, transient

receptor potential canonical. Diagram adapted from Nilius & Flockerzi (2014), Tang et al. (2018), Vazquez et al. (2004). 24

Figure 1.6 The fruits and leaves of Ficus schwarzii. Photos courtesy by Prof Kuan-Hon Lim.....33

Figure 1.7 Chemical structure of schwarzinicine A, which was obtained naturally as a scalemic mixture (4:1 ratio of (+)/ (-)). 34

Figure 1.8 The structures of two phenylethylamine analogues of schwarzinicine A, namely (A) N-phenethyl-1,2,3,4-tetrahydronaphthalen-2-amine (FK244) and (B) 1-(furan-2-yl)-N-phenethylpentan-3-amine (PM20).....37

Figure 1.9 Illustration of an organ bath set-up. Isometric tension of isolated tissues is recorded by a force transducer connected to a laptop. The tissue is submerged in the Krebs solution with constant aeration, jacketed by circulating water at 37 °C. Change of Krebs solution in washes is done by emptying the solution through drainage first then adding fresh Krebs solution.....40

Figure 1.10 Microscopic view of an adult C. elegans. Its unique features made it a versatile organism in the modern pipelines of drug discovery. 43

Figure 1.11 Mode of action of fura-2 AM as a ratiometric Ca^{2+} sensor in cell-based assays. Abbreviations: Ca^{2+}, calcium ion; EC, extracellular; IC, intracellular; PM, plasma membrane. Diagram adapted from Li (2019). 45

Figure 1.12 Healthy adherent HEK 293 cells at 50% confluency under 4x objectives lens. They appear to have epithelial morphology, which is slightly oval to pyramidal shape with hair-like filopodia.....46

Figure 2.1 Chemical structures of (A) schwarzinicine A and (B) FK244. 50

Figure 2.2 Synthesis of N-phenethyl-1,2,3,4-tetrahydronaphthalen-2-amine (FK244). 51

Figure 2.3 Illustration of tissues of interest mounted on holders. The approach in (A) depicts the manner of mounting aortic, tracheal, and bronchiole rings to a glass rod, while (B) depicts the method of tying bladder strips to a metal rod. 60

Figure 2.4 Illustration of a representative isometric tension trace recording showing that the tissue was challenged twice with KCl to test its viability. The difference in magnitude was measured and used to calculate the average KCl-induced contraction.....67

Figure 2.5 Illustration of a representative isometric tension trace recording showing the analysis of drug-induced (A) contraction and (B) relaxation in smooth muscle tissue. 68

Figure 2.6 Chemical structures of (A) FK244, (B) nifedipine, (C) SKF-96365 and (D) Pyr3. 70

Figure 2.7 Effect of FK244 on rat isolated (A) aorta, (B) bladder and (C) trachea at the basal tone. Tissue responses have been expressed as the percentage

of KCl-induced tone. Data are shown as the mean ± SEM of 5 to 6 animals. Abbreviation: KCl, potassium chloride. *72*

Figure 2.8 Effect of FK244 in (A) rat isolated aorta, bladder and trachea pre-contracted with phenylephrine or carbachol. Relaxation effect of FK244 compared to vehicle control in (B) aortic rings, (C) bladder strips and (D) tracheal rings. Aortic tissue responses have been expressed as the percentage of phenylephrine-induced tone while bladder and tracheal tissues responses have been expressed as the percentage of carbachol-induced tone. Data are shown as the mean ± SEM of 5 to 7 animals. Abbreviations: CCH, carbachol; PE, phenylephrine. *73*

Figure 2.9 Effect of FK244 in (A) vascular tissues, (B) airway tissues and (C) porcine tissues. Tissue responses have been expressed as the percentage of agonist-induced tone. Data are shown as the mean ± SEM of 5 to 8 animals. Abbreviations: CCH, carbachol; PE, phenylephrine, PB, porcine bronchiole; PPA, porcine pulmonary artery; RA, rat aorta; RT, rat trachea. *76*

Figure 2.10 Effect of FK244 in endothelium-intact (E+) and -denuded (E-) aortae. Representative tracings of vehicle control CRCs in (A) E+ aorta and (B) E- aorta, as well as FK244 CRCs in (C) E+ aorta and (D) E- aorta. (E) Cumulative CRCs of vehicle control and FK244 in E+ and E- rat isolated aortae. Aortic tissue relaxation has been expressed as the percentage of phenylephrine-induced tone. Data are shown as the mean ± SEM of 5 to 6 animals. Abbreviation: PE, phenylephrine. *78*

Figure 2.11 Effect of L-NAME with inhibition on eNOS on FK244-induced relaxation. Tissue responses have been expressed as the percentage of phenylephrine-induced tone. Data are shown as the mean ± SEM of 6 animals. Abbreviations: L-NAME, N^G-nitro-L-arginine methyl ester; PE, phenylephrine. *80*

Figure 2.12 Effect of cyclic nucleotides in FK244-induced vasorelaxation. Tissues were pre-treated with (A) forskolin and (B) ODQ for 30 minutes before FK244 CRCs were constructed. Tissue responses have been expressed as the percentage of phenylephrine-induced tone. Data are shown as the mean ± SEM of 5 to 8 animals. Abbreviation: PE, phenylephrine. *81*

Figure 2.13 Effect of adrenoceptor-antagonists on FK244-induced vasorelaxation in rat aortae. Aortic rings were pre-incubated with (A) prazosin, (B) rauwolscine, and (C) propranolol followed by CRCs to FK244. Tissue responses have been expressed as the percentage of KCl-induced tone for prazosin- and rauwolscine-treated aortic rings. For propranolol-treated aortic rings, tissue responses have been expressed as the percentage of phenylephrine-induced tone. Data are shown as the mean ± SEM of 5 to 6 animals. Abbreviations: KCl, potassium chloride; PE, phenylephrine. *83*

Figure 2.14 Effect of K^+ channel blockers on FK244-induced vasorelaxation. Tissues were exposed to (A) 4-AP, (B) $BaCl_2$, (C) glibenclamide and (D) TEA, before performing cumulative CRCs to FK244 under raised vascular tone. Tissue responses have been expressed as the percentage of

phenylephrine-induced tone. Data are shown as the mean ± SEM of 6 animals. Abbreviations: 4-AP, 4-aminopyridine, $BaCl_2$, barium chloride, PE, phenylephrine, TEA, tetraethylammonium chloride.....84

Figure 2.15 Effect of FK244 on aortic tissues pre-constricted with (A) phenylephrine, KCl and U46619. Cumulative CRCs of FK244 with vehicle control when pre-contracted with (B) phenylephrine, (C) KCl and (D) U46619. Tissue responses were expressed as the percentage of contractile agent-induced contraction. Data are shown as the mean ± SEM of 5 to 6 animals. Abbreviations: KCl, potassium chloride; PE, phenylephrine.....87

Figure 2.16 Effect of FK244 treatment in the aortic rings on the vascular contraction elicited by the contractile agents. Cumulative CRCs to (A) phenylephrine, (B) KCl, (C) serotonin and (D) U46619 was demonstrated in the presence of FK244. Tissue responses were expressed as the percentage of KCl-induced contraction. Data are shown as the mean ± SEM of 5 to 7 animals. Abbreviations: KCl, potassium chloride; PE, phenylephrine. 90

Figure 2.17 Reversibility of FK244 shown in phenylephrine-induced contraction. Tissue responses were expressed as the percentage of KCl-induced contraction. Data are shown as the mean ± SEM of 6 animals. Two-way ANOVA followed by Bonferroni's post hoc test was used to compare FK244 to vehicle control at the first and second addition of phenylephrine. Abbreviations: KCl, potassium chloride, PE, phenylephrine.....92

Figure 2.18 Vasorelaxation effect of FK244 and Ca^{2+} channel blockers. Cumulative CRCs was compared between FK244 and (A) SOCC/non-selective TRPC inhibitors (2-APB, Pyr6, SKF-96365), (B) TRPC-selective inhibitors (HC-070, Pyr3), and (C) VGCC inhibitors (nifedipine, verapamil). Tissue relaxations were expressed as the percentage of phenylephrine-induced contraction. Data are shown as the mean ± SEM of 5 to 7 animals. Abbreviations: 2-APB, 2-aminoethoxydiphenyl borate, PE, phenylephrine; SOCC, store-operated Ca^{2+} channel; TRPC, transient receptor potential canonical; VGCC, voltage-gated Ca^{2+} channel.....94

Figure 2.19 Effect of Ca^{2+} channel blockers on phenylephrine-induced contraction in the vasculature. The Ca^{2+} channel blockers used were (A) SOCC/non-selective TRPC inhibitors (2-APB, Pyr6, SKF-96365), (B) TRPC-selective inhibitors (Pyr3), and (C) VGCC inhibitors (nifedipine, verapamil). Tissue responses were expressed as the percentage of KCl-induced contraction. Data are shown as the mean ± SEM of 5 to 7 animals. Abbreviations: 2-APB, 2-aminoethoxydiphenyl borate; KCl, potassium chloride; PE, phenylephrine; SOCC, store-operated Ca^{2+} channel; TRPC, transient receptor potential canonical; VGCC, voltage-gated Ca^{2+} channel. 97

Figure 2.20 Effect of FK244 on (A) phenylephrine-, (B) KCl- and (C) U46619-induced contraction in normal Krebs and Ca^{2+}-free Krebs solution. Tissue responses were recorded at 0, 30, and 60 minutes after the addition of each contractile agent and were expressed as the percentage of KCl-induced contraction. Data are shown as the mean ± SEM of 5 to 6

animals. Two-way ANOVA followed by Bonferroni's post hoc test was used to compare vehicle control and FK244 treatment in either normal or Ca^{2+} free Krebs separately at each time point. Abbreviations: KCl, potassium chloride, PE, phenylephrine.....100

Figure 2.21 Effect of (A/B/C) Ca^{2+} channel blockers and (D) FK244 on $CaCl_2$-induced contraction in rat isolated aortic rings bathed in Ca^{2+}-free Krebs solution. The Ca^{2+} channel blockers used were (A) SOCC/non-selective TRPC inhibitors (2-APB, Pyr6, SKF-96365), (B) TRPC- selective inhibitors (Pyr3), and (C) VGCC inhibitors (nifedipine, verapamil). Tissue contractions were expressed as the percentage of KCl-induced contraction in Ca^{2+}-containing Krebs solution. Data are shown as the mean ± SEM of 5 to 7 animals. Abbreviations: 2-APB, 2-aminoethoxydiphenyl borate; $CaCl_2$, calcium chloride; KCl, potassium chloride; SOCC, store-operated Ca^{2+} channel; TRPC, transient receptor potential canonical; VGCC, voltage-gated Ca^{2+} channel. 103

Figure 2.22 Effect of FK244-induced relaxation in the presence of different Ca^{2+} channel blockers. CRCs to FK244 were performed in the presence of SOCC/non-selective TRPC inhibitors – (A) 2-APB, (B) Pyr6, (C) SKF-96365; TRPC- selective inhibitors – (D) Pyr3; and VGCC inhibitors – (E) nifedipine, (F) verapamil. Tissue relaxations were expressed as the percentage of phenylephrine-induced contraction. Data are shown as the mean ± SEM of 5 to 6 animals. Abbreviations: 2-APB, 2-aminoethoxydiphenyl borate; PE, phenylephrine; SOCC, store-operated Ca^{2+} channel; TRPC, transient receptor potential canonical; VGCC, voltage-gated Ca^{2+} channel. 106

Figure 2.23 Schematic diagram depicting the regulation of Ca^{2+} dynamic by phenylephrine, serotonin, KCl and U46619, to induce VSM contraction. Activation of phenylephrine α_1-adrenoceptors and serotonin 5-HT_{2A} receptors initiate G_q protein signal transduction, whereas $G_{12/13}$ protein is believed to be coupled to U46619-activated TP receptors in the VSM. Downstream effectors of phenylephrine, serotonin and KCl activate TRPC and VGCC channels. Solid pointed solid arrow denotes downstream effectors activation, blunt arrow denotes downstream effectors inhibition. Dotted arrows denote flow of Ca^{2+}. Abbreviations: Ca^{2+}, calcium ion; CaM, calmodulin; CRAC, Ca^{2+} release-activated channels; DAG, diacylglycerol; EC, extracellular; GTP, guanosine-5'-triphosphate; IC, intracellular; IP_3, inositol-1,4,5-trisphosphate; IP_3R, IP_3 receptor; KCl, potassium chloride; MLC, myosin light chain; MLCK, MLC kinase; MLCP, MLC phosphatase; MLC-P, phosphorylated MLC; NSCC, non-selective cation channels; ORAI, Ca^{2+} release-activated Ca^{2+} channel modulator; PE, phenylephrine; PIP_2, phosphatidylinositol 4,5-bisphosphate; PKC, protein kinase C; RhoA, Ras homolog family member A; ROCC, receptor-operated Ca^{2+} channels; ROCK, Rho-associated protein kinase; RyR, ryanodine receptor; SERCA, sarco/endoplasmic reticulum Ca^{2+}-ATPase; SOCC, store-operated Ca^{2+} channels; SR, sarcoplasmic reticulum; STIM, stromal interaction molecule; TRPC, transient receptor potential canonical; VGCC, voltage-gated Ca^{2+} channels.....116

Figure 3.1 Chemical structures of (A) schwarzinicine A and (B) PM20.....125

Figure 3.2 Synthesis of 1-(furan-2-yl)-N-phenethylpentan-3-amine (PM20).....126

Figure 3.3 Chemical structures of (A) PM20, (B) nifedipine, (C) SKF-96365 and (D) Pyr3. 132

Figure 3.4 Effect of PM20 on rat isolated (A) aorta, (B) bladder and (C) trachea at the basal tone. Tissue responses have been expressed as the percentage of KCl-induced tone. Data are shown as the mean ± SEM of 5 to 6 animals. Abbreviation: KCl, potassium chloride.....134

Figure 3.5 Effect of PM20 in (A) rat isolated aorta, bladder and trachea pre-contracted with phenylephrine or carbachol. Relaxation effect of PM20 compared to vehicle control in (B) aortic rings, (C) bladder strips and (D) tracheal rings. Aortic tissue responses have been expressed as the percentage of phenylephrine-induced tone while bladder and tracheal tissues responses have been expressed as the percentage of carbachol-induced tone. Data are shown as the mean ± SEM of 5 to 6 animals. Abbreviations: CCH, carbachol; PE, phenylephrine. 136

Figure 3.6 Effect of PM20 in endothelium-intact (E+) and -denuded (E-) aortae. Representative tracings of PM20 CRCs in (A) E+ aorta and (B) E- aorta, as well as (C) cumulative CRCs of vehicle control and PM20 in E+ and E- rat isolated aortae. Aortic tissue relaxation has been expressed as the percentage of phenylephrine-induced tone. Data are shown as the mean ± SEM of 5 to 6 animals. Abbreviation: PE, phenylephrine. 138

Figure 3.7 Effect of pre-exposure of L-NAME on PM20-induced vasorelaxation. Tissue responses have been expressed as the percentage of phenylephrine-induced tone. Data are shown as the mean ± SEM of 5 animals. Abbreviations: L-NAME, N^G-nitro-L-arginine methyl ester; PE, phenylephrine. 140

Figure 3.8 Effect of cyclic nucleotides against PM20-induced vasorelaxation. Tissues were pre-treated with (A) forskolin and (B) ODQ for 30 minutes before the construction of cumulative CRCs to PM20. Tissue responses have been expressed as the percentage of phenylephrine-induced tone. Data are shown as the mean ± SEM of 5 to 8 animals. Abbreviation: PE, phenylephrine. 141

Figure 3.9 Effect of adrenoceptor-antagonists on PM20-induced vasorelaxation in rat aortae. Aortic rings were pre-incubated with (A) prazosin, (B) rauwolscine, and (C) propranolol for 30 minutes before the construction of cumulative CRCs to PM20. Tissue responses have been expressed as the percentage of KCl-induced tone for prazosin- and rauwolscine-treated aortic rings. For propranolol-treated aortic rings, tissue responses have been expressed as the percentage of phenylephrine-induced tone. Data are shown as the mean ± SEM of 5 to 6 animals. Abbreviations: KCl, potassium chloride; PE, phenylephrine. 143

Figure 3.10 Effect of K^+ channel blockers on PM20-induced relaxation. Cumulative CRCs to PM20 were carried out after tissues were pre-incubated with a single dose of (A) 4-AP, (B) $BaCl_2$, (C) glibenclamide and (D) TEA.

Tissue responses have been expressed as the percentage of phenylephrine-induced tone. Data are shown as the mean ± SEM of 6 animals. Abbreviations: 4-AP, 4-aminopyridine, $BaCl_2$, barium chloride, PE, phenylephrine, TEA, tetraethylammonium chloride.....144

Figure 3.11 Effect of increasing concentration of PM20 on aortic rings pre-contracted with (A) phenylephrine, KCl and U46619. Cumulative CRCs of PM20 with vehicle control when pre-contracted with (B) phenylephrine, (C) KCl and (D) U46619. Tissue responses were expressed as the percentage of contractile agent-induced contraction. Data are shown as the mean ± SEM of 5 to 6 animals. Abbreviations: KCl, potassium chloride; PE, phenylephrine. 147

Figure 3.12 Effect of PM20 treatment in the aortic rings on the vascular contraction elicited by the contractile agents. Cumulative CRCs to (A) phenylephrine, (B) KCl, (C) serotonin and (D) U46619 was demonstrated in the presence of PM20. Tissue responses were expressed as the percentage of KCl-induced contraction. Data are shown as the mean ± SEM of 5 to 7 animals. Abbreviations: KCl, potassium chloride; PE, phenylephrine. 150

Figure 3.13 Reversibility of PM20 shown in phenylephrine-induced contraction. Tissue responses were expressed as the percentage of KCl-induced contraction. Data are shown as the mean ± SEM of 5 to 6 animals. Two-way ANOVA followed by Bonferroni's post hoc test was used to compare PM20 to vehicle control at the first and second addition of phenylephrine. Abbreviations: KCl, potassium chloride, PE, phenylephrine. 152

Figure 3.14 Vasorelaxation effect of PM20 and Ca^{2+} channel blockers. Cumulative CRCs was compared between PM20 and (A) SOCC/non-selective TRPC inhibitors (2-APB, Pyr6, SKF-96365), (B) TRPC- selective inhibitors (HC-070, Pyr3), and (C) VGCC inhibitors (nifedipine, verapamil). Tissue relaxations were expressed as the percentage of phenylephrine-induced contraction. Data are shown as the mean ± SEM of 5 to 7 animals. Abbreviations: 2-APB, 2-aminoethoxydiphenyl borate, PE, phenylephrine; SOCC, store-operated Ca^{2+} channel; TRPC, transient receptor potential canonical; VGCC, voltage-gated Ca^{2+} channel....154

Figure 3.15 Effect of PM20 on (A) phenylephrine-, (B) KCl- and (C) U46619-induced contraction in normal Krebs and Ca^{2+}-free Krebs solution. Tissue responses were recorded at 0, 30, and 60 minutes after the addition of each contractile agent and were expressed as the percentage of KCl-induced contraction. Data are shown as the mean ± SEM of 5 to 6 animals. Two-way ANOVA followed by Bonferroni's post hoc test was used to compare vehicle control and PM20 treatment in either normal or Ca^{2+} free Krebs separately at each time point. Abbreviations: KCl, potassium chloride, PE, phenylephrine.....157

Figure 3.16 Effect of (A/B/C) Ca^{2+} channel blockers and (D) PM20 on $CaCl_2$-induced contraction in rat isolated aortic rings bathed in Ca^{2+}-free Krebs solution. The Ca^{2+} channel blockers used were (A) SOCC/non-selective TRPC inhibitors (2-APB, Pyr6, SKF-96365), (B) TRPC- selective inhibitors (Pyr3), and (C) VGCC inhibitors (nifedipine, verapamil).

Tissue contractions were expressed as the percentage of KCl-induced contraction in Ca^{2+}-containing Krebs solution. Data are shown as the mean ± SEM of 5 to 6 animals. Abbreviations: 2-APB, 2-aminoethoxydiphenyl borate; $CaCl_2$, calcium chloride; KCl, potassium chloride; SOCC, store-operated Ca^{2+} channel; TRPC, transient receptor potential canonical; VGCC, voltage-gated Ca^{2+} channel. 160

Figure 3.17 Effect of PM20-induced relaxation in the presence of different Ca^{2+} channel blockers. CRCs to PM20 were performed in the presence of SOCC/non-selective TRPC inhibitors – (A) 2-APB, (B) Pyr6, (C) SKF-96365; TRPC- selective inhibitors – (D) Pyr3; and VGCC inhibitors – (E) nifedipine, (F) verapamil. Tissue relaxations were expressed as the percentage of phenylephrine-induced contraction. Data are shown as the mean ± SEM of 5 to 6 animals. Abbreviations: 2-APB, 2-aminoethoxydiphenyl borate; PE, phenylephrine; SOCC, store-operated Ca^{2+} channel; TRPC, transient receptor potential canonical; VGCC, voltage-gated Ca^{2+} channel. 163

Figure 4.1 Effect of FK244 and PM20 on the lifespan of C. elegans. Heat-killed E. coli, DMSO and nemadipine A acted as the controls. The lifespan of the worms has been expressed as percentage of mean survival. Data are shown as mean ± SD of one representative biological replicate (n/N = 1/3). Abbreviation: DMSO, dimethyl sulfoxide.....192

Figure 4.2 Effect of carbachol-induced vasorelaxation in endothelium-intact (E+) and -denuded (E-) SD aorta, as well as in SHR isolated aorta. Tissue responses have been expressed as the percentage of phenylephrine-induced tone. Data are shown as the mean ± SEM of 4 to 5 animals. Abbreviations: PE, phenylephrine; SD, Sprague-Dawley rats; SHR, spontaneously hypertensive rats.....194

Figure 4.3 Vasorelaxation effect of FK244 and PM20 in SHR. The results of (A) FK244 and (B) PM20 in SHR isolated aortic rings were compared to vehicle controls and SD rats. Tissue responses have been expressed as the percentage of phenylephrine-induced tone. Data are shown as the mean ± SEM of 5 to 6 animals. Abbreviations: PE, phenylephrine; SD, Sprague-Dawley rats; SHR, spontaneously hypertensive rats.....196

Figure 4.4 Vasorelaxation effect of FK244 and PM20 in diabetic and non-diabetic rats. The effects of (A) FK244 and (B) PM20 in diabetic rats were compared to vehicle control and non-diabetic rats. Tissue responses have been expressed as the percentage of phenylephrine-induced tone. Data are shown as the mean ± SEM of 9 to 12 animals. Abbreviation: D, diabetic rats; ND, non-diabetic rats; PE, phenylephrine. 197

Figure 4.5 Cumulative CRCs of FK244 and PM20 in (A) SHR and (B) diabetic rats. Tissue responses have been expressed as the percentage of phenylephrine-induced tone. Data are shown as the mean ± SEM of 6 to 11 animals. Abbreviations: D, diabetic rats; PE, phenylephrine; SHR, spontaneously hypertensive rats.....198

Figure 4.6 Effect of FK244 in (A) SHR isolated aorta, bladder and trachea. Relaxation effect of FK244 were compared to their respective vehicle controls

(DMSO) in (B) aortic rings (C) bladder strips and (D) tracheal rings. Aortic tissue responses have been expressed as the percentage of phenylephrine-induced tone while bladder and tracheal tissues responses have been expressed as the percentage of carbachol-induced tone. Data are shown as the mean ± SEM of 5 to 8 animals. Abbreviations: CCH, carbachol; PE, phenylephrine. 200

Figure 4.7 Effect of FK244 on SNP-induced relaxation in SHR isolated aortic rings. Tissue responses have been expressed as the percentage of phenylephrine-induced contraction. Data represent the mean values ± SEM of 5 animals. Abbreviations: PE, phenylephrine; SNP, sodium nitroprusside.....202

Figure 4.8 Effect of FK244 on phenylephrine-induced contraction in SHR aortic rings. Cumulative CRCs to phenylephrine were constructed in the presence of 10 µM and 100 µM of FK244. Tissue responses have been expressed as the percentage of KCl-induced contraction. Data are shown as the mean ± SEM of 5 to 6 animals. Abbreviations: KCl, potassium chloride, PE, phenylephrine. 203

Figure 4.9 Concentration-dependent effect of FK244 on $CaCl_2$-induced contraction in SHR isolated aortic rings bathed in Ca^{2+}-free Krebs solution. Tissue responses have been expressed as the percentage of KCl-induced contraction. Data are shown as the mean ± SEM of 5 to 6 animals. Abbreviations: KCl, potassium chloride; $CaCl_2$, calcium chloride.....205

Figure 5.1 Illustration of a 96-well plate seeded with cells, representing one biological replicate. Each experiment was repeated six times (column 1 – 6) using the same compound, generating six technical replicates (n/N = 1/6). Column 7 to 12 in the 96-well plate (grey columns) were not utilised in all the experiments. 222

Figure 5.2 Grid etched on a haemocytometer. Cells fell on the top and left border of the centre grid (indicated with green border) was included but excluded on the right and bottom border (indicated with red border). Diagram adapted from Science ABC (2021). 222

Figure 5.3 FK244 inhibited Ca^{2+} influx via TRPC3 and TRPC6 channels. Representative $[Ca^{2+}]_i$ measurements recorded in a single 96-well plate (N = 6), measuring the inhibition of OAG-mediated Ca^{2+} influx by 0.1 – 100 µM FK244 in (A) (Tet+) HEK T-REx™ cells expressing hTRPC3 and (B) WT HEK 293 cells overexpressing hTRPC6. Concentration-response curves to FK244 were plotted for experiments in (C) hTRPC3 and (D) hTRPC6. Responses were calculated at 90 – 140 seconds compared to baseline $[Ca^{2+}]_i$ at 0 – 55 seconds. Data are shown as mean ± SEM (hTRPC3: n/N = 4/24; hTPRC6: n/N = 5/30). Abbreviations: DMSO, dimethyl sulfoxide; TRPC, transient receptor potential canonical. 227

Figure 5.4 PM20 inhibited Ca^{2+} influx via TRPC3 and TRPC6 channels. Representative $[Ca^{2+}]_i$ measurements recorded in a single 96-well plate (N = 6), measuring the inhibition of OAG-mediated Ca^{2+} influx by 0.1 – 100 µM PM20 in (A) (Tet+) HEK T-REx™ cells expressing hTRPC3 and

(B) WT HEK 293 cells overexpressing hTRPC6. Concentration-response curves to PM20 were plotted for experiments in (C) hTRPC3 and (D) hTRPC6. Responses were calculated at 90 – 140 seconds compared to baseline $[Ca^{2+}]_i$ at 0 – 55 seconds. Data are shown as mean ± SEM (hTRPC3: n/N = 5/30; hTPRC6: n/N = 5/30). Abbreviations: DMSO, dimethyl sulfoxide; TRPC, transient receptor potential canonical.....229

Figure 5.5 FK244 and PM20 did not induce Ca^{2+} influx via TRPC3 and TRPC6 activation. Representative $[Ca^{2+}]_i$ measurements recorded in a single 96-well plate (n/N = 1/6), showing (A) FK244 and (B) PM20 did not shift basal Ca^{2+} level in TRPC3 -expressing HEK cells. Similarly, no influx of Ca^{2+} was recorded in TRPC6-expressing HEK cells after addition of (C) FK244 and (D) PM20. Abbreviations: DMSO, dimethyl sulfoxide; TRPC, transient receptor potential canonical. 230

Figure 5.6 Representative Ca^{2+} recordings showing FK244 and PM20 did not evoke intracellular Ca^{2+} release in WT cells in Ca^{2+}-containing and Ca^{2+}-free environment (n/N = 1/6). In Ca^{2+}-containing SBS, 0.3 – 100 µM of (A) FK244 and (B) PM20 did not cause an increase in $[Ca^{2+}]_i$ through store depletion like thapsigargin. A similar observation was recorded in Ca^{2+}-free SBS containing 0.3 – 100 µM of (C) FK244 and (D) PM20. Abbreviations: Ca^{2+}, calcium ion; DMSO, dimethyl sulfoxide; TRPC, transient receptor potential canonical; WT, wild type.....231

Figure 6.1 Schematic diagram illustrating the purported vasorelaxation mechanisms of FK244 and PM20 in rat isolated aorta. Pharmacological inhibitors are shown in red font. Solid pointed solid arrow denotes downstream effectors activation, blunt arrow denotes downstream effectors inhibition. Dotted arrows denote flow of Ca^{2+}. The pathways inhibited by FK244 and PM20 are indicated with red crosses. Question mark indicates the possible inhibition of FK244 and PM20 on TRPC1/4/5 channels. Abbreviations: 2-APB, 2-aminoethoxydiphenyl borate; 4-AP, 4-aminopyridine; AC adenylyl cyclase; ATP adenosine triphosphate; $BaCl_2$ barium chloride; Ca^{2+}, calcium ion; CaM, calmodulin; cAMP, 3'-5'-cyclic adenosine monophosphate; cGMP, 3'-5'-cyclic guanosine monophosphate; CRAC, Ca^{2+} release-activated channels; DAG, diacylglycerol; eNOS endothelial nitric oxide synthase; GTP, guanosine-5'-triphosphate; IP_3, inositol-1,4,5-trisphosphate; IP_3R, IP_3 receptor; L-arg, L-arginine; MLC, myosin light chain; MLCK, MLC kinase; MLCP, MLC phosphatase; MLC-P, phosphorylated MLC; NO nitric oxide; NSCC, non-selective cation channels; ORAI, Ca^{2+} release-activated Ca^{2+} channel modulator; PIP_2, phosphatidylinositol 4,5-bisphosphate; PKA protein kinase A; PKC, protein kinase C; PKG, protein kinase G; PLC; phospholipase C; ROCC, receptor-operated Ca^{2+} channels; RyR, ryanodine receptor; SERCA, sarco/endoplasmic reticulum Ca^{2+}-ATPase; sGC soluble guanylyl cyclase; SOCC, store-operated Ca^{2+} channels; SR, sarcoplasmic reticulum; STIM, stromal interaction molecule; TEA tetraethylammonium chloride; TRPC, transient receptor potential canonical; VGCC, voltage-gated Ca^{2+} channels. 251

Tables

Table 1.1 Expression of TRPC3 and TRPC6 mRNAs and proteins in VSM preparations. 22

Table 1.2 Pathophysiology of TRPC-related hypertension. 26

Table 1.3 Examples of plant-derived alkaloids with antihypertensive activity. 29

Table 1.4 Chemical structure and physicochemical analysis of schwarzinicine A using Lipinski's Rule of Five and Veber's rule. The values that have exceeded the limit are highlighted in red.....36

Table 2.1 Summary of drugs and their details. 56

Table 2.2 Chemical structure and physicochemical analysis of FK244, nifedipine, SKF-96365 and Pyr3 using Lipinski's Rule of Five and Veber's rule. 71

Table 2.3 Maximum tissue response (E_{max}) and potency (pEC_{50}) of FK244 in rat isolated aorta, bladder and trachea after being induced contraction with their respective contractile agents. 74

Table 2.4 Maximum tissue response (E_{max}) and potency (pEC_{50}) of FK244-induced vasorelaxation with prior treatment of K^+ blockers in rat isolated aortic rings.....85

Table 2.5 Maximum tissue response (E_{max}) and potency (pEC_{50}) of vehicle control and FK244 derived from the respective CRCs with phenylephrine, KCl or U46619 as the pre-contractile agent. 88

Table 2.6 Maximum tissue response (E_{max}) and potency (pEC_{50}) of phenylephrine, KCl, serotonin and U46619 in the presence of FK244 (10 µM, 30 µM, 100 µM) and their respective vehicle controls. 91

Table 2.7 Maximum tissue response (E_{max}) and potency (pEC_{50}) of FK244 and known Ca^{2+} channel blockers in rat isolated aortic rings.....95

Table 2.8 Maximum tissue response (E_{max}) and potency (pEC_{50}) of phenylephrine following pre-exposure of known Ca^{2+} channel blockers in aortic tissues. 98

Table 2.9 Maximum tissue response (E_{max}) of phenylephrine, KCl and U46619-induced contraction in normal Krebs and Ca^{2+}-free Krebs solution in the presence of FK244. 101

Table 2.10 Maximum tissue response (E_{max}) of $CaCl_2$ CRCs following pre-exposure of vehicle control, FK244 or Ca^{2+} channel blockers. 104

Table 2.11 Maximum tissue response (E_{max}) and potency (pEC_{50}) of FK244 in the presence of different Ca^{2+} channel blockers. 107

Table 3.1 Chemical structure and physicochemical analysis of PM20, nifedipine, SKF-96365 and Pyr3 using Lipinski's Rule of Five and Veber's rule. 133

Table 3.2 Comparison of the maximum tissue response (E_{max}) and potency (pEC_{50}) of vehicle and PM20 in rat isolated aorta, bladder and trachea after being induced contraction with their respective contractile agents. 137

Table 3.3 Maximum tissue relaxation (E_{max}) and potency (pEC_{50}) of PM20-induced vasorelaxation with prior treatment of K^+ blockers in rat isolated aortic rings.....145

Table 3.4 Maximum response (E_{max}) and pEC_{50} values of vehicle control and PM20 derived from the respective CRCs with phenylephrine, KCl or U46619 as the pre-contractile agonist. 148

Table 3.5 Summary of the maximum tissue responses (E_{max}) and potency (pEC_{50}) of the contractile response of phenylephrine, KCl, serotonin and U46619 in the presence of PM20 (10 µM, 30 µM, 100 µM) and their respective vehicle controls.....151

Table 3.6 Summary of the maximum tissue relaxation (E_{max}) and potency (pEC_{50}) of PM20 and known Ca^{2+} channel blockers in rat isolated aortic rings.155

Table 3.7 Maximum tissue response (E_{max}) of phenylephrine, KCl and U46619-induced contraction in normal Krebs and Ca^{2+}-free Krebs solution in the presence of PM20.....158

Table 3.8 Maximum tissue response (E_{max}) and pEC_{50} of $CaCl_2$ CRCs following pre-exposure to vehicle control, PM20 or Ca^{2+} channel blockers. 161

Table 3.9 Maximum relaxation (E_{max}) and pEC_{50} values of PM20 in the presence of different Ca^{2+} channel blockers. 164

Table 4.1 Summary of chemicals and their details. 182

Table 4.2 Details on stock and final concentration, concentration of DMSO, and volume of stock solution and heat-killed E. coli required during preparation of plates. 185

Table 4.3 Summary of the mean lifespan for nematodes exposed to control (heat-killed E. coli), vehicle control (DMSO 5%), nemadipine A and FK244. 193

Table 4.4 Summary of the mean lifespan for nematodes exposed to control (heat-killed E. coli), vehicle control (DMSO 5%), nemadipine A and PM20. 193

Table 4.5 Comparison of the maximum percentage response (E_{max}) and potency (pEC_{50}) of vehicle control, FK244 and PM20 in aortae isolated from SD rats and SHR.....196

Table 4.6 Comparison of the maximum percentage response (E_{max}) and potency (pEC_{50}) of vehicle control, FK244 and PM20 in aortae isolated from non-diabetic and diabetic rats.....197

Table 4.7 Comparison of the maximum percentage response (E_{max}) and potency (pEC_{50}) of vehicle and FK244 in SHR isolated aorta, bladder and trachea after induced contraction with their respective contractile agents. 201

Table 4.8 Maximum response (E_{max}) and pEC_{50} values derived from phenylephrine's CRCs after pre-exposure to vehicle control and FK244 (10 µM, 100 µM). 204

Table 4.9 Maximum tissue response (E_{max}) of $CaCl_2$ derived from respective CRCs in the presence of vehicle control or FK244. 206

Table 5.1 Summary of chemicals and their details. *219*

Table 6.1 Pharmacological comparison between FK244 and PM20. ..... *247*

Table 6.2 Comparison between the parent compound schwarzinicine A and its analogues FK244 and PM20. ..... *249*

Table of Contents

Abstract i

Publications / Awards iii

Acknowledgements v

Declaration vi

Abbreviations vii

Figures and tables xiii

Chapter 1 Introduction 1

1.1 Hypertension 1

1.1.1 Regulation of blood pressure 2

1.1.2 Pathophysiology of hypertension 6

1.1.3 Antihypertensive therapy and limitations 9

1.1.4 Cost of antihypertensive drug therapy and limitations 11

1.2 Resistant Hypertension 11

1.2.1 Interventions and limitations 11

1.3 Ca^{2+} signalling in VSM 13

1.3.1 Ca^{2+} release from the intracellular stores 13

1.3.2 Ca^{2+} entry from the extracellular space 13

1.3.3 Ca^{2+} sequestration and extrusion 14

1.3.4 Ca^{2+}-dependent mechanisms of VSM contraction and relaxation 17

1.3.5 Ca^{2+}-independent regulation of VSM contraction and relaxation 18

1.4 TRPC channels in the vasculature 20

1.4.1 Expression of TRPC3 and TRPC6 in the vasculature 21

1.4.2 Structure of TRPC3 and TRPC6 channels 23

1.4.3 Involvement of TRPC3 and TRPC6 channels in CVDs 25

1.5 Natural products in drug discovery 27

1.5.1 Medicinal plants and alkaloids with antihypertensive effects 27
1.5.2 Schwarzinicine A as a lead compound 32
1.5.2.1 Background 32
1.5.2.2 Biological and physicochemical properties of schwarzinicine A ...34
1.5.2.3 Synthetic schwarzinicine analogues 37
1.6 Research approaches 38
1.6.1 Isolated tissue bath 38
1.6.2 *Caenorhabditis elegans (C. elegans)* 41
1.6.3 Fluorometric intracellular Ca^{2+} recordings 44
1.6.3.1 HEK 293 cell as an expression system for TRPC channels.....46
1.7 Research aim 47

Chapter 2 Pharmacological investigation of *N*-phenethyl-1,2,3,4-tetrahydronaphthalen-2-amine (FK244)49

2.1 Introduction.....49
2.1.1 Schwarzinicine A and FK244 49
2.1.2 Synthesis of *N*-phenethyl-1,2,3,4-tetrahydronaphthalen-2-amine (FK244) 51
2.1.3 Lipinski's Rule of Five and Veber's rule.....52
2.2 Significance of study 54
2.3 Materials and methods 54
2.3.1 Analysis of physicochemical properties on FK244 and other commonly used Ca^{2+} channel blockers.....54
2.3.2 Drugs and solutions.....55
2.3.3 Isolated tissue preparations 58
2.3.3.1 Rat isolated tissues 58
2.3.3.2 Porcine isolated tissues 58
2.3.4 Organ bath setup 59
2.3.5 Isometric tension recordings 61
2.3.5.1 Effect of FK244 on rat isolated tissues at basal tension and raised muscle tone 61
2.3.5.2 Effect of FK244 on porcine pulmonary artery and bronchiole pre-contracted with phenylephrine and carbachol.....61

2.3.5.3 Role of endothelium on FK244-induced relaxation.....62

2.3.5.4 Role of NO in FK244-induced relaxation.....62

2.3.5.5 Role of cAMP and cGMP in FK244-induced relaxation.....62

2.3.5.6 Role of α-, β- adrenoceptors in FK244-induced relaxation 63

2.3.5.7 Role of K^+ channels in FK244-induced relaxation 63

2.3.5.8 Effect of FK244 on aorta pre-contracted with different contractile agents 64

2.3.5.9 Effect of FK244 on the contractile response induced by different contractile agents 64

2.3.5.10 Reversibility of FK244's inhibition against phenylephrine-induced contraction.....64

2.3.5.11 Effect of Ca^{2+} channel blockers in rat isolated aorta pre-contracted with phenylephrine.....65

2.3.5.12 Effect of Ca^{2+} channel blockers on phenylephrine-induced contraction.....65

2.3.5.13 Effect of FK244 on intracellular Ca^{2+}-induced vasoconstriction ...65

2.3.5.14 Effect of FK244 on contractile responses to Ca^{2+} re-introduction .66

2.3.5.15 Effect of Ca^{2+} channel blockers on FK244-induced relaxation 66

2.3.6 Data analysis 67

2.4 Results 70

2.4.1 Physicochemical properties of FK244 obey Lipinski's and Veber's rule analysis 70

2.4.2 FK244-induced smooth muscle relaxation was observed in rat isolated aorta, bladder and trachea at raised vascular tone but not at basal tone 72

2.4.3 FK244 was equally efficacious but less potent in porcine tissues 75

2.4.4 FK244 induced similar relaxation profile in endothelium-intact (E+) and -denuded (E-) rat isolated aortae.....77

2.4.5 Presence of L-NAME did not reduce FK244-induced relaxation 80

2.4.6 Forskolin and ODQ did not affect FK244-induced vasorelaxation 81

2.4.7 FK244-induced relaxation was not influenced by α- and β-adrenoceptor antagonists 82

2.4.8 FK244-induced relaxation was not influenced by K^+ channel blockers 84

2.4.9 FK244 relaxation profile was not similar across different contractile agents 86

2.4.10 FK244 attenuated the CRCs of phenylephrine, KCl and serotonin but not U46619 89

2.4.11 Contraction to phenylephrine recovered after FK244-treated tissues were washed 92

2.4.12 FK244 exhibited similar vasorelaxant properties as verapamil 93

2.4.13 Ca^{2+} channel blockers of different mechanism of actions showed divergent responses in phenylephrine-induced contraction 96

2.4.14 Pre-incubation with FK244 did not affect intracellular-induced contraction mediated by different contractile agents 99

2.4.15 Extracellular Ca^{2+}-induced contraction was suppressed by FK244 102

2.4.16 TRPC-selective inhibitors attenuated FK244's vasorelaxation effect . 105

2.5 Discussion 108

2.5.1 Physicochemical properties of FK244 – a theoretical calculation 108

2.5.2 Tissue selectivity of FK244 109

2.5.3 Role of endothelium and NO 111

2.5.4 Role of cyclic nucleotides 111

2.5.5 Role of adrenoceptors 112

2.5.6 Role of K^+ channels 112

2.5.7 Role of contractile agents 112

2.5.8 Reversibility of FK244 as an inhibitor to phenylephrine-induced contraction 117

2.5.9 Role of intra- and extracellular Ca^{2+} 118

2.5.10 Relaxation profiles of FK244 and other Ca^{2+} channel blockers 119

2.5.11 Role of extracellular Ca^{2+}-permeable channels 120

2.6 Chapter summary 123

Chapter 3 Pharmacological investigation of 1-(furan-2-yl)-*N*-phenethylpentan-3-amine (PM20) 124

3.1 Introduction.....124

3.1.1 Schwarzinicine A and PM20 124

3.1.2 Synthesis of 1-(furan-2-yl)-*N*-phenethylpentan-3-amine (PM20).....125

3.2 Significance of study.....127

3.3 Materials and methods.....127

3.3.1 Analysis of physicochemical properties on PM20 and Ca^{2+} channel blockers.....127

3.3.2 Drugs and solutions.....127

3.3.3 Rat isolated tissue preparations.....128

3.3.4 Organ bath setup 128

3.3.5 Isometric tension recordings.....128

3.3.5.1 Effect of PM20 on rat isolated tissues at basal tension and raised muscle tone 128

3.3.5.2 Role of endothelium on PM20-induced relaxation.....128

3.3.5.3 Role of NO in PM20-induced relaxation.....129

3.3.5.4 Role of cAMP and cGMP in PM20-induced relaxation.....129

3.3.5.5 Role of α-, β- adrenoceptors in PM20-induced relaxation.....129

3.3.5.6 Role of K^+ channels in PM20-induced relaxation 129

3.3.5.7 Effect of PM20 on aorta pre-contracted with different contractile agents 129

3.3.5.8 Effect of PM20 on the contractile response induced by different contractile agents 130

3.3.5.9 Reversibility of PM20's inhibition against phenylephrine-induced contraction.....130

3.3.5.10 Effect of PM20 compared to the CRCs of Ca^{2+} channel blockers in rat isolated aorta.....130

3.3.5.11 Effect of PM20 on intracellular Ca^{2+}-induced vasoconstriction...130

3.3.5.12 Effect of PM20 on contractile responses to Ca^{2+} re-introduction.130

3.3.5.13 Effect of Ca^{2+} channel blockers on PM20-induced relaxation 131

3.3.6 Data analysis 131

3.4 Results.....132

3.4.1 Physicochemical properties of PM20 obey Lipinski's and Veber's rule analysis 132

3.4.2 PM20 did not induce tissue contraction at basal tone but relaxed pre-contracted smooth muscle tissues 134

3.4.3 PM20 induced similar relaxation in endothelium-intact (E+) and -denuded (E-) rat isolated aortae 138

3.4.4 Incubation with L-NAME did not suppress PM20-induced relaxation 140

3.4.5 PM20-induced relaxation was not affected by forskolin and ODQ 141

3.4.6 PM20-induced relaxation was not influenced by α- and β-adrenoceptor antagonists 142

3.4.7 PM20-induced relaxation was not affected by K^+ channel blockers 144

3.4.8 PM20 was the most potent in relaxing phenylephrine-induced contraction 146

3.4.9 PM20 attenuated maximum tissue contraction induced by phenylephrine, KCl and serotonin but not U46619 149

3.4.10 Contraction to phenylephrine recovered after PM20-treated tissues were washed 152

3.4.11 PM20 displayed similar vasorelaxation profiles as nifedipine and verapamil 153

3.4.12 PM20 has no effect on intracellular Ca^{2+}-induced contraction mediated by phenylephrine, KCl and U46619 156

3.4.13 PM20 suppressed extracellular Ca^{2+}-induced contraction in rat aortae 159

3.4.14 PM20-induced relaxation was diminished in the presence of TRPC-selective inhibitors 162

3.5 Discussion 165

3.5.1 Physicochemical properties of PM20 – a theoretical calculation 165

3.5.2 Tissue selectivity of PM20 166

3.5.3 Role of endothelium and NO 167

3.5.4 Role of cyclic nucleotides 167

3.5.5 Role of adrenoceptors 168

3.5.6 Role of K^+ channels 168

3.5.7 Role of contractile agents 169

3.5.8 Reversibility of PM20 as an inhibitor to phenylephrine-induced contraction 171

3.5.9 Role of intra- and extracellular Ca^{2+} 171

3.5.10 Relaxation profiles of PM20 and other Ca^{2+} channel blockers.....174

3.5.11 Role of extracellular Ca^{2+}-permeable channels 174

3.6 Chapter summary.....175

Chapter 4 Effects of FK244 and PM20 on the lifespan of *C. elegans* and *in vitro* pharmacological evaluation in disease models 176

4.1 Introduction.....176

4.1.1 Toxicity assessment 176

4.1.2 *glp-4* mutated *C. elegans* 177

4.1.3 Vascular pathologies in SHR 177

4.1.4 Hypertension and diabetes 179

4.1.5 STZ-induced diabetic rat model.....179

4.2 Significance of study 180

4.3 Materials and methods 181

4.3.1 Drugs and solutions.....181

4.3.2 Toxicity screening.....183

4.3.2.1 *C. elegans* strain.....183

4.3.2.2 Culturing of *C. elegans* 183

4.3.2.3 Preparation of NGM and *E. coli* for routine maintenance 183

4.3.2.4 Worm chunking 184

4.3.2.5 Preparation of plates for lifespan assay 184

4.3.2.6 Age synchronisation.....185

4.3.2.7 Lifespan assay 186

4.3.3 Blood pressure measurement in SHR 187

4.3.4 Induction of diabetes in Wistar rats 187

4.3.5 Rats isolated tissue preparation.....188

4.3.6 Organ bath set-up 188

4.3.7 Isometric tension recordings 189

4.3.7.1 Effect of endothelium integrity on carbachol-induced relaxation 189

4.3.7.2 Effect of FK244 and PM20 on SHR and diabetic rat isolated aorta pre-contracted by phenylephrine.....189

4.3.7.3 Effect of FK244 on SHR isolated trachea and bladder pre-contracted by carbachol 189

4.3.7.4 Effect of FK244 in NO/cGMP-induced vasorelaxation 189

4.3.7.5 Effect of FK244 on phenylephrine-induced contraction 190

4.3.7.6 Effect of FK244 on contractile response to Ca^{2+} re-introduction 190

4.3.8 Data analysis 190

4.4 Results 191

4.4.1 FK244 and PM20 did not affect the lifespan of the worms at a lower concentration 191

4.4.2 Carbachol-induced relaxation in SHR isolated aortae was attenuated compared to SD 194

4.4.3 FK244 and PM20 induced vasorelaxation in SHR and diabetic rat aortae at raised vascular tone 195

4.4.4 FK244 was more potent than PM20 in SHR aortic tissues but equally effective in diabetic rat isolated aortae 198

4.4.5 FK244 induced relaxation on aortic, tracheal and bladder smooth muscle tissues of SHR 199

4.4.6 Presence of FK244 did not affect SNP-induced vasorelaxation in SHR 202

4.4.7 FK244 attenuated phenylephrine-induced contraction in SHR 203

4.4.8 FK244 inhibited Ca^{2+}-induced contraction in SHR 205

4.5 Discussion 207

4.5.1 Effect of FK244 and PM20 on the lifespan of *C. elegans* 207

4.5.2 Endothelium impairment in SHR 209

4.5.3 Relaxation profiles of FK244 and PM20 in disease models 209

4.5.4 Pharmacological evaluation of FK244 in SHR-isolated aortae 212

4.6 Chapter summary 213

Chapter 5 Effects of FK244 and PM20 on TRPC3 and TRPC6 channels and internal Ca^{2+} store in HEK 293 cells 214

5.1 Introduction.....214

5.1.1 Role of TRPC3 and TRPC6 in Ca^{2+} signalling.....214

5.1.2 TRPC3 and TRPC6 channels as therapeutic targets.....216

5.2 Significance of study.....217

5.3 Materials and methods.....217

5.3.1 Drugs and materials.....217

5.3.2 Sub-culturing human TRPC3-expressing (Tet+) HEK T-REx^{TM} and wild-type (WT) HEK 293 adherent cells.....220

5.3.3 Transfection of TRPC6 channel in WT cells.....220

5.3.4 Plating cells for experiments.....221

5.3.5 Fluorometric intracellular Ca^{2+} recordings.....223

5.3.5.1 Effects of FK244 and PM20 on OAG-mediated TRPC channel activation.....223

5.3.5.2 Effects of FK244 and PM20 on basal Ca^{2+} level via TRPC3 and TRPC6 channels.....224

5.3.5.3 Effects of FK244 and PM20 on intracellular Ca^{2+} store.....224

5.3.6 Data analysis.....225

5.4 Results.....226

5.4.1 FK244 and PM20 suppressed TRPC-mediated Ca^{2+} influx in HEK 293 cells.....226

5.4.2 FK244 and PM20 did not affect basal Ca^{2+} level through activation of TRPC3 and TRPC6 channels.....230

5.4.3 FK244 and PM20 did not affect intracellular store Ca^{2+} release.....231

5.5 Discussion.....232

5.6 Chapter summary.....235

Chapter 6 General discussion 236

6.1 Introduction..... 236

6.2 Functional role of FK244 and PM20 in VSM tissue..... 236

6.3 Ca^{2+} modulation property of FK244 and PM20 242

6.4 Analogues vs the parent compound: A comparison between FK244, PM20 and schwarzinicine A..... 249

6.5 Purported mechanism of actions of FK244 and PM20 250

6.6 Toxicity of FK244 and PM20 on the lifespan in *C. elegans* 252

6.7 Clinical potential of FK244 and PM20 253

6.8 Limitations of study..... 255

6.9 Future work..... 259

6.9.1 Functional assay..... 259

6.9.2 TRPC expression 260

6.9.3 Cell-based assay..... 260

6.9.4 *In vivo* assay..... 263

6.9.5 Binding assay..... 263

6.10 Concluding statements 264

Appendix A Synthesis of FK244 265

Appendix B Ethics approval – SD rats..... 267

Appendix C Synthesis of PM20..... 273

Appendix D Ethics approval – SHR 278

Appendix E Ethics approval – Wistar rats 283

Appendix F Activation of TRPC3 and TRPC6 channels by OAG..... 284

References 285

Chapter 1 Introduction

1.1 Hypertension

Hypertension, more commonly known as high blood pressure, is a condition where one's blood pressure is persistently raised. Clinically, hypertension is diagnosed when a patient has a systolic blood pressure/diastolic blood pressure (SBP/DBP) higher than 140/90 mmHg (Malaysian Society of Hypertension, 2018; NICE, 2019; Whelton, Carey, Aronow, et al., 2018).

Globally, the number of people with hypertension was estimated at 1.13 billion (World Health Organization, 2013; Bin Zhou, Bentham, Di Cesare, et al., 2017). Hypertension affects 6.4 million people in Malaysia and 13.5 million people in the United Kingdom (UK) (Institute for Public Health, 2020; NICE, 2019). Sedentary lifestyle, diet high in sodium and saturated fats, diabetes, obesity and smoking are contributing factors to the development of hypertension (Unger, Borghi, Charchar, et al., 2020; Whelton et al., 2018). Most hypertensive cases remained undiagnosed as it rarely presents with any symptoms in the early stage. When blood pressure has remained high and uncontrolled for a significant amount of time, the patient may experience dizziness, shortness of breath, nosebleed and even chest pain.

Hypertension is one of the risk factors for cardiovascular diseases (CVDs). When CVDs are not properly managed, it increases the risk of lethal events such as myocardial infarction or stroke (Fuchs & Whelton, 2020). CVDs are reported to be the number one leading cause of death in Malaysia and worldwide (Malaysian Society of Hypertension, 2018; World Health Organization, 2017). National Institute for Health and Care Excellence (NICE) UK reported that for every 2 mmHg increment in SBP, the risk of mortality of ischaemic heart disease and stroke increased by 7% to 10%, respectively. It is estimated that in each year, 4.9 million of death incidents are caused by ischaemic heart disease, while haemorrhagic stroke and ischaemic stroke account for 2 million and 1.5 million of deaths (Forouzanfar et al., 2017).

1.1.1 Regulation of blood pressure

The autonomic nervous system is known for cardiovascular regulation. It controls blood pressure by modulating cardiac output and peripheral vascular resistance. Numerous endogenous vasodilators and constrictors regulate peripheral vascular resistance. The vascular endothelium is a monolayer of cells that separates the blood and tissues. It was found in the interior lining of the wall of arteries, veins, and capillaries. The endothelium regulates vascular permeability by maintaining the extravasation of solutes, hormones, and fluid between intra- and extra-vascular compartments, achieving a balanced vascular tone and blood pressure. Since the discovery of vasodilators such as prostaglandin I_2 (PGI_2), nitric oxide (NO), and endothelium-derived hyperpolarising factors (EDHFs), the participation of endothelium in the blood pressure regulation has become more apparent (Furchgott & Vanhoutte, 1989; Furchgott & Zawadzki, 1980; Weksler, Marcus, & Jaffe, 1977). Endothelium-derived NO, cyclooxygenase (COX)-derived PGI_2 and EDHFs are released in response to endogenous stimuli, such as neuropeptides (e.g. substance P), acetylcholine (ACh), bradykinin and mechanical stimuli like shear stress (Marti, Gheorghiade, Kalogeropoulos, et al., 2012). Besides, endothelial-dependent vasoconstrictors such as endothelin (ET), thromboxane A_2 (TXA_2), and reactive oxygen species (ROS), are also the key players in maintaining vascular tone.

Physiological stimuli such as shear stress and stretch contribute to blood pressure control. Under normal physiological conditions, low shear stress in the vasculature produces NO through the activation of endothelial nitric oxide synthase (eNOS) via kinases such as phosphatidylinositol-3-kinase (PI3K)/protein kinase B (AKT), protein kinase A (PKA), protein kinase C (PKC) signalling pathways (Kong, Qu, Li, et al., 2017; Sriram, Laughlin, Rangamani, et al., 2016). This major vasodilator NO is converted from L-arginine through an enzymatic process of eNOS in the endothelial cells. NO produced then diffuses to the neighbouring vascular smooth muscle (VSM), relaxes the blood vessels by binding to soluble guanylyl cyclase (sGC). Activation of sGC converts guanosine-5'-triphosphate (GTP) to 3’-5’-cyclic guanosine monophosphate (cGMP) by cleaving two phosphate groups. cGMP activates protein kinase G (PKG), which promotes vasorelaxation through dephosphorylation of phosphate-bound myosin light chain (MLC). Furthermore, NO is also known to downregulate the activity of ET-1 on ET receptors subtype A and B. ET-1

predominantly activates ET_A receptors on VSM cells (VSMCs), where it induces an increase in intracellular calcium concentration ($[Ca^{2+}]_i$) and leads to vascular contraction (Khalil, 2011). As $[Ca^{2+}]_i$ elevated due to the stimulation of ET-1 on endothelial ET_B receptors, it contributes to the production of PGI_2 and EDHFs (Houde, Desbiens, & D'Orléans-Juste, 2016).

Another major group of mediators that elicit relaxation are known as the EDHFs. Putative EDHF includes hydrogen peroxide (H_2O_2), epoxyeicosatrienoic acids (EETs), C-natriuretic peptide (CNP), carbon monoxide (CO), and hydrogen sulphide (H_2S) (Sandoo, Veldhuijzen van Zanten, Metsios, et al., 2015). Multiple pathways are involved in the relaxation responses produced by endogenous EDHFs, such as the synergistic interaction with NO and activation of sGC and PKG, leading to cGMP-induced relaxation. Moreover, EDHFs are known to induce COX-1-dependent release of PGI_2 and hyperpolarise the VSM plasma membrane through the opening of potassium ion (K^+) channels (Félétou, 2011). Endothelium-derived hyperpolarisation involves the activation of endothelial small- and intermediate-conductance calcium ion (Ca^{2+})-activated K^+ (SK_{Ca} and IK_{Ca}) channels, resulting in the inhibition of Ca^{2+} influx via voltage-gated Ca^{2+} channels (VGCCs) in smooth muscle layer (Félétou, 2011).

COX exists in two isoforms – COX-1 and COX-2, where both convert arachidonic acid to PGH_2, the common metabolite for the synthesis of TXA_2 by thromboxane synthase and PGI_2 by prostacyclin synthase (Caughey, Cleland, Penglis, et al., 2001). PGI_2 causes vasorelaxation by increasing the concentration of 3'-5'-cyclic adenosine monophosphate (cAMP) through adenylyl cyclase (AC) activation in the VSMC. cAMP accumulation inhibits the activity of MLC kinase (MLCK), thereby preventing vascular contraction caused by Ca^{2+}. On the other hand, COX-derived TXA_2 is known as a potent vasoconstrictor. It stimulates smooth muscle thromboxane prostanoid (TP) receptors and downstream G_q receptor activation (Félétou, Köhler, & Vanhoutte, 2010). The elevation of Ca^{2+} following G_q receptor activation leads to vasoconstriction.

Arterial baroreceptors, located at the aortic arch and carotid sinus, are a group of mechanosensors that detect changes in blood pressure (Wehrwein & Joyner, 2013). They are stimulated by rising blood flow and pressure that stretch the vessel wall. Shear stress diminishes the sympathetic output in healthy vessels (Armstrong & Moore, 2019). Moreover, baroreceptor-mediated reflex rapidly upregulates parasympathetic activity

to maintain the total peripheral resistance and cardiac output within a normalised range (Lobo, Sobotka, & Pathak, 2017). Activation of the sympathetic and parasympathetic systems in response to blood pressure changes, evoke the release of neurotransmitters such as ACh and noradrenaline. Endothelial synthesis of ACh requires mitochondrial-generated acetyl-coenzyme A and choline (Wilson, Lee, & McCarron, 2016). The effect of adrenaline, a hormone secreted by the adrenal medulla, in the regulation of vascular tone is also critical (Guyenet, 2006; Giuseppe Mancia & Grassi, 2014). ACh binds to muscarinic receptors expressed on the vasculature. Muscarinic receptors are either coupled to $G_{q/11}$ proteins (M_1, M_3, and M_5 subtypes) that increases $[Ca^{2+}]_i$ via phospholipase C (PLC) activation or $G_{i/o}$ proteins (M_2 and M_4 subtypes) that attenuates cAMP-dependent signalling (Sandow, Senadheera, Grayson, et al., 2012). ACh evokes vasorelaxation by activating M_3 receptors that are predominantly expressed on the endothelial cells (Tangsucharit, Takatori, Zamami, et al., 2016). The increase of Ca^{2+} in vascular endothelial cells triggers a wide range of signal transduction pathways, including the activation of eNOS that synthesises NO, prostaglandins production and the release of EDHFs (Kellogg, Zhao, Coey, et al., 2005; Nguyen, Lee, Park, et al., 2013).

Circulating endogenous catecholamines – noradrenaline and adrenaline, act on adrenoceptors. Stimulation of α-adrenoceptors on VSM elicits vasoconstriction and increases blood pressure. However, activation of β_2-adrenoceptors that are primarily expressed on VSMC produces a prominent vasorelaxant effect (Wallukat, 2002). The occupation of catecholamines on these adrenoceptors contributes complexly to the adrenergic regulation of vascular resistance. For example, α_1-adrenoceptor is linked to G_q protein that promotes extracellular Ca^{2+} influx and releases Ca^{2+} from sarcoplasmic reticulum (SR) store. Meanwhile, α_2-adrenoceptor activates inhibitory G_i protein that limits vasorelaxation by inhibiting AC's activity and reducing the production of second messenger cAMP. G_s protein is responsible for β_2-adrenoceptors downstream signalling upon cellular activation by noradrenaline and adrenaline. They oppose the effects of G_i protein, where it stimulates cAMP-dependent PKA and vasorelaxation (Goldstein, 2010).

Bidirectional interactions between the autonomic control and renin-angiotensin-aldosterone system (RAAS) also play crucial roles in regulating blood pressure. Renin released from the kidney acts on angiotensinogen, forming angiotensin (AT) I.

Subsequently, angiotensin converting enzyme (ACE) rapidly converts AT I into AT II. Under normal physiological vascular resistance, AT II is an important vasoactive substance that maintains vascular tone. AT II stimulates aldosterone secretion by acting on AT receptors found in the adrenal gland and vasopressin secretion at the posterior pituitary gland (Fountain & Lappin, 2018; Oparil, Zaman, & Calhoun, 2003). Aldosterone stimulates water and sodium ion (Na^+) reabsorption in the nephrons, increasing the circulating blood volume and blood pressure. AT II demonstrates a positive ionotropic effect on the cardiac muscle that increases cardiac output, further driving the sympathetic activity (Ames, Atkins, & Pitt, 2019; Oparil et al., 2003). Furthermore, AT II is also a potent vasoconstrictor that couples to G_q protein receptors, which mediate Ca^{2+} sensitisation to elicit vasoconstriction and increase blood pressure (Kuo & Ehrlich, 2015; Wynne, Chiao, & Webb, 2009).

On the other hand, hormones such as atrial natriuretic peptide (ANP) and brain natriuretic peptide (BNP) are antagonistic to RAAS. They reverse the reabsorption of Na^+, counterbalance the release of renin, aldosterone and vasopressin. ANP hormone encourages the release of vasodilators such as NO and PGI_2. Within this peptide family, C-type natriuretic peptide (CNP), mainly synthesised and found in endothelial cells, also possess a blood-pressure-lowering effect (Fu, Ping, Wang, et al., 2018; Richards, 2007; Sarzani, Spannella, Giulietti, et al., 2017). These natriuretic peptides promote vascular relaxation by the opening of large-conductance Ca^{2+}-activated K^+ channel (BK_{Ca}), ATP-sensitive K^+ channel (K_{ATP}) channels and reduce cell proliferation (Félétou, 2011; Lumsden, Khambata, & Hobbs, 2010; Pandey, 2008; Wilkins, Redondo, & Brown, 1997).

All these mechanisms described above are constitutively active to maintain basal vascular tone. They are essential in response to any fluctuations in cardiac output and blood pressure to prevent disruption in vascular homeostasis. Any chronic perturbations may disturb the balance between vasorelaxation and vasoconstriction, increasing the risk of progression into vascular pathologies and hypertension. If left untreated, cardiovascular events such as aneurysm, stroke and heart attack may occur.

1.1.2 Pathophysiology of hypertension

Baroreceptor reflex reduces the fluctuation in arterial blood pressure. Resetting of the baroreceptor reflex was observed in hypertensive patients (G. Mancia, Ludbrook, Ferrari, et al., 1978). It alters the sensitivity of baroreceptors and overdrives sympathetic responses (Grassi, Cattaneo, Seravalle, et al., 1998; Judy & Farrell, 1979; Matsukawa, Gotoh, Hasegawa, et al., 1991). In addition, excess sympathetic stimulation could be attributed greatly to increased release of noradrenaline and enhanced sensitivity of adrenergic receptors. This then raised the cytosolic Ca^{2+} level and leads to vasoconstriction. The activation of β_1-adrenoceptors by noradrenaline also induces renin secretion, augmenting the vascular tone through RAAS (Ames et al., 2019; Saxena, 1992). A high concentration of AT II is supposed to inhibit kidney renin secretion. However, this negative feedback mechanism was suppressed in hypertensive patients, where chronic activation of RAAS perpetuates the development of hypertension (A. J. Miller & Arnold, 2019; Seely, Moore, Rogacz, et al., 1989).

Patients with hypertension usually have elevated cardiac output and increased peripheral vascular resistance. The latter is mainly characterised by endothelial dysfunction and VSM remodelling. Enhanced vascular tone due to damaged endothelial cell damaged was first demonstrated in 1980 (Furchgott & Zawadzki, 1980). Damaged endothelial lining disrupts the synthesis and mechanism of action of vasoactive substances. For instance, elevated ROS which causes oxidative stress was reported to enhance the modulation of AT receptors by AT II in SHR (Wassmann, Bäumer, Strehlow, et al., 2001). Endothelial dysfunction and oxidative stress are associated with arterial stiffness which commonly represented in CVDs such as primary or secondary hypertension and heart failure (Marti et al., 2012). Endothelial dysfunction also dysregulates depolarisation and vasoconstriction in VSMCs due to reduced relaxing factors such as NO, PGI_2, and EDHFs (Félétou, Verbeuren, & Vanhoutte, 2009). At the same time, the production of contracting factors such as ET-1 and TXA_2 may be increased (Wynne et al., 2009). When blood flow against the endothelium surface at a high pressure, the high physiological shear force promotes the formation of inflammatory markers such as C-reactive protein (CRP). Cytokine-activated CRP diminishes the effect of eNOS while augments the effect of ET-1 (S. Verma, Buchanan, & Anderson, 2003). Chronic dysregulation of eNOS, NO and ET-1 initiates atherosclerotic lesion, and contribute to increased blood pressure (Deanfield, Halcox,

& Rabelink, 2007). An imbalance production of vascular relaxing and contracting factors owing to endothelial dysfunction severely impaired the control of vascular tone. Furthermore, the generation of relaxing factors such as NO and the conversion of arachidonic acid into PGI_2 rely strongly on intracellular Ca^{2+} release or extracellular Ca^{2+} entry. These processes show a multifaceted physiological role for Ca^{2+} in regulating vascular tone and blood pressure (Triggle, Samuel, Ravishankar, et al., 2012).

A healthy vascular wall has three layers of tissues; the outermost layer of connective tissues (tunica adventitia), the middle layer with sheets of smooth muscle cells (tunica media) and the innermost layer lined by endothelium (tunica intima) (**Figure 1.1**). Vascular remodelling involves the thickening of tunica media and has been implicated in hypertension. Under constantly elevated blood pressure, the rise in $[Ca^{2+}]_i$ contributes to vascular remodelling, which is the alteration of the structure of vessels, particularly the resistance arteries. In addition, long term vasoconstriction encourages the deposition of collagen or fibronectin which reduces the size of lumen (Intengan & Schiffrin, 2001). Inflammation-induced atherosclerosis, impaired endothelium, apoptosis are also known to trigger VSMC proliferation (Intengan & Schiffrin, 2001). Moreover, persistent elevation of ROS, AT II and ETs was found to induce vascular growth by engaging the epidermal growth factor receptor (EGFR) (Saito & Berk, 2001). They creates a pro-inflammatory and -hypertrophic environment, causing the build-up of proliferative tissue mass (Beevers, Lip, & O'brien, 2001; Intengan & Schiffrin, 2001). The reduction in the size of vessel lumen raised the peripheral vascular resistance, worsen the homeostatic blood pressure control (Didion, 2016). Treatment with Ca^{2+} channel blockers such as nifedipine and amlodipine was found to reduce the thickness of tunica media in the vessels of hypertensive rats, showing that Ca^{2+} modulation plays a role in vascular cell growth and has an impact on blood pressure (Sharifi, Li, Endemann, et al., 1998; Stead, Werstiuk, & Lee, 2000).

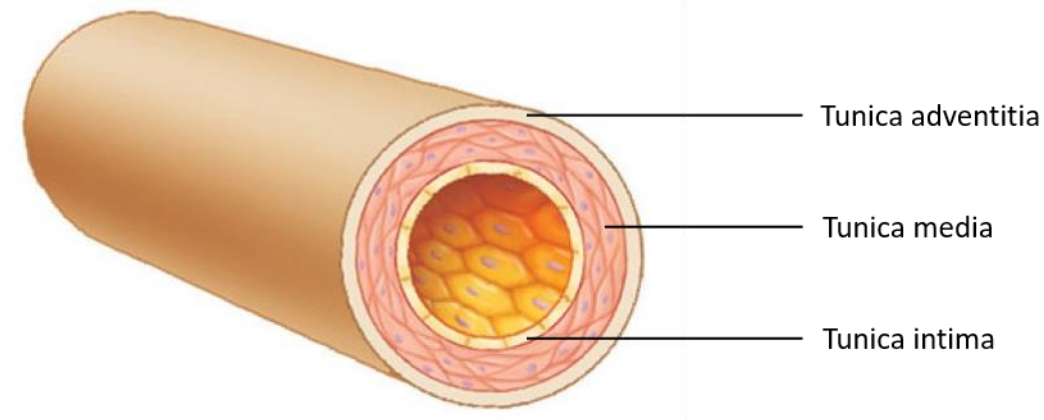


Figure 1.1 Structures of the artery, consisting of the outermost layer called tunica adventitia, a middle section of tunica media, and an inner layer of tunica intima. *Diagram adapted from Stanfield, (2005).*

1.1.3 Antihypertensive therapy and limitations

According to NICE UK guidelines and Clinical Practice Guidelines in Malaysia, hypertension can be categorised into a few stages. Stage 1 hypertension is classified as having clinic blood pressure of 140/90 mmHg and above; stage 2 with a blood pressure of 160/100 mmHg and above and stage 3 hypertension as having SBP of 180 mmHg and above (Malaysian Society of Hypertension, 2018; NICE, 2019). Categorising hypertension according to its severity helps with medicine prescribing. Non-pharmacological management such as weight reduction, increasing physical activity, reducing salt, alcohol and fat consumption is recommended for improving the overall health of hypertensive patients (Erejuwa, Gan, Romani, et al., 2019). However, when non-pharmacological management fails to bring down the blood pressure to a healthy level, pharmacological intervention is necessary to reduce the burden of hypertension and secondary cardiovascular risk.

Patients diagnosed with hypertension are usually treated with low-dose monotherapy. A few types of antihypertensive can be prescribed concurrently to ensure the blood pressure is controlled within the desired range (Malaysian Society of Hypertension, 2018; NICE, 2019). As shown in **Figure 1.2**, the choice of first-line antihypertensive offered to patients under 55 years is either an ACE inhibitor or an angiotensin-II receptor blocker (ARB). ACE inhibitors such as ramipril, lisinopril, perindopril, and ARB, including candesartan, losartan, and valsartan, are routinely prescribed for clinical use. For patients over 55 years, Ca^{2+} channel blockers will be offered as their first-line antihypertensive. If patients fail to achieve their target blood pressure measurement, a combination of Ca^{2+} channel blocker and ACE or ARB will be initiated as their second-line treatment (**Figure 1.2**). Combination therapy is preferred as it mitigates the risk of developing adverse effects to antihypertensive drugs when used at higher doses. However, increasing the dose of the first-line medication can be an alternative to adding a second drug to the regimen if the dose is best tolerated.

Dihydropyridines (DHPs) form the mainstay of Ca^{2+} channel blockers therapy for hypertension. The first-generation nifedipine and nicardipine were proven effective in treating hypertension. However, their clinical use is limited by the rapid onset and short duration of vasodilatory action (Weiss & Koschak, 2014). A slow-release formulation of DHPs improved the increased therapeutic effects of second-generation DHPs. Amlodipine and felodipine are examples of the third-generation DHPs which possess

more stable pharmacokinetics (Coca, Mazón, Aranda, et al., 2013). Highly lipophilic lercanidipine and lacidipine are characterised as the fourth-generation DHPs (Thomas F. Lüscher & Cosentino, 1998). They have stable activity, a lower rate of side effects, and are more vascular selective (Grassi, Robles, Seravalle, et al., 2017).

A thiazide-like diuretic will only be considered as a step-3 treatment when the blood pressures are inadequately controlled despite the first two medications (**Figure 1.2**) (Malaysian Society of Hypertension, 2018; NICE, 2019).

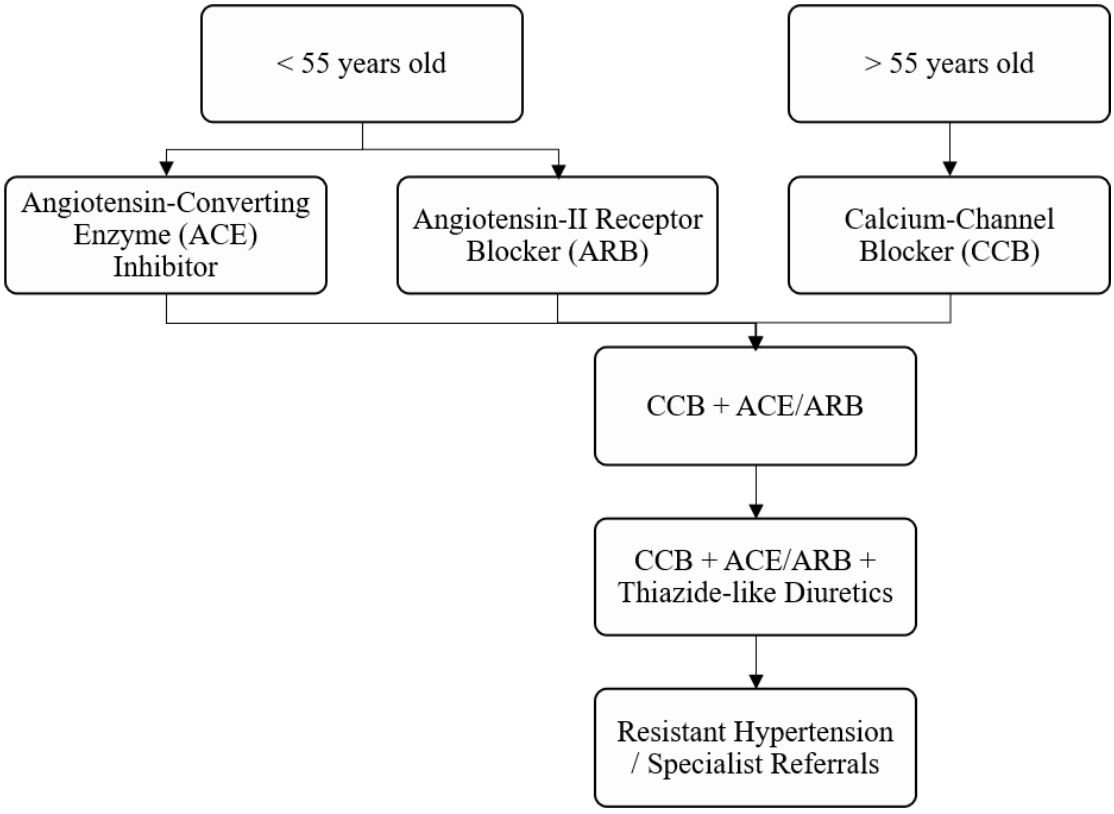


Figure 1.2 Summary of the treatment for hypertension **(Malaysian Society of Hypertension, 2018; NICE, 2019).**

1.1.4 Cost of antihypertensive drug therapy and limitations

The average cost of antihypertensive medications was approximately $9 billion per year (Wierzejska, Giernaś, Lipiak, et al., 2020). The figure was projected to $9.4 billion worldwide in the year 2025 (World Health Organization, 2013). In 2016, the Ministry of Health Malaysia had spent about RM608 million on antihypertensive medications (Malaysian Society of Hypertension, 2018). RM54 million was spent on amlodipine alone, as it was the most prescribed antihypertensive medication in Malaysia (Fong & Shanizza, 2020).

The financial burden of hypertension increased with other healthcare costs such as consultation, diagnostic tests, hypertension-associated hospitalisation, and complications. According to the National Health and Morbidity Survey commissioned by the Ministry of Health Malaysia in 2019, 6.4 million people suffer from hypertension in Malaysia (Institute for Public Health, 2020). However, only 2.9 million of them are diagnosed and managed with medications. Despite medical treatment, there are only 45% of these patients have controlled blood pressure. On the other hand, in Malaysia's primary care setting, more than one-third of hypertensive patients surveyed had a combination of two or more antihypertensive drugs. Yet, their blood pressure was not controlled (Teh, Lim, Tong, et al., 2020).

1.2 Resistant Hypertension

Patients will be referred to a specialist if their blood pressure cannot be controlled and maintained under 140/90 mmHg with at least three antihypertensive medicines. This condition is classified as resistant hypertension (Calhoun, Jones, Textor, et al., 2008; Malaysian Society of Hypertension, 2018; NICE, 2019). Globally, the prevalence of resistant hypertension is around 7 – 13% of all patients treated for hypertension (Chia & Ching, 2014; Persell, 2011; Sinnott, Smeeth, Williamson, et al., 2017). Patients categorised as having resistant hypertension are excluded from poor adherence to treatment, white coat effect and poor blood pressure measuring techniques.

1.2.1 Interventions and limitations

Interventions are available for patients with resistant hypertension after specialist assessment. A further drug can be added to patients' drug regimens. Spironolactone is prescribed if the blood potassium level is lower than 4.5 mmol/l (NICE, 2019). α and β-blockers such as prazosin, carvedilol, and labetalol are prescribed for resistant

hypertension (NICE, 2019). Centrally-acting sympathomimetics such as clonidine and methyldopa can cause severe rebound hypertension if not weaned properly (Alviar, Devarapally, Nadkarni, et al., 2013; Yaxley & Thambar, 2015). Hydralazine and minoxidil sometimes are prescribed for resistant hypertension with a high dose diuretic as they can cause problematic water retention (Mann, 2011; Yaxley & Thambar, 2015). Pharmacological management in resistant hypertension increases the risk of adverse events in patients, especially those with co-morbidities.

Apart from pharmacological treatment, renal sympathetic nerve ablation, more commonly known as renal denervation (RDN), has been proposed as an alternative method to treat resistant hypertension. This invasive technique employs radiofrequency or ultrasound to ablate nerves of the renal arteries, hoping to reduce the blood pressure by inhibiting sympathetic stimulation (Reilly & White, 2016). Coppolino et al. (2017) reviewed that there is no evidence that RDN provides better blood pressure control compared to standard treatment. It also increased the incidence of bradycardia in patients who underwent RDN (Coppolino, Pisano, Rivoli, et al., 2017). This is further supported by other randomised clinical trials, concluding that RDN did not significantly reduce SBP compared to the control group (Bhatt, Kandzari, O'Neill, et al., 2014; Reilly & White, 2016; Schlaich, Schultz, & Shetty, 2016). Joint UK societies and NICE UK do not recommend renal denervation as an alternative treatment for resistant hypertension in clinical settings due to concerns over its safety, effectiveness and costs (Lobo, De Belder, Cleveland, et al., 2015; NICE, 2019).

Treating resistant hypertension remains challenging. With 7 – 13% of hypertensive patients diagnosed with resistant hypertension later, 5% of these patients will still have uncontrolled blood pressure despite an optimised antihypertensive treatment (Feig, Roy, & Cody, 2010; Pimenta & Calhoun, 2016). Its main challenge is that it manifests with other co-morbidities such as diabetes, chronic kidney disease (CKD) and atherosclerosis, complicating the pathophysiology and thus limiting the treatment options. Currently, there is no drug indicated explicitly for resistant hypertension as current medications for hypertension showed limited efficacy in treating resistant hypertension. As pharmacological and surgical treatments are inadequate to control resistant hypertension, the current state of hypertension management implies a need to develop new medicine with a novel mechanism of action that can address the issues with resistant hypertension.

1.3 Ca^{2+} signalling in VSM

For years, the role of Ca^{2+} has always been the interest among researchers in search of answers to the regulation of muscle tone. The contractility of vascular tissues is known to be mediated by various modulators that affect $[Ca^{2+}]_i$ level via different signalling pathways.

1.3.1 Ca^{2+} release from the intracellular stores

When VSMC is stimulated by G_q-receptor activation, PLC catalyses the hydrolysis of phosphatidylinositol 4,5-bisphosphate (PIP_2), generating inositol-1,4,5-trisphosphate (IP_3) and 1,2-diacyl-*sn*-glycerol (DAG) (**Figure 1.3**). When IP_3 binds to IP_3 receptors embedded on the SR membrane, Ca^{2+} confined within its lumen is pumped out into the cytosol through IP_3 receptors (**Figure 1.3**) (Kuo & Ehrlich, 2015). A localised increase in $[Ca^{2+}]_i$ triggers the opening of ryanodine receptors (RyRs), permeating further Ca^{2+} efflux from internal stores (**Figure 1.3**) (Van Petegem, 2012). This process amplifies the Ca^{2+} signal required for inducing vascular contraction, which is defined as Ca^{2+}-induced Ca^{2+} release (CICR) (**Figure 1.3**) (Fellner & Arendshorst, 2007).

1.3.2 Ca^{2+} entry from the extracellular space

Active entry of Ca^{2+} into VSMCs is required to sustain the intracellular Ca^{2+} oscillations during smooth muscle contraction. A few mechanisms of Ca^{2+} entry has been reported in VSMCs, including voltage-dependent Ca^{2+} entry, receptor-operated Ca^{2+} entry (ROCE), and store-operated Ca^{2+} entry (SOCE) (Ghosh, Syed, Prada, et al., 2017; C. H. Lee, Poburko, Sahota, et al., 2001). When cytosolic Ca^{2+} increases, Ca^{2+}-activated chloride channels (CaCCs) are activated to produce spontaneous transient inward current (STIC) by exporting chloride ion (Cl^-) out of the cell (**Figure 1.3**) (Amberg & Navedo, 2013; McGeown, 2010). Examples of CaCCs found in VSMCs are transmembrane member 16A/anoctamin-1 (TMEM16A/Ano1) and bestrophin (Bulley & Jaggar, 2014; Leblanc, Forrest, Ayon, et al., 2015). This effect accumulates and gradually depolarises the plasma membrane. Depolarisation can also be produced by high extracellular K^+. Following depolarisation, the opening of L-type VGCCs allows Ca^{2+} influx from the extracellular medium, promoting vascular contraction on a positive feedback mechanism (**Figure 1.3**). Ca^{2+} influx through L-type VGCCs can also occur when second messenger DAG activates PKC (**Figure 1.3**) (Amberg & Navedo, 2013; Somlyo & Somlyo, 2000; Sun, Gu, & Haddad, 2003). Voltage-dependent extracellular Ca^{2+} entry has long been recognised as the main mechanism of Ca^{2+} entry into smooth

muscle cells, predominantly facilitated by L-type VGCCs. On top of that, the paradigm has also recognised the role of T-type VGCCs in vascular myogenic constriction (Hill-Eubanks, Werner, Heppner, et al., 2011; Kuo, Wölfle, & Hill, 2011).

Both ROCE and SOCE falls under the category of non voltage-dependent Ca^{2+} entry. Since the discovery of TRPC channels, they have been frequently proposed as the molecular components that regulate ROCE and SOCE during vascular contraction (Xingjuan Chen, Sooch, Demaree, et al., 2020; J. J. Lopez, Jardin, Sanchez-Collado, et al., 2020; Ong, De Souza, & Ambudkar, 2016). ROCE via receptor-operated Ca^{2+} channels (ROCCs) like TRPC channels can be stimulated by producing second messengers from G_q receptor activation, such as DAG (**Figure 1.3**) (detailed in **section 5.1.1**). Direct ROCE can also be activated by agonists gating various ionotropic receptors such as purinergic receptors or glutamate receptors (Dong, Hsu, Koziol-White, et al., 2021; Harhun, Sukhanova, Gordienko, et al., 2015). As the name suggests, SOCE is described as a Ca^{2+} entry that occurred through store-operated Ca^{2+} channels (SOCCs) following store depletion. Store depletion activates stromal interaction molecule (STIM). Subsequently, it interacts with Ca^{2+} release-activated Ca^{2+} channel modulator (Orai) protein to form the STIM-Orai complex, which then allows Ca^{2+} influx through TRPC channels (**Figure 1.3**) (detailed in **section 5.1.1**) (Gudlur, Zeraik, Hirve, et al., 2020; Prakriya & Lewis, 2015). Lastly, the operation of Na^+-Ca^{2+} exchanger (NCX) in the reverse mode mediated by TRPC6 channels represents a further mechanism of extracellular Ca^{2+} influx in VSMCs (**Figure 1.3**) (Lemos, Poburko, Liao, et al., 2007).

1.3.3 Ca^{2+} sequestration and extrusion

Eliminating intracellular Ca^{2+} is crucial to regulate Ca^{2+} homeostasis and maintain vascular tone. When cytosolic Ca^{2+} is raised from intracellular store release, a negative feedback mechanism generates a spontaneous transient outward current (STOC), which activates K^+ channels such as BK_{Ca} (**Figure 1.3**) (Jackson, 2017; McGeown, 2010). Hyperpolarisation due to the efflux of K^+ reduces the opening of L-type VGCCs (**Figure 1.3**) (Félétou et al., 2010). When Ca^{2+} entry is restricted, the vascular tone slowly reverts to the basal level (Berridge, 2008). Furthermore, the extrusion of cytosolic Ca^{2+} across the plasma membrane is also regulated via adenosine 5'-triphosphate (ATP)-dependent plasma membrane Ca^{2+}-ATPase (PMCA) or NCX (**Figure 1.3**). NCX removes one Ca^{2+} in exchange for three Na^+ in the cell (Kuo & Ehrlich, 2015).

On the other hand, fluctuations in $[Ca^{2+}]_i$ is also maintained by removing surplus Ca^{2+} presents in the cytosol back into internal stores of SR. Mitochondrial Ca^{2+} uniporter functions rapidly when $[Ca^{2+}]_i$ is elevated at a high concentration, around 1 µM (**Figure 1.3**) (Berridge, Bootman, & Roderick, 2003; Fan, Zhang, Tsai, et al., 2020). Activation of sarco/endoplasmic reticulum Ca^{2+}-ATPase (SERCA) pumps, which are expressed on the SR membrane, facilitates the sequestration of Ca^{2+} back into intracellular stores (**Figure 1.3**) (Nazer & Van Breemen, 1998). Conversely, pharmacological inactivation of SERCA pumps by thapsigargin or cyclopiazonic acid leads to store Ca^{2+} depletion, which increases the cytosolic Ca^{2+} level by disrupting the Ca^{2+} homeostasis (Dettbarn & Palade, 1998).

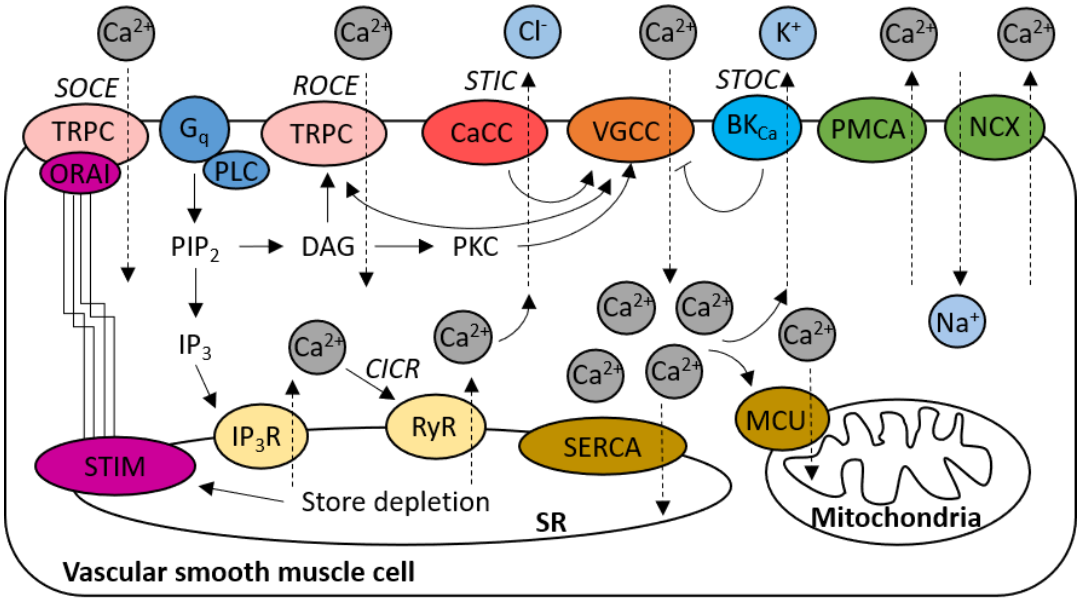


Figure 1.3 Overview of Ca^{2+} signalling pathways entering or exiting VSMCs. Individual subcellular Ca^{2+} events are italicised. *Solid pointed solid arrow denotes downstream effectors activation, blunt arrow denotes downstream effectors inhibition. Dotted arrows denote flow of ions. Abbreviations: BK_{Ca}, large-conductance Ca^{2+}-activated K^+ channel; Ca^{2+}, calcium ion; CaCC, Ca^{2+}-activated chloride channels; CICR, Ca^{2+}-induced Ca^{2+} release; Cl^-, chloride ion; DAG, diacylglycerol; IP_3, inositol-1,4,5-trisphosphate; IP_3R, IP_3 receptor; K^+, potassium ion; MCU, mitochondrial uniporter; NCX, Na^+-Ca^{2+} exchanger; ORAI, Ca^{2+} release-activated Ca^{2+} channel modulator; PIP_2, phosphatidylinositol 4,5-bisphosphate; PKC, protein kinase C; PLC; phospholipase C; PMCA, plasma membrane Ca^{2+}-ATPase; ROCE, receptor-operated Ca^{2+} entry; RyR, ryanodine receptor; SERCA, sarco/endoplasmic reticulum Ca^{2+}-ATPase; SOCE, store-operated Ca^{2+} entry; SR, sarcoplasmic reticulum; STIC, spontaneous transient inward current; STIM, stromal interaction molecule; STOC, spontaneous transient outward current; TRPC, transient receptor potential canonical; VGCC, voltage-gated Ca^{2+} channels.*

1.3.4 Ca^{2+}-dependent mechanisms of VSM contraction and relaxation

VSM contractility is known to involve receptors and ion channels such as G-protein coupled receptors (GPCRs), K^+, and Ca^{2+} channels, which are expressed on the plasma membrane of the endothelial and VSMCs (Brinks & Eckhart, 2010; Hill-Eubanks et al., 2011). Activation and inhibition of these receptors and ion channels affect downstream Ca^{2+} mobilisation. Changes in $[Ca^{2+}]_i$ are central to vascular tone regulation (Amberg & Navedo, 2013; González-Cobos & Trebak, 2011).

Resting membrane potential at approximately -50 to -30 mV contains less than 100 nM free intracellular Ca^{2+} (Hill-Eubanks et al., 2011). At this point, the membrane potential is adequate to permit the opening of L-type VGCCs. In other words, an influx of Ca^{2+} through a small cluster of L-type VGCCs happens continuously at a steady state (Kuo & Ehrlich, 2015; Navedo, Amberg, Votaw, et al., 2005). There is also some Ca^{2+} leaked from intracellular stores (Poburko, Lhote, Szado, et al., 2004). This low concentration of Ca^{2+} is essential to sustain the vascular myogenic tone, which is important in maintaining blood pressure.

To elicit VSM contraction, cytosolic Ca^{2+} has to be raised to 300 nM – 1 µM by either extracellular or intracellular sources of Ca^{2+}, or a combination of both (Hill-Eubanks et al., 2011; C. H. Lee et al., 2001) As the global $[Ca^{2+}]_i$ increases as shown in **Figure 1.4**, Ca^{2+} binds to regulatory protein calmodulin (CaM) to form Ca^{2+}-CaM complex. It then stimulates an enzymatic process where MLCK activates MLC by phosphorylation. It involves converting ATP to adenosine 5'-diphosphate (ADP), attaching the free phosphate group to MLC. The phosphorylated MLC then attaches to the actin of the thin filament, forming cross bridges and initiates smooth muscle contraction (S. Ahmed & Warren, 2018).

The opposing reaction favours vascular relaxation, which removes Ca^{2+} out of the cell or back into the intracellular compartment. As $[Ca^{2+}]_i$ decreases, Ca^{2+} dissociates from CaM. Consequently, the activity of myosin light chain phosphatase (MLCP) increases and catalyses the dephosphorylation of MLC (S. Ahmed & Warren, 2018). The cross-bridge formation between actin and myosin uncouples, resulting in vasorelaxation.

1.3.5 Ca^{2+}-independent regulation of VSM contraction and relaxation

It is worth mentioning that a part of the molecular mechanism for vascular contraction and relaxation does not rely on Ca^{2+}.

Activation of GPCR, particularly $G_{12/13}$ subtype, catalyses the interaction of Ras homolog family, member A (RhoA) with GTP. The RhoA-GTP unit then stimulates downstream Rho-associated protein kinase (ROCK), attenuating the activity of MLCP (**Figure 1.4**). Ca^{2+}-dependent pathways and RhoA/ROCK pathway synergistically enhance the contraction in VSM by keeping most MLC phosphorylated.

This unbalanced effect that weighs towards phosphorylated MLC and contraction is reversed when NO diffuses from vascular endothelial cells to smooth muscle cells. It binds to sGC, converting GTP to cGMP (**Figure 1.4**). cGMP-activated PKG promotes the activity of MLCP, encouraging the dephosphorylation of phosphate-bound MLC (Sandoo et al., 2015). Similarly, G_s activation augments vasorelaxation but via a different mechanism. G_s-mediated activation of AC produces cAMP from ATP, leading to activation of PKA (**Figure 1.4**). Instead of promoting MLCP, active PKA targets MLCK, which hinders the phosphorylation of free MLC and reduces VSM contractile responsiveness (Al-Shboul, 2018; Rigor, Shen, Pivetti, et al., 2013).

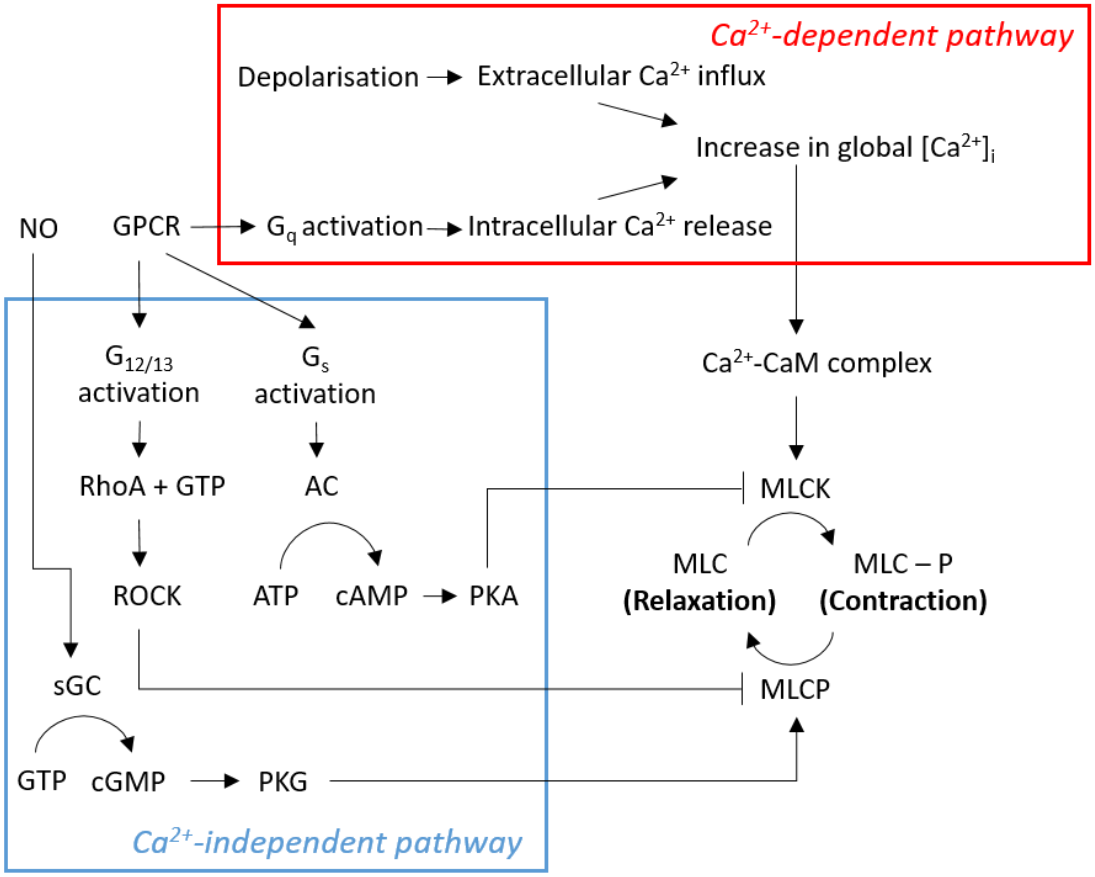


Figure 1.4 Schematic diagram of Ca^{2+}-dependent (red box) and Ca^{2+}-independent (blue box) VSM contraction and relaxation mechanisms. *These two pathways are interlinked to regulate smooth muscle tone. Pointed arrows denote downstream effectors activation; blunt arrows denote downstream effectors inhibition. Abbreviations: $[Ca^{2+}]_i$, intracellular Ca^{2+} concentration; AC, adenylyl cyclase; ATP, adenosine 5'-triphosphate, CaM, calmodulin; cAMP, 3'-5'-cyclic adenosine monophosphate; cGMP, 3'-5'-cyclic guanosine monophosphate; Ca^{2+}, calcium ion; GPCR: G-protein coupled receptor; GTP, guanosine-5'-triphosphate; MLC, myosin light chain; MLCK, MLC kinase; MLCP, MLC phosphatase; MLC-P, phosphorylated MLC; NO, nitric oxide; PKA, protein kinase A; PKG, protein kinase G; RhoA, Ras homolog family member A; ROCK, rho-associated protein kinase; sGC, soluble guanylyl cyclase. Diagram adapted from S. Ahmed & Warren (2018).*

1.4 TRPC channels in the vasculature

Transient receptor potential (TRP) superfamily, first identified in *Drosophila* fly in 1989, exists as six subfamilies; TRPC (canonical), TRPM (melastatin), TRPV (vanilloid), TRPP (polycystin), TRPML (mucolipin), and TRPA (ankyrin), due to similarity in amino acid sequence (Montell & Rubin, 1989; Nilius, Owsianik, Voets, et al., 2007). Among these subfamilies, TRPC homologue was discovered to play a significant role in regulating cellular Ca^{2+} homeostasis. They are a group of non-selective cation channels (NSCCs), which mainly modulate Ca^{2+} and Na^{+} across the plasma membrane to maintain the cell's physiological functions (Bouron, Kiselyov, & Oberwinkler, 2015; Wes, Chevesich, Jeromin, et al., 1995). There are seven subtypes in TRPC channels, from TRPC1 – TRPC7 channels. Within this family, they can be divided into three main subgroups based on highly conserved homologies, namely TRPC1/4/5, TRPC3/6/7 and TRPC2 (Hofmann, Schaefer, Schultz, et al., 2002; Montell, Birnbaumer, Flockerzi, et al., 2002). TRPC2 channels are pseudogene in humans and therefore not expressed.

In this thesis, the notation TRPC3, TRPC6 etc., are used to denote different TRPC protein subtypes. TRPC3/6 etc., denotes any TRPC channels incorporating these channels or that composed of TRPC3 and/or TRPC6 etc., as homo- or heteromultimeric channels in any ratio. On the other hand, TRPC3:C3 and TRPC6:C6 etc., denote specific homomultimeric TRPC channels.

1.4.1 Expression of TRPC3 and TRPC6 in the vasculature

All TRPC channels were present and functional in smooth muscle cells and endothelial cells of different animal species (Albert, Saleh, & Large, 2009; Earley & Brayden, 2015). Among these TRPC channels, TRPC3 and TRPC6 are the TRPC subtypes involved in the regulation of vasoconstriction and myogenic responses (Álvarez-Miguel, Cidad, Pérez-García, et al., 2017; Dietrich, Mederos y Schnitzler, Gollasch, et al., 2005; R. Inoue, Jensen, Shi, et al., 2006; Kochukov, Balasubramanian, Noel, et al., 2012; Martín-Bórnez, Galeano-Otero, Del Toro, et al., 2020; Thilo, Baumunk, Krause, et al., 2009). TRPC3 and TRPC6 show around 80% amino acid sequence homology and share similar functional properties (Boulay, Zhu, Peyton, et al., 1997). Although TRPC7 is homologous to TRPC3 and TRPC6, it remains as one of the least studied TRPC channels. Its physiological roles in the vasculature are vaguely discerned. This could be due to the expression of TRPC7 is limited to a few cell types, mostly detected in non-vascular related sites such as the central nervous system and lung tissues (X. Zhang & Trebak, 2014). Therefore, the focus of this thesis is placed on the abundantly expressed TRPC3 and TRPC6 channels in the vasculature, which their vascular roles are clearly connected to *in vivo* functional responses.

Expression of mammalian TRPC3 and TRPC6 has been widely reported in the vasculature (Albert et al., 2009; Beech, Muraki, & Flemming, 2004). In addition, TRPC6 has consistently shown higher expression levels than TRPC3 homologue in rat aorta and pulmonary artery (Facemire, Mohler, & Arendshorst, 2004; Y. Yu, Fantozzi, Remillard, et al., 2004). **Table 1.1** has provided strong evidence of the expression of TRPC3 and TRPC6 mRNA and proteins in the VSM of different mammalian species. There were some discrepancies where TRPC3 was not expressed in adult and embryonic rat aortae (**Table 1.1**) (Jung, Strotmann, Schultz, et al., 2002; Poburko et al., 2004; Soboloff, Spassova, Xu, et al., 2005). The variation between rat species, the reliability and effectiveness of TRPC antibodies could contribute to the inconsistency. The detection of mRNA and protein could also be limited by the expression level of TRPC3 (Beech et al., 2004).

Table 1.1 Expression of TRPC3 and TRPC6 mRNAs and proteins in VSM preparations.

Smooth muscle types	TRPC3	TRPC6	References
Rat thoracic aorta	✓	✓	(Facemire et al., 2004) (Liu, Yang, He, et al., 2009)
	×	✓	(Poburko et al., 2004)
Embryonic rat thoracic aorta (A7r5)	×	✓	(Jung et al., 2002) (Soboloff et al., 2005)
Rat carotid artery	✓	-	(Noorani, Noel, & Marrelli, 2011) (J. Chen, Crossland, Noorani, et al., 2009)
Rat caudal artery	✓	✓	(Mita, Ito, Taira, et al., 2010)
Human, rat cerebral artery	✓	✓	(Adebiyi, Zhao, Narayanan, et al., 2010) (Reading, Earley, Waldron, et al., 2005) (Welsh, Morielli, Nelson, et al., 2002) (Yip, Chan, Leung, et al., 2004)
Rat renal preglomerular artery	✓	✓	(Facemire et al., 2004) (Fellner & Arendshorst, 2002)
Human, rat pulmonary artery	✓	✓	(Y. Yu, Sweeney, Zhang, et al., 2003) (Y. Yu et al., 2004)
Human, rabbit coronary artery	✓	✓	(J. Shi, Ju, Large, et al., 2012) (Yip et al., 2004)

1.4.2 Structure of TRPC3 and TRPC6 channels

TRPC3 and TRPC6 channels are voltage-independent NSCCs as they do not possess a voltage-sensing domain (Nilius et al., 2007). Between the cytoplasmic NH_2 and COOH termini lies the six transmembrane segments TM1 – TM6, where the putative pore-forming loop is located between TM5 and TM6 (**Figure 1.5**) (Vazquez, Wedel, Aziz, et al., 2004).

There are four ankyrin repeats at the N-terminus, a coiled-coil, and a caveolin binding region (**Figure 1.5**). At the opposite end, a highly conserved EWKFAR motif in *Drosophila* and mammalian TRP, a proline-rich motif, a CIRB region for CaM and IP_3 receptor binding, as well as a similarly structured coiled-coil, are located at the C-terminus (**Figure 1.5**). The coiled coils at both termini are the interaction sites for homo- or heterotetrameric assembly of various TRPC subtypes. It also controls oligomerisation with other coiled-containing protein motifs such as STIM proteins when SOCE takes place (Nilius & Flockerzi, 2014; Tang, Guo, Zheng, et al., 2018; Vazquez et al., 2004). Structural analyses have shown that TRPC3 and TRPC6 relied on coiled-coil to either form homotetramers among themselves or heterotetrameric channels made up of other TRPC subtypes such as TRPC1/3 (J. Chen et al., 2009; Lintschinger, Balzer-Geldsetzer, Baskaran, et al., 2000; Liu, Bandyopadhyay, Singh, et al., 2005), TRPC1/4/5/6 (Nilius & Flockerzi, 2014), TRPC3/6 (Álvarez-Miguel et al., 2017; Hofmann et al., 2002), TRPC6/7(Maruyama, Nakanishi, Walsh, et al., 2006).

Glycosylation patterns found on the extracellular loop contribute to the different constitutive activity of TRPC3 and TRPC6 subtypes (**Figure 1.5**) (Nilius & Flockerzi, 2014; Vazquez et al., 2004). Glycosylation for TRPC3 channels occurs only on the first extracellular loop from *N*-terminus, which is believed to lead to a non-selective conductance for both mono- and divalent cations. Conversely, TRPC6 channels have the first and second extracellular loop glycosylated, showing a more Ca^{2+}-selective permeability (Bacsa, Tiapko, Stockner, et al., 2020; Hofmann, Obukhov, Schaefer, et al., 1999; Kamouchi, Philipp, Flockerzi, et al., 1999).

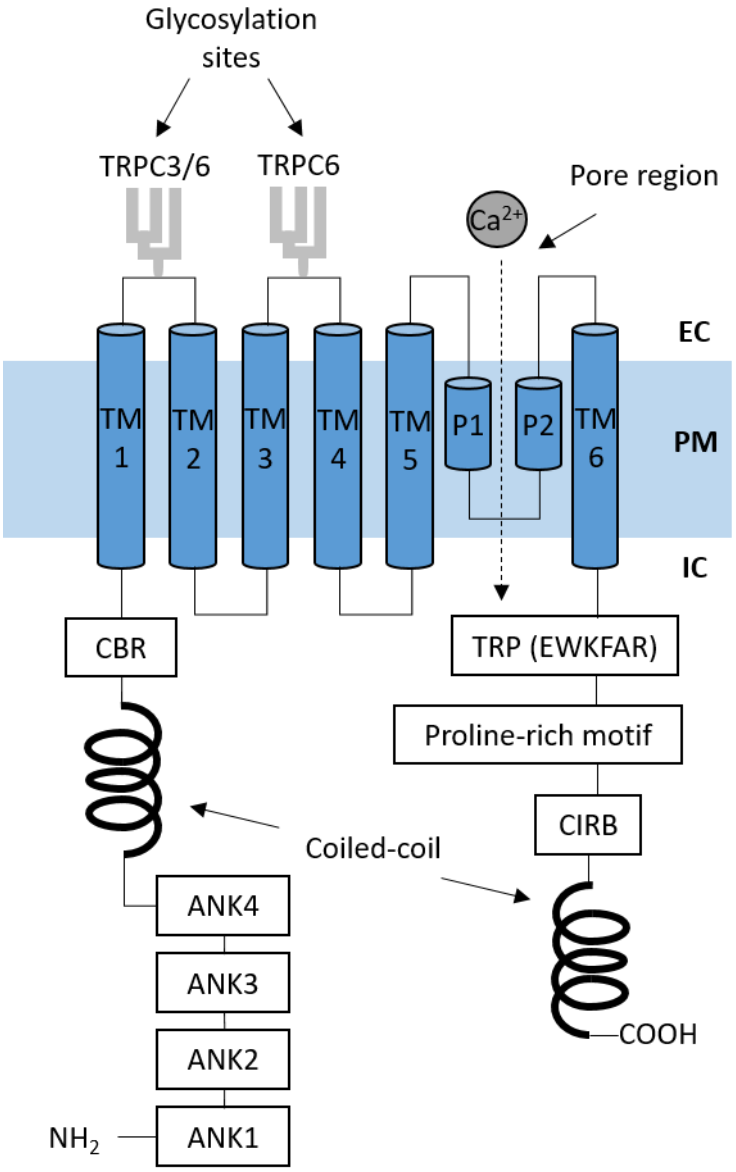


Figure 1.5 Structural representation of TRPC3 and TRPC6 channels as Ca^{2+}-permeable plasmalemmal ion channels. *Abbreviations: ANK, ankyrin; CBR, caveolin binding region; CIRB, calmodulin/IP_3 receptor binding region; COOH, carboxyl terminus; EC, extracellular; IC, intracellular; NH_2, amino terminus; P, pore; PM, plasma membrane; TM, transmembrane; TRP, transient receptor potential; TRPC, transient receptor potential canonical. Diagram adapted from Nilius & Flockerzi (2014), Tang et al. (2018), Vazquez et al. (2004).*

1.4.3 Involvement of TRPC3 and TRPC6 channels in CVDs

Regulation of Ca^{2+} homeostasis in VSM is viewed as one of the main mechanisms for controlling blood pressure. In fact, TRPC3 and TRPC6 channels were found to be involved in the pathophysiology of hypertension and other CVDs (Schilling, 2001; Thilo, Loddenkemper, Berg, et al., 2009; Thilo, Scholze, Liu, et al., 2008; Y. Yu et al., 2004). Evidence from experiments using disease models have suggested TRPC3 and TRPC6 channels are potential therapeutic targets for CVDs such as hypertension (Thilo, Baumunk, et al., 2009; Thilo, Loddenkemper, et al., 2009), cardiac hypertrophy (Wu, Eder, Chang, et al., 2010), and atrial fibrillation (Harada, Luo, Qi, et al., 2012).

Expression of TRPC6 through calcineurin-nuclear factor of activated T-cells (NFAT) pathway activation was found to upregulated in models of heart failure. This observation has suggested the possibility of pathologic cardiac remodelling and cardiomyopathy *in vivo* (Kuwahara, Wang, McAnally, et al., 2006). The importance of TRPC3 and TRPC6 channels in the cardiovascular system has been further emphasised in the last decade (Earley & Brayden, 2015; H. Wang, Cheng, Tian, et al., 2020). Compelling evidence indicates that they are functionally important in regulating vascular contractility via the regulation of Ca^{2+} dynamics. The functional role of TRPC3 and TRPC6 channels has been studied using genetic knockout mice, where evidence showed they regulate agonist-mediated vascular contractility (Álvarez-Miguel et al., 2017; Kochukov et al., 2012). Changes to these TRPC channels have been linked to vascular pathologies such as hypertension and pulmonary oedema (Weissmann, Sydykov, Kalwa, et al., 2012). The expressions of TRPC3 and TRPC6 channels were found to increase Ca^{2+} influx in VSMCs isolated from hypertensive animals and patients. Through Ca^{2+}-dependent signal transduction, this upregulation of functional TRPC3 and TRPC6 channels is believed to augment vascular contraction.(Dietrich, Mederos y Schnitzler, Gollasch, et al., 2005; Liu, Scholze, Zhu, et al., 2005, 2006; Thilo, Loddenkemper, et al., 2009). Further evidence that support the association of systemic hypertension with the changes in expression and function of TRPC channels are listed in **Table 1.2**.

Table 1.2 Pathophysiology of TRPC-related hypertension.

Evidence	References
• TRPC3 channel contributes more to the depolarization in hypertensive VSMCs. • TRPC3/6 heteromultimerisation and proportion were affected by increased TRPC3 channel expression.	(Álvarez-Miguel et al., 2017)
• High salt intake elevated TRPC3 mRNA levels and expression in hypertensive individuals. • Pyr3, a selective TRPC3 inhibitor, reduced TRPC3-mediated SOCE that was causally related to SBP.	(Y. Hu, Xia, Li, et al., 2020)
• TRPC3 maintains calcium homeostasis at a cytoplasmic and mitochondrial level. • SHR showed augmented mitochondrial TRPC3 expression and activity, which led to Ca^{2+} dysregulation. • Inhibition of TRPC3 by telmisartan and Pyr3, ameliorated hypertension through reducing excessive mitochondrial ROS production, ATP content and H_2O_2 synthesis.	(Bin Wang, Xiong, Lin, et al., 2017)
• Aldosterone-induced TRPC6 expression was found to modulate homeostasis of Ca^{2+} via ROCCs in VSMCs, which influenced vascular contractility in hypertensive rats.	(Bae, Kim, Lee, et al., 2007)
• Upregulation of TRPC1 and TRPC6 mRNA increased with age and SBP and may be involved in VSMC proliferation carotid arterial remodelling in SHRs.	(Lin, Hong, Zou, et al., 2015)
• Enhanced protein expression of TRPC1, TRPC3 and TRPC5 was detected in the mesenteric arterioles from SHR. • Increased vasomotion and Ca^{2+} influx was reduced by verapamil, a VGCC blocker, and SKF-96365, a non-selective TRPC channel blocker. • Chronic administration of ARB such as telmisartan and candesartan diminished TRPC1, TRPC3 and TRPC5 protein expression *in vivo*.	(Xiaoping Chen, Yang, Ma, et al., 2010)

1.5 Natural products in drug discovery

To date, adequate management of high blood pressure with optimised pharmacological treatment is still a global challenge. Advances in pharmacological management is one of the efforts needed to address the substantial public health burden posed by hypertension. Drug development is the process of identifying chemical compounds that can treat diseases and be transformed into therapeutic agents. It encompasses three main phases, including target discovery, preclinical research and clinical trials. Plants or traditional remedies have great chemical diversity for discovering novel molecular entities with medicinal properties. 16% of the total number of FDA-approved drugs in the year 2018 were derived from natural products, highlighting the dominant role of natural resources in recent drug discovery (de la Torre & Albericio, 2019). For instance, salicin, first isolated from willow bark in 1826, was used as an analgesic and antipyretic (Montinari, Minelli, & De Caterina, 2019). Its structure was optimised into salicylic acid and then acetylsalicylic acid, commonly known as aspirin. Throughout its usage in clinics, aspirin is also indicated as an antiplatelet agent to treat cardiovascular diseases (Miner & Hoffhines, 2007). Recently, aspirin was even found to reduce the risk of developing colorectal cancer, showing the ever-growing discovery on the medicinal properties of plant-derived compounds (Burn, Sheth, Elliott, et al., 2020; Singh-Ranger, 2018; Soualy, Deutsch, Benallaoua, et al., 2020).

1.5.1 Medicinal plants and alkaloids with antihypertensive effects

Accumulating literature has reported the increasing therapeutic potentials of bioactive compounds in plants, such as flavonoids, terpenes, tannins, steroids and alkaloids, on hypertension (R. R. Bai, Wu, & Xu, 2015; T. Verma, Sinha, Bansal, et al., 2021).

The extract of *Hibiscus sabdariffa*, commonly known as rosella, presented blood pressure lowering effects (M. G. Abubakar, Ukwuani, Mande, et al., 2015; Mojiminiyi, Dikko, Muhammad, et al., 2007). Polyphenols such as anthocyanins, particularly delphinidin-3-sambubioside and cyanidin-3-sambubioside, have been identified for its antihypertensive, antioxidant and cholesterol-lowering activities (Hopkins, Lamm, Funk, et al., 2013; Majdoub, Diouri, Arena, et al., 2019; Yang, Peng, Chan, et al., 2010). Furthermore, evidence also reported its antihypertensive effects were mediated by endothelium-derived NO/3'-5'-cyclic guanosine monophosphate (cGMP) pathway and the inhibition of Ca^{2+} influx (Ajay, Chai, Mustafa, et al., 2007).

Besides, Ca^{2+}-mediating compounds isolated from plants have encouraged the search for new antihypertensive compounds in plant extracts. For example, 2,7-dihydroxy-3,4,9-trimethoxyphenantrene was believed to be responsible for the Ca^{2+} antagonistic effects and subsequent vasorelaxation of the methanolic extract of an orchid species, *Laelia anceps* (Vergara-Galicia, Ortiz-Andrade, Rivera-Leyva, et al., 2010). The same group of researchers reported that the extract of another orchid species, *Laelia autumnalis*, also acted as a smooth muscle relaxant by inhibiting Ca^{2+} influx and increasing cGMP production (Vergara-Galicia, Ortiz-Andrade, Castillo-España, et al., 2008). Furthermore, organic and aqueous extracts of *Jatropha gossypiifolia* (bellyache bush) showed an endothelium-independent inhibition of Ca^{2+}-induced vasoconstriction (Abreu, Marinho, Paes, et al., 2003). The reduced contractile response in ileal smooth muscle by coriander extract and fractions was associated with inhibitory actions on muscarinic receptors and Ca^{2+} influx (Jabeen, Bashir, Lyoussi, et al., 2009).

Among the bioactive compounds, alkaloids are widely reported to exhibit vasorelaxant and antihypertensive effects. Alkaloids are compounds containing heterocyclic nitrogen in their chemical structures. It was thought that the biological impacts of alkaloids are linked to the amine group and the associated alkalinity (Matsuura & Fett-Neto, 2015). Plant-derived alkaloids often display diverse medicinal use, as they have a wide range of activities such as antihypertensive, antitumour and antibacterial effects. Among them, the alkaloids which are well known for their therapeutic uses include morphine, quinine, vincristine and caffeine (Fester, 2010). In **Table 1.3**, some active alkaloid constituents isolated from medicinal plants are listed, together with their putative antihypertensive mode of action.

Table 1.3 Examples of plant-derived alkaloids with antihypertensive activity.

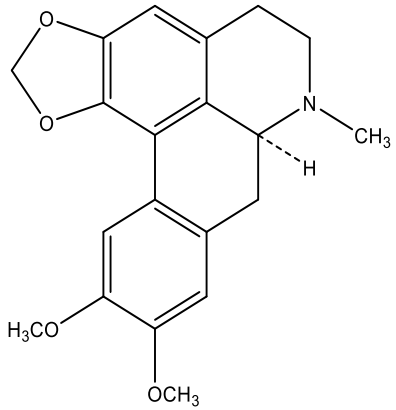
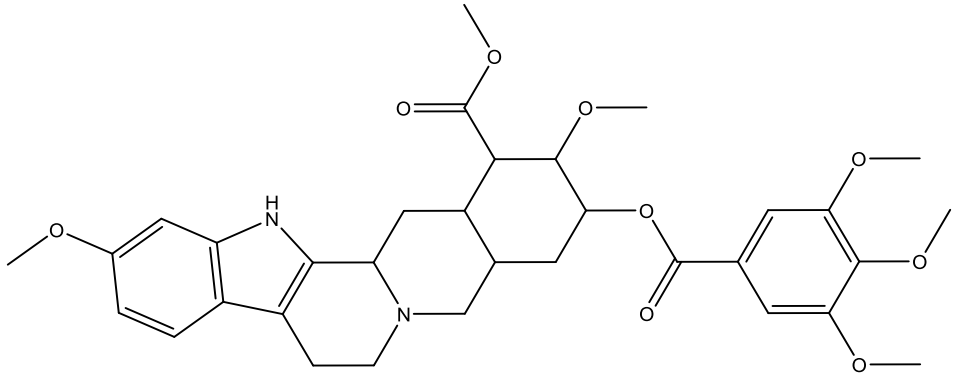
Plant species	Plant part	Alkaloid	Mode of actions	References
Lindera megaphylly **(Spicewood, Wu Yao)**	Root	(+)-Dicentrines 	• α_1-adrenoceptor antagonism	(C. C. Chen, Huang, Ou, et al., 1991; S.-M. Yu, Hsu, Ko, et al., 1992; S.-M. Yu, Kang, Chen, et al., 1993)
Rauwolfia serpentina **(Devil pepper, Indian snakeroot)**	Root bark	Reserpine 	• Depletion of biogenic amine (e.g., serotonin, noradrenaline) in neurotransmission	(Lobay, 2015; Vakil, 1955; T. Verma et al., 2021)

Table 1.3 Examples of plant-derived alkaloids with antihypertensive activity. (continued)

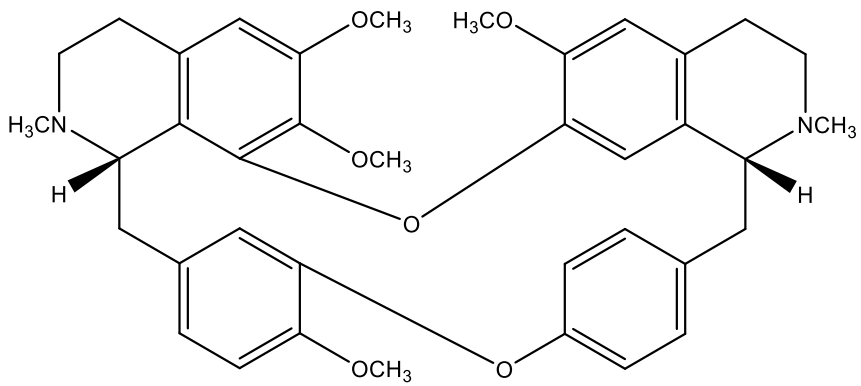
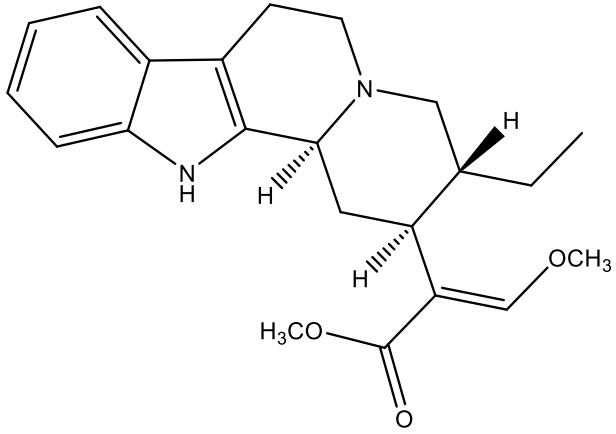
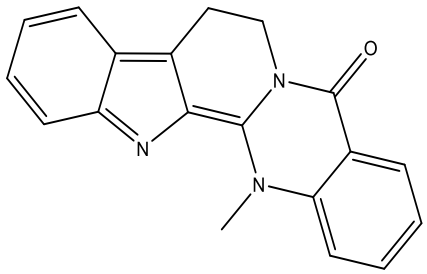
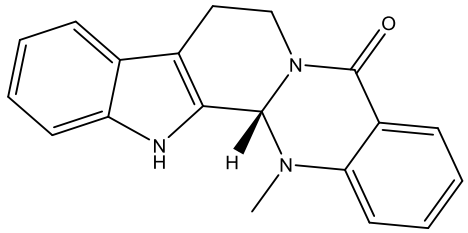
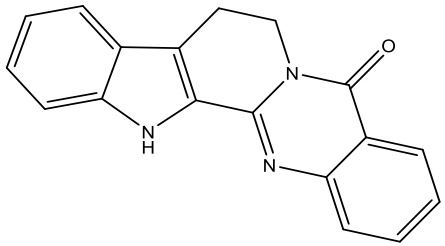
Plant species	Plant part	Alkaloid	Mode of actions	References
Stephania tetrandra **(Han Fang Ji, traditional chinese medicine)**	Stem bark	Tetrandrine 	• Selective blockage of L-type VGCCs • Interaction with α_1- adrenoceptor	(Iturriaga-Vásquez, Miquel, Ivorra, et al., 2003; Ivorra, Cercós, Zafra-Polo, et al., 1992; Zafra-Polo, Tormos, Cortes, et al., 1993)
Uncaria macrophylla **(Gambir plant, Gou Teng)**	Stem and leaf	Dihydrocorynantheine 	• Ca^{2+} channel blockade • K^+ channel activation	(J. S. Shi, Yu, Chen, et al., 2003; K. Wang, Zhou, Wang, et al., 2011)

Table 1.3 Examples of plant-derived alkaloids with antihypertensive activity. (continued)

Plant species	Plant part	Alkaloid	Mode of actions	References
Evodia rutaecarpa **(Wu Zhu Yu, traditional Chinese medicine)**	Fruit	Dehydroevodiamine 	• Endothelium dependent • α_1-adrenoceptor blockade • Ca^{2+} channel blockade • K^+ channel activation	(Chiou, Liao, Shum, et al., 1996)
		Evodiamine 	• Activation of transient receptor potential vanilloid (TRPV1) channel	(C. P. Hu, Xiao, Deng, et al., 2002)
		Rutaecarpine 	• Increase eNOS activity • Production of cGMP • Attenuation of L-type VGCC activity	(Tian, Li, & Xu, 2019; G. J. Wang, Wu, Chen, et al., 1999)

1.5.2 Schwarzinicine A as a lead compound

1.5.2.1 Background

Past studies have attested that alkaloids extracted from plants are valuable sources to search for vasoactive agents. Around the world, there are a few *Ficus* species that had their alkaloid contents reported and investigated for therapeutic potentials, namely *F. hispida* (Jia, Wu, Li, et al., 2020), *F. fistulosa* (H. J. Zhang, Tamez, Aydogmus, et al., 2002), *F. septica* (Kubo, Yatsuzuka, Matsushima, et al., 2016), *F. nota* (Latayada, Uy, Akihara, et al., 2017), and *F. hirta* (Wan, Chen, Li, et al., 2017). The genus *Ficus*, which is a large group of fig-bearing trees, belongs to the family Moraceae. The genus contains over 800 species that are widely distributed and cultivated in tropical regions (Berg & Corner, 2005). While fig fruits of some species are consumed as food, most of the medicinal actions described for the selected *Ficus* species that have been studied came from the leaves and bark (Philip Lansky & Maaria Paavilainen, 2011). Modern ethnomedical uses of the leaves from *Ficus* species include pain relief as well as treating bruises, cough and diarrhoea (Philip Lansky & Maaria Paavilainen, 2011). They can also be applied externally for haemorrhoids, pruritis or eczema (Lansky, Paavilainen, Pawlus, et al., 2008).

In our research group, the abundance of *Ficus schwarzii* in Malaysia has prompted the investigation of the alkaloid content in the plant. Crude alkaloid extracts were obtained from the leaves of *Ficus schwarzii* (**Figure 1.6**). Early studies within our research group have shown that it exhibited cytotoxic effects on colorectal adenocarcinoma (HT-29) cells (I. B. Abubakar, Lim, & Loh, 2015). Subsequently, seven novel phenylethylamine alkaloids were isolated from the extract, namely schwarzinicines A – G (Krishnan, Lee, Yap, et al., 2020). Among these compounds, schwarzinicine A, *N*-(3,4-dimethoxyphenethyl)-1,4-bis(3,4-dimethoxyphenyl)butan-2-amine, was isolated with the highest yield (**Figure 1.7**). Having said that, the yield of schwarzinicine A from *Ficus schwarzii* was still considered low, with only 385 mg (equivalent to 0.002%) isolated from approximately 20 kg of dried leaves (Krishnan et al., 2020).



Figure 1.6 The fruits and leaves of Ficus schwarzii. *Photos courtesy by Prof Kuan-Hon Lim.*

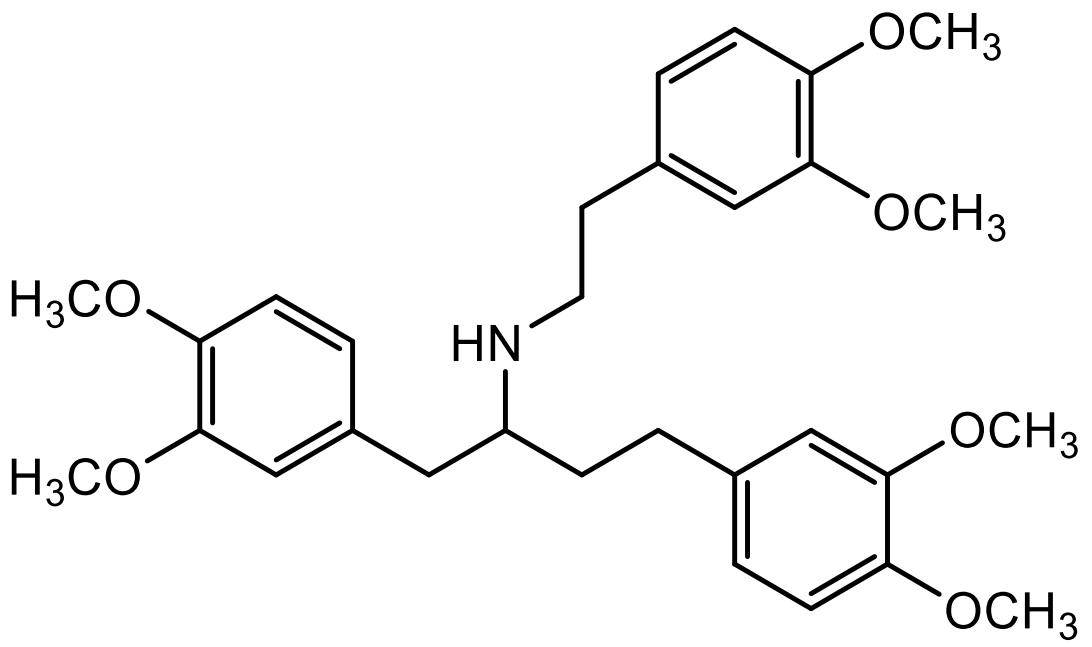


Figure 1.7 Chemical structure of schwarzinicine A, which was obtained naturally as a scalemic mixture (4:1 ratio of (+)/ (-)).

1.5.2.2 Biological and physicochemical properties of schwarzinicine A

Earlier findings reported that schwarzinicine A exhibited overt vasorelaxation properties with a profile similar to dobutamine (Krishnan et al., 2020). Following these initial observations, follow-up studies had found that schwarzinicine A demonstrated its potential role as a Ca^{2+} channel modulator when it exhibited a higher vasorelaxant effect when compared to other Ca^{2+} channel blockers such as verapamil and nifedipine (Loong, 2016).

Further investigations suggested that schwarzinicine A-induced vasorelaxation in rat aortae was mediated via the blockage of Ca^{2+} influx. In a Ca^{2+}-free environment, schwarzinicine A markedly suppressed the contractile response to re-addition of calcium chloride ($CaCl_2$) in a concentration-dependent manner, affecting extracellular Ca^{2+} entry in a similar way to nifedipine and SKF-96365 (Loong, 2016). Ca^{2+} imaging measurement revealed that schwarzinicine A also displayed a Ca^{2+} inhibitory property by blocking Ca^{2+} entry in rat's dorsal root ganglion cells (Loong, 2016). These observations provide additional evidence that schwarzinicine A could affect Ca^{2+} influx via a mechanism different from an L-type Ca^{2+} channel blocker.

To measure the intracellular Ca^{2+} dynamics by schwarzinicine A in transient receptor potential canonical (TRPC) channels, human embryonic kidney (HEK) cells overexpressing human TRPC3 and TRPC6 channels were employed. These channel

subtypes were chosen based on their functional roles in vascular regulation reported in some studies (Álvarez-Miguel et al., 2017; Dietrich, Mederos y Schnitzler, Gollasch, et al., 2005; R. Inoue et al., 2006; Kochukov et al., 2012; Martín-Bórnez et al., 2020; Thilo, Baumunk, et al., 2009). Fluorometric intracellular Ca^{2+} recordings confirmed its inhibition of hTRPC3-, and hTRPC6-mediated Ca^{2+} influx into HEK 293 cells with half-maximal inhibitory concentration (IC_{50}) values of 3 and 7 µM, respectively (unpublished data).

All in all, one of schwarzinicine A's mechanisms of action interferes with the cellular Ca^{2+} dynamics across the cell membrane with the involvement of TRPC channels. The evidence gathered suggested that schwarzinicine A blocks Ca^{2+} influx through multiple TRPC channels to exert a substantial vascular relaxation response in a functional vascular tissue. It also revealed schwarzinicine A as a non-selective TRPC channel blocker.

Despite promising biological activities, plant-derived schwarzinicine A has less favourable physicochemical properties, potentially affecting its *in vivo* pharmacokinetic profile. Virtual screening using Lipinski's Rule of Five and Veber's rule was carried out to evaluate the drug-likeness of schwarzinicine A, as a good balance between physicochemical properties and biological efficacy is imperative for it to become a successful therapeutic agent. Analyses revealed that the molecular weight (MW) and the number of rotatable bonds in schwarzinicine A exceeded the limits set in both rules (highlighted in red, **Table 1.4**). Rotatable bonds increase the flexibility of a compound. Together with high MW, these characteristics negatively influence the permeability of schwarzinicine A across the plasma membrane, which could lead to low oral bioavailability (Zerroug, Belaidi, BenBrahim, et al., 2019).

Lipinski, Lombardo, Dominy, et al., (1997) stated that a compound should be evaluated with caution if it failed to meet two out of four rules. On the other hand, Veber, Johnson, Cheng, et al., (2002) recommended compliance of both parameters when predicting good absorption and bioavailability of a compound. Although the tenets of Lipinski's and Veber's rules are helpful to predict the drug-likeness of schwarzinicine A, there are still many orally available drugs that do not entirely follow the rules, such as atorvastatin and montelukast (IUPHAR database, 2015). Furthermore, compounds

from natural origins are more likely to violate these rules (M. Ahmed, Hasani, Kalyaanamoorthy, et al., 2021; Veber et al., 2002).

Table 1.4 Chemical structure and physicochemical analysis of schwarzinicine A using Lipinski's Rule of Five and Veber's rule. *The values that have exceeded the limit are highlighted in red.*

Physicochemical properties	Schwarzinicine A
Lipinski's Rule of Five	
Hydrogen bond donor (HBD ≤ 5)	1
Hydrogen bond acceptor (HBA ≤ 10)	7
Molecular weight (MW < 500 Da)	510
Partition coefficient (LogP ≤5)	4.76
Lipinski's rule violations	1
Veber's rule	
Rotatable bond (≤10)	15
Topological polar surface area (tPSA ≤ 140 Å^2)	67.41
Veber's rule violations	1

1.5.2.3 Synthetic schwarzinicine analogues

Due to the low isolation yield of naturally occurring schwarzinicine A and its less satisfactory physicochemical properties, efforts were put into synthesising analogues that share the same pharmacophore as schwarzinicine A. Pharmacological studies on schwarzinicine A have provided a promising basis for the development of synthetic analogues (F. K. Lee, Krishnan, Muhamad, et al., 2021).

Through preliminary structure-activity relationship (SAR) studies, Dr Fong-Kai Lee from the School of Pharmacy has successfully identified several structural features that are associated with improved potency, in addition to discovering analogues with significantly improved potency. *N*-Phenethyl-1,2,3,4-tetrahydronaphthalen-2-amine and 1-(furan-2-yl)-*N*-phenethylpentan-3-amine, designated as FK244 and PM20, respectively (**Figure 1.8**), are amongst the more potent analogues that were discovered. The analogue design was directed as such that FK244 and PM20 have similar vasorelaxation profiles as schwarzinicine A, as well as improved physicochemical properties (detailed in **Chapter 2** and **Chapter 3**). This project focused mainly on elucidating the pharmacological effects and mechanism of actions for both FK244 and PM20. Although the molecular mechanisms for schwarzinicine A were not entirely determined, these findings pinpoint the most relevant pathways for further investigation on FK244 and PM20, especially the purported inhibitory effect on Ca^{2+} mobilisation via TRPC channels.

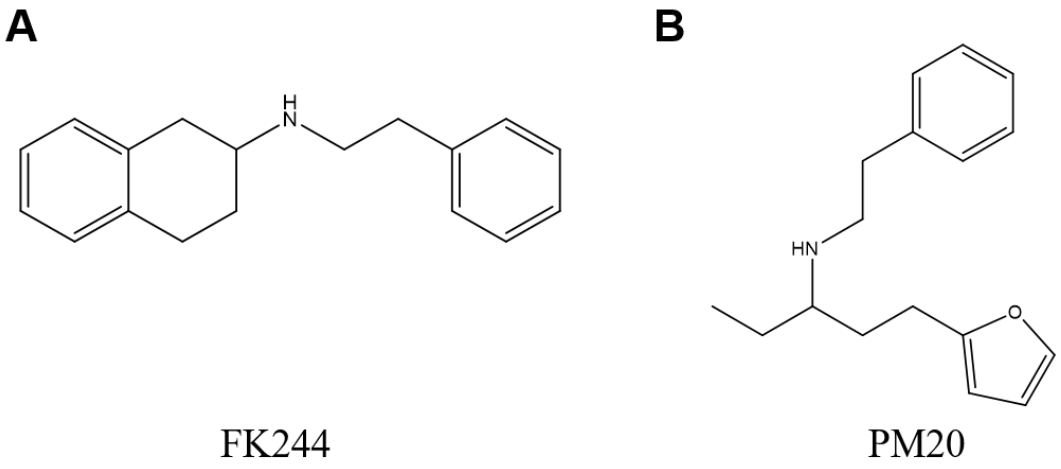


Figure 1.8 The structures of two phenylethylamine analogues of schwarzinicine A, namely (A) N-phenethyl-1,2,3,4-tetrahydronaphthalen-2-amine (FK244) and (B) 1-(furan-2-yl)-N-phenethylpentan-3-amine (PM20).

1.6 Research approaches

The diversity of natural plant compounds provides an interesting pool of chemical entities for drug discovery and development. Optimisation of the structure of schwarzinicine A has given rise to two analogues – FK244 and PM20, with improved biological and physicochemical properties. This section reviewed a few methodologies employed in this study to screen the pharmacological activities of FK244 and PM20.

1.6.1 Isolated tissue bath

In vitro isolated tissue bath assay is a well-standardised technique to evaluate smooth muscle function in animal tissues upon the addition of desired drugs or compounds. The general principles of the tissue bath system involve measuring the concentration-dependent contraction and relaxation of smooth muscle tissues under isometric tension. The tissue contractile force can be used to determine the efficacy and potency of the compound of interest by calculating its maximum tissue response (E_{max}) and half-maximal effective concentration (EC_{50}). The contractile force exerted by a compound can be manipulated and compared by exogenously administering other compounds with opposing effects or of known mechanisms of action (Jespersen, Tykocki, Watts, et al., 2015).

The organ bath apparatus consists of isolated smooth muscle tissues placed in a double-layered glass bath containing physiological salt solution in the inner lumen and circulating heated water at 37 ± 1 °C in the outer jacket (**Figure 1.9**). The organ bath system also delivers carbogen gas continuously to the living tissues. Carbogen gas is made up of 95% oxygen (O_2) and 5% carbon dioxide (CO_2). The tissue of interest is mounted in place by two stainless-steel hooks; the bottom stirrup is attached to a vertical rod while the top stirrup is connected to an isometric force transducer via a silk thread (**Figure 1.9**). In the beginning of the experiment, a passive tension is applied by mechanically stretching the resting smooth muscle preparation, creating an isometric tension (Watson, Magnussen, & Rabe, 1998). Changes in the muscle tone will be measured as forces and recorded by the force transducer (**Figure 1.9**). Then, the data are converted to digital signals using a data acquisition system and shown on a laptop (**Figure 1.9**) (Jespersen et al., 2015; Kullmann, Daugherty, de Groat, et al., 2014; Semenov, Herlihy, & Brenner, 2012).

The size of the tissue chamber can be changed to accommodate experiments on various isolated tissues. A low volume glass bath is preferred when measuring smaller vessels or when the drug samples acquired are in a small amount. Tissues can be obtained from mice, rats, guinea pigs and pigs. Examples of isolated smooth muscle tissues used are vascular rings (aorta, artery, vein) (Moohammadaree, Changtam, Wicha, et al., 2015), gastrointestinal tissues (ileum, stomach, duodenum) (Mohamed. Shabi, Rameshkannan, Haja Nazeer, et al., 2018), airways (trachea, bronchus) (M. K. Lee, Lim, Millns, et al., 2018; Semenov et al., 2012), urinary and reproductive tissues (bladder, ureter, vas deferens, uterus) (Colabufo, Pagliarulo, Berardi, et al., 2007; Zafra-Polo et al., 1993).

This pharmacological technique remains an important facet in drug development owing to its simplicity and reproducibility. The main consideration is that the tissue is immersed in an environment that highly mimics the *in vivo* physiological conditions. Thus, it enables the demonstration of the tissue's physiological reaction to drugs, integrating all cellular mechanisms and functioning as a whole (Jespersen et al., 2015; Leloup, Van Hove, De Moudt, et al., 2019). Most importantly, the isometric tension recordings encapsulate a wide range of information, which is useful to investigate the pharmacological effects of FK244 and PM20, as well as for drug target(s) characterisation. This technique allows us to better envisage how the analogues would work *in vivo*, providing more meaningful outcomes when screening for potential therapeutic agents.

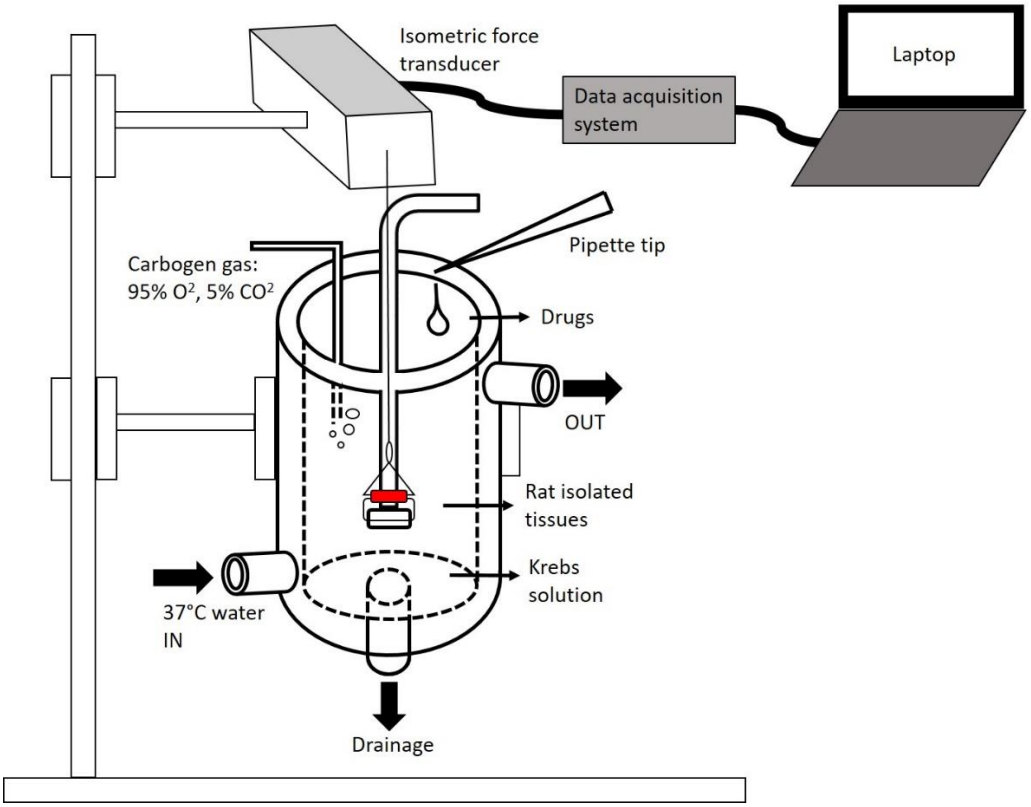


Figure 1.9 Illustration of an organ bath set-up. *Isometric tension of isolated tissues is recorded by a force transducer connected to a laptop. The tissue is submerged in the Krebs solution with constant aeration, jacketed by circulating water at 37 °C. Change of Krebs solution in washes is done by emptying the solution through drainage first then adding fresh Krebs solution.*

1.6.2 *Caenorhabditis elegans (C. elegans)*

Closely related to pharmacology, toxicology is also an indispensable part of the drug development process. *In vivo* toxicity screening in mammals are currently the gold standard in the pharmaceutical industry, especially when *in vitro* findings could not consistently be reproduced *in vivo* (Giacomotto & Ségalat, 2010; Hirsch & Schildknecht, 2019). Traditionally, the drug target must be identified in high-throughput screening and then carry out toxicity screening in mammals (Giacomotto & Ségalat, 2010). Around 70% of drug candidates suffer attrition at the preclinical validation stage when they do not show satisfactory pharmacokinetic properties and safety profiles (Kramer, Sagartz, & Morris, 2007).

Moreover, *in vivo* mammalian experiments are associated with high cost, low output, and controversial debates on ethical issues. At present, it is still unrealistic to terminate the use of all animals in finding the next breakthrough in therapeutic strategies (Barré-Sinoussi & Montagutelli, 2015). Nonetheless, efforts were made to develop alternative animal models which have a lower hierarchy of moral importance. Following primates, dogs and rodents, increasing studies use invertebrates such as *C. elegans* to balance animal welfare and quality scientific output relevant to human diseases (Franco, Sandøe, & Olsson, 2018). Small whole-animal toxicity screening in *C. elegans* during lead optimisation is gaining momentum to identify safer bioactive compounds at an earlier stage (C. K. Leung, Wang, Malany, et al., 2013; Xiong, Pears, & Woollard, 2017). Toxicity data obtained using *C. elegans* are within the context of a whole animal and do not rely on the initial characterisation of drug targets (Giacomotto & Ségalat, 2010).

C. elegans is a free-living soil nematode about 1 mm in length (**Figure 1.10**). Not only is it useful in toxicology studies, but it is also widely used in biomedical research including neuroscience, cardiovascular and ageing (Fitsanakis, 2012; Putcha & Johnson, 2004; Tissenbaum, 2015). Since its discovery in the 1960s, its genome, the nervous system and anatomy are fully mapped and described (Brenner, 1974; The C. elegans Sequencing Consortium, 1998). Phylogenetic analyses showed that they express genes that are homologous in humans, thus making them a remarkable model organism to study human physiology and related diseases (Shaye & Greenwald, 2011). With only over 1000 somatic cells, its capability of undergoing genetic crosses to alter specific genes has catalysed the progress in understanding fundamental human genetics and disease pathophysiology (Tenor & Aballay, 2008).

C. elegans exists primarily as hermaphrodite (XX). It can self-fertilise and generate homozygous worms with identical genetic makeup. In contrast, male *C. elegans* only exist in 0.1% of the worm's population. *C. elegans* is easy to propagate with a short life cycle. When the nematodes are raised under 16 °C, their growth is slowed down. It takes them about 5 days to reach adulthood compared to 3 days under 20 – 25 °C (Gómez-Orte, Cornes, Zheleva, et al., 2018). Variability in nematode's developmental process provides flexibility in planning experimental work.

One gravid worm can lay up to an average of 300 eggs in its adulthood (Schafer, 2005). These characteristics are highly favourable among the scientific community as it vastly increases the sample size without raising ethical concerns. Despite the large brood size, the maintenance cost is relatively inexpensive due to its small size and low demand for space. *C. elegans* is grown on agar plates or liquid cultures added with *Escherichia coli (E. coli)* as the main food source. The larvae of *C. elegans* can also be kept in liquid nitrogen as cryopreserved stocks for at least 6 months. Similar to *in vitro* techniques, the frozen stock can be thawed to revive the worms (Schafer, 2005).

C. elegans is optically transparent throughout its lifespan. This distinctive characteristic has added value to studies on compound toxicity, where changes such as egg-laying defect, paralysis and death can be easily observed. A basic screening based on the survival of *C. elegans* infected with human pathogenic bacteria was used to identify novel antimicrobial agents (Moy, Ball, Anklesaria, et al., 2006). The development of high-resolution microscopy and imaging techniques have revolutionised research using *C. elegans*. Nematodes tagged with fluorescent markers can be imaged clearly under the microscope, enabling the measurement of drug toxicity effects on the cellular response (Breimann, Preusser, & Preibisch, 2019).

Large-scale screening using *C. elegans* is not entirely without limitations as their data cannot replace all studies in mammals. They are not shortcuts to human treatment but serve to complement *in vitro* screenings for bioactive, non-toxic compounds (Nass & Hamza, 2007). This model organism provides the foundation for further understanding the potential drug-induced toxicity of FK244 and PM20 that are relevant to human physiology.

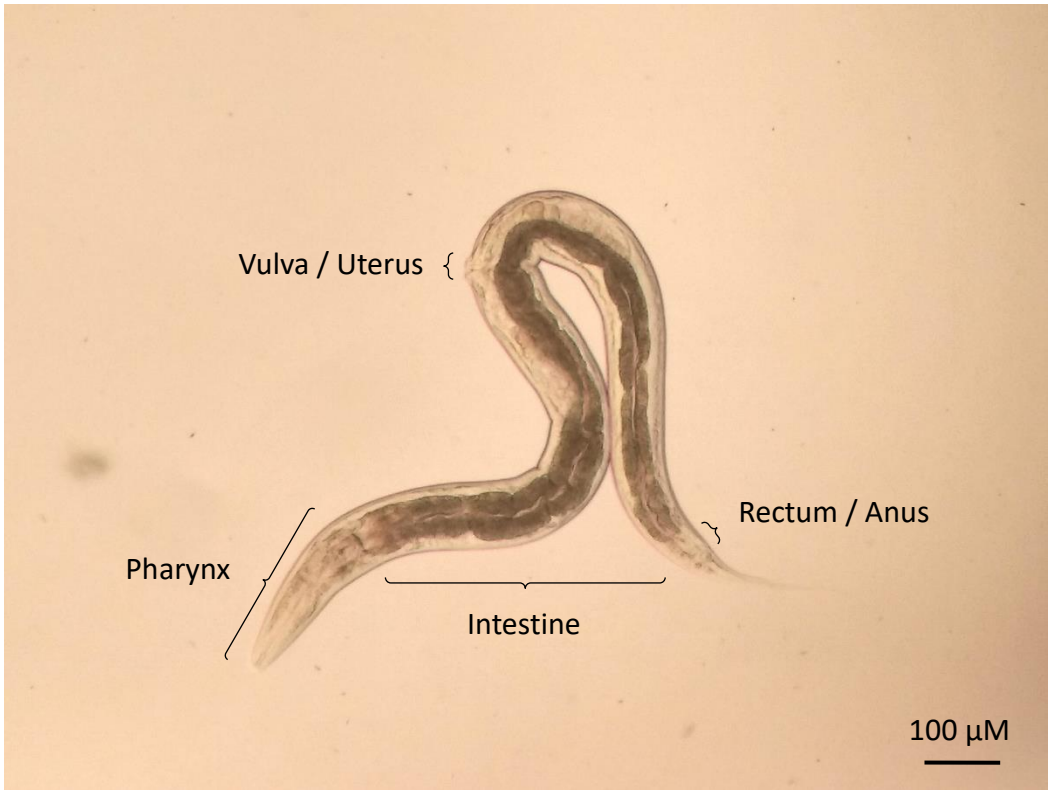


Figure 1.10 Microscopic view of an adult C. elegans. *Its unique features made it a versatile organism in the modern pipelines of drug discovery.*

1.6.3 Fluorometric intracellular Ca^{2+} recordings

One of the fundamental regulatory mechanisms for smooth muscle contractility is Ca^{2+} mobilisation. It is facilitated by a wide range of intracellular and extracellular mechanisms in smooth muscle cells (Berridge, 2008). To study isolated receptor channels and their underlying role in mediating Ca^{2+} signals, it is critical to measure the changes of Ca^{2+} level in isolated living cells. Fluorometric intracellular Ca^{2+} recording is a reliable experimental technique to examine these Ca^{2+} fluxes *in vitro*. Fluorescence detection using fluorescent Ca^{2+} indicators can reveal important information on Ca^{2+} signal transduction within the cell's intracellular compartments and through channel proteins.

The lipid-soluble fluorescent Ca^{2+} indicator, fura-2 acetoxymethyl (AM) ester has been widely used to measure $[Ca^{2+}]_i$ due to its ability to pass through plasma membrane without disrupting cellular functions (Takahashi, Camacho, Lechleiter, et al., 1999). To detect the changes in $[Ca^{2+}]_i$, cells are first loaded with fura-2 AM. Fura-2 AM has a Ca^{2+}-selective chelator and a fluorophore (**Figure 1.11**). Intracellular esterase cleaves the AM groups on fura-2 AM and produces charged fura-2 which is entrapped within the cells (**Figure 1.11**). Fura-2 loaded cells are excitable with ultraviolet light at the wavelengths of 340 and 380 nm, whereas the emitted fluorescence spectrum is between 505 to 520 nm. The dual excitation wavelength of fura-2 changes when it captures cytosolic Ca^{2+}, permitting the quantitative determination of $[Ca^{2+}]_i$ (**Figure 1.11**) (Grienberger & Konnerth, 2012; Grynkiewicz, Poenie, & Tsien, 1985; Li, 2019). This trait makes it stands out from other non-ratiometric Ca^{2+} sensitive dyes such as quin-2, fluo-3 or fluo-4 (Hideharu & Haruo, 1994).

Fluorometric intracellular Ca^{2+} recording remains popular in biomedical research. It has been employed to study pathological modulation of Ca^{2+} in smooth muscles (Dorn, Becker, & Davis, 1992; Lindsey & Songu-Mize, 2010). It has also been proven useful in exploring new roles for Ca^{2+}-permeable channels within the realm of vascular pharmacology (C. C. Bauer, Boyle, Porter, et al., 2010; Tosun, Paul, & Rapoport, 1998; Urena, del Valle-Rodriguez, & Lopez-Barneo, 2007). As growing evidence revealed additional mechanisms underlying Ca^{2+} transport across the plasma membrane, more drug targets were identified to encourage the development of potential therapeutic agents (Just, Chenard, Ceci, et al., 2018; T. Maier, Follmann, Hessler, et al., 2015; Rubaiy, Ludlow, Henrot, et al., 2017; Schleifer, Doleschal, Lichtenegger, et al., 2012).

In short, investigation on intracellular Ca^{2+} dynamics and its regulation through receptor channels can be performed jointly with functional studies to characterise the potential targets of FK244 and PM20.

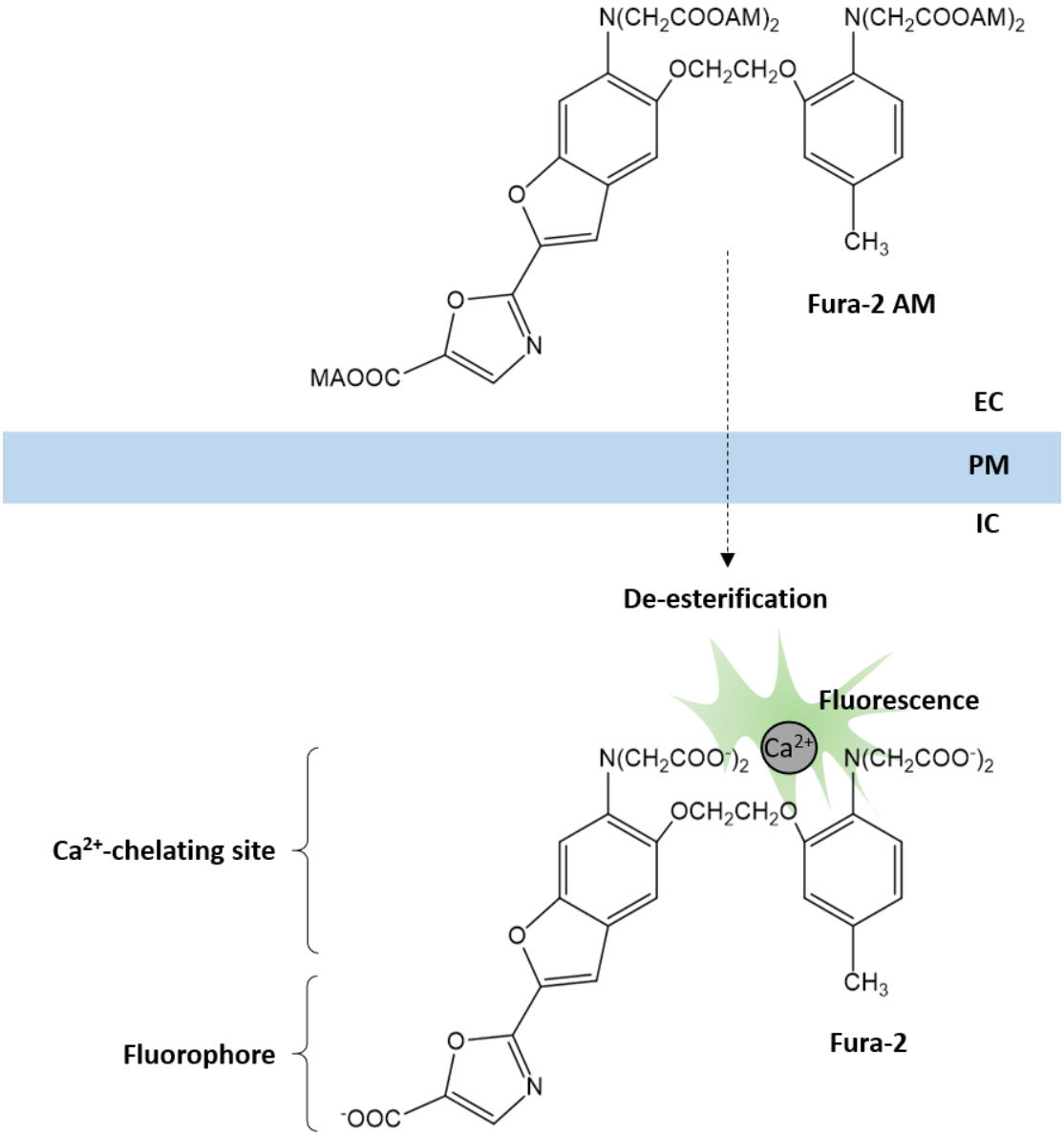


Figure 1.11 Mode of action of fura-2 AM as a ratiometric Ca^{2+} sensor in cell-based assays. *Abbreviations: Ca^{2+}, calcium ion; EC, extracellular; IC, intracellular; PM, plasma membrane. Diagram adapted from Li (2019).*

1.6.3.1 HEK 293 cell as an expression system for TRPC channels

HEK 293 cells were foetal kidney cells originally derived and cultured from an aborted female foetus (**Figure 1.12**) (Graham, Smiley, Russell, et al., 1977). Since the 1980s, it has been one of the most common cell lines used in cell-based assays across different research fields. It is widely preferred due to its low maintenance needs, requiring only basic high-glucose media, broad-spectrum antibiotics, and a humidified incubator to grow. Their growth doubles every 36 hours, making it simple for research replication. However, their high reproducibility also comes with a cost; their cell health deteriorates when the passage number increases (P. Thomas & Smart, 2005).

HEK 293 cells remain a desirable choice to use as a transient TRPC expression system (Capra, Busnelli, Perenna, et al., 2013; L. P. He, Hewavitharana, Soboloff, et al., 2005), and also generate stable TRPC-transfected cells (Durocher, Perret, & Kamen, 2001; Estacion, Sinkins, Jones, et al., 2006; Gibon, Tu, Bohic, et al., 2011). HEK 293 cell is suitable as the host cell line for heterologous TRPC channels expression owing to its high accuracy in transfection and rapid amplification of recombinant proteins (P. Thomas & Smart, 2005). They are often utilised to carry out high throughput screening to search for potential therapeutic agents and characterise novel drug targets (de la Peña & Gomis, 2019; M. Miller, Wu, Xu, et al., 2016)

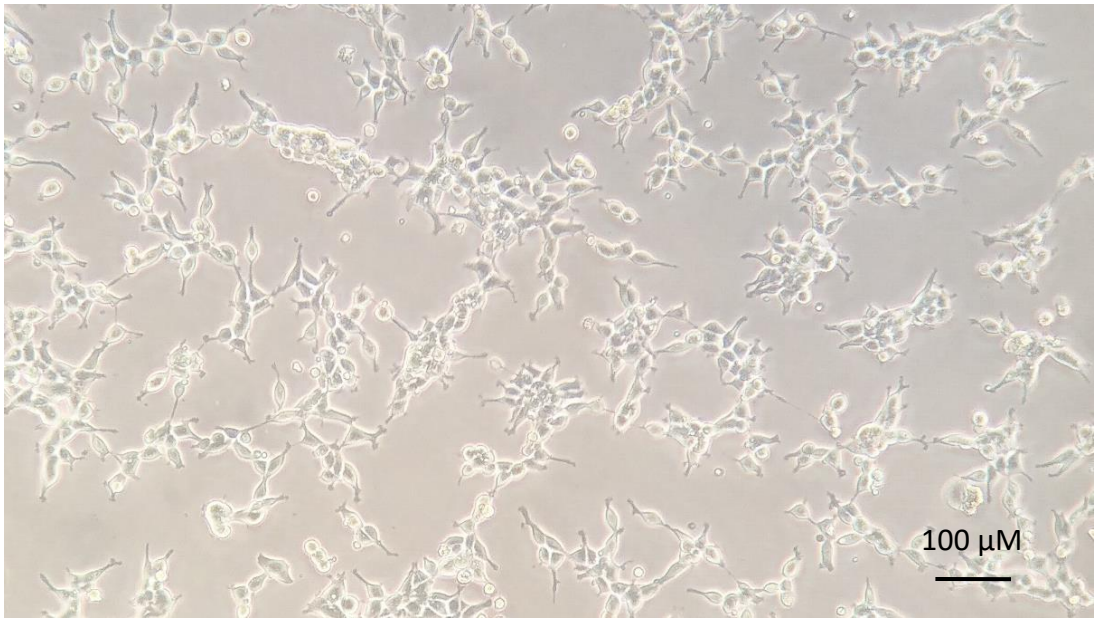


Figure 1.12 Healthy adherent HEK 293 cells at 50% confluency under 4x objectives lens. *They appear to have epithelial morphology, which is slightly oval to pyramidal shape with hair-like filopodia.*

1.7 Research aim

Globally, approximately 1.13 billion people suffer from hypertension (World Health Organization, 2013; Bin Zhou et al., 2017). Prevalence of resistant hypertension is around 7 – 13% of all patients diagnosed with hypertension (Chia & Ching, 2014; Persell, 2011; Sinnott et al., 2017). As hypertension is inadequately controlled by current pharmacological and surgical treatments, this situation necessitates the development of new medicine with a novel mechanism of action(s) to improve the clinical management of resistant hypertension.

Studies have reported alkaloids isolated from natural sources can exhibit antihypertensive effects by acting as VSM relaxants (C. C. Chen et al., 1991; Iturriaga-Vásquez et al., 2003; G. J. Wang et al., 1999; K. Wang et al., 2011). Recently, a novel plant phenylethylamine alkaloid, *N*-(3,4-dimethoxyphenethyl)-1,4-bis(3,4-dimethoxyphenyl)butan-2-amine, coined as schwarzinicine A was isolated from the leaves of a local fig species, *Ficus schwarzii*. It was reported that schwarzinicine A exerts overt vasorelaxation (Krishnan et al., 2020). These initial observations had led to the synthesis of *N*-phenethyl-1,2,3,4-tetrahydronaphthalen-2-amine (FK244) and 1-(furan-2-yl)-*N*-phenethylpentan-3-amine (PM20) based on the pharmacophore of schwarzinicine A. This research aims to investigate FK244's and PM20's potential role as Ca^{2+} channel modulators, as well as characterisation of their pharmacological effects using the rat isolated aorta as a native system. It is hypothesised that FK244 and PM20, being the analogues of lead compound schwarzinicine A, will also be able to exert vasorelaxation by modulating Ca^{2+} dynamics with improved pharmacological profiles. This study was designed to determine the vasorelaxant effects and mechanism of action for FK244 and PM20, with a specific focus on Ca^{2+} mobilisation.

The overall objectives of this research were:

i. To elucidate the functional activity and mechanism of action of FK244 (**Chapter 2**) and PM20 (**Chapter 3**) using rat isolated aorta and its effects on other smooth muscles such as rat isolated trachea and bladder

ii. To determine the toxicity of FK244 and PM20 by evaluating the lifespan of *C. elegans* fed with these compounds (**Chapter 4**)

iii. To assess the efficacy and potency of FK244 and PM20 using spontaneously hypertensive rats (SHR) and streptozotocin (STZ)-induced diabetic rats as disease models (**Chapter 4**)

iv. To investigate Ca^{2+} modulation of FK244 and PM20 through TRPC3 and TRPC6 channels at the cellular level using HEK 293 cell line (**Chapter 5**)

Chapter 2 Pharmacological investigation of *N*-phenethyl-1,2,3,4-tetrahydronaphthalen-2-amine (FK244)

2.1 Introduction

2.1.1 Schwarzinicine A and FK244

Schwarzinicine A, *N*-(3,4- dimethoxyphenethyl)-1,4-bis(3,4-dimethoxyphenyl)butan-2-amine, is a plant-derived phenylethylamine isolated from the leaves of a local fig plant species, *Ficus schwarzii*. Early studies within our research group have shown that it exhibited vasorelaxation activities in porcine coronary and pulmonary arteries as well as rat aorta (Loong, 2016). Previous findings have shown that the vasorelaxation effects demonstrated by schwarzinicine A was due to the blocking of plasma Ca^{2+} channels. Using fluorometric intracellular Ca^{2+} recordings, inhibition on TRPC3 and TRPC6 channels were identified as schwarzinicine A's targeted Ca^{2+} channels.

Due to the low isolation yield of schwarzinicine A from natural sources, efforts were put in to chemically synthesise analogues of schwarzinicine A in a much more scalable and sustainable way (F. K. Lee et al., 2021). As a result, Dr Fong-Kai Lee and Prof Kuan-Hon Lim (School of Pharmacy) have successfully synthesised a range of analogues that are structurally similar to schwarzinicine A. Subsequently, the comparison of vasorelaxation activity of schwarzinicine A and its analogues was carried out to study their SAR (F. K. Lee et al., 2021). It aimed at determining the pharmacophore of schwarzinicine A, which is the chemical group(s) that is responsible for inducing biological activities in an organism (F. K. Lee et al., 2021; M. E. Maier, 2015).

There are many strategies for studying SAR. One of the most common strategies used is simplification. Removing complex side chains and fragments would simplify the structure of analogues. By comparing these analogues with the parent compound, the auxophores, which are the groups that do not contribute to the activities of the compound, can be identified (C. He, Preiss, Wang, et al., 2017). As schwarzinicine A has a large and complex scaffold, some of the chemical groups were not essential to elicit its biological activities. In the first round of the simplification process, all the 3,4-dimethoxy ($-OCH_3$) groups on the three phenyl rings were completely removed to reduce its structural complexity (**Figure 2.1**). It was found that the removal of all

methoxy groups did not affect the activities of analogues compared to schwarzinicine A (F. K. Lee, 2020).

Furthermore, one out of three aromatic rings was removed one at a time. These have led to the synthesis of a series of schwarzinicine A analogues that possessed less complex structural scaffolds. SAR study has shown that only two out of three rings were required to retain the vasorelaxant activities of analogues (F. K. Lee, 2020). Interestingly, the efficacy of analogues was less than 100% when none of the two rings retained was an aromatic ring. Therefore, to achieve more than 100% relaxation effects in rat isolated aorta, at least one of the two rings after the simplification process has to be an aromatic ring.

Another strategy used in the SAR study of schwarzinicine A was rigidification. As the name suggests, it is a process that locks the conformations of a compound by reducing the number of rotatable bonds. Bond rotation allows the existence of many alternative conformations of a compound, some of which may be inactive and do not bind to the receptor's active site to evoke biological effects. This strategy was aimed to lock schwarzinicine A in its potentially active conformation to get an analogue with improved potency. Through rigidification, the rotatable bonds connecting rings B and C in schwarzinicine A were restricted, resulting in the formation of *N*-phenethyl-1,2,3,4-tetrahydronaphthalen-2-amine with an aminotetralin ring (indicated with red-coloured bonds, **Figure 2.1**). The structure has a phenethylamine unit connected to an aminotetralin via an aliphatic fragment. This analogue was designated as FK244.

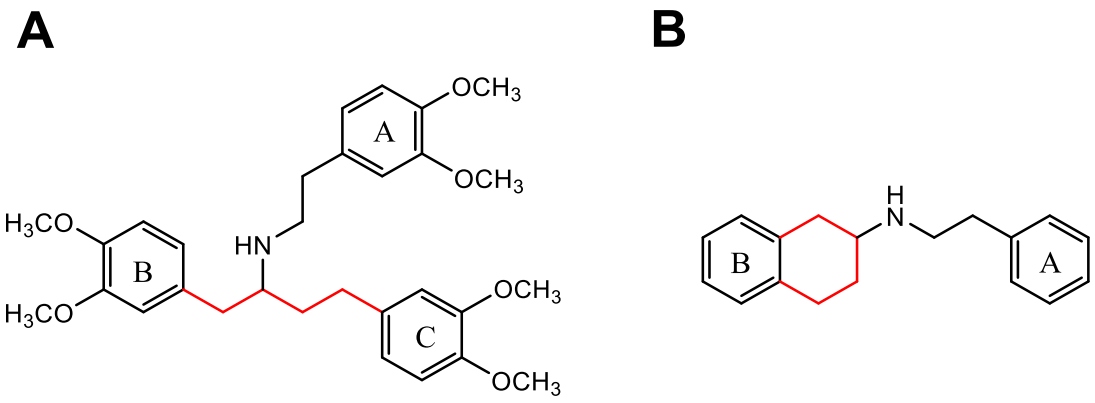


Figure 2.1 Chemical structures of (A) schwarzinicine A and (B) FK244.

2.1.2 Synthesis of *N*-phenethyl-1,2,3,4-tetrahydronaphthalen-2-amine (FK244)

As shown in **Figure 2.2**, FK244 **(2)** was synthesised in a one-step reaction of reductive amination between ketone **(1)** and phenethylamine with sodium triacetoxyborohydride ($NaBH(OAc)_3$). To a stirring solution of β-tetralone **(1)** (397.2 mg, 2.72 mM, 1 equivalent) in 1,2-dichloroethane ($ClCH_2CH_2Cl$) (10 ml) was added phenethylamine (0.38 ml, 3.09 mM, 1.1 equivalent), $NaBH(OAc)_3$ (935.7 mg, 4.41 mM, 1.6 equivalent) and acetic acid (AcOH) (0.16 ml, 2.8 mM, 1 equivalent). The solution was stirred at room temperature for 25 hours before the addition of 1 M sodium hydroxide (NaOH) solution (10 ml). The mixture was then extracted with ethyl acetate (EtOAc) (3 × 20 ml). The combined organic layer was washed with brine (10 ml) and subsequently dried with sodium sulphate (Na_2SO_4) before concentrated *in vacuo*. The crude product was purified by centrifugal radial thin-layer chromatography (TLC) using an eluent system of diethyl ether (Et_2O)-hexane (1:2). The product extracted was *N*-phenethyl-1,2,3,4-tetrahydronaphthalen-2-amine (FK244) as a brown oil (529.9 mg, 2.11 mM). The yield of FK244 was 78%. The purity of FK244 was at least 99% by nuclear magnetic resonance (NMR). FK244 was characterised by ^{1}H NMR, ^{13}C NMR, infrared spectroscopy (IR) and high resolution electrospray ionisation mass spectrometry (HRESIMS). Data of characterisation are shown in **Appendix A**. SAR study and synthesis of FK244 were carried out by Dr Fong-Kai Lee, from the University of Nottingham Malaysia.

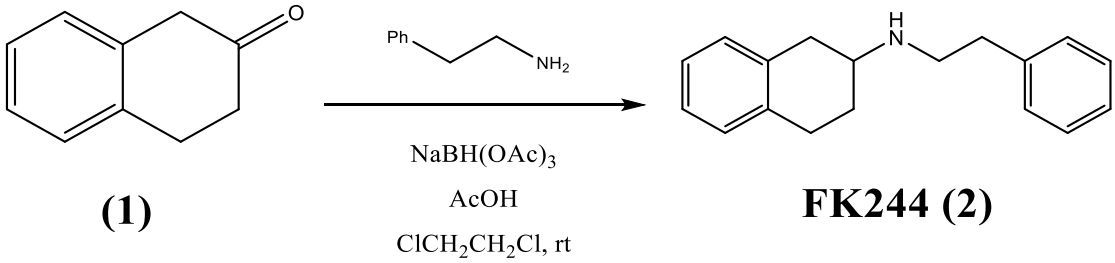


Figure 2.2 Synthesis of N-phenethyl-1,2,3,4-tetrahydronaphthalen-2-amine (FK244).

2.1.3 Lipinski's Rule of Five and Veber's rule

In the drug discovery process, solubility, pharmacokinetic and pharmacological properties of a compound are important factors to determine its potential to be an efficacious and safe drug. Hence, Lipinski's and Veber's analyses (Lipinski et al., 1997; Veber et al., 2002) were used to determine the drug-likeness and the potential oral bioavailability of FK244 and PM20.

Lipinski's reported four key physicochemical parameters that are important indicators of orally active drugs which have good pharmacokinetic profiles. The parameters are no more than 5 hydrogen bond donors (HBDs), no more than 10 hydrogen bond acceptors (HBAs), no more than 500 Dalton (Da) of MW and a partition coefficient (logP) equal to or less than 5 (Lipinski et al., 1997). They have cut off values at multiple of five; hence this analysis is also named as the 'Lipinski's Rule of Five'. Compounds that do not obey these rules were found more likely to have poor absorption and permeation (Lipinski et al., 1997).

Lipinski's analysis states the higher the number of HBA, the lower the permeability and absorption of the compound across the phospholipid bilayer. Similarly, an excessive number of HBD decreases the permeability of compound across the plasma membrane. HBD is counted as heteroatoms bond with hydrogen, while HBA is any heteroatoms bond without a positive charge. However, to give an effective rule for the prediction of oral bioavailability, Odović et al. (2017) stated that HBA excludes any halogens, nitrogen in pyrrole ring and aromatic oxygen and sulphur. Molecules with high MW are less likely to be orally active than low MW compounds as high MW impedes intestinal absorption. In addition, logP describes the solubility of a compound in two immiscible solvents (Lipinski et al., 1997). It measures the lipophilicity of the compound. Lipophilicity can be tested by using the shake-flask method or high-performance liquid chromatography (HPLC). In the shake-flask method, the commonly used solvents are octan-1-ol and water (Işık, Levorse, Mobley, et al., 2020). The compound should be tested at a pH when all its molecules are in an unionised, neutral form. Hydrophilicity and hydrophobicity directly affect a compound's oral bioavailability, absorption, distribution, metabolism, excretion (ADME) properties, and interactions with receptors.

Furthermore, Veber et al. (2002) also investigated the influence of rotatable bonds and polar surface area on oral bioavailability in rats. They have concluded that compounds that have 10 or less rotatable bonds and polar surface area equal to or less than 140 square angstrom ($Å^2$) are more likely to have high bioavailability. Rotatable bonds are any single bonds that have no hydrogen atom. However, correction factors are applied to exclude C-N bond as it is non-rotatable but fall within the definition of rotatable bonds. Moreover, high polar surface area reduces intestinal absorption (Veber et al., 2002). Topological polar surface area (tPSA) is closely related to total hydrogen bond count, the number of HBD and HBA as hydrogen affects the polarity of a compound. Literature has shown that tPSA is superior to logP in correlating the drug permeation rate (Ghose, Viswanadhan, & Wendoloski, 1998; Odović et al., 2017).

2.2 Significance of study

The chemical nomenclature of *N*-phenethyl-1,2,3,4-tetrahydronaphthalen-2-amine was first revealed in a study on the vasopressor activity of synthetic phenethylamine compounds (Allewelt & Day, 1941). However, no further information is published on its biological activity since 1941. This chapter aims to elucidate the pharmacological effects and mechanism of action of FK244 in VSM tissue (rat aorta) using the organ bath technique.

These were the objectives of this chapter:

i. To predict the drug-likeness of FK244 using Lipinski's Rule of Five and Veber's rule
ii. To investigate the effects of FK244 in rat and porcine smooth muscle tissues
iii. To investigate the main vasorelaxation mechanisms of FK244 in rat arterial smooth muscle
iv. To study the relaxation effects of FK244 against different contractile agents
v. To assess the reversibility of FK244's inhibition against phenylephrine-induced contraction
vi. To determine the role of FK244 in regulating Ca^{2+} homeostasis
vii. To evaluate the Ca^{2+}-inhibiting mechanism of FK244 using known Ca^{2+} channel blockers

2.3 Materials and methods

2.3.1 Analysis of physicochemical properties on FK244 and other commonly used Ca^{2+} channel blockers

Lipinski's Rule of Five and Veber's rule were used to evaluate the potential drug-likeness and oral bioavailability of FK244. Nifedipine, SKF-96365 and Pyr3 were used as reference compounds. The rationale for choosing nifedipine is because it is a marketed oral medication for hypertension, targeting L-type VGCC. SKF-96365, a non-selective TRPC blocker and Pyr3, a selective TRPC3 inhibitor, were used in comparison to FK244, although they are not used clinically and made available in oral dosage form. Currently, there is no formulated oral dosage form for TRPC inhibitors approved for use clinically.

The structures of these compounds were drawn, and the values for logP, MW, and tPSA were calculated using ChemDraw Profession (version 16.0.1.4, PerkinElmer

Informatics Inc.). The number of HBD, HBA, and rotatable bond, were determined using online tool Molinspiration Cheminformatics (2002)

For the reference compounds, all the data were extracted from the International Union of Basic and Clinical Pharmacology (IUPHAR), which was created in collaboration with the British Pharmacological Society (BPS) (IUPHAR database, 2015).

2.3.2 Drugs and solutions

Details of the drugs including their brands, solvent used, stock concentration, and final dimethyl sulfoxide (DMSO) concentration in the bath are listed in **Table 2.1**. FK244 was dissolved in 100% DMSO to make up a stock solution of 100 mM. Lower concentrations of FK244 and other drugs were prepared in a 10-fold serial dilution from 100 mM stock solutions. They include: 10 mM (DMSO 75%), 1 mM (DMSO 50%), 100 μM (DMSO 25%), 10 μM (purified water), 1 μM (purified water) and 100 nM (purified water). The final concentration of DMSO in the organ bath solution did not exceed 0.3%, while methanol did not exceed 0.05%.

Standard Krebs-Ringer buffer solution (referred to as normal Krebs throughout the thesis) was prepared on the day of experiment with the following composition (mM): sodium chloride (NaCl) 120, potassium chloride (KCl) 5.4, magnesium sulphate ($MgSO_4$) 1.2, potassium dihydrogen phosphate (KH_2PO_4) 1.2, sodium bicarbonate ($NaHCO_3$) 25, *D*-glucose 11.7, and $CaCl_2$ 1.26 (Loong, Tan, Lim, et al., 2015). After dissolving all the salts in purified water, Krebs solution was aerated with carbogen gas for at least 15 minutes. In experiments where Ca^{2+}-free Krebs was required, $CaCl_2$ was omitted.

Table 2.1 Summary of drugs and their details.

Drugs	Company, Country	Solvent	Stock concentration (M)	Final DMSO concentration in bath (%)
(*R*)-(−)-phenylephrine hydrochloride	Sigma-Aldrich, USA	Purified water	0.1	N/A
1-[2-(4-Methoxyphenyl)-2-[3-(4-methoxyphenyl)propoxy]ethyl-1*H*-imidazole hydrochloride (SKF-96365)	Tocris Bioscience, UK	DMSO 100%	0.1	0.075
11-Dideoxy-9*α*,11*α*-methanoepoxy prostaglandin F_{2a} (U46619)	Tocris Bioscience, UK	DMSO 100%	0.1	0.3
1*H*-[1,2,4]Oxadiazolo[4,3-*a*]quinoxalin-1-one (ODQ)	Tocris Bioscience, UK	DMSO 100%	0.1	0.05
2-Aminoethoxydiphenyl borate (2-APB)	Tocris Bioscience, UK	DMSO 100%	0.1	0.1
4-Aminopyridine (4-AP)	Tocris Bioscience, UK	Purified water	0.1	N/A
Barium chloride ($BaCl_2$)	Sigma-Aldrich, USA	Purified water	1	N/A
Calcium chloride	Chemiz, Malaysia	Purified water	1.0	N/A
Carbamylcholine chloride (Carbachol)	Nacalai Tesque, Japan	Purified water	0.1	N/A
Ethyl-1-(4-(2,3,3-trichloroacrylamide)phenyl)-5-(trifluoromethyl)-1*H*-pyrazole-4-carboxylate (Pyr3)	Sigma-Aldrich, USA	DMSO 100%	0.1	0.075
Ethylene glycol-bis(2-aminoethylether)-*N*,*N*,*N′*,*N′*-tetraacetic acid (EGTA)	Sigma-Aldrich, USA	NaOH 10 N	0.1 / pH 8.0	N/A

Table 2.1 Summary of drugs and their details. (continued)

Drugs	Company, Country	Solvent	Stock concentration (M)	Final DMSO concentration in bath (%)
Forskolin	Tocris Bioscience, UK	DMSO 75%	0.01	≈ 0
Glibenclamide	Tokyo Chemical Industry (TCI), Japan	DMSO 100%	0.1	0.075
***N*-[4-[3,5-Bis(trifluoromethyl)-1*H*-pyrazol-1-yl]phenyl]-3-fluoro-4-pyridinecarboxamide (Pyr6)**	Sigma-Aldrich, USA	DMSO 100%	0.1	0.075
***N*^{G}-Nitro-*L*-arginine methyl ester (L-NAME) hydrochloride**	Tocris Bioscience, UK	Purified water	0.1	N/A
Nifedipine	Nacalai Tesque, Japan	DMSO 100%	0.1	0.075
Potassium chloride (KCl)	Chemiz, Malaysia	Purified water	3	N/A
Prazosin	TCI, Japan	Methanol 50%	0.01	0.05 (methanol)
Propranolol	Merck Millipore, USA	Purified water	0.1	N/A
Rauwolscine	Tocris Bioscience, UK	Purified water	0.01	N/A
Serotonin hydrochloride	Tocris Bioscience, UK	Purified water	0.1	N/A
Tetraethylammonium chloride (TEA)	Tocris Bioscience, UK	Purified water	0.1	N/A
Verapamil	TCI, Japan	Purified water	0.1	N/A

2.3.3 Isolated tissue preparations

2.3.3.1 Rat isolated tissues

Ethics approval (UNMC12, **Appendix B)** was obtained from the University of Nottingham's Animal Welfare and Ethics Review Body (AWERB), which follows the UK Animals (Scientific Procedures) Act 1986. This study also adheres to Animal Research: Reporting of In Vivo Experiments (ARRIVE) guidelines and complies with all international, national and institutional policies. Normotensive adult male Sprague–Dawley (SD) rats (233 – 591 g; 2-3 months old) were obtained from the animal house at University Putra Malaysia (UPM), Malaysia, where they were housed under standard condition (12:12 light-dark cycle from 8 a.m.-8 p.m.; 18 – 20 °C) and allowed free access to food pellet and water.

Methods used in tissue preparation were adopted from (Loong et al., 2015). The rats were euthanised using CO_2. Then, the rat thoracic aorta, trachea and bladder were excised and immediately placed in Krebs-Ringer bicarbonate solution (pH 7.4). The connective tissues were subsequently cleaned off from the aorta and trachea and cut into 4 mm and 2 mm rings, respectively. The bladder was divided in half in the sagittal plane and trimmed into a 5 × 2 mm (length × width) rectangular strip.

2.3.3.2 Porcine isolated tissues

Porcine pulmonary artery and bronchiole were isolated from lungs of freshly slaughtered white hybrid pigs of either sex (≈ 50 kg, 4 – 6 months old) obtained from a local abattoir in Nottingham, UK. First-order pulmonary artery and bronchiole were placed in cold aerated Krebs solution at 4 °C overnight, with an additional 2% Ficoll added to the Krebs solution for bronchiole storage. The next day, connective tissues were cleaned off from the arteries and bronchioles and cut into 4 mm rings with less than 5 mm in diameter. Isolation of porcine tissues described in this subsection was carried out by Ms Yin-Ying Saw at the University of Nottingham UK.

2.3.4 Organ bath setup

The tissues were immersed in a 30 ml double-layered glass bath containing 10 ml Krebs solution at 37 ± 1 °C with continuous aeration of carbogen gas. The tracheal and aorta rings were hooked between two stainless-steel hooks, with the bottom stirrup attached to a glass rod and the top stirrup connected to an isometric force transducer (MLTF050/ST, ADInstruments, USA), with a silk thread (**Figure 2.3A**). The bottom end of the bladder strips was tied to a metal rod, while another end was tied and connected to the force transducer using silk thread (**Figure 2.3B**). Tissues were allowed to equilibrate in the bathing medium for 30 minutes under a passive tension of 19.6 mN (2 g) for rat aortic rings, 9.8 mN (1 g) for tracheal rings and bladder strips (Loong et al., 2015). For porcine tissues, passive tension of 39.2 mN (4 g) and 19.6 mN (2 g) were applied on pulmonary artery and bronchiole, respectively (Rashid, Heer, Garle, et al., 2013). Changes in the muscle tension were recorded by the force transducer connected to a PowerLab data acquisition unit (PL26T04, ADInstruments, Australia) through LabChart v8.1.13 available on the laptop (EliteBook 8470p, Hewlett-Packard, USA). After 30 minutes, tissue viability was established by testing their response to 60 mM of KCl twice (Baik, Sohn, Ok, et al., 2011). The tissue was rinsed with Krebs solution and allowed 15 minutes for tension recovery. The average contraction induced by 60 mM KCl was used as a reference value (100%) in data analysis (detailed in **section 2.3.6**). After twice KCl exposure, the preparations were left to equilibrate for a minimum of 30 minutes to reach a stable basal tension before starting the experimental protocol.

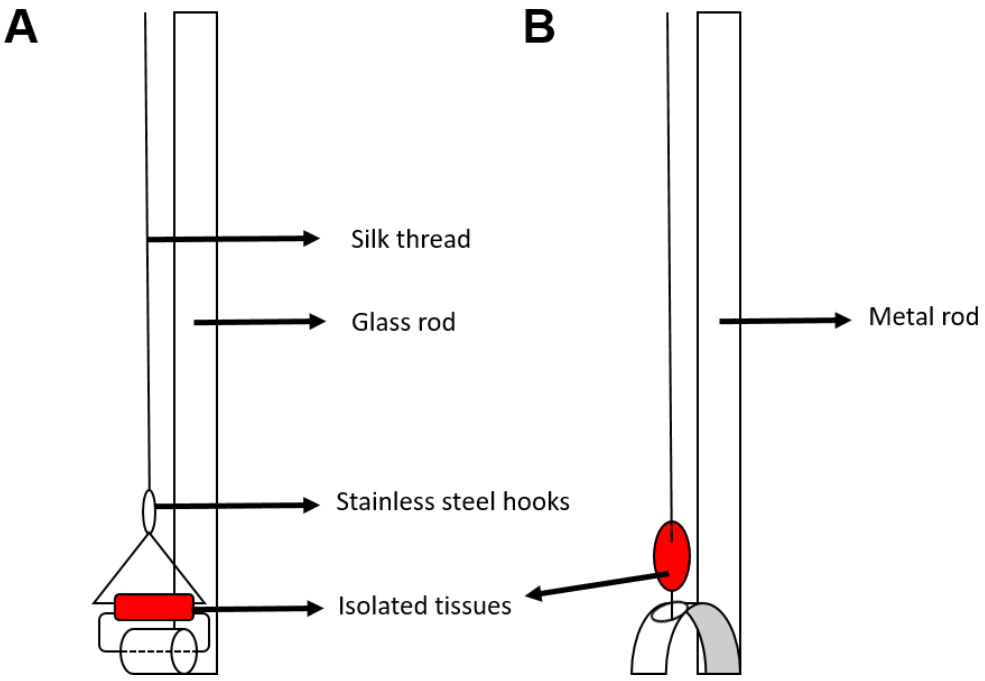


Figure 2.3 Illustration of tissues of interest mounted on holders. *The approach in (A) depicts the manner of mounting aortic, tracheal, and bronchiole rings to a glass rod, while (B) depicts the method of tying bladder strips to a metal rod.*

2.3.5 Isometric tension recordings

2.3.5.1 Effect of FK244 on rat isolated tissues at basal tension and raised muscle tone

To investigate the effect of FK244 on smooth muscle at basal tension (without the addition of contractile agonists), cumulative concentration-response curves (CRCs) to FK244 (0.1 nM to 100 μM) were constructed using rat isolated aorta, bladder and trachea. Each concentration was added either at an interval of 7 minutes or after the responses have plateaued if there was any change in tension.

In another series of experiments, the rat isolated aortic tissues were pre-contracted with a submaximal concentration of phenylephrine (100 nM), whereas bladder and tracheal tissues were pre-contracted with carbachol (1 μM). A submaximal concentration of phenylephrine or carbachol is the concentration where approximately 70% of KCl-induced contraction tone was achieved in respective tissues (EC_{70}). Once a stable tone was reached, cumulative CRCs to FK244 were constructed to study their effects on pre-contracted rat isolated aorta (0.1 nM to 100 μM), bladder (3 nM to 100 μM) and trachea (0.1 nM to 100 μM). A shorter range of concentrations was used in bladder tissue to reduce the effect of prolonged compound sensitisation on the spontaneous rhythmic myogenic contraction in the bladder tissue. Cumulative CRCs of vehicle control (DMSO) was carried out in an identical manner as FK244.

2.3.5.2 Effect of FK244 on porcine pulmonary artery and bronchiole pre-contracted with phenylephrine and carbachol

To compare the efficacy and potency of FK244 in other species than rat, porcine pulmonary artery and bronchiole were used. Porcine tissues were used because of their close resemblance to human anatomy and physiology (Swindle, Makin, Herron, et al., 2012). They were pre-contracted with phenylephrine (pulmonary artery) and carbachol (bronchiole) to submaximal tension. The pre-contractile agent was added cumulatively instead of at a fixed concentration due to the highly variable porcine tissue responsiveness. In contrast to laboratory rats which were raised under controlled conditions, variable environmental factors when raising domestic pigs and their genetic diversity affect porcine tissue responsiveness greatly. Concentrations of phenylephrine and carbachol used to pre-contract porcine pulmonary artery and bronchiole were approximately 20 μM to 396 μM and 4.7 nM to 100 nM, respectively. Following the pre-contraction, vehicle control or FK244 (0.1 nM to 100 μM) were added cumulatively

into the bath to construct CRCs. The experiments described in this subsection were carried out by Ms Yin-Ying Saw at the University of Nottingham UK.

2.3.5.3 Role of endothelium on FK244-induced relaxation

To prepare endothelium-denuded aortic rings, the endothelium of aortic rings was mechanically removed by gentle abrasion of the intimal surface of the rings using blunt tip forceps. The absence of endothelium was tested by pre-contracting the aortic tissues with submaximal concentration of phenylephrine (100 nM) before adding carbachol (1 µM), a muscarinic agonist. Carbachol was used instead of ACh due to its resistance to acetylcholinesterase degeneration. These submaximal concentrations of phenylephrine and carbachol were chosen based on the concentration where they induced response at approximately 70% of their maximum induced contraction (EC_{70}). Successful denudation was validated by less than 10% relaxation induced by carbachol (Panthiya, Pantan, Tocharus, et al., 2019).

After washing with Krebs solution and equilibrated for 15 minutes, endothelium-denuded aortic rings were pre-contracted phenylephrine (100 nM) again. Once a stable tone was reached, cumulative CRCs to FK244 (0.1 nM to 100 µM) were constructed. In control group, vehicle control (DMSO) was added into the bath in the same manner.

2.3.5.4 Role of NO in FK244-induced relaxation

The involvement of endothelium-derived NO was further verified in a separate experiment using L-NAME, an eNOS inhibitor. Aortic rings were pre-incubated with L-NAME (100 µM) (Arsyad & Dobson, 2016) for 30 minutes and pre-contracted with phenylephrine (100 nM). Then, cumulative CRCs to FK244 (0.1 nM to 100 µM) were constructed. In control groups, vehicle control (purified water) was used to pre-incubate the aortic rings and experiment was repeated in the same manner.

2.3.5.5 Role of cAMP and cGMP in FK244-induced relaxation

To investigate whether FK244-induced relaxation involved cyclic nucleotides, the aortic rings were pre-incubated with forskolin (10 nM) (S. -M Yu & Kuo, 1995), an AC activator, or ODQ (1 µM) (Badran, Baydoun, Samaha, et al., 2019), an sGC inhibitor, for 30 minutes. Subsequently, a single concentration of phenylephrine (100 nM – 3 µM) was added to contract the aortic rings. When a stable tone of phenylephrine was achieved, cumulative CRCs to FK244 (0.1 nM to 100 µM) were carried out. In

control group, vehicle control (DMSO) was used to pre-incubate the aortic rings and experiment was repeated in the same manner.

2.3.5.6 Role of α-, β- adrenoceptors in FK244-induced relaxation

To examine whether FK244 elicit vasorelaxation by inhibiting α- adrenoceptors or activating β-adrenoceptors, aortic rings were pre-incubated with prazosin (10 μM) (Skomedal, Aass, & Osnes, 1984), an α_1-adrenoceptor antagonist, rauwolscine (10 μM) (Ok, Bae, Shim, et al., 2012), an α_2-adrenoceptor antagonist or propranolol (3 μM) (Jiang, Xia, Wang, Song, & Bruce, 2005), a non-selective β-adrenoceptor antagonist. After a 30-minute incubation, KCl (60 mM) was used to pre-contract prazosin- and rauwolscine-treated aortic rings. For propranolol-treated aortic rings, a single concentration of phenylephrine (100 nM – 3 μM) was used for pre-contraction. When the response has stabilised, cumulative CRCs to FK244 (0.1 nM to 100 μM) were constructed. In control groups, vehicle control (methanol or purified water) was used to pre-incubate the aortic rings and experiment was repeated in the same manner.

2.3.5.7 Role of K^+ channels in FK244-induced relaxation

To determine whether FK244-induced relaxation involve K^+ channels, experiments were conducted by pre-incubating the aortic rings with 4-aminopyridine (4-AP, 1 mM), a voltage-gated K^+ (K_v) channel blocker; barium chloride ($BaCl_2$, 1 mM), an inwardly rectifying K^+ (K_{ir}) channel blocker, glibenclamide (10 μM), an K_{ATP} channel blocker; and tetraethylammonium chloride (TEA, 5 mM), a Ca^{2+}-activated K^+ (K_{Ca}) channel blocker, for 30 minutes (Panthiya et al., 2019; Wicha, Tocharus, Nakaew, et al., 2015). After the pre-contraction to a single concentration of phenylephrine (100 nM – 3 μM) has stabilised, construction of cumulative CRCs to FK244 (0.1 nM to 100 μM) were carried out. In control groups, vehicle control (DMSO or purified water) was used to pre-incubate the aortic rings and experiment was repeated in the same manner.

2.3.5.8 Effect of FK244 on aorta pre-contracted with different contractile agents

To compare the efficacy and potency of FK244 in the presence of contractile agonists of different mechanisms, the aortic rings were pre-contracted with either phenylephrine (100 nM), KCl (60 mM), or U46619 (300 nM). These concentrations were chosen as the concentration when the tissues achieved a submaximal response of 70 to 80% (EC_{70-80}) in respective cumulative CRCs. After the contraction has stabilised, cumulative CRCs to vehicle control (DMSO) or FK244 (3 nM to 300 μM) were constructed. Serotonin, a 5-hydroxytryptamine (5-HT) agonist, was not used in this experiment because a stable tone could not be established in aortic tissues.

2.3.5.9 Effect of FK244 on the contractile response induced by different contractile agents

Cumulative CRCs of phenylephrine (0.1 nM to 300 μM), KCl (10 μM to 300 mM), serotonin (0.1 nM to 300 μM), and U46619 (0.1 nM to 3 μM) were constructed after pre-incubation with vehicle control (DMSO) or FK244 (10 μM, 30 μM, 100 μM) for 30 minutes. These three concentrations were chosen based on FK244 cumulative CRCs in pre-contracted aortic rings (**Figure 2.8B**), where they achieved maximum tissue relaxation (EC_{90-100}) in the aortic tissues. It was hypothesised that FK244 could demonstrate a concentration-dependent inhibition on the contractile response of phenylephrine, KCl, serotonin and U46619.

2.3.5.10 Reversibility of FK244's inhibition against phenylephrine-induced contraction

This protocol set out to determine whether phenylephrine-induced contraction will recover after FK244 is removed by washing. Aortic rings were pre-treated either with vehicle control (DMSO) or FK244 (10 μM) for 30 minutes before the addition of a single concentration of phenylephrine (10 μM). Then, the aortic rings were thoroughly rinsed with Krebs solution and left for 30 minutes to return to a stable basal tone. Subsequently, the tissues were challenged with another addition of phenylephrine (10 μM).

2.3.5.11 Effect of Ca^{2+} channel blockers in rat isolated aorta pre-contracted with phenylephrine

To assess the efficacy and potency of known Ca^{2+} channel blockers in inducing vasorelaxation, aortic rings were pre-contracted with phenylephrine (100 nM) prior to performing cumulative CRCs to SOCC/non-selective TRPC inhibitors: 2-aminoethoxydiphenyl borate (2-APB), Pyr6, SKF-96365; TRPC-selective inhibitors: HC-070, Pyr3; and VGCC inhibitors: nifedipine and verapamil. The range of concentration used in constructing CRCs was from 0.1 nM to 100 μM, except for HC-070, only up to 30 μM due to solubility issue. Cumulative CRCs of FK244 obtained in **Figure 2.8B** were put together for further analysis.

2.3.5.12 Effect of Ca^{2+} channel blockers on phenylephrine-induced contraction

This protocol investigated the possible involvement of Ca^{2+} channel blockers in phenylephrine-induced vasocontraction signalling pathways. Aortic rings were pre-treated with Ca^{2+} channel blockers for 30 minutes prior to construction of cumulative CRCs to phenylephrine (0.1 nM to 300 μM). The Ca^{2+} channel blocker used for pre-incubation were either 2-APB (100 μM) (Bishara, Murphy, & Hill, 2002), nifedipine (10 μM) (Garcia, Pereira, Gutierrez, et al., 2016), Pyr3 (10 μM) (Kiyonaka, Kato, Nishida, et al., 2009), Pyr6 (10 μM) (Schleifer et al., 2012), SKF-96365 (10 μM) (Baik et al., 2011; Singh, Hildebrand, Garcia, et al., 2010; Zagranichnaya, Wu, & Villereal, 2005), or verapamil (10 μM) (Baik et al., 2011). The concentration used for incubation was based on the $EC_{70\text{-}90}$ from the CRCs in **section 2.4.12** and backed by literature. Vehicle (DMSO) was used as control to pre-incubate the aortic rings and experiment was repeated in the same manner.

2.3.5.13 Effect of FK244 on intracellular Ca^{2+}-induced vasoconstriction

To investigate the influence of FK244 on the contraction induced by intracellular Ca^{2+} stores, aortic rings were pre-incubated with FK244 (10 μM) for 30 minutes in Ca^{2+}-free Krebs containing 1 mM EGTA (Fransen, Van Hove, Leloup, et al., 2015). EGTA is routinely used to chelate free Ca^{2+} in the external environment. Subsequently, a single concentration of either phenylephrine (10 μM), KCl (60 mM) or U46619 (300 nM) was added into the bath for 1 hour to evoke intracellular Ca^{2+}-induced contraction. This series of experiments were repeated in Ca^{2+}-containing Krebs (normal Krebs).

2.3.5.14 Effect of FK244 on contractile responses to Ca^{2+} re-introduction

To investigate whether FK244 affects extracellular Ca^{2+}-induced contraction, aortic rings were pre-incubated with vehicle control (DMSO) or FK244 (10 μM, 30 μM, 100 μM) in Ca^{2+}-free Krebs solution for 30 minutes. After 30 minutes of pre-incubation, KCl (60 mM) was added to the aortic rings for 15 minutes to induce plasma membrane depolarisation. Then, $CaCl_2$ was cumulatively re-introduced to the bathing medium (1 μM to 3 mM).

The experiment was repeated by incubating the aortic rings with either 2-APB (100 μM), Pyr3 (10 μM), Pyr6 (10 μM), SKF-96365 (10 μM), nifedipine (10 μM) or verapamil (10 μM) to assess the efficacy of these Ca^{2+} channel blockers in mediating Ca^{2+}-induced contraction.

2.3.5.15 Effect of Ca^{2+} channel blockers on FK244-induced relaxation

Aortic rings were pre-incubated with a range of Ca^{2+} channel blockers for 30 minutes. Similar to **section 2.3.5.11**, the Ca^{2+} channel blocker used for pre-incubation in the aortic rings were SOCC/non-selective TRPC inhibitors: 2-APB (100 μM), Pyr6 (10 μM), SKF-96365 (10 μM); TRPC-selective inhibitors: Pyr3 (10 μM); and VGCC inhibitors: nifedipine (10 μM) and verapamil (10 μM). The concentration used for incubation was based on the EC_{70-90} from the CRCs in **section 2.4.12** and backed by literature. Following pre-contraction with a single concentration of phenylephrine (300 nM – 10 μM), CRCs to FK244 (0.1 nM to 100 μM) were carried out. The concentration of phenylephrine used to pre-contract the aortic tissues was determined by the EC_{70} of phenylephrine CRCs in the presence of respective Ca^{2+} channel blockers (**section 2.4.13**). In control groups, vehicle control (DMSO or purified water) was used to pre-incubate the aortic rings and experiment was repeated in the same manner.

2.3.6 Data analysis

Mean KCl-induced contraction (*y*) was obtained by averaging value 'a' and 'b' (**Figure 2.4**). The value was used in data analysis of some experiments (**Figure 2.7**, **Figure 2.13A**, **B**, **Figure 2.15C**, **Figure 2.16**, **Figure 2.17**, **Figure 2.19**, **Figure 2.20**, **Figure 2.21**). Tissues with an average contraction of less than 3.9 mM (0.4 g) were discarded and excluded from data analysis.

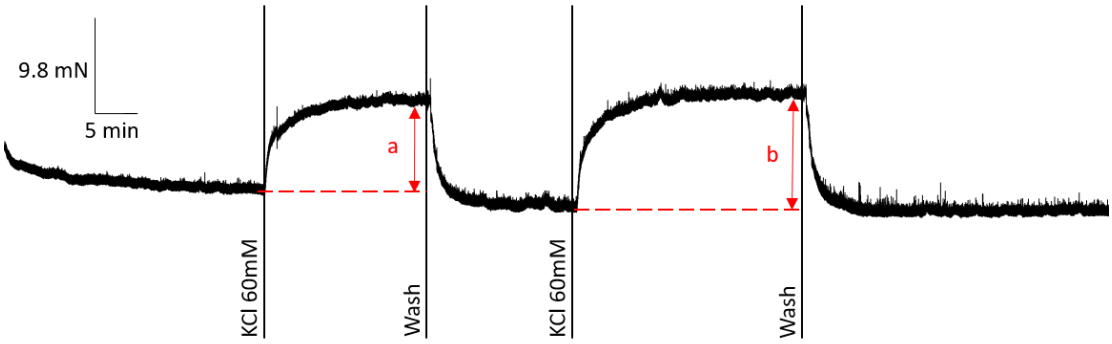


Figure 2.4 Illustration of a representative isometric tension trace recording showing that the tissue was challenged twice with KCl to test its viability. *The difference in magnitude was measured and used to calculate the average KCl-induced contraction.*

In **Figure 2.5A**, an example of a trace recording was shown to depict the analysis of tissue contraction, whereas **Figure 2.5B** shows a trace recording of a relaxation response. When measuring the tissue response, the percentage of tissue response was calculated using the formula below:

$$\frac{\textbf{Magnitude of tissue contraction or relaxation } (\boldsymbol{x})}{\textbf{Magnitude of contraction induced by precontractile agent } (\mathbf{y})} \times \mathbf{100}\%$$

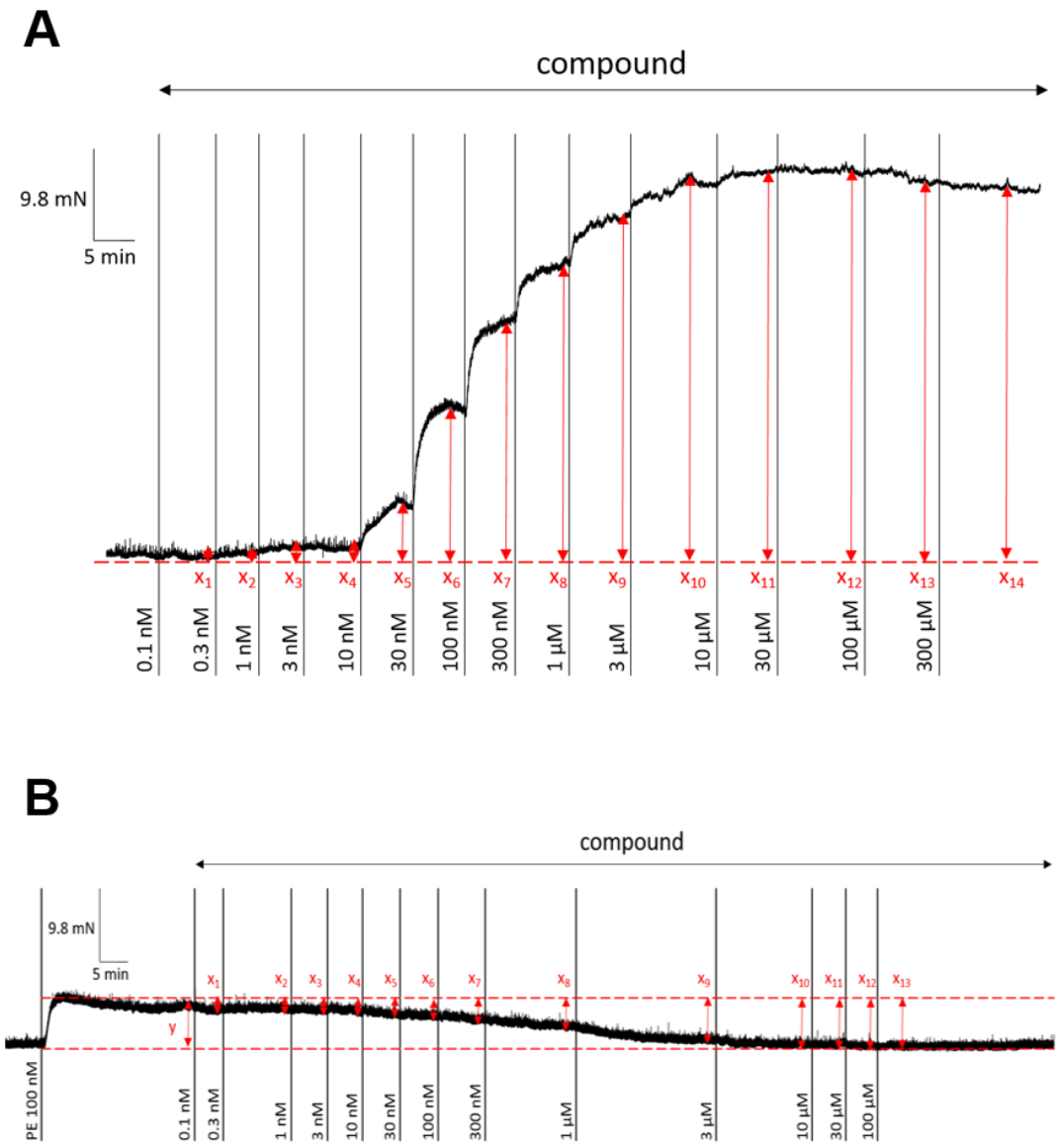


Figure 2.5 Illustration of a representative isometric tension trace recording showing the analysis of drug-induced (A) contraction and (B) relaxation in smooth muscle tissue.

Data were presented as mean ± standard error of mean (SEM), with n number refers to the number of separate animals used in each group. Percentage concentration-responses were presented in a non-linear regression curve using three parameters equation in GraphPad Prism (version 8.2.1 for Windows, GraphPad Software, La Jolla California USA), with Hill slope constrained to 1. E_{max} and EC_{50} were derived from the non-linear regression analysis of the obtained CRCs. Potency, represented by the pEC_{50} values, were calculated as the negative logarithm of EC_{50}. In GraphPad Prism, $logEC_{50}$ is computed as the midpoint of a sigmoid CRC plotted on a log scale as the x-axis. $logEC_{50}$ is closer to Gaussian distribution compared to EC_{50} values. Hence the potency is represented by pEC_{50} (also to remove the confusion of negative values).

In circumstances when the response has not plateaued and E_{max} cannot be calculated, E_{max} would be derived from the response generated at the highest concentration tested (**Figure 2.7**, **Figure 2.8C, D**, **Figure 2.9**, **Figure 2.13A, B**, **Figure 2.15C, D**, **Figure 2.16A, B**, **Figure 2.18A, B**, **Figure 2.21**). pEC_{50} of non-plateaued CRCs were not determined in this study as the plateaued response was not achieved. In cases where estimated pEC_{50} was calculated from a non-plateaued curve, it was for comparison and discussion purposes. It would be calculated from a normalised non-linear regression curve fit where the curve assumed the maximum tissue response as 100%. Estimated pEC_{50} is the concentration that produced 50% relaxation with maximum tissue response obtained in the experiment as 100%.

When Hill slope is constrained to 1, it assumed one-to-one binding between the ligand and receptor. This is recommended when the research sets to determine E_{max} and potency of a compound, without compromising the statistical power when data lie outside the curve fit (Wenner, Wilson, Davis, et al., 2011). It is also sensible to constrain Hill slope when there are limited data points with obvious plateau (Motulsky & Christopoulos, 2003). Fitting Hill slope equation may provide additional information about drug-ligand interaction at binding sites, however, pharmacokinetics and pharmacodynamics are not the focus of this study.

Statistical analysis was performed using unpaired Student's *t*-test to compare between control group and treatment group (**Figure 2.7**, **Figure 2.8B** – **D**, **Figure 2.9C**, **Figure 2.11**, **Figure 2.12**, **Figure 2.13**, **Figure 2.14C**, **Figure 2.15B** – **D**, **Figure 2.22**). One-way Analysis of Variance (ANOVA) followed by post hoc test was also used to compare the effects of three or more groups. Bonferroni's post hoc test was used when only specific pairs were compared in **Figure 2.9A**, **B**, **Figure 2.10E**, **Figure 2.18**. Dunnett's post hoc test was used to compare vehicle control/FK244 with all other treatment groups in **Figure 2.14A**, **B**, **D**, **Figure 2.16**, **Figure 2.19**, **Figure 2.21**. Tukey's post hoc test compares all possible combinations within groups in **Figure 2.8A**, **Figure 2.15A**. Two-way ANOVA with Bonferroni's post hoc test was used to analyse data in **Figure 2.17** and **Figure 2.20**. A single ANOVA was used to compare the data in **Figure 2.18** and **Figure 3.14**, **Figure 2.20** and **Figure 3.15**, **Figure 2.21** and **Figure 3.16**. Results with $p < 0.05$ were considered statistically significant. Individual significance was indicated in asterisk symbol in table, where '****' shows $p < 0.0001$, '***' shows $p < 0.001$, '**' shows $p < 0.01$ and '*' shows $p < 0.05$.

2.4 Results

2.4.1 Physicochemical properties of FK244 obey Lipinski's and Veber's rule analysis

Figure 2.6 shows the chemical structures of FK244, nifedipine, SKF-96365 and Pyr3. Their physicochemical parameters are presented in **Table 2.2**. Nifedipine, a DHP Ca^{2+} channel blocker targeting L-type VGCC, is the first-line treatment indicated for hypertension. SKF-96365, a TRPC channel blocker, and Pyr3, a TRPC3-selective blocker were included in the analysis as reference compounds. All the compounds followed Lipinski's and Veber's rule with no violation in the analysis. They possess favourable drug-like molecular properties, including less than 5 HBAs, less than 10 HBDs, logP value within 5, and less than 140 $Å^2$ of tPSA. FK244 has a MW of 251.37 Da, which is the lowest among all compounds. Corresponding to its small structure, it also has the least rotatable bonds and tPSA. On the other hand, SKF-96365 has 10 rotatable bonds, which is borderline violating the Veber's rule.

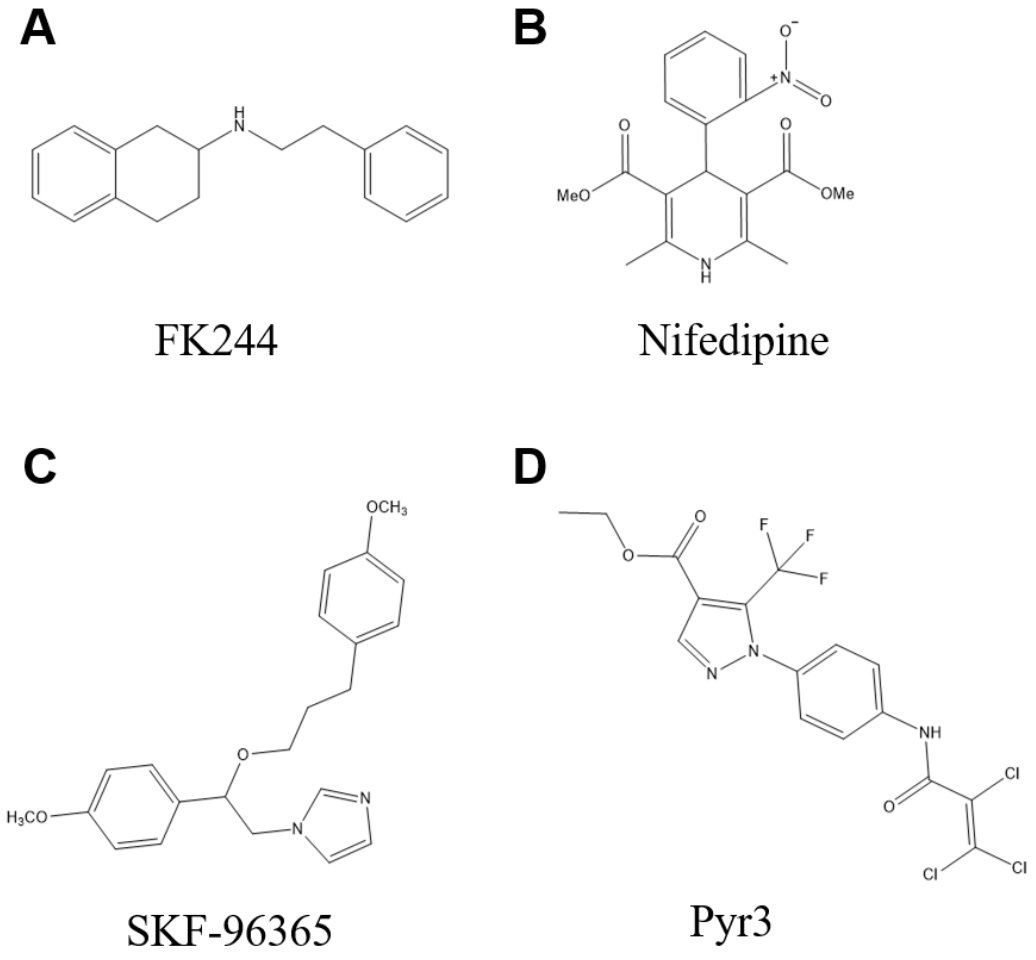


Figure 2.6 Chemical structures of (A) FK244, (B) nifedipine, (C) SKF-96365 and (D) Pyr3.

Table 2.2 Chemical structure and physicochemical analysis of FK244, nifedipine, SKF-96365 and Pyr3 using Lipinski's Rule of Five and Veber's rule.

Compound	FK244	Nifedipine	SKF-96365	Pyr3
Lipinski's Rule of Five				
Hydrogen bond donor (HBD ≤ 5)	1	1	0	1
Hydrogen bond acceptor (HBA ≤ 10)	1	5	2	5
Molecular weight (MW < 500 Da)	251.37	346.12	366.19	454.98
Partition coefficient (LogP ≤ 5)	3.97	3.31	3.94	4.59
Lipinski's rule violations	0	0	0	0
Veber's Rule				
Rotatable bond (≤10)	4	6	10	8
Topological polar surface area (tPSA ≤ 140 Å^2)	12.03	107.77	45.51	72.7
Veber's rule violations	0	0	0	0

2.4.2 FK244-induced smooth muscle relaxation was observed in rat isolated aorta, bladder and trachea at raised vascular tone but not at basal tone

At basal tone, FK244 did not evoke any response in the aortic rings compared to the vehicle control (E_{max}: vehicle control: 5.6 ± 1.5%; FK244: 5.5 ± 9.5%; p = 0.9878) (**Figure 2.7A**). Similarly, the presence of FK244 did not have any observable effect in the bladder smooth muscle (E_{max}: vehicle control: 2.7 ± 1.2%; FK244: -2.4 ± 2.3%; p = 0.0857) (**Figure 2.7B**). Moreover, trachea smooth muscle at basal tone did not respond to the presence of FK244 at any concentration. (E_{max}: vehicle control: 11.1 ± 7.0%; FK244: 1.3 ± 2.4%; p = 0.2203) (**Figure 2.7C**).

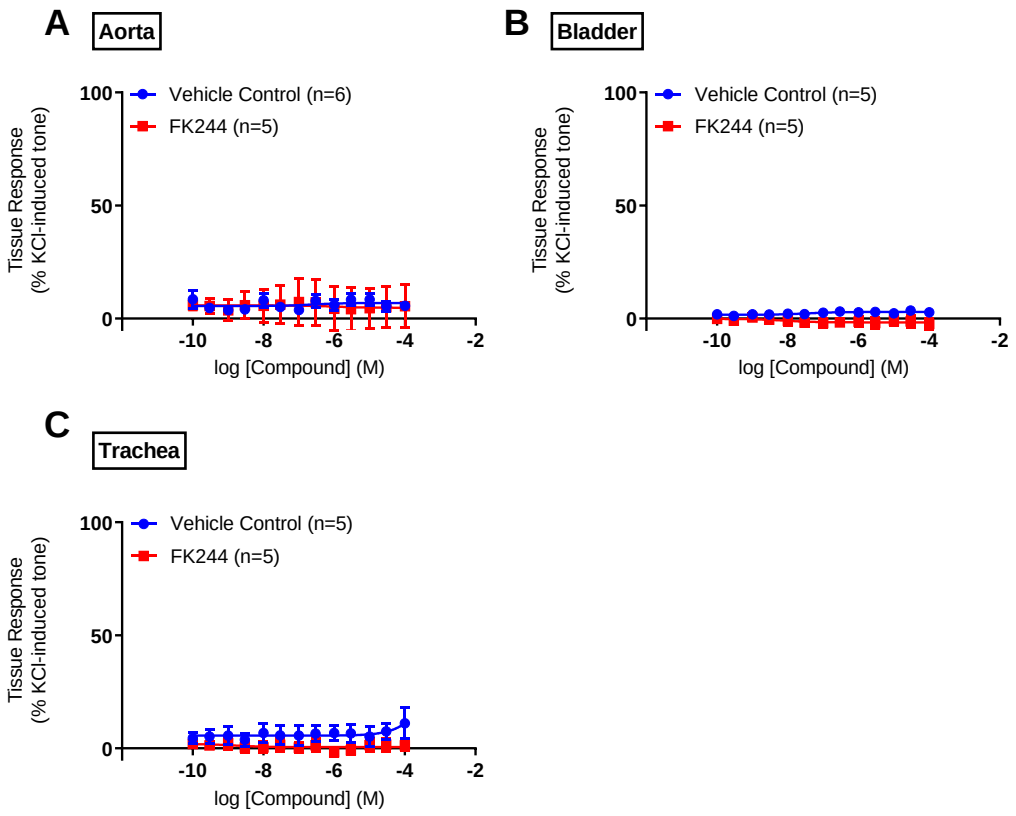


Figure 2.7 Effect of FK244 on rat isolated (A) aorta, (B) bladder and (C) trachea at the basal tone. *Tissue responses have been expressed as the percentage of KCl-induced tone. Data are shown as the mean ± SEM of 5 to 6 animals. Abbreviation: KCl, potassium chloride.*

Cumulative addition of FK244 elicited relaxation in different smooth muscle tissues (**Figure 2.8A**). FK244 induced significant relaxation in the aortic, bladder and tracheal smooth muscle tissues (**Figure 2.8B, C, D)**. The values of E_{max} and pEC_{50} of FK244 in these three smooth muscle tissue types are summarised in **Table 2.3**. Results have shown that FK244 significantly induced vasorelaxation in all tissues compared to

vehicle control (**Table 2.3**). E_{max} of FK244 in bladder (b) was significantly lower than in aorta (a) (b vs a; $p = 0.0003$) and trachea (t) (b vs t; $p = 0.0029$). In contrast, FK244 was equally efficacious in aorta and trachea ($p = 0.2876$). On the other hand, FK244 exhibited considerably higher potency (pEC_{50}) in aorta compared to bladder and trachea (a vs b; $p < 0.0001$; a vs t; $p < 0.0001$), but the potency of FK244 did not differ much in the bladder and trachea smooth muscle (b vs t; $p = 0.1648$). Comparison between aorta, bladder and trachea was made using one-way ANOVA followed by Tukey's post hoc test. pEC_{50} of FK244 in bladder and trachea was an estimation from non-plateaued CRCs, they were used in statistical analysis to compare with pEC_{50} of FK244 in aorta.

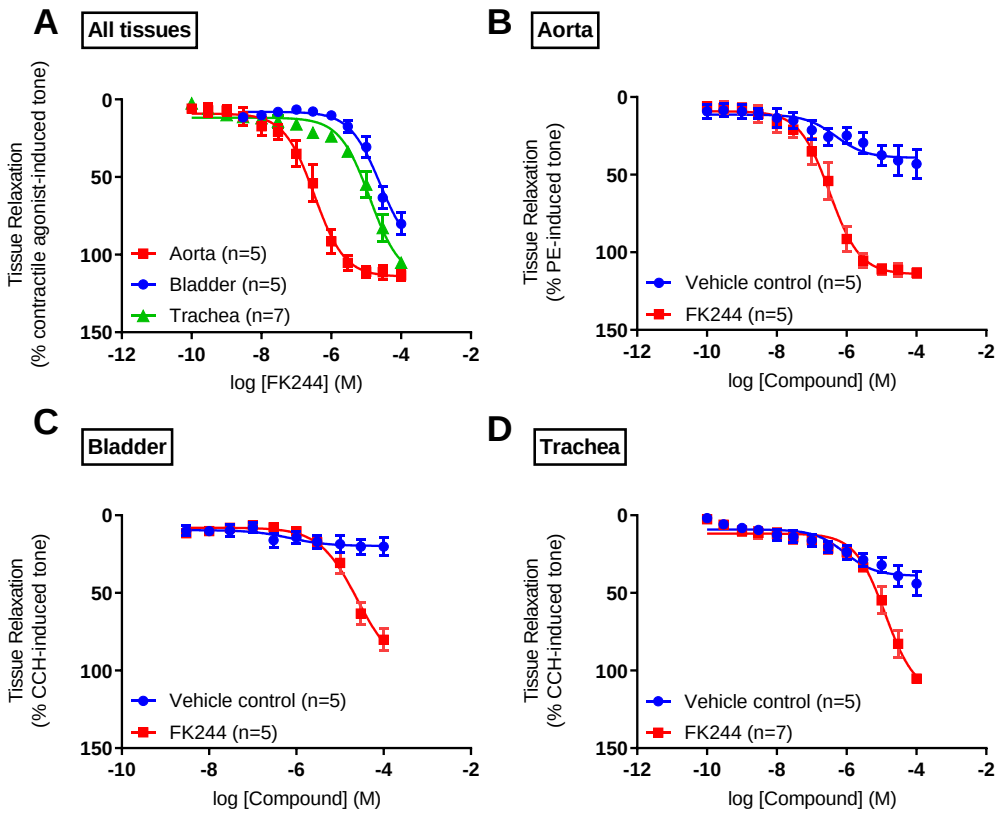


Figure 2.8 Effect of FK244 in (A) rat isolated aorta, bladder and trachea pre-contracted with phenylephrine or carbachol. *Relaxation effect of FK244 compared to vehicle control in (B) aortic rings, (C) bladder strips and (D) tracheal rings. Aortic tissue responses have been expressed as the percentage of phenylephrine-induced tone while bladder and tracheal tissues responses have been expressed as the percentage of carbachol-induced tone. Data are shown as the mean ± SEM of 5 to 7 animals. Abbreviations: CCH, carbachol; PE, phenylephrine.*

Table 2.3 Maximum tissue response (E_{max}) and potency (pEC_{50}) of FK244 in rat isolated aorta, bladder and trachea after being induced contraction with their respective contractile agents.

Tissue	Treatment	E_{max} (%)	pEC_{50}
Aorta	Vehicle control	43.1 ± 9.4	ND
	FK244	114.9 ± 3.4 **** ($p < 0.0001$)	6.49 ± 0.15
Bladder	Vehicle control	20.2 ± 5.9	ND
	FK244	80.1 ± 7.0 *** ($p = 0.0002$)	4.88 ± 0.10 †
Trachea	Vehicle control	44.1 ± 7.7	ND
	FK244	105.2 ± 2.8 **** ($p < 0.0001$)	5.24 ± 0.13 †

Unpaired Student's test was used to compare the E_{max} between vehicle and FK244 treatment in aorta, bladder and trachea tissues. Individual p-values were stated in the respective columns. Data are shown as mean ± SEM of 5 to 7 animals. Abbreviation: ND, not determined. †Estimated pEC_{50} was calculated based on maximum tissue response.

2.4.3 FK244 was equally efficacious but less potent in porcine tissues

FK244 exhibited overt vasorelaxation effects in rat isolated smooth muscles. Therefore, this experiment was conducted to compare its efficacy in porcine tissues. Even though both rat aorta and porcine pulmonary artery are blood vessels and were pre-contracted by the same agent – phenylephrine, FK244 exhibited significantly higher potency in rat aorta compared to porcine pulmonary artery albeit having similar magnitude of relaxation (E_{max}: rat aorta: 114.9 ± 3.4%; porcine pulmonary artery: 105.2 ± 6.4%; p = 0.6346; pEC_{50}: rat aorta: 6.49 ± 0.15; porcine pulmonary artery: 5.20 ± 0.08; $p < 0.0001$) (**Figure 2.9A**).

Furthermore, since FK244 showed full relaxation close to 100% in rat airway tissues, its efficacy and potency were compared using porcine airway tissues. Results revealed that FK244 was equally efficacious but significantly less potent in porcine bronchiole (E_{max}: rat trachea: 105.2 ± 2.8%; porcine bronchiole: 96.6 ± 4.7%; p = 0.9566; pEC_{50}: rat trachea: 5.24 ± 0.13; porcine bronchiole: 4.51 ± 0.07; p = 0.0015) (**Figure 2.9B**). Relaxation effect of FK244 was significant in porcine pulmonary artery (**Figure 2.9A**) and bronchiole (**Figure 2.9B**) compared to vehicle control (E_{max}: vehicle control: porcine pulmonary artery: 22.2 ± 6.5%, $p < 0.0001$; porcine bronchiole: 18.2 ± 15.7%; p = 0.0014). The statistical analysis was done using one-way ANOVA with Bonferroni's post-hoc test.

Interestingly, when comparing the potency of FK244 in vasculature and airways of both species, FK244 seemed to be more vascular-selective than airways-selective (porcine pulmonary artery vs porcine bronchiole: E_{max}: p = 0.6157; pEC_{50}: p = 0.0020, unpaired Student's *t*-test) (rat aorta vs rat trachea: refer to **section 2.4.2**) (**Figure 2.9C**).

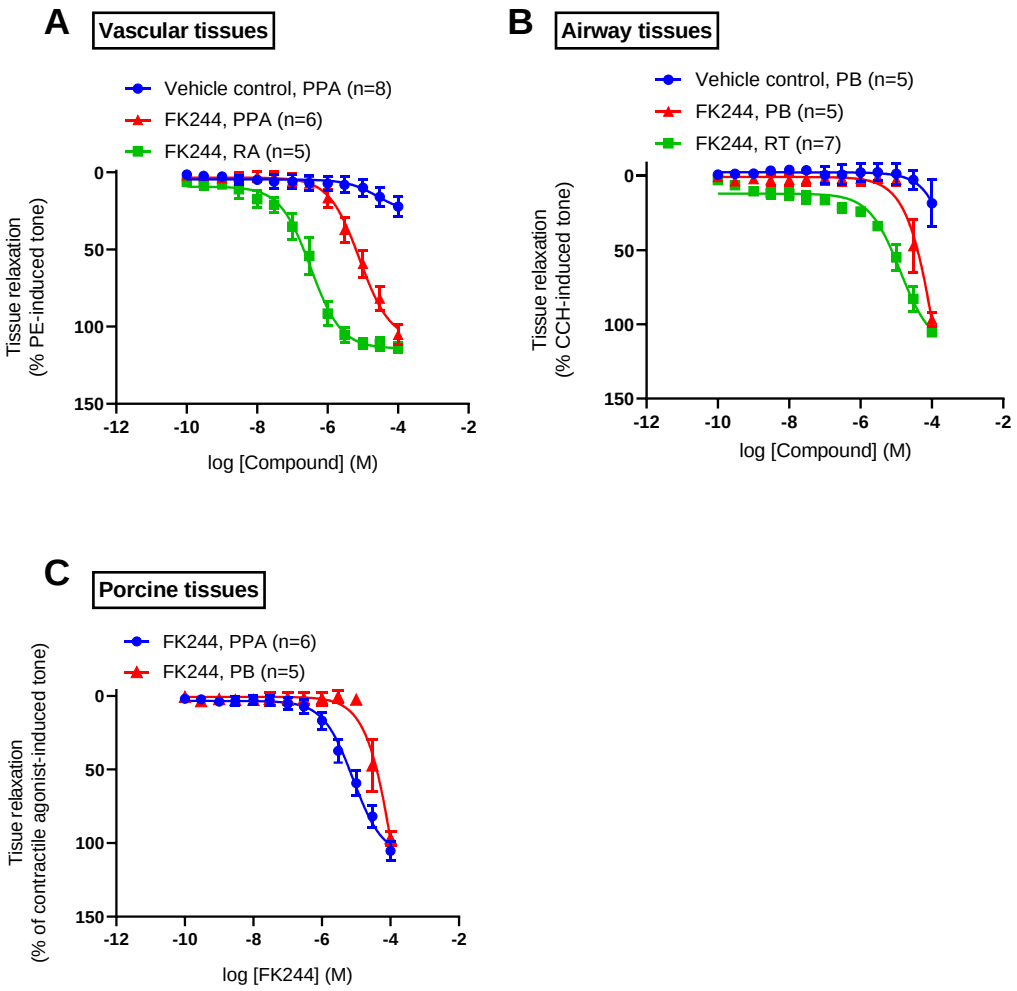
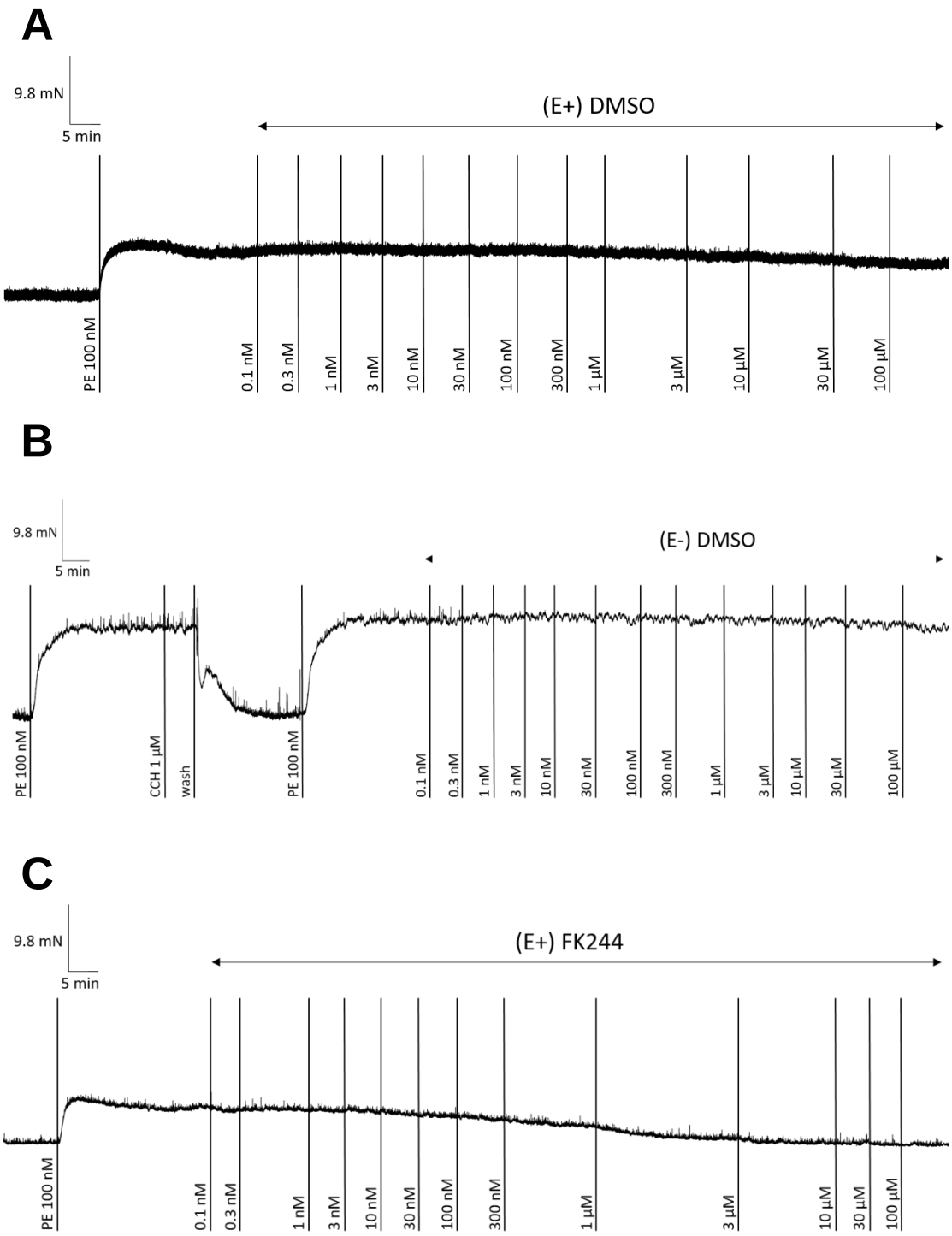


Figure 2.9 Effect of FK244 in (A) vascular tissues, (B) airway tissues and (C) porcine tissues. *Tissue responses have been expressed as the percentage of agonist-induced tone. Data are shown as the mean ± SEM of 5 to 8 animals. Abbreviations: CCH, carbachol; PE, phenylephrine, PB, porcine bronchiole; PPA, porcine pulmonary artery; RA, rat aorta; RT, rat trachea.*

2.4.4 FK244 induced similar relaxation profile in endothelium-intact (E+) and -denuded (E-) rat isolated aortae

Cumulative addition of FK244 has induced noticeable relaxation in rat aortae. Therefore, the involvement of endothelium in FK244-induced vasorelaxation was investigated. Aortic relaxation in **Figure 2.8B** was incorporated in the graph below (**Figure 2.10E**) to make a comparison between the effect of FK244 in endothelium-intact and -denuded rings. Significant vasorelaxation was achieved in the CRCs of FK244 compared to vehicle control in endothelium-intact ('Aorta' in **Table 2.3**) and -denuded aortic rings (E-, E_{max}: vehicle control: 26.7 ± 3.9%; FK244: 124.1 ± 3.4%; $p < 0.0001$). Endothelium has no significant impact on the relaxation profile of FK244 (E_{max}: E+: 114.9 ± 3.4%; E-: 124.1 ± 3.4%; $p = 0.7914$; pEC_{50}: E+: 6.49 ± 0.15; E-: 6.21 ± 0.08; $p > 0.9999$). Statistical analysis was done using one-way ANOVA with Bonferroni's post-hoc test. Representative tracing recordings of this experiment were depicted in **Figure 2.10A** – **D**.



(Figure continued on the next page)

Figure 2.10 Effect of FK244 in endothelium-intact (E+) and -denuded (E-) aortae. *Representative tracings of vehicle control CRCs in (A) E+ aorta and (B) E- aorta, as well as FK244 CRCs in (C) E+ aorta and (D) E- aorta. (E) Cumulative CRCs of vehicle control and FK244 in E+ and E- rat isolated aortae. Aortic tissue relaxation has been expressed as the percentage of phenylephrine-induced tone. Data are shown as the mean ± SEM of 5 to 6 animals. Abbreviation: PE, phenylephrine.*

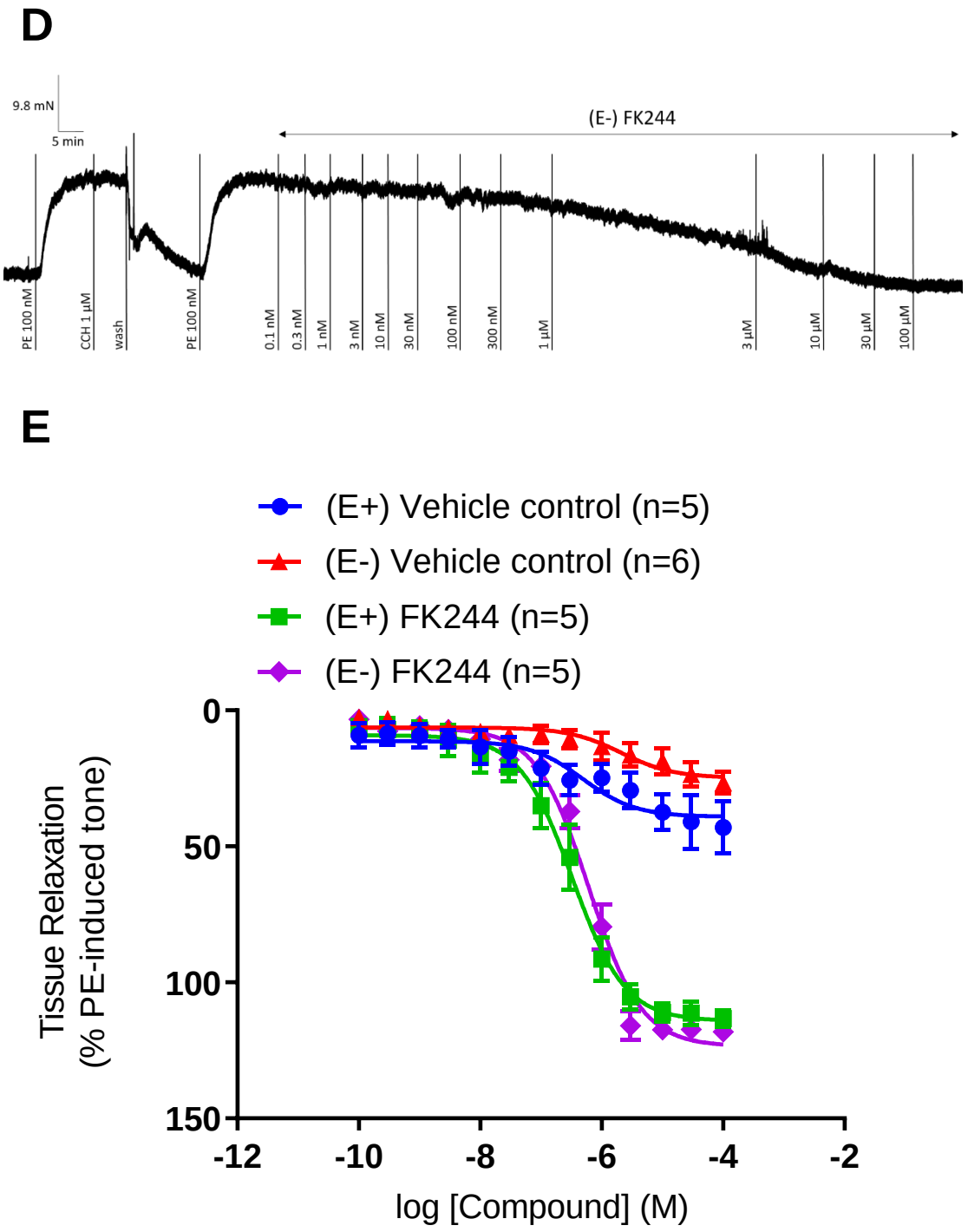


Figure 2.10 Effect of FK244 in endothelium-intact (E+) and -denuded (E-) aortae. *Representative tracings of vehicle control CRCs in (A) E+ aorta and (B) E- aorta, as well as FK244 CRCs in (C) E+ aorta and (D) E- aorta. (E) Cumulative CRCs of vehicle control and FK244 in E+ and E- rat isolated aortae. Aortic tissue relaxation has been expressed as the percentage of phenylephrine-induced tone. Data are shown as the mean ± SEM of 5 to 6 animals. Abbreviation: PE, phenylephrine. (continued)*

2.4.5 Presence of L-NAME did not reduce FK244-induced relaxation

L-NAME was used to exclude the participation of endothelium-derived NO in FK244-induced vasorelaxation. Incubation with L-NAME, an eNOS inhibitor, did not reduced FK244 relaxation in the aortic rings (E_{max}: vehicle control: 107.8 ± 4.4%; L-NAME: 113.4 ± 2.1%; p = 0.2765) (**Figure 2.11**). The potency of FK244 was similar in aortic tissues pre-exposed to vehicle control and L-NAME (pEC_{50}: vehicle control: 6.24 ± 0.23; L-NAME: 6.06 ± 0.08; p = 0.4770). Statistical analysis was done with unpaired Student's *t*-test.

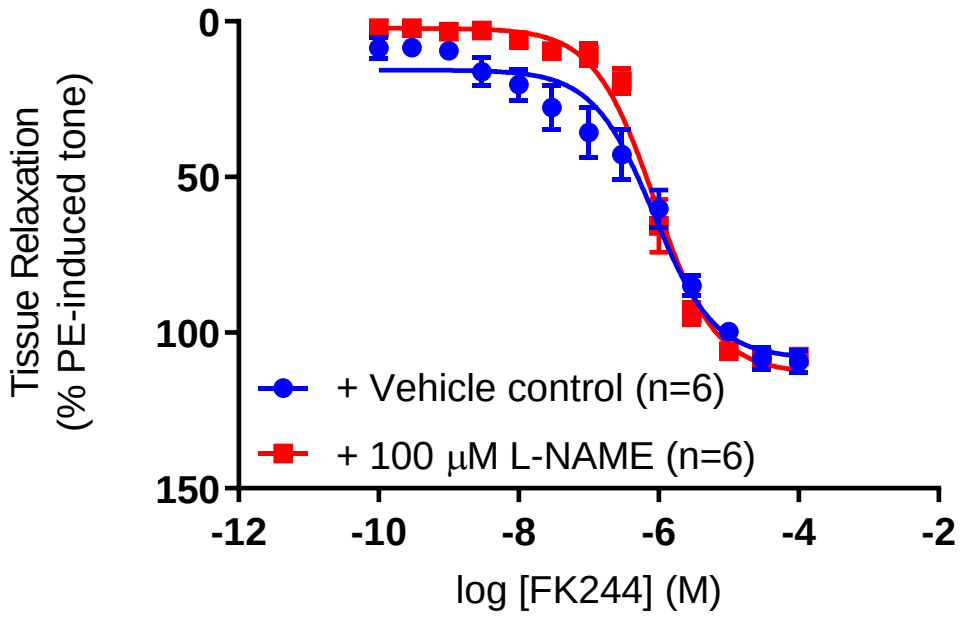


Figure 2.11 Effect of L-NAME with inhibition on eNOS on FK244-induced relaxation. *Tissue responses have been expressed as the percentage of phenylephrine-induced tone. Data are shown as the mean ± SEM of 6 animals. Abbreviations: L-NAME, N^G-nitro-L-arginine methyl ester; PE, phenylephrine.*

2.4.6 Forskolin and ODQ did not affect FK244-induced vasorelaxation

Forskolin, an AC activator did not potentiate FK244-induced vasorelaxation in terms of its efficacy and potency (E_{max}: vehicle control: 121.7 ± 4.1%; forskolin: 120.7 ± 5.3%; p = 0.8854; pEC_{50}: vehicle control: 5.58 ± 0.19; forskolin: 5.60 ± 0.11; p = 0.9099) (**Figure 2.12A**). Furthermore, ODQ-induced inhibition on sGC did not reduce the efficacy and potency of FK244 (E_{max}: vehicle control: 128.7 ± 6.7%; ODQ: 127.6 ± 2.9%; p = 0.8733; pEC_{50}: vehicle control: 6.00 ± 0.18; ODQ: 6.05 ± 0.17; p = 0.8243) (**Figure 2.12B**). Statistical analysis was done with unpaired Student's *t*-test.

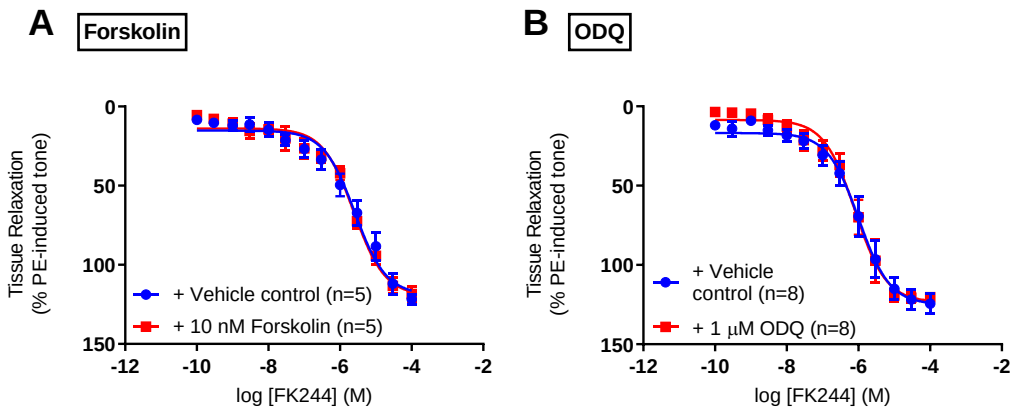


Figure 2.12 Effect of cyclic nucleotides in FK244-induced vasorelaxation. *Tissues were pre-treated with (A) forskolin and (B) ODQ for 30 minutes before FK244 CRCs were constructed. Tissue responses have been expressed as the percentage of phenylephrine-induced tone. Data are shown as the mean ± SEM of 5 to 8 animals. Abbreviation: PE, phenylephrine.*

2.4.7 FK244-induced relaxation was not influenced by α- and β-adrenoceptor antagonists

Prazosin, rauwolscine, and propranolol were used to investigate whether adrenoceptors are the therapeutic target of FK244. In **Figure 2.13A**, the magnitude of maximum tissue relaxation in the presence of α_1-adrenoceptor antagonist – prazosin, was similar to vehicle control (E_{max}: vehicle control: 114.1 ± 2.5%; prazosin: 108.9 ± 1.1%; $p = 0.0870$; estimated pEC_{50}: vehicle control: 5.40 ± 0.10; prazosin: 5.43 ± 0.11; $p = 0.8928$). Similarly, rauwolscine-induced α_2-adrenoceptor inhibition did not affect the maximum relaxation and potency of FK244 (E_{max}: vehicle control: 107.7 ± 5.4%; rauwolscine: 108.6 ± 2.1%; $p = 0.8894$; estimated pEC_{50}: vehicle control: 5.30 ± 0.11; rauwolscine: 5.03 ± 0.11; $p = 0.1170$) (**Figure 2.13B**). Meanwhile, aortic rings exposed to propranolol did not show any significance in FK244-induced relaxation (E_{max}: vehicle control: 107.8 ± 4.4%; propranolol: 107.7 ± 2.7%; $p = 0.9898$; pEC_{50}: vehicle control: 6.24 ± 0.23; propranolol: 6.08 ± 0.28; $p = 0.6778$) (**Figure 2.13C**). Statistical analysis was done with unpaired Student's *t*-test.

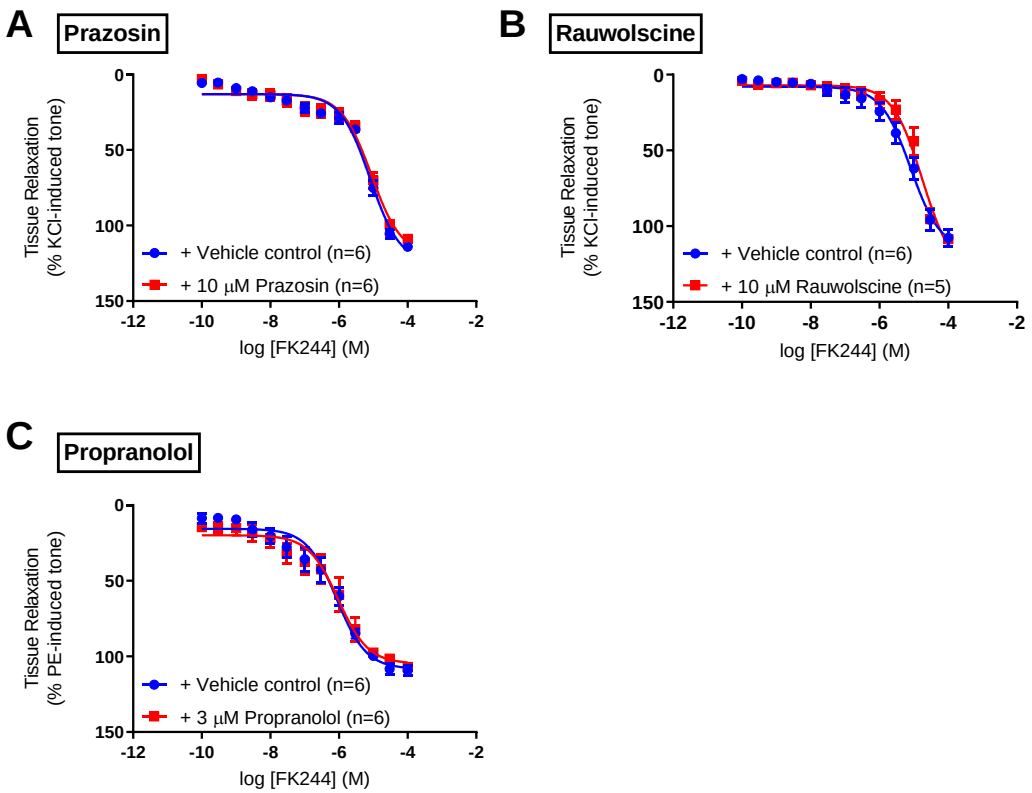


Figure 2.13 Effect of adrenoceptor-antagonists on FK244-induced vasorelaxation in rat aortae. *Aortic rings were pre-incubated with (A) prazosin, (B) rauwolscine, and (C) propranolol followed by CRCs to FK244. Tissue responses have been expressed as the percentage of KCl-induced tone for prazosin- and rauwolscine-treated aortic rings. For propranolol-treated aortic rings, tissue responses have been expressed as the percentage of phenylephrine-induced tone. Data are shown as the mean ± SEM of 5 to 6 animals. Abbreviations: KCl, potassium chloride; PE, phenylephrine.*

2.4.8 FK244-induced relaxation was not influenced by K^+ channel blockers

Aortic rings were pre-treated with 4-AP (K_v channel blocker), $BaCl_2$ (K_{ir} channel blocker), glibenclamide (K_{ATP} channel blocker) and TEA (K_{Ca} channel blocker) to determine whether the vascular relaxant effect of FK244 involves the opening of K^+ channels. Presence of 4-AP (**Figure 2.14A**), $BaCl_2$ (**Figure 2.14B**), glibenclamide (**Figure 2.14C**) and TEA (**Figure 2.14D**) had no influence on the efficacy and potency of FK244. The values of E_{max} and pEC_{50} of FK244-induced relaxation in the presence of vehicle controls and all four K^+ channel blockers are summarised in **Table 2.4**.

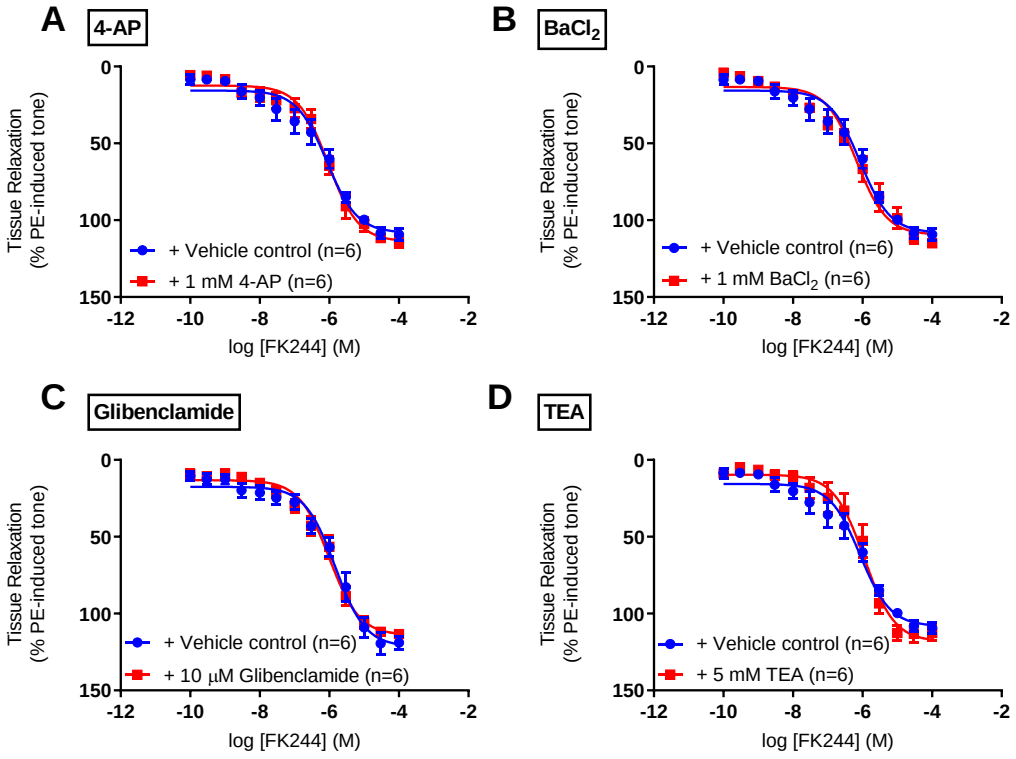


Figure 2.14 Effect of K^+ channel blockers on FK244-induced vasorelaxation. *Tissues were exposed to (A) 4-AP, (B) $BaCl_2$, (C) glibenclamide and (D) TEA, before performing cumulative CRCs to FK244 under raised vascular tone. Tissue responses have been expressed as the percentage of phenylephrine-induced tone. Data are shown as the mean ± SEM of 6 animals. Abbreviations: 4-AP, 4-aminopyridine, $BaCl_2$, barium chloride, PE, phenylephrine, TEA, tetraethylammonium chloride.*

Table 2.4 Maximum tissue response (E_{max}) and potency (pEC_{50}) of FK244-induced vasorelaxation with prior treatment of K^+ blockers in rat isolated aortic rings.

Treatment	E_{max} (%)	pEC_{50}
Vehicle control (H_2O)	107.8 ± 4.4	6.24 ± 0.23
+ 1 mM 4-AP	116.2 ± 3.2 (p = 0.2156)	5.97 ± 0.10 (p = 0.6137)
+ 1 mM $BaCl_2$	114.0 ± 2.4 (p = 0.4365)	6.09 ± 0.22 (p = 0.8925)
+ 5 mM TEA	117.7 ± 3.1 (p = 0.1203)	6.01 ± 0.17 (p = 0.7388)
Vehicle control (DMSO)	122.6 ± 5.2	5.80 ± 0.08
+ 10 µM Glibenclamide	115.3 ± 2.4 (p = 0.2257)	6.01 ± 0.15 (p = 0.2436)

One-way ANOVA followed by Dunnett's post hoc test was used to compare between 4-AP, $BaCl_2$, TEA, with vehicle control (H_2O). Unpaired Student's t-test was used to compare between glibenclamide with vehicle control (DMSO). Individual p-values were stated in the respective columns. Data are shown as mean ± SEM of 6 animals.

2.4.9 FK244 relaxation profile was not similar across different contractile agents

FK244 displayed distinct relaxation profile with different contractile agents (**Figure 2.15A**). FK244 exhibited similar maximum relaxation response in both KCl- and phenylephrine-induced tone (p = 0.4669; **Table 2.5**) but a slight reduced in response compared to U46619-induced contraction (p = 0.0495). There was no difference in the efficacy between U46619- and phenylephrine-induced contraction (p = 0.3444; **Figure 2.15A** and **Table 2.5**).

On the other hand, FK244 exhibited the highest potency in aortic rings pre-contracted with phenylephrine in comparison to KCl (p = 0.0001) and U46619 (p < 0.0001). The potency of FK244 was approximately 200-fold higher in relaxing phenylephrine-contracted aortae than U46619-contracted aortae. FK244 was also 20-time more potent in relaxing phenylephrine-induced contraction than KCl-induced contraction. FK244 was also more potent in relaxing aorta pre-contracted with KCl compared to U46619 (p = 0.0044). Statistical analysis mentioned was done with one-way ANOVA with Tukey's post hoc test by comparing the effects between all three groups.

Comparing the relaxation profiles across all three contractile agents, FK244 achieved E_{max} at approximately 10 µM in phenylephrine-contracted aortic tissues. On the contrary, FK244-induced relaxation did not plateau in KCl- or U46619-contracted tissues. Hence, the potency was estimated from maximum tissue relaxation. In addition, the relaxation only started to manifest at 10 µM in aortic rings pre-contracted with U46619.

Results also showed that FK244 effectively induced vasorelaxation in all groups compared to vehicle control (**Figure 2.15B** – **D**). The values of E_{max} and pEC_{50} for vehicle controls and FK244-induced vasorelaxation in the presence of phenylephrine, KCl and U46619 are summarised in **Table 2.5**.

.

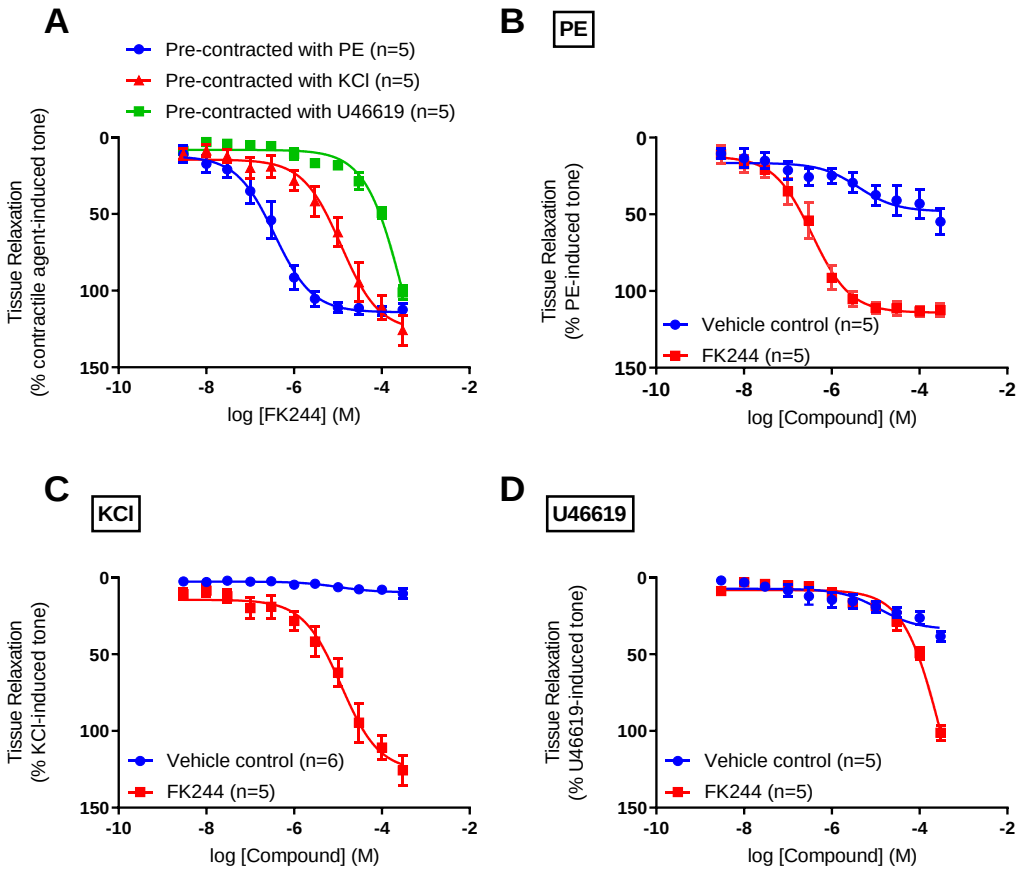


Figure 2.15 Effect of FK244 on aortic tissues pre-constricted with (A) phenylephrine, KCl and U46619. *Cumulative CRCs of FK244 with vehicle control when pre-contracted with (B) phenylephrine, (C) KCl and (D) U46619. Tissue responses were expressed as the percentage of contractile agent-induced contraction. Data are shown as the mean ± SEM of 5 to 6 animals. Abbreviations: KCl, potassium chloride; PE, phenylephrine.*

Table 2.5 Maximum tissue response (E_{max}) and potency (pEC_{50}) of vehicle control and FK244 derived from the respective CRCs with phenylephrine, KCl or U46619 as the pre-contractile agent.

Contractile agonist	Treatment	E_{max} (%)	pEC_{50}
Phenylephrine	Vehicle control	54.9 ± 8.5	ND
	FK244	114.5 ± 3.4 *** (p = 0.0002)	6.46 ± 0.14
KCl	Vehicle control	10.4 ± 3.3	ND
	FK244	125.6 ± 9.6 **** (p < 0.0001)	5.07 ± 0.24 †
U46619	Vehicle control	38.3 ± 3.3	ND
	FK244	101.2 ± 4.8 **** (p < 0.0001)	4.15 ± 0.06 †

Unpaired Student's t-test was used to compare phenylephrine, KCl or U46619 with their respective vehicle controls. Individual p-values were stated in the respective columns. Data are shown as mean ± SEM of 5 to 6 animals. Abbreviations: KCl, potassium chloride; ND, not determined. †Estimated pEC_{50} was calculated based on maximum tissue response.

2.4.10 FK244 attenuated the CRCs of phenylephrine, KCl and serotonin but not U46619

When the aortic rings were pre-treated with 10 μM of FK244, it shifted the CRC of phenylephrine to the right but preserved the E_{max} of phenylephrine-induced contraction. When the concentration of FK244 was raised to 30 μM and 100 μM, it suppressed the maximum contractile response of phenylephrine (**Figure 2.16A**). The potency of phenylephrine was not determined for pre-incubation of 30 μM and 100 μM FK244 because the tissue contraction has not plateaued.

Aortic rings incubated with FK244 at all concentration significantly attenuated the E_{max} of KCl (**Figure 2.16B**). The potency was not determined as the maximum contraction has not plateaued in all groups.

Results also revealed that 10 μM of FK244 did not attenuate serotonin-induced contraction and its potency in aortic tissues (**Figure 2.16C**). When the concentration of FK244 used for pre-incubation was raised to 30 μM and 100 μM, the overall trend was that it attenuated the maximum contractile response of serotonin-induced contraction compared to vehicle control. The potency of serotonin was not altered with 30 μM of FK244 but reduced slightly with 100 μM of FK244.

Both the E_{max} and pEC_{50} of U46619 was not affected by pre-incubation with FK244 at all concentrations tested (**Figure 2.16D**).

~1 to 3-fold shift in potency with minor significance was observed in serotonin or U46619-induced contraction in the presence of FK244 of various concentration. However, the decrease in potency was remarkably high in phenylephrine-induced contraction, where 10 μM of FK244 has reduced the potency of phenylephrine about 123-fold. The E_{max} and pEC_{50} values of contractile agonists-induced contraction are summarised in **Table 2.6**.

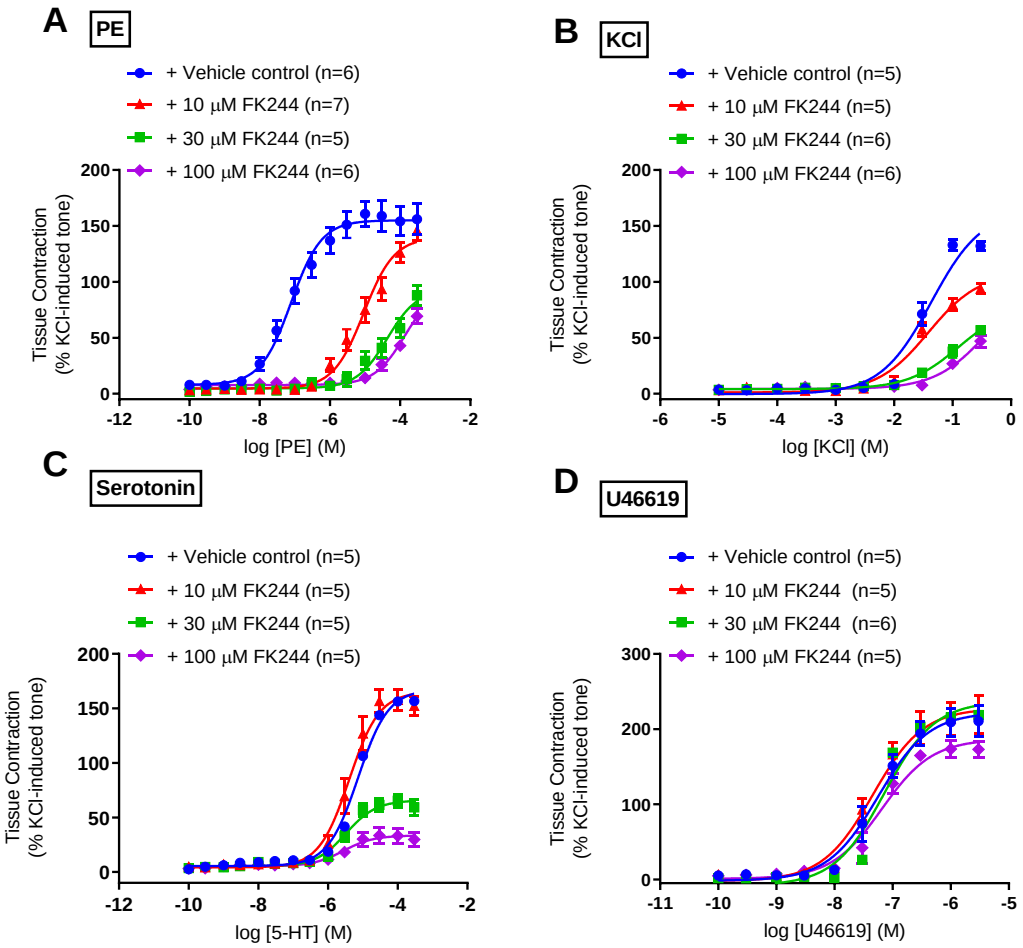


Figure 2.16 Effect of FK244 treatment in the aortic rings on the vascular contraction elicited by the contractile agents. *Cumulative CRCs to (A) phenylephrine, (B) KCl, (C) serotonin and (D) U46619 was demonstrated in the presence of FK244. Tissue responses were expressed as the percentage of KCl-induced contraction. Data are shown as the mean ± SEM of 5 to 7 animals. Abbreviations: KCl, potassium chloride; PE, phenylephrine.*

Table 2.6 Maximum tissue response (E_{max}) and potency (pEC_{50}) of phenylephrine, KCl, serotonin and U46619 in the presence of FK244 (10 µM, 30 µM, 100 µM) and their respective vehicle controls.

Treatment	Phenylephrine		KCl		Serotonin		U46619	
	E_{max} (%)	pEC_{50}	E_{max} (%)	pEC_{50}	E_{max} (%)	pEC_{50}	E_{max} (%)	pEC_{50}
Vehicle control	155.4 ± 13.0	7.09 ± 0.01	132.1 ± 4.4	ND [#]	170.3 ± 11.7	5.10 ± 0.15	226.2 ± 22.6	7.26 ± 0.13
FK244 + 10 µM	145.9 ± 9.4 (p = 0.8082)	5.00 ± 0.13 **** (p < 0.0001)	93.8 ± 4.5 **** (p < 0.0001)	ND [#]	166.9 ± 9.0 (p =0.9860)	5.38 ± 0.13 (p = 0.1852)	230.3 ± 25.5 (p = 0.9987)	7.34 ± 0.10 (p = 0.8941)
+ 30 µM	87.9 ± 8.6 *** (p = 0.0003)	ND [#]	56.8 ± 2.3 **** (p < 0.0001)	ND [#]	66.0 ± 6.8 **** (p < 0.0001)	5.48 ± 0.06 (p = 0.0579)	238.4 ± 28.1 (p = 0.9652)	7.12 ± 0.05 (p = 0.6674)
+ 100 µM	69.2 ± 6.7 **** (p < 0.0001)	ND [#]	47.0 ± 5.5 **** (p < 0.0001)	ND [#]	33.6 ± 7.0 **** (p < 0.0001)	5.52 ± 0.05 * (p = 0.0331)	189.1 ± 12.1 (p = 0.5742)	7.20 ± 0.14 (p = 0.9735)

One-way ANOVA followed by Dunnett's post hoc test was used to compare FK244 at each concentration to the vehicle control in their respective contractile agent groups. Individual p-values were stated in the respective columns. Data are shown as the mean ± SEM of 5 to 7 animals. Abbreviation: ND, not determined. [#]pEC_{50} was not determined as the maximum contraction was not achieved.

2.4.11 Contraction to phenylephrine recovered after FK244-treated tissues were washed

It was demonstrated in the previous experiment that FK244 inhibited phenylephrine-induced contraction. This protocol examined the reversibility of the action of FK244 on the inhibition of phenylephrine-induced contraction. When the aortic rings were pre-incubated with 10 µM of FK244, the contractile response to the first addition of 10 µM phenylephrine was significantly diminished (E_{max}: Vehicle control: 139.0 ± 12.1%; FK244: 76.1 ± 7.9%; p = 0.0006) (**Figure 2.17**). Subsequently, the aortic tissues were thoroughly rinsed with Krebs solution to remove any residual vehicle or FK244 in the bath solutions. When the tissues were added with phenylephrine the second time, the contraction to phenylephrine has recovered and was similar to the response achieved in vehicle control (E_{max}: Vehicle control: 110.1 ± 10.0%; FK244: 85.1 ± 10.2%; p = 0.1958) (**Figure 2.17**). Moreover, the magnitude of contraction to second phenylephrine in FK244-treated tissues seemed higher than the first addition when FK244 was present in the bath solution (FK244 first vs second phenylephrine addition: 76.1 ± 7.9% vs 85.1 ± 10.2%).

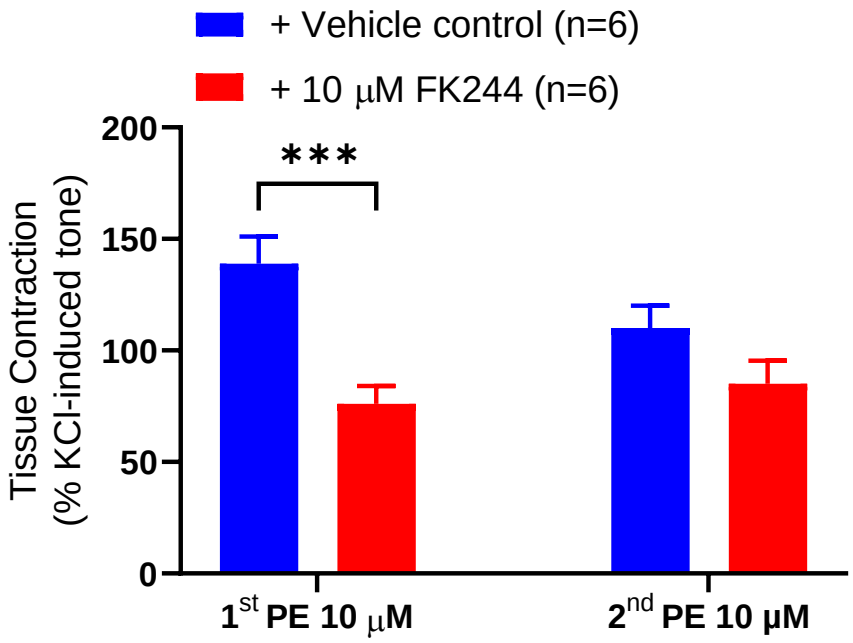


Figure 2.17 Reversibility of FK244 shown in phenylephrine-induced contraction. *Tissue responses were expressed as the percentage of KCl-induced contraction. Data are shown as the mean ± SEM of 6 animals. Two-way ANOVA followed by Bonferroni's post hoc test was used to compare FK244 to vehicle control at the first and second addition of phenylephrine. Abbreviations: KCl, potassium chloride, PE, phenylephrine.*

2.4.12 FK244 exhibited similar vasorelaxant properties as verapamil

A comparison was made between the vasorelaxation effect of FK244 and a range of Ca^{2+} channel blockers with different mechanism of actions (**Figure 2.18**). For the ease of visualisation, CRCs of FK244 and other Ca^{2+} channel blockers were categorised in different panels according to their putative mechanism of action. This arrangement does not affect the statistical analysis, where comparison was made altogether.

FK244 achieved the highest relaxation effect among all compounds. E_{max} of FK244 was significantly higher than the rest of the Ca^{2+} channel blockers that target more selectively towards TRPC channels and SOCC, namely 2-APB, SKF-96395 (**Figure 2.18A**), and Pyr3 (**Figure 2.18B**). On the contrary, E_{max} of FK244 was similar to verapamil, a non-DHP VGCC blocker and nifedipine, a DHP L-type VGCC blocker (**Figure 2.18C**). Its vasorelaxation effect was also comparable to Pyr6 (**Figure 2.18A**), a SOCC mediator, and HC-070 (**Figure 2.18B**), a putative TRPC4/5 channels blocker.

E_{max} of each Ca^{2+} channel blocker was expressed relative to the corresponding E_{max} of FK244 and presented as the relative E_{max}. The relaxation magnitude of FK244 (see relative E_{max} in **Table 2.7**) was higher than all the Ca^{2+} channel blockers, as the relative E_{max} of all Ca^{2+} channel blockers was less than 1. The difference in E_{max} was the most prominent between FK244 and Pyr3 (-43.5%), followed by SKF-96395 (-27.7%), 2-APB (-26.5%), HC-070 (-24.5%), and finally Pyr6 (-23.6%).

FK244 also demonstrated its potential as a Ca^{2+} channel blocker by possessing potency within the micromolar range as to all the Ca^{2+} channel blockers tested (**Table 2.7**). Evidently, nifedipine was the most potent compound among these Ca^{2+} channel blockers, with a potency ~19 fold higher than FK244. The values for E_{max} and pEC_{50} for all compounds are summarised in **Table 2.7**.

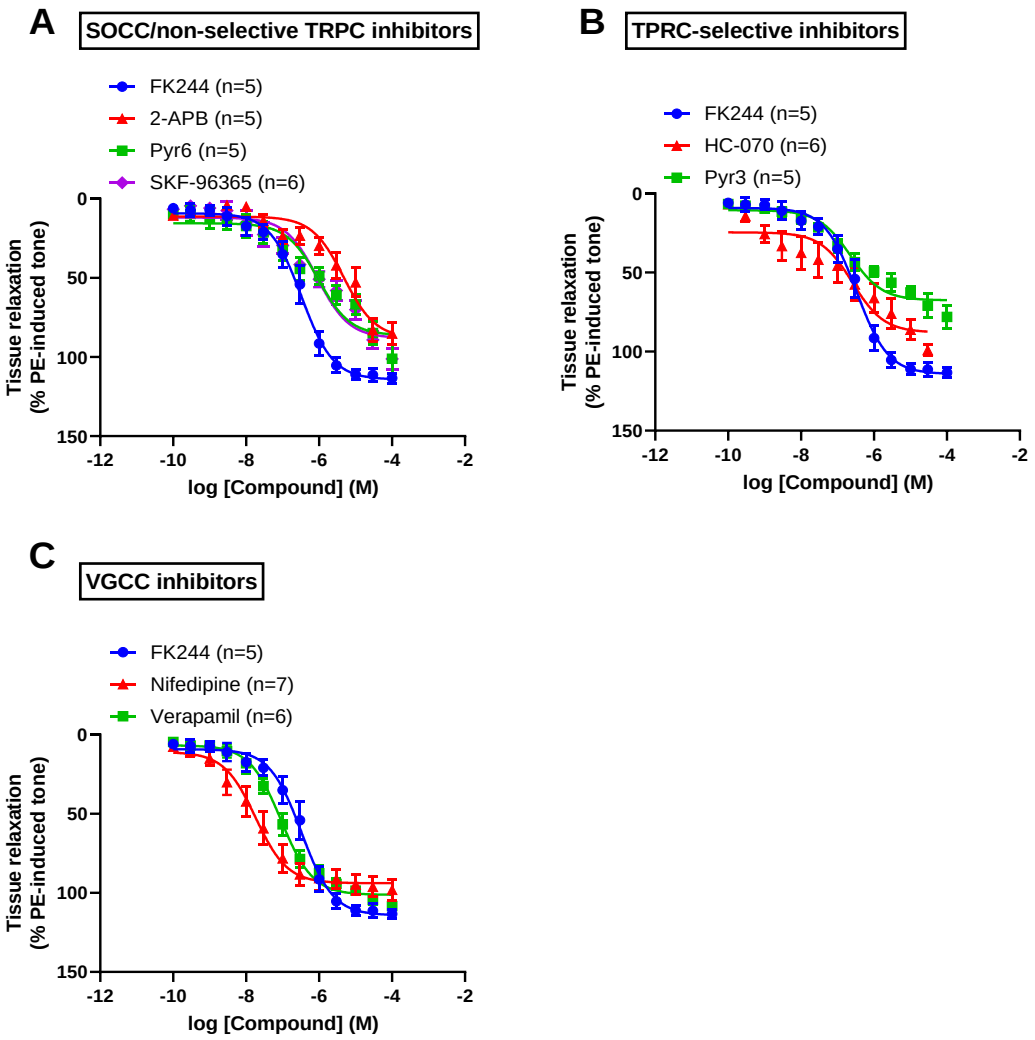


Figure 2.18 Vasorelaxation effect of FK244 and Ca^{2+} channel blockers. *Cumulative CRCs was compared between FK244 and (A) SOCC/non-selective TRPC inhibitors (2-APB, Pyr6, SKF-96365), (B) TRPC-selective inhibitors (HC-070, Pyr3), and (C) VGCC inhibitors (nifedipine, verapamil). Tissue relaxations were expressed as the percentage of phenylephrine-induced contraction. Data are shown as the mean ± SEM of 5 to 7 animals. Abbreviations: 2-APB, 2-aminoethoxydiphenyl borate, PE, phenylephrine; SOCC, store-operated Ca^{2+} channel; TRPC, transient receptor potential canonical; VGCC, voltage-gated Ca^{2+} channel.*

Table 2.7 Maximum tissue response (E_{max}) and potency (pEC_{50}) of FK244 and known Ca^{2+} channel blockers in rat isolated aortic rings.

Treatment	E_{max} (%)	Relative E_{max}	pEC_{50}
FK244	114.9 ± 3.4	1	6.49 ± 0.15
2-APB	88.4 ± 5.8 * (p = 0.0387)	0.77	5.42 ± 0.27 † (p = 0.5246)
HC-070	90.5 ± 1.9 (p = 0.0527)	0.79	6.88 ± 0.54 † (p > 0.9999)
Nifedipine	94.7 ± 6.0 (p = 0.1734)	0.82	7.77 ± 0.21 (p = 0.1206)
Pyr3	71.4 ± 6.3 **** (p < 0.0001)	0.62	6.50 ± 0.28 † (p > 0.9999)
Pyr6	91.3 ± 8.1 (p = 0.0994)	0.79	5.97 ± 0.33 † (p > 0.9999)
SKF-96365	87.2 ± 6.8 * (p = 0.0166)	0.76	6.41 ± 0.46 † (p > 0.9999)
Verapamil	101.8 ± 2.2 (p > 0.9999)	0.89	7.03 ± 0.10 (p > 0.9999)

One-way ANOVA followed by Bonferroni's post hoc test was used to compare the vasorelaxation effect of all the Ca^{2+} channel blockers to FK244. Individual p-values were stated in the respective columns. Data are shown as the mean ± SEM of 5 to 7 animals. †Estimated pEC_{50} was calculated based on maximum tissue response.

2.4.13 Ca^{2+} channel blockers of different mechanism of actions showed divergent responses in phenylephrine-induced contraction

Phenylephrine-induced contraction was performed in the presence of Ca^{2+} channel blockers to investigate the Ca^{2+} channels involved in the aortic contraction. For the ease of visualisation, CRCs of vehicle control and Ca^{2+} channel blockers were categorised in different panels according to their putative mechanism of action. This arrangement does not affect the statistical analysis, as the comparison was made altogether.

By comparing to vehicle control, the contractile effect of phenylephrine in the vascular tissue dropped significantly following pre-treatment of SOCC/non-selective TRPC inhibitors – 2-APB, SKF-96365 (**Figure 2.19A**) and VGCC inhibitors – nifedipine, verapamil (**Figure 2.19C**). Unlike other Ca^{2+} channel blockers, Pyr3, a TRPC3-selective inhibitor (**Figure 2.19B**) and Pyr6, a SOCC inhibitor (**Figure 2.19A**), did not influence the tissue contractility to phenylephrine at 10 µM.

At 100 µM, 2-APB appeared to have similar suppression effect on phenylephrine-induced vasoconstriction compared to 10-fold less nifedipine and SKF-96365 at 10 µM (**Table 2.8**). The potency of phenylephrine was not affected in the presence of all Ca^{2+} channel blockers tested (**Table 2.8**). The values for E_{max} and pEC_{50} for phenylephrine after incubation with Ca^{2+} channel blockers are summarised in **Table 2.8**.

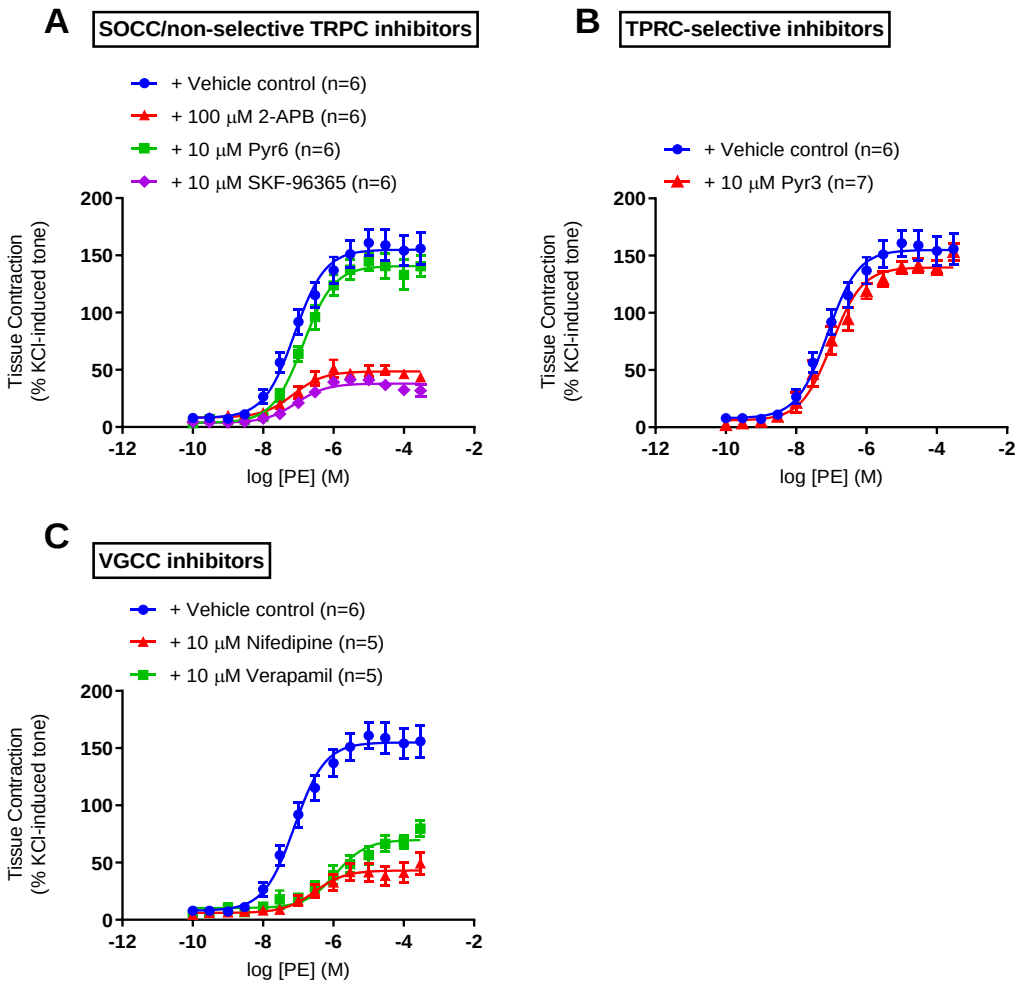


Figure 2.19 Effect of Ca^{2+} channel blockers on phenylephrine-induced contraction in the vasculature. *The Ca^{2+} channel blockers used were (A) SOCC/non-selective TRPC inhibitors (2-APB, Pyr6, SKF-96365), (B) TRPC- selective inhibitors (Pyr3), and (C) VGCC inhibitors (nifedipine, verapamil). Tissue responses were expressed as the percentage of KCl-induced contraction. Data are shown as the mean ± SEM of 5 to 7 animals. Abbreviations: 2-APB, 2-aminoethoxydiphenyl borate; KCl, potassium chloride; PE, phenylephrine; SOCC, store-operated Ca^{2+} channel; TRPC, transient receptor potential canonical; VGCC, voltage-gated Ca^{2+} channel.*

Table 2.8 Maximum tissue response (E_{max}) and potency (pEC_{50}) of phenylephrine following pre-exposure of known Ca^{2+} channel blockers in aortic tissues.

Treatment	E_{max} (%)	pEC_{50}
Vehicle control	155.4 ± 12.0	7.09 ± 0.10
+ 100 µM 2-APB	48.7 ± 3.9 **** (p < 0.0001)	7.10 ± 0.15 (p > 0.9999)
+ 10 µM Nifedipine	44.2 ± 8.2 **** (p < 0.0001)	6.43 ± 0.27 (p = 0.1538)
+ 10 µM Pyr3	141.3 ± 4.8 (p = 0.5642)	6.99 ± 0.19 (p = 0.9980)
+ 10 µM Pyr6	141.3 ± 9.1 (p = 0.5965)	6.84 ± 0.07 (p = 0.8864)
+ 10 µM SKF-96365	38.5 ± 2.5 **** (p < 0.0001)	7.01 ± 0.15 (p = 0.9996)
+ 10 µM Verapamil	66.2 ± 8.9 **** (p < 0.0001)	6.60 ± 0.44 (p = 0.4002)

One-way ANOVA followed by Dunnett's post hoc test, comparing all treatment groups to vehicle control. Individual p-values were stated in the respective columns. Data are shown as the mean ± SEM of 5 to 7 animals.

2.4.14 Pre-incubation with FK244 did not affect intracellular-induced contraction mediated by different contractile agents

Aortic rings treated with FK244 (10 μM) were either immersed in Ca^{2+}-free Krebs or Ca^{2+}-containing Krebs (normal Krebs) solution to examine its effect on intracellular Ca^{2+} release upon the addition of different contractile agents. In **Figure 2.20A**, aortic rings pre-incubated with FK244 in normal Krebs showed significant suppression in phenylephrine-induced contraction compared to those pre-incubated with vehicle control. Without external Ca^{2+}, phenylephrine evoked a feeble contraction in vehicle-treated aortic rings as a direct effect of the mobilisation of store intracellular Ca^{2+}. Similar observations were noted in FK244-treated tissues (**Figure 2.20A** and **Table 2.9**). It was observed that this tone of contraction dropped over 1 hour in both treatments - vehicle control and FK244 (**Figure 2.20A**).

By comparing to vehicle control, FK244 consistently suppressed the contractile response in normal Krebs over the course of an hour. KCl managed to induce a marginal contraction in the absence of Ca^{2+} in both treatments (**Figure 2.20B** and **Table 2.9**).

Tissue contraction to U46619 treated with FK244 in both normal and Ca^{2+}-free Krebs was not significantly different from vehicle control (**Figure 2.20C** and **Table 2.9**). Moreover, the contraction induced by U46619 over the 1 hour was sustained and stable (**Figure 2.20C**). This observation supports the earlier findings in **section 2.4.10**, where pre-incubation of 10 μM FK244 did not affect the U46619's cumulative CRC. The E_{max} values of contractile agent-induced contraction are summarised in **Table 2.9**.

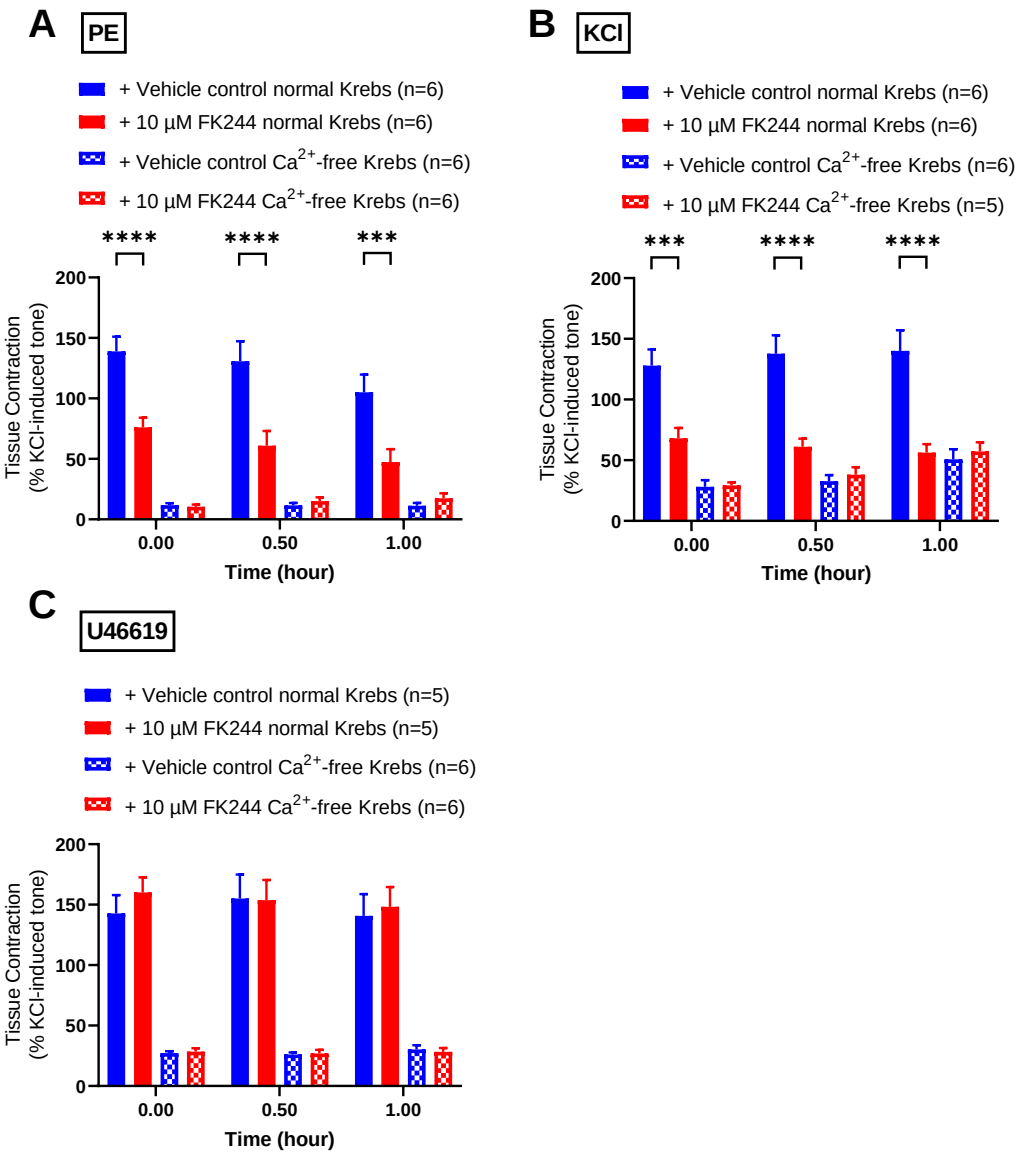


Figure 2.20 Effect of FK244 on (A) phenylephrine-, (B) KCl- and (C) U46619-induced contraction in normal Krebs and Ca^{2+}-free Krebs solution. *Tissue responses were recorded at 0, 30, and 60 minutes after the addition of each contractile agent and were expressed as the percentage of KCl-induced contraction. Data are shown as the mean ± SEM of 5 to 6 animals. Two-way ANOVA followed by Bonferroni's post hoc test was used to compare vehicle control and FK244 treatment in either normal or Ca^{2+} free Krebs separately at each time point. Abbreviations: KCl, potassium chloride, PE, phenylephrine.*

Table 2.9 Maximum tissue response (E_{max}) of phenylephrine, KCl and U46619-induced contraction in normal Krebs and Ca^{2+}-free Krebs solution in the presence of FK244.

		E_{max} (%)					
		Phenylephrine		**KCl**		**U46619**	
Treatment	**Time (hour)**	**Normal Krebs**	**Ca^{2+} free Krebs**	**Normal Krebs**	**Ca^{2+} free Krebs**	**Normal Krebs**	**Ca^{2+} free Krebs**
Vehicle control	**0**	139.0 ± 12.1	11.8 ± 1.7	127.9 ± 13.3	28.0 ± 5.5	142.7 ± 15.3	27.2 ± 1.6
	0.5	130.8 ± 16.5	11.6 ± 2.1	137.8 ± 15.1	32.7 ± 5.1	155.0 ± 19.9	26.1 ± 1.6
	1	105.1 ± 14.6	11.3 ± 2.3	140.1 ± 17.0	50.8 ± 8.3	140.8 ± 17.9	30.3 ± 3.4
FK244	**0**	76.1 ± 7.9 **** ($p < 0.0001$)	10.5 ± 1.8 ($p > 0.9999$)	68.2 ± 8.4 **** ($p < 0.0001$)	29.2 ± 2.6 ($p > 0.9999$)	160.1 ± 12.4 ($p = 0.8786$)	28.4 ± 2.7 ($p > 0.9999$)
	0.5	60.9 ± 12.1 **** ($p < 0.0001$)	15.1 ± 3.2 ($p = 0.9996$)	61.1 ± 6.7 **** ($p < 0.0001$)	38.1 ± 6.2 ($p = 0.9982$)	153.8 ± 16.7 ($p > 0.9999$)	26.9 ± 3.1 ($p > 0.9999$)
	1	47.4 ± 10.6 **** ($p < 0.0001$)	17.3 ± 4.3 ($p = 0.9944$)	56.3 ± 7.0 **** ($p < 0.0001$)	57.3 ± 7.5 ($p = 0.9955$)	148.3 ± 16.4 ($p = 0.9969$)	28.3 ± 3.1 ($p > 0.9999$)

Two-way ANOVA followed by Bonferroni's post hoc test was used to compare between vehicle control and FK244 treatment in either normal or Ca^{2+} free Krebs separately at each time point. Individual p-values were stated in the respective columns. Data are shown as mean ± SEM of 5 to 6 animals.

2.4.15 Extracellular Ca^{2+}-induced contraction was suppressed by FK244

The role of extracellular Ca^{2+} in FK244-induced relaxation was investigated. 2-APB, Pyr6 and SKF-96365 are non-selective TRPC inhibitors which modulate SOCC, has shown to inhibit $CaCl_2$-induced contraction to different extend (**Figure 2.21A**). Interestingly, Pyr3 being a selective inhibitor to TRPC3 at 10 μM, was not able to suppress $CaCl_2$-induced contraction (**Figure 2.21B**). Lastly, nifedipine and verapamil as VGCC inhibitors greatly reduced tissue contraction to Ca^{2+}, where almost no contraction was observed (**Figure 2.21C**).

All FK244-treated aortic rings showed a significant reduction in tissue contraction when $CaCl_2$ was re-introduced into a Ca^{2+}-free environment (**Figure 2.21D**). This effect is concentration-dependent, observed in 10 μM, 30 μM and 100 μM of FK244. Total suppression of response was observed in the presence of 100 μM.

The values of E_{max} are summarised in **Table 2.10**. The potency of $CaCl_2$ was not calculated as maximum tissue response has not plateaued in all tissues, especially in the case of 100 μM of FK244, 10 μM of nifedipine, SKF-96365 and verapamil, where extremely low tissue responses were recorded.

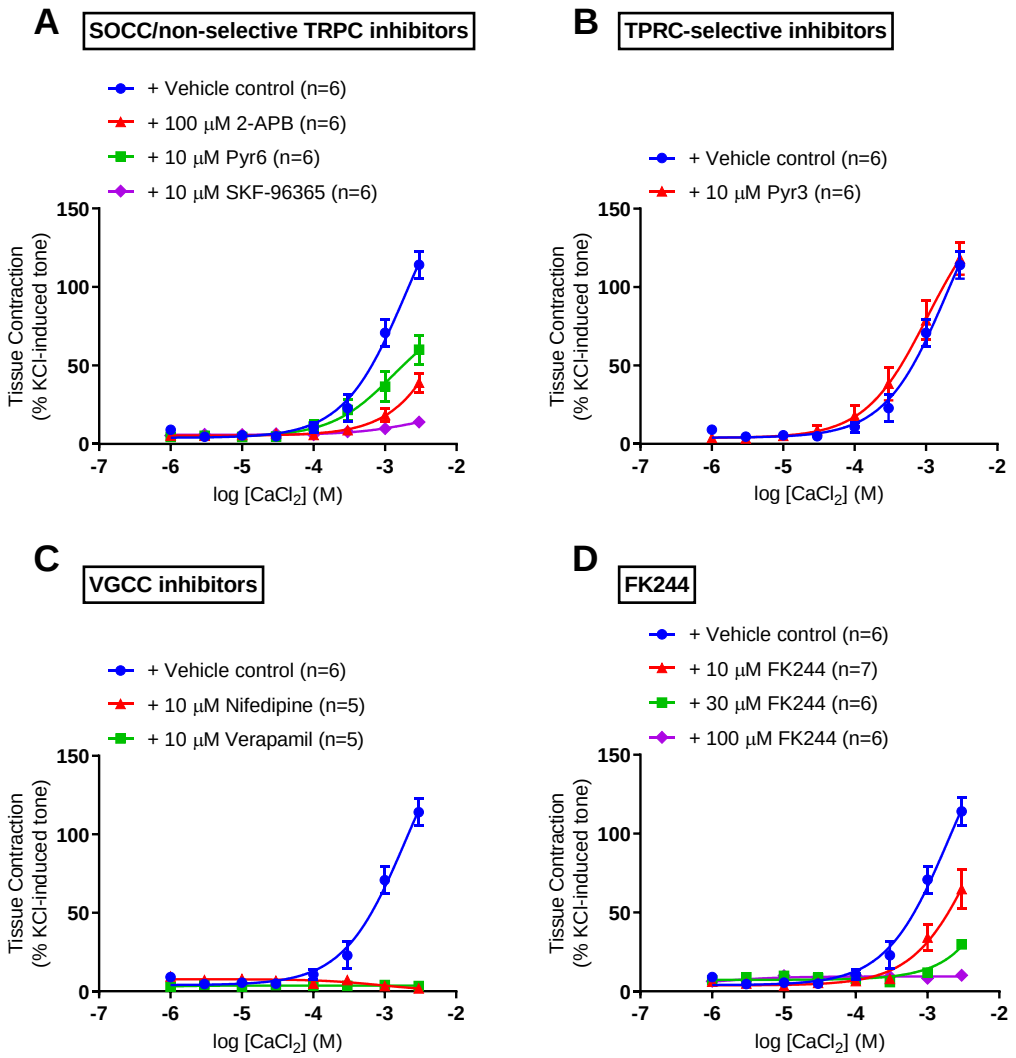


Figure 2.21 Effect of (A/B/C) Ca^{2+} channel blockers and (D) FK244 on $CaCl_2$-induced contraction in rat isolated aortic rings bathed in Ca^{2+}-free Krebs solution. *The Ca^{2+} channel blockers used were (A) SOCC/non-selective TRPC inhibitors (2-APB, Pyr6, SKF-96365), (B) TRPC- selective inhibitors (Pyr3), and (C) VGCC inhibitors (nifedipine, verapamil). Tissue contractions were expressed as the percentage of KCl-induced contraction in Ca^{2+}-containing Krebs solution. Data are shown as the mean ± SEM of 5 to 7 animals. Abbreviations: 2-APB, 2-aminoethoxydiphenyl borate; $CaCl_2$, calcium chloride; KCl, potassium chloride; SOCC, store-operated Ca^{2+} channel; TRPC, transient receptor potential canonical; VGCC, voltage-gated Ca^{2+} channel.*

Table 2.10 Maximum tissue response (E_{max}) of $CaCl_2$ CRCs following pre-exposure of vehicle control, FK244 or Ca^{2+} channel blockers.

Treatment	E_{max} (%)	
Vehicle control	114.1 ± 8.7	
+ 10 µM FK244	64.8 ± 12.1	**** ($p < 0.0001$)
+ 30 µM FK244	29.7 ± 2.9	**** ($p < 0.0001$)
+ 100 µM FK244	10.1 ± 3.7	**** ($p < 0.0001$)
+ 100 µM 2-APB	38.9 ± 6.1	**** ($p < 0.0001$)
+ 10 µM Nifedipine	1.7 ± 0.7	**** ($p < 0.0001$)
+ 10 µM Pyr3	118.1 ± 10.3	($p = 0.9994$)
+ 10 µM Pyr6	60.0 ± 9.3	**** ($p < 0.0001$)
+ 10 µM SKF-96365	13.9 ± 2.7	**** ($p < 0.0001$)
+ 10 µM Verapamil	3.2 ± 0.9	**** ($p < 0.0001$)

One-way ANOVA followed by Dunnett's post hoc test was used to compare all the treatment groups to vehicle control. Individual p-values were stated in the respective columns. Data are shown as the mean ± SEM of 5 to 7 animals.

2.4.16 TRPC-selective inhibitors attenuated FK244's vasorelaxation effect

A series of experiments were performed using a few Ca^{2+} channel blockers to examine the effect of FK244 against Ca^{2+} dynamics. The presence of TRPC-related inhibitors such as 2-APB (**Figure 2.22A**), Pyr6 (**Figure 2.22B**), SKF-96365 (**Figure 2.22C**) and Pyr3 (**Figure 2.22D**), have significantly reduced the aortic relaxant responses to FK244 (**Table 2.11**). In contrast, pre-incubation of VGCC blockers, nifedipine (**Figure 2.22E**) and verapamil (**Figure 2.22F**), did not affect the efficacy of FK244-induced relaxation (**Table 2.11**). As shown in **Table 2.11**, the rank order of the largest effect on E_{max} recorded was Pyr6 (-35.6%) > SKF-96365 (-28.8%) >2-APB (-19.8%) > Pyr3 (-17.9%).

In terms of potency, the pEC_{50} of FK244 was reduced in Pyr6- and SKF-96395-treated aortic rings but not affected in the presence of 2-APB, nifedipine, Pyr3 and verapamil (**Table 2.11**). Interestingly, Pyr6 and SKF-96365 increased the potency of FK244 by ~ 5.5-fold and ~5.1-fold compared to the vehicle control group. The values of E_{max} and potency of FK244 are summarised in **Table 2.11**.

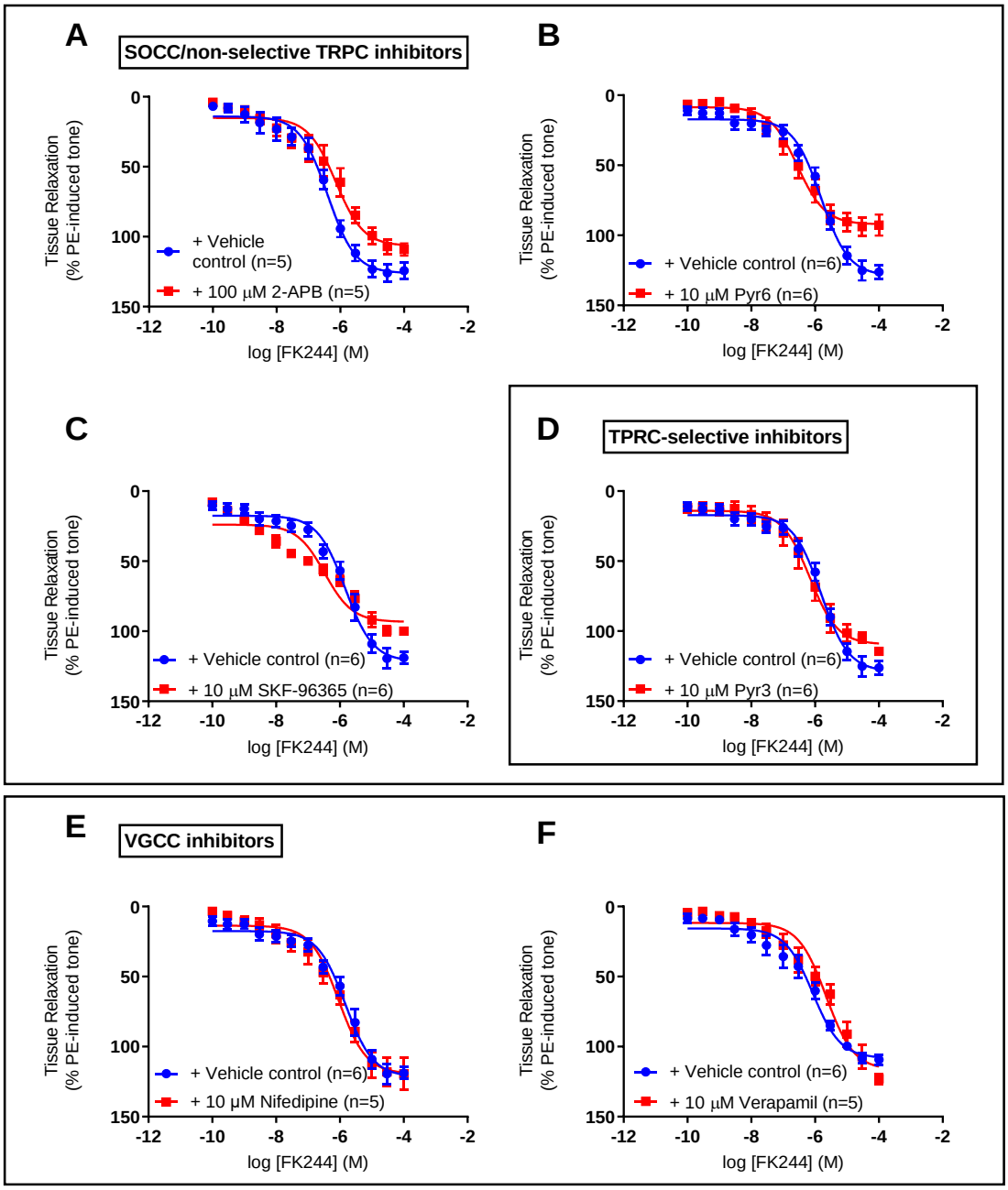


Figure 2.22 Effect of FK244-induced relaxation in the presence of different Ca^{2+} channel blockers. *CRCs to FK244 were performed in the presence of SOCC/non-selective TRPC inhibitors – (A) 2-APB, (B) Pyr6, (C) SKF-96365; TRPC- selective inhibitors – (D) Pyr3; and VGCC inhibitors – (E) nifedipine, (F) verapamil. Tissue relaxations were expressed as the percentage of phenylephrine-induced contraction. Data are shown as the mean ± SEM of 5 to 6 animals. Abbreviations: 2-APB, 2-aminoethoxydiphenyl borate; PE, phenylephrine; SOCC, store-operated Ca^{2+} channel; TRPC, transient receptor potential canonical; VGCC, voltage-gated Ca^{2+} channel.*

Table 2.11 Maximum tissue response (E_{max}) and potency (pEC_{50}) of FK244 in the presence of different Ca^{2+} channel blockers.

Treatment	E_{max} (%)	pEC_{50}
Vehicle control	126.0 ± 5.5	6.41 ± 0.04
+ 100 µM 2-APB	106.2 ± 4.9 * (p = 0.0267)	6.31 ± 0.28 (p =0.7451)
Vehicle control	122.6 ± 5.2	5.78 ± 0.08
+ 10 µM Nifedipine	120.3 ± 10.5 (p = 0.8379)	6.08 ± 0.15 (p = 0.1236)
Vehicle control	129.5 ± 5.8	5.81 ± 0.07
+ 10 µM Pyr3	111.5 ± 2.3 * (p = 0.0168)	6.16 ± 0.18 (p = 0.1054)
Vehicle control	129.5 ± 5.8	5.81 ± 0.07
+ 10 µM Pyr6	93.8 ± 6.5 ** (p = 0.0022)	6.55 ± 0.20 ** (p = 0.0057)
Vehicle control	122.6 ± 5.2	5.80 ± 0.08
+ 10 µM SKF-96395	93.9 ± 3.4 *** (p = 0.0009)	6.51 ± 0.18 ** (p = 0.0054)
Vehicle control	107.8 ± 4.4	6.24 ± 0.23
+ 10 µM Verapamil	116.7 ± 7.9 (p = 0.3278)	5.79 ± 0.30 (p = 0.2643)

Unpaired Student's t-test was used to compare each treatment with their respective vehicle controls. Individual p-values were stated in respective columns. Data are shown as mean ± SEM of 5 to 6 animals.

2.5 Discussion

In this chapter, experiments were designed to examine the pharmacological properties of FK244 and elucidate its mechanism of action using the organ bath techniques.

2.5.1 Physicochemical properties of FK244 – a theoretical calculation

In drug development, Lipinski's and Veber's rule are commonly used for hit selection an early stage. A lower number of HBA and HBD indicates higher plasma membrane permeability (Lipinski, Lombardo, Dominy, et al., 2012). FK244 has a low MW and the least number of HBA and HBD when compared to nifedipine, SKF-96365 and Pyr3. Its MW is almost half of Pyr3 and substantially lower than nifedipine. This suggests that FK244 is likely to have better oral absorption and high cell permeability.

A negative logP value is less favourable due to the compound being more polar and thus affecting its permeability through the phospholipid bilayer. Drugs with moderate logP value that ranged from 0 to 3 usually demonstrate optimal gastrointestinal absorption via passive diffusion mechanism (Ghose et al., 1998; Veber et al., 2002). FK244 has a high logP value close to 4, indicating that it is less polar and has low aqueous solubility. Odović et al. (2017) found that most clinically available drugs have logP within the range of 2.24 to 5.23. FK244 has a similar logP to nifedipine, a Ca^{2+} channel blocker widely used in treating hypertension (Odović et al., 2017). Therefore, FK244 is predicted to have a lower attrition possibility in the drug development process.

Besides, studies highlighted that the less rotatable bonds a compound has, the more likely it will have optimal receptor interaction (Veber et al., 2002; Zerroug et al., 2019). Having reduced molecular flexibility was found to be an important predictor of good oral bioavailability apart from MW. In Veber's analysis, FK244 possesses the least number of rotatable bonds and the lowest tPSA among all four reference compounds. Therefore, it will be less challenging to determine the conformation of FK244 that targets the binding site of the target protein.

Lipinski's rule is not a set of strict rules to eliminate potentially beneficial compounds. It is well known that many orally active drugs were reported to have violated Lipinski's rules, especially naturally occurring compounds (Petit, Meurice, Kaiser, et al., 2012). FK244 obeyed Lipinski's and Veber's rule, suggesting it is likely to exhibit desired drug-like properties and good pharmacokinetic profiles.

2.5.2 Tissue selectivity of FK244

FK244 did not produce any observable effect against the aortic, bladder and trachea tissues at basal tone as it did not produce any measurable change in tissue tension. Adding phenylephrine, an α_1–adrenergic receptors agonist, to induce the vascular contraction of the aortic segments mimics the effect of stretched blood vessels in hypertension. Similarly, carbachol, a muscarinic receptor agonist, was used to induce contractions in airways tissues isolated from rats and swine, as well as rat isolated bladder tissues. Preparation of isolated airways and bladder strips are used in functional assays for modelling clinical conditions such as airways constriction in asthmatic patients and overactive bladder associated with urinary frequency (Schneider, Fetscher, Krege, et al., 2004; Semenov et al., 2012). Studies have reported that phenylephrine induced weak contraction in rat trachea and bladder tissues compared to muscarinic agonists due to limited expression of α-adrenoceptors in these preparations (Michel & Vrydag, 2006; Vornanen, 1982). Therefore, carbachol was used as the contractile agents for tracheal and bladder tissues in this study. Phenylephrine and carbachol stimulate contraction by activating the adrenergic receptors (α_1) in the vasculature and muscarinic (M_3) receptors in the airways or bladder, respectively, and both receptors are coupled to G_q receptor (Fleichman, Schneider, Fetscher, et al., 2004; Proskocil & Fryer, 2005; Schneider et al., 2004). G_q protein activation contributes to the pathologies of vascular and airway diseases (Carr, Koziol-White, Zhang, et al., 2016; Keys, Greene, Koch, et al., 2002). Focusing on the G_q protein regulation is important to ensure that the biochemical signalling is similar in all the tissues tested with FK244. FK244 reduced the tissue contractions evoked by these agonists in rat and porcine smooth muscle tissues, suggesting the presence of target proteins affected by FK244. These initial observations in the aorta have led to a few possibilities of the target(s) of FK244, which included affecting adrenoreceptors or interfering with the downstream signalling mechanism upon activation of the G_q receptors.

The potency of FK244-induced relaxation in the aorta was approximately 40-fold higher compared to the bladder and approximately 18-fold higher compared to the trachea. FK244 was also around 5-fold more potent in porcine pulmonary arteries compared to porcine bronchiole. These findings suggest that FK244-induced relaxation is more vascular-selective than other smooth muscle tissues after this initial

investigation in two different species of animals. Tissue selectivity of FK244 is a desirable property when evaluating its ability to cause potential adverse effect *in vivo*.

Interestingly, FK244 is shown to be more potent in rat thoracic aorta than in porcine pulmonary artery. Structural and physiological variables in different vascular beds may contribute to the observed difference in FK244's relaxation profile. The pulmonary artery, as part of the pulmonary circulation, has thinner and less muscular walls compared to the thoracic aorta, which originated from the systemic circuit (Prasad, 2000). The SBP/DBP in the pulmonary circuit was reported to be around 25/10 mmHg, while the more commonly known blood pressure of 120/80 mmHg represents the pressure of the systemic circulation (Chamarthy, Kandathil, & Kalva, 2018). This shows that the vessels in pulmonary circulation, particularly the pulmonary arteries, regulate pulmonary blood pressure and have no contribution to the systemic blood pressure. The potential therapeutic benefits of FK244 in treating pulmonary arterial hypertension (PAH) has motivated the testing of its vasorelaxation effect in pulmonary arteries. The results have shown that it may have less contribution in treating PAH. PAH is defined as having mean pulmonary arterial pressure beyond 25 mmHg (Chamarthy et al., 2018). High dosage of Ca^{2+} channel blockers such as nifedipine and diltiazem are used in treating idiopathic PAH: 120 – 240 mg of nifedipine or 240 – 900 mg of diltiazem (Galiè, Humbert, Vachiery, et al., 2016; Ministry of Health, 2011; NICE, 2007). Their usage in managing PAH is not encouraged as the patient responsiveness to these treatments is low and often cause systemic hypotension with a negative inotropic effect (Barst, McGoon, Torbicki, et al., 2004; Kiely, Elliot, Sabroe, et al., 2013; Medarov & Judson, 2015). Pathophysiology of PAH includes vascular remodelling, arterial wall stiffness and endothelial dysfunction (Tuder, Marecki, Richter, et al., 2007). Therefore, the current guidelines recommend short-acting vasodilators such as ET receptor antagonists (ERAs), phosphodiesterase (PDE) 5 inhibitors and sGC stimulators as PAH-specific therapy (Galiè et al., 2016; Ministry of Health, 2011; NICE, 2007). These drugs act on the vascular endothelium and VSM, with ERAs blocking the G_q protein-coupled ET receptors, whereas PDE5 inhibitors and sGC stimulators intervene the NO/cGMP pathways (Duarte, Hanson, & Machado, 2013; Enevoldsen, Sahana, Wehland, et al., 2020; Khalil, 2011; Preston, 2008). Taken together, NO/cGMP pathways and G_q-protein signal transduction are likely to be the underlying mechanisms in maintaining a balanced vascular tone in pulmonary arteries.

With a reduced FK244's potency observed in the pulmonary artery, it may reflect that FK244's vasorelaxation mechanism is less sensitive via these pathways. However, more experiments were carried out to verify its effect on the endothelium, NO/cGMP pathways and G_q downstream signalling transduction.

2.5.3 Role of endothelium and NO

The vascular endothelium plays a vital role in vasorelaxation. Endothelial cells synthesise NO by activating eNOS as well as the produce mediators such as PGI_2 through the activation of COX (Bauer & Sotníková, 2010; Bonaventura et al., 2008; Heimlich & Pollock, 2014; Nilius & Droogmans, 2001). Besides, EDHFs, such as endogenous H_2O_2, H_2S, and K^+, hyperpolarise the VSM plasma membrane, resulting in vasorelaxation (V. Bauer & Sotníková, 2010; Rang, Dale, Flower, et al., 2012; P. S. Wong, Roberts, & Randall, 2015). L-NAME served to eliminate the residual endothelial NO within the system by inhibiting the activity of eNOS, testing the possible involvement of NO in FK244-induced relaxant responses. Our results showed that the removal of endothelium and pre-incubation with L-NAME has no significant impact on FK244-induced vasorelaxation. FK244-induced vasorelaxation was endothelium-independent and not through increasing the production of these endothelial relaxation factors, particularly NO.

2.5.4 Role of cyclic nucleotides

Forskolin, an AC activator, and ODQ, an sGC inhibitor, were used to investigate whether cAMP/cGMP pathway is involved in FK244-induced relaxation. Activation of AC increases the level of cytosolic cAMP via the conversion of ATP, triggering downstream PKA-dependent Ca^{2+} desensitisation. The activity of MLCK was reduced and MLCP activity was increased, promoting de-phosphorylation of MLC and evoke vasorelaxation (Amberg & Navedo, 2013). On the other hand, when ODQ inhibited NO-activated sGC, less cGMP was generated and hence reduced cGMP/PKG-dependent vasorelaxation. The potency of FK244 was increased by pre-incubation with vehicle control (DMSO) compared to the CRC of FK244 in **section 2.4.2**. DMSO 1% and above was reportedly caused smooth muscle relaxation by generating NO from endothelial cells and induced Ca^{2+} desensitization (Kaneda, Sasaki, Urakawa, et al., 2016; Shiga, Hirano, Nishimura, et al., 2007). Throughout the study, although the concentration of DMSO in the organ bath solution did not exceed 0.3%, it is possible that its cellular effect could still contribute to the enhancement of FK244 vasorelaxant

effect. All in all, compared to vehicle control, incubation with forskolin and ODQ neither augment nor diminish FK244-induced vasorelaxation, implying that FK244 does not act via cAMP- or cGMP-dependent pathways.

Low potency of FK244 in the pulmonary artery (**section 2.5.2**), the lack of effects of endothelium, L-NAME (**section 2.5.3**) and ODQ (**section 2.5.4**) on FK244-induced relaxation, have further indicate that FK244 does not involve in endothelium- and NO/cGMP-mediated vasorelaxation.

2.5.5 Role of adrenoceptors

Prazosin, rauwolscine and propranolol were used in our study to assess whether FK244 relaxed the vascular tone by inhibiting adrenoceptors in the aorta. Adrenergic blockers, such as prazosin and propranolol, are clinically indicated for hypertension and CVDs. They interfere with the ligand binding to G_q and $G_{s/i}$ protein, respectively, to reduce sympathetic drive (Gordon & Kittleson, 2008; Stamper, Lieberman, & Drake, 2009; Vasudevan, Mohan, Goswami, et al., 2011). Our results demonstrated that FK244 has no adrenergic effect as the inhibition of adrenoceptors did not affect the vascular effect exhibited by FK244.

2.5.6 Role of K^+ channels

There are a few K^+ channels subtypes present in the vasculatures, namely K_v, $K_{ir,}$ K_{ATP}, K_{Ca} channels (Brayden, 1996; Jackson, 2017; Ledoux, Werner, Brayden, et al., 2006; Sobey, 2001). The opening of K^+ channels facilitates K^+ efflux and hyperpolarise the membrane potential. This is followed by the closure of VGCCs and reversing vasocontraction (Ledoux et al., 2006). In the present study, pre-incubation with 4-AP, $BaCl_2$, TEA and glibenclamide did not reduce FK244-induced vasorelaxation. It is unlikely that FK244's mechanism of action is related to opening the K^+ channels and hyperpolarisation.

2.5.7 Role of contractile agents

FK244 has displayed the highest potency in reducing contraction to phenylephrine, followed by KCl and then lastly, U46619. In the reverse experiment, FK244 also selectively suppressed phenylephrine-, KCl- and serotonin-induced vasoconstriction but not U46619-induced vasoconstriction. These findings may be attributable to varied mechanisms of actions of different contractile agents in the VSMC, as illustrated in **Figure 2.23**.

The potency of FK244 was reduced in aortic preparations pre-contracted with KCl rather than phenylephrine. High K^+ may lead to impaired ability of the VSM to relax, which subsequently prevented vasorelaxant responses to FK244. These findings may be indicative of a contribution of K^+ channel opening and hyperpolarisation to FK244's mechanisms of action. It is unlikely that the opening of K^+ channel contributes to FK244-induced relaxation as the selective K^+ channel blockers did not reduce FK244-induced vasorelaxation. However, FK244's relaxation mechanism could interfere with plasma membrane depolarisation. KCl increases VSM tone by depolarising the plasma membrane and allowing the influx of Ca^{2+} through L-type VGCCs (P. H. Ratz, Berg, Urban, et al., 2005). KCl is routinely used as a receptor-independent contractile agent to bypass GPCR stimulation. Despite lacking voltage sensors in TRPC channels, TRPC3 and TRPC6 channels in particular, can mediate Ca^{2+} entry secondary to membrane depolarisation and the activation of VGCCs, where VGCCs act as the main channels of extracellular Ca^{2+} influx to induce contraction (Estacion et al., 2006; Falcón, Galeano-Otero, Martín-Bórnez, et al., 2020; Soboloff et al., 2005; Welsh et al., 2002). It was reported in another study that KCl-induced contraction involves Ca^{2+} entry through 2-APB-sensitive TRP channels (P. H. Ratz & Berg, 2006). The authors suggested that increasing $[Ca^{2+}]_i$ during KCl depolarisation may translocate activated ROCK to caveolin (P. H. Ratz et al., 2005). Caveolin, a protein required to form a cove-like structure at the plasma membrane, binds to TRPC channels and induce SOCE (Brazer, Singh, Liu, et al., 2003; Lockwich, Singh, Liu, et al., 2001; Nilius & Flockerzi, 2014). In short, a reduction in the potency of KCl-induced contraction has implied that L-type VGCCs and TRPC channels were likely to be inhibited by FK244.

In vascular tissues, the vasoconstriction effects of phenylephrine, serotonin and U46619 are mediated by the α_1-adrenoceptors, 5-HT_{2A} receptors, and TP receptors, respectively. Upon binding to their specific receptors, phenylephrine, serotonin and U46619 activate G_q protein. G_q signalling activates PLC to breakdown PIP_2 into DAG and IP_3. DAG and its downstream effector PKC, elevate $[Ca^{2+}]_i$ through the activation of L-type VGCCs (Fransen et al., 2015; Touyz, Alves-Lopes, Rios, et al., 2018) and TRPC channels (Amberg & Navedo, 2013; Hill-Eubanks et al., 2011). In the VSMCs, DAG can directly activate ROCCs such as TRPC3 and TRPC6 channels by generating an inwardly rectifying cationic current. It then leads to Ca^{2+} mobilisation through TRPC channels, independent of PKC (Hofmann et al., 1999; Nilius & Flockerzi, 2014; H. Yan,

Zhang, Wong, et al., 2019). TRPC6 channel was also suggested to be a component of NSCCs that is activated by α_1-adrenoceptors (R. Inoue, Okada, Onoue, et al., 2001).

Another product of PLC – IP_3, binds to IP_3 receptors embedded in the membrane of SR (Touyz et al., 2018). Elevation of cytosolic Ca^{2+}, either by external Ca^{2+} influx through L-type VGCCs or store Ca^{2+} release through IP_3 receptors, triggers the opening of RyRs in a process called CICR. Activation of IP_3 receptors and RyRs releases Ca^{2+} from the SR store into the cytosol and elevates $[Ca^{2+}]_i$. Upon Ca^{2+} store depletion, STIM, a Ca^{2+}-sensor protein anchored in the SR membrane, couples with Orai located at the plasma membrane to form an SR/plasma membrane junction to allow Ca^{2+} influx (Gudlur et al., 2020; Soboloff, Rothberg, Madesh, et al., 2012). This process is widely known as SOCE, which increases cellular Ca^{2+} level through the opening of SOCCs located at the plasma membrane (Amberg & Navedo, 2013; Jairaman & Prakriya, 2013; Spassova, Soboloff, He, et al., 2004). Ca^{2+} release-activated Ca^{2+} (CRAC) channels form the subset of SOCCs, where the Orai component was the pore-forming subunits of the CRAC channels (Prakriya, Feske, Gwack, et al., 2006; Prakriya & Lewis, 2015; Vig, Beck, Billingsley, et al., 2006). The depolarising Ca^{2+} current through SOCE was also identified as the CRAC current (I_{CRAC}) (Jairaman & Prakriya, 2013). An increasing number of studies have also pointed out TRPC channels play a role in SOCE by coupling with STIM1/Orai1 pore-forming subunit that makes up of SOCC (Z. Liu & Khalil, 2018; J. Shi, Miralles, Birnbaumer, et al., 2017). Evidence has shown that TRPC1/4/5 channels comprise another part of the SOCC by coupling to the STIM/Orai complex to facilitate Ca^{2+} influx. STIM/Orai complex also binds to TRPC3/6 channels (except TRPC7) when TRPC1/4/5 heterotetramerise with TRPC3/6 (K. P. Lee, Yuan, Hong, et al., 2010; Yuan, Zeng, Huang, et al., 2007). TPRC and STIM/Orai communication also lead to the opening of L-type Ca^{2+} channels, which induces a huge Ca^{2+} influx and ultimately, vascular contraction (Falcón et al., 2020; Samanta, Bakowski, Amin, et al., 2020; Soboloff et al., 2005).

Regardless of the target receptors, the Ca^{2+} influx mechanism of these contractile agonists relies mainly on Ca^{2+}-permeable channels such as L-type VGCC and TRPC channel. There is evidence showing TRPC1 – 4 channels are involved in serotonin's downstream signalling pathway in the human pulmonary artery (Rodat-Despoix, Aires, Ducret, et al., 2009; Varghese, Hong, & Weir, 2006). From our results, it was evident that FK244 may, although not exclusively, inhibit extracellular Ca^{2+} influx through L-

type VGCC, as it suppressed the contraction caused by phenylephrine, KCl and serotonin. It is also likely that FK244 also modulates G_q-downstream messengers, inhibits Ca^{2+} influx through TRPC channels due to FK244's excellent activity in suppressing phenylephrine-induced contraction at low concentration.

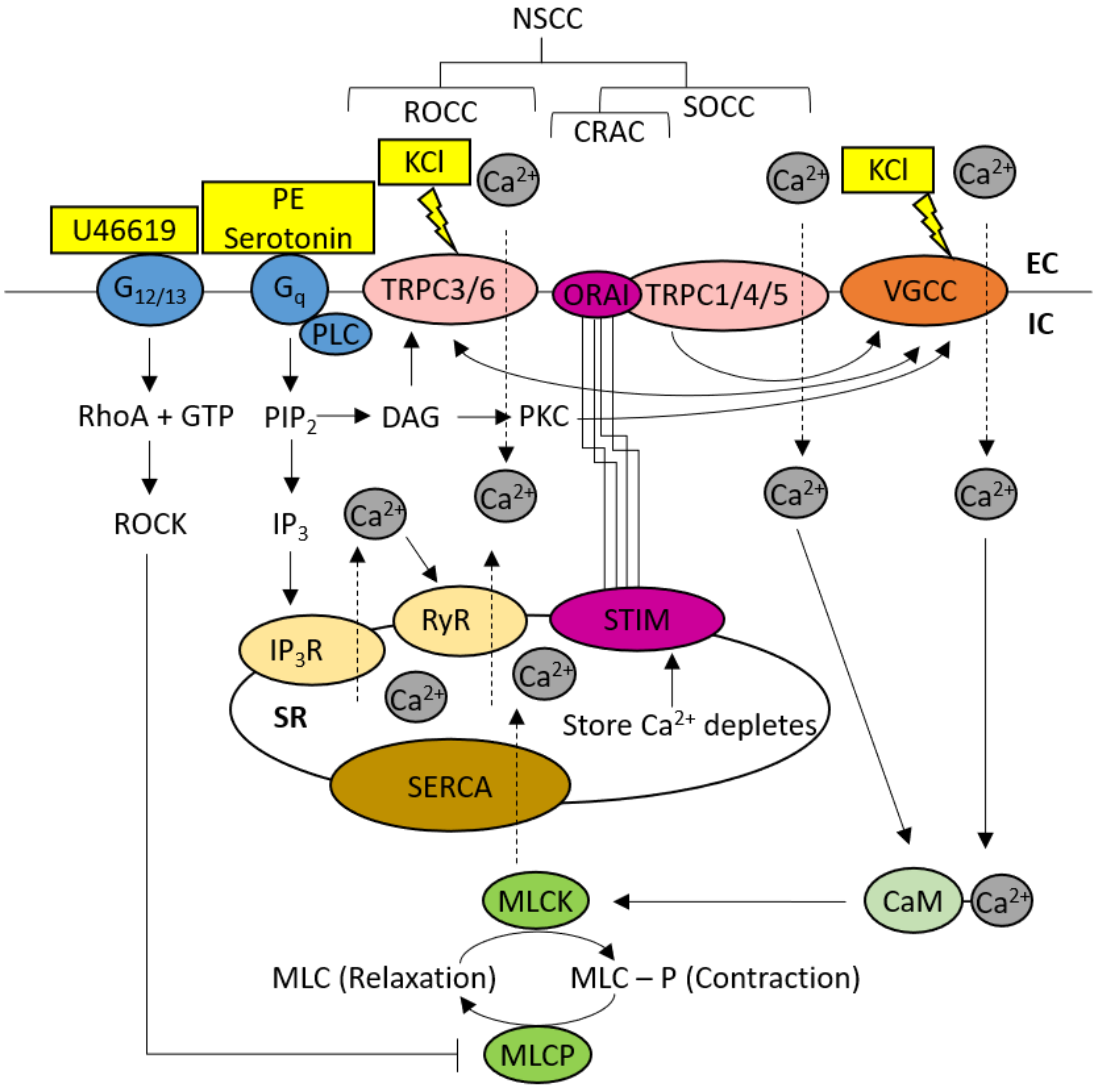


Figure 2.23 Schematic diagram depicting the regulation of Ca^{2+} dynamic by phenylephrine, serotonin, KCl and U46619, to induce VSM contraction. *Activation of phenylephrine α_1-adrenoceptors and serotonin 5-HT_{2A} receptors initiate G_q protein signal transduction, whereas $G_{12/13}$ protein is believed to be coupled to U46619-activated TP receptors in the VSM. Downstream effectors of phenylephrine, serotonin and KCl activate TRPC and VGCC channels. Solid pointed solid arrow denotes downstream effectors activation, blunt arrow denotes downstream effectors inhibition. Dotted arrows denote flow of Ca^{2+}. Abbreviations: Ca^{2+}, calcium ion; CaM, calmodulin; CRAC, Ca^{2+} release-activated channels; DAG, diacylglycerol; EC, extracellular; GTP, guanosine-5'-triphosphate; IC, intracellular; IP_3, inositol-1,4,5-trisphosphate; IP_3R, IP_3 receptor; KCl, potassium chloride; MLC, myosin light chain; MLCK, MLC kinase; MLCP, MLC phosphatase; MLC-P, phosphorylated MLC; NSCC, non-selective cation channels; ORAI, Ca^{2+} release-activated Ca^{2+} channel modulator; PE, phenylephrine; PIP_2, phosphatidylinositol 4,5-bisphosphate; PKC, protein kinase C; RhoA, Ras homolog family member A; ROCC, receptor-operated Ca^{2+} channels; ROCK, Rho-associated protein kinase; RyR, ryanodine receptor; SERCA, sarco/endoplasmic reticulum Ca^{2+}-ATPase; SOCC, store-operated Ca^{2+} channels; SR, sarcoplasmic reticulum; STIM, stromal interaction molecule; TRPC, transient receptor potential canonical; VGCC, voltage-gated Ca^{2+} channels.*

It is worth to scrutinise the non-response of FK244 in U46619-mediated contraction. In **Figure 2.15D**, FK244 at 100 μM had caused 23% relaxation in U46619-precontracted tissue compared to vehicle control. This difference was also noted in **Figure 2.16D**, where U46619-induced contraction was attenuated approximately 37% with incubation of 100 μM of FK244 compared to vehicle control. Apart from G_q proteins activation, U46619-activated TP receptors also coupled to $G_{12/13}$ proteins (Nakahata, 2008; Offermanns, 2006). Following $G_{12/13}$ protein activation, GTP-bound RhoA activates ROCK and subsequently inhibits MLCP activity to sustain smooth muscle contraction (**Figure 2.23**) (Alapati, McKenzie, Blair, et al., 2007; García-Redondo, Briones, Martínez-Revelles, et al., 2015; Grann, Comerma-Steffensen, Arcanjo, et al., 2016; McKenzie, MacDonald, & Shaw, 2009). The activity of U46619 was GTP-dependent, which involved RhoA-GTP activation and ROCK in eliciting vasoconstriction in U46619-treated tissues (Baldassare, Tarver, Henderson, et al., 1993; Gohla, Schultz, & Offermanns, 2000). Increase Ca^{2+} sensitisation by regulating the MLC phosphorylation level is independent of $[Ca^{2+}]_i$. It was said to contribute to the tonic phase in agonist-induced contraction in the VSMC (Fukata, Kaibuchi, Amano, et al., 2001; Somlyo & Somlyo, 2000). A study has shown that in rat aorta, U46619 depend less on extracellular Ca^{2+} influx and VGCC to elicit its contractile effect compared to serotonin (Tasaki, Hori, Ozaki, et al., 2003). Taken together, activation of U46619 in rat aortic smooth muscle may be predominantly coupled to $G_{12/13}$ receptor instead of G_q receptor in this experimental setting. It can be reasonably believed that FK244 does not entail the Ca^{2+}-independent RhoA/ROCK pathway through $G_{12/13}$ receptor to elicit its vascular effect. This could explain the lack of influence in U46619-induced contraction by FK244.

2.5.8 Reversibility of FK244 as an inhibitor to phenylephrine-induced contraction

It was found that FK244's inhibition on phenylephrine-induced contraction was reversible by washing the tissue with fresh Krebs solution. The contraction to phenylephrine was higher after washing, although the contraction did not recover to the percentage as high as the first phenylephrine-induced contraction in vehicle-treated tissue. One possible explanation is that α_1-adrenoceptor-mediated desensitisation may mask the reversible effect of FK244. Reduced responsiveness to α_1-adrenoceptor-agonist stimulation may occur in isolated tissues due to repeated plasma membrane excitation, depletion of ATP as fuel resources, exhaustion of contraction coupling

process or enhance NO synthesis in the endothelium (Arce, Vicente, Segura, et al., 2017; Gürdal, Can, & Uğur, 2005). Studies have also reported that prolonged exposure of at least 1 hour to α_1-adrenoceptor-agonist such as phenylephrine promoted desensitisation of α_1-adrenoceptors by receptor internalisation and reduced turnover rate of PIP_2 (Lurie, Tsujimoto, & Hoffman, 1985; S. Y. Wang, Song, Xu, et al., 2007). In this study, following 30-minute incubation with vehicle control or FK244, phenylephrine was added into the bath for an hour both before and after washing with Krebs solution. Therefore, it is sensible to suggest desensitisation of α_1-adrenoceptors may account for the reduction of second phenylephrine-induced contraction in both vehicle- and FK244-treated tissues. In short, after FK244 has been washed out with fresh Krebs solution, phenylephrine still managed to stimulate contraction with no loss of response in the same tissue. This finding indicates that the action of FK244 is reversible.

2.5.9 Role of intra- and extracellular Ca^{2+}

This study also questioned whether the vasorelaxation effect of FK244 was due to the inhibition of intracellular Ca^{2+} store depletion or extracellular Ca^{2+} influx. Ca^{2+} mobilisation is an essential physiological process that regulates the vascular tone. In **Figure 2.20**, the phasic contraction was high with external Ca^{2+} but attenuated in the presence of FK244, except in U46619-contracted tissues. In the absence of external Ca^{2+}, the initial phasic contraction after G_q activation was markedly reduced, and the tonic contraction afterwards remained low. The phasic contraction was reported to be initiated by the Ca^{2+} release from the intracellular store through IP_3 receptors and RyRs, while additional external Ca^{2+} influx is required to sustain the high tonic contraction (Burt, 2003; Fransen et al., 2015; Van Petegem, 2012). When Ca^{2+} was chelated by EGTA in the external environment, a similar percentage of contraction were obtained for phenylephrine-, KCl- and U46619-induced contraction in both the control and FK244-treated groups. The agonist-induced contraction was measured over an hour because the tonic contraction from store Ca^{2+} release was reported to be slowly increasing (Fernández-Tenorio, Porras-González, Castellano, et al., 2011; Fransen et al., 2015). Store Ca^{2+} release from IP_3 receptors and RyRs (via CICR) was responsible for the aortic contraction without external Ca^{2+} (Fernández-Tenorio et al., 2011; Urena et al., 2007). In Ca^{2+}-free environment, the small phasic contraction induced by KCl was likely due to the increase in cytosolic free Ca^{2+} from intracellular store, while the tonic contraction was stimulated by KCl-mediated Ca^{2+} sensitisation mechanism (P. H.

Ratz & Berg, 2006), where MLCK was activated to facilitate MLC phosphorylation and contraction. This sensitisation of agonist often does not require any changes in $[Ca^{2+}]_i$ (Himpens, Kitazawa, & Somlyo, 1990). Our findings suggest that FK244 is less likely to regulate intracellular Ca^{2+} store release but is more probably to reduce external Ca^{2+} influx that is associated with tonic contractile response.

It has been reported that Ca^{2+} influx in the VSMC is driven by the activation of various channels, such as VGCCs and TRPC channels (Amberg & Navedo, 2013; Berridge, 2008; Hill-Eubanks et al., 2011). A high concentration of K^+ was added into the organ bath to depolarise the plasma membrane. When the activation threshold for L-type VGCC is reached, the channels open up, allowing the influx of Ca^{2+} from the external environment to induce contraction (Berridge, 2008). The current paradigm focuses on the direct activation of L-type VGCCs upon membrane depolarisation. However, based on the literature, we hypothesised that TRPC channels are actually involved in the initial influx of Ca^{2+} to reach the activation threshold for L-type VGCC following membrane depolarisation (Falcón et al., 2020; Soboloff et al., 2005). The aortic tissues which were previously treated with different concentration of FK244 significantly suppressed Ca^{2+}-induced contractions in a concentration-dependent manner. With 100 µM of FK244, smooth muscle contraction was abolished. Hence, FK244 was likely to induce vasorelaxation by regulating extracellular Ca^{2+}-permeable channels. Our findings propose that FK244 does not mediate intracellular Ca^{2+} store and is expected to reduce extracellular Ca^{2+} influx by regulating VGCCs or Ca^{2+}-permeable TRPC channels.

2.5.10 Relaxation profiles of FK244 and other Ca^{2+} channel blockers

Comparing the relaxant profiles of FK244 with other Ca^{2+} channel blockers has revealed that FK244 is as potent as TRPC channels blockers and VGCCs blockers but is more efficacious than 2-APB, Pyr3, and SKF-96365. Among these Ca^{2+} channel blockers, the rank of vasorelaxant response for these compounds is: FK244 > verapamil > nifedipine > Pyr6 > HC-070 > 2-APB > SKF-96365 > Pyr3. This observation indicates that FK244 may target TRPC channels with similar potency, but FK244 may target other signalling pathways on top of TRPC channels inhibition to achieve more than 100% of vasorelaxation. FK244 showed comparable E_{max} as nifedipine and verapamil, suggesting it may also target VGCCs.

The estimated pEC_{50} of HC-070, Pyr3 and SKF-96365 is close to FK244's potency. Pyr3 was reported to be a selective blocker to TRPC3 channels with an IC_{50} of 0.8 µM ($pEC_{50} \approx 6.09$) (Kiyonaka et al., 2009). HC-070 was reported to be a potent TRPC4, 5 channels with an IC_{50} of 46 nM to TRPC4 channels ($pEC_{50} \approx 7.34$) and 9.3 nM ($pEC_{50} \approx 8.03$) to TRPC5 channels. It also has an inhibitory effect on TRPC3 channels, but at a higher IC_{50} of 1 µM ($pEC_{50} \approx 6$) (Just et al., 2018). SKF-96365 has been characterised as a non-selective TRPC channels blocker which mediates ROCE and SOCE, with IC_{50} around 5 – 25 µM ($pEC_{50} \approx 5.30 – 4.60$) (R. Inoue et al., 2001; Merritt, Armstrong, Benham, et al., 1990; Okada, Shimizu, Wakamori, et al., 1998). The reported IC_{50} values for Pyr3 corroborated with the pEC_{50} value observed in this study. This implies that Pyr3-induced relaxation in the rat aorta was mediated by TRPC3 channel inhibition expressed on the VSMC. For HC-070, the pEC_{50} obtained in isometric tension recordings was similar to its reported IC_{50} for TRPC3/4/5 channels (Just et al., 2018). This suggests that the vasculature effect of HC-070 is likely to include the inhibition of TRPC3 channels in addition to TRPC4 and TRPC5 channels. Vascular relaxation via both TRPC4 and TRPC5 channels may be minimal as no relaxation effect was observed at the nanomolar range of concentrations of HC-070. SKF-96365 also showed similar potency, but whether by the means of inhibiting ROCE-related TRPC3/6 or SOCE-related TRPC4/5 was not clear yet. To summarise the efficacy and potency of SOCC and TRPC inhibitors, it can be said that for an overt relaxation to occur, a compound is required to inhibit multiple TRPC channels including TRPC3/4/5/6 channels. Observing from all the CRCs of Ca^{2+} channel blockers, it can be suggested that : 1) selective inhibition of only TRPC3 channels by Pyr3 would not produce a large tissue relaxation; 2) non-selective inhibition of a combination of TRPC channels by 2-APB, HC-070 and SKF-96365, did not produce a relaxation as substantial as FK244; 3) Inhibition of VGCCs, the major Ca^{2+}-permeable channel involve in smooth muscle contraction, is necessary to produce a profound vasorelaxation, as observed in nifedipine and verapamil CRCs. Consistent with previous findings, FK244 is likely to modulate VGCCs and TRPC channels.

2.5.11 Role of extracellular Ca^{2+}-permeable channels

SKF-96395, being a non-selective TRPC inhibitor, has suppressed phenylephrine-induced contraction at a similar magnitude as nifedipine and verapamil. The inhibition on L-type VGCCs by DHP nifedipine, and phenylalkylamine verapamil, is well

established and their roles in modulating Ca^{2+} are relatively simple and straightforward (Pignier & Potreau, 2000). On top of that, verapamil was also found to block other VGCCs such as P/Q-type (Nimmrich & Gross, 2012), R-type (Cai, Mulle, & Yue, 1997), N-type (Diochot, Richard, Baldy-Moulinier, et al., 1995) and T-type VGCC (Bergson, Lipkind, Lee, et al., 2011), albeit at higher concentrations compared to L-type VGCC inhibition. Inhibition of VGCCs by verapamil may have more clinical importance in cardiac diseases because it predominantly inhibits cardiac VGCCs, whereas nifedipine is more vascular-selective (Pérez-Vizcaíno, Tamargo, Hof, et al., 1993). On the other hand, the molecular target of SKF-96365 in mediating Ca^{2+} dynamics is still debatable. It was initially described as a ROCE and voltage-gated Ca^{2+} entry inhibitor (Merritt et al., 1990). It did not inhibit the channel itself but rather an unknown entity involved in the ROCE and voltage-gated Ca^{2+} entry pathway. Various studies have used SKF-96365 as a ROCC inhibitor (Baik et al., 2011), TRPC3 inhibitor (Zhu, Jiang, & Birnbaumer, 1998), SOCE/I_{CRAC} inhibitor (Kiselyov, Xu, Mozhayeva, et al., 1998), TPRC-mediated SOCE inhibitor (Sabourin, Bartoli, Antigny, et al., 2016; Zagranichnaya et al., 2005) and NSCC inhibitor (Garcia et al., 2016) to elucidate the influence of ROCE and SOCE in physiological processes. NSCC is an umbrella term for all channels that permeate cation into the cell, including TRPC channels. TRPC channels are mainly categorised into ROCC which includes TRPC3/6/7 and SOCC, which includes TRPC1/4/5 (Nilius & Flockerzi, 2014). The role of individual TRPC subtypes in isolated tissues is yet to be defined due to the possibility of heterotetramerisation. The concentration of SKF-96365 used in literature was within the range of 3 – 40 µM, showing that the non-selective inhibition of ROCC and SOCC by SKF-96365 is within this range. FK244 at 100 µM has abolished the $CaCl_2$-induced contraction, which has the same effect as SKF-96935, nifedipine or verapamil at 10-fold lower concentration of 10 µM. These results indicate the ability of FK244 to block Ca^{2+} influx via all classes of VGCCs or NSCCs is not as profound as these known Ca^{2+} channel blockers. The presence of SKF-96365 reduced the vasorelaxation effect of FK244, whereas pre-incubation with nifedipine and verapamil did not affect FK244-induced vasorelaxation. An attempt to explain these findings consists in purporting that 1) FK244 may compete with SKF-96365 to block ROCC and SOCC in the VSM, 2) FK244 may simultaneously inhibit other plasmalemmal Ca^{2+} permeable channels on top of SKF-96365-sensitive signalling pathways, 3) the two potent VGCC blockers may have shadowed the relaxation effect of FK244.

As a SOCC inhibitor (Schleifer et al., 2012; Z. K. Sweeney, Minatti, Button, et al., 2009; Yonetoku, Kubota, Miyazaki, et al., 2008), Pyr6 was described to specifically inhibit the Orai proteins that interact with TRPC channels to facilitate SOCE pathway (Xingjuan Chen et al., 2020; Schleifer et al., 2012; Silva & Ballejo, 2019). Pyr3 is a pyrazole compound that selectively blocks TRPC3 channels (Kiyonaka et al., 2009). Pyr3 and Pyr6 did not suppress phenylephrine-induced contraction. Their high selectivity against TRPC3 channels and Orai/SOCE inhibition could be the reason that they were hardly effective to reduce phenylephrine-induced contraction. As mentioned, phenylephrine evoked extracellular Ca^{2+} entry via multiple Ca^{2+} sensitive channels such as L-type VGCCs and TRPC channels involved in both ROCE and SOCE pathways. The presence of Pyr3 also did not attenuate $CaCl_2$-induced contraction which includes external Ca^{2+} influx following KCl-mediated membrane depolarisation, suggesting that TRPC3 channels play a minor role in facilitating Ca^{2+} influx following membrane depolarisation compared to L-type VGCCs. On the other hand, Pyr6-induced Orai inhibition affected Ca^{2+} influx through SOCCs, explains that SOCC plays a bigger role in facilitating extracellular Ca^{2+} influx compared to TRPC3 channel alone. Both FK244 and Pyr6 at 10 µM, inhibited $CaCl_2$-induced contraction to a similar magnitude. This observation connotes the idea that FK244 perhaps has a vasorelaxation mechanism similar to Pyr6, which is through SOCC or Orai inhibition. Incubation with Pyr3 and Pyr6 also reduced the efficacy of FK244, indicating that FK244 is likely to be a TRPC3 channel or SOCC inhibitor. Investigation on the extent of FK244's inhibition on VGCC and TRPC channels had been carried out by incubating nifedipine and Pyr3 to simultaneously block VGCCs and TRPC channels prior to the addition of FK244. Despite varying the incubation concentration, no contraction was observed with the addition of $CaCl_2$ and phenylephrine (data not shown), rendering organ bath as an ineffective method to examine the extent of FK244 inhibition on two different classes of Ca^{2+}-permeable channels.

2-APB was initially reported as an IP_3 receptors inhibitor (Maruyama, Kanaji, Nakade, et al., 1997) It was found later that 2-APB is more likely to independently inhibits SOCE through SOCC, with little Ca^{2+} modulation effect on IP_3 receptors (Bishara et al., 2002; Bootman, Collins, Mackenzie, et al., 2002; Broad, Braun, Lievremont, et al., 2001; Gregory, Rychkov, & Barritt, 2001). Other studies also reported that 2-APB inhibits TRPC channels which synergistically suppresses phenylephrine-induced

contraction with L-type VGCC blocker – nifedipine (Lievremont, Bird, & Putney, 2005; P. H. Ratz & Berg, 2006). As discussed, phenylephrine evokes ROCE through VGCC, TPRC3 and TRPC6 channels, at the same time induces Ca^{2+} release from the SR store through IP_3 receptors and RyRs. To sustain phenylephrine-induced contraction, apart from continuous Ca^{2+} influx via L-type VGCC, depletion of SR store will prompt Ca^{2+} refilling via SOCE pathway to complete the cycle of intracellular Ca^{2+}-induced contraction. Phenylephrine- and $CaCl_2$-induced contraction were diminished by the presence of 2-APB, showing that 2-APB may block both SOCCs and TRPC channels as indicated in the literature. 100 µM of 2-APB showed a higher suppression in $CaCl_2$-induced contraction compared to 10 µM of Pyr6. This could be the result of difference in concentration used for incubation. 2-APB significantly reduced the E_{max} of FK244, further supporting that SOCCs as part of TRPC channels may be the binding targets of FK244.

It is worth to mention that signalling cascades upon compound activation or inhibition is not always straightforward and usually intertwine with other physiological processes within the cells. In a native environment, functional TRPC3 and TRPC6 channels can form heterotetramers with each other (Goel, Sinkins, & Schilling, 2002; Hofmann et al., 2002). Accumulating evidence has shown that not only do TRPC3 and TRPC6 channels involve in ROCE, but they are also sensitive to SOCE when they interact with Orai or form heteromultimeric channels with TRPC1/4/5 channels (Liao, Erxleben, Yildirim, et al., 2007; Liu, Bandyopadhyay, et al., 2005; Séguéla, Ase, Grant, et al., 2014; Zagranichnaya et al., 2005). The assembly of heteromultimeric TRPC channels in native tissues has overlapping roles in mediating ROCE and SOCE, which could explain the sensitivity of FK244 on both ROCC and SOCC regulated by 2-APB, Pyr3, Pyr6, SKF-96365.

2.6 Chapter summary

The findings in the functional studies of this chapter have shown new evidence on the modulation of Ca^{2+} by FK244. It primarily inhibits extracellular Ca^{2+} influx to exert a vasorelaxant activity within the micromolar range. FK244-mediated vasorelaxation involved greatly in the downstream signalling pathway of phenylephrine, pointing towards G_q-coupled downstream effector in general. It appears to modulate these Ca^{2+} channels including TRPC channels and L-type VGCCs.

Chapter 3 Pharmacological investigation of 1-(furan-2-yl)-*N*-phenethylpentan-3-amine (PM20)

3.1 Introduction

3.1.1 Schwarzinicine A and PM20

In Chapter 2, it was mentioned that a few SAR strategies had been used to optimise the pharmacophore of schwarzinicine A to generate analogues that are more efficacious and potent than schwarzinicine A. Using the simplification method, it is more cost-effective to eliminate redundant structures, thus, generating a simpler but equally (or more) effective compounds. Simpler structures are also likely to have reduced toxicity when ineffective functional groups are removed (S. Z. Wang, Dong, & Sheng, 2019). In schwarzinicine A, all the 3,4-dimethoxy (-OCH_3) groups were removed as they have no effect on vasorelaxant activity in SAR studies (F. K. Lee et al., 2021).

Subsequently, the 3,4-dimethoxyphenyl group (ring B) that is present in schwarzinicine A was simplified to a methyl group (**Figure 3.1**). As mentioned in Chapter 2, the vasorelaxant effect of analogues was retained when two rings were present and one of which must be an aromatic ring. Ring variation is another SAR strategy to improve binding to the target receptor (Wood, 2005). This step could potentially improve the selectivity of the analogue. Therefore, the 3,4-dimethyoxyphenyl group (ring C) in schwarzinicine A was replaced with a 2-furyl group (**Figure 3.1**). Furan ring is one of the aromatic ring options used in drug optimisation (Polêto, Rusu, Grisci, et al., 2018). Although it does not have the same valency as the benzene group in schwarzinicine A, isosteric replacement is a step to generate compounds with improved lipophilicity or metabolism (Lima & Barreiro, 2012). Lastly, it was found that up to two-carbon in an alkyl chain extended from the central amine was tolerable for analogue's vasorelaxation activity. This chemical structure was remained unchanged in synthesising schwarzinicine A analogues (F. K. Lee et al., 2021).

These modifications yield 1-(furan-2-yl)-*N*-phenethylpentan-3-amine as the novel analogue that exhibited promising vasorelaxant activity as compared to schwarzinicine A. The analogue was designated as PM20.

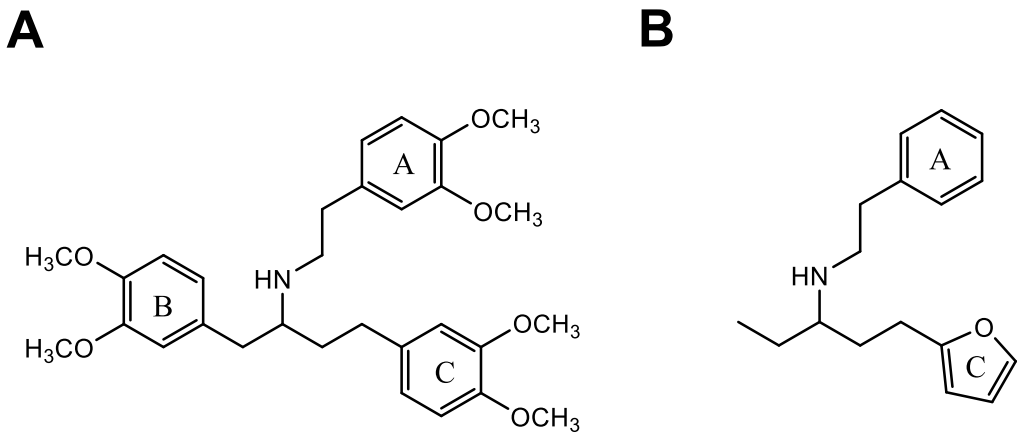


Figure 3.1 Chemical structures of (A) schwarzinicine A and (B) PM20.

3.1.2 Synthesis of 1-(furan-2-yl)-*N*-phenethylpentan-3-amine (PM20)

As illustrated in **Figure 3.2**, the synthesis of PM20 **(4)** was carried out first by converting the commercially available carboxylic acid **(1)** to Weinreb amide **(2)**. Then, the aminde reacted with ethylmagnesium bromide to produce ketone **(3)** with a yield of 71%. Preparation steps to yield intermediate **(2) (3)** are reported in detail in **Appendix C** (**Appendix C.1** and **Appendix C.2**).

To obtain PM20 **(4)** in **Figure 3.2**, reductive amination of ketone **(3)** was done with $NaBH(OAc)_3$ in the presence of phenethylamine. In the reductive amination step, phenethylamine (0.21 ml, 1.71 mM, 1.1 equivalent), $NaBH(OAc)_3$ (529.1 mg, 2.50 mM, 1.6 equivalent) and AcOH (0.09 ml, 1.57 mM, 1 equivalent) was added to a stirring solution of 1-(furan-2-yl)pentan-3-one **(3)** (231.9 mg, 1.52 mM, 1 equivalent) in $ClCH_2CH_2Cl$ (8 ml). The solution was stirred at room temperature for 24 hours before adding 6 ml of 1 M NaOH solution. The mixture was then extracted with EtOAc (3 × 10 ml). The combined organic layer was washed with brine and dried with Na_2SO_4 before concentrated *in vacuo*. The crude product was purified by centrifugal radial TLC using an eluent system of Et_2O-hexane (1:2). The product extracted was 1-(furan-2-yl)-*N*-phenethylpentan-3-amine (PM20) **(4)** as a colourless oil (182.8 mg, 0.71 mM). The yield of PM20 was 47%. The purity of 1-(furan-2-yl)-*N*-phenethylpentan-3-amine was at least 99% by NMR. PM20 was characterised by IR, HRESIMS, ^{1}H NMR (**Appendix C.3**) and ^{13}C NMR (**Appendix C.4**). IR (neat): ν_{max} 3331, 2928, 2867, 1454, 1143, 1007 cm^{-1}; HRESIMS *m/z* 258.1864 $[M + H]^+$ (calculated for $C_{17}H_{24}NO$, 258.1858). SAR study and synthesis of PM20 were performed by Dr Fong-Kai Lee, from the University of Nottingham Malaysia.

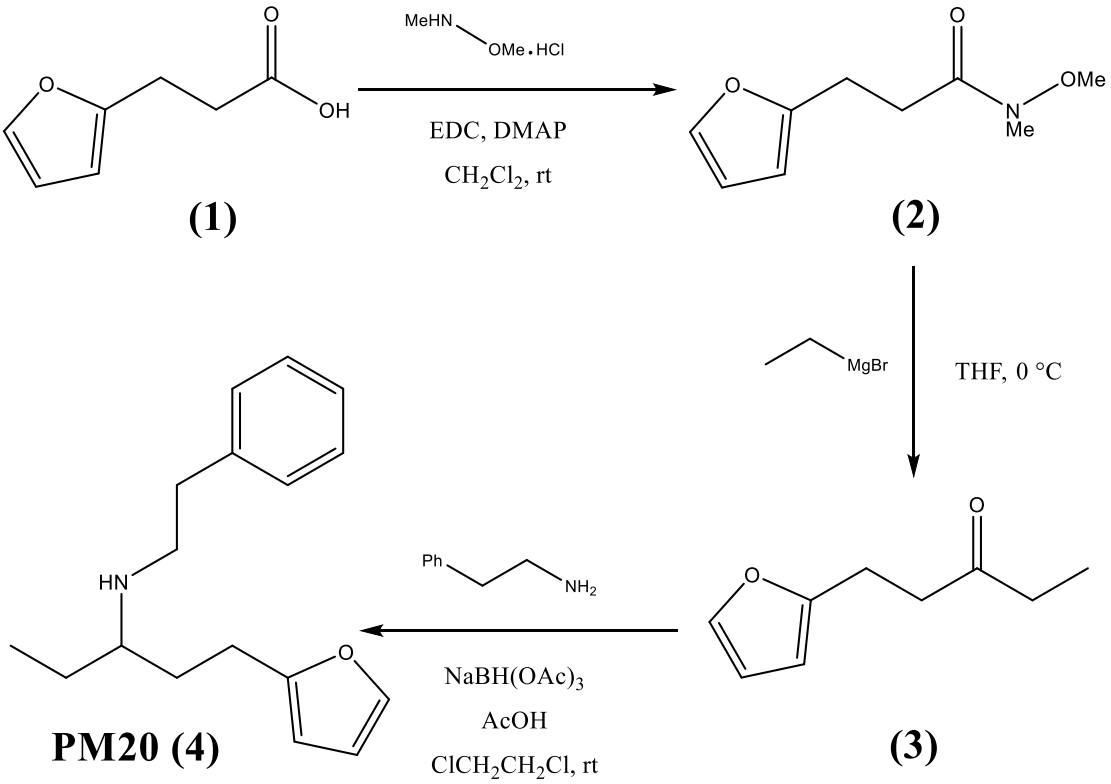


Figure 3.2 Synthesis of 1-(furan-2-yl)-N-phenethylpentan-3-amine (PM20).

3.2 Significance of study

PM20 is a novel phenylethylamine that shares similar pharmacophore with its parent compound, schwarzinicine A. However, its biological activity was not assessed previously and therefore unknown. Using the same technique employed in **Chapter 2** (FK244), this chapter aims to investigate the pharmacological effects and mechanism of action of PM20 in a VSM tissue (rat aorta) using the organ bath technique.

These were the objectives of this chapter:

i. To evaluate the drug-likeness of PM20 using Lipinski's Rule of Five and Veber's rule
ii. To investigate the effect of PM20 in rat isolated smooth muscles at basal and pre-contracted tone
iii. To elucidate the main vasorelaxation mechanisms of PM20 in rat arterial smooth muscle
iv. To study the relaxation effect of PM20 against different contractile agents
v. To assess the reversibility of PM20's inhibition against phenylephrine-induced contraction
vi. To assess the role of PM20 in mediating Ca^{2+} dynamics
vii. To evaluate the Ca^{2+}-inhibiting mechanism of PM20 using known Ca^{2+} channel blockers

3.3 Materials and methods

3.3.1 Analysis of physicochemical properties on PM20 and Ca^{2+} channel blockers

Drug-likeness prediction of PM20, nifedipine, Pyr3 and SKF-96365 was carried out as described in **section 2.3.1** using Lipinski's Rule of Five and Veber's rule.

3.3.2 Drugs and solutions

Drugs used in this chapter were the same as in **section 2.3.2**. Please refer to **Table 2.1** for the details of the drugs including their brands, solvent used, stock concentration, and final DMSO concentration in the organ bath. PM20 was dissolved in 100% DMSO to make up a stock solution of 100 mM. It was diluted in an identical manner as FK244. Normal and Ca^{2+}-free Krebs solutions were made as described in **section 2.3.2**.

3.3.3 Rat isolated tissue preparations

All experiments conducted in this chapter used smooth muscle tissues isolated from adult male SD rats (233–591 g; 2-3 months old) purchased from UPM, Malaysia (Ethics approval reference number: UNMC12). This study follows the UK Animals (Scientific Procedures) Act 1986, ARRIVE guidelines and complies with all international, national and institutional policies. The procedures used for isolation of aorta, trachea and bladder tissues have been described in **section 2.3.3.1**.

Pharmacological investigation of PM20 was not carried out in porcine pulmonary artery and bronchiole as the results obtained in FK244 have shown that phenylethylamine alkaloids exhibited more pronounced effects in rat isolated tissues.

3.3.4 Organ bath setup

The aortic rings, tracheal rings and bladder strips were mounted to the organ bath assembly and equilibrated as described in **section 2.3.4**.

3.3.5 Isometric tension recordings

The experiment protocols in this section were adapted from **section 2.3.5**.

3.3.5.1 Effect of PM20 on rat isolated tissues at basal tension and raised muscle tone

Cumulative CRCs to vehicle control (DMSO) or PM20 (0.1 nM to 100 μM) were constructed in at basal tone. In another series of experiments, the same method was repeated in rat isolated aorta, bladder and trachea, with prior pre-contraction using 100 nM phenylephrine (aorta) or 1 μM carbachol (bladder and trachea). Once a stable tone was achieved, each concentration was added either at an interval of 7 minutes or after the responses have plateaued if there was any change in tension.

3.3.5.2 Role of endothelium on PM20-induced relaxation

Endothelium-denuded aortic rings were prepared and validated as described in **section 2.3.5.3**. Endothelium-denuded aortic rings were pre-contracted with phenylephrine (100 nM). Once a stable tone was reached, cumulative CRCs to vehicle control or PM20 (0.1 nM to 100 μM) were constructed.

3.3.5.3 Role of NO in PM20-induced relaxation

Aortic rings were pre-incubated with L-NAME (100 μM) for 30 minutes, followed by pre-contraction with phenylephrine (100 nM). Next, cumulative CRCs to PM20 (0.1 nM to 100 μM) were constructed. In control group, vehicle control (purified water) was used to pre-incubate the aortic rings and experiment was repeated in the same manner.

3.3.5.4 Role of cAMP and cGMP in PM20-induced relaxation

Aortic rings were pre-incubated with forskolin (10 nM) or ODQ (1 μM) for 30 minutes, followed by pre-contraction with a single concentration of phenylephrine (100 nM – 3 μM). Then, cumulative CRCs to PM20 (0.1 nM to 100 μM) were constructed. In control group, vehicle control (DMSO) was used to pre-incubate the aortic rings and experiment was repeated in the same manner.

3.3.5.5 Role of α-, β- adrenoceptors in PM20-induced relaxation

Aortic rings were pre-incubated with prazosin (10 μM), rauwolscine (10 μM) and propranolol (3 μM) for 30 minutes. Then, KCl (60 mM) was used to pre-contract prazosin- and rauwolscine-treated aortic rings. For propranolol-treated aortic rings, a single concentration of phenylephrine (100 nM – 3 μM) was used for pre-contraction. When the response has stabilised, cumulative CRCs to PM20 (0.1 nM to 100 μM) were constructed. In control groups, vehicle control (methanol or purified water) was used to pre-incubate the aortic rings and experiment was repeated in the same manner.

3.3.5.6 Role of K^+ channels in PM20-induced relaxation

Aortic rings were pre-incubated with 4-AP (1 mM), TEA (5 mM), $BaCl_2$ (1 mM) or glibenclamide (10 μM) for 30 minutes. Then, a single concentration of phenylephrine (100 nM – 3 μM) was added into the bath to pre-contract the aortic rings. After the contraction has stabilised, cumulative CRCs to PM20 (0.1 nM to 100 μM) were constructed. In control groups, vehicle control (DMSO or purified water) was used to pre-incubate the aortic rings and experiment was repeated in the same manner.

3.3.5.7 Effect of PM20 on aorta pre-contracted with different contractile agents

Aortic rings were pre-contracted with either phenylephrine (100 nM), KCl (60 mM), or U46619 (300 nM). After the contraction has stabilised, cumulative CRCs to vehicle control (DMSO) or PM20 (0.1 nM to 100 μM) were constructed.

3.3.5.8 Effect of PM20 on the contractile response induced by different contractile agents

Aortic rings were pre-incubated with vehicle control (DMSO) or PM20 (10 μM, 30 μM, 100 μM) for 30 minutes. These three concentrations were chosen based on PM20 cumulative CRCs in pre-contracted aortic rings (**Figure 3.5B**), where they achieved maximum tissue relaxation (EC_{90-100}) in the aortic tissues. Then, cumulative CRCs of phenylephrine (0.1 nM to 300 μM), KCl (10 μM to 300 mM), serotonin (0.1 nM to 300 μM), and U46619 (0.1 nM to 3 μM) were constructed.

3.3.5.9 Reversibility of PM20's inhibition against phenylephrine-induced contraction

Aortic rings were pre-treated either with vehicle control (DMSO) or PM20 (10 μM) for 30 minutes before the addition of a single concentration of phenylephrine (10 μM). Then, the aortic rings were thoroughly rinsed with Krebs solution and left for 30 minutes to return to a stable basal tone. Subsequently, the tissues were challenged with another addition of phenylephrine (10 μM).

3.3.5.10 Effect of PM20 compared to the CRCs of Ca^{2+} channel blockers in rat isolated aorta

To compare the vasorelaxation profiles of PM20 and known Ca^{2+} channel blockers, cumulative CRCs of PM20 (**Figure 3.5B**) was analysed together with other Ca^{2+} channel blockers (2-APB, HC-070, nifedipine, Pyr3, Pyr6, SKF-96365 and verapamil) in **section 2.4.12**.

3.3.5.11 Effect of PM20 on intracellular Ca^{2+}-induced vasoconstriction

Aortic rings were pre-incubated with PM20 (10 μM) for 30 minutes in Ca^{2+}-free Krebs supplemented with 1 mM EGTA. Subsequently, a single concentration of either phenylephrine (10 μM), KCl (60 mM) or U46619 (300 nM) was added into the bath for 1 hour to evoke intracellular Ca^{2+}-induced contraction. This series of experiments were repeated in Ca^{2+}-containing Krebs (normal Krebs). The results obtained with PM20 were analysed together with the results of vehicle control (DMSO) in **section 2.4.14**.

3.3.5.12 Effect of PM20 on contractile responses to Ca^{2+} re-introduction

Aortic rings were pre-incubated with vehicle control (DMSO) or PM20 (10 μM, 30 μM, 100 μM) in Ca^{2+}-free Krebs solution for 30 minutes. Next, KCl (60 mM) was added for 15 minutes to induce plasma membrane depolarisation. $CaCl_2$ was then cumulatively

re-introduced to the bath (1 µM to 3 mM). The results obtained with PM20 were analysed together with the results of Ca^{2+} re-introduction in the presence of various Ca^{2+} channel blockers (2-APB (100 µM), Pyr3 (10 µM), Pyr6 (10 µM), SKF-96365 (10 µM), nifedipine (10 µM) and verapamil (10 µM)) in **section 2.4.15**.

3.3.5.13 Effect of Ca^{2+} channel blockers on PM20-induced relaxation

Aortic rings were pre-incubated with a range of Ca^{2+} channel blockers for 30 minutes. The Ca^{2+} channel blocker used in pre-incubation was either 2-APB (100 µM), nifedipine (10 µM), Pyr3 (10 µM), Pyr6 (10 µM), SKF-96365 (10 µM), or verapamil (10 µM). Following pre-contraction with a single concentration of phenylephrine (300 nM – 10 µM), cumulative CRCs to PM20 (0.1 nM to 100 µM) were carried out. In control groups, vehicle control (DMSO or purified water) was used to pre-incubate the aortic rings and experiment was repeated in the same manner.

3.3.6 Data analysis

Similar methods for data analysis were used as described in **section 2.3.6**. All data were presented as mean ± SEM of *n* number of separate animals. CRCs of compounds were fitted using a non-linear regression curve with a three-parameter equation in GraphPad Prism. E_{max} and EC_{50} were derived from the curve fit, and EC_{50} was converted into pEC_{50}. When the response has not plateaued, E_{max} was taken as the response produced at the highest concentration tested, while pEC_{50} was not routinely calculated except for **Figure 3.5**, **Figure 3.9**, **Figure 3.11**, **Figure 3.14**. They were calculated to make relative comparison with those regression curve fit that has plateaued. Statistical analysis was performed using unpaired Student's *t*-test to compare between control group and treatment group (**Figure 3.4**, **Figure 3.5B** – **D**, **Figure 3.7**, **Figure 3.8**, **Figure 3.9**, **Figure 3.10**, **Figure 3.11B** – **D**, **Figure 3.17**). One-way ANOVA followed by Bonferroni's (**Figure 3.6C**, **Figure 3.14**), Dunnett's (**Figure 3.12**, **Figure 3.16**), or Tukey's (**Figure 3.5A**, **Figure 3.11A**) post hoc test was also used to compare the effects of three or more groups. Two-way ANOVA with Tukey's post hoc test was used to analyse data in **Figure 3.13** and **Figure 3.15**. Results with $p < 0.05$ were considered statistically significant. Individual significance was indicated in asterisk symbol in table, where '****' shows $p < 0.0001$, '***' shows $p < 0.001$, '**' shows $p < 0.01$ and '*' shows $p < 0.05$.

3.4 Results

3.4.1 Physicochemical properties of PM20 obey Lipinski's and Veber's rule analysis

Evaluation of PM20's drug-likeness using Lipinski's and Veber's rule revealed that it obeys all the set criteria. PM20 has the simplest structure and correspondingly the lowest MW among all compounds, including nifedipine, SKF-96365 and Pyr3 (**Figure 3.3**, **Table 3.1**). Besides, its number of HBD and HBA were well within the limit of 5 and 10 in respective criteria. LogP value of PM20 was close to 5, second to Pyr3, which is the highest among the compounds compared. PM20 possesses 8 rotatable bonds and has the smallest tPSA compared to other compounds, which further showed that it satisfied Veber's drug-likeness analysis.

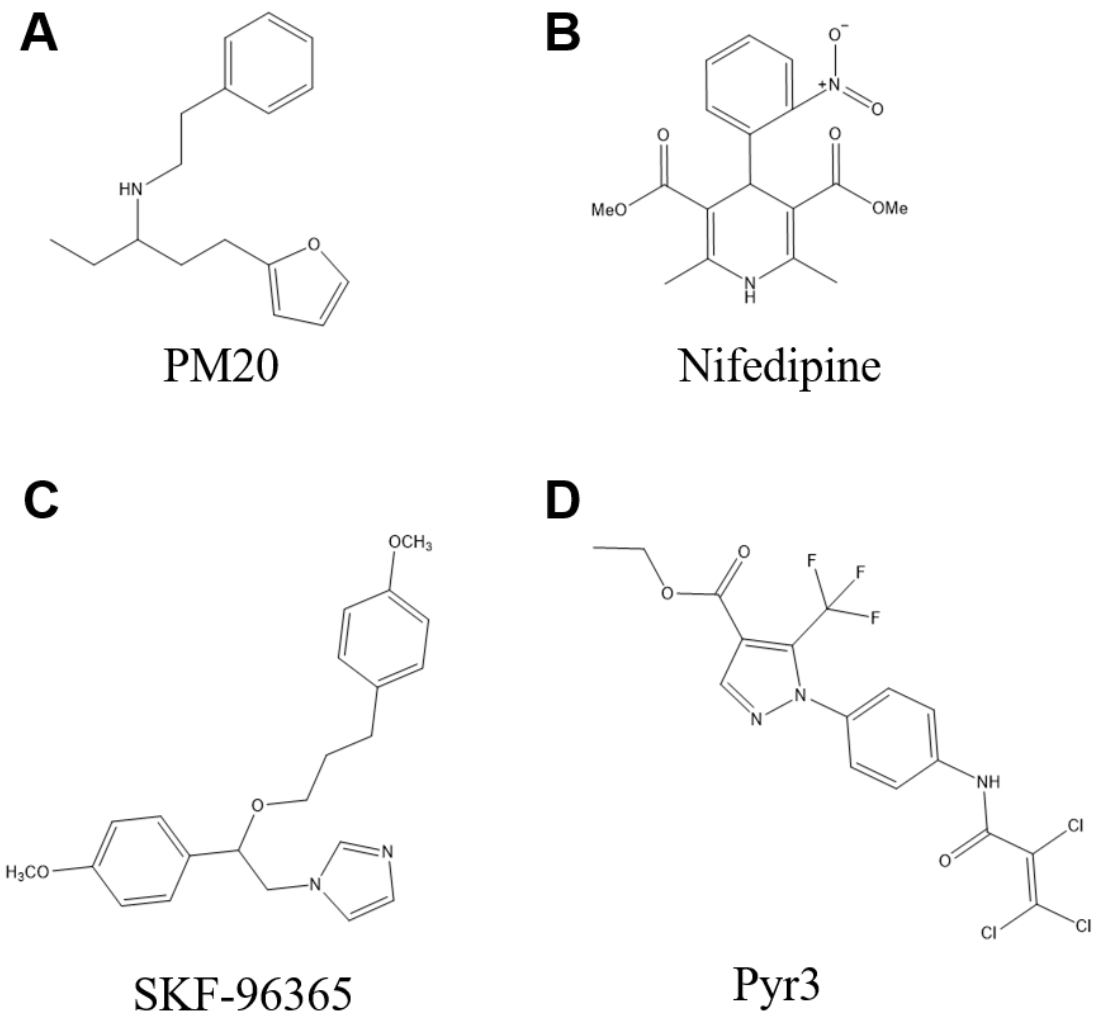


Figure 3.3 Chemical structures of (A) PM20, (B) nifedipine, (C) SKF-96365 and (D) Pyr3.

Table 3.1 Chemical structure and physicochemical analysis of PM20, nifedipine, SKF-96365 and Pyr3 using Lipinski's Rule of Five and Veber's rule.

Compound	PM20	Nifedipine	SKF-96365	Pyr3
Lipinski's Rule of Five				
Hydrogen bond donor (HBD ≤ 5)	1	1	0	1
Hydrogen bond acceptor (HBA ≤ 10)	2	5	2	5
Molecular weight (MW < 500 Da)	257.38	346.12	366.19	454.98
Partition coefficient (LogP ≤ 5)	4.07	3.31	3.94	4.59
Lipinski's rule violations	0	0	0	0
Veber's Rule				
Rotatable bond (≤10)	8	6	10	8
Topological polar surface area (tPSA ≤ 140 Å^2)	25.17	107.77	45.51	72.70
Veber's rule violations	0	0	0	0

3.4.2 PM20 did not induce tissue contraction at basal tone but relaxed pre-contracted smooth muscle tissues

When the tissues were set with only passive tension, cumulative presence of PM20 did not induce significant contraction or relaxation in rat isolated aorta (E_{max}: vehicle control: 5.8 ± 2.5%; PM20: 6.8 ± 2.6%; p = 0.8021) (**Figure 3.4A**), bladder (E_{max}: vehicle control: 3.3 ± 1.8%; PM20: 11.8 ± 3.1%; p = 0.0528) (**Figure 3.4B**) and trachea (E_{max}: vehicle control: 5.4 ± 4.4%; PM20: -9.9 ± 5.5%; p = 0.0827) (**Figure 3.4C**) compared to vehicle control.

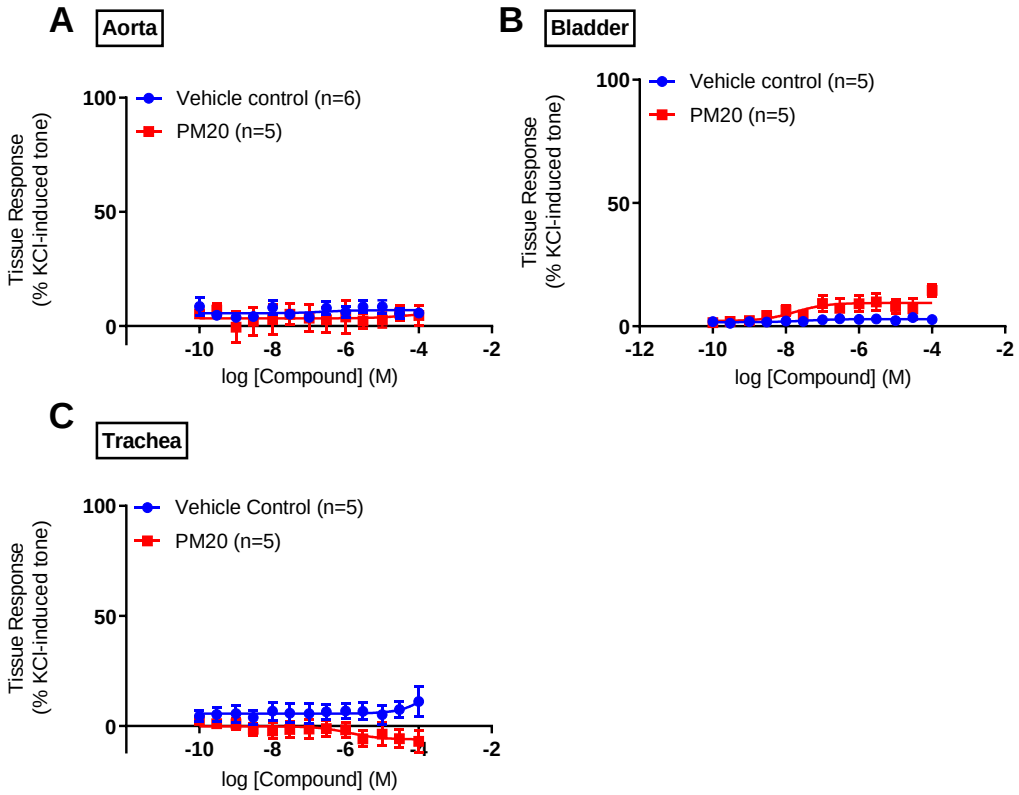


Figure 3.4 Effect of PM20 on rat isolated (A) aorta, (B) bladder and (C) trachea at the basal tone. *Tissue responses have been expressed as the percentage of KCl-induced tone. Data are shown as the mean ± SEM of 5 to 6 animals. Abbreviation: KCl, potassium chloride.*

In another series of experiments, the smooth muscle tissues were pre-contracted with contractile agonists. Cumulative addition of PM20 elicited relaxation in all smooth muscle tissues tested (**Figure 3.5A**). PM20 managed to induce significant relaxation compared to vehicle control in all the smooth muscle tissues (**Table 3.2**) namely the aorta (**Figure 3.5B**), bladder (**Figure 3.5C**) and trachea (**Figure 3.5D**).

By comparing the E_{max} as stated in **Table 3.2**, the maximum tissue relaxation induced by PM20 in all three tissues was not significantly different from each other (a vs b; p = 0.2849; a vs t; p = 0.9424; b vs t; p = 0.1709). PM20 was more potent in aorta (a) when compared to bladder (b) (a vs b; $p < 0.0001$) and trachea (t) (a vs t; p = 0.0002). However, its potency was similar between bladder and trachea (b vs t; p = 0.5238). The comparison between aorta, bladder and trachea was made using one-way ANOVA followed by Tukey's post hoc test. pEC_{50} of PM20 in bladder and trachea was an estimation from non-plateaued CRCs, they were used in statistical analysis to compare with pEC_{50} of PM20 in aorta.

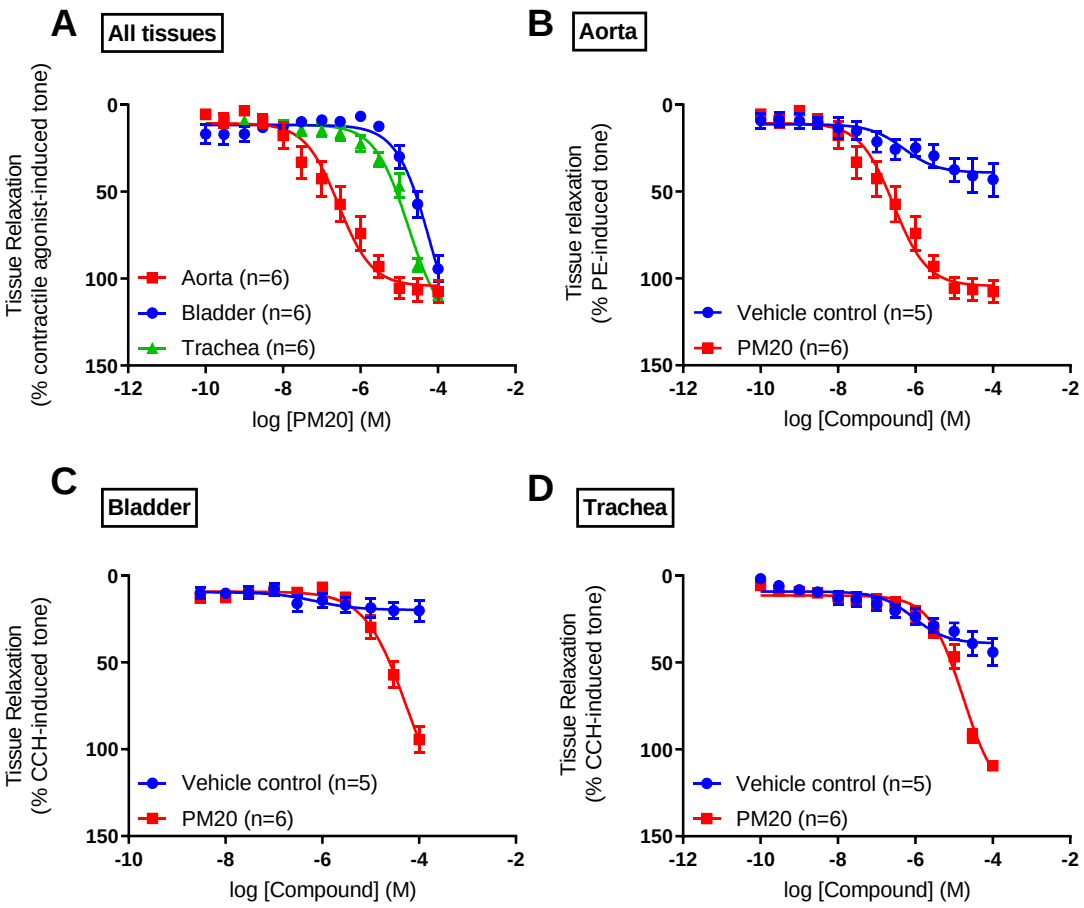


Figure 3.5 Effect of PM20 in (A) rat isolated aorta, bladder and trachea pre-contracted with phenylephrine or carbachol. *Relaxation effect of PM20 compared to vehicle control in (B) aortic rings, (C) bladder strips and (D) tracheal rings. Aortic tissue responses have been expressed as the percentage of phenylephrine-induced tone while bladder and tracheal tissues responses have been expressed as the percentage of carbachol-induced tone. Data are shown as the mean ± SEM of 5 to 6 animals. Abbreviations: CCH, carbachol; PE, phenylephrine.*

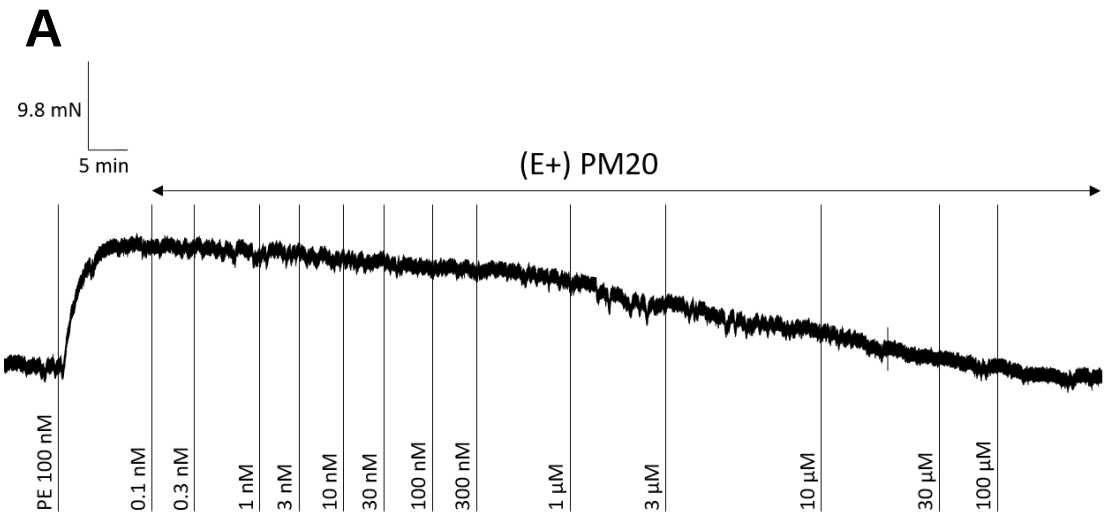
Table 3.2 Comparison of the maximum tissue response (E_{max}) and potency (pEC_{50}) of vehicle and PM20 in rat isolated aorta, bladder and trachea after being induced contraction with their respective contractile agents.

Tissue	Treatment	E_{max} (%)	pEC_{50}
Aorta	Vehicle control	43.1 ± 9.4	ND
	PM20	106.8 ± 6.1 *** (p = 0.0002)	6.69 ± 0.32
Bladder	Vehicle control	20.2 ± 5.9	ND
	PM20	94.4 ± 7.3 **** (p < 0.0001)	4.74 ± 0.20 †
Trachea	Vehicle control	44.1 ± 7.6	ND
	PM20	109.4 ± 1.8 **** (p < 0.0001)	5.08 ± 0.11 †

Unpaired Student's test was used to compare the E_{max} between vehicle and PM20 treatment in aorta, bladder, and trachea. Individual p-values were stated in the respective columns. Data are shown as mean ± SEM of 5 to 6 animals. Abbreviation: ND, not determined. †Estimated pEC_{50} was calculated based on maximum tissue response.

3.4.3 PM20 induced similar relaxation in endothelium-intact (E+) and -denuded (E-) rat isolated aortae

To determine if PM20-induced vasorelaxation is endothelium-dependent, the reduction of vascular tone by PM20 was compared between endothelium-intact and -denuded aortic rings (**Figure 3.6C**). Aortic relaxation in **Figure 3.5B** was incorporated in **Figure 3.6C** to depict the effect of endothelium in PM20-induced vasorelaxation. Cumulative addition of PM20 has achieved significant relaxation in both endothelium-intact (E+, 'Aorta' in **Table 3.2**) and denuded (E-) aortic tissues compared to vehicle control (E-, E_{max}: vehicle control: 26.7 ± 3.9%; PM20: 105.4 ± 10.3%; $p < 0.0001$). Moreover, vasorelaxation profile of PM20 was not altered in the presence or absence of endothelium (E_{max}: E+: 106.8 ± 6.1%; E-: 105.4 ± 10.3%; $p > 0.9999$; pEC_{50}: E+: 6.69 ± 0.32; E-: 6.44 ± 0.26; $p > 0.9999$).Statistical analysis was done using one-way ANOVA with Bonferroni's post-hoc test. Representative tracing recordings of PM20 cumulative CRCs were depicted in **Figure 3.6A** and **B**. Data for vehicle controls are shared between PM20 and FK244 (**section 2.4.4**), therefore, representative tracing recordings for vehicle controls are not shown.



(Figure continued on the next page)

Figure 3.6 Effect of PM20 in endothelium-intact (E+) and -denuded (E-) aortae. *Representative tracings of PM20 CRCs in (A) E+ aorta and (B) E- aorta, as well as (C) cumulative CRCs of vehicle control and PM20 in E+ and E- rat isolated aortae. Aortic tissue relaxation has been expressed as the percentage of phenylephrine-induced tone. Data are shown as the mean ± SEM of 5 to 6 animals. Abbreviation: PE, phenylephrine.*

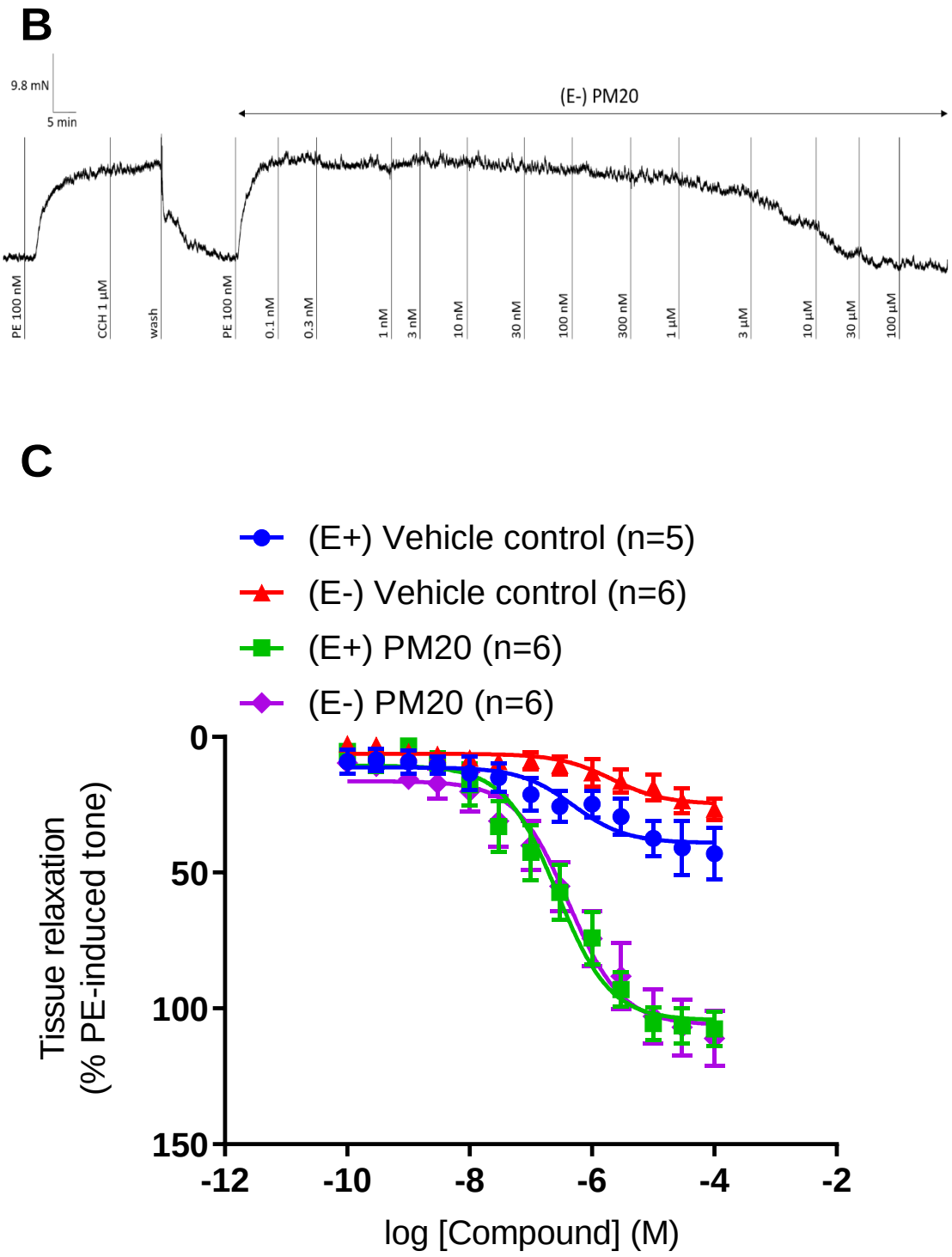


Figure 3.6 Effect of PM20 in endothelium-intact (E+) and -denuded (E-) aortae. ***Representative*** *tracings of PM20 CRCs in (A) E+ aorta and (B) E- aorta, as well as (C) cumulative CRCs of vehicle control and PM20 in E+ and E- rat isolated aortae. Aortic tissue relaxation has been expressed as the percentage of phenylephrine-induced tone. Data are shown as the mean ± SEM of 5 to 6 animals. Abbreviation: PE, phenylephrine. (continued)*

3.4.4 Incubation with L-NAME did not suppress PM20-induced relaxation

To exclude the effect endothelium-derived NO on PM20-induced relaxation, L-NAME was used to incubate the aortic rings. Pre-incubation with L-NAME did not alter relaxation caused by PM20 (E_{max}: vehicle control: 116.7 ± 7.6%; L-NAME: 116.3 ± 4.0%; p = 0.9585) (**Figure 3.7**). The potency of PM20 was similar in vehicle control- and L-NAME-treated tissues (pEC_{50}: vehicle control: 5.73 ± 0.28; L-NAME: 5.67 ± 0.06; p = 0.7484). Statistical analysis was done with unpaired Student's *t*-test.

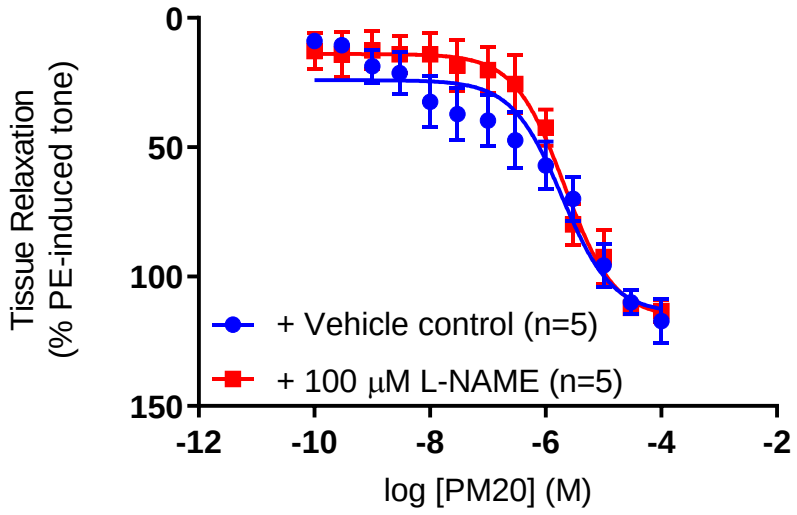


Figure 3.7 Effect of pre-exposure of L-NAME on PM20-induced vasorelaxation. *Tissue responses have been expressed as the percentage of phenylephrine-induced tone. Data are shown as the mean ± SEM of 5 animals. Abbreviations: L-NAME, N^G-nitro-L-arginine methyl ester; PE, phenylephrine.*

3.4.5 PM20-induced relaxation was not affected by forskolin and ODQ

PM20-induced vasorelaxation was unaffected in terms of its efficacy and potency despite the presence of forskolin (E_{max}: vehicle control: 127.7 ± 3.5%; forskolin: 128.3 ± 3.1%; p = 0.1761; pEC_{50}: vehicle control: 6.12 ± 0.28; forskolin: 5.93 ± 0.11; p = 0.5365) (**Figure 3.8A**). Furthermore, the suppressant effect of ODQ on sGC did not have significant effect on PM20-induced relaxation (E_{max}: vehicle control: 110.6 ± 3.5%; ODQ: 1147 ± 3.3%; p = 0.4280; pEC_{50}: vehicle control: 5.90 ± 0.11; ODQ: 5.68 ± 0.10; p = 0.1647) (**Figure 3.8B**). Statistical analysis was done with unpaired Student's *t*-test.

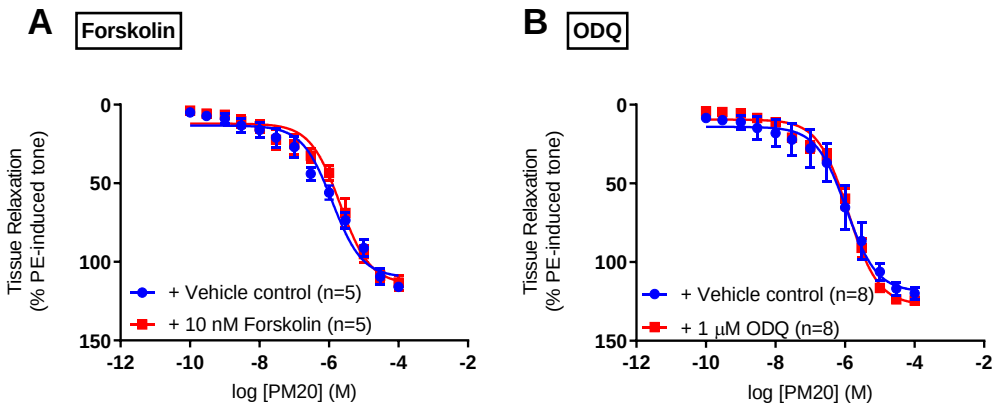


Figure 3.8 Effect of cyclic nucleotides against PM20-induced vasorelaxation. *Tissues were pre-treated with (A) forskolin and (B) ODQ for 30 minutes before the construction of cumulative CRCs to PM20. Tissue responses have been expressed as the percentage of phenylephrine-induced tone. Data are shown as the mean ± SEM of 5 to 8 animals. Abbreviation: PE, phenylephrine.*

3.4.6 PM20-induced relaxation was not influenced by α- and β-adrenoceptor antagonists

Prazosin, rauwolscine, and propranolol were used to investigate the role of adrenoceptors in PM20's vasorelaxation mechanism. The presence of prazosin did not exert any effect on the maximum tissue relaxation induced by PM20 (E_{max}: vehicle control: 110.3 ± 6.0%; prazosin: 113.2 ± 4.8%; p = 0.7237; estimated pEC_{50}: vehicle control: 5.86 ± 0.30; prazosin: 5.59 ± 0.23; p = 0.5045) (**Figure 3.9A**). Similarly, α_2-adrenoceptor inhibited by rauwolscine did not affect the maximum relaxation and potency elicited by PM20 (E_{max}: vehicle control: 115.1 ± 5.4%; rauwolscine: 108.7 ± 1.9%; p = 0.2956; estimated pEC_{50}: vehicle control: 5.27 ± 0.06; rauwolscine: 5.17 ± 0.15; p = 0.5678) (**Figure 3.9B**). When the aortic rings were pre-incubated with propranolol, the differences in magnitude of PM20-induced relaxation and its potency in eliciting relaxation were insignificant compared to pre-incubation with vehicle control (E_{max}: vehicle control: 116.7 ± 7.6%; propranolol: 114.8 ± 6.4%; p = 0.8529; pEC_{50}: vehicle control: 5.76 ± 0.28; propranolol: 6.36 ± 0.25; p = 0.1478) (**Figure 3.9C**). Statistical analysis was performed with unpaired Student's *t*-test.

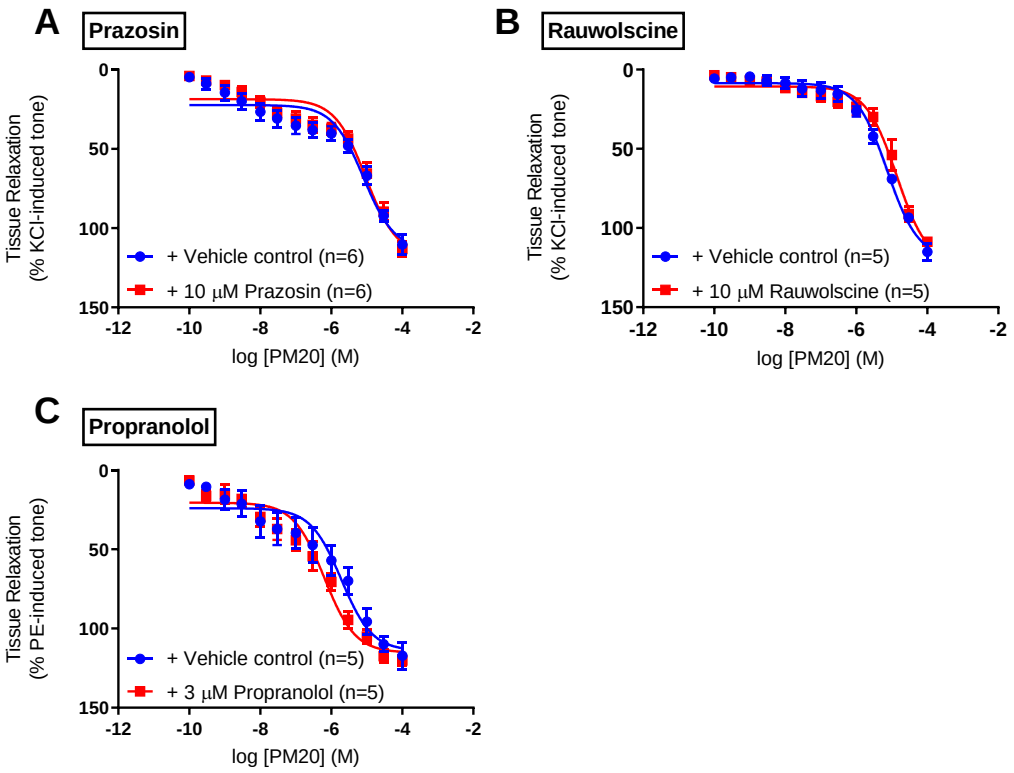


Figure 3.9 Effect of adrenoceptor-antagonists on PM20-induced vasorelaxation in rat aortae. *Aortic rings were pre-incubated with (A) prazosin, (B) rauwolscine, and (C) propranolol for 30 minutes before the construction of cumulative CRCs to PM20. Tissue responses have been expressed as the percentage of KCl-induced tone for prazosin- and rauwolscine-treated aortic rings. For propranolol-treated aortic rings, tissue responses have been expressed as the percentage of phenylephrine-induced tone. Data are shown as the mean ± SEM of 5 to 6 animals. Abbreviations: KCl, potassium chloride; PE, phenylephrine.*

3.4.7 PM20-induced relaxation was not affected by K^+ channel blockers

K^+ channel blockers such as 4-AP (K_v channel blocker), $BaCl_2$ (K_{ir} channel blocker), glibenclamide (K_{ATP} channel blocker) and TEA (K_{Ca} channel blocker) were used to determine whether the vascular effect of PM20 involves the opening of K^+ channels. Presence of 4-AP (**Figure 3.10A**), $BaCl_2$ (**Figure 3.10B**), glibenclamide (**Figure 3.10C**) and TEA (**Figure 3.10D**) had no significant effect on the relaxation profile of PM20. The values of E_{max} and pEC_{50} for PM20-induced relaxation in the presence of vehicle controls and all four K^+ channel blockers are summarised in **Table 3.3**.

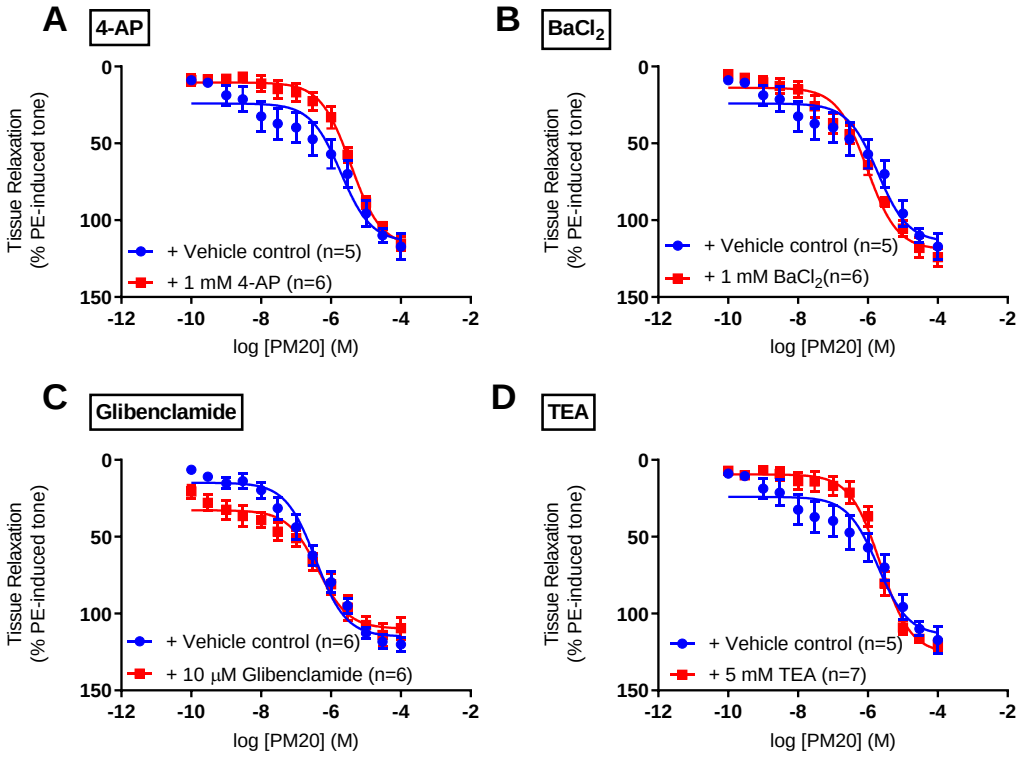


Figure 3.10 Effect of K^+ channel blockers on PM20-induced relaxation. *Cumulative CRCs to PM20 were carried out after tissues were pre-incubated with a single dose of (A) 4-AP, (B) $BaCl_2$, (C) glibenclamide and (D) TEA. Tissue responses have been expressed as the percentage of phenylephrine-induced tone. Data are shown as the mean ± SEM of 6 animals. Abbreviations: 4-AP, 4-aminopyridine, $BaCl_2$, barium chloride, PE, phenylephrine, TEA, tetraethylammonium chloride.*

Table 3.3 Maximum tissue relaxation (E_{max}) and potency (pEC_{50}) of PM20-induced vasorelaxation with prior treatment of K^+ blockers in rat isolated aortic rings.

Treatment	E_{max} (%)	pEC_{50}
Vehicle control (H_2O)	116.7 ± 7.6	5.76 ± 0.28
+ 1 mM 4-AP	117.3 ± 1.9 (p = 0.9997)	5.46 ± 0.07 (p = 0.3903)
+ 1 mM $BaCl_2$	119.6 ± 7.4 (p = 0.9605)	6.12 ± 0.16 (p = 0.2762)
+ 5 mM TEA	126.9 ± 1.8 (p = 0.3673)	5.64 ± 0.08 (p = 0.8967)
Vehicle control (DMSO)	117.1 ± 5.4	6.50 ± 0.23
+ 10 µM Glibenclamide	111.2 ± 6.5 (p = 0.5074)	6.40 ± 0.21 (p = 0.7564)

One-way ANOVA followed by Dunnett's post hoc test was used to compare between 4-AP, $BaCl_2$, TEA, with vehicle control (H_2O). Unpaired Student's t-test was used to compare between glibenclamide with vehicle control (DMSO). Individual p-values were stated in the respective columns. Data are shown as mean ± SEM of 5 to 7 animals.

3.4.8 PM20 was the most potent in relaxing phenylephrine-induced contraction

PM20 displayed distinct relaxation profile with different contractile agents (**Figure 3.11A**). PM20 generated the highest relaxation effect in aortae pre-contracted with KCl, however, the maximum relaxation was not significantly higher compared to phenylephrine-induced contraction (p = 0.6138) and U46619-induced contraction (p = 0.0643). Moreover, there was also no difference in terms of the efficacy between phenylephrine- and U46619-induced contraction (p = 0.2796).

On the other hand, PM20 exhibited the highest potency in aortic rings pre-contracted with phenylephrine, followed by U46619 (p = 0.0060 vs phenylephrine) and lastly KCl (p = 0.0010 vs phenylephrine) (**Figure 3.11A**). The potency of PM20 in relaxing phenylephrine-contracted aortae was approximately 33.9-fold higher than relaxing KCl-contracted aortae. It was also about 14.8-fold more potent compared to the potency in U46619-contracted aortae. The pEC_{50} of PM20 was similar in U46619- and KCl-contracted aortae (p = 0.5185). Statistical analysis was done with one-way ANOVA with Tukey's post hoc test by comparing the effects between all three groups.

In general, the relaxation profile of PM20 in aortic rings pre-contracted with KCl and U46619 showed similar trend. PM20-induced relaxation did not plateau in KCl- or U46619-contracted tissues, therefore, the potency was estimated. It is worth noting that at 10 µM of PM20, the relaxation has reached its maximum in phenylephrine-contracted aortae, while it only achieved half-maximal relaxation in U46619-contracted aortae (**Figure 3.11A**).

Results also showed that PM20 effectively induced vasorelaxation in all groups compared to vehicle control (**Figure 3.11B – D**). The values of E_{max} and pEC_{50} for vehicle control- and PM20-induced vasorelaxation in the presence of phenylephrine, KCl and U46619 are summarised in **Table 3.4**.

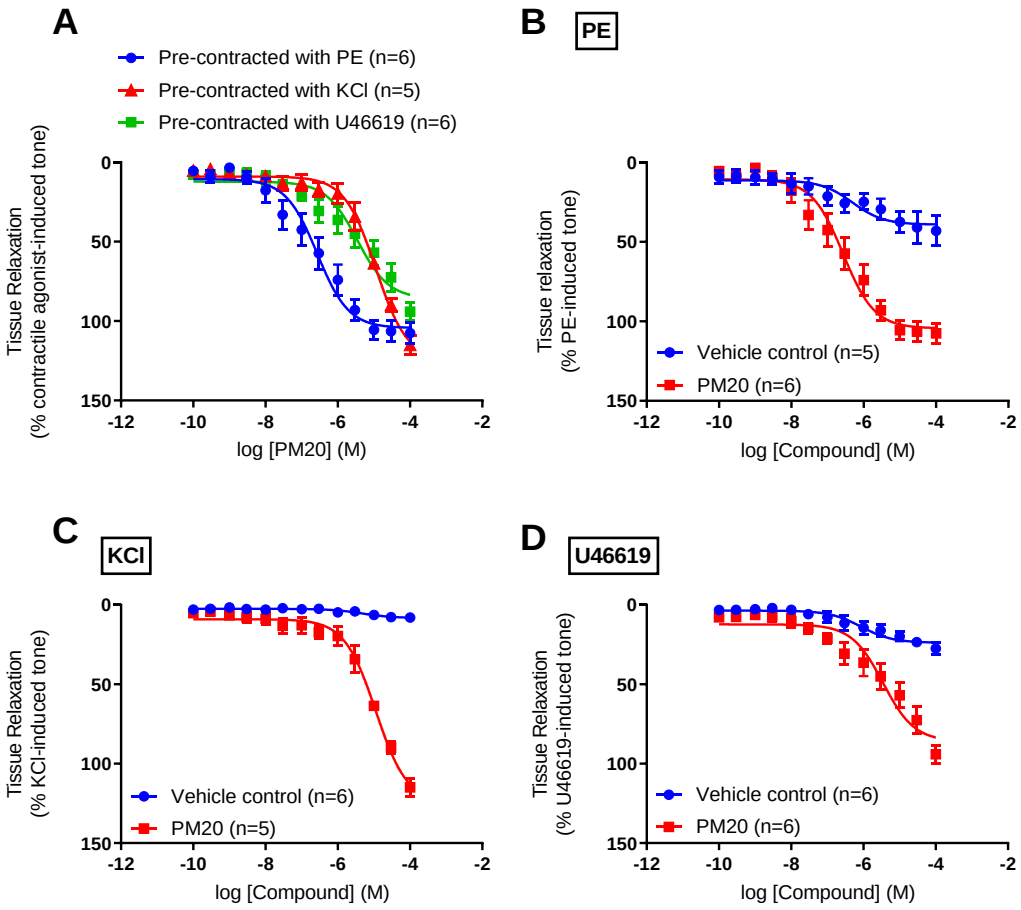


Figure 3.11 Effect of increasing concentration of PM20 on aortic rings pre-contracted with (A) phenylephrine, KCl and U46619. *Cumulative CRCs of PM20 with vehicle control when pre-contracted with (B) phenylephrine, (C) KCl and (D) U46619. Tissue responses were expressed as the percentage of contractile agent-induced contraction. Data are shown as the mean ± SEM of 5 to 6 animals. Abbreviations: KCl, potassium chloride; PE, phenylephrine.*

Table 3.4 Maximum response (E_{max}) and pEC_{50} values of vehicle control and PM20 derived from the respective CRCs with phenylephrine, KCl or U46619 as the pre-contractile agonist.

Contractile agonist	Treatment	E_{max} (%)	pEC_{50}
Phenylephrine	Vehicle control	43.1 ± 9.4	ND
	PM20	106.8 ± 6.1 *** (p = 0.0002)	6.69 ± 0.32
KCl	Vehicle control	8.0 ± 2.6	ND
	PM20	114.9 ± 5.7 **** (p < 0.0001)	5.16 ± 0.06 †
U46619	Vehicle control	27.4 ± 3.4	ND
	PM20	94.0 ± 5.6 **** (p < 0.0001)	5.52 ± 0.18 †

Unpaired Student's t-test was used to compare phenylephrine, KCl or U46619 with their respective vehicle controls. Individual p-values were stated in the respective columns. Data are shown as mean ± SEM of 5 to 6 animals. Abbreviations: KCl, potassium chloride; ND, not determined. †Estimated pEC_{50} was calculated based on maximum tissue response.

3.4.9 PM20 attenuated maximum tissue contraction induced by phenylephrine, KCl and serotonin but not U46619

Pre-treatment of PM20 at 10 μM has lowered the potency of phenylephrine, which was shown as the rightward shift in phenylephrine's CRC. However, the E_{max} of phenylephrine-induced contraction was unaffected. When the pre-incubation concentration of PM20 was increased to 30 μM and 100 μM, it suppressed the maximum contractile response of phenylephrine (**Figure 3.12A**). The potency of phenylephrine was not determined for pre-incubation of 30 μM and 100 μM PM20 because the tissue contraction has not plateaued.

PM20 significantly attenuated the E_{max} of KCl in a concentration-dependent manner (**Figure 3.12B**). The potency was not determined as the maximum tissue contraction has not plateaued in all the groups.

Our findings have shown that 10 μM of PM20 attenuated the E_{max} of serotonin-induced contraction in the aortic tissues (**Figure 3.12C**). With a higher pre-incubation concentration of PM20 at 30 μM and 100 μM, it diminished the maximum contractile response of serotonin compared to vehicle control. The potency of serotonin was not altered with pre-exposure to all concentrations of PM20.

E_{max} and pEC_{50} of U46619 was unaltered in the presence of PM20 at all concentrations tested (**Figure 3.12D**).

To highlight the overt effect of PM20 on phenylephrine-induced contraction, 10 μM of PM20 has reduced the potency of phenylephrine by ~81.3 fold to the right. This level of suppression was not observed in serotonin or U46619-induced contraction, where only ~1.3 to 1.6-fold shift in potency was observed. The E_{max} and pEC_{50} values of contractile agent-induced contraction are summarised in **Table 3.5**.

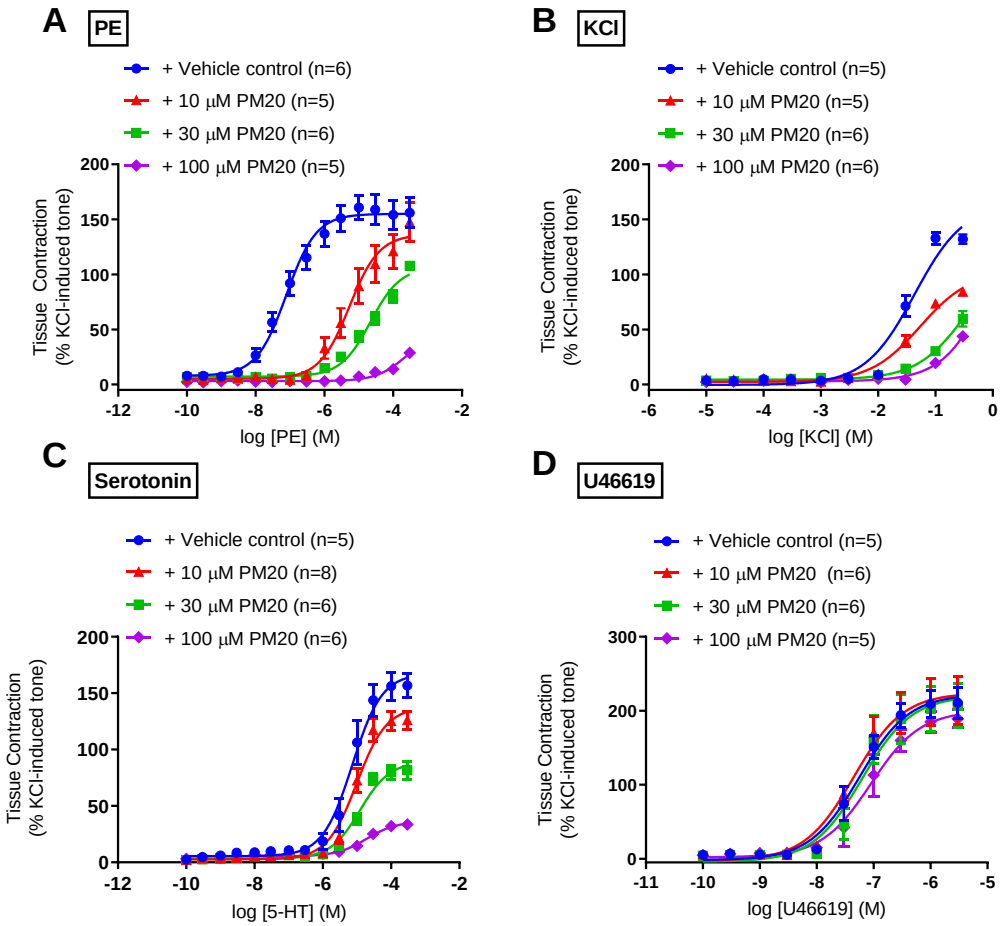


Figure 3.12 Effect of PM20 treatment in the aortic rings on the vascular contraction elicited by the contractile agents. *Cumulative CRCs to (A) phenylephrine, (B) KCl, (C) serotonin and (D) U46619 was demonstrated in the presence of PM20. Tissue responses were expressed as the percentage of KCl-induced contraction. Data are shown as the mean ± SEM of 5 to 7 animals. Abbreviations: KCl, potassium chloride; PE, phenylephrine.*

Table 3.5 Summary of the maximum tissue responses (E_{max}) and potency (pEC_{50}) of the contractile response of phenylephrine, KCl, serotonin and U46619 in the presence of PM20 (10 µM, 30 µM, 100 µM) and their respective vehicle controls.

Treatment	Phenylephrine		KCl		Serotonin		U46619	
	E_{max} (%)	pEC_{50}	E_{max} (%)	pEC_{50}	E_{max} (%)	pEC_{50}	E_{max} (%)	pEC_{50}
Vehicle control	155.4 ± 12.0	7.09 ± 0.10	132.1 ± 4.4	ND [#]	170.3 ± 11.7	5.10 ± 0.15	226.2 ± 22.6	7.26 ± 0.13
PM20 + 10 µM	147.7 ± 18.3 (p = 0.9296)	5.18 ± 0.22 **** (p < 0.0001)	84.2 ± 3.5 **** (p < 0.0001)	ND [#]	138.5 ± 8.3 * (p = 0.0402)	4.98 ± 0.06 (p = 0.6953)	226.7 ± 34.8 (p > 0.9999)	7.36 ± 0.10 (p = 0.8616)
+ 30 µM	107.8 ± 3.5 * (p = 0.0130)	ND [#]	59.7 ± 7.1 **** (p < 0.0001)	ND [#]	90.5 ± 8.6 **** (p < 0.0001)	4.92 ± 0.09 (p = 0.4876)	221.7 ± 32.2 (p = 0.9989)	7.15 ± 0.08 (p = 0.8508)
+ 100 µM	28.8 ± 4.9 **** (p < 0.0001)	ND [#]	43.8 ± 4.2 **** (p < 0.0001)	ND [#]	36.4 ± 4.7 **** (p < 0.0001)	4.79 ± 0.11 (p = 0.1151)	204.8 ± 13.0 (p = 0.9194)	7.02 ± 0.17 (p = 0.4070)

One-way ANOVA followed by Dunnett's post hoc test was used to compare PM20 at each concentration to the vehicle control in their respective group. Individual p-values were stated in the respective columns. Data are shown as the mean ± SEM of 5 to 8 animals. Abbreviation: ND, not determined. [#]pEC_{50} was not determined as the maximum contraction was not achieved.

3.4.10 Contraction to phenylephrine recovered after PM20-treated tissues were washed

It was determined in the previous experiment that PM20 inhibited phenylephrine-induced contraction. This protocol examined the reversibility of PM20. When the aortic rings were pre-incubated with 10 μM of PM20, the contractile response to the first addition of 10 μM phenylephrine was significantly diminished (E_{max}: Vehicle control: 139.0 ± 12.1%; PM20: 92.7 ± 6.7%; $p = 0.0052$) (**Figure 3.13**). Subsequently, the aortic tissues were thoroughly rinsed with Krebs solution to remove any residual vehicle or PM20 in the bath solutions. When the tissues were added with phenylephrine the second time, the contraction to phenylephrine has recovered and was similar to the response achieved in vehicle control (E_{max}: Vehicle control: 110.1 ± 10.0%; PM20: 106.4 ± 4.1%; $p > 0.9999$) (**Figure 3.13**). Moreover, the magnitude of contraction to second phenylephrine addition in PM20-treated tissues seemed higher than the first addition when PM20 was present in the bath solution (PM20 first vs second phenylephrine addition: 92.7 ± 6.7% vs 106.4 ± 4.1%).

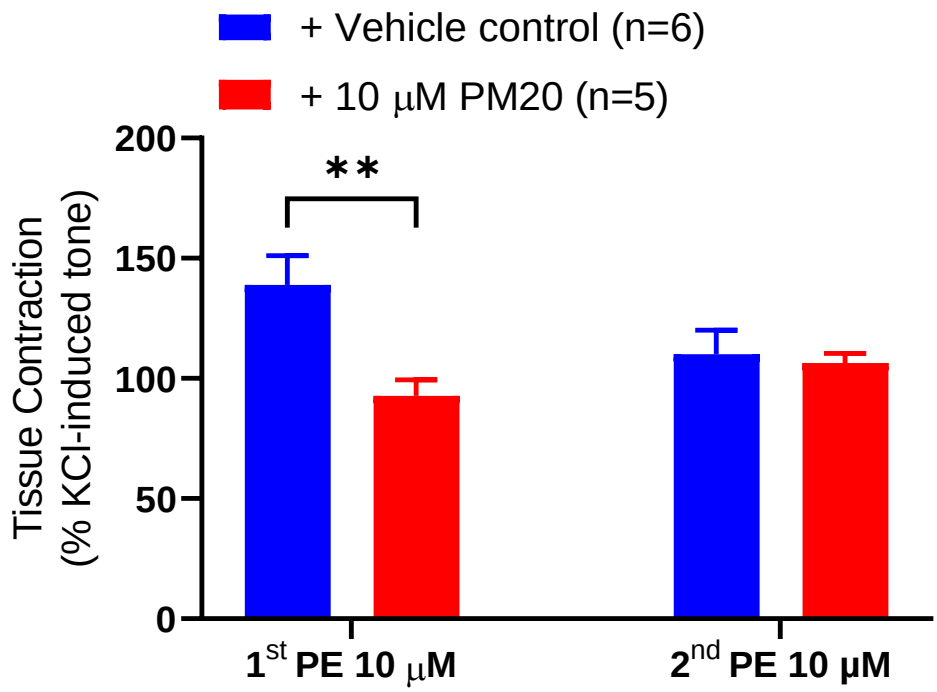


Figure 3.13 Reversibility of PM20 shown in phenylephrine-induced contraction. *Tissue responses were expressed as the percentage of KCl-induced contraction. Data are shown as the mean ± SEM of 5 to 6 animals. Two-way ANOVA followed by Bonferroni's post hoc test was used to compare PM20 to vehicle control at the first and second addition of phenylephrine. Abbreviations: KCl, potassium chloride, PE, phenylephrine.*

3.4.11 PM20 displayed similar vasorelaxation profiles as nifedipine and verapamil

A comparison was made between the vasorelaxation effect of PM20 and a range of Ca^{2+} channel blockers with different mechanism of actions (**Figure 3.14**). For the ease of visualisation, CRCs of PM20 and other Ca^{2+} channel blockers were categorised in different panels according to their putative mechanism of actions. This arrangement does not affect the statistical analysis, where comparison was made altogether.

The order of E_{max} induced by all the compounds tested, from the highest to the lowest, was PM20 > verapamil > nifedipine > Pyr6 > HC-070 > 2-APB > SKF-96365 > Pyr3. PM20, being the compound that achieved the most relaxation effect in the aorta, showed a significantly higher relaxation effect than Pyr3 (**Figure 3.14B**), which relaxed the least in the aorta. Their difference in efficacy was 35.4% (**Table 3.6**). Only PM20, VGCC inhibitors – nifedipine and verapamil had achieved a plateaued relaxation in the aorta (**Figure 3.14C**).

Other than that, the E_{max} and pEC_{50} of PM20 was similar to the rest of the Ca^{2+} channel blockers, namely non-selective TRPC channel inhibitors – 2-APB, Pyr6, SKF-96395 (**Figure 3.14A**), TRPC1/4/5 inhibitor HC-070 (**Figure 3.14B**) and VGCC inhibitors – nifedipine and verapamil (**Figure 3.14C**). Relative E_{max} of each Ca^{2+} channel blocker was expressed relative to the corresponding E_{max} of PM20. The vasorelaxation caused by PM20 (see relative E_{max} in **Table 3.6**), shown with a value of 1, was higher than all the Ca^{2+} channel blockers, which can be seen with relative E_{max} values less than 1. PM20's potency was slightly higher than the estimated potency of 2-APB (~18.6 fold), Pyr3 (~1.5 fold), Pyr6 (~5.2 fold) and SKF-96395 (~1.9 fold), but slightly lower than HC-070 (~1.6 fold) (**Table 3.6**). Nonetheless, the potency of PM20 was not significantly different from other Ca^{2+} channel blockers. The values of E_{max} and pEC_{50} for all compounds are summarised in **Table 3.6**.

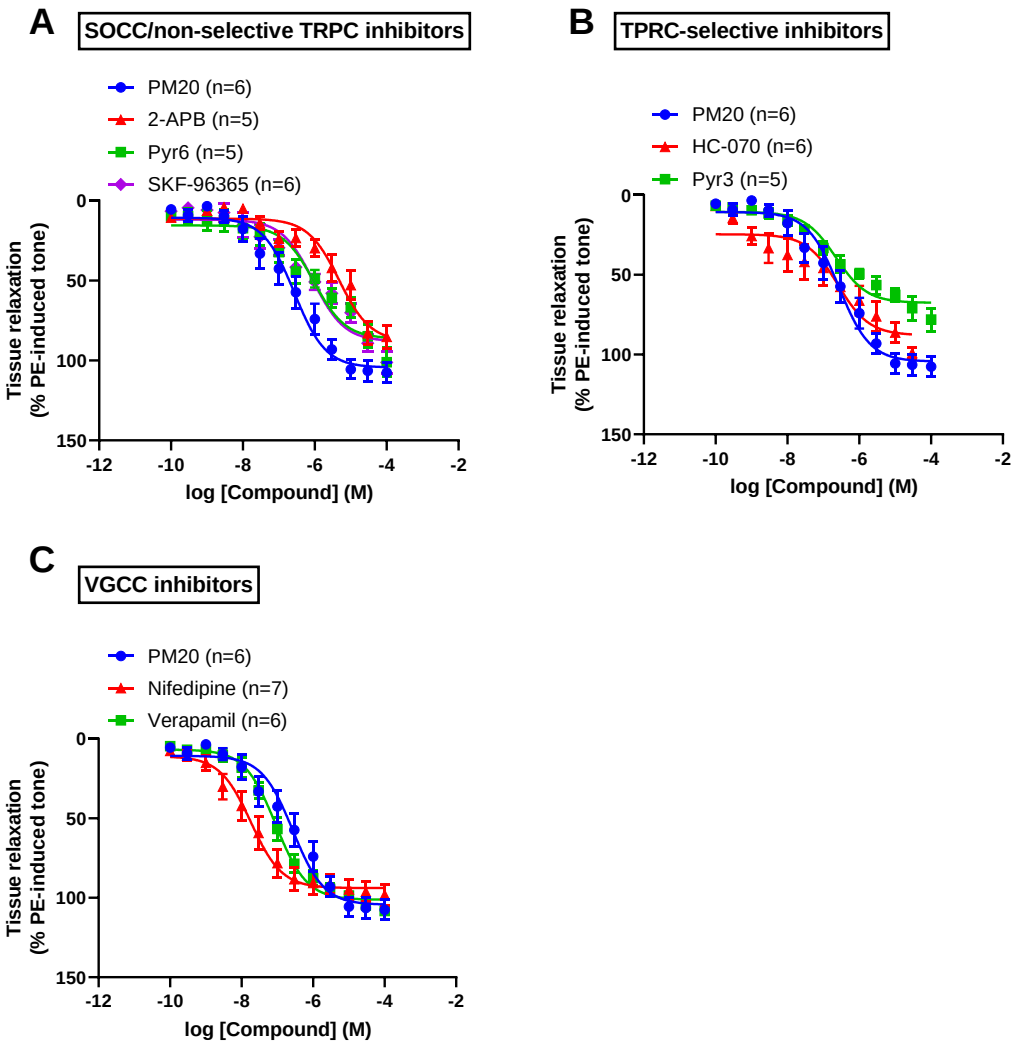


Figure 3.14 Vasorelaxation effect of PM20 and Ca^{2+} channel blockers. *Cumulative CRCs was compared between PM20 and (A) SOCC/non-selective TRPC inhibitors (2-APB, Pyr6, SKF-96365), (B) TRPC- selective inhibitors (HC-070, Pyr3), and (C) VGCC inhibitors (nifedipine, verapamil). Tissue relaxations were expressed as the percentage of phenylephrine-induced contraction. Data are shown as the mean ± SEM of 5 to 7 animals. Abbreviations: 2-APB, 2-aminoethoxydiphenyl borate, PE, phenylephrine; SOCC, store-operated Ca^{2+} channel; TRPC, transient receptor potential canonical; VGCC, voltage-gated Ca^{2+} channel.*

Table 3.6 Summary of the maximum tissue relaxation (E_{max}) and potency (pEC_{50}) of PM20 and known Ca^{2+} channel blockers in rat isolated aortic rings.

Treatment	E_{max} (%)	Relative E_{max}	pEC_{50}
PM20	106.8 ± 6.1	1	6.69 ± 0.32
2-APB	88.4 ± 5.8 (*p* = 0.3623)	0.83	5.42 ± 0.27 † (*p* = 0.1574)
HC-070	90.5 ± 1.9 (*p* = 0.5154)	0.85	6.88 ± 0.54 † (*p* > 0.9999)
Nifedipine	94.8 ± 6.0 (*p* > 0.9999)	0.89	7.77 ± 0.21 (*p* = 0.2552)
Pyr3	71.4 ± 6.3 *** (*p* = 0.0009)	0.67	6.50 ± 0.28 † (*p* > 0.9999)
Pyr6	91.3 ± 8.1 (*p* = 0.8189)	0.85	5.97 ± 0.33 † (*p* > 0.9999)
SKF-96365	87.2 ± 6.8 (*p* = 0.1847)	0.82	6.41 ± 0.46 † (*p* > 0.9999)
Verapamil	101.8 ± 2.2 (*p* > 0.9999)	0.95	7.03 ± 0.10 (*p* > 0.9999)

One-way ANOVA followed by Bonferroni's post hoc test, comparing the vasorelaxation effect of all the Ca^{2+} channel blockers to PM20. Individual p-values were stated in the respective columns. Data are shown as the mean ± SEM of 5 to 7 animals. †Estimated pEC_{50} was calculated based on maximum tissue response.

3.4.12 PM20 has no effect on intracellular Ca^{2+}-induced contraction mediated by phenylephrine, KCl and U46619

Aortic rings treated with PM20 (10 μM) were either immersed in Ca^{2+}-free Krebs or Ca^{2+}-containing Krebs (normal Krebs) solution for 1 hour to examine its effect on intracellular Ca^{2+} release upon the addition of different contractile agents. In **Figure 3.15A**, aortic rings pre-incubated with PM20 in normal Krebs reduced phenylephrine-induced contraction compared to those pre-incubated with vehicle control. This suppression was significant at 0 and 0.5 hours but not at 1 hour (**Table 3.7**). It was observed that the tone of contraction induced by phenylephrine gradually decreasing over a period of 1 hour in aortae treated with vehicle and PM20 (**Table 3.7**). In parallel experiments, the presence of PM20 in Ca^{2+} free Krebs did not affect the contraction induced by phenylephrine. Without external Ca^{2+}, phenylephrine only managed to induce a weak contraction which the magnitude was similar in both vehicle-and PM20-treated aortic rings (**Figure 3.15A** and **Table 3.7**).

In **Figure 3.15B**, PM20 consistently suppressed the contraction evoked by KCl in normal Krebs for 1 hour. Absence of Ca^{2+} has led to a small contraction by KCl in both treatments, which gradually increased over time (**Figure 3.15B** and **Table 3.7**).

PM20 did not suppress U46619-induced contraction regardless of the presence of external Ca^{2+} (**Figure 3.15C** and **Table 3.7**). Moreover, the contraction induced by U46619 over the 1 hour was sustained and stable. This observation supports the earlier findings in **Figure 3.12D**, where 10 μM of PM20 did not affect U46619's cumulative CRC. The E_{max} values of contractile agent-induced contraction are summarised in **Table 3.7**.

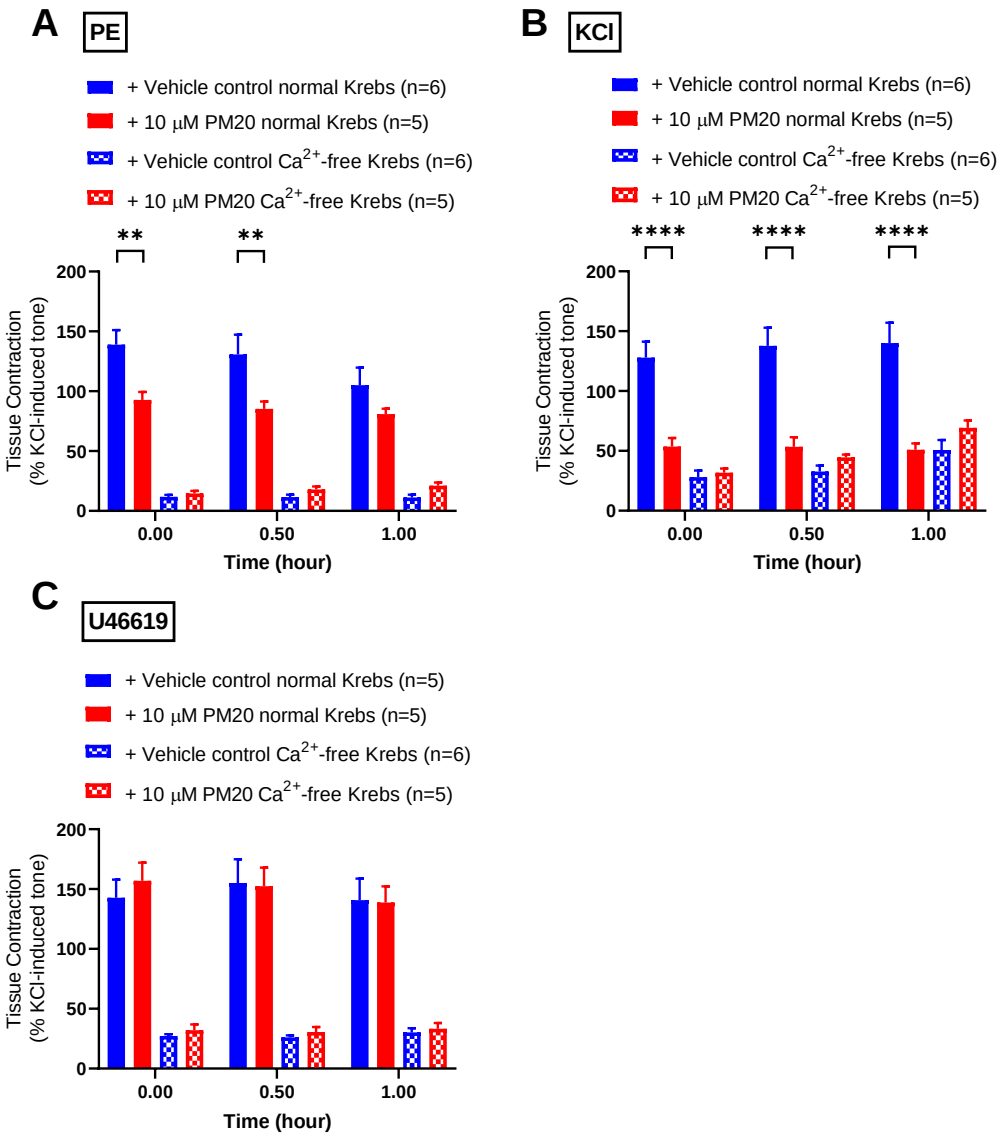


Figure 3.15 Effect of PM20 on (A) phenylephrine-, (B) KCl- and (C) U46619-induced contraction in normal Krebs and Ca^{2+}-free Krebs solution. *Tissue responses were recorded at 0, 30, and 60 minutes after the addition of each contractile agent and were expressed as the percentage of KCl-induced contraction. Data are shown as the mean ± SEM of 5 to 6 animals. Two-way ANOVA followed by Bonferroni's post hoc test was used to compare vehicle control and PM20 treatment in either normal or Ca^{2+} free Krebs separately at each time point. Abbreviations: KCl, potassium chloride, PE, phenylephrine.*

Table 3.7 Maximum tissue response (E_{max}) of phenylephrine, KCl and U46619-induced contraction in normal Krebs and Ca^{2+}-free Krebs solution in the presence of PM20.

		E_{max} (%)					
		Phenylephrine		**KCl**		**U46619**	
Treatment	**Time (hour)**	**Normal Krebs**	**Ca^{2+} free Krebs**	**Normal Krebs**	**Ca^{2+} free Krebs**	**Normal Krebs**	**Ca^{2+} free Krebs**
Vehicle control	**0**	139.0 ± 12.1	11.8 ± 1.7	127.9 ± 13.3	28.0 ± 5.5	142.7 ± 15.3	27.2 ± 1.6
	0.5	130.8 ± 16.5	11.6 ± 2.1	137.8 ± 15.1	32.7 ± 5.1	155.0 ± 19.9	26.1 ± 1.6
	1	105.1 ± 14.6	11.3 ± 2.3	140.1 ± 17.0	50.8 ± 8.3	140.8 ± 17.9	30.3 ± 3.4
PM20	**0**	92.7 ± 6.7 ** (p = 0.0021)	14.6 ± 2.2 (p = 0.9999)	53.5 ± 7.3 **** (p < 0.0001)	31.8 ± 3.5 (p = 0.9997)	156.9 ± 15.1 (p = 0.9452)	32.0 ± 5.0 (p = 0.9995)
	0.5	85.3 ± 6.1 ** (p = 0.0027)	18.0 ± 2.5 (p = 0.9924)	53.4 ± 8.1 **** (p < 0.0001)	44.7 ± 2.2 (p = 0.9347)	152.4 ± 15.5 (p > 0.9999)	30.6 ± 4.1 (p = 0.9997)
	1	80.9 ± 4.6 (p = 0.3165)	21.0 ± 2.6 (p = 0.9525)	51.0 ± 5.2 **** (p < 0.0001)	69.2 ± 6.3 (p = 0.6932)	138.8 ± 13.4 (p > 0.9999)	33.3 ± 4.8 (p > 0.9999)

Two-way ANOVA followed by Bonferroni's post hoc test was used to compare between vehicle control and PM20 treatment in either normal or Ca^{2+} free Krebs separately at each time point. Individual p-values were stated in the respective columns. Data are shown as mean ± SEM of 5 to 6 animals.

3.4.13 PM20 suppressed extracellular Ca^{2+}-induced contraction in rat aortae

Following previous results, the role of extracellular Ca^{2+} in PM20-induced relaxation was investigated. Pre-treatment with PM20 at 10, 30 and 100 µM significantly decreased the contraction induced by cumulative addition of $CaCl_2$ compared to vehicle control treatment (**Figure 3.16D**). Attenuation of tissue contraction by PM20 was concentration dependent. PM20 at 100 µM completely abolished $CaCl_2$-induced contraction.

The effect of Ca^{2+} channel blockers on $CaCl_2$-induced contraction shown in **Figure 3.16A** – **C**, are the same as **Figure 2.21A** – **C** (**section 2.4.15**). Non-selective TRPC inhibitor – 2-APB, SKF-96365 and Pyr6 (**Figure 3.16A**), significantly suppressed $CaCl_2$-induced contraction at different extent, with the exception of TRPC3-selective inhibitor – Pyr3 (**Figure 3.16B**). Moreover, total suppression of tissue response was observed in the presence of 10 µM of nifedipine and verapamil (**Figure 3.16C**). The rank order of maximum tissue contraction in the presence of these Ca^{2+} channel blockers, from the lowest to highest, was nifedipine < verapamil < SKF-96365 < 2-APB < Pyr6 < Pyr3 (**Table 3.8**).

The values of E_{max} are summarised in **Table 3.8**. The potency of $CaCl_2$ was not calculated as maximum tissue response has not plateaued in all tissues, especially in the case of 100 µM of PM20, nifedipine, SKF-96365 and verapamil, where extremely low tissue responses were recorded.

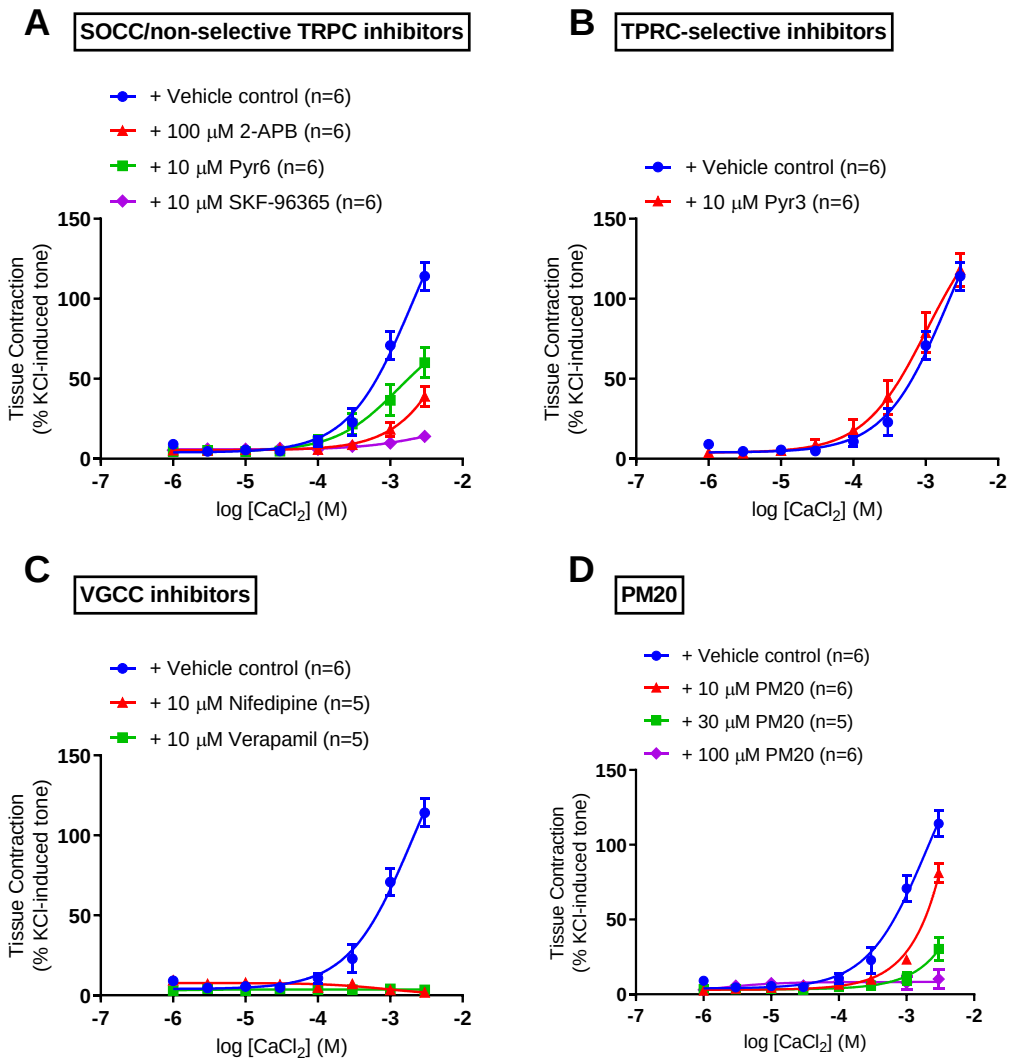


Figure 3.16 Effect of (A/B/C) Ca^{2+} channel blockers and (D) PM20 on $CaCl_2$-induced contraction in rat isolated aortic rings bathed in Ca^{2+}-free Krebs solution. *The* ***Ca^{2+}*** *channel blockers used were (A) SOCC/non-selective TRPC inhibitors (2-APB, Pyr6, SKF-96365), (B) TRPC- selective inhibitors (Pyr3), and (C) VGCC inhibitors (nifedipine, verapamil). Tissue contractions were expressed as the percentage of KCl-induced contraction in Ca^{2+}-containing Krebs solution. Data are shown as the mean ± SEM of 5 to 6 animals. Abbreviations: 2-APB, 2-aminoethoxydiphenyl borate; $CaCl_2$, calcium chloride; KCl, potassium chloride; SOCC, store-operated Ca^{2+} channel; TRPC, transient receptor potential canonical; VGCC, voltage-gated Ca^{2+} channel.*

Table 3.8 Maximum tissue response (E_{max}) and pEC_{50} of $CaCl_2$ CRCs following pre-exposure to vehicle control, PM20 or Ca^{2+} channel blockers.

Treatment	E_{max} (%)	
Vehicle control	114.1 ± 8.7	
+ 10 µM PM20	81.1 ± 6.1	* (p = 0.0181)
+ 30 µM PM20	30.2 ± 7.8	**** (p < 0.0001)
+ 100 µM PM20	10.1 ± 6.1	**** (p < 0.0001)
+ 100 µM 2-APB	38.9 ± 6.1	**** (p < 0.0001)
+ 10 µM Nifedipine	1.7 ± 0.7	**** (p < 0.0001)
+ 10 µM Pyr3	118.1 ± 10.3	(p = 0.9994)
+ 10 µM Pyr6	60.0 ± 9.3	**** (p < 0.0001)
+ 10 µM SKF-96365	13.9 ± 2.7	**** (p < 0.0001)
+ 10 µM Verapamil	3.2 ± 0.9	**** (p < 0.0001)

One-way ANOVA followed by Dunnett's post hoc test, comparing all the treatment groups to vehicle control. Individual p-values were stated in the respective columns. Data are shown as the mean ± SEM of 5 to 6 animals.

3.4.14 PM20-induced relaxation was diminished in the presence of TRPC-selective inhibitors

These experiments assessed whether Ca^{2+} channels are implicated in PM20-induced relaxation. The presence of SOCC/non-selective TRPC inhibitors – 2-APB (**Figure 3.17A**), Pyr6 (**Figure 3.17B**) and SKF-96365 (**Figure 3.17C**) had diminished the E_{max} of PM20-induced relaxation (**Table 3.9**). Similarly, the maximum tissue relaxation effect of PM20 was significantly reduced by Pyr3, a TRPC3-selective inhibitor (**Figure 3.17D**). On the contrary, PM20-induced relaxation in the aortic rings was not affected by pre-incubation with nifedipine (**Figure 3.17E**) and verapamil (**Figure 3.17F**). As shown in **Table 3.9**, the rank order of the largest effect on PM20's E_{max} was Pyr6 (-23.1%), followed by 2-APB (-21.4%), Pyr3 (-19.0%) and lastly, SKF-96365 (-15.3%). The potency of PM20 was not altered in the presence of all the Ca^{2+} channel blockers compared to vehicle control treatment (**Table 3.9**). The values of E_{max} and potency of PM20 are summarised in **Table 3.9**.

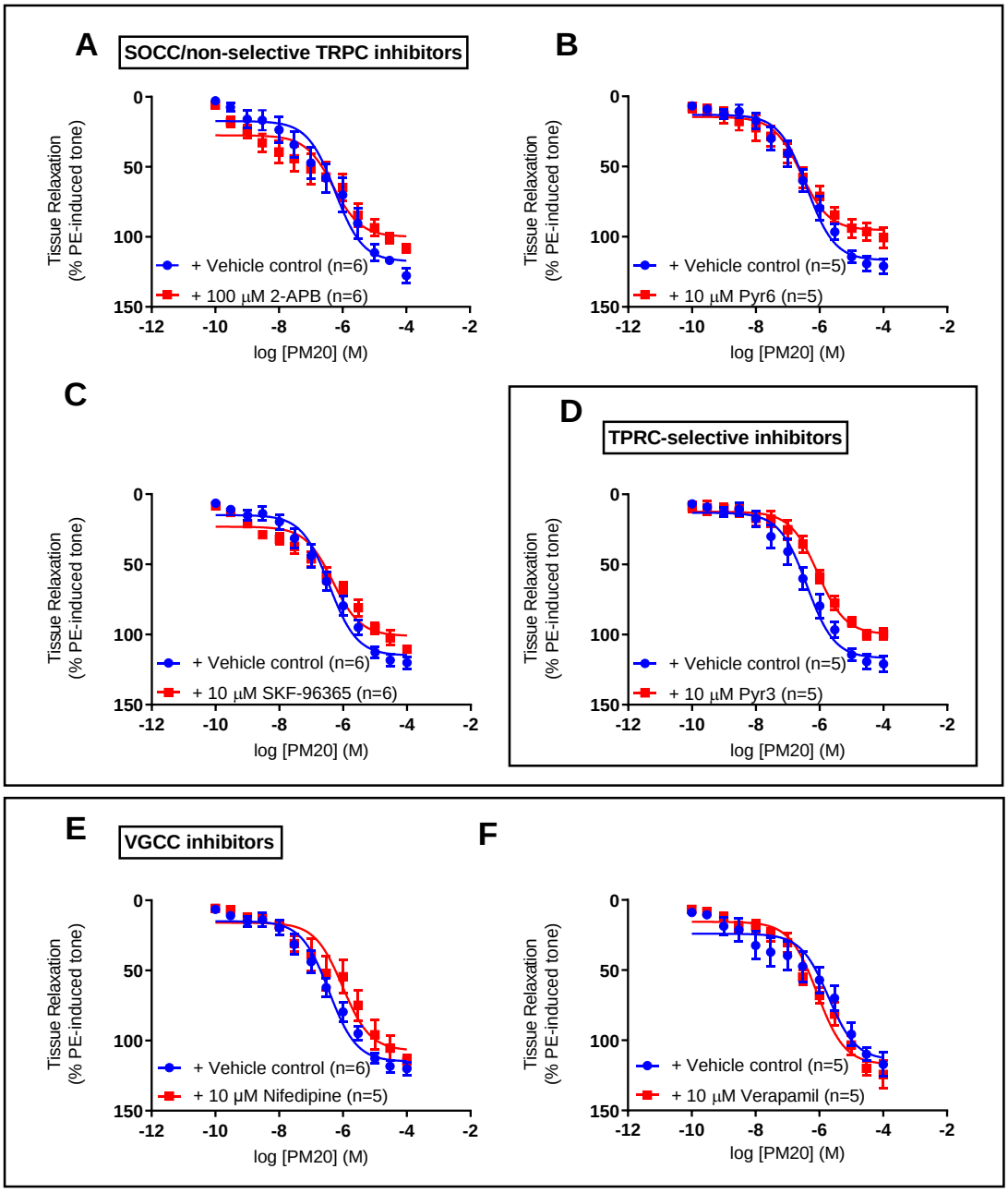


Figure 3.17 Effect of PM20-induced relaxation in the presence of different Ca^{2+} channel blockers. *CRCs to PM20 were performed in the presence of SOCC/non-selective TRPC inhibitors – (A) 2-APB, (B) Pyr6, (C) SKF-96365; TRPC- selective inhibitors – (D) Pyr3; and VGCC inhibitors – (E) nifedipine, (F) verapamil. Tissue relaxations were expressed as the percentage of phenylephrine-induced contraction. Data are shown as the mean ± SEM of 5 to 6 animals. Abbreviations: 2-APB, 2-aminoethoxydiphenyl borate; PE, phenylephrine; SOCC, store-operated Ca^{2+} channel; TRPC, transient receptor potential canonical; VGCC, voltage-gated Ca^{2+} channel.*

Table 3.9 Maximum relaxation (E_{max}) and pEC_{50} values of PM20 in the presence of different Ca^{2+} channel blockers.

Treatment	E_{max} (%)	pEC_{50}
Vehicle control	123.3 ± 5.3	6.30 ± 0.34
+ 100 µM 2-APB	101.9 ± 6.0 * (p = 0.0231)	6.78 ± 0.50 (p = 0.4393)
Vehicle control	117.1 ± 5.4	6.50 ± 0.23
+ 10 µM Nifedipine	108.6 ± 5.5 (p = 0.3075)	6.10 ± 0.32 (p = 0.3311)
Vehicle control	119.4 ± 6.0	6.45 ± 0.28
+ 10 µM Pyr3	100.5 ± 3.3 * (p = 0.0242)	6.06 ± 0.09 (p = 0.2236)
Vehicle control	119.4 ± 6.0	6.45 ± 0.28
+ 10 µM Pyr6	96.4 ± 6.3 * (p = 0.0292)	6.60 ± 0.20 (p = 0.6842)
Vehicle control	117.1 ± 5.4	6.50 ± 0.23
+ 10 µM SKF-96395	101.7 ± 3.2 * (p = 0.0359)	6.35 ± 0.18 (p = 0.6226)
Vehicle control	114.3 ± 6.7	5.76 ± 0.28
+ 10 µM Verapamil	123.7 ± 8.2 (p = 0.3931)	5.99 ± 0.26 (p = 0.5627)

Unpaired Student's t-test was used to compare each treatment with their respective vehicle controls. Individual p-values were stated in the respective columns. Data are shown as mean ± SEM of 5 to 6 animals. Abbreviation: 2-APB, 2-aminoethoxydiphenyl borate.

3.5 Discussion

This chapter investigated the pharmacological properties of another analogue of schwarzinicine A coined as PM20.

3.5.1 Physicochemical properties of PM20 – a theoretical calculation

Poor biopharmaceutical properties and pharmacokinetic profiles of potential drug candidates remain the primary reasons behind the high drug attrition rate in the drug development industry (Meanwell, 2011). Early evaluation of the drug-likeness of PM20 would be beneficial in providing useful information about its potential oral bioavailability. All physicochemical properties of PM20 fall within Lipinski's Rule of Five and Veber's rule, suggesting an increased likelihood of high oral absorption.

PM20 has the least MW among all the compounds such as nifedipine, SKF-96365 and Pyr3. As MW increases, solubility and permeability across membrane decrease. On the opposite, plasma protein binding increases with MW (Meanwell, 2011). In Meanwell's study, compounds with MW less than 300 have plasma protein binding around 72% and bioavailability of 18% in the rats. When the MW increases to about 500, the binding increases to 98.2%, but bioavailability reduced to 10%. This analysis suggests that PM20 may have lower plasma protein binding but slightly higher bioavailability than other reference compounds. Binding too strongly to plasma protein is less desirable as it may affect the level of unbound drugs in the blood and produce less drug effect (C.-Y. Ma, Yang, Zhang, et al., 2008).

LogP contributes to the prediction of compound's membrane permeability. It is also the key descriptor to predict ADME properties of compounds (Hou, Li, Zhang, et al., 2009; Hou & Wang, 2008). Compounds with logP less than or equal to 5 have been shown to have optimised binding to the target, good permeation through phospholipid bilayer and without having to compromise their aqueous solubility for drug absorption (Benet, Hosey, Ursu, et al., 2016). Aqueous solubility can also be affected by the number of hydrogen bonds, which Lipinski et al. (1997) has stated that a compound's HBD should be less than or equal to 5, while HBA should be less than or equal to 10. Forming a high number of intermolecular hydrogen bonds may affect drug absorption from the intestine to the blood, consequently reduce oral bioavailability (Alex, Millan, Perez, et al., 2011). All the compounds, including PM20, nifedipine, SKF-96365 and Pyr3, have logP ranging from 3 to 5 and a low number of HBA/HBD. Nifedipine is marketed as an oral

Ca^{2+} channel blockers with satisfactory *in vivo* pharmacokinetics, including its ADME (Raemsch & Sommer, 1983; Renwick, Robertson, Macklin, et al., 1988). This indicates that PM20 is also likely to be orally available as they have similar physiochemical profiles.

The molecular structure of PM20 is less flexible compared to SKF-96365. It has only 8 rotatable bonds compared to 10 in SKF-96365. Increasing number of rotatable bond and tPSA negatively impact the compounds' bioavailability. Veber et al. (2002) has shown that the number of compounds with oral bioavailability of more than 20% was decreased by half when the number of rotatable bonds was more than 7. Almost all compounds with tPSA less or equal to 140 $Å^2$ have a bioavailability greater than 80%. Therefore, a reasonable degree of conformational constraint in PM20's structure is desirable to increase its target binding specificity. The rigidity in PM20 may also enhance interaction at binding sites to elicit its drug effect (Lawson, Maccoss, & Heer, 2018).

Lipinski's and Veber's analyses facilitate rapid selection and prioritisation of the lead compound from a library of analogues. Due to its simplicity, not all marketed drugs obey the Lipinski's or Veber's rule, such as atorvastatin and montelukast (IUPHAR database, 2015). They both have MW higher than 500 Da and logP more than 5, yet, these drugs are available in oral formulation. These rules were initially put together in attempt to associate compounds' physicochemical properties with their oral bioavailability through retrospective analysis. Therefore, these rules must be exercised with caution as they are relatively straightforward and might not accurately predict complex pharmacokinetics *in vivo*.

3.5.2 Tissue selectivity of PM20

Initial pharmacological evaluation of PM20 has shown that it did not affect the basal tension of the tissues. PM20 was not capable of causing contraction or relaxation on smooth muscle tissues without the presence of active tension. The speculation was further supported when PM20 managed to evoke relaxant effects in the presence of contractile agonists – phenylephrine and carbachol. PM20 at low concentration managed to relax vascular tone induced by phenylephrine. In contrast, PM20-induced relaxation in bladder and trachea occurred at a much higher concentration. Its potency in the aorta was approximately 41-fold higher compared to the trachea and 89-fold

higher compared to the bladder. These observations indicate that PM20 is more selective for aortic tissue as it was the most efficacious and potent in aortic tissues. Therefore, subsequent experiments were conducted using rat aortic segments. PM20 could be antagonising the effect of phenylephrine as an inhibitor at α-adrenoceptors, or it may target downstream effectors in G_q signal transduction pathway upon stimulation by phenylephrine (O'Connell, Jensen, Baker, et al., 2014).

3.5.3 Role of endothelium and NO

Removing the endothelium by denudation has eliminated the effects of NO and EDHFs on PM20-induced vasorelaxation. Pre-incubating the endothelium-intact aorta with L-NAME, on the other hand, inhibited the activity of eNOS and thereby reducing the production of NO from L-arginine (Küng, Moreau, Takase, et al., 1995). Should PM20's vasorelaxant effect requires both endothelium and VSM, denudation or pre-incubation with L-NAME would have reduced its effect in the aortic tissue. The tissue response evoked by PM20 did not differ between endothelium-intact and -denuded aortic segments. Furthermore, the magnitude of relaxation induced by PM20 was similar in the presence or absence of L-NAME. These findings have shown that PM20-induced vasorelaxation is independent of endothelium and NO.

3.5.4 Role of cyclic nucleotides

Cyclic nucleotide cGMP and cAMP are important second messengers in regulating smooth muscle relaxation. If PM20-induced relaxation is regulated via cAMP pathways, additional forskolin that activates AC and subsequently increases cAMP level would potentiate PM20-induced relaxation. On the other hand, treatment with ODQ has inhibited sGC and halted the conversion of GTP to cGMP. Inhibition of sGC activity would diminish the effect of PM20, should it act via the cGMP pathway. However, the presence of forskolin and ODQ did not influence the relaxation profile of PM20, indicating that PM20-induced relaxation does not involve in modulating the level of cAMP and cGMP.

3.5.5 Role of adrenoceptors

Results have shown that PM20 reduced the aortic contractile responses to phenylephrine, a G_q protein-coupled α_1-adrenoceptor agonist. PM20 could be antagonising the effect of phenylephrine at α-adrenoceptors to evoke a relaxation response. Therefore, experiments were designed to investigate the involvement of adrenoceptors in PM20-induced relaxation. Relaxation to PM20 in aortic tissue pre-exposed to α-adrenoceptor antagonists such as prazosin (α_1-selective) and rauwolscine (α_2-selective) did not show any significant difference. Furthermore, PM20 could be activating β-adrenoceptor to evoke a relaxation response in the aorta. However, aortic tissues pre-treated with propranolol, a non-selective β-adrenoceptor antagonist did not attenuate the relaxation effect of PM20. These findings have demonstrated that PM20-induced relaxation was independent of adrenoceptors.

3.5.6 Role of K^+ channels

The opening of K^+ channels that hyperpolarises the plasma membrane through the efflux of K^+, is one of the possible relaxation mechanisms found in VSM. Conversely, closure of K^+ channels reduces the hyperpolarising current and the extent of membrane hyperpolarisation, which increases VSM contractility (Jackson, 2000; Jiang et al., 2005; Ledoux et al., 2006; Sobey, 2001). If PM20 evoked vasorelaxation by activating the K^+ channels, pre-incubating the tissues with K^+ channel blockers would contravene and suppress the relaxation effect of PM20. Four K^+ channel blockers were used in this study, namely 4-AP (K_v channel blocker), $BaCl_2$ (K_{ir} channel blocker), glibenclamide (K_{ATP} channel blocker) and TEA (K_{Ca} channel blocker). According to the results obtained, there were no significant changes to PM20-induced relaxation in tissues pre-incubated with K^+ channels inhibitors compared to vehicle control, suggesting that vasorelaxation induced by PM20 does not involve K^+ channels such as K_v, K_{ir}, K_{ATP}, and K_{Ca} channels.

Ca^{2+} influx through L-type VGCCs and CICR via RyRs has been indicated upon K^+ channel blocker-induced membrane depolarisation (Jackson, 2017). In the experiment, phenylephrine was added after pre-treatment with K^+ channel blockers to evoke an active contraction, which involved Ca^{2+} influx. Due to the insensitivity of PM20 to K^+ channel blockers, it is likely that PM20-induced relaxation in these tissues was linked to the downstream inhibition of Ca^{2+} influx via Ca^{2+}-permeable channels instead of K^+ channels activation.

3.5.7 Role of contractile agents

In these series of experiment, contractile agent KCl and TXA mimetic U46619 were used to replace phenylephrine in the experiment to investigate the relaxation profile of PM20. PM20 displayed similar efficacy in reducing the contraction induced by all three agents but exhibited the highest potency in relaxing phenylephrine-induced contraction.

As discussed in the previous chapter (**Figure 2.23**), phenylephrine downstream signalling pathway evokes ROCE through L-type VGCCs, TPRC3 and TRPC6 channels, at the same time induces Ca^{2+} release from the SR store through IP_3 receptors and RyRs (McGeown, 2004; Putney, 2009). Apart from continuous Ca^{2+} influx via L-type VGCC, depletion of SR store will prompt Ca^{2+} refilling from the external source via SOCE pathway to sustain phenylephrine-induced contraction. Accumulating evidence has suggested that TRPC1/4/5 channels form part of the subunits of SOCC, while other subunits involved in mediating SOCE current includes STIM and Orai components (Jairaman & Prakriya, 2013; F. P. Leung, Yung, Yao, et al., 2008; Prakriya & Lewis, 2015). Interestingly, TRPC-induced SOCE also interacts with L-type VGCCs to form a Ca^{2+} signalling complex, but the underlying mechanisms remain elusive (Ávila-Medina, Calderón-Sánchez, González-Rodríguez, et al., 2016; Spinelli & Trebak, 2016). Based on our results, L-type VGCCs, TRPC channels involved in ROCE (TRPC3/6) and SOCE (TRPC1/4/5) pathways, could be the targets of PM20. This inference was supported when pre-incubation with PM20 attenuated the contractile response by phenylephrine.

It has been long established that the external application of a high concentration of K^+ evokes membrane depolarisation and subsequently open L-type VGCCs, which allow Ca^{2+} entry to stimulate smooth muscle contraction (**Figure 2.23**). In addition to the more commonly known route of Ca^{2+} entry through L-type VGCCs, depolarisation induced by high concentration of KCl also releases Ca^{2+} from SR (Kobayashi, Kanaide, & Nakamura, 1985, 1986). After KCl has depleted store Ca^{2+}, 2-APB-sensitive TRPC channels will facilitate external Ca^{2+} influx to replenish store Ca^{2+} (**Figure 2.23**) (P. H. Ratz & Berg, 2006). Our findings have shown that PM20 reduced tissue pre-contraction by KCl. However, this inhibition occurred at a relatively high concentration of PM20 compared to the inhibition of phenylephrine. One possible explanation is that the TRPC channels activated during KCl depolarisation were more likely to be only related to store depletion, which is the store-operated TRPC1/4/5 channels. Phenylephrine on the

other hand, could have activated DAG-sensitive TRPC3/6 channels (ROCCs) on top of TRPC1/4/5 (SOCCs) after store-depletion through IP_3 receptors and RyRs. With more TRPC subtypes activated in phenylephrine, PM20 could exert relaxation at lower potency. Generally, these findings have further supported the postulation that PM20 is likely to inhibit TRPC-related channels and L-type VGCCs.

U46619, a potent vasoconstrictor, is known to couple to G_q protein as one of the second messenger pathways upon activation on TP receptors (Nakahata, 2008; Offermanns, 2006). This may explain PM20's sensitivity on U46619-precontracted aortic rings, but the relaxation only observed at high concentration of PM20. From the results obtained, the contraction by U46619 observed in VSMC may not be solely via G_q activation. Pre-incubation with PM20 did not affect the contractile force of U46619 in rat aortae. TP receptors are also coupled to $G_{12/13}$, which leads to downstream RhoA/ROCK pathway activation and substantial Ca^{2+} sensitisation by inhibiting the activity of MLCP (Pang, Guo, Su, et al., 2005; Sakurada, Okamoto, Takuwa, et al., 2001). The RhoA/ROCK pathway is a non-G_q sensitive mechanism, which is independent of Ca^{2+} influx through L-type VGCC (Alapati et al., 2007; Grann et al., 2016; Nobe & Paul, 2001). Both G_q and $G_{12/13}$-mediated RhoA/ROCK pathways could be coupled to U46619 in the VSM, but our results suggest that the latter is likely to be more dominant in mediating U46619's vasoconstriction in our experiment setting (**Figure 2.23**).

The results have also shown that pre-incubation with increasing concentration of PM20 had caused a rightward shift of serotonin's CRCs. As previously discussed, serotonin evoked vascular contraction by activating 5-HT_{2A} receptors (Varghese et al., 2006; Villazon, Padin, Cadavid, et al., 2002; Watts, 2002). The contraction is linked to the G_q downstream signalling pathway, which then coupled to PKC and the opening of L-type VGCC (McKune & Watts, 2001). On the other hand, serotonin also played a role in regulating Ca^{2+} influx via SOCC by stimulating TRPC1 – 4 channels (Rodat-Despoix et al., 2009; Varghese et al., 2006). Since a high concentration of PM20 managed to inhibit serotonin-induced contraction, thus suggesting that PM20 may modulate these key ion channels involved in serotonin-induced contraction.

PM20 at 10 µM did not affect serotonin-induced contraction, but it has reduced the potency of phenylephrine-induced contraction. Although both agonists are heavily implicated in G_q transduction pathway, the rate of G_q activation is subject to receptor

density and receptor-specific binding kinetic (Falkenburger, Dickson, & Hille, 2013). The expression and density of 5-HT_{2A} and α_1-adrenergic receptors were not controlled and measured in our experiment, which may affect downstream IP_3 and DAG production from PIP_2 (Falkenburger et al., 2013; Mak, 2013). Also, when Ca^{2+} is released from IP_3-sensitive SR store, DAG activity and downstream PKC-mediated signalling can be catalysed depending on the rising $[Ca^{2+}]_i$ (De Pittà, Ben-Jacob, & Berry, 2019). Different extent of G_q stimulation upon agonists' activation complicates the role of second messengers and diversifies the responses in $[Ca^{2+}]_i$ regulation (Himpens et al., 1990; P. H. Ratz et al., 2005). Combining all these plausible factors, G_q-coupled phenylephrine and serotonin have shown different contraction profiles in vehicle control groups. Despite at same concentration, PM20 was more effective in suppressing the contraction evoked by phenylephrine instead of serotonin, indicating that PM20 could be more sensitive to the changes in Ca^{2+} homeostasis occurred with phenylephrine.

At this point, we could not exclude PM20's role on store Ca^{2+} release. The role of PM20 in mediating store Ca^{2+}-induced contraction will be discussed in **section 3.5.9**.

3.5.8 Reversibility of PM20 as an inhibitor to phenylephrine-induced contraction

Pre-treatment with PM20 markedly reduced phenylephrine-induced contraction compared to aortic rings treated with vehicle control. The concentration of PM20 used was at its near-maximal (EC_{90-100}) activity. However, after removing PM20 from the bath solution, it restored the rings' ability to contract upon stimulation by phenylephrine. The tissue contraction is comparable to those pre-treated with vehicle control, indicating that its inhibition was reversible through washing.

3.5.9 Role of intra- and extracellular Ca^{2+}

Ca^{2+} undeniably plays a central role in regulating the vascular tone. From previous results, there are possibilities that PM20 may modulate plasmalemmal L-type VGCCs, Ca^{2+}-permeable TRPC channels and inhibit the release of intracellular Ca^{2+} from SR. Therefore, experiments were designed to investigate the role of PM20 in modulating intra- and extracellular Ca^{2+} dynamic. The results have shown that the contractile response of phenylephrine, KCl was suppressed by PM20, but it did not affect U46619-induced contraction in normal Krebs solution. These findings agree with previous

inference, where PM20 is likely to inhibit L-type VGCCs and TRPC channels but has no role in mediating Ca^{2+} sensitisation via the RhoA/ROCK pathway.

The observations in Ca^{2+}-free Krebs have offered more insights into the PM20's mechanism in modulating intracellular Ca^{2+} store release. Its presence did not reduce phenylephrine-, KCl- and U46619-induced contraction in Ca^{2+}-free Krebs solution. The addition of phenylephrine causes a spontaneous release of intracellular Ca^{2+} from the SR through IP_3 receptors (Putney, 2009). Continuous Ca^{2+} release would also cause a positive feedback loop to allow more Ca^{2+} release via RyRs, where they co-operatively amplify cytosolic Ca^{2+} level (McGeown, 2004). As mentioned, CICR is the activation of RyRs in respond to rising of $[Ca^{2+}]_i$ (**Figure 2.23**). Other than phenylephrine, a high concentration of KCl has also been shown to induce Ca^{2+}release from SR through RyRs in Ca^{2+}-free physiological salt solution, which leads to a rise in cytosolic Ca^{2+} level (Kobayashi et al., 1985, 1986). The release of store Ca^{2+} via IP_3 receptors and RyRs to evoke depolarisation-induced smooth muscle contraction was also reported in other studies (Fellner & Arendshorst, 2007; Urena et al., 2007; I. Y. Wang, Bai, Sanderson, et al., 2010). Similarly, U46619 can also increase $[Ca^{2+}]_i$ via IP_3 receptors, RyRs and PKC-mediated pathways upon its activation on G_q receptors (Himpens et al., 1990; Nobe & Paul, 2001). In the study conducted by Himpens et al. (1990),the contractile force generated by U46619 in a Ca^{2+} free environment was significantly attenuated compared to Ca^{2+}-containing solution, which is consistent with our findings. Taken together, phenylephrine, KCl and U46619 induced Ca^{2+} release from SR store via IP_3 receptors and RyRs to evoke a feeble contraction in a Ca^{2+}-free environment. Since PM20 did not affect the tissue contraction to these contractile agents compared to vehicle control, it is not likely to inhibit store Ca^{2+} depletion via these channels to generate vasorelaxation effect.

In addition, Fransen et al. (2015) has suggested that the initial phasic contraction in the VSM is associated with Ca^{2+} release from SR, while the sustained tonic contraction relies on external Ca^{2+} influx. Comparing the contractile response of all three contractile agents in normal and Ca^{2+}-free Krebs has demonstrated the necessity of external Ca^{2+} to sustain high contractile force in aortic tissues throughout the 1 hour. Besides, PM20 could only reduce the magnitude of contraction in Ca^{2+}-containing Krebs, indicating its role mainly inhibits extracellular Ca^{2+}-dependent contraction.

From the above results, the study was then focused on verifying the role of PM20 in regulating Ca^{2+} mobilisation in VSM. PM20 blocked vasoconstriction in a concentration-dependent manner when $CaCl_2$ was added in Ca^{2+}-free Krebs solution, further confirming that its vasorelaxant effect involves the inhibition of extracellular Ca^{2+} influx via plasmalemmal ion channels. There is a part of L-type VGCCs directly activated upon membrane depolarisation, at the same time, TRPC channels also facilitate the initial influx of Ca^{2+} until it reaches the activation threshold for more L-type VGCC activation (Falcón et al., 2020; Soboloff et al., 2005). When TRPC-selective inhibitors such as 2-APB, Pyr6, and SKF blocked SOCE and ROCE, they attenuated the tissue contraction upon re-addition of external Ca^{2+}. Pyr3, a TRPC3 inhibitor that only inhibits a particular subtype of TRPC, did not suppress tissue contraction towards Ca^{2+}. On the contrary, when L-type VGCCs were blocked by nifedipine and verapamil, they abolished the tissue contraction completely. These findings suggest that: 1) majority of Ca^{2+} influx is through L-type VGCCs for tissue contraction; 2) blocking TRPC channels would result in Ca^{2+} influx through other Ca^{2+}-permeable routes (possibly through L-type VGCCs) to induce contraction; 3) a non-selective inhibition on all TRPC subtypes is required to cause a certain degree of attenuation in tissue contraction force. When comparing the inhibition effects of PM20 with these Ca^{2+} channel blockers, we can see that a lower concentration of PM20 did not inhibit $CaCl_2$-induced vasoconstriction completely, but a higher concentration did. Therefore, at a low concentration of PM20 at 10 and 30 μM, it is likely that PM20 selectively blocks the SOCE and ROCE via TRPC channels. On the other hand, it is postulated that high concentration of PM20 at 100 μM may has some off-target inhibition, which was not selective towards TRPC channels. Subsequently, it inhibited all components involved in extracellular Ca^{2+} influx, including L-type VGCCs.

3.5.10 Relaxation profiles of PM20 and other Ca^{2+} channel blockers

PM20 has also demonstrated its potential to be a Ca^{2+} channel blocker by possessing efficacy and potency comparable to all the Ca^{2+} channel blockers tested except Pyr3. As discussed previously, Pyr3 evoked relaxation through TRPC3 inhibition, whereas HC-070, a potent TRPC4/5 inhibitor, has to block TRPC3 on top of TRPC1/4/5 to reduce the contractile force induced by phenylephrine in the VSM (Just et al., 2018; Kiyonaka et al., 2009). This observation suggests that the relaxant effect of PM20 requires the inhibition of a few TRPC subtypes rather than selectively blocking one subtype. This inference can also be further supported when PM20 vasorelaxation was similar to non-selective TRPC inhibitors – 2-APB, Pyr6 and SKF-96365.

Although PM20's relaxant profile was statistically similar to all Ca^{2+} channel blockers, it displayed the highest efficacy in inducing vasorelaxation among all compounds. Unlike all the CRCs of TRPC inhibitors, PM20's CRC has reached a plateau similar to nifedipine and verapamil. These observations indicate a possibility of PM20 exhibiting TPRC channel inhibition at low concentration but may also block VGCCs at high concentration.

3.5.11 Role of extracellular Ca^{2+}-permeable channels

Consistent with the findings in FK244 (**section 2.4.16**), the efficacy of PM20 was reduced by pre-treating the aortic rings with 2-APB, Pyr3, Pyr6 and SKF-96365. Pyr3 is a TRPC3-selective inhibitor, while Pyr6 is a SOCC inhibitor which also plays a role in inhibiting the assembly of Orai subunit to TRPC channels (Schleifer et al., 2012; Silva & Ballejo, 2019; Z. K. Sweeney et al., 2009; Yonetoku et al., 2008). On the other hand, 2-APB and SKF-96365 have been characterised as a non-selective TRPC channels blockers that mediate ROCE and SOCE pathways (Bishara et al., 2002; Broad et al., 2001; Gregory et al., 2001; R. Inoue et al., 2001; Merritt et al., 1990; Okada et al., 1998). In agreement with the discussion point made previously, the results obtained in these experiments have revealed that PM20 is likely to inhibit TRPC channels. It is interesting when pre-incubation of nifedipine and verapamil did not influence PM20-induced relaxation. In coherence with previous inference, these data suggest that the mechanism of relaxation exhibited by PM20 might be different from VGCC blockers, and the ability of PM20 in inhibiting VGCCs may not be as profound as nifedipine and verapamil.

The presence of all these Ca^{2+} channel blockers did not affect the potency of PM20. This gave us a subtle clue that PM20 has pharmacological effects slightly different from each of these compounds. However, this interpretation on potency (pEC_{50}) may need considerations from other perspectives, such as their binding affinity towards target receptors, non-specific target binding as well as competitive/non-competitive inhibition. Isometric tension recordings could not provide direct evidence to PM20's mechanism of action to permit discussion from these aspects.

Furthermore, formation of heterotetrameric TRPC channels is feasible between different subtypes. They usually co-assemble based on their sequence homology, i.e., TRPC1/4/5 subgroup and TRPC3/6/7 subgroup (Hofmann et al., 2002). To date, the mechanism of TRPC's heteromultimerisation in native tissue is unknown. Furthermore, cross-association has been detected across subgroups with combinations such as TRPC1:C6, TRPC1:C3, and TRPC3:C6. These heterotetramers were demonstrated to display characteristics of both store-operated and receptor-operated TRPC channels (Goel et al., 2002; Liu, Bandyopadhyay, et al., 2005; Y. Yu et al., 2003). Therefore, PM20 could be targeting multiple TRPC channels subtypes, including heterotetramers. This explains its reduced sensitivity against tissues treated with TRPC inhibitors – 2-APB, Pyr3, Pyr6, and SKF-96365, while its potency remains unaffected.

3.6 Chapter summary

PM20 has displayed the desired drug-likeness profile in Lipinski's and Veber's analysis. It produces an endothelium-independent vasorelaxation in rat isolated aortic rings. The findings in the functional studies have eliminated other possible vasorelaxant mechanisms of PM20, including NO, cyclic nucleotide second messengers, adrenoceptors and K^+ channels. The present study shows evidence of PM20's potential mode of action, which is through the inhibition of transmembrane Ca^{2+} influx with negligible effect on intracellular Ca^{2+} store. The current data support the hypothesis that PM20 tends to block TRPC channels and L-type VGCCs which both are largely involved in phenylephrine-induced contraction.

Chapter 4 Effects of FK244 and PM20 on the lifespan of *C. elegans* and *in vitro* pharmacological evaluation in disease models

4.1 Introduction

4.1.1 Toxicity assessment

Evaluation of the potential drug candidate's safety profile is an essential part of the drug discovery process. The pre-clinical toxicological screening is critical to examine any potential adverse drug events and assess their severity. Toxicity profiling was only being systematically developed in the 1920s, when J. W. Trevan, a British biologist introduced the median lethal dose (LD_{50}) test to study the toxicity of drugs like cocaine, insulin and digitalis extract in frog model (Trevan, 1927). *In vivo* toxicity testing then became widely practised using rodents, cats, dogs and rabbit in biomedical research to study the effect of compounds, drugs or even environmental pollutants. In the 1960s, the Replace, Reduce, Refine (3Rs) approach was encouraged for more ethical use of animal in scientific studies.

With the focus of reducing the number of animal used in scientific experiments, *C. elegans* model, is widely used as a scientific model in many biomedical studies (Apfeld & Alper, 2018; Leiser, Jafari, Primitivo, et al., 2016; Sherman & Harel, 2019). Its usage as a screening tool in therapeutic or toxicity screening of compounds is gaining momentum ever since the genetic features of *C. elegans* are established and described. Many studies have employed *C. elegans* model to evaluate compounds' toxicity to neurons (Boyd, McBride, Rice, et al., 2010; Fitsanakis, 2012), genetic expression (Honnen, 2017; Sendoel, Maida, Zheng, et al., 2014), as well as high-throughput screening for the targets of toxicity (Lucanic, Garrett, Gill, et al., 2018).

Such model organism provides an ethical free *in vivo* environment which can improve cellular-to-animal translation of compounds that have previously shown promising effects (Bulterijs & Braeckman, 2020). Highly conserved genetic regulation and physiology in *C. elegans* hold great opportunities at reducing the number of vertebrates used in biomedical research (Betschinger & Knoblich, 2004; M. C. K. Leung, Williams, Benedetto, et al., 2008; Putcha & Johnson, 2004). Acute and chronic compound exposure in *C. elegans* provides a preliminary toxicological spectrum before initiating

the investigation in large animal models such as rodents, dogs or rabbits (L. Shen, Xiao, Ye, et al., 2009).

4.1.2 *glp-4* mutated *C. elegans*

glp-4 in chromosome *I* of *C. elegans* is the gene responsible for normal proliferation of germ cells. When *glp-4* was mutated with 20 mM of ethyl methane sulphonate for 4 hours, the mutation at the allele *bn2* was revealed to be a temperature-sensitive allele (Beanan & Strome, 1992). Subsequent analysis found that the mutation arrested prophase in the mitotic cell cycle. This arrest led to the disruption of meiotic cell division and prevented the germ cells from differentiating into gametes in both XX and XO *C. elegans*. This germ-line mutated sterile strain named SS104 [*glp-4 (bn2) I*] reproduces freely at 16 °C but become sterile at 25 °C. Young adults of SS104 strain grown under 25 °C only have an average of only 12 germ nuclei in their gonad arms compared to 900 germ nuclei in wild-type *C. elegans* (Beanan & Strome, 1992). Interestingly, the arrest is reversible when the sterile worms are placed under 16 °C again, reversing the germ-line proliferation phenotype. Reversed fertile SS104 displayed wild-type behaviour but have a reduced progeny size (Beanan & Strome, 1992). SS104 strain is used widely in *C. elegans*' lifespan studies as it exhibits wild-type physiology and prevents the possible confounding effect of worm reproduction when raised at restrictive temperature of 25 °C (Alper, McElwee, Apfeld, et al., 2010; Jakobsen, Bojer, Marinus, et al., 2013; H. J. Lee, Noormohammadi, Koyuncu, et al., 2019; McColl, Killilea, Hubbard, et al., 2008; Poulsen, Schøler, Nielsen, et al., 2014). This characteristic provides a great advantage as it eases the process of enumeration of alive and dead worms in a population.

4.1.3 Vascular pathologies in SHR

High blood pressure and blood flow in SHR increase shear stress on the vessels. They promote vascular remodelling in SHR. The vasculature in SHR is usually characterised by having inward eutrophic remodelling, where the structure involves decreased wall and lumen diameters but with unaltered media cross-sectional area (Intengan & Schiffrin, 2001). Another study reported a hypertrophic remodelling of the thoracic aorta in SHR, where the wall of the aorta was found thicker compared to normotensive rats (Török & Kristek, 2001). The varied types of vascular remodelling suggest that vascular remodelling may depend on the severity of hypertension. Furthermore, some

evidence has indicated that vessels' thickening was already existed prior to developing high blood pressure in SHR (R. Lee, 1985; Rizzoni, Castellano, Porteri, et al., 1994).

Distorted Ca^{2+} dynamics is believed to be implicated in excessive vascular remodelling in SHR (De Mello, 2016; Fellner & Arendshorst, 2002). Proliferating pulmonary arterial smooth muscle cell (PASMC) was found to have increased expression of TRPC1 due to excessive store Ca^{2+} depletion (Golovina, Platoshyn, Bailey, et al., 2001; M. Sweeney, Yu, Platoshyn, et al., 2002). ATP-mediated TRPC4 expression was reported to amplify Ca^{2+} influx via store-operated pathway which modulated the proliferation activity of PASMC (S. Zhang, Remillard, Faniozzi, et al., 2004). Pyr3-treated hypertensive rats significantly improved the reduction in wall and lumen diameter in the basilar artery smooth muscle cells (BASMC) of hypertensive rats, suggesting a possible role of TRPC3 in the pathophysiological vascular remodelling in hypertension (M. Wang, Tang, Ma, et al., 2016).

Furthermore, the expression of TMEM16A, which is a component of CaCC, was found to be elevated in the arteries of SHR. Ca^{2+}-activated Cl^- efflux via CACCs leads to membrane depolarisation and subsequently opening of VGCC (Goto, Ohtsubo, & Kitazono, 2018). Upregulation of TMEM16A and CaCC deteriorates endothelial function and intensifies blood pressure (M. M. Ma, Gao, Guo, et al., 2017). Application of a TMEA16A inhibitor, T16Ainh-A01, was shown to inhibit single CaCC currents in rabbit pulmonary artery myocytes and exhibit anti-contractile effects in isolated mouse and human arteries (Davis, Shi, Pritchard, et al., 2013). This finding corroborates the reduction of blood pressure in SHR by T16Ainh-A01-induced inhibition on CaCC (Bingxiang Wang, Li, Huai, et al., 2015). Evidence indicates that K_{ir} channels, CaCCs, and TRPV4 also involved in EDHF-mediated relaxation. In hypertensive rat models, downregulation of SK_{Ca}, IK_{Ca} channels and TRPV4 reduced hyperpolarisation in the myoendothelial gap junctions, preventing vascular relaxation. In addition, the activation of SK_{Ca} and IK_{Ca} channels generates endothelium-dependent hyperpolarisation, which becomes impaired in hypertension.

Vascular pathologies in SHR are numerous and complex, which all have an impact on the development of hypertension and sustained high blood pressure. Thus, it contributes to an increased risk of comorbidity such as diabetes (Rizzoni & Rosei, 2006).

4.1.4 Hypertension and diabetes

Diabetes mellitus is a chronic metabolic illness diagnosed by persistently having HbA1c of 48 mmol/mol (6.5%) or fasting blood glucose of 7.0 mmol/l or greater (NICE, 2020). The relationship between hypertension and diabetes are often tied by vascular injury. Oxidative stress is viewed as the common aetiology in these two metabolic disorders. As mentioned, when AT II causes oxidative stress, it stimulates the production of ROS and causes endothelial dysfunction in hypertensive patients (Cheung & Li, 2012). Endothelium dysfunction has also been consistently reported in diabetic patients. Hyperglycaemia induces apoptotic processes in the endothelial cell through β_1-integrin signalling pathway and consequently impairs NO production and its activity and (Avogaro, Albiero, Menegazzo, et al., 2011). Atherosclerosis may be the consequence when the integrity of vasculature is compromised under this vicious cycle. Hence, diabetes is closely related to cardiovascular pathologies, especially hypertension.

A study revealed that half of the patients with primary hypertensive were resistant to insulin (Reaven, 2011). Elevation in blood pressure and structural remodelling of vessels alter the delivery of insulin to cells and exacerbate comorbidities (Salvetti, Brogi, Di Legge, et al., 1993). Insulin resistance in diabetic patients with impaired glucose absorption in skeletal muscle, adipose, liver and vascular tissues, is suggested to cause oxidative stress and endothelial dysfunction. Furthermore, disruption in glucose signalling may increase sodium reabsorption in the kidneys, thereby activating the RAAS-mediated AT II pathways that increases the blood pressure (Govindarajan, Sowers, & Stump, 2006).

4.1.5 STZ-induced diabetic rat model

Diabetic rodent models are often used to study the pathophysiological mechanism of diabetes (Morita, Ouchi, Terada, et al., 2018; Yaroshevskii, 1979). By injecting STZ intravenously to rodents, this antineoplastic agent induces necrosis of pancreatic β-cells. Loss of insulin-producing β cells disrupts the regulation of blood glucose level and manifests as hyperglycaemia. Vascular dysfunction associated with hyperglycaemia has been reported in STZ-induced diabetic rat models, due to decreased plasma NO level, glutathione peroxidase activity as well as elevated lipid peroxidation (Saleh, Bayoumi, El-Eraky, et al., 2013). Impaired vascular function in hyperglycaemic rats was manifested by a reduced reactivity towards noradrenaline stimulation, NO- and

ACh-dependent vasodilation. Furthermore, increased vascular oxidative stress through ROS formation also plays an important role in the setting of STZ-induced diabetes, which reduces NO bioavailability and leads to further diabetic vascular complications (Hink, Li, Mollnau, et al., 2001; Oelze, Knorr, Schuhmacher, et al., 2011; L. F. Zhang, Zalewski, Liu, et al., 2003). These indications were backed by immunohistochemical evidence that detects raise in superoxide anion and nitrotyrosine, a marker indicating the reduction in NO bioavailability in the arteriole sections of STZ-induced diabetic rats (Davidson, Kleinschmidt, Oltman, et al., 2007).

4.2 Significance of study

The findings in Chapter 2 and 3 have presented evidence that FK244- and PM20-induced vasorelaxation in aortic segments obtained from normotensive rats. Therefore, the current chapter aimed to investigate the toxicity of both compounds by studying their effects on the lifespan of *C. elegans.* The second aim was to evaluate the effects of FK244 and PM20 (*ex vivo*) in rat disease models for hypertension and diabetes.

These were the objectives of this chapter:

i. To evaluate the effect of FK244 and PM20 on the lifespan of *C. elegans*
ii. To examine the vascular endothelial integrity of SHR isolated aorta
iii. To construct CRCs to FK244 and PM20 in pre-contracted aortic tissues isolated from SHR and diabetic rat
iv. To investigate the effect of FK244 in SHR isolated trachea and bladder
v. To examine the role of FK244 in NO/cGMP-induced vasorelaxation in SHR-isolated aorta
vi. To study the effect of FK244 against phenylephrine- and $CaCl_2$-induced contraction in SHR aortae

4.3 Materials and methods

4.3.1 Drugs and solutions

Table 4.1 summarised the chemicals used in the lifespan assay. KPO_4 was prepared by slowly adding 1 M of dipotassium hydrogen phosphate (K_2HPO_4) to 1 M of KH_2PO_4 to reach a pH of 6.0. $MgSO_4$, $CaCl_2$ were dissolved in purified water to make stock solutions of 1 M. KPO_4, $MgSO_4$, and $CaCl_2$ were autoclaved at 121 °C for 20 minutes. Cholesterol was dissolved in 95% ethanol to make a stock solution of 5 mg/ml. Streptomycin was dissolved in sterile purified water to make a stock solution of 100 mg/ml. Cholesterol and streptomycin were sterilised by filtering through a membrane filter of 0.2 µM pore size. Sterile membrane filtration technique was used as streptomycin and cholesterol denature under high temperature. All these sterile stock solutions were kept refrigerated at 4 °C and used up to a month.

M9 buffer (pH 7.4) was prepared with the following composition: KH_2PO_4 3 g/l, disodium hydrogen phosphate (Na_2HPO_4) 6 g/l, NaCl 5 g/l, and $MgSO_4$ 1 mM. First, KH_2PO_4, Na_2HPO_4, and NaCl were dissolved in purified water and autoclaved at 121 °C for 20 minutes. Sterile $MgSO_4$ was then added to the solution after it was cooled. M9 buffer was kept refrigerated at 4 °C and used up to a month.

2× lysis buffer was freshly made every time age-synchronisation of *C. elegans* was performed. 5 ml of 2× lysis buffer contained the following: 2 ml of sodium hypochlorite (household bleach Clorox®), 0.5 ml of 10N NaOH and 2.5 ml of sterile purified water.

For organ bath experiments, phenylephrine, carbachol, sodium nitroprusside (SNP) and $CaCl_2$ were dissolved in purified water to make up stock solution mentioned in **Table 4.1**. 10-fold serial dilution was conducted to dilute the stock solution and used to perform CRCs in isometric tension recordings. FK244 and PM20 used in both isometric tension recordings and lifespan assay was dissolved in 100% DMSO as 100 mM stock. Lower concentrations of FK244 and PM20 were prepared in a 10-fold serial dilution from 100 mM stock solutions. They include: 10 mM (DMSO 75%), 1 mM (DMSO 50%), 100 µM (DMSO 25%), 10 µM (purified water), 1 µM (purified water) and 100 nM (purified water). Krebs solution was prepared as described in **section 2.3.2**.

Table 4.1 Summary of chemicals and their details.

Drugs	Company, Country	Solvent	Stock concentration (M, unless stated otherwise)
(*R*)-(−)-phenylephrine hydrochloride	Sigma-Aldrich, USA	Purified water	0.1
Calcium chloride ($CaCl_2$)	Chemiz, Malaysia	Purified water	1.0
Carbamylcholine chloride (Carbachol)	Nacalai Tesque, Japan	Purified water	0.1
Cholesterol	Sigma-Aldrich, USA	95% ethanol	5 mg/ml
K_2HPO_4 (Dipotassium hydrogen phosphate)	Chemiz, Malaysia	Purified water	1
KH_2PO_4 (Potassium dihydrogen phosphate)	Chemiz, Malaysia	Purified water	1M or 3g/l
$MgSO_4$ (Magnesium sulphate)	Chemiz, Malaysia	Purified water	1
Na_2HPO_4 (Disodium hydrogen phosphate)	Chemiz, Malaysia	Purified water	6 g/l
NaCl (Sodium chloride)	Chemiz, Malaysia	Purified water	5g/l
NaOH (Sodium hydroxide)	Thermo Fisher Scientific, USA	-	10
Nemadipine A	Santa Cruz, Texas, USA	DMSO	0.01
Potassium chloride (KCl)	Chemiz, Malaysia	Purified water	3
Sodium nitroprusside (SNP)	Sigma-Aldrich, USA	Purified water	0.1
Streptomycin sulphate	Nacalai Tesque, Japan	Purified water	100 mg/ml

4.3.2 Toxicity screening

4.3.2.1 *C. elegans* strain

SS104 strain [*glp-4 (bn2) I*] (Beanan & Strome, 1992) was obtained from the Caenorhabditis Genetics Centre (CGC), University of Minnesota. In lifespan assay, SS104 is commonly used as they are fertile at 16 °C but progeny production is halted when the experiment was carried out at 25 °C (Jakobsen et al., 2013; Poulsen et al., 2014). This characteristic is desirable because young larvae will affect the counting of living adult worms that were initially exposed to the drugs in the beginning of the experiment.

4.3.2.2 Culturing of *C. elegans*

As mentioned, *C. elegans* was routinely maintained at 16 °C to propagate freely. They were cultured on 6 cm petri dishes containing nematode growth media (NGM) seeded with *E. coli* OP50 as their food source. To prevent contamination, the worms are transferred to new plates every 4 to 5 days when the food source has depleted. All the experimental work on *C. elegans* exercised sterile techniques. All solutions, materials and equipment were kept sterile to prevent contamination on *C. elegans*. All methods used in *C. elegans* experiment were adapted from Wong, Kong, Lee, et al. (2016) and Sutphin & Kaeberlein (2009).

4.3.2.3 Preparation of NGM and *E. coli* for routine maintenance

NGM agar was prepared with the following composition: NaCl 3 g/l, bacteriological agar 20 g/l, bacteriological peptone 2.5 g/l, $MgSO_4$ 1 mM, $CaCl_2$ 1 mM, KPO_4 25 mM, cholesterol 5 µg/ml, and streptomycin 100 µg/ml. NaCl, bacteriological agar, and bacteriological peptone were first dissolved in purified water and autoclaved at 121 °C for 20 minutes. The sterile media was cooled down to approximately 55 °C before adding $MgSO_4$, $CaCl_2$, KPO_4, cholesterol, and streptomycin. The NGM was swirled gently to mix the solution evenly throughout. Then, 10 ml of NGM was carefully poured into a 6 cm petri dish and allowed to solidify for 1 hour.

When the NGM solidified, it was seeded with a layer of *E. coli* on top. *E. coli* glycerol stock stored at -80 °C was thawed. Using the streak plate technique, the thawed bacteria were diluted and grown on Luria Bertani (LB) agar at 37 °C overnight. The following day, a single colony of *E. coli* was inoculated into a sterile LB broth supplemented with 100 µg/ml of streptomycin. The bacteria were cultured at 37 °C in an incubator shaker

overnight (about 16 – 17 hours for optimum bacteria growth). The bacteria were cultured in a circular shaking motion at a speed of 250 rpm to ensure sufficient aeration, avoid bacterial clusters and achieve prolific bacterial reproduction.

The next day, the cloudy LB broth was redistributed equally in a few 50 ml falcon tubes. The broth was centrifuged (Eppendorf® Centrifuge 5810R) with a speed of 4000 rpm for 25 minutes at 4 °C to harvest bacteria pellets. After discarding the supernatant, the bacteria were resuspended and concentrated 25-fold in fresh, sterile LB broth. To maintain *C. elegans* population, 300 µl of *E. coli* were seeded on top of the NGM, in the centre of each 6 cm plate.

4.3.2.4 Worm chunking

This technique was used to transfer a population of *C. elegans* from a 'starved' plate where the *E. coli* have all been consumed by the worms, to a new plate. This technique reduces the chances of contamination in the agar plates and prevents *C. elegans* larvae becoming dauer. Dauer larvae can be found when the growth of worms is interrupted due to lacking food source. A flamed and cooled spatula was used to cut a piece of NGM agar with worms on top, measuring approximately 1 cm^3 in size. This piece of agar was transferred to a new plate containing fresh *E. coli*. The agar was carefully flipped upside down to allow the worms to crawl out of the chunk and access the bacterial lawn sooner. The piece of agar was removed once most of the worms has moved to the new plate. The new plate containing worms was maintained at 16 °C.

4.3.2.5 Preparation of plates for lifespan assay

NGM was prepared according to the method described in **section 4.3.2.3**. 5 ml of NGM was poured in 3.5 cm petri dish (Jet Bio-Filtration, China) and allowed to solidify.

Concentrated *E. coli* OP50 was cultured and resuspended in fresh LB broth using the methods described in **section 4.3.2.3**. It was then heated for 30 minutes at 80 °C in a 1.5 ml tube using a thermoblock (Eppendorf® Thermomixer® R). Heat-killed bacteria was required to prevent any potential effect of the compounds towards live *E. coli*, thereby affecting the lifespan of *C. elegans*. 3.5 cm petri dishes used in the assay were seeded with 50 µl of bacteria. The plates were let dried in a bio-safety cabinet for 2 – 3 hours before storing at 4 °C. Heat-killed *E. coli* OP50 was used as the control. Nemadipine A (20 µM) (Santa Cruz, Texas, USA), a DHP Ca^{2+} channel blocker which is effective in *C. elegans*, was added to heat-killed *E. coli* and used as the positive

control (Kwok, Ricker, Fraser, et al., 2006; S. H. Park, Park, Kim, et al., 2013). In addition, FK244 or PM20 (3 µM, 10 µM) were used to determine its toxicity. These concentrations of FK244 and PM20 were chosen based on its $EC_{90\text{-}100}$ in pre-contracted rat isolated aorta (**Figure 2.8B** and **Figure 3.5B**). Nemadipine A was dissolved in 75% DMSO to make up 10 mM stock solution and further diluted into 1 mM (DMSO 50%) and 100 µM (DMSO 25%). These diluted solutions of nemadipine A, FK244 or PM20 were mixed with heat-killed *E. coli*. 5% of DMSO was used as vehicle control in lifespan assay to rule out the effect of solvent. Assuming the food source is always in excess for 30 worms, **Table 4.2** shows the reconstitution of DMSO, nemadipine A, and FK244 in heat-killed *E. coli*, to make up to 50 µl in volume and be seeded on one 3.5 cm plate.

Table 4.2 Details on stock and final concentration, concentration of DMSO, and volume of stock solution and heat-killed E. coli required during preparation of plates.

Compound	**Stock concentration**	**Final concentration**	**Concentr-ation of solvent, DMSO (%)**	**Volume of stock solution (ml)**	**Volume of heat-killed *E. coli* (ml)**
Control	-	-	-	-	50
DMSO	100%	5%	5	2.5	47.5
Nemadipine A	100 µM	20 µM	5	10	40
FK244/PM20	10 µM	3 µM	0.75	15	35
FK244/PM20	100 µM	10 µM	2.5	5	45

4.3.2.6 Age synchronisation

Age synchronisation was carried out to ensure all the worms on the plates are hatched from the eggs at the same time, in order to eliminate variation in their lifespan due to age difference. First, a plate full of gravid adult worms and eggs on the NGM agar was prepared by chunking the worms in new plates and incubated at 16 °C for 3 – 4 days. Gravid worms can be seen with numerous eggs in their uterus using a stereomicroscope (Nikon SMZ745). 5 ml of M9 buffer was measured and poured onto the plates containing gravid worms. The solution was pipetted up and down a few times to flush the worms off the plates. The M9 buffer now containing worms was then transferred

into a 15 ml falcon tube and mixed with 5 ml of freshly made 2× lysis buffer. The mixture was vortexed vigorously for 5 minutes to break the worms' cuticle and release the eggs from the uterus. The eggs are covered by chitin shell, so while they are resistant to the bleaching agent, the bleach removes the contaminants. The solution was then centrifuged at 1800 rpm for 1 minute at room temperature. The supernatant was discarded, and the egg pellet was mixed gently with 5 ml of fresh M9 buffer. These washing steps consisting centrifugation and resuspension with M9 buffer were repeated twice to ensure a thorough washout of the lysis buffer. The final supernatant was discarded, and the eggs were seeded on a few new plates. When the M9 has evaporated, the plates were kept at 25 °C for 48 hours to grow sterile *C. elegans* for the experiment. Eggs harvested from a single plate were considered as one biological replicate.

4.3.2.7 Lifespan assay

48 hours after egg preparation, 30 adult *C. elegans* were picked individually using a worm picker made by mounting an L-shaped platinum wire into the tip of a glass pasture pipette. It was flamed and cooled each time before using it to transfer the worms from the age-synchronised plate to the plates for assay. This picking technique allowed fix number and specific worms to be picked for the experiment. These synchronised population of *C. elegans* were fed with heat-killed *E. coli*, or containing either DMSO (5%), nemadipine A (20 μM), or FK244 (3 μM, 10 μM), to test the compounds' toxicity. Lifespan assay was carried out on three plates concurrently (representing three technical replicates) using the worms from one biological replicate (n/N = 1/3). The number of live and dead *C. elegans* were counted at the interval of one or two days using stereomicroscope (R. R. Wong et al., 2016). The worms were scored dead if they failed to respond to a gentle touch with the worm picker. The worms were censored if it is missing or dried on the wall of petri dish. The assay was conducted until all worms within the population were dead. Throughout the experiment, the worms were kept at 25 °C to halt egg-laying properties and eliminate confusion while scoring worm mortality. Lifespan assay was further conducted using another two biological replicates which gave rise to n/N = 3/9 for each tested compound. Lifespan assay was repeated by replacing FK244 with PM20.

4.3.3 Blood pressure measurement in SHR

Ethics approval (UNMC18, **Appendix D**) was obtained from the University of Nottingham's AWERB, following the UK Animals (Scientific Procedures) Act 1986. This study also adheres to ARRIVE guidelines and complies with all international, national guidelines and institutional policies. SHRs (336 – 497 g; 3 – 4 months old) were purchased from Monash University, Malaysia campus, where they were housed under standard condition (12 hours light-dark cycle from 8 a.m. – 8 p.m.; 23 ± 1°C) and allowed free access to food pellet and water.

Methods used in SHR blood pressure measurement were adopted from Cheng, Ton, Tan, et al., (2017). Every week, SBP/DBP of the SHRs were measured using the Mouse and Rat Tail Cuff Blood Pressure System (IITC Life Sciences, Los Angeles, USA). The rats were kept in a cylindrical plastic holder one at a time to restrict their movement during the measurement of blood pressure. The rats were placed into a ventilated chamber at 32 °C for 15 – 20 minutes to allow the dilatation of caudal arteries. After acclimatising them, the tail was passed through the hole of the tail-cuff which was connected to a pulse transducer. The system was switched on and the SBP/DBP readings were recorded. The readings were repeated three times to get an average reading of SBP/DBP for each rat. The SBP/DBP of SHRs used for this study ranged between 284 – 338 /169 – 308 mmHg. The blood pressure of SHRs was measured by Mr Boon-Hee Goh from Monash University, Malaysia campus.

The rats were euthanised using CO_2 and sacrificed on the day of the experiment by a laboratory technician at Monash University. Rat aorta, bladder and trachea were isolated on the spot and transported back to the University of Nottingham Malaysia for organ bath studies.

4.3.4 Induction of diabetes in Wistar rats

Ethics approval (Reference number: 2018-210807/PHARM/R/AHAJ) was obtained from the Institutional Animal Care and Use Committee (IACUC), University of Malaya (**Appendix E**). Non-diabetic (293 – 428 g) and diabetic (321 – 402 g) male Wistar rats were obtained from University Malaya (UM), Malaysia. They were housed on a 12-hour light-dark cycle with free access to high-fat or normal diet and distilled water under controlled temperature and humidity.

Type 2 diabetes rat model was induced in 8-week old male Wistar rats using a combination of high-fat diet and low-dose STZ (Mansor, Gonzalez, Cole, et al., 2013; Skovsø, 2014). The rats were given unrestricted high-fat diet or normal diet purchased from Biosystems Corporation®, Singapore. A high-fat diet (C1090-60; Altromin) consists 60% kcal of fat, 16% kcal of protein and 24% kcal of carbohydrate, were given to rats for 3 weeks to induce type 2 diabetes. On the other hand, control non-diabetic rats were fed with a normal diet (1320; Altromin), consisting 11% kcal of fat, 24% kcal of protein and 65% kcal of carbohydrate. On day 14, the fasted rats fed with a high-fat diet were administered a single dose of 30 mg/kg STZ via intraperitoneal injection (IP). STZ was reconstituted in citrate buffer (30 mM citric acid and 20 mM sodium citrate, pH 4) immediately before the injection. The diet was continued further for another three weeks in both diabetic and non-diabetic rats. Blood glucose was monitored weekly with blood sampled from the lateral tail vein using a glucometer (Accu Check Performa®, Roche Diagnostics, France).

On the day of sacrifice, the blood glucose level was within the range of 5.9 – 8.8 mmol/l for non-diabetic rats and 9.2 – 29.0 mmol/l for diabetic rats. The rats were sacrificed with an IP injection of 50 mg/kg sodium pentobarbital (Euthatal, Merial Animal Health / Boehringer Ingelheim, Germany).

The experimental procedures described in this subsection were carried out by Dr Shin-Yee Fung and Mr Alvin Chee-Sum Yap from the Department of Molecular Medicine, University of Malaya. After they sacrificed the animals, the rat aorta, bladder and trachea were isolated and transported back to the University of Nottingham Malaysia for organ bath studies.

4.3.5 Rats isolated tissue preparation

Rats' aorta, trachea and bladder were removed and prepared for experiments according to the methods described in **section 2.3.3.1**.

4.3.6 Organ bath set-up

The aortic rings, tracheal rings and bladder strips were mounted to the organ bath assembly and equilibrated as described in **section 2.3.4**.

4.3.7 Isometric tension recordings

4.3.7.1 Effect of endothelium integrity on carbachol-induced relaxation

To assess the endothelium integrity in SHR isolated aortae, the aortic rings were added carbachol (1 μM) after pre-contracting with phenylephrine (100 nM). Successful denudation was validated by less than 10% relaxation induced by carbachol (Panthiya, Pantan, Tocharus, et al., 2019). The experiment was repeated using normal and denuded aortic rings from SD rats. This experiment was carried out by Dr Kayatri Govindaraju.

4.3.7.2 Effect of FK244 and PM20 on SHR and diabetic rat isolated aorta pre-contracted by phenylephrine

Hypertensive and diabetic rat models were used to investigate the vasorelaxation effect of FK244 and PM20 in disease models. The rat isolated tissues were pre-contracted with phenylephrine (100 nM). Cumulative CRCs to vehicle control (DMSO), FK244 and PM20 (0.1 nM to 100 μM) were constructed using isolated aorta from SHRs, non-diabetic and diabetic rats. Each concentration was added either at an interval of 7 minutes or after the responses plateau if there was any tension change. The results in SHRs were compared to normotensive SD rats (results from **Figure 2.8B** and **Figure 3.5B**), whereas the results in diabetic rats were compared to non-diabetic rats.

4.3.7.3 Effect of FK244 on SHR isolated trachea and bladder pre-contracted by carbachol

Being the more potent compound in SHR aortae (results in **section 4.4.4**), FK244 was chosen for further pharmacological testing. The rat isolated trachea and bladder were pre-contracted with carbachol (1 μM). After the contraction tone stabilised, cumulative CRCs to vehicle and FK244 (3 nM to 100 μM) were constructed in rat isolated trachea and bladder. Concentrations at 0.1 nM – 1 nM were omitted due to their negligible effects in smooth muscle relaxation as seen in normotensive rats (**Figure 2.8C**, **D** and **Figure 3.5C**, **D**).

4.3.7.4 Effect of FK244 in NO/cGMP-induced vasorelaxation

To investigate the involvement of NO/cGMP pathway in FK244 mechanism of action, SHR isolated aortic rings were incubated with FK244 (10 μM) for 30 minutes followed by pre-contraction with phenylephrine (100 nM). After the raised vascular tone has stabilised, cumulative addition of SNP (0.01 nM – 3 μM), a NO donor was performed in the aortic rings.

4.3.7.5 Effect of FK244 on phenylephrine-induced contraction

To investigate if FK244 involves in the contraction mechanism of phenylephrine, SHR isolated aortic rings were pre-incubated with vehicle control or FK244 (10 μM and 100 μM) for 30 minutes. Subsequently, cumulative CRCs of phenylephrine (0.1 nM to 300 μM) were constructed.

4.3.7.6 Effect of FK244 on contractile response to Ca^{2+} re-introduction

This protocol examined the role of FK244 in mediating extracellular Ca^{2+} influx. Aortic rings were pre-incubated with vehicle control, FK244 (10 μM, 30 μM, 100 μM) in Ca^{2+}-free Krebs solution. After 30 minutes of pre-incubation, KCl (60 mM) was added to the aortic rings for 15 minutes to induce plasma membrane depolarisation. Then, $CaCl_2$ was cumulatively re-introduced to the bathing medium (1 μM to 3 mM).

4.3.8 Data analysis

The overall survival of the worms has been expressed as mean lifespan ± SD for n/N = 1/3. n number refers to independent experiments and N number refers to the number of replicates in one experiment. SD was used to quantify the variability within one biological replicate. GraphPad Prism was used to generate the survival curve which illustrated the percentage of live worms in the plates over time. Statistical analyses were performed using Kaplan-Meier non-parametric analysis and log-rank (Mantel-Cox) test in StatView 5.01 (SAS Institute Inc.). The pair-wise comparison was considered significant if *p*-values less than 0.05 ($p < 0.05$).

For isometric tension recordings, methods used in data analysis were described in **section 2.3.6**. Statistical analyses were performed using unpaired Student's *t*-test to compare between control group and treatment group (**Figure 4.6B – D**, **Figure 4.7**). One-way ANOVA followed by Bonferroni's (**Figure 4.3**, **Figure 4.4, Figure 4.5**), Dunnett's (**Figure 4.8**, **Figure 4.9**), or Tukey's (**Figure 4.2**, **Figure 4.6A**) post hoc test was also used to compare the effects of three or more groups. Results with $p < 0.05$ were considered statistically significant. Individual significance was indicated in asterisk symbol in table, where '****' shows $p < 0.0001$, '***' shows $p < 0.001$, '**' shows $p < 0.01$ and '*' shows $p < 0.05$.

4.4 Results

4.4.1 FK244 and PM20 did not affect the lifespan of the worms at a lower concentration

In parallel to pharmacological studies, the toxicity of FK244 and PM20 were assessed *in vivo* using *C. elegans*. Worms exposed to 5% of DMSO, the vehicle used to dissolve all the compounds, and 3 µM of FK244, have a mean lifespan similar to the heat-killed *E. coli*, which was around 18 days (**Figure 4.1A**, **Table 4.3**). They did not seem to affect the lifespan of the worms. However, exposure of 10 µM of FK244 had significantly reduced the mean lifespan of the worms to 15.78 days. In contrast, nemadipine A, a DHP compound known to target Ca^{2+} channel blocker in *C. elegans*, has shown to increase the survival of the worms, with a mean lifespan of 20.29 days.

In another batch of *C. elegans*, the worms treated with PM20 displayed a similar lifespan assay trend. Generally, 5% of DMSO and 3 µM of PM20 did not reduce or increase the worms' survival, with a mean lifespan of around 17 days (**Figure 4.1B**). Like the results yielded with FK244, exposure of 10 µM of PM20 in the worm population also has a reduced mean lifespan of 16.37 days. The population of *C. elegans* had a slight increase mean lifespan of 18.33 days when fed with 20 µM of nemadipine A. **Table 4.3** and **Table 4.4** summarise the mean lifespan for *C. elegans* fed with control (heat-killed *E. coli*), vehicle control (DMSO 5%), nemadipine A, FK244 or PM20.

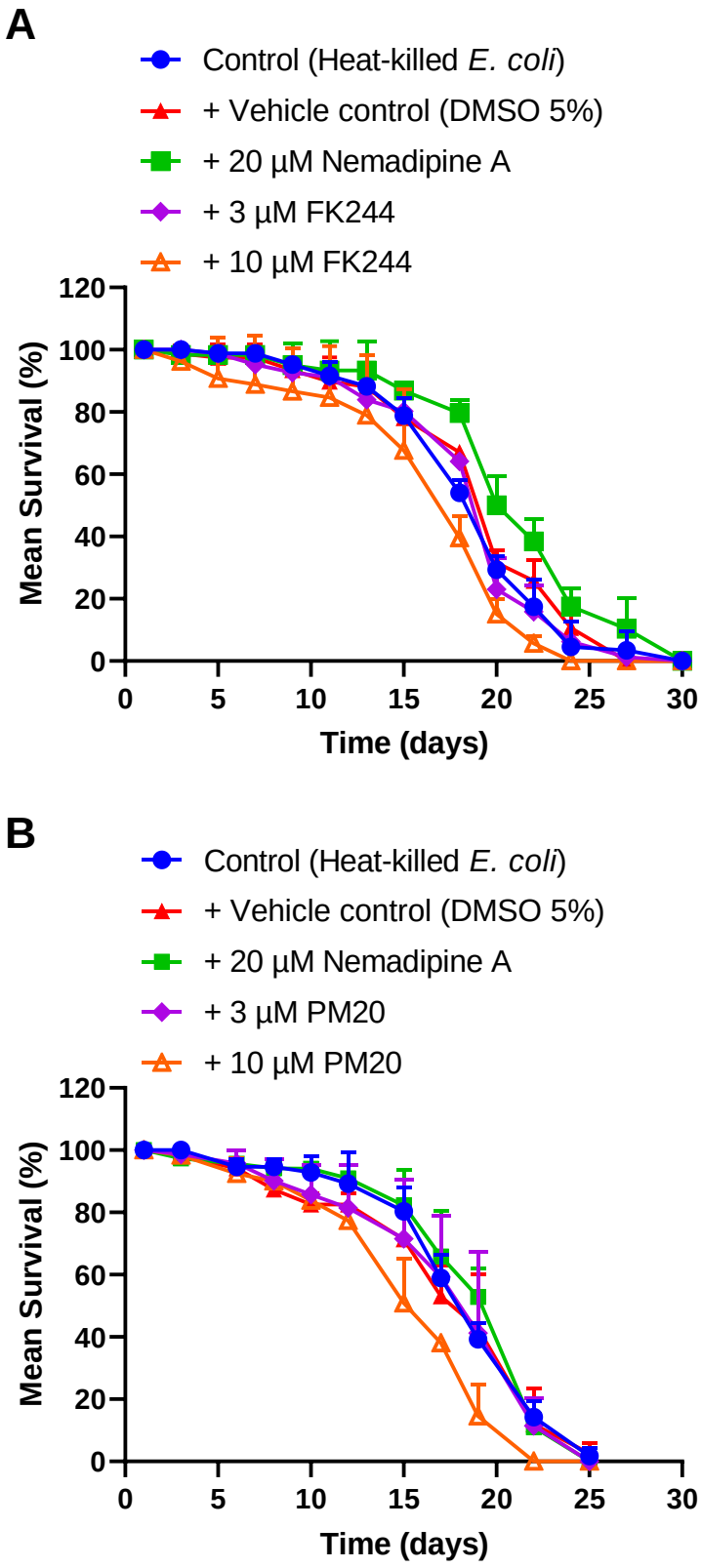


Figure 4.1 Effect of FK244 and PM20 on the lifespan of C. elegans. *Heat-killed E. coli, DMSO and nemadipine A acted as the controls. The lifespan of the worms has been expressed as percentage of mean survival. Data are shown as mean ± SD of one representative biological replicate (n/N = 1/3). Abbreviation: DMSO, dimethyl sulfoxide.*

Table 4.3 Summary of the mean lifespan for nematodes exposed to control (heat-killed E. coli), vehicle control (DMSO 5%), nemadipine A and FK244.

Treatment group	Mean lifespan (day)
Control	18.11 ± 0.50
Vehicle control	18.44 ± 0.59 (*p* = 0.3396)
+ 20 µM Nemadipine A	20.29 ± 0.73 ** (*p* = 0.0027)
+ 3 µM FK244	17.97 ± 0.53 (*p* = 0.9707)
+ 10 µM FK244	15.78 ± 0.73 ** (*p* = 0.0095)

Logrank Mantel-Cox test, pair-wise comparison was used to compare all compounds to control. Individual p-values were stated in the respective columns. Data are shown as the mean ± SD of one representative biological replicate (n/N = 1/3).

Table 4.4 Summary of the mean lifespan for nematodes exposed to control (heat-killed E. coli), vehicle control (DMSO 5%), nemadipine A and PM20.

Treatment group	Mean lifespan (day)
Control	17.86 ± 0.63
Vehicle control	17.04 ± 0.81 (*p* = 0.7128)
+ 20 µM Nemadipine A	18.33 ± 0.57 (*p* = 0.5920)
+ 3 µM PM20	17.43 ± 0.63 (*p* = 0.9260)
+ 10 µM PM20	16.37 ± 0.53 * (*p* = 0.0324)

Logrank Mantel-Cox test, pair-wise comparison was used to compare all compounds to control. Individual p-values were stated in the respective columns. Data are shown as the mean ± SD of one representative biological replicate (n/N = 1/3).

4.4.2 Carbachol-induced relaxation in SHR isolated aortae was attenuated compared to SD

In SD rats, the addition of carbachol has reduced phenylephrine-induced contraction by 72.7 ± 6.4% (**Figure 4.2**). This reduction was significantly different from the carbachol-induced contraction observed in SHR isolated aortic rings, where the reduction was only 8.3 ± 3.4% ($p < 0.0001$) (**Figure 4.2**). After the vascular endothelium of SD rats was denuded, carbachol-induced relaxation was minimal, at 6.6 ± 1.4% (**Figure 4.2**). The tissue relaxation in denuded SD aortae was similar compared to in SHR aortae ($p = 0.9627$), whereas it was also significantly lower than the vasorelaxation measured in normal SD aortae ($p < 0.0001$).

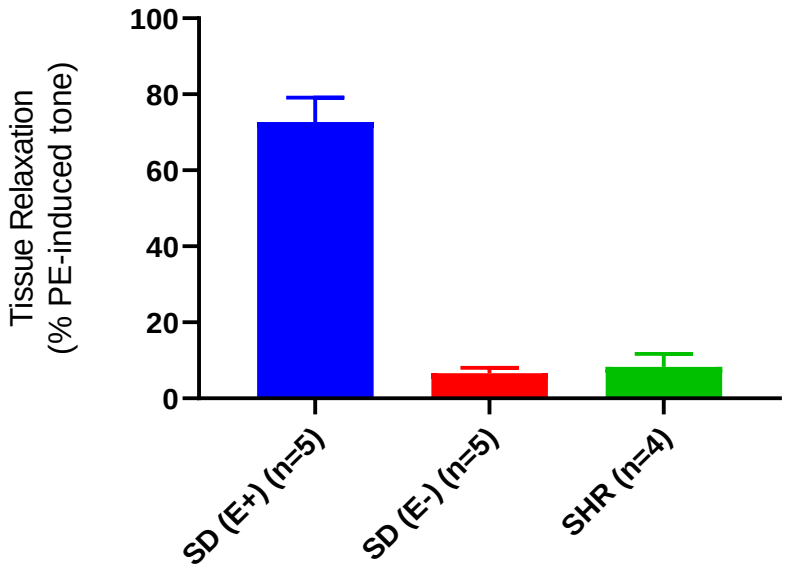


Figure 4.2 Effect of carbachol-induced vasorelaxation in endothelium-intact (E+) and -denuded (E-) SD aorta, as well as in SHR isolated aorta. *Tissue responses have been expressed as the percentage of phenylephrine-induced tone. Data are shown as the mean ± SEM of 4 to 5 animals. Abbreviations: PE, phenylephrine; SD, Sprague-Dawley rats; SHR, spontaneously hypertensive rats.*

4.4.3 FK244 and PM20 induced vasorelaxation in SHR and diabetic rat aortae at raised vascular tone

This experiment investigated the effects of FK244 and PM20 in two disease models, namely the SHRs and diabetic rats.

Statistical analysis showed that the E_{max} and pEC_{50} in SD and SHR were not significantly different (**Table 4.5**). FK244 (**Figure 4.3A**) and PM20 (**Figure 4.3B**) were equally efficacious and potent in both SD rats and SHRs (E_{max}: FK244: $p > 0.9999$; PM20: $p > 0.9999$; pEC_{50}: FK244: $p > 0.9999$; PM20: $p = 0.7069$). In addition, the efficacy and potency of FK244 (**Figure 4.4A**) and PM20 (**Figure 4.4B**) were also not affected in non-diabetic or diabetic rats (E_{max}: FK244: $p > 0.9999$; PM20: $p > 0.9999$; pEC_{50}: FK244: $p > 0.9999$; PM20: $p > 0.9999$).

The efficacy of FK244 and PM20 in SD, SHR, non-diabetic and diabetic rats were all significantly higher than their respective vehicle controls (**Table 4.5** and **Table 4.6**). Potency wise, FK244 and PM20 have shown to have similar potency compared to the vehicle control. Exception was noted for diabetic rats exposed to cumulatively increasing of FK244, where its potency was significantly lower than the vehicle control in diabetic rats (**Table 4.6**).

Furthermore, when the results were compared among all the CRCs of vehicle control, statistical analyses have shown that the E_{max} and pEC_{50} in SD and SHR, non-diabetic and diabetic rats, were not significantly different ($p > 0.05$).

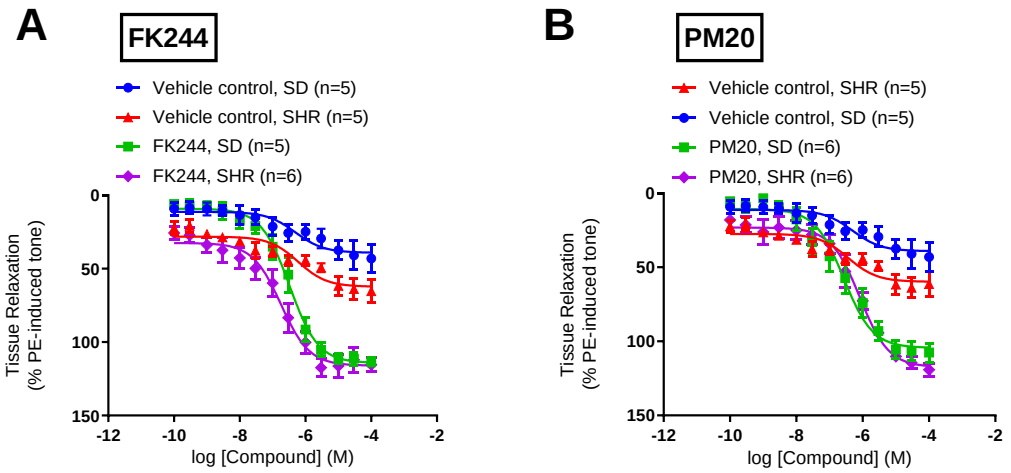


Figure 4.3 Vasorelaxation effect of FK244 and PM20 in SHR. *The results of (A) FK244 and (B) PM20 in SHR isolated aortic rings were compared to vehicle controls and SD rats. Tissue responses have been expressed as the percentage of phenylephrine-induced tone. Data are shown as the mean ± SEM of 5 to 6 animals. Abbreviations: PE, phenylephrine; SD, Sprague-Dawley rats; SHR, spontaneously hypertensive rats.*

Table 4.5 Comparison of the maximum percentage response (E_{max}) and potency (pEC_{50}) of vehicle control, FK244 and PM20 in aortae isolated from SD rats and SHR.

Treatment	Strain	E_{max} (%)	pEC_{50}
Vehicle control	SD	43.1 ± 9.4	6.45 ± 0.25
	SHR	65.3 ± 7.7	6.72 ± 0.38
FK244	SD	114.9 ± 3.4 **** ($p < 0.0001$)	6.49 ± 0.15 ($p > 0.9999$)
	SHR	116.6 ± 6.1 **** ($p < 0.0001$)	6.86 ± 0.23 ($p > 0.9999$)
PM20	SD	106.8 ± 6.1 **** ($p < 0.0001$)	6.69 ± 0.32 ($p > 0.9999$)
	SHR	117.5 ± 3.1 **** ($p < 0.0001$)	6.11 ± 0.10 ($p = 0.7045$)

A single one-way ANOVA with Bonferroni's post-hoc test was used to compare between: vehicle control SD and SHR; FK244 SD and SHR; PM20 SD and SHR; vehicle control SD and FK244 SD; vehicle control SHR and FK244 SHR, vehicle control SD and PM20 SD; vehicle control SHR and PM20 SHR. Individual p-value was stated in the respective column, comparing FK244 or PM20 in SD or SHR, to the vehicle control. Data are shown as mean ± SEM of 5 to 6 animals.

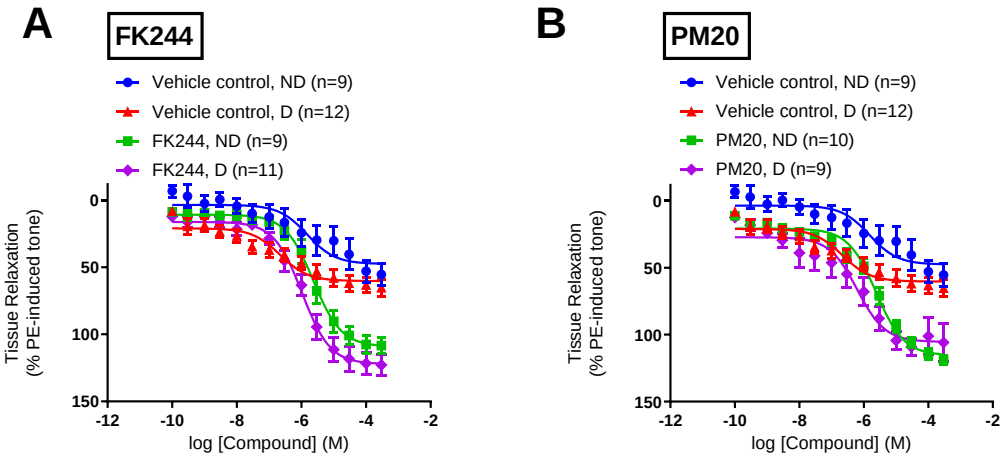


Figure 4.4 Vasorelaxation effect of FK244 and PM20 in diabetic and non-diabetic rats. *The effects of (A) FK244 and (B) PM20 in diabetic rats were compared to vehicle control and non-diabetic rats. Tissue responses have been expressed as the percentage of phenylephrine-induced tone. Data are shown as the mean ± SEM of 9 to 12 animals. Abbreviation: D, diabetic rats; ND, non-diabetic rats; PE, phenylephrine.*

Table 4.6 Comparison of the maximum percentage response (E_{max}) and potency (pEC_{50}) of vehicle control, FK244 and PM20 in aortae isolated from non-diabetic and diabetic rats.

Treatment	Strain	E_{max} (%)	pEC_{50}
Vehicle control	Non-diabetic	55.3 ± 8.2	5.87 ± 0.38
	Diabetic	65.2 ± 6.1	7.09 ± 0.25
FK244	Non-diabetic	113.1 ± 5.9 **** ($p < 0.0001$)	5.60 ± 0.18 ($p > 0.9999$)
	Diabetic	123.8 ± 8.0 **** ($p < 0.0001$)	5.96 ± 0.12 * ($p = 0.0110$)
PM20	Non-diabetic	116.9 ± 4.3 **** ($p < 0.0001$)	5.71 ± 0.19 ($p > 0.9999$)
	Diabetic	114.1 ± 5.6 **** ($p < 0.0001$)	6.22 ± 0.37 ($p = 0.1407$)

A single one-way ANOVA with Bonferroni's post-hoc test was used to compare between: vehicle control non-diabetic and diabetic; FK244 non-diabetic and diabetic; PM20 non-diabetic and diabetic; vehicle control non-diabetic and FK244 non-diabetic; vehicle control diabetic and FK244 diabetic, vehicle control non-diabetic and PM20 non-diabetic; vehicle control diabetic and PM20 diabetic. Individual p-value was stated in the respective column, comparing FK244 or PM20 in non-diabetic or diabetic, to the vehicle control. Data are shown as mean ± SEM of 9 to 12 animals.

4.4.4 FK244 was more potent than PM20 in SHR aortic tissues but equally effective in diabetic rat isolated aortae

Using the results obtained in **section 4.4.3**, another comparison was made to compare the efficacy and potency of FK244 and PM20 in two disease models: the SHR and diabetic rats. As FK244 and PM20 are analogues, the more efficacious or potent candidate was chosen to undergo further pharmacological tests. This step was taken to minimise the number of animals used and increase the cost-effectiveness of this study.

Comparing the vasorelaxation effects of FK244 and PM20, they are equally efficacious (E_{max}: FK244: 116.6 ± 6.1%, PM20: 117.5 ± 3.1%; $p > 0.9999$) (**Figure 4.5A**). However, FK244 demonstrated a slightly higher potency in reducing the phenylephrine-induced contraction in the aortic rings of SHR (pEC_{50}: FK244: 6.86 ± 0.23; PM20: 6.11 ± 0.10; $p = 0.0292$) (**Figure 4.5A**).

On the other hand, there was no significant difference in the efficacy and potency of FK244 and PM20 in diabetic rat isolated aortae rings (E_{max}: FK244: 123.8 ± 8.0%; PM20: 114.1 ± 5.6%; $p > 0.9999$; pEC_{50}: FK244: 5.96 ± 0.12; PM20: 6.22 ± 0.37; $p > 0.9999$) (**Figure 4.5B**). As FK244 is shown to be the more potent compound in relaxing SHR aortic rings, it was used as the analogue in further pharmacological tests using tissues from SHRs and not from diabetic rats.

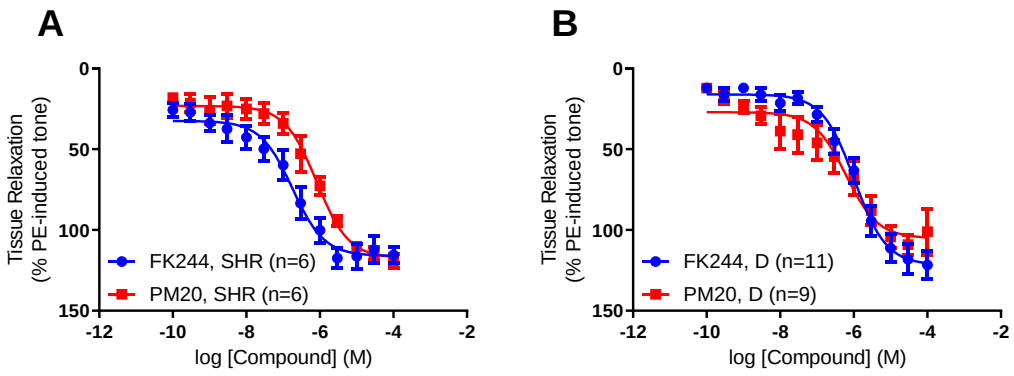


Figure 4.5 Cumulative CRCs of FK244 and PM20 in (A) SHR and (B) diabetic rats. *Tissue responses have been expressed as the percentage of phenylephrine-induced tone. Data are shown as the mean ± SEM of 6 to 11 animals. Abbreviations: D, diabetic rats; PE, phenylephrine; SHR, spontaneously hypertensive rats.*

4.4.5 FK244 induced relaxation on aortic, tracheal and bladder smooth muscle tissues of SHR

FK244 showed relaxation in SHR isolated aortic, tracheal and bladder tissues pre-contracted with the respective pre-contractile agent (**Figure 4.6A**). FK244 induced the highest relaxation in rat isolated aorta among all three types of tissues (**Table 4.7**) The maximum percentage of relaxation in aorta (a) was significantly higher than in bladder (b) (a vs b; $p < 0.0001$), but has no difference compared to trachea (t) (a vs t; $p = 0.5100$). In addition, the maximum percentage of relaxation in the trachea was also higher than in the bladder (t vs b; $p < 0.0001$).

Moreover, pEC_{50} of FK244-induced relaxation was observed around 7 in the aorta (**Figure 4.6B**). On the other hand, pEC_{50} of FK244-induced relaxation occurred approximately 40-fold lower in the bladder (**Figure 4.6C**) and 50-fold lower in the trachea (**Figure 4.6D**) (**Table 4.7**). Comparing the potency across tissues, aorta was significantly more potent than bladder (a vs b; $p = 0.0003$) and trachea (a vs t; $p < 0.0001$), whereas the bladder was equipotent to trachea (b vs t; $p = 0.9548$). Comparison between aorta, bladder and trachea tissues was made using one-way ANOVA followed by Tukey's post hoc test. The values of E_{max} and pEC_{50} of vehicle control and FK244 in these three smooth muscle tissues were summarised in **Table 4.7**.

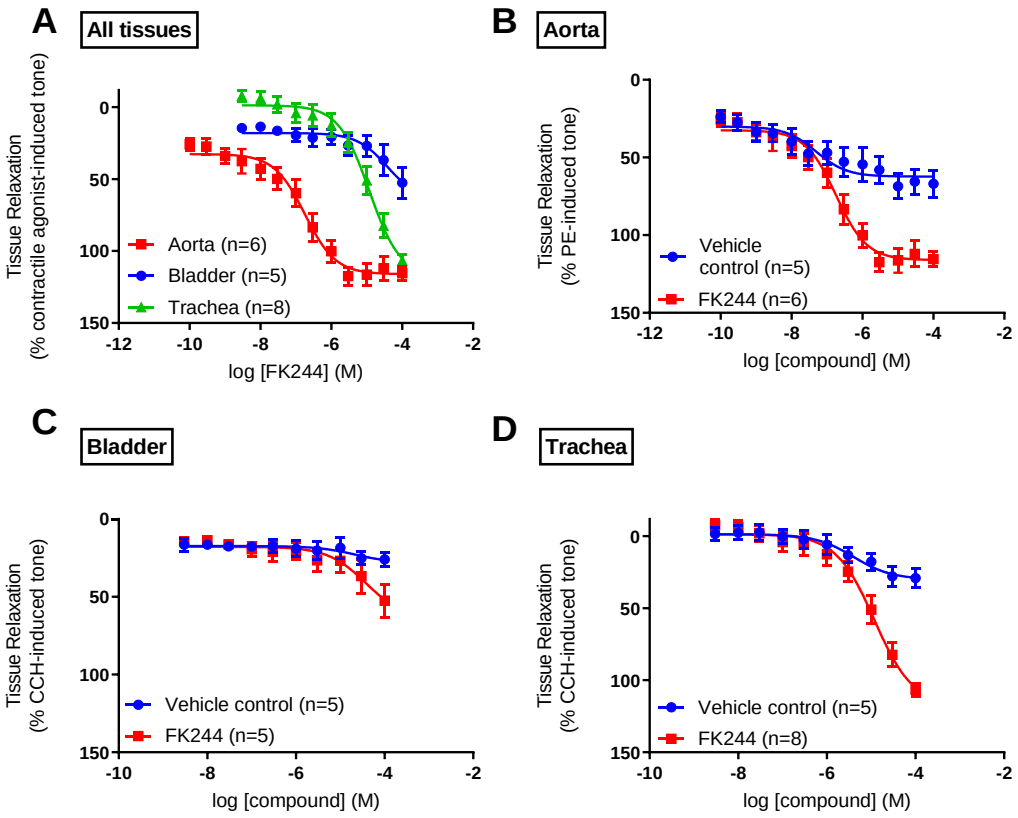


Figure 4.6 Effect of FK244 in (A) SHR isolated aorta, bladder and trachea. *Relaxation effect of FK244 were compared to their respective vehicle controls (DMSO) in (B) aortic rings (C) bladder strips and (D) tracheal rings. Aortic tissue responses have been expressed as the percentage of phenylephrine-induced tone while bladder and tracheal tissues responses have been expressed as the percentage of carbachol-induced tone. Data are shown as the mean ± SEM of 5 to 8 animals. Abbreviations: CCH, carbachol; PE, phenylephrine.*

Table 4.7 Comparison of the maximum percentage response (E_{max}) and potency (pEC_{50}) of vehicle and FK244 in SHR isolated aorta, bladder and trachea after induced contraction with their respective contractile agents.

Tissue	Treatment	E_{max} (%)	pEC_{50}
Aorta	Vehicle control	67.0 ± 8.7	ND
	FK244	116.6 ± 6.1 *** (p = 0.0010)	6.86 ± 0.23 (p = 0.5637)
Bladder	Vehicle control	26.0 ± 4.4	ND
	FK244	52.5 ± 10.5 * (p = 0.0479)	5.26 ± 0.32 † ** (p = 0.0086)
Trachea	Vehicle control	29.0 ± 6.5	ND
	FK244	106.6 ± 4.3 **** (p < 0.0001)	5.17 ± 0.10 † ** (p = 0.0063)

Unpaired Student's test was used to compare between vehicle control and FK244 treatment in aorta, bladder, and trachea tissues. Individual p-values were stated in the respective columns. Data are shown as mean ± SEM of 5 to 8 animals. Abbreviations: ND, not determined. †Estimated pEC_{50} was calculated based on maximum tissue response.

4.4.6 Presence of FK244 did not affect SNP-induced vasorelaxation in SHR

To investigate whether FK244's mechanism involves NO/cGMP pathway, SNP, a NO donor was used. Unpaired Student's *t*-test showed no difference between the potency of vehicle control and FK244-treated aortic rings in SNP-induced relaxation. (pEC_{50}: vehicle control: 8.53 ± 0.23; FK244: 8.31 ± 0.26; $p = 0.5426$) (**Figure 4.7**). Meanwhile, the presence of FK244 did not affect the maximum aortic relaxation to SNP (E_{max}: vehicle control: 114.3 ± 2.7%; FK244: 112.8 ± 9.0%; $p = 0.8825$) (**Figure 4.7**).

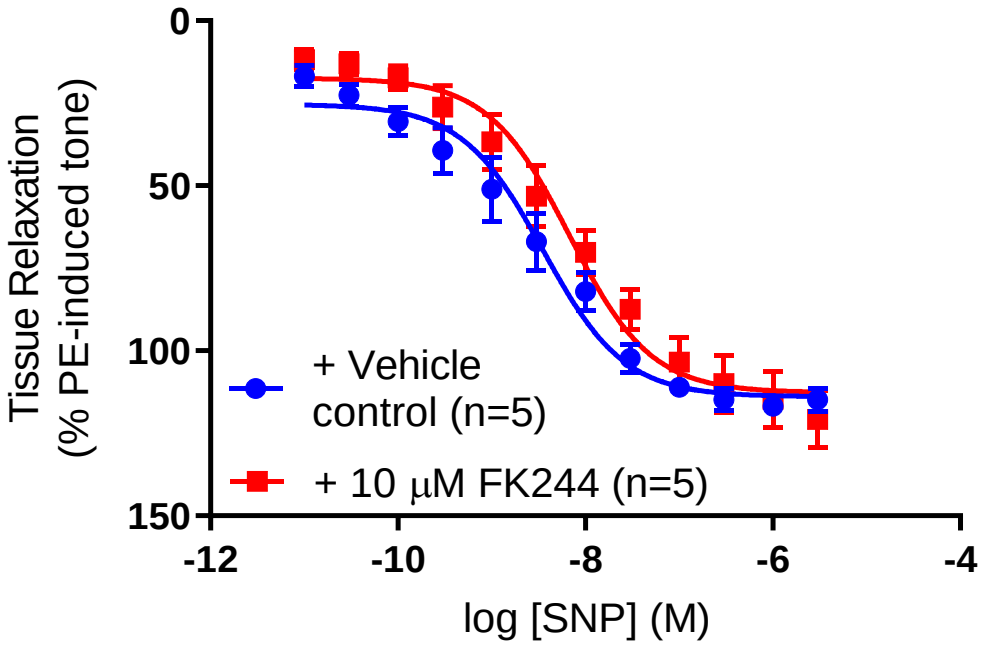


Figure 4.7 Effect of FK244 on SNP-induced relaxation in SHR isolated aortic rings. *Tissue responses have been expressed as the percentage of phenylephrine-induced contraction. Data represent the mean values ± SEM of 5 animals. Abbreviations: PE, phenylephrine; SNP, sodium nitroprusside.*

4.4.7 FK244 attenuated phenylephrine-induced contraction in SHR

Phenylephrine CRC was used to evaluate whether FK244 interferes with phenylephrine-induced vasoconstriction. 10 μM FK244 shifted the curve to the right and reduced the maximum percentage of phenylephrine-induced contraction (**Figure 4.8**). A further reduction in the efficacy and potency of phenylephrine-induced contraction was observed when the aortic rings were pre-exposed to 100 μM of FK244 (**Figure 4.8**). The E_{max} and pEC_{50} values of phenylephrine-induced contraction are summarised in **Table 4.8**.

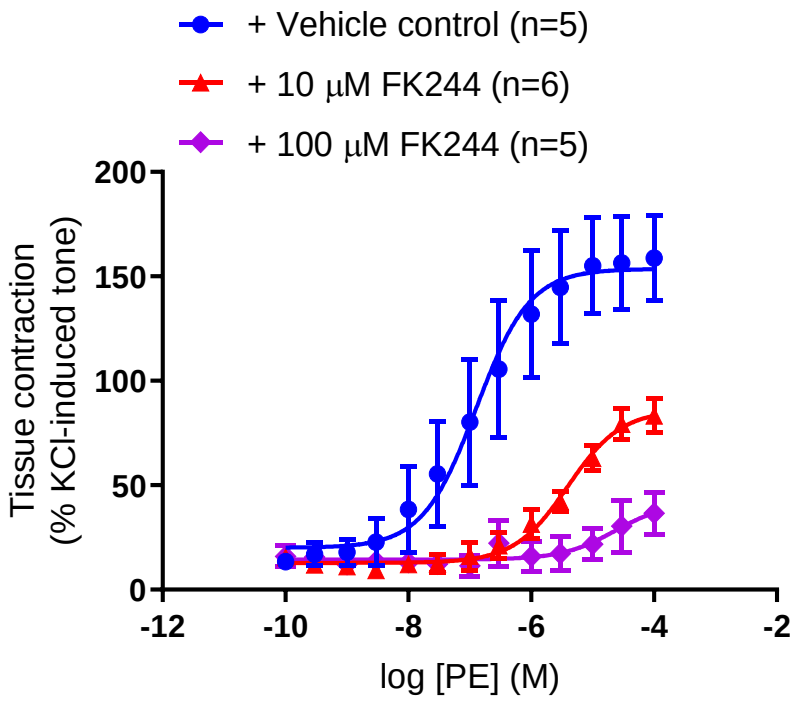


Figure 4.8 Effect of FK244 on phenylephrine-induced contraction in SHR aortic rings. *Cumulative CRCs to phenylephrine were constructed in the presence of 10 μM and 100 μM of FK244. Tissue responses have been expressed as the percentage of KCl-induced contraction. Data are shown as the mean ± SEM of 5 to 6 animals. Abbreviations: KCl, potassium chloride, PE, phenylephrine.*

Table 4.8 Maximum response (E_{max}) and pEC_{50} values derived from phenylephrine's CRCs after pre-exposure to vehicle control and FK244 (10 µM, 100 µM).

Treatment	E_{max} (%)	pEC_{50}
Vehicle control	158.6 ± 21.2	6.75 ± 0.33
+ 10 µM FK244	83.3 ± 8.2 ** (p = 0.0033)	5.76 ± 0.26 * (p = 0.0471)
+ 100 µM FK244	36.6 ± 10.3 **** (p < 0.0001)	5.24 ± 0.27 ** (p = 0.0053)

One-way ANOVA with Dunnett's post hoc test was used to compare FK244-treated tissue to vehicle control. Individual p-values were stated in the respective columns. Data are shown as mean ± SEM of 5 to 6 animals.

4.4.8 FK244 inhibited Ca^{2+}-induced contraction in SHR

Overall, pre-incubation with increasing concentrations of FK244 showed a concentration-dependent reduction in tissue contraction when $CaCl_2$ was re-introduced into a Ca^{2+}-free environment (**Figure 4.9**). Starting from 10 μM, 30 μM to 100 μM, FK244 has caused significant attenuation on the magnitude of $CaCl_2$-induced contraction compared to vehicle control (**Table 4.9**). Pre-incubation of 100 μM FK244 almost abolished the aortic contraction. The E_{max} values of $CaCl_2$-induced contraction in the presence of FK244 are summarised in **Table 4.9**. The potency of $CaCl_2$ was not calculated as maximum tissue responses were not achieved.

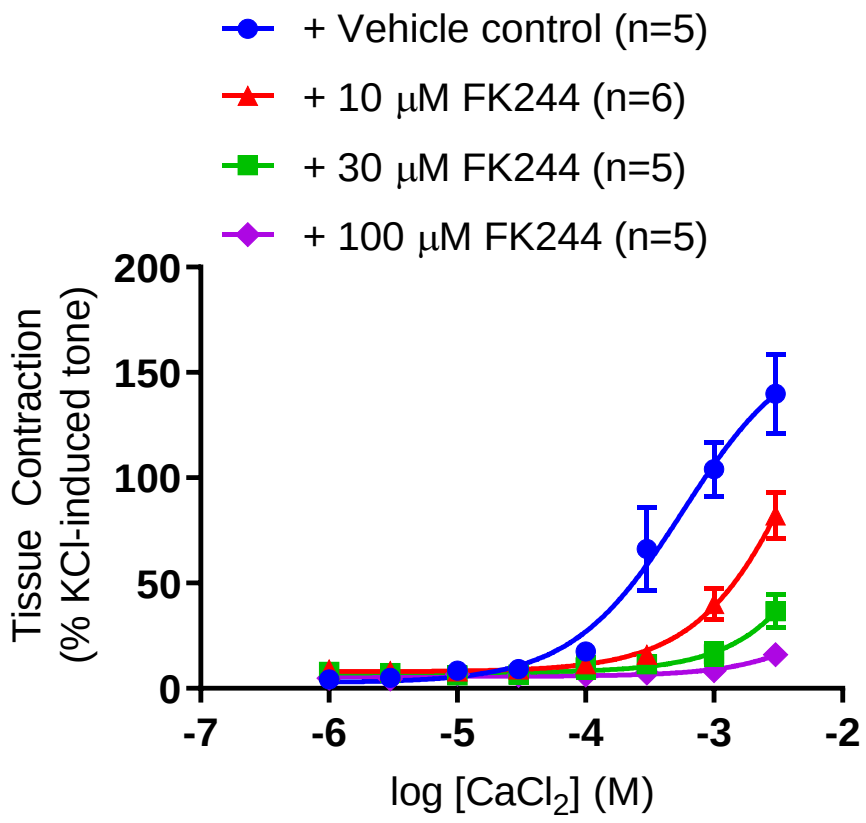


Figure 4.9 Concentration-dependent effect of FK244 on $CaCl_2$-induced contraction in SHR isolated aortic rings bathed in Ca^{2+}-free Krebs solution. *Tissue responses have been expressed as the percentage of KCl-induced contraction. Data are shown as the mean ± SEM of 5 to 6 animals. Abbreviations: KCl, potassium chloride; $CaCl_2$, calcium chloride.*

Table 4.9 Maximum tissue response (E_{max}) of $CaCl_2$ derived from respective CRCs in the presence of vehicle control or FK244.

Treatment	E_{max} (%)
Vehicle control	140.0 ± 18.8
+ 10 µM FK244	82.1 ± 10.8 ** (p = 0.0065)
+ 30 µM FK244	36.6 ± 8.1 **** (p < 0.0001)
+ 100 µM FK244	16.0 ± 4.6 **** (p < 0.0001)

One-way ANOVA with Dunnett's post hoc test was used to compare FK244-treated tissues to vehicle control. Individual p-values were stated in the respective columns. Data are shown as the mean ± SEM of 5 to 6 animals.

4.5 Discussion

This chapter first examined the *in vivo* toxicity of FK244 and PM20 in *C. elegans*. Furthermore, considering FK244 and PM20 have shown overt vasorelaxation activities in normotensive SD isolated aortae, this chapter also investigated their vasorelaxation effects in two disease models, namely the SHRs and diabetic rats.

4.5.1 Effect of FK244 and PM20 on the lifespan of *C. elegans*

For a compound to be safely indicated in a clinical setting, a balance of its therapeutic and toxic effects is imperative. *C. elegans* is an established *in vivo* model organism used to predict the toxicity of a compound. In the lifespan assay, heat-killed *E. coli* was used as the control to benchmark against the toxicity of FK244 and PM20. Besides, 5% of DMSO was used as vehicle control in this study to exclude any toxicity due to the combination of vehicle and drug. 5% DMSO did not have any effect on the lifespan of *C. elegans*. The obtained result agrees with the findings in worms after egg-laying phase, where their lifespan was not affected after exposure to 1% DMSO (Frankowski, Alavez, Spilman, et al., 2013).

Continuous treatment of *C. elegans* with 10 μM of FK244 and PM20 had reduced the lifespan of *C. elegans*. Although this concentration induced E_{max} in rat isolated tissues, this concentration likely causes toxicity and subsequently reduce the lifespan in the whole organism. In contrast, a lower concentration of 3 μM did not pose toxicity nor reduce the percentage of mortality among the worms. These findings provide useful evidence to determine the range of concentration should FK244 and PM20 be tested *in vivo*.

Nemadipine A is a DHP that antagonises the α_1-subunit of L-type VGCC, encoded by the gene *egl-19* in *C. elegans*. Although nemadipine A and nifedipine share similar potency in patch-clamp studies, it was reported that nemadipine A achieved a superior inhibition on L-type VGCC in whole-worm assay compared to nifedipine due to ester and halogen substituents in nemadipine A's structure. (Kwok et al., 2006). Conventionally used Ca^{2+} channel blockers such as nifedipine and amlodipine could not show robust phenotypic changes in the nematodes (Kwok et al., 2006). As this study focused on Ca^{2+} channel blockers, therefore nemadipine A was used as a positive control in this lifespan assay instead of other Ca^{2+} channel blockers used in isometric tension recordings.

On the other hand, nemadipine A increased the survival of *C. elegans* compared to the control groups in both experiments (FK244 and PM20), even though the difference was not significant in the batch treated with PM20. Nemadipine A with a concentration of 5 µM and above was reported to stunt the growth of *C. elegans* (Kwok et al., 2006). This may explain their extended lifespan in both experiments where they grow and age at a slower rate. It has been previously described that 2 µM of nemadipine A had significantly increased the lifespan of *C. elegans*. However, the exact median lifespan was not reported (Zullo, Drake, Aron, et al., 2019). Nemadipine A did not drastically reduce the lifespan of *C. elegans* as one would expect from a toxic compound. Conversely, it stunted the growth of *C. elegans* which was demonstrated by an increased lifespan. This could be interpreted as a physiological-tolerated toxic effect.

This study investigated the effect of a fixed concentration on the lifespan of *C. elegans*. The dose-survival graph was not constructed with increasing concentration of FK244 or PM20, hence their LD_{50} was not deduced. Although lifespan assay is an important indication in early drug development, it can be unpredictable. Toxicity may be affected by the high dose, uncontrolled dosage and prolonged treatment (or rather a constant submersion) of *C. elegans* in the drug-containing bacteria lawn. It is worth noting that any increase or decrease in the lifespan of *C. elegans* in the results was not due to bacterial metabolism, toxins or host-microbe interaction in the worms, as live *E. coli* have been destroyed under high temperature.

In this assay, the endpoint parameter measured to define toxicity was the death of worms. However, the *in vivo* toxicity of a compound is a gradual process that builds up over time and ultimately leads to death. In *C. elegans*, apart from worm mortality, studies have used other functional parameters to measure a compound's toxicity, for instance, feeding rate (Kong, Aziz, Kakarla, et al., 2019), worm motility (Aitlhadj & Stürzenbaum, 2013) and fertility (S. Y. Lee & Kang, 2017).

4.5.2 Endothelium impairment in SHR

Studies have reported vascular endothelium dysfunction in SHR when endothelium-dependent relaxation induced by ACh or carbachol was suppressed (Bolton, Lang, & Takewaki, 1984; T F Lüscher & Vanhoutte, 1986). Furchgott and Zawadski (1980) have shown that endothelial cells are required for ACh-induced vascular relaxation. The presence of ACh in SHR's atherosclerotic coronary artery also evoked a paradoxical contraction possibly due to the release of vasoactive substances, providing inferential links between endothelium dysfunction and CVDs (Ludmer, Selwyn, Shook, et al., 1986; T F Lüscher & Vanhoutte, 1986).

It was established that with an intact endothelium, carbachol activates the most abundantly expressed M_3 receptors, which then catalyses the conversion of L-arginine to NO (Dowd, 2017). NO diffuses to VSMC and causes the conversion of GTP to cGMP by activating sGC. Subsequently, activation of PKG by cGMP leads to Ca^{2+} desensitisation through MLCP activity. Aortic rings with carbachol-induced relaxation of more than 80% were considered intact, whereas less than 10% was deemed damaged (Arsyad & Dobson, 2016). In the results obtained, worsening of endothelial function was inferred when phenylephrine-contracted aortic rings isolated from SHR did not produce more than 10% of relaxation upon addition of carbachol. Its meagre reduction in the contractile response induced by phenylephrine was comparable to those in endothelium-denuded SD aortae. This finding further supports the evidence from previous literature where endothelium dysfunction was suggested in SHR.

4.5.3 Relaxation profiles of FK244 and PM20 in disease models

The lowest concentration of these two compounds in SHRs and diabetic rats has caused an unusually high relaxation – around 30%. This was shown to be the vehicle effect as DMSO has induced a similar magnitude of relaxation. Both FK244 and PM20 displayed similar efficacy and potency in eliciting vasorelaxation in the aorta of SHR and diabetic rats compared to normotensive SD rats and non-diabetic rats, respectively. This observation indicates that FK244 and PM20 are equally effective in the vasculature of healthy and pathological states. As introduced, hypertension and diabetes are two inter-connected metabolic syndromes, which both share common underlying pathophysiological mechanisms that incur damages to the vasculature, especially the arteries. Vascular damage in the diabetic rats used in this study was assumed based on the evidence in the literature (**section 4.1.5**). The pathophysiology of TRPC channels

has been reported in SHR and diabetic rats. The expression of TRPC1 and TRPC6 channels was doubled in the caudal artery of diabetic rats (Mita, Ito, et al., 2010), whereas arterial remodelling in SHR also involved upregulation of TRPC1 and TRPC6 (Lin et al., 2015). In the coronary artery of SHR, TRPC1 was found downregulated and TRPC3 was upregulated, but phenylephrine-induced contraction in the artery was found unaffected (Noorani et al., 2011). Besides, evidence has shown increased activity of L-type VGCCs current in SHR (Ohya, Tsuchihashi, Kagiyama, et al., 1998) and enhanced L-type VGCCs sensitivity in STZ-induced diabetic rats (R. Wang, Wu, Tang, et al., 2000). These findings agree with those reported by Pratt, Bonnett, Ludwig, et al. (2002), where they found that the mRNA and protein expression of L-type VGCCs were amplified in the mesenteric arteries of SHR. The alteration in characteristics of L-type VGCC and TRPC channel may contribute to the abnormalities in vascular tone. Despite these changes of L-type VGCC and TRPC channels in disease states as suggested in the literature, the consistency of the functional responses induced by FK244 and PM20 in hypertensive and diabetic models is favourable as they remained effective.

Enhanced vascular contraction was reported in SHR due to increased VSMC-synthesised TXA_2 (Nademi, Lu, & Dickhout, 2020) and impaired endothelium (Dohi, Kojima, & Sato, 1996; Félétou et al., 2009; Wilson, Zhang, Buckley, et al., 2019) which led to the dysregulation of vasodilation pathways, particularly NO/cGMP-mediated relaxation (Arce et al., 2017; Brozovich, Nicholson, Degen, et al., 2016). Apart from endothelium dysfunction, increased store-Ca^{2+} release and Ca^{2+} influx from external space were found to be accounted for the heightened myogenic tone to phenylephrine in mesenteric arteries isolated from hypertensive rats (Linde, Karashima, Raina, et al., 2012). Accumulating evidence has also pointed out that upregulation of TRPC1/3/5/6 in different vascular beds of SHR was the reason behind the increase in myogenic contraction in SHR, where the contraction could be inhibited by TRPC channels blockers 2-APB and SKF-96365 (Xiaoping Chen et al., 2010; Liu et al., 2009; M. Wang et al., 2016). Similar augmentation in contractile response was reported in the aorta of STZ-induced diabetic rats due to increased extracellular Ca^{2+} influx in VSM and reduced endothelial relaxing substances such as NO and PGI_2 (Okon, Szado, Laher, et al., 2003; Xavier, Davel, Rossoni, et al., 2003). Contradicting these studies, we observed that phenylephrine-induced contraction in SHR was not higher than that in

SD rats. Furthermore, the phenylephrine-induced contraction was not augmented in STZ-induced diabetic rats compared to non-diabetic rats prior to constructing CRCs against FK244 and PM20. Although our results were not widely observed in other studies, these findings were not uncommon. Low contractility has been reported in the arteries of diabetic rats due to reduced extracellular Ca^{2+} entry (Mita, Kuramoto, Ito, et al., 2010). Moreover, abnormal intracellular Ca^{2+} modulation due to defect SR pumps and intracellular Ca^{2+} leakage to the external environment had contributed to the low tissue contraction in SHR aortae (Low, Kwan, & Daniel, 1993). In our experiments, the reduced responsiveness towards adrenergic stimulation in SHR was hypothesised as an adaptation towards morbidity-caused vascular complications or a manifestation of VSM contractility dysfunction. The variation in results compared to the majority of the literature may also depends on the severity of hypertension, disease progression, age of SHR, and the type of blood vessels used in SHR experiments (Hadjiisky, Peyri, & Grosgogeat, 1987).

Even though phenylephrine-induced contraction was not augmented in SHR, it was pointed out that the $CaCl_2$-induced contraction was higher in SHR than in SD rats. Increasing concentration of Ca^{2+} had induced a higher contractile response in SHR aortae (**Figure 4.9**), whereas lower aortic contractility was recorded in SD rat aortae (**Figure 2.21**, **Figure 3.16**). Elevated mitochondrial TRPC3-mediated Ca^{2+} uptake was found to be associated with increased mitochondrial ROS production in SHR (Bin Wang et al., 2017). The expression level of TRPC3 mRNA was significantly higher in SHR fed with a high-salt diet. Similarly, TRPC3-mediated SOCE increased in hypertensive patients with high salt intake (Y. Hu et al., 2020). TRPC6 expression was also upregulated in hypertensive rats, raising the ROCC current and contributing to hypercontractility in the vasculature (Bae et al., 2007). The comparison between SHR and SD rats in this study was nonetheless limited to functional but not molecular differences. The results have been interpreted with caution by considering that Wistar-Kyoto (WKY) rat is the appropriate normotensive control strain for SHR due to the similarity in their genetic makeup. Future studies should be performed using WKY to verify the effect of FK244 and PM20 in disease models (detailed in **section 6.8** and **section 6.9.1**).

The relaxation induced by FK244 and PM20 was not affected despite the evidence of impaired endothelium in SHR. This indication corroborates the vasorelaxation effect of

FK244 and PM20 was mostly exerted on the VSMC. This observation was supported by the findings in earlier chapters, where the relaxation profiles of FK244 and PM20 were unaffected in endothelium-denuded SD aortae.

4.5.4 Pharmacological evaluation of FK244 in SHR-isolated aortae

FK244 was selected to undergo further pharmacological testing as its potency was superior to PM20 in SHR. In past chapters, FK244 had shown selectivity against SD isolated aorta. This was consistently seen in SHR isolated aortae as its relaxation effects were the most prominent in vascular tissues, compared to the bladder and tracheal smooth muscle. The vascular selectivity of FK244 is highly desirable as it is intended to reduce blood pressure without inducing off-site smooth muscle relaxation. Selective molecular targeting cannot be flawless and absolute. Still, with careful selection of concentration range and dose, unwanted side effects and even toxicity can be reduced, as demonstrated with marketed drugs such as heart-selective digoxin.

Since the integrity of endothelium was shown to be impaired in SHR, the level of endogenous NO level was questionable. Therefore, it was unreliable to use L-NAME, an endothelium-dependent eNOS inhibitor, to investigate the role of NO/cGMP pathway in FK244-induced vasorelaxation. On the other hand, the relaxation response to SNP was reported to have no difference in endothelium intact- and denuded arteries (Gericke, Steege, Manicam, et al., 2014). Hence, it is justified to use SNP, an NO donor, to evaluate the NO-dependent signalling pathway of FK244 in SHR-isolated aorta. NO generated by the degradation of SNP diffuses to the VSMC, activates sGC and subsequently induces cGMP-mediated vasorelaxation. The results showed that the presence of NO did not augment vasorelaxation induced by FK244, showing that NO/cGMP pathway is unlikely to be the mechanism of FK244.

Our findings have shown that FK244 effectively reduced phenylephrine-induced contractile sensitivity in SHR's VSMC. FK244 also reduced phenylephrine's potency in the vessels, indicating its mechanism interfered with phenylephrine's contractile mechanism. There are multiple mechanisms in which phenylephrine induces vasoconstriction in SHR-isolated aortae. Phenylephrine activates G_q receptors, triggers a rapid phasic contraction, which was caused by IP_3-mediated intracellular Ca^{2+} release from store compartments (Linde et al., 2012). At the same time, DAG was also generated alongside IP_3 from the hydrolysis of PIP_2. DAG was a putative TRPC3 and

TRPC6 activator which directly initiate Ca^{2+} influx in response to G_q stimulation. Following phasic contraction, the tonic phase was then sustained by external Ca^{2+} influx through VGCCs. Our results also showed that the presence of FK244 inhibited $CaCl_2$-induced contraction. Combining these two observations, FK244 was likely blocking extracellular Ca^{2+} influx after membrane depolarisation. The presence of FK244 could be inhibiting L-type VGCCs which were activated by KCl-induced depolarisation, thereby reducing $CaCl_2$-induced vascular contractility.

Furthermore, Fransen et al. (2015) has mentioned that phenylephrine-induced contraction relies half on the Ca^{2+} influx through L-type VGCCs and another half through NSCCs. As mentioned before, NSCCs are diverse cation channels which includes all the ROCCs and SOCCs, where TRPC channels belong (Malczyk, Erb, Veith, et al., 2017). These NSCCs could be TRPC1/4/5 channels and DAG-sensitive TRPC3/6 channels. Evidence obtained from phenylephrine-induced contraction and $CaCl_2$-induced contraction have delineated an alternative mode of action of FK244, which is inhibition of extracellular Ca^{2+} influx via TRPC3 and TRPC6 channels. Nevertheless, their role in modulating VSMC's Ca^{2+} dynamic via other TRPC subtypes and L-type VGCCs may also account for the reduction in contractile response mediated by phenylephrine and $CaCl_2$ in the aortae of SHR.

4.6 Chapter summary

In summary, this chapter presented preliminary findings on the toxicity of FK244 and PM20. The findings provided valuable insights in identifying a sensible dosage selection when commencing chronic exposure toxicity studies in other model organisms. This could reduce the usage and number of vertebrates in the later stage of pre-clinical testing. In addition, the results in this chapter have shown that the efficacy and potency of FK244 and PM20 were preserved in disease models. Their effectiveness in relaxing pre-constricted aortae in hypertensive and diabetic rat models has demonstrated promising evidence for them to be pursued as therapeutic agents for hypertension and vascular complications in diabetic patients. This work also shed light on the pharmacological effect of FK244 in SHR aortae. Compelling data have revealed FK244's selectivity against VSM with minimal endothelium-dependent effect. Moreover, Ca^{2+} modulation via L-type VGCCs and TRPC channels may be the dominant mechanism responsible for FK244-induced vasorelaxation in isolated aortic tissues.

Chapter 5 Effects of FK244 and PM20 on TRPC3 and TRPC6 channels and internal Ca^{2+} store in HEK 293 cells

5.1 Introduction

Gathering the findings from Chapter 2 and 3, FK244 and PM20 reduced phenylephrine-induced contraction and demonstrated extracellular Ca^{2+}-inhibiting properties. Phenylephrine-induced G_q activation is known to generate second messenger DAG that can directly activate TRPC3 and TRPC6 channels (Hofmann et al., 1999). As TRPC3 and TRPC6 channels also reportedly play more roles in vascular contractility compared to other TRPC subtypes, this evidence prompted further investigation on these two channels.

5.1.1 Role of TRPC3 and TRPC6 in Ca^{2+} signalling

Compare to large-conductance L-type VGCCs, Ca^{2+} permeability through TRPC channels during vasoconstriction are relatively low. The conductance of cation varies between TRPC subtypes. TRPC3 channels conducts both Ca^{2+} and Na^{+} currents relatively equally, whereas TRPC6 channels favour divalent cation conductance (permeability ratio P_{Ca}/P_{Na} : TRPC3 = 1.6; TRPC6 = 5.0) (Bacsa et al., 2020; Hofmann et al., 1999; Kamouchi et al., 1999).

Growing literature demonstrated that the molecular mechanisms of TRPC3 and TRPC6 in modulating Ca^{2+} dynamics are complex in nature. Studies have offered novel insights on TRPC3- and TRPC6-mediated Ca^{2+} regulatory mechanisms, including 1) direct Ca^{2+} transport through the pore region of TRPC channels, 2) modulation of Na^{+} permeability, which indirectly affects Ca^{2+} homeostasis, and 3) functional interaction with other Ca^{2+}-permeable channels by recruiting signalling messengers (Bacsa et al., 2020; Kiselyov, Kim, Zeng, et al., 2005).

Assembly of TRPC homo- or heterotetramers upon specific signal transduction is essential for Ca^{2+} permeation across the plasma membrane (Bacsa et al., 2020). The formation of multimeric proteins is usually confined within the TRPC1/4/5 and TRPC3/6 subgroups (Goel et al., 2002; Hofmann et al., 2002). TRPC3/6 channels primarily function as receptor-operated ion channels, whereas activation of TRPC1/4/5 channels is regulated by internal store Ca^{2+} level (Alonso-Carbajo, Kecskes, Jacobs, et

al., 2017; Hofmann et al., 1999). The key upstream event for receptor-operated activation of TRPC3 and TRPC6 is the cleavage of PIP_2 to IP_3 and DAG via PLC pathway (H. Wang et al., 2020). Both TRPC3 and TRPC6 channels can be activated independently from PKC, directly by DAG, including other cell-permeable DAG analogues such as 1-stearoyl-2-arachidonyl-*sn*-glycerol (SAG) and 1-oleoyl-2-acetyl-*sn*-glycerol (OAG) (Hofmann et al., 1999). OAG is metabolised to its corresponding phosphatidic acid through the action of a DAG kinase (R. Inoue et al., 2001; Kiyonaka et al., 2009). A recent study has revealed that the putative binding site for DAG, OAG in TRPC3 and TRPC6 channels is likely to be lipid-sensing site (Lichtenegger, Tiapko, Svobodova, et al., 2018).

On the other hand, controversial evidence has also described the involvement of TRPC3 and TRPC6 channels in store-operated mechanisms when they cross-associate with the TRPC1/4/5 subgroups. The DAG-sensitive TRPC3 and TRPC6 can be altered depending on $[Ca^{2+}]_i$ (Bacsa et al., 2020). They respond to store-depletion and permit SOCE when they heterotetramerise (Strübing, Krapivinsky, Krapivinsky, et al., 2003; Yuan et al., 2007). Examples of functional store-operated heteromultimeric complexes include TRPC1/3 (Alkhani, Ase, Grant, et al., 2014; J. Chen et al., 2009; Lintschinger et al., 2000; Liu, Bandyopadhyay, et al., 2005), TRPC4/6 (B. Zhang, Liu, Roos, et al., 2018), and TRPC1/6 (Bréchard, Melchior, Plançon, et al., 2008). The molecular mechanism of SOCE begins when intracellular Ca^{2+} pool depletes. STIM1 and STIM2 which located on the SR membrane, sense reduction in SR store Ca^{2+}. These STIM Ca^{2+}-sensing proteins then oligomerise with Orai located at the plasma membrane. The activated complex formed by STIM and Orai is regarded as the component of CRAC channels, forming part of the SOCC. Subsequently, STIM-Orai complexes undergo a series of translocation and reorganisation processes to interact with TRPC3/6 channels on the plasma membrane. They form the primary domain for SOCE to conduct I_{CRAC} (J. J. Lopez, Jardin, Albarrán, et al., 2020).

5.1.2 TRPC3 and TRPC6 channels as therapeutic targets

As the physiological function of TRPC3 and TRPC6 channels are still ill-defined, the development of compounds that can inhibit these channels would be desirable for pharmacological studies. Targeting the diverse Ca^{2+} regulation mechanisms of TRPC3 and TRPC6 channels is an area of growing interest. The development of the functional characterisation and pharmacology of these TRPC channels has been slow until recently, when a number of novel selective small molecules have been discovered (H. Wang et al., 2020). Thus, in many earlier cardiovascular disorder functional studies, non-selective TRPC channel inhibitors such as SKF-96365 and 2-APB was used (P. H. Ratz & Berg, 2006; Sabourin et al., 2016; Singh et al., 2010). Initially, SKF-96365 was reported as a novel ROCE inhibitor with an IC_{50} of 8.5 µM. Albeit its inhibition potency against TRPC6 channels was as low as 2 µM (Harteneck, Klose, & Krautwurst, 2011), it was also found to inhibit voltage-gated Ca^{2+} entry (Clementi & Meldolesi, 1996; Singh et al., 2010), rendering it a non-selective TRPC blocker. Another popular non-selective TRPC blocker, 2-APB, is widely used in studies investigating the role of IP_3 receptors in regulating SOCE mechanisms (Bootman et al., 2002; Splettstoesser, Florea, & Büsselberg, 2007). It soon became apparent that 2-APB had a much broader profile when it was shown to block TRPC channels (Tesfai, Brereton, & Barritt, 2001; Xu, Zeng, Boulay, et al., 2005).

Only in the past decade, more research focused on developing new molecules as TRPC modulators (H. Wang et al., 2020). For instance, Pyr3 was synthesised as a TRPC3-selective inhibitor (Kiyonaka et al., 2009), DS88790512 as a TRPC6-selective inhibitor (Motoyama, Nagata, Kobayashi, et al., 2018) and HC-070 as a potent TRPC1/4/5 inhibitor with potency at nanomolar range (Just et al., 2018). By combining the broad and selective-TPRC modulators in research, their physiological functions can be revealed to provide deeper insights to develop interesting lead structures for drug development.

5.2 Significance of study

TRPC3 and TRPC6 channels are functionally important in regulating vascular contractility via the regulation of Ca^{2+} dynamics. mRNA of TRPC3 and TRPC6 were detected in SD rat isolated aorta (Facemire et al., 2004). Therefore, this chapter aimed to determine the modulation of Ca^{2+} by FK244 and PM20 via TRPC3 and TRPC6 channels using fluorometric Ca^{2+} recordings.

These were the objectives of this chapter:

i. To characterise the inhibition of FK244 and PM20 on TRPC3- and TRPC6-mediated Ca^{2+} influx in HEK 293 cells
ii. To determine the activation of TRPC3 and TRPC6 by FK244 and PM20 by measuring basal $[Ca^{2+}]_i$
iii. To examine the effects of FK244 and PM20 on intracellular Ca^{2+} store

5.3 Materials and methods

The methods used in cell culture (**section 5.3.2**), transfection (**section 5.3.3**) and fluorometric intracellular Ca^{2+} recordings (**section 5.3.4** and **5.3.5**) were adopted from (Minard, Bauer, Chuntharpursat-Bon, et al., 2019).

5.3.1 Drugs and materials

WT HEK 293 cells used for all cell culture experiments were from passage 23 to 35. hTRPC3-expressing (Tet+) HEK 293 T-REx™ cells were cultured from passage 11 to 23. The term 'plating media' used in this thesis was referred to Dulbecco's Modified Eagle Media GlutaMAX™ (DMEM; Invitrogen, Paisley, UK) supplemented with 10% fetal bovine serum (FBS) and 100 units/ml, 100 ug/ml of penicillin-streptomycin. It was used to culture both cell lines in 75 cm^2 flasks. (Tet+) HEK T-REx™ cells are HEK 293 cells overexpressing tetracycline-inducible recombinant proteins. Therefore, (Tet+) HEK T-REx™ cells expressing TRPC3 channel proteins had to be cultured in 'growth media'. It was referred to the plating media which has been supplemented with an additional 10 μg/ml of blasticidin and 400 μg/ml of zeocin. They were used solely in culturing (Tet+) HEK T-REx™ cells to maintain a stable expression of the tetracycline repressor protein and the selection of stable hTRPC3-expressing cells. On the other hand, WT cells do not overexpress a particular protein of interest (i.e., TRPC3). Hence, there was no need for additional blasticidin and zeocin in the media to aid the selection of desired cells.

Details of the drugs, including their brands, solvent used, stock concentration, and final concentration used in cell culture experiments, are listed in **Table 5.1**. Standard buffer solution (SBS) was prepared with the following composition (mM): NaCl 130, KCl 5, $MgCl_2$ 1.2, glucose 8, HEPES 10, and $CaCl_2$ 1.5. In Ca^{2+}-free SBS, $CaCl_2$ was replaced with 0.4 mM EGTA (Sigma, USA). The pH was adjusted to 7.4 using 1 M of NaOH. FK244 and PM20 were made up as 100 mM stock in 100% DMSO. Lower concentrations of FK244 and PM20 from 0.1 mM to 30 mM, were serially diluted from 100 mM stock solutions using 100% DMSO. They were further diluted 1:1000 in recording buffer (SBS + 0.01% pluronic F-127) before being added to cells.

Table 5.1 Summary of chemicals and their details.

Chemicals	Company, Country	Solvent	Stock concentration	Final concentration
1-oleoyl-2-acetyl-*sn*-glycerol (OAG)	Sigma-Aldrich, UK	DMSO 100%	100 mM	100 µM
Blasticidin	Invivogen, California, USA	DMEM	10 mg/ml	10 µg/ml
Fetal bovine serum (FBS)	Sigma-Aldrich, UK	DMEM	100%	10%
Fura-2 acetoxymethyl ester (Fura-2 AM)	Molecular Probes, UK	DMSO 100%	1 mM	1 µM
Penicillin-streptomycin	ThermoFisher Scientific, UK	DMEM	10,000 units/mL, 10,000 µg/mL penicillin-streptomycin	100 units/ml, 100 ug/ml penicillin-streptomycin
Pluronic F-127	Sigma-Aldrich, UK	DMSO	10%	0.01%
Poly-D-lysine	VWR, Lutterworth, UK	Phosphate-buffered saline (PBS)	1 mg/ml	50 µg/ml
Tetracycline	Sigma-Aldrich, UK	Purified water	1 mg/ml	1 µg/ml
Thapsigargin	Sigma-Aldrich, UK	DMSO 100%	5 mM	1 µM
Zeocin	Invivogen, California, USA	DMEM	100 mg/ml	400 µg/ml

5.3.2 Sub-culturing human TRPC3-expressing (Tet+) HEK T-REx™ and wild-type (WT) HEK 293 adherent cells

Cells were passaged with a ratio of 1:10 every 3 to 4 days. Growth media was aspirated from the culture flask containing hTRPC3-expressing (Tet+) HEK 293 T-REx™ cells. 10 ml PBS (Sigma-Aldrich, USA), without $CaCl_2$ and magnesium chloride ($MgCl_2$), was added gently to the side of the flask to wash the cells. This step was to remove any residual serum, calcium, and magnesium, which could possibly inhibit the action of trypsin. After removing PBS, 2 ml of pre-warmed trypsin (0.25%, ThermoFisher Scientific) was added to the flask. The flask was rocked gently back and forth to ensure trypsin was evenly coated the cell layer which was adhered to the bottom of the flask. The flask was placed in a humidified incubator with 5% CO_2 at 37 °C for two minutes. Then, detached cells were washed off the surface several times using 8 ml pre-warmed plating media. The media containing cells was transferred to a 15 ml conical tube and centrifuged at 100 g for 5 minutes at room temperature. The supernatant was discarded. The cell pellet was re-suspended with 5 ml of fresh plating media. New cell culture vessel was seeded at a dilution of 1:10, with 0.5 ml of cells suspension added to 9.5 ml of growth media. For sub-culturing wild-type (WT) HEK 293 cells, all the steps were identical, with the exception that all growth media used was replaced with plating media. After sub-culturing was carried out, all the cells were maintained at 37 °C in a 5% CO_2 humidified incubator.

5.3.3 Transfection of TRPC6 channel in WT cells

A 6-well culture plate (Costar®, Corning Incorporated, USA) was initially coated with 1 ml of 50 µg/ml poly-D-lysine solution for 30 minutes before rinsing off twice with 1 ml PBS. 1 x 10^6 WT HEK 293 cells/well (approximately 40 - 60% confluence) were plated in 2 ml of plating media 24 hours before transfection. The cells were grown overnight at 37 °C in a humidified incubator with 5% CO_2. The next day, the cells were transfected using human TRPC6 (hTRPC6) cloned into pcDNA3 (stock 1.15 µg/µl) and jetPRIME® transfection reagent (VWR, Lutterworth, UK) in a ratio of 1:3 (2 µg: 6 µl). TRPC6 cloned into pcDNA3 was obtained from Dr Melanie Ludlow (Beech Lab, Leeds Institute of Cardiovascular and Metabolic Medicine, University of Leeds). Transfection mix was prepared by diluting 2 µg of hTRPC6 in 200 µL jetPRIME® buffer. After a brief vortex, 6 µl of jetPRIME® transfection reagent was added to the mix. The mix was then incubated at room temperature for 10 minutes before being added to the cells.

4 to 6 hours later, the plating media was replaced with fresh pre-warmed plating media. The cells were then cultured for another 24 hours at 37 °C in a 5% CO_2 incubator to be ready for plating.

5.3.4 Plating cells for experiments

Pellet of hTRPC3-expressing (Tet+) HEK T-REx^{TM} cells and TRPC6-transfected WT cells were obtained by centrifuge using methods described in **section 5.3.2**. These cell pellets were re-suspended in 5 ml of plating media. 48 wells, half of a black, clear-bottom poly-D-lysine coated 96-well cell culture microplate (CELLCOAT®, Greiner Bio-One, Germany) were used in one single experiment (**Figure 5.1**). Each well required 90% confluency, which is approximately 50,000 cells in 100 µl of plating media. For counting the number of the cells, 100 µl of cell suspension was diluted 1:4 in 300 µl of plating media. After mixing thoroughly, 10 µl of diluted cell suspension was pipetted on a haemocytometer. The number of cells in the centre of the grid (1 x 1 mm^2) were counted (**Figure 5.2**). Cells that fell on the top and left border of the centre grid were included, whereas cells on the bottom and right border were excluded (**Figure 5.2**). The height between the haemocytometer slide and glass coverslip was 0.1 mm, therefore the volume was 0.1 mm^3. The number of cells per ml (1000 mm^3 equivalent) was calculated as follow:

$$\textbf{Number of cells per ml} = \textbf{Average number of cells} \times \textbf{4 (dilution factor)} \times 10^4$$

To account for transfer error during pipetting, 6 ml of plating media containing 3×10^6 cells were prepared for plating 48 wells. The volume of cell suspension needed was calculated as follow:

$$\textbf{Volume of cell suspension needed} = \frac{3 \times 10^6}{\textbf{Number of cells per ml}}$$

In a 15 ml conical tube, the required volume of cell suspension was added and topped up with plating media to make up 6 ml. For hTRPC3-expressing (Tet+) HEK T-REx^{TM} cells, 6 µl of tetracycline was added to the cells to induce the overexpression of relevant TRPC protein. After mixing gently, 100 µl of plating media containing 50,000 cells were plated onto a 96-well plate. The 96-well plate containing cells were kept overnight at 37 °C in a 5% CO_2 humidified incubator.

Compounds	1	2	3	4	5	6	7	8	9	10	11	12
A 0 µM (DMSO)												
B 0.1 µM												
C 0.3 µM												
D 1 µM												
E 3 µM												
F 10 µM												
G 30 µM												
H 100 µM												

Figure 5.1 Illustration of a 96-well plate seeded with cells, representing one biological replicate. *Each experiment was repeated six times (column 1 – 6) using the same compound, generating six technical replicates (n/N = 1/6). Column 7 to 12 in the 96-well plate (grey columns) were not utilised in all the experiments.*

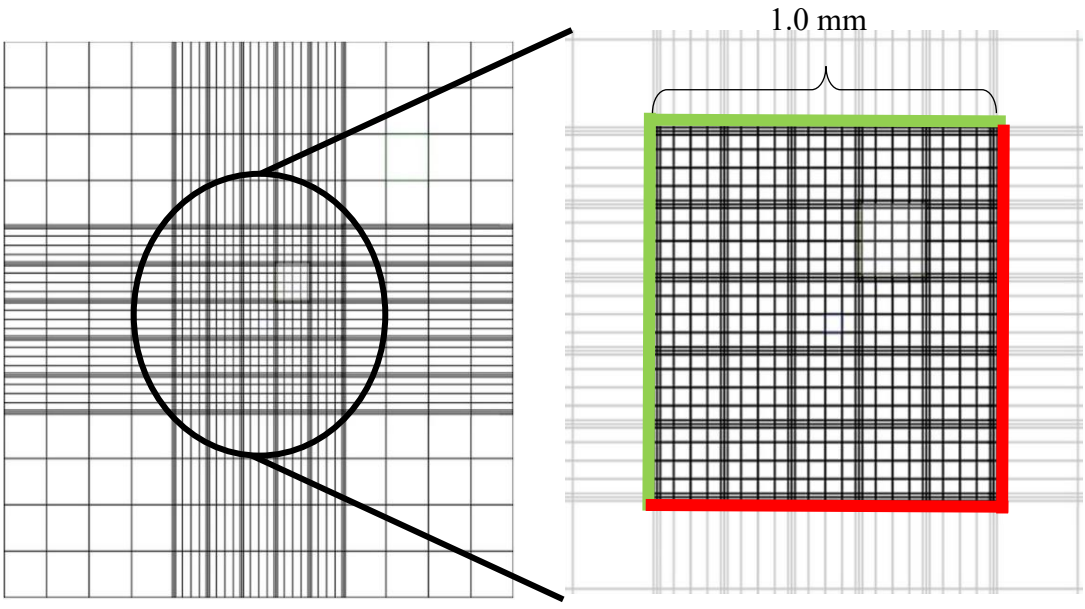


Figure 5.2 Grid etched on a haemocytometer. *Cells fell on the top and left border of the centre grid (indicated with green border) was included but excluded on the right and bottom border (indicated with red border). Diagram adapted from Science ABC (2021).*

5.3.5 Fluorometric intracellular Ca^{2+} recordings

5.3.5.1 Effects of FK244 and PM20 on OAG-mediated TRPC channel activation

As described in **section 5.3.4**, all the cells were plated at 90% confluence 24 hours before the experiment. The next day, in the dark room, the media was removed before loading 50 µl of SBS, containing 2 µM fura-2 AM and 0.01% pluronic F-127 to the cells. Pluronic F-127 was used to increase the solubility of fura-2 AM in SBS. The cells were incubated for 1 hour at 37 °C. After that, fura-2 AM was removed and the cells were washed twice with 100 µl of fresh SBS. This step was followed by the addition of 80 µl recording buffer. Recording buffer was made up of SBS with 0.01% pluronic F-127, containing either vehicle control (DMSO 0.1%), and FK244 with concentration (in µM) of 0.1, 0.3, 1, 3, 10, 30, and 100. The cells were then incubated at room temperature for another 30 minutes prior to the experiment.

30 minutes later, fluorometric Ca^{2+} measurements were carried out at room temperature (21 ± 3 °C) on FlexStation 3 Multimode Microplate Reader (Molecular Devices, San Jose, USA). Fura-2 loaded cells were excited at wavelengths of 340 and 380 nm. Emitted fluorescence was recorded at 510 nm. For one technical replicate, measurements were made every 5 seconds for 5 minutes. Baseline recordings were measured from 0 – 55 seconds. At 60 seconds, 80 µl of compound buffer containing 200 µM OAG (TRPC3 and TRPC6 channel activator) was automatically pipetted from the compound plate to the cell plate. Compound buffer was also added with FK244 (0.1 – 100 µM), DMSO 0.1% and 0.01% pluronic F-127 to maintain their constant concentration throughout the measurements. The addition of recording and compound buffer was executed using automated liquid handling by the FlexStation following pre-defined plate layouts and settings. The experiment ended when all six technical replicates were completed. The final concentration of DMSO in the experiment was 0.1%.

This experiment was performed on hTRPC3-expressing (Tet+) HEK T-REx^{TM} cells and hTRPC6-expressed WT HEK 293 cells. In addition, this experiment was repeated using PM20 in replacement of FK244.

5.3.5.2 Effects of FK244 and PM20 on basal Ca^{2+} level via TRPC3 and TRPC6 channels

hTRPC3-expressing (Tet+) HEK T-REx^{TM} cells were plated and incubated with fura-2 AM using the method described in **section 5.3.5.1**. After removing fura-2 AM and washing the cells with fresh SBS, the cells were left to incubate for another 30 minutes. Immediately before the experiment, the SBS was replaced with 80 µl of recording buffer, which was made up of SBS containing 0.01% pluronic F-127 and 0.2% DMSO (to match with 0.2% DMSO in the compound buffer). The final concentration of DMSO in the experiment was 0.2%. Subsequently, Ca^{2+} measurements were carried out using the similar setting as mentioned in **section 5.3.5.1**. At 60 seconds, 80 µl of compound buffer was automatically pipetted from the compound plate to the cells. Compound buffer was prepared using SBS with 0.01% pluronic F-127, containing either vehicle control (DMSO 0.2%), 200 µM OAG, FK244 with concentrations (in µM) of 20, 60, and 200. These concentrations were halved when pipetted into the cells as the volume of buffer doubled.

The same experiment was performed on hTRPC6-expressed WT HEK 293 cells. Moreover, this protocol was repeated by replacing FK244 with PM20, on TRPC3- and TRPC6-expressing HEK 293 cells. In this series of experiments, only the three highest concentrations of FK244 and PM20 were used. This was decided based on the results in **sections 5.4.1** and **5.4.2**, as the three highest concentrations were close to or higher than the IC_{50}.

5.3.5.3 Effects of FK244 and PM20 on intracellular Ca^{2+} store

WT HEK 293 cells were plated and incubated with fura-2 AM following the method described in **section 5.3.5.1**. After removing fura-2 AM and washing the cells with fresh SBS, the cells were left to incubate for another 30 minutes. Immediately before the experiment, the SBS was replaced with 80 µl of recording buffer, which was made up of SBS containing 0.01% pluronic F-127 and 0.2% DMSO (to match with 0.2% DMSO in the compound buffer). The final concentration of DMSO in the experiment was 0.2%. Subsequently, Ca^{2+} measurements were carried out using the similar setting as mentioned in **section 5.3.5.1**. At 60 seconds, 80 µl of compound buffer was automatically pipetted from the compound plate to the cells. Compound buffer was prepared using SBS with 0.01% pluronic F-127, containing either vehicle control (DMSO 0.2%), 2 µM thapsigargin, and FK244 with concentrations (in µM) of 0.6, 2,

6, 20, 60, and 200. These concentrations were halved when pipetted into the cells as the volume of buffer doubled. The lowest concentration of FK244 (0.2 µM, halved equal to 0.1 µM) was not tested as it has shown insignificant difference to vehicle in **section 5.4.1**. The same experiments were repeated with PM20.

In Ca^{2+}-free recordings, the protocols for FK244 and PM20 were repeated, with the exception that the recording buffer and compound buffer were made up using Ca^{2+}-free SBS containing 0.4 mM EGTA.

5.3.6 Data analysis

Data were presented as the mean ± SEM, with n number refers to the number of independent experiments performed on cultured cells. Data were obtained from 4 – 5 independent experiments (n = 4 – 5). Each experiment consisted of six technical replicates (six wells on each row of a 96-well plate), represented by N = 6. The amplitude of intracellular Ca^{2+} recordings was measured from 90 – 140 seconds for TRPC3 and TRPC6 channels. This interval was chosen because it was the time interval of peak fluorescence amplitude. CRCs were constructed by expressing the response of activator as the percentage of baseline measurements at 0 – 55 seconds. CRCs were fitted with a 4-parameter nonlinear regression fit using GraphPad Prism. IC_{50} for TRPC3 and TRPC6 channels was derived from the curve fit. Potency was calculated, which is represented by pIC_{50} – the negative logarithm of IC_{50}.

5.4 Results

5.4.1 FK244 and PM20 suppressed TRPC-mediated Ca^{2+} influx in HEK 293 cells

The effect of FK244 on TRPC3-mediated Ca^{2+} influx was investigated using (Tet+) HEK T-REx^{TM} cells overexpressing TRPC3 channels. As seen in **Figure 5.3A** and **B**, exogenous application of 100 µM OAG at 60 seconds caused an increase in fluorescence due to Ca^{2+} influx following TRPC3 and TRPC6 channels. This increase of $[Ca^{2+}]_i$ was reduced by pre-incubation with FK244 in a concentration-dependent manner (**Figure 5.3A**). At the highest concentration tested, 100 µM of FK244 completely inhibited the influx of Ca^{2+} through TRPC3 in response to OAG. Our data revealed that the IC_{50} was 14 µM (pIC_{50} 4.9), with Hill slope = -1.4 (**Figure 5.3C**).

Similar protocols were followed to investigate the activity of FK244 against WT HEK 293 cells transfected with hTRPC6. TRPC6-mediated Ca^{2+} entry was evidently reduced by FK244, with complete inhibition was observed at 100 µM (**Figure 5.3B**). The IC_{50} for TRPC6 inhibition was 15 µM (pIC_{50} 4.8), with Hill slope = -1.5 (**Figure 5.3D**).

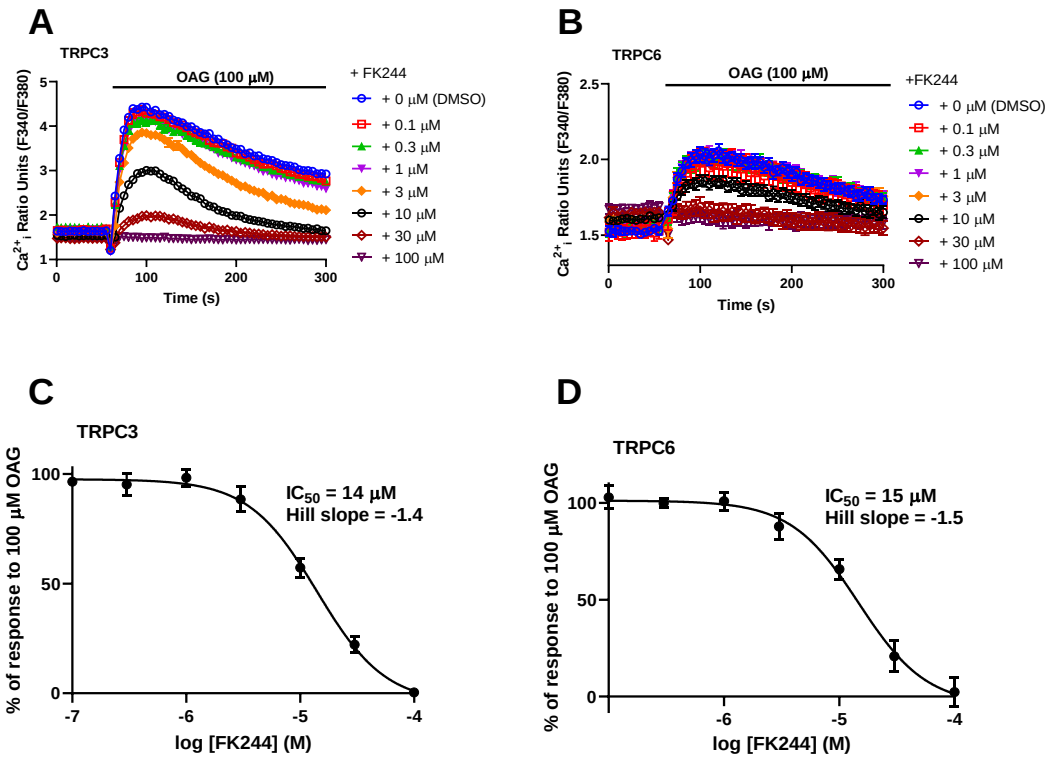


Figure 5.3 FK244 inhibited Ca^{2+} influx via TRPC3 and TRPC6 channels. *Representative $[Ca^{2+}]_i$ measurements recorded in a single 96-well plate (N = 6), measuring the inhibition of OAG-mediated Ca^{2+} influx by 0.1 – 100 µM FK244 in (A) (Tet+) HEK T-REx™ cells expressing hTRPC3 and (B) WT HEK 293 cells overexpressing hTRPC6. Concentration-response curves to FK244 were plotted for experiments in (C) hTRPC3 and (D) hTRPC6. Responses were calculated at 90 – 140 seconds compared to baseline $[Ca^{2+}]_i$ at 0 – 55 seconds. Data are shown as mean ± SEM (hTRPC3: n/N = 4/24; hTPRC6: n/N = 5/30). Abbreviations: DMSO, dimethyl sulfoxide; TRPC, transient receptor potential canonical.*

Similar protocols were used to determine whether PM20 inhibits TRPC3 and TRPC6 channels. In **Figure 5.4A**, it can be seen that increasing concentration of PM20 reduced Ca^{2+} entry via activated TRPC3 channels upon the application of 100 µM OAG at 60 seconds. At the highest concentration tested, 100 µM of PM20 completely inhibited the influx of Ca^{2+} through TRPC3 in response to OAG.

In addition, OAG-induced Ca^{2+} influx was monitored in hTRPC6-expressing HEK cells in the presence of PM20. PM20 suppressed OAG-mediated Ca^{2+} influx in HEK cells overexpressing hTRPC6 (**Figure 5.4B**) in a concentration-dependent manner. Complete inhibition of OAG-mediated increase of $[Ca^{2+}]_i$ via TRPC6 was achieved at 100 µM.

The results showed that the IC_{50} of PM20 for TRPC3 and TRPC6 channels was similar, with values of 14 µM (pIC_{50} = 4.9, **Figure 5.4C**) and 13 µM (pIC_{50} = 4.9, **Figure 5.4D**) respectively. Hill slope values of -1.8 and -1.4 were obtained for TRPC3 and TRPC6 channels. For both channels, vehicle control (DMSO 0.1%) had no effect on the Ca^{2+} influx in the cells.

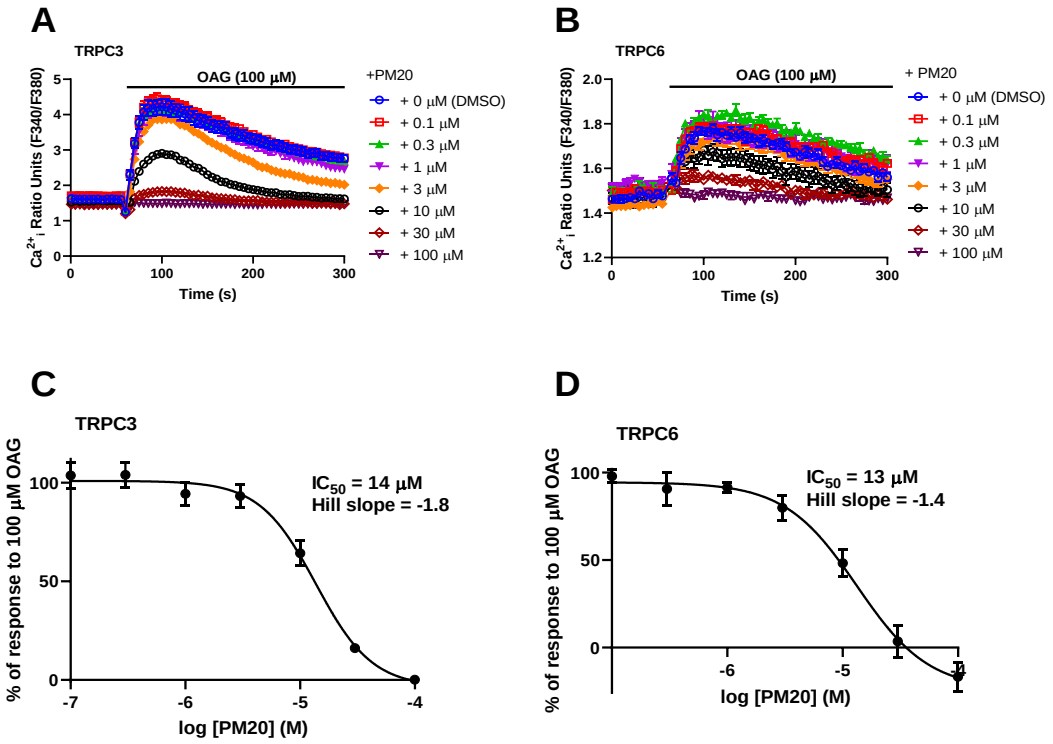


Figure 5.4 PM20 inhibited Ca^{2+} influx via TRPC3 and TRPC6 channels. *Representative $[Ca^{2+}]_i$ measurements recorded in a single 96-well plate (N = 6), measuring the inhibition of OAG-mediated Ca^{2+} influx by 0.1 – 100 µM PM20 in (A) (Tet+) HEK T-REx™ cells expressing hTRPC3 and (B) WT HEK 293 cells overexpressing hTRPC6. Concentration-response curves to PM20 were plotted for experiments in (C) hTRPC3 and (D) hTRPC6. Responses were calculated at 90 – 140 seconds compared to baseline $[Ca^{2+}]_i$ at 0 – 55 seconds. Data are shown as mean ± SEM (hTRPC3: n/N = 5/30; hTPRC6: n/N = 5/30). Abbreviations: DMSO, dimethyl sulfoxide; TRPC, transient receptor potential canonical.*

5.4.2 FK244 and PM20 did not affect basal Ca^{2+} level through activation of TRPC3 and TRPC6 channels

At 60 seconds, each row of cells was injected with either DMSO, OAG or FK244/PM20. FK244 (**Figure 5.5A**) and PM20 (**Figure 5.5B**) did not show an increase in Ca^{2+} influx in hTRPC3-expressing (Tet+) HEK 293 T-REx^{TM} cells before and after 60 seconds. OAG, a known TRPC3 activator, showed a sharp increase in Ca^{2+} influx when it was applied to the cells at 60 seconds. In TRPC6-transfected WT HEK 293 cells, there was no change in fura-2 fluorescence after the cells were added with FK244 (**Figure 5.5C**) and PM20 (**Figure 5.5D**).

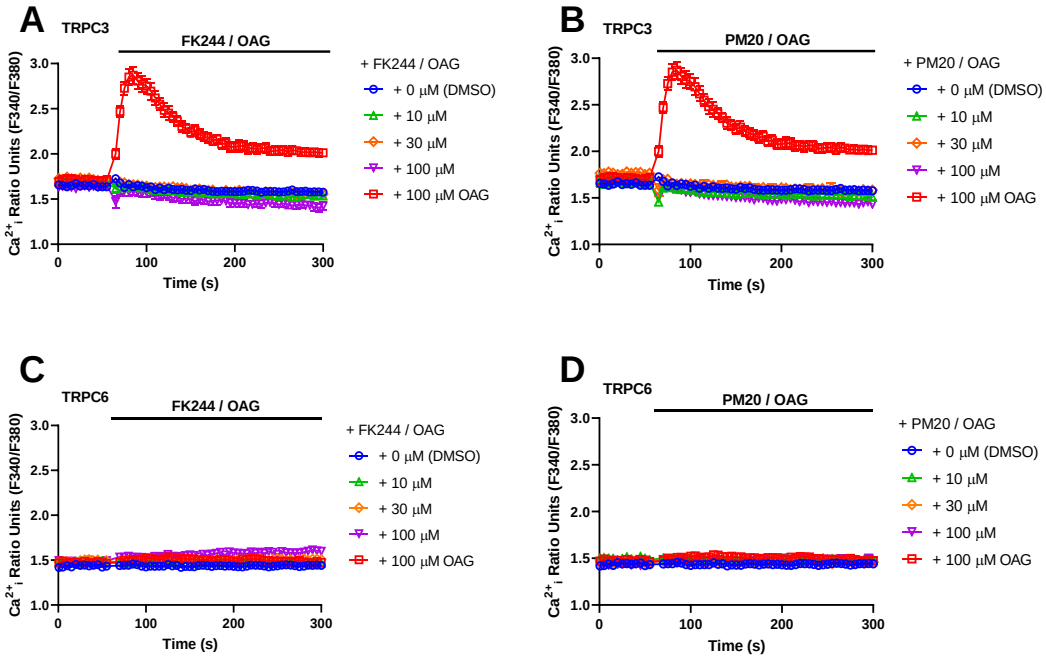


Figure 5.5 FK244 and PM20 did not induce Ca^{2+} influx via TRPC3 and TRPC6 activation. *Representative $[Ca^{2+}]_i$ measurements recorded in a single 96-well plate (n/N = 1/6), showing (A) FK244 and (B) PM20 did not shift basal Ca^{2+} level in TRPC3 -expressing HEK cells. Similarly, no influx of Ca^{2+} was recorded in TRPC6-expressing HEK cells after addition of (C) FK244 and (D) PM20. Abbreviations: DMSO, dimethyl sulfoxide; TRPC, transient receptor potential canonical.*

5.4.3 FK244 and PM20 did not affect intracellular store Ca^{2+} release

To investigate the effects of FK244 and PM20 on intracellular Ca^{2+} store, WT HEK 293 cells were incubated in Ca^{2+}-containing or Ca^{2+}-free SBS before the addition of FK244 or PM20. Without activator OAG, FK244 (**Figure 5.6A**) and PM20 (**Figure 5.6B**) did not induce any changes in baseline $[Ca^{2+}]_i$ with Ca^{2+} presented in the external environment. There was no intracellular Ca^{2+} store depletion induced by FK244 (**Figure 5.6C**) and PM20 (**Figure 5.6D**) without the presence of external Ca^{2+}. 1 µM thapsigargin was used the positive control in this experiment. Thapsigargin, a SERCA pump inhibitor, evoked intracellular Ca^{2+} release into the cytosol, thus causing an increase in the fluorescence. In Ca^{2+}-containing SBS, the cytosolic $[Ca^{2+}]_i$ was increasing continuously. However, in Ca^{2+}-free SBS, the Ca^{2+} release peaked at approximately 150 seconds and was not sustained throughout.

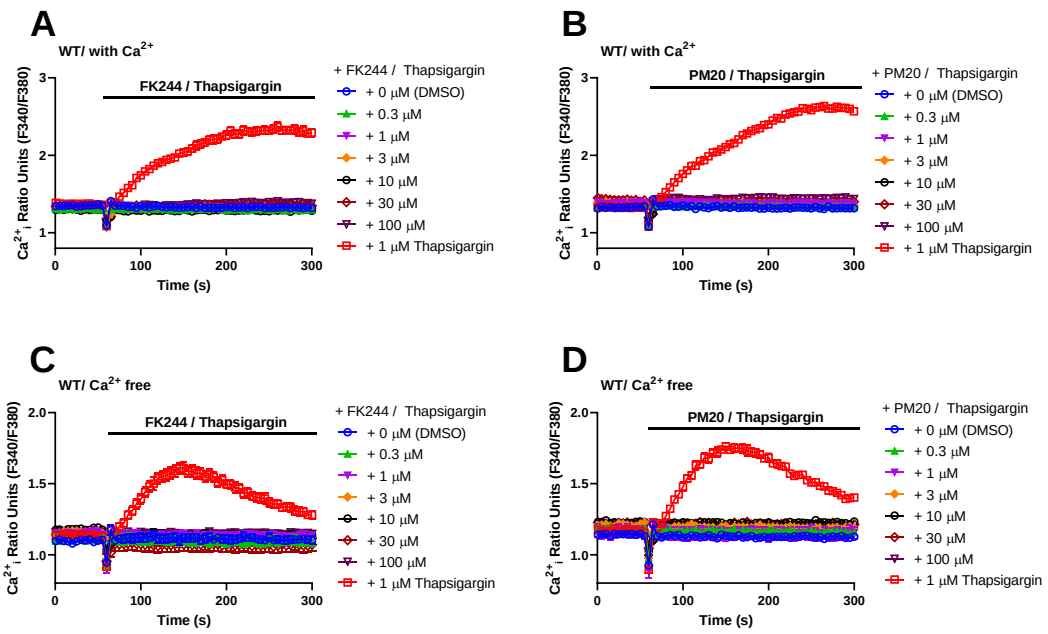


Figure 5.6 Representative Ca^{2+} recordings showing FK244 and PM20 did not evoke intracellular Ca^{2+} release in WT cells in Ca^{2+}-containing and Ca^{2+}-free environment (n/N = 1/6). *In Ca^{2+}-containing SBS, 0.3 – 100 µM of (A) FK244 and (B) PM20 did not cause an increase in $[Ca^{2+}]_i$ through store depletion like thapsigargin. A similar observation was recorded in Ca^{2+}-free SBS containing 0.3 – 100 µM of (C) FK244 and (D) PM20. Abbreviations: Ca^{2+}, calcium ion; DMSO, dimethyl sulfoxide; TRPC, transient receptor potential canonical; WT, wild type.*

5.5 Discussion

In this chapter, the investigation of FK244 and PM20 in regulating Ca^{2+} were carried out, focusing on TRPC3 and its closely related channel – TRPC6. TRPC3 and TRPC6 channels are functionally important in regulating vascular contractility via the regulation of Ca^{2+} dynamics. They were chosen based on their functional roles in vascular regulation reported in the literature (Álvarez-Miguel et al., 2017; Dietrich, Mederos y Schnitzler, Gollasch, et al., 2005; R. Inoue et al., 2006; Kochukov et al., 2012; Martín-Bórnez et al., 2020; Thilo, Baumunk, et al., 2009). In order to measure the intracellular Ca^{2+} dynamics modulated by FK244 and PM20 in TRPC3:C3 and TRPC6:C6 channels, HEK 293 cells overexpressing human TRPC3 and TRPC6 channels were employed.

The data revealed that exogenous application of OAG, a cell-permeable analogue of DAG which activates TRPC3 and TRPC6 channels, showed an increase in fluorescence due to the influx of Ca^{2+}. It was demonstrated that FK244 and PM20 were able to cause a concentration-dependent inhibition on both OAG-mediated TRPC3 and TRPC6 activation with pIC_{50}(s) close to 5. Their potency for Ca^{2+} inhibition was at a low micromolar range (IC_{50}: 13 – 15 μM), which are similar to the IC_{50} value reported for TRPC3-selective inhibitor – Pyr3, at 0.8 μM (Kiyonaka et al., 2009). Recently, there are some small molecules identified as TRPC6 blockers such as DS88790512 (IC_{50}: 11 nM) and ribemansides A and B (IC_{50}: 24.5 and 25.6 μM). DS88790512 was approximately a 1000-time more potent than FK244 and PM20 (Motoyama et al., 2018), whereas ribemansides A and B have similar potency to FK244 and PM20 (Baoping Zhou, Wang, Zhang, et al., 2018). Despite this, there is no information on their selectivity against other TRPC subtypes (Motoyama et al., 2018; H. Wang et al., 2020; Baoping Zhou et al., 2018).

It was vital to evaluate the ability of FK244 and PM20 to regulate basal $[Ca^{2+}]_i$ through the activation of TRPC3 and TRPC6 channels. The results demonstrated that FK244 and PM20 are not activators of TRPC3 and TRPC6 channels in HEK 293 cells overexpressing these channels. There was no change in fura-2 fluorescence when the cells were added with FK244 or PM20 of their three highest concentration (10, 30 and 100 μM). These three concentrations were chosen because they have shown a certain extent of inhibition on TRPC3 and TRPC6-mediated Ca^{2+} influx. Besides, FK244 and PM20 do not act pharmacologically similar to OAG, as they did not induce Ca^{2+} influx

by activating TRPC3 and TRPC6. The findings indicate that FK244 and PM20 do not mobilise basal Ca^{2+} without the presence of an activator such as OAG.

In WT cells, FK244 and PM20 did not affect the resting $[Ca^{2+}]_i$ like thapsigargin, in both Ca^{2+}-containing and Ca^{2+}-free SBS. SR acts as a large reserve for intracellular Ca^{2+} (Kho, Lee, Jeong, et al., 2010). It stores Ca^{2+} via activated SERCA, which can be inhibited by thapsigargin. When thapsigargin inhibited Ca^{2+} reuptake through SERCA, the disruption to Ca^{2+} homeostasis and accumulation of cytosolic Ca^{2+} level was reflected by the elevation of fluorescence. Apart from SERCA inhibition, compound-induced increasing fluorescence at resting $[Ca^{2+}]_i$ could be due to store Ca^{2+} release through the activation of IP_3 receptors, RyRs or basal Ca^{2+} entry via Ca^{2+}-permeable channels such as L-type VGCCs or TRPC channels. However, the results showed that FK244 and PM20 did not alter the fluorescence recorded in WT cells, confirming that they do not induce intracellular store Ca^{2+} depletion by activating IP_3 receptors, RyRs or inhibiting SERCA. They also do not stimulate basal Ca^{2+} entry by activating plasmalemmal Ca^{2+}-permeable ion channels.

It is worth mentioning that the fluorescent Ca^{2+} ratio in TRPC3- and TRPC6-expressed HEK cells were of different values, with TRPC3 channels generating a higher Ca^{2+} ratio in the assays conducted. hTRPC3 gene was incorporated as part of the genome of the cells, hence when cultured, TRPC3 channels were readily expressed in a stable, tetracycline-inducible cell line (HEK T-REx™ cells). When tetracycline was added to the cells a day before the experiment, it induced a robust TRPC3 protein expression in the majority of the cells, and cells which did not induce TRPC3 channels had been killed (Condreay, Witherspoon, Clay, et al., 1999). On the other hand, the TRPC6-overexpressed system was prepared through transient transfection in WT HEK 293 cells. They were transiently transfected using hTRPC6-containing pcDNA3 plasmid. In TRPC6 assays, only transfected cells may express TRPC6 channels, thus contributing a less reliable expression level. When comparing transient expression with stable incorporation in an inducible cell line for a particular channel, the signal is always higher in the stable, inducible cell lines (Geron, Hazan, & Priel, 2017). In the experiments conducted, different Ca^{2+} ratios might be due to fewer cells are transfected in TRPC6-expressed HEK cells. It is also plausible that the quality and quantity of expressed TRPC channel was better with tetracycline-induced expression. HEK T-REx™ cells undergo selection by tetracycline which eliminates cells without

expressing TRPC3 channels. On the other hand, the WT cells overexpressing TRPC6 channels had not undergone any selection process hence it can be affected by transfection efficiency. As Ca^{2+} recordings in TRPC3 and TRPC6 channels were conducted using different overexpression systems, comparing the difference in amplitude of Ca^{2+} ratios may yield less useful inference.

Even though TRPC3 and TRPC6 are highly homologous, their underlying Ca^{2+} influx mechanism in response to OAG is likely to be different. TRPC3 and TRPC6 channels have distinct permeability ratios towards Ca^{2+} and Na^{+}, with TRPC3 channels having a lower Ca^{2+} selectivity compared to TRPC6 channels (permeability ratio, P_{Ca}/P_{Na}: TRPC3 = 1.6; TRPC6 = 5.0) (Bacsa et al., 2020; Hofmann et al., 1999; Kamouchi et al., 1999). Difference in Ca^{2+}-permeability has made them to have distinct functional roles in regulating VSM contractility and other cellular systems (Boulay et al., 1997; Dietrich, Mederos y Schnitzler, Gollasch, et al., 2005; Klein, Mentrup, Timmen, et al., 2020; Zhu, Jiang, Peyton, et al., 1996). The distinction between functions of TRPC3 and TRPC6 was demonstrated in another study where TRPC3 mediated agonist-induced depolarisation in cerebral artery SMC, while TRPC6 played a role in pressure-induced depolarisation which potentiates myogenic tone (Reading et al., 2005). Nevertheless, functional roles of TRPC3 and TRPC6 channels may overlap to compensate for missing mechanisms. It was found that TRPC3 was upregulated in TRPC6-knockout mice when unexpected enhancement in vascular reactivity was detected (Dietrich, Mederos y Schnitzler, Gollasch, et al., 2005).

OAG-induced Ca^{2+} influx in TRPC-6 transfected WT HEK cells may not be apparent in the experiment that assessed basal $[Ca^{2+}]_i$ via TRPC6 channel activation. As mentioned in the previous paragraph, transfection efficiency can be affected by many factors such as purity and the amount of DNA, dilution medium, the ratio of transfection reagent and transfection duration. Although these factors have been optimised in the methods, the confluency and the quality of HEK cells may vary in each experiment. Cells viability and protein expression were reported to be influenced by the passage number, and these can reduce the transfection efficiency (Ponce, Castillo, Hinojosa, et al., 2018). The passage number of WT HEK 293 cells used in TRPC6 activation experiment were P33 and P35. Passage number up to 60 for HEK 293 cells is not uncommon. However, lower passage number of 20- 30 is encouraged for transfection

procedures (P. Thomas & Smart, 2005). The effect of high passage number on TRPC6-transfection efficiency was not ruled out, hence minimal effect of OAG was observed.

Current findings could not reveal the binding site of FK244 and PM20 on TRPC3 and TRPC6 channels. It was not possible to verify that the inhibition of FK244 and PM20 on TRPC3 and TRPC6 channels were mediated by direct interaction with the channels or inhibition on the activation pathway of OAG. OAG, as an analogue to the endogenous DAG, may activate these channels directly and indirectly via a PKC-dependent mechanism (González-Cobos & Trebak, 2011; Venkatachalam, Zheng, & Gill, 2003). Despite this, preliminary tests were done to show that OAG-activated Ca^{2+} influx was only recorded in HEK T-REx^{TM} cells treated with tetracycline and WT HEK 293 cells transfected with hTRPC6 plasmid (**Appendix F**). These findings suggested OAG-induced fluorescence was mediated by the overexpressed TRPC3 and TRPC6 channels. Therefore, FK244 and PM20 are most likely to be inhibitors to the channels themselves.

5.6 Chapter summary

To summarise, current data showed evidence on the modulation of Ca^{2+} by phenylethylamine alkaloids - FK244 and PM20. The results from this chapter affirmed the role of FK244 and PM20 as TRPC3 and TRPC6 inhibitors which suppressed extracellular Ca^{2+} influx. They are inhibitors of both homomeric TRPC3:C3 and TRPC6:C6 channels, with similar potency. They are not activators and have no role in intracellular Ca^{2+} store depletion. The inhibition of phenylethylamine alkaloids FK244 and PM20 on TRPC3 and TRPC6 channels could bring pharmacological significance in clinical use.

Chapter 6 General discussion

6.1 Introduction

In this study, Lipinski's and Veber's rules were employed to assess the drug-likeness of the phenylethylamine alkaloids. The parent compound, schwarzinicine A, was found to have violated one of Lipinski's and Veber's rules. These physicochemical rules are relatively simple to apply, and the values for the parameters involved can be calculated easily. It is noted that these are just guidelines that provide a weak correlation to oral bioavailability and drugs pharmacokinetics especially hepatic and renal metabolism (Hou et al., 2009). Therefore, we did not take the violations of schwarzinicine A as a hard cut-off. Instead of rejecting it as a potential drug for further development, the analyses have indicated some potentials for improving the drug design. Through lead optimisation on the pharmacophore of schwarzinicine A, both FK244 and PM20 were synthesised.

6.2 Functional role of FK244 and PM20 in VSM tissue

The study began by elucidating the pharmacological effects of FK244 and PM20 in VSM tissue using the organ bath technique.

Before carrying out functional evaluation on FK244 and PM20, these two compounds had undergone drug-likeness analyses to predict their oral bioavailability based on their physicochemical properties. **Table 6.1** lists the similarities and differences between FK244 and PM20. Both the compounds obeyed Lipinski's Rule of Five and Veber's rule without any violation (**Table 6.1**), showing they are likely to have more favourable pharmacokinetic properties (greater oral bioavailability) compared to schwarzinicine A.

In organ bath assays, FK244 and PM20 relaxed the pre-contracted smooth muscle tissues in the rat aorta, bladder, and trachea. The efficacy for PM20 was similar in all smooth muscle tissue. However, FK244 was slightly less efficacious in relaxing the bladder tissue than aortic and tracheal tissues (**Table 6.1**). FK244 and PM20 achieved more than 100% efficacy in pre-contracted aortic and tracheal tissues, indicating a relaxation beyond basal tone. However, they did not manipulate the basal tone in quiescent tissues. FK244 and PM20 could behave differently on passive stretch or active tone due to the presence of agonists. Another possible explanation is that the aortae may have retained some active tension induced by KCl during the tissue viability test prior to pre-contraction with phenylephrine.

Potency wise, they managed to reduce phenylephrine-induced contraction in the aorta at a higher potency compared to the carbachol-induced contraction in the bladder and trachea (**Table 6.1**). Moreover, both the compounds possessed similar potency in inducing relaxation in the bladder and tracheal tissues. As FK244 and PM20 most likely relaxed the aortic tissues through inhibition of VGCCs and TRPC channels, it is indicative that there could be a lower expression of TRPC channels in the bladder and trachea. Although phenylephrine and carbachol are associated with the G_q signalling pathway, there is also a possibility that carbachol-induced contraction is less mediated through TRPC channels in the bladder and tracheal tissues, thus, affecting the efficacy and potency of FK244 and PM20.

In addition to rat tissues, the relaxant effect of FK244 was also tested in the porcine bronchiole and pulmonary artery. Overall, FK244 has shown a reduced potency against murine and porcine airway tissues compared to vascular tissues. FK244 also showed selectivity for the thoracic aorta from the systemic circulation over the pulmonary artery of the pulmonary circuit. Nevertheless, its efficacy remained similar in all tissues tested. The aortic selectivity reflected by higher potency has prompted us to investigate the mechanism of actions of FK244 and PM20 in rat aorta. One possible mechanism to relax the pre-contracted aortae was antagonising α-adrenoceptors or interfering with G_q downstream signalling pathways in the VSM.

The plausible effects of FK244 and PM20 affecting the adrenoceptors have also been ruled out using prazosin, rauwolscine and propranolol (**Table 6.1**). In addition, the vasorelaxation effect of FK244 and PM20 was not potentiated when forskolin, an AC activator, increased intracellular cAMP level (**Table 6.1**). Based on these data, neither FK244 nor PM20 induced relaxation by activating β-adrenoceptors and downstream regulation of the AC level.

Furthermore, regulation of the vascular tone can be modulated by a few signal transduction pathways. These include the vascular endothelium and the production of NO, which play important roles in relaxing the vasculature. It was found that removing the endothelium and eliminating NO using L-NAME did not affect the relaxant response of FK244 and PM20 (**Table 6.1**). Furthermore, ODQ-induced sGC inhibition that decreased the level of cGMP did not reduce the relaxant profile of FK244 and

PM20 (**Table 6.1**). These findings produced evidence that FK244 and PM20 do not exert vasorelaxation effects via the endothelium-modulated NO/cGMP pathways.

Vasorelaxation induced by FK244 and PM20 via the activation of K^+ channels was also investigated. Electrochemical gradient allows K^+ to diffuse out of the cells via the opening of K^+ channels, leads to an increase in hyperpolarisation current and vasorelaxation (Jackson, 2000). In the VSM, four main classes of K^+ channels were expressed: K_v, K_{ir}, K_{ATP}, and K_{Ca} channels (Jackson, 2017). The inhibition of these channels did not suppress the relaxant effect of FK244 and PM20 (**Table 6.1**). Therefore, their roles in regulating these ion channels were excluded.

As a piece of supplementary information, a preliminary test was done to examine the reversibility of FK244 and PM20 on phenylephrine-induced contraction. FK244 and PM20 initially suppressed phenylephrine-induced contraction, but the contraction has recovered after washing out the compounds. The results showed that the relaxation effects of both compounds are reversible (**Table 6.1**).

Since FK244 and PM20 produced vasorelaxation effects in phenylephrine-contracted aortae, U46619 and KCl were used as the alternative vasocontractile agents to explore the relaxation characteristics of these compounds. Both FK244 and PM20 exhibited the highest potency against phenylephrine-contracted aortic tissue, and the potency of relaxation was significantly higher than that in KCl- and U46619-induced contraction (**Table 6.1**). A marked difference was noticed when FK244 produced a higher relaxation in KCl-contracted aortae than in U46619-contracted aortae (**Table 6.1**). On the other hand, the efficacy in PM20 was comparable in all three pre-contractile agents (**Table 6.1**). It was interesting to learn that FK244 and PM20 exhibited slightly different potency in relaxing aortae pre-contracted by KCl. FK244 had a higher potency against KCl-contracted aortae compared to U46619-contracted aortae (**Table 6.1**). These findings were different for PM20, where it relaxed aortae pre-contracted by KCl and U46619 at similar potency (**Table 6.1**). Compared to PM20, FK244 has higher efficacy and potency against KCl but not U46619 suggests that FK244 could play more role in the KCl contractile mechanism mediated by membrane depolarisation (P. H. Ratz et al., 2005).

Based on these findings, a series of reverse protocols were carried out whereby the aortic tissues were pre-incubated with FK244 and PM20 before the contractile agents

were added. These contractile agents were phenylephrine, KCl, U46619 and serotonin. The results corroborated with the previous observations. FK244 and PM20 attenuated the contractile effects of phenylephrine, KCl and serotonin (**Table 6.1**). They did not appear to have any significant suppression on the contractility induced by U46619 (**Table 6.1**). U46619-induced contraction was not suppressed by pre-incubation of FK244 and PM20 in these reverse protocols (**Figure 2.16D**, **Figure 3.12D**). However, FK244 and PM20 induced closed to 100% vascular relaxation in response to U46619-induced tone (**Figure 2.15D**, **Figure 3.11D**). It was suggested that U46619 is likely to mediate vasocontraction via $G_{12/13}$-mediated RhoA/ROCK pathway instead of the G_q pathway, which FK244 and PM20 predominantly act on. This incoherent evidence could be due to the sequence of tissue stimulation by compounds with opposing actions. In the first protocol, FK244 or PM20 antagonised the active tone induced by a single concentration of U46619. Conversely, in the reverse protocol, U46619 was added cumulatively after a single concentration of FK244 or PM20 was added into the bath to oppose their inhibitory action. Furthermore, we cannot entirely exclude the effect of time that FK244 and PM20 were present in the bath. The tissues were stimulated cumulatively and continuously with FK244 or PM20 for about two hours in the first protocol. However, FK244 or PM20 was used to treat the tissue for only 30 minutes. Different mechanisms of action may underlie the acute (in CRCs) versus moderate (30 minutes pre-incubation) relaxation effects of FK244 and PM20 on the responses to U46619. These observations imply a possibility that FK244 and PM20 are more effective in relaxing contracted vasculature rather than preventing vascular contraction.

Another notable observation was that at a low incubation concentration of 10 μM, FK244 did not diminish serotonin-induced contraction, but PM20 did (**Table 6.1**). From these experiments, the relaxation mechanism(s) involved in FK244 and PM20 was hypothesised to be inhibiting G_q signalling pathways. Moreover, Ca^{2+} mobilisation within the cell or entry from extracellular space has been long appreciated for its role in modulating vascular contractility. Therefore, these findings also showed that the regulation of Ca^{2+} via TRPC channels and L-type VGCCs which are implicated in phenylephrine's signal transduction could be the key mechanism underlying the relaxation effects of FK244 and PM20.

A few TRPC channels and VGCCs inhibitors were selected as the positive controls in our study. These include non-selective TRPC inhibitors – 2-APB, SKF-96365;

Orai/SOCC blocker – Pyr6; TRPC1/4/5-selective inhibitor – HC-070; TRPC3-selective inhibitor – Pyr3; and VGCC inhibitors – nifedipine and verapamil. 2-APB, SKF-96365 and Pyr6 are also labelled as SOCC inhibitors because TRPC channels and Orai component mediate SOCE pathway that form part of the SOCCs. The characterisation of FK244 and PM20 with these Ca^{2+} channel blockers has presented slight differences between them in terms of their pharmacological properties. The efficacy of FK244 was comparable to HC-070, Pyr6, nifedipine and verapamil but significantly higher than 2-APB, Pyr3 and SKF-96365 (**Table 6.1**). PM20 has similar efficacy to all the Ca^{2+} channel blockers tested but was only significantly higher than Pyr3 (**Table 6.1**). On the other hand, the potency of FK244 and PM20 was not significantly different from all the Ca^{2+} channel blockers but lower than nifedipine (**Table 6.1**). Considered the evidence gathered in this study, we postulate that inhibition of TRPC3 alone by Pyr3 could only produce a partial vasorelaxation response. However, inhibition of multiple TRPC channels subtypes may be required to observe a maximal vascular response in FK244 and PM20.

A few Ca^{2+} channel blockers, namely 2-APB, SKF-96365, nifedipine and verapamil, had substantially reduced phenylephrine-induced contraction, except Pyr3 and Pyr6. As Pyr3 and Pyr6 are selective against TRPC3 and Orai/SOCE, respectively, these findings suggest that non-selective TRPC channels inhibition or VGCCs inhibition are essential to suppress aortic contraction to phenylephrine. These Ca^{2+} channel blockers suppressed phenylephrine-induced contraction at varied extent, highlighting the complexity of cellular Ca^{2+} signalling and the interplay between L-type VGCCs and TRPC channels in regulating Ca^{2+} influx (Ávila-Medina et al., 2016; Berridge et al., 2003; González-Cobos & Trebak, 2011; J. J. Lopez, Jardin, Sanchez-Collado, et al., 2020).

In the second part of the functional studies, the effects of FK244 and PM20 were tested in disease models. Vascular remodelling, such as VSMC proliferation and atherosclerosis, was a prominent feature reported in SHR aorta (Hadjiisky et al., 1987; Török & Kristek, 2001). In addition, the functional effects of FK244 and PM20 were also tested in STZ-induced diabetic rats, as diabetes is a comorbidity of hypertension. Diabetes and hypertension share common vascular complications, such as endothelial dysfunction, arterial stiffness, increased predisposition of dyslipidemia and atherosclerosis (Petrie, Guzik, & Touyz, 2018). In the present study, endothelium

impairment in SHR aortae was established due to its low response to carbachol-induced relaxation. It was found that FK244 and PM20 displayed consistent relaxation profiles even in impaired vasculature. Moreover, vascular remodelling and dysfunction as reported in diabetic rats, did not affect the vascular effects of FK244 and PM20.

FK244 was selected to proceed with pharmacological testing in SHR aorta as it exhibited a higher potency than PM20 in SHR (**Table 6.1**). Like the findings obtained in SD rats, vasorelaxation induced by FK244 was not enhanced in the presence of the NO donor – SNP. This ruled out the endothelial involvement of FK244 in mediating NO/cGMP pathway. Furthermore, FK244 has reduced the contraction to phenylephrine and $CaCl_2$ in SHR. The available evidence suggests that FK244 is likely to inhibit extracellular Ca^{2+} influx via phenylephrine-regulated mechanisms. It may block Ca^{2+} entry via DAG-sensitive TRPC3 and TRPC6, SOCE via TRPC1/4/5, or L-type VGCCs upon membrane depolarisation. The putative mechanisms of FK244 in SD rat is likely to be the same as in SHR.

However, it is worth noting that in the presence of FK244, there was a noticeable difference in the tissue contractility of SD and SHR towards phenylephrine stimulation. The presence of FK244 at 10 µM significantly reduced the maximum contraction induced by phenylephrine in SHR aortic rings (**Figure 4.8**) but failed to alter the contractile response in normotensive SD aortic rings (**Figure 2.16A**). In Chapter 4, it was discussed that phenylephrine-induced contraction in SHR was generally lower than that observed in SD rats in our experimental set-up. Abnormal intracellular Ca^{2+} modulation due to defect SR pumps and intracellular Ca^{2+} leakage to the external space could attribute to the discrepancies in functional effects observed (Low et al., 1993). On the contrary, functional upregulation of L-type VGCCs in SHR compared to normotensive control has been described to enhance Ca^{2+} current recorded in patch clamp electrophysiology, which proportionately influenced blood pressure levels (Cox & Rusch, 2002). The complexities of protein expression in hypertensive vascular pathophysiology are further underscored in TRPC channels. TRPC3 channels were found upregulated in TRPC6 knockout mice, which said to be responsible for the elevated blood pressure and tissue contractility towards phenylephrine (Dietrich, Mederos y Schnitzler, Gollasch, et al., 2005). These findings contrast with the results reported by Noorani et al. (2011),where upregulation of TRPC3 and downregulation of TRPC1 observed in SHR did not affect phenylephrine-induced contraction. The

discrepancies could be due to the difference in animal species and the type of vessels used, as these factors may have different vascular physiology. Dietrich et al. (2005) utilised mice aorta and mesenteric arteries, whereas Noorani et al. (2011) utilised rat carotid artery. As we did not observe any increase in SHR aortic contractile response earlier, this could mean that there was no functional upregulation of Ca^{2+}-permeable channels in our SHR aortic preparations. This ruled out the possibility of a more efficacious inhibition on upregulated L-type VGCCs or TRPC channels by FK244 in SHR aortae. However, the different suppression effect of 10 μM FK244 on phenylephrine may be due to increased susceptibility to its targeted channels in pathological states. This postulation is supported when nifedipine showed a greater inhibitory effect on the basal tone of mesenteric arteries obtained from SHR (Cox & Rusch, 2002). Therefore, it can be reasonably believed that Ca^{2+} leakage and enhanced target binding by FK244 mediated this suppression towards phenylephrine in SHR.

In summary, we have demonstrated that phenylethylamine analogues – FK244 and PM20, managed to induce vasorelaxation in the aorta isolated from both normotensive and hypertensive models. The functional data have provided convincing evidence that FK244 and PM20 with similar chemical structures, elicited similar pharmacological effects in aortic smooth muscle tissues. They generated vasorelaxation effects in response to pre-contraction of phenylephrine, KCl and U46619. Besides, they also suppressed the contraction induced by phenylephrine, KCl and serotonin. These findings point towards the possibilities in the regulation of Ca^{2+} dynamic by FK244 and PM20.

6.3 Ca^{2+} modulation property of FK244 and PM20

Smooth muscle contraction depends on rising $[Ca^{2+}]_i$. One of the key inferences made from isometric tension recordings was that both analogues could modulate Ca^{2+} dynamic via the inhibition of TRPC channels and L-type VGCCs, which are activated in phenylephrine's downstream signal transduction. This notion supported the findings where pre-treatment with FK244 and PM20 effectively attenuated the $CaCl_2$-induced contraction in Ca^{2+}-free Krebs solution. Inhibition of extracellular Ca^{2+} entry by FK244 was noted even in SHR. The efficacy of FK244 and PM20 was reduced by pre-incubation of TRPC blockers, which includes 2-APB, Pyr3, Pyr6 and SKF-96365 (**Table 6.1**). The presence of Pyr6 and SKF-96365 in the bath had reduced the potency of FK244. However, the potency of PM20 was unaltered in the presence of other Ca^{2+}

channel blockers (**Table 6.1**). These findings further confirmed that FK244 and PM20 might interfere with extracellular Ca^{2+}-permeability across non-specific inhibition on TRPC channels and L-type VGCCs with varied sensitivity.

To investigate the postulation proposed based on the evidence obtained from organ bath studies, Ca^{2+} recordings were used to directly observe the effect of FK244 and PM20 on instantaneous intracellular Ca^{2+} dynamic. The activity of FK244 and PM20 against TRPC3- and TRPC6-mediated Ca^{2+} influx was examined. Both the compounds managed to reduce the fluorescent signals in TRPC3 and TRPC6-overexpressing HEK 293 cells. They were able to suppress OAG-induced extracellular Ca^{2+} influx via TRPC3 and TRPC6 in cellular assays (**Table 6.1**). These data also support previous inference where the relaxation responses evoked by FK244 and PM20 in the VSM were due to extracellular Ca^{2+} influx inhibition. We observed that FK244 and PM20 has a similar potency in inhibiting TRPC3 and TRPC6 (**Table 6.1**). High sequence homology between TRPC3 and TRPC6 channels may underpin the relatively close potency of FK244 and PM20 against these channels. Different TRPC channel subtypes can form heterotetrameric channels. Accumulating evidence reported the detection of native heterotetrameric TRPC channels in the vasculature such as TRPC1:C6, TRPC1:C3 and TRPC3:C6 channels (Goel et al., 2002; Liu, Bandyopadhyay, et al., 2005; Y. Yu et al., 2003). Co-expression of these heterotetrameric channels may reduce the strict definition of SOCE being regulated by TRPC1/4/5 and ROCE by TRPC3/6 (Kiselyov et al., 1998; Lintschinger et al., 2000; Zagranichnaya et al., 2005; B. Zhang et al., 2018). The changes in the functional roles of TRPC channels associated with heteromultimerisation remain largely unexplored. Therefore, the vasorelaxation recorded in native tissues could likely be dependent on the inhibition of Ca^{2+} influx through homo- and/or heteromultimeric TRPC complexes, including those containing TRPC3 and TRPC6 channels.

The inhibition on OAG-induced Ca^{2+} influx by FK244 and PM20 was noticeable at 10 µM, which they then achieved a complete inhibition at 100 µM. Looking at the CRCs obtained from organ bath experiments, the vasorelaxation induced by FK244 and PM20 occurred at a much lower concentration, around 100 nM. However, we cannot make a direct comparison based on the potency of FK244 and PM20 from organ bath experiments and Ca^{2+} recordings because their affinity towards different receptors may differ (Motulsky & Christopoulos, 2003). Nevertheless, these observations have

suggested that FK244 and PM20 could be inhibiting other Ca^{2+}-permeable ion channels or heteromultimeric TRPC channels to eliciting overt vasorelaxation in the VSM, on top of TRPC3 and TRPC6 inhibition.

In this study, TRPC3 and TRPC6-overexpressed systems were employed due to their substantial roles documented in modulating vascular Ca^{2+} dynamic and contractility stimulated by phenylephrine. TRPC6 channels was the indispensable component in phenylephrine-activated current in rabbit portal vein myocytes (R. Inoue et al., 2001). Between TRPC3 and TRPC6 channels, there are some differences in their role in contribution to vascular tone. High blood pressure recorded in hypertensive mice was contributed more by TRPC3 activation than TRPC6 (Álvarez-Miguel et al., 2017). Thilo et al. (2009) also observed that the expression of TRPC3 was more prominent in hypertensive patients, while the expression of TRPC6 remained unaltered.

The inhibitory effects of FK244 and PM20 on other TRPC subtypes, namely TRPC1, TRPC4, TRPC5 and TPRC7, cannot be excluded, thus require further investigation. The expression of TRPC 1 and TRPC5 channels was upregulated in VSMC isolated from SHR and hypertensive patients (Xiaoping Chen et al., 2010; Liu et al., 2006). TRPC5 channel was also proposed as a mechanosensor in baroreflex regulation of blood pressure in mice (Lau, Shen, Wong, et al., 2016). Endothelial TRPC4 channels were reported to regulate vascular tone by increasing Ca^{2+} influx through the SOCE pathway, which elevate eNOS activity and NO production (Freichel, Suh, Pfeifer, et al., 2001). While TRPC4 is widely studied for Ca^{2+} modulation property, its significance in hypertension is not widely recognised (Lindsey & Songu-Mize, 2010; Martín-Bórnez et al., 2020; Nilius & Flockerzi, 2014; Nilius et al., 2007). Although TRPC7 channels can be directly activated by PLC-derived DAG (Hofmann et al., 1999), the expression of TRPC7 was not consistent across all types of the vasculature. TRPC7 was only found in the endothelial cells but not in the smooth muscle cells of human coronary and cerebral arteries (Yip, Chan, Leung, et al., 2004). In rat species, the mRNA of TRPC7 was not detected in the aorta and pre-glomerular resistance vessels (Facemire et al., 2004) but was expressed in cultured A7r5 rat aortic smooth muscle cells (Jung et al., 2002; Maruyama et al., 2006). FK244 and PM20 should ideally be characterised against other TRPC channels, i.e., TRPC1, TRPC4 and TRPC5 channels, to further elucidate their role in regulating Ca^{2+} influx via different TRPC subtypes.

The evidence in fluorometric Ca^{2+} recordings was consistent with the findings in functional assays. FK244 and PM20 did not induce a contraction or relaxation in the smooth muscles at the basal tone. Ca^{2+} recording studies then revealed that FK244 and PM20 did not enhance or reduce basal $[Ca^{2+}]_i$ in TRPC3-, TRPC6-overexpressing cells and WT HEK 293 cells (**Table 6.1**). These results implied that at basal $[Ca^{2+}]_i$, they do not induce Ca^{2+} influx via Ca^{2+}-permeable channels or store Ca^{2+} release. Additionally, they have no role in stimulating Ca^{2+} efflux or Ca^{2+} sequestration into SR because there was no change in baseline $[Ca^{2+}]_i$ as reportedly noted in other compounds (Jeon, Yoo, Jung, et al., 2020; Minard et al., 2019; Qin, Hou, Zhang, et al., 2014; Serres, Yang, & Jouannet, 1994). They were not behaving as activators of TRPC3, TRPC6 channels or other Ca^{2+}-permeable channels present in WT HEK 293 cells. Hence it was anticipated that no smooth muscle contraction would be detected at the basal tone in functional studies. These observations also demonstrated that the presence of an activator such as OAG or phenylephrine was essential to observe the vasorelaxant effects of FK244 and PM20, in both the cases of inhibiting Ca^{2+} signals in cellular assays and inducing functional relaxation in the vasculature.

In organ bath experiments, pre-incubation with FK244 and PM20 in Ca^{2+}-free Krebs solution did not enhance or suppress aortic tissue contraction to phenylephrine, KCl and U46619. The observation agrees with the results in Ca^{2+} recordings, where FK244 and PM20 did not deplete store Ca^{2+} like thapsigargin in WT HEK 293 cells exposed to a buffer without external Ca^{2+} (**Table 6.1**). Thapsigargin inhibits the SERCA pump which prevents Ca^{2+} reuptake into SR. Consequently, the build-up of cytosolic Ca^{2+} level increases the Ca^{2+} signals observed in experiments. Following thapsigargin-induced store depletion, the influx of Ca^{2+} from the extracellular medium, termed as SOCE, sustains the cytoplasmic Ca^{2+} oscillation (Earley & Brayden, 2015; Thastrup, 1990). On the contrary, the absence of extracellular Ca^{2+} depletes intracellular Ca^{2+} stores and reduces cytosolic Ca^{2+} levels (Nazer & Van Breemen, 1998). Our data are consistent with this description of SOCE, where the Ca^{2+} signal induced by thapsigargin was continuously rising in Ca^{2+}-containing buffer, but the signal could not be sustained in Ca^{2+}-free buffer. This suggests that no external Ca^{2+} influx was taking place via the SOCE pathway to sustain the Ca^{2+} signal. Therefore, these observations in fluorometric Ca^{2+} recordings and functional studies complement each other. Unlike thapsigargin,

FK244 and PM20 do not regulate intracellular Ca^{2+} store and induce SOCE at baseline when no activator was present.

In short, although the inhibition of L-type VGCCs could not be entirely ruled out based on the current findings, the present study demonstrated one major role of FK244 and PM20 in modulating Ca^{2+} dynamic is via TRPC3 and TRPC6 channels.

Table 6.1 Pharmacological comparison between FK244 and PM20.

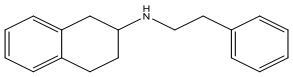
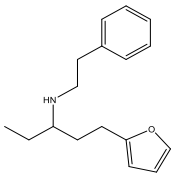
	FK244	**PM20**
Analogues		
Similarities		
Lipinski's and Veber's rule violation	0	
pEC_{50} in ABT	A > B & T	
Tissue selectivity (SD rat and SHR)	A > B & T	
Relaxation-independent factors	Endothelium, adrenoceptors, K^+ channels, cyclic nucleotides	
Compound reversibility	Reversible	
pEC_{50} vs other Ca^{2+} channel blockers	Similar to all Ca^{2+} channel blockers (2-APB, HC-070, nifedipine, Pyr3, Pyr6, SKF-96365 and verapamil)	
Suppression on contractile agents	Suppressed phenylephrine-, KCl- and serotonin-induced contraction, but not U46619-induced contraction	
E_{max} in the presence of other Ca^{2+} channel blockers	Reduced by TRPC-inhibitors (2-APB, Pyr3, Pyr6 and SKF-96365)	
General mechanism	Inhibition on extracellular Ca^{2+} influx	
Fluorometric intracellular Ca^{2+} recordings	• Inhibition on OAG-mediated Ca^{2+} influx via TRPC3 and TRPC6 (IC_{50}: 13 – 15 μM) • Do not alter baseline $[Ca^{2+}]_i$ • Do not regulate intracellular Ca^{2+} store	

Table 6.1 Pharmacological comparison between FK244 and PM20. (continued)

Analogues	**FK244**	**PM20**
	Differences	
E_{max} in ABT	B < A & T	All the same
E_{max} against pre-contractile agents	• Phenylephrine = KCl • Phenylephrine = U46619 • KCl > U46619	• Phenylephrine = KCl = U46619
pEC_{50} against pre-contractile agents	• Phenylephrine > KCl • Phenylephrine > U46619 • KCl > U46619	• Phenylephrine > KCl • Phenylephrine > U46619 • KCl = U46619
Suppression on the effect of contractile agents	Did not suppress serotonin at low concentration (10 μM)	Suppressed serotonin at low concentration (10 μM)
pEC_{50} in SHR	Higher (pEC_{50}: 6.86 ± 0.23)	Lower (pEC_{50}: 6.11 ± 0.10)
E_{max} vs other Ca^{2+} channel blockers	Higher than 2-APB, HC-070, Pyr3, Pyr6, SKF-96365	Higher than Pyr3 only
pEC_{50} in the presence of other Ca^{2+} channel blockers	Reduced by Pyr6 and SKF-96365	Not affected

Abbreviations: 2-APB, 2-aminoethoxydiphenyl borate; A, aorta; B, bladder; KCl, potassium chloride; SD, Sprague-Dawley, SHR, spontaneously hypertensive rat; T, trachea.

6.4 Analogues vs the parent compound: A comparison between FK244, PM20 and schwarzinicine A

This study was extended from previous work which examined the mechanism of a natural compound isolated from *Ficus schwarzii*, schwarzinicine A. Although these three compounds possess the same pharmacophore, the physiochemical properties of FK244 and PM20 did not violate Lipinski's and Veber's rules (**Table 6.2**), showing an improvement in the potential drug-likeness and oral bioavailability compared to the parent compound schwarzinicine A. These three compounds produced marked vasorelaxation effects in rat isolated aorta. From the studies carried out by Krishnan's group (2020), FK244 and PM20 have maintained a comparable E_{max} as schwarzinicine A (**Table 6.2**). Both analogues are as potent as schwarzinicine A in relaxing the VSM tissues (**Table 6.2**).

Both FK244 and PM20 demonstrated Ca^{2+} modulating property like schwarzinicine A. Unexpectedly, the comparison has revealed their potency against TRPC3 and TRPC6 channels was lower than schwarzinicine A (**Table 6.2**). Structural difference is among the reasons that can contribute to the difference in potency, as it could affect one's binding affinity and transcellular permeability. Drug development success relies on compounds that have more balanced pharmacokinetics, pharmacological and toxicity profiles.

Table 6.2 Comparison between the parent compound schwarzinicine A and its analogues FK244 and PM20.

Compounds	TRPC subtypes	Schwarzinicine A	FK244	PM20
Lipinski's and Veber's rule violation	N/A	2	0	0
E_{max} (%, rat aorta)	N/A	119.3 ± 3.6 [a]	114.9 ± 3.4	106.8 ± 6.1
pEC_{50} (rat aorta)	N/A	5.69 [a,b]	6.49	6.69
IC_{50} (μM) (pIC_{50}) (HEK 293 cells)	TRPC3	3 (5.52)	14 (4.85)	14 (4.85)
	TRPC6	7 (5.15)	15 (4.82)	13 (4.88)

[a] *Values extracted from Krishnan, Lee, Yap, et al., 2020*
[b] *Reported as EC_{50} (μM) = 2.01 ± 0.67 (pEC_{50} ≈ 5.69)*

6.5 Purported mechanism of actions of FK244 and PM20

In summary, the putative vasorelaxation mechanism of FK244 and PM20 in rat isolated aorta is summarised in **Figure 6.1**. Functional studies have excluded their effects on adrenoceptors, cAMP, and K^+ channels. The vasorelaxation effects of FK244 and PM20 were also independent of endothelium and NO/cGMP-mediated pathways. They are likely to inhibit the plasmalemmal Ca^{2+} permeable channels since they reduced extracellular Ca^{2+}-induced contraction but did not modulate store-Ca^{2+}. The presence of 2-APB, SKF-96365, Pyr3 and Pyr6 had reduced the relaxation profiles of FK244 and PM20. Therefore, it was hypothesised that FK244 and PM20 inhibit NSCCs, specifically TRPC channels. Inhibition on L-type VGCCs is also likely, as VGCCs are the major Ca^{2+}-permeable ion channels that mediate smooth muscle contraction. These postulations were partly confirmed in fluorometric Ca^{2+} recordings, where FK244 and PM20 have both shown inhibition towards TRPC3- and TRPC6-mediated Ca^{2+} influx. Moreover, they did not affect basal $[Ca^{2+}]_i$, substantiated the findings recorded in organ bath experiments. Collectively, we have shown evidence supporting the role of FK244 and PM20 as vasorelaxants by modulating TRPC channels in rat isolated aorta.

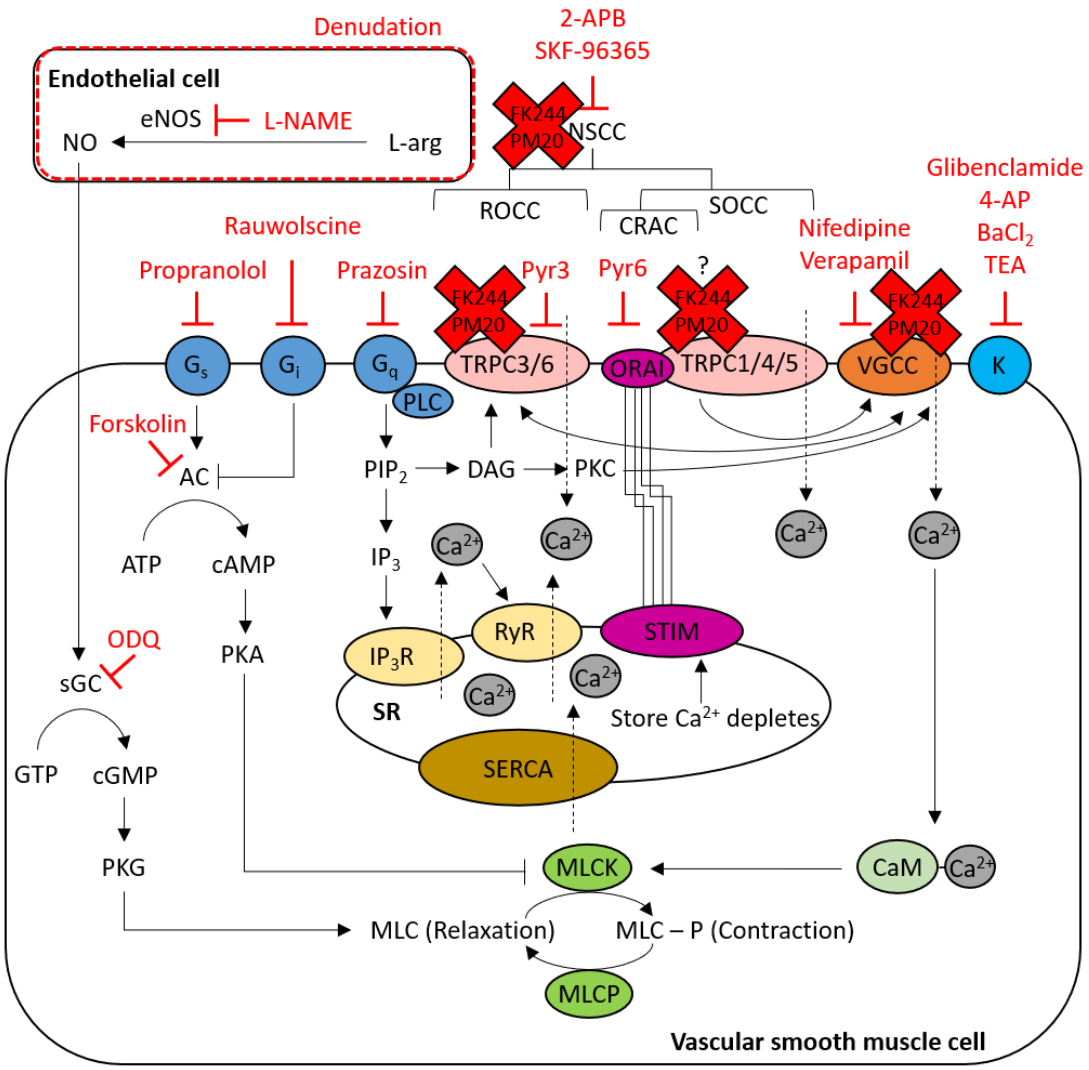


Figure 6.1 Schematic diagram illustrating the purported vasorelaxation mechanisms of FK244 and PM20 in rat isolated aorta. *Pharmacological inhibitors are shown in red font. Solid pointed solid arrow denotes downstream effectors activation, blunt arrow denotes downstream effectors inhibition. Dotted arrows denote flow of Ca^{2+}. The pathways inhibited by FK244 and PM20 are indicated with red crosses. Question mark indicates the possible inhibition of FK244 and PM20 on TRPC1/4/5 channels. Abbreviations: 2-APB, 2-aminoethoxydiphenyl borate; 4-AP, 4-aminopyridine; AC adenylyl cyclase; ATP adenosine triphosphate; $BaCl_2$ barium chloride; Ca^{2+}, calcium ion; CaM, calmodulin; cAMP, 3'-5'-cyclic adenosine monophosphate; cGMP, 3'-5'-cyclic guanosine monophosphate; CRAC, Ca^{2+} release-activated channels; DAG, diacylglycerol; eNOS endothelial nitric oxide synthase; GTP, guanosine-5'-triphosphate; IP_3, inositol-1,4,5-trisphosphate; IP_3R, IP_3 receptor; L-arg, L-arginine; MLC, myosin light chain; MLCK, MLC kinase; MLCP, MLC phosphatase; MLC-P, phosphorylated MLC; NO nitric oxide; NSCC, non-selective cation channels; ORAI, Ca^{2+} release-activated Ca^{2+} channel modulator; PIP_2, phosphatidylinositol 4,5-bisphosphate; PKA protein kinase A; PKC, protein kinase C; PKG, protein kinase G; PLC; phospholipase C; ROCC, receptor-operated Ca^{2+} channels; RyR, ryanodine receptor; SERCA, sarco/endoplasmic reticulum Ca^{2+}-ATPase; sGC soluble guanylyl cyclase; SOCC, store-operated Ca^{2+} channels; SR, sarcoplasmic reticulum; STIM, stromal interaction molecule; TEA tetraethylammonium chloride; TRPC, transient receptor potential canonical; VGCC, voltage-gated Ca^{2+} channels.*

6.6 Toxicity of FK244 and PM20 on the lifespan in *C. elegans*

This study also employed *C. elegans* as a model organism to assess the *in vivo* toxicity of FK244 and PM20. In drug development, toxicity evaluation of potential drug candidates is vital before approving their use in humans. It aimed to strike a balance between the compound's therapeutic effects and adverse effects. Toxicity assessments using *C. elegans* have demonstrated promising inter-species predictability between *C. elegans* and rats (Williams & Dusenbery, 1988; Wittkowski, Marx-Stoelting, Violet, et al., 2019). The application of compounds in nematodes *C. elegans* has been developed to refine this process, which was usually carried out in rodents.

In this study, the lifespan of *C. elegans* was used as the parameter to evaluate the toxicity of FK244 and PM20. The death of *C. elegans* was marked as the endpoint of this toxicity test. The mean lifespan of *C. elegans* had been significantly reduced by the higher concentration of FK244 and PM20 at 10 µM, but not at 3 µM. Therefore, exposure to 10 µM of FK244 and PM20 may pose toxicity in higher-ranked animals like rodents. In functional assays using organ bath technique, 10 µM of FK244 and PM20 was the concentration that first achieved a 100% vasorelaxation in isolated tissues. This toxicity test could help us to identify the range of concentration and cumulative dosage to be administered in rodents for future *in vivo* toxicity and pharmacokinetics testing. From the results, perhaps 3 µM or its equivalent dosage in mg/kg would be a more suitable concentration to be started in rodents, albeit ADME-related issues still need to be taken into consideration.

This toxicity assay aimed to improve the prediction of toxicity in humans while being cost-effective. One of the strengths of using *C. elegans* for toxicity testing was that it could provide a high number of *in vivo* replicates in a short time, with a rather economical set-up (Hunt, 2017). It also highlights the effort in exercising the 3Rs principle, considering the possible reduction in the number of rats or other animals that would be used for future *in vivo* experiments. Furthermore, this experiment model utilised fewer amount of test compounds compared to drug administration in rats. Ideally, toxicity assessment should be carried out both *in vitro* using human cells and *in vivo* using the whole organism with intact systems to have a more accurate prediction of the toxicity of FK244 and PM20. Using *C. elegans* closes the gap on the limitation between cell-specific and mammalian *in vivo* toxicity experiments. Since most mammalian genes were conserved in *C. elegans* and extensive mutation strains of *C.*

elegans are available, future work could focus on elucidating the toxicity mechanism induced by a high concentration of FK244 and PM20 at a molecular level.

6.7 Clinical potential of FK244 and PM20

Currently, there is no antihypertensive medication approved for clinical use that is known to modulate TRPC channels. FK244 and PM20 may present significant therapy advancement for hypertension due to increasing evidence on the functions of TRPC channels in regulating vascular contractility (Adebiyi et al., 2010; Liu et al., 2009). TRPC channels may be an important target for pharmacological intervention to reduce smooth muscle tone and arterial blood pressure. Upregulation of TRPC channels have been described in hypertension (Liu et al., 2006; Thilo, Baumunk, et al., 2009; Thilo, Loddenkemper, et al., 2009), vascular remodelling (M. Wang et al., 2016), cardiac hypertrophy (Wu et al., 2010), and atrial fibrillation (Harada et al., 2012; Ju, Lee, Trajanovska, et al., 2015).

Patients with high blood pressure were managed with antihypertensive drugs such as adrenergic blockers, Ca^{2+} channel blockers, ACE inhibitors, and diuretics. Most patients who have uncontrolled hypertension require at least two or more antihypertensive medications to achieve a satisfactory blood pressure target (Malaysian Society of Hypertension, 2018). Poorly controlled hypertension is also known as resistant hypertension. The prevalence of resistant hypertension was 12% in the Asian population (Naseem, Adam, Khan, et al., 2017) and 7% in the UK (Sinnott et al., 2017). Not only these patients are subjected to a higher risk of developing cardiovascular complications, but they may also experience adverse drug reactions due to the increased dosage as per treatment guidelines (NICE, 2019).

Given that hypertension is a modifiable risk factor for CVD, the ability of phenylethylamines FK244 and PM20 to evoke overt relaxation responses selectively in aortic smooth muscle tissues could potentially be clinically relevant for treating hypertension and related vascular diseases. The concrete evidence of FK244 and PM20 modulating Ca^{2+} dynamic via plasmalemmal TRPC channels provide a basis for the development of FK244 and PM20 as antihypertensive agents. Since both of them could inhibit TRPC channels and possibly L-type VGCCs, they may be used as a substitute for nifedipine, an L-type VGCC blocker that has no effect on TRPC channels (J. R. Lopez, Uryash, Faury, et al., 2020), especially in clinical conditions where inhibition

of both types of channels are required. As current treatments indicate a gap in achieving clinical efficacy, FK244 and PM20 serve as another option in combination therapy and may mitigate the side effects caused by high-dose antihypertensive drug regimen.

In addition, the assembly of homo/heterotetramers in native tissues presented new insights into the pathophysiology of hypertension and cardiovascular complications (Álvarez-Miguel et al., 2017). These compounds characterised against TRPC channels may act as pharmacological probes that catalyse the research in this field. They could be used to study the contribution of homo- and heteromultimeric TRPC channels in dysregulation of Ca^{2+} dynamic and altered vascular tone. Moreover, the pharmacophore of FK244 and PM20 has laid the foundation for future investigation on the structural and functional relationship of TRPC channels in disease vasculature.

6.8 Limitations of study

Measuring isometric tension using the organ bath technique can only suggest the plausible inhibition mechanisms of FK244 or PM20. It does not allow us to pinpoint the inhibition on specific Ca^{2+}-permeable ion channels involved in each signalling mechanism or show evidence of their interaction with ion channels. The downstream signalling mechanisms upon receptor activation in the VSM are complex as they interact with one another physiologically in the tissue. For example, phenylephrine stimulates α_1-adrenoceptors and releases store Ca^{2+} by the generation of second messenger IP_3. Simultaneously, the generation of DAG also induces Ca^{2+} influx through L-type VGCCs and NSCCs, notably TRPC3/6 channels. Depletion of store Ca^{2+} activates SOCE via NSCCs like TRPC 1/4/5 channels. The rising of global $[Ca^{2+}]_i$ stimulates further CICR from the SR store by activating RyRs (Amberg & Navedo, 2013; Putney, Broad, Braun, et al., 2001). This example is reiterated to emphasise that the organ bath technique is not able to isolate a single Ca^{2+} signalling mechanism in native tissues even though a selective agonist (phenylephrine) is used. Therefore, in the case of phenylephrine, the inhibition on L-type VGCCs by FK244 and PM20 could not be excluded from the experiments conducted using the organ bath technique, despite showing inhibition on TRPC3 and TRPC6 channels in fluorometric Ca^{2+} recordings.

The organ bath technique also limits the evidence by observing only the compounds' effects on the contractility of the VSM. It could not investigate when a non-contractile Ca^{2+} mobilisation is involved. For instance, thapsigargin depleted store Ca^{2+} by inhibiting the SERCA pump located at the SR membrane. A rise in fluorescent signal was detected in Ca^{2+} recordings (**Figure 5.6**). However, no contraction was observed when thapsigargin was added to the aortic smooth muscle tissues in the organ bath (Govindaraju, 2019). Moreover, we intended to investigate the effect of FK244 or PM20 to attenuate OAG-induced contraction in functional studies. Such experiments would provide corroborative evidence supporting their ability to inhibit TRPC3/6 channels in VSM. Surprisingly, OAG, a well-characterised TRPC3/6 activator and Hyp9, a TRPC6 channel activator (Leuner, Kazanski, Muller, et al., 2007) did not evoke aortic tissue contraction in our experiment setting (data not shown). TRPC activation alone may not be sufficient to evoke noticeable contraction that our apparatus is sensitive enough to detect. These observations noted with thapsigargin, OAG and Hyp9 have demonstrated the limitation of correlating the modulation of Ca^{2+} dynamic with

the tissues' isometric tension. The use of fluorometric Ca^{2+} recordings could be a more appropriate method to measure the effect of FK244 on non-contractile Ca^{2+} dynamic.

In this study, the inhibitory effects of FK244 and PM20 on TRPC3 and TRPC6 channels have been elucidated. The characterisation of these two compounds may have been more robust with fluorometric intracellular Ca^{2+} screening done on other TRPC subtypes (e.g., TRPC1, TRPC4, TRPC5). It is essential to learn their effects on all TRPC channel subtypes as they are known to form heterotetramers in native tissues (Dietrich, Mederos y Schnitzler, Kalwa, et al., 2005; Nilius & Flockerzi, 2014). The mechanism of TRPC homo- and heterotetramers formation and their physiological roles in different vascular beds have been scarcely explored. The assembly of heteromultimeric TRPC channels in a native environment has diverse and ill-defined roles on Ca^{2+} mobilisation pathways (Maruyama et al., 2006). Although homotetramers of TRPC3 or TRPC6 channels are mostly formed in heterologous overexpression system, the formation of heteromultimeric channels *in vivo* with different association patterns may alter their functional properties (Hofmann et al., 2002; Nilius & Flockerzi, 2014). TRPC3 and TRPC6 channels are able to heterotetramerise owing to their closely related homologues with 85% similarity in amino acid sequence (Boulay et al., 1997; Goel et al., 2002; Hofmann et al., 2002). Receptor-operated TRPC3 and TRPC6 were reported to be involved in the signalling pathway of store-dependent Ca^{2+} influx when they heterotetramerised with other subunits of TRPC (Liu, Bandyopadhyay, et al., 2005; Séguéla et al., 2014; Zagranichnaya et al., 2005). Moreover, heterologous system overexpressing TRPC3 and TRPC6 has been shown to have altered homeostasis of Ca^{2+}, Na^{+}, K^{+}, and zinc ion (Zn^{2+}). Therefore, cell-based assays could not fully reproduce their functions under physiological conditions (Chevallet, Jarvis, Harel, et al., 2014; Gibon et al., 2011; Löf, Blom, & Törnquist, 2008). These factors have complicated the elucidation of the pharmacological mechanism of FK244 and PM20 under physiological conditions, where multiple Ca^{2+} routes are implicated. Also, the compounds' potency (IC_{50}) on homotetrameric TRPC channels in fluorometric Ca^{2+} recordings could not be directly compared with their potency (pEC_{50}) obtained from organ bath studies due to this reason.

The concern of transfection efficacy of TRPC3 and TRPC6 channels was noted as they were not determined in this study. Regarding TRPC3 channels, although the cells had initially undergone transfection, antibiotic selection by blasticidin and zeocin in

established stable cell lines had eliminated all the non-transfected cells. The only characterisation performed was to test them with OAG. OAG is a well-characterised activator of TRPC3/6 channels (Dietrich, Mederos y Schnitzler, Kalwa, et al., 2005; Hofmann et al., 1999). Non-induced cells showed no response to OAG, whereas the induced ones did. This is similar for TRPC6 channels – non-transfected cells showed no response to OAG, whereas those transfected with TRPC6 did (**Appendix F**). The transfection efficacy is commonly assessed by using a recombinant fluorescent-tagged protein to calculate the percentage of cells that are expressing the protein. However, it is worth bearing in mind that using fluorescent protein tagging approach may not be all desirable in case the tagged construct behaves differently to the endogenous protein and may affect the functional readout (i.e., calcium response) (M. Ratz, Testa, Hell, et al., 2015). Although there is a correlation between the amount of protein expressed and the fluorescent signal measured, assessing transfection efficiency is not as relevant as characterising the expression of TRPC channels with OAG. Even when the transfection efficiency is high, but if there is only a small number of functional channels, the ion channel activity of an overexpressed protein could not be recorded. Hence, it is more important to determine the functional response of the TRPC proteins with a well-characterised activator – OAG, that is absent in non-transfected or non-induced stable cells. Nonetheless, the transfection efficacy is identified as a limitation of this study and should be determined in future experiments to strengthen the evidence using an over-expression system.

Another experimental limitation is the methods used in conducting lifespan assay on *C. elegans*. The nematodes were exposed to food source (heat-killed *E. coli*) added with a compound of interest instead of injecting it directly into them. Conducting lifespan assay on solid culture in our experiment did not permit the quantification of the exact compound concentration ingested by *C. elegans*. Compound administration in *C. elegans* through microinjection is still in its infancy. It is labour-intensive, technically challenging, expensive and often leads to inconsistent results (Song, Dong, & Liu, 2016). Microinjection is only used to induce a compound to a specific site in immobilised *C. elegans* or when the compound cannot be dissolved in NGM agar or *E. coli* (Ghaemi, Tong, Gupta, et al., 2020). Furthermore, the manual counting of the nematodes, which is prone to research bias, could be improved by an automated lifespan assay. Detecting dead *C. elegans* by processing video recordings or time-lapse images

of the worms is worth exploring in the future to improve the reproducibility of the assay as well as scale up the sample size (H.-E. H. Park, Jung, & Lee, 2017).

Our study compared the *in vitro* vasorelaxation effects of FK244 and PM20 between normotensive SD rats and SHRs. This comparison may be disputable as WKY rat is a more established strain used as the control in experiments carried out with SHR (Coyle, 1986; S. Shen, Xia, & Qiao, 2015), rendering the comparison between SD rat and SHR less scientifically relevant to hypertension. WKY rats are a strain of normotensive rats that have similar genetic makeup as SHR. They are both inbred strains that have their genetic materials preserved down the generations. It was reported that there is actually a substantial genetic divergence between SHR and WKY rat due to variation in breeders, and the inbreeding of WKY rat only commenced 10 years after SHR (Louis & Howes, 1990; Nabika, Nara, Ikeda, et al., 1991; Zhang-James, Middleton, & Faraone, 2013). Historically, the inbred WKY rat was generated from outbred Wistar rat, showing the possibility of WKY rat preserving some of the genetic background from Wistar rat (Zhang-James et al., 2013). Furthermore, SD rats have been compared to SHRs in non-molecular studies to examine their differences in biochemical parameters (T. Inoue, Moriya, Goto, et al., 1995) as well as the antihypertensive effects of compounds in functional assays (Kim, Jo, Choi, et al., 2018). Environmental factors were shown to influence the vascular physiology and blood pressure of SHR, showing that genetic makeup is not the sole contributor to blood pressure control (Azar, Sharp, & Lawson, 2011; Cierpial & McCarty, 1991; Oron-Herman, Kamari, Grossman, et al., 2008). Fundamentally, this research aimed to study the functional effects of FK244 and PM20 in normotensive SD rats and SHR based on the *in vitro* aortic functions. Indeed, we observed similar relaxation profiles between these two strains despite their genetic heterogeneity.

6.9 Future work

The findings in this study point towards the Ca^{2+}-inhibiting mechanism of FK244 and PM20 in vascular tissues via TRPC3 and TRPC6 channels. These results have highlighted the need for some key future experiments to overcome the limitations in current work. Therefore, further investigations are required to evaluate other possible modes of inhibition of FK244 and PM20.

6.9.1 Functional assay

In this study, the functional responses of FK244 and PM20 were measured in rat thoracic aorta. Future work should investigate the vasorelaxant properties of PM20 and FK244 in human isolated arteries. Isolated vessels from WKY rats should also be used to clearly compare the effect of FK244 and PM20 on tissue contractility and TRPC function with SHR. These investigations could provide concrete evidence that corroborates the notion that FK244 and PM20 are potential antihypertensive agents. Smaller resistance vessels such as mesenteric arteries (Bridges, Williams, Pointer, et al., 2011) and renal interlobar arteries (Stannov, Brasen, Salomonsson, et al., 2019) contribute to peripheral resistance, thus are more relevant to hypertension physiology. Smaller arteries have reduced diameter compared to the aorta, therefore, encounter greater resistance. They are the primary vessels that play significant roles in influencing the arterial blood pressure when they undergo vasoconstriction and relaxation (Chaudhry, Miao, & Rehman, 2020). To better relate their vascular effects to antihypertensive activity, future experiments on FK244 and PM20 could be extended in smaller resistance arteries (< 300 μm internal diameter), such as the mesenteric arteries using wire myograph (Anwar, Samaha, Ballan, et al., 2017; Watts, 2002).

The effects of FK244 and PM20 on $G_{12/13}$-related Ca^{2+} sensitising RhoA/ROCK pathway remain unexplored. Despite the subtle evidence provided in experiments using U46619-induced contraction, a more direct approach may be investigated through a direct inhibition on RhoA/ROCK pathway using Y-27632, a ROCK inhibitor (Uehata, Ishizaki, Satoh, et al., 1997). Reduced kinase activity decreases Ca^{2+} sensitivity and promotes smooth muscle relaxation. If the presence of Y-27632 did not enhance the relaxation profile of FK244 or PM20, then their effects on RhoA/ROCK pathway can be reasonably excluded.

TRPC1 – 4 channels were suggested to be involved in serotonin-induced Ca^{2+} influx human pulmonary artery (Rodat-Despoix et al., 2009). A non-specific TRPC inhibitor such as SKF-96365 could be used to confirm this inference in rat aorta. Should the Ca^{2+} influx be partly mediated via TRPC channels, the presence of SKF-96365 would attenuate serotonin-induced aortic contraction. In addition, pre-incubation with nifedipine could also examine the extent of L-type VGCC involvement in serotonin-induced vasocontraction.

Apart from using SNP, another interesting method to investigate the involvement of FK244 in SHR's NO/cGMP pathways is to employ ODQ, an sGC inhibitor. It provides direct evidence on FK244's vasorelaxation mechanism. If the inhibition of cGMP did not diminish the relaxation of FK244 in the SHR aortae, it implies that FK244 does not induce vasorelaxation via cGMP-dependent pathways.

6.9.2 TRPC expression

Although literature reviewed the expression of TRPC channels in rat aorta, the quantification of TRPC channels in SD and SHR aortae used in this study was not performed. Sodium dodecyl sulphate-polyacrylamide gel electrophoresis (SDS-PAGE) and western blotting can be done to detect each TRPC isoforms isolated from homogenised aortic tissues by using TRPC-specific polyclonal antibodies (Mita, Ito, et al., 2010; Wu et al., 2010). Immunohistochemistry is also one of the most used methods for protein detection. TRPC detection with antibodies allows us to identify and localise the expression of TRPC protein within the smooth muscle layers (Erac, Selli, Kosova, et al., 2010). The results obtained generate valuable links between TRPC protein expressions in the aorta and the relaxation profiles of FK244 and PM20. Quantifying the protein expression in the bladder and trachea could also provide valuable insight into the varying potency of FK244 and PM20 in different smooth muscles.

6.9.3 Cell-based assay

More work should be done to investigate the effect of FK244 and PM20 in modulating L-type VGCC using the fluorescent Ca^{2+} recordings technique. CRCs to FK244 and PM20 should be constructed In HEK 293 cells transiently transfected with L-type VGCCs (Rosa, Yamaguchi, & Morad, 2013; J. R. Thomas & Lee, 2016). Alternatively, Bay K8644, an L-type VGCC agonist or nifedipine, L-type VGCC inhibitor, can be

employed to examine the inhibitory effect of FK244 and PM20 on Ca^{2+} influx through L-type VGCCs (Fransen et al., 2015).

Although this study was heavily focused on inhibiting upstream extracellular Ca^{2+} influx from inducing relaxation, it is also important to note that vascular tone can be regulated by intracellular Ca^{2+} clearance after an active contraction (Gros, Afroze, You, et al., 2003). These mechanisms involved Ca^{2+} sequestration into SR via SERCA, Ca^{2+} extrusion out of the cytosol via PMCA or NCX (Fierro, DiPolo, & Llano, 1998; Schuh, Quaschning, Knauer, et al., 2003). These three channels accounted for 89 – 97% of intracellular Ca^{2+} clearance (L. Chen, Koh, & Hille, 2003). Therefore, the regulation of intracellular Ca^{2+} by FK244 and PM20 through Ca^{2+} clearance instead of inhibition should be further explored in cell-based assays to complement the findings in functional studies. For example, the possible opposing actions of FK244 and PM20 on thapsigargin-induced store depletion could be visualised using fluorometric Ca^{2+} recordings. If FK244 or PM20 are to be NCX activators, their pharmacological actions could be examined using SEA 0400, a potent NCX inhibitor (F. Yan, Lu, Zhang, et al., 2020) in rat aortic smooth muscle cells. On the other hand, caloxin, a peptide developed as a PMCA inhibitor (Chaudhary, Walia, Matharu, et al., 2001; Pande, 2011), could be used to assess the regulation of FK244 and PM20 on cytosolic Ca^{2+} through PMCA (Pande, Mallhi, Sawh, et al., 2006).

It is also crucial to characterise the selectivity of FK244 and PM20 against other TRPC subtypes such as TRPC1, TRPC4, TRPC5 and TRPC7. The findings from these experiments can be used to distinguish the role of FK244 and PM20 in facilitating ROCE and SOCE, which involve different TRPC subtypes or a combination of heteromultimeric TRPC channels. Expressing concatemers such as TRPC1/4, TRPC1/5 (Rubaiy et al., 2017), TRPC3/6, and TRPC6/7 (Maruyama et al., 2006) can elucidate the inhibitory activities of FK244 and PM20 in heteromultimeric TRPC channels. Results produced by a gene-silencing approach using anti-sense strategy to knockdown TRPC3 and TRPC6 (Dietrich, Mederos y Schnitzler, Gollasch, et al., 2005) in aortic smooth muscle cells could corroborate the evidence of the ability of FK244 and PM20 in targeting these channels and modulating smooth muscle tone. Similar experiments can be carried out in native VSMCs to establish the physiological relevance of their inhibition in the vasculature.

Evidence has shown the possibilities of TRPC3 and TRPC6 channels engage not only in ROCE but also SOCE under certain circumstances, such as during the assembly of STIM1/Orai1 complex in response to store-Ca^{2+} depletion (Alkhani et al., 2014; Yuan et al., 2007; Zagranichnaya et al., 2005). To investigate the interaction between the analogues and STIM1/Orai1, electrophysiology experiments can be done using STIM1-knockdown VSMCs. Patch clamp electrophysiology utilises electric current to measure the activity of ion channels in the cell membrane. Further pharmacological characterisation of FK244 and PM20 using patch clamp recordings would be useful in providing more evidence to confirm their activities against TRPC channels in a native system. It can also exclude their possible effects on intracellular Ca^{2+} signalling pathways. Experiments can be done to record the whole-cell and single-channel cation currents passing through TRPC channels expressed in VSMCs under controlled voltage in the presence of FK244 or PM20 (J. Shi, Miralles, Birnbaumer, et al., 2017). Putative SOCC blockers such as SKF-96365 and 2-APB can be used as positive controls.

6.9.4 *In vivo* assay

Toxicity testing using nematodes *C. elegans* has provided valuable clues on the safety profiles of FK244 and PM20 in a whole organism. Dose-response curves can be constructed to determine the LD_{50} for FK244 and PM20 in *C. elegans* (Charão, Souto, Brucker, et al., 2015). Besides, elucidating the effects of FK244 and PM20 on other toxicity endpoints, including the growth, motility and reproduction of *C. elegans* (Kong et al., 2019), will generate valuable evidence regarding their underlying toxicity mechanism. This assay can be repeated in other *C. elegans* strain that carry certain gene mutations for coded for Ca^{2+} channels found in the pharyngeal muscles, for example, *egl-19* (mutation in α_1-subunit of L-type VGCC) and *unc-36* (mutation in α_2-subunit of L-type VGCC) (Lainé, Frøkjær-Jensen, Couchoux, et al., 2011).

Furthermore, this study has obtained useful evidence to advance the toxicity study *in vivo* using larger animals. Following once-daily oral administration of FK244 or PM20 at their pre-determined LD_{50}, toxicity screening for 28 days can be carried out by examining any sign of toxicity such as diarrhoea, reduction in body weight and mortality. Blood sample evaluation can be performed alongside to investigate any alteration to the haematological parameters and biochemical indicators after being fed FK244 or PM20. Necropsy should be done as the next step to assess any histological changes in the vascular tissues, heart, kidney and liver, which are the main organs affected in hypertension (Al-Afifi, Alabsi, Bakri, et al., 2018; Nath & Yadav, 2015).

6.9.5 Binding assay

Since FK244 and PM20 inhibit TRPC3 and TRPC6 channels, the compounds' binding site can be identified using the Nobel Prize-winning method – cryogenic electron microscopy. This technique combines two important steps: freezing large protein using liquid nitrogen and electron microscopy, to generate a high-resolution, three-dimensional image of the protein structure. Accumulating studies have employed this technique to determine TRPC channels' structure when interacting with pharmacological agents (Y. Bai, Yu, Chen, et al., 2020; Duan, Li, Chen, et al., 2019; Tang et al., 2018). Mapping out the interaction sites of FK244 and PM20 in TRPC3 and TRPC6 channels allow us to characterise their mechanisms and binding to other proteins/ion channels. At the same time, it also facilitates the study of SAR between phenylethylamines and TRPC channels, providing robust information for subsequent analogue synthesis.

6.10 Concluding statements

For the first time, this study characterised the pharmacological activities of FK244 and PM20 as vasorelaxants against TRPC channels. Mechanism of actions and the protein target(s) of these two analogues were elucidated. The findings have successfully answered the objectives set for this study (**section 1.7**) and can be concluded as follows:

(i) In functional studies, FK244 and PM20 elicited concentration-dependent relaxation in rat isolated smooth muscle tissues (aorta, bladder, and trachea). They were more effective in relaxing VSM tissue.

(ii) The relaxant effect of FK244 was also observed in porcine pulmonary arteries and bronchioles with similar efficacy but lower potency. The results demonstrated that the relaxation effect of FK244 is not species-specific. It may also be more useful in managing systemic hypertension than pulmonary hypertension.

(iii) Evidence has excluded the influence of endothelium on FK244/PM20-induced vasorelaxation. The plausible effects of FK244 and PM20 affecting the NO, cAMP/cGMP, α/β-adrenoceptors and K^+ channels (K_v, K_{ir}, K_{ATP}, K_{Ca} channels) have also been ruled out.

(iv) Isometric tension recordings also revealed that the observed effects of FK244 and PM20 were inhibiting extracellular Ca^{2+} influx via plasmalemmal Ca^{2+}-permeable channels such as L-type VGCCs and TRPC channels. They did not influence intracellular store Ca^{2+} depletion induced by contractile agents.

(v) Exposure to FK244 and PM20 at lower concentration did not reduce the lifespan and was non-toxic towards *C. elegans*. The compounds appeared to pose toxicity at a higher concentration as they slightly reduced the lifespan of *C. elegans*.

(vi) *In vitro* experiments conducted using rat isolated aortae from SHR and STZ-induced diabetic rats have shown that FK244 and PM20 were equally effective in the vasculature of disease rat models. Vasorelaxation effect of FK244 in SHR was also likely to be inhibition of extracellular Ca^{2+} entry.

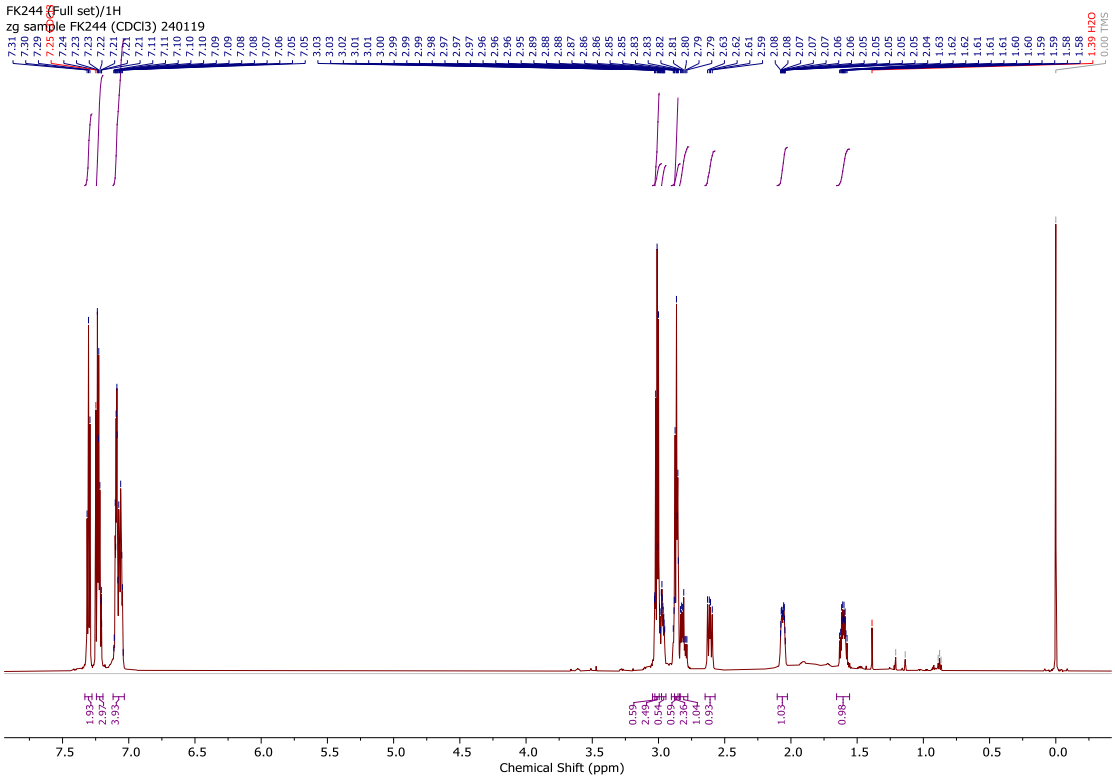
(vii) Fluorometric intracellular Ca^{2+} recordings showed that FK244 and PM20 were able to block OAG-mediated Ca^{2+} influx in TRPC3- and TRPC6-overexpressing HEK 293 cells.

Appendix A Synthesis of FK244

IR (neat): ν_{max} 3306, 3023, 2920, 2838, 1492, 1452, 1124 cm^{-1}.

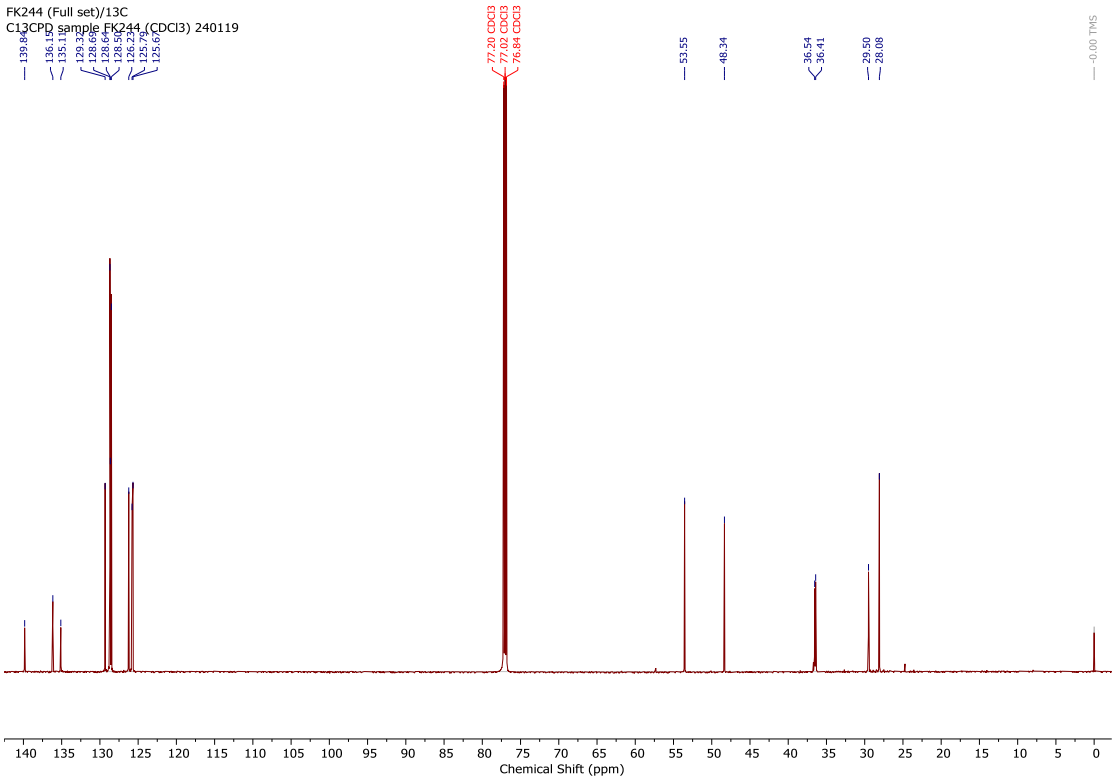
HRESIMS *m/z* 252.1750 $[M + H]^+$ (calculated for $C_{18}H_{22}N$, 252.1752).

^1H NMR ($CDCl_3$, 700 MHz): δ 7.30 (t, *J* = 7.6 Hz, 2H), 7.24 – 7.19 (m, 3H), 7.12 – 7.03 (m, 4H), 3.01 (t, *J* = 7.3 Hz, 2H), 3.05 – 2.98 (m, 1H), 2.98 – 2.94 (m, 1H), 2.90 – 2.84 (m, 1H), 2.86 (t, *J* = 7.3 Hz, 2H), 2.81 (ddd, *J* = 16.8, 10.9, 5.7 Hz, 1H), 2.61 (dd, *J* = 15.6, 9.4 Hz, 1H), 2.10 – 2.03 (m, 1H), 1.60 (dtd, *J* = 12.6, 10.5, 5.7 Hz, 1H) (**Appendix A.1**).



Appendix A.1 ^1H NMR spectrum of* N*-phenethyl-1,2,3,4-tetrahydronaphthalen-2-amine (FK244) ($CDCl_3$, 700 MHz).

^{13}C NMR ($CDCl_3$, 175 MHz): δ 139.8, 136.2, 135.1, 129.3, 128.7, 128.6, 128.5, 126.2, 125.8, 125.7, 53.6, 48.3, 36.5, 36.4, 29.5, 28.1 (**Appendix A.2**).



Appendix A.2 ^{13}C NMR spectrum of* N*-phenethyl-1,2,3,4-tetrahydronaphthalen-2-amine (FK244) ($CDCl_3$, 175 MHz).

Appendix B Ethics approval – SD rats

The University of Nottingham

Animal Welfare and Ethical Review Body

Cover Form applicable to the use of animals in non-regulated procedures

Title of Study: **Investigation on the effect of natural product extracts and compounds on the isolated rat smooth muscles**

Name of Applicant: **Kang Nee TING**

School: **Life Sciences (Malaysia Campus)**

AWERB REF: UNMC12

1. Requests to use animals in non-regulated procedures must incorporate the information required below in the format requested for project licence applicants. The completed form should be returned electronically to the bsu@nottingham.ac.uk. When approved a protocol reference number will be provided to the applicant and must be used when ordering animals for use in the non-regulated study.

Its purpose is to highlight the key points in the proposed programme of work and to provide an executive summary in non-technical language accessible to the lay members of the Animal Welfare and Ethical Review Body.

Your application must be accompanied by this summary written in non-technical terms. You should complete this summary template. We expect that, for all but the most complex of studies, you will be able to provide a satisfactory summary using 500 to 1,000 words.

Study Title (max. 50 characters)	In-vitro organ bath experiments investigating effects of natural product extracts and isolated compounds on rat smooth muscles.		
Key Words (max. 5 words)	Isolated tissues; aorta; bladder; airway		
Expected duration of the study (yrs)	4 years (this is formed part of PhD projects, BSc Biomedical Sciences, MPharm year 4 research projects and a grant application to be submitted to the Malaysia government)		
Purpose of the study	Basic research	**Yes**	
	Translational and applied research		No
	Regulatory use and routine production		No
	Protection of the natural environment in the interests of the health or welfare of humans or animals		No
	Preservation of species		No
	Higher education or training	**Yes**	
	Forensic enquiries		No
	Maintenance of colonies of genetically altered animals[1]		No

1

The University of Nottingham

Describe the objectives of the study (e.g. the scientific unknowns or scientific/clinical needs being addressed)	This application is divided into two main objectives: 1. MPharm year 3 and BSc Biomedical Sciences research projects: To enable students to further understand the pharmacology of smooth muscles including understanding the process of research in natural product drug discovery. 2. PhD projects: This forms part of the research skills training. In vitro organ bath technique will be one of the methodology to be included in the thesis. There are currently 3 students under my supervision using this technique of experiments
What are the potential benefits likely to derive from this study (how science could be advanced or humans or animals could benefit from the project)?	1. Students will gain a better understanding of the pharmacology of the smooth muscles in different vascular beds where technical skills will be gained as part of their training in undergraduate or postgraduate level. 2. These experiments will provide new information on the effect of active extracts and compounds isolated from the natural flora on isolated smooth muscles from the airways, bladder and aorta. We are moving to test new compounds synthesize based on the skeletal structure of novel compounds isolated from local plant species. 3. In Malaysia, the skills on isolated organ bath are limited and this forms part of an important technique for drug discovery.
What species and approximate numbers of animals do you expect to use over what period of time?	Adult rats will be utilised for these experiments. With the current set up, it is estimated about 3 to 4 animals will be used weekly.
What procedures will be conducted?	All animals will be sacrificed by an experienced animal technician according to the methods described in Schedule 1 of the UK Animals (Scientific Procedures) Act 1986.
In the context of what you propose to do to the animals, what are the expected adverse effects and the likely/expected level of severity? What will happen to the animals at the end?	No treatments will be carried out on living animals. After humane killing, the tissues will be removed for isolated organ bath experiments.

The University of Nottingham

Application of the 3Rs	
1. Replacement State why you need to use animals and why you cannot use non-animal alternatives	The study of some of the pharmacology can only be meaningful when carried out in complex integrated tissues from animals. We have tried carrying out some experiments on primary smooth muscle cell lines and to date this has not been successful. Cell lines only provide limited information on the effects of the compounds and extracts that we have been working with. Answering a direct question, for example whether a compound would dilate the airway is only possible from investigations on the isolated smooth muscle rings.
2. Reduction Explain how you will assure the use of minimum numbers of animals	The maximum number of different organs from each animal will be utilised. For example, the aorta, bladder and airways (bronchus and trachea) will be used from each rat.
3. Refinement Explain the choice of species and why the animal model(s) you will use are the most refined, having regard to the objectives. Explain the general measures you will take to minimise welfare costs (harms) to the animals.	At present no other sources of animal tissues are available but, for future planning, sourcing animal tissues from sheep obtained from local slaughter houses will be considered to minimise the use of rats in these experiments.
4. Housing and Care Please confirm that animals will be housed and cared for according to the requirements of the UK Animals (Scientific Procedures) Act 1986 draft Code of Practice for the care and accommodation of animals (February 2013) **or** provide details and justification for alternative housing and care standards.	Animals will be purchased from the animal facilities in University Putra Malaysia (UPM) and University Kebangsaan Malaysia (UKM) Both of these animal facilities are governed by their own institutional animal care and use committee (IACUC). They adhere to the Malaysian code of practice for the care and use of animals for scientific purposes which are consistent with the UK Home Office regulations. Information on the facility can be found here http://www.vet.upm.edu.my/eiacuc.html (UPM) http://www.kkl.ukm.my:8080/laru/wp-content/uploads/2013/03/UKMAEC-GUIDELINE-2007.pdf (UKM)

The University of Nottingham

5. Humane Killing Please confirm that animals will be humanely killed using an appropriate method of humane killing detailed in Schedule 1 of the UK Animals (Scientific Procedures) Act 1986 **or** provide details and justification for alternative methods of killing.	Animals will be killed by concussion of the brain and/or exposure to carbon dioxide gas. Death is confirmed by dislocation of the neck.
For Office Use Only	
Will the study be subject to Retrospective Assessment?	Yes | No | Date due:

Committee use only

Comments by NACWO:

The proposed project appears appropriate with no welfare issues providing animals are humanely killed by trained and competent staff.
Neil Yates
05.09.13

Amendment 07/12/16
The request to source animals from an additional University is reasonable and confirmation has been received that both animal providers adhere to the Malaysian Code of Practice. However additional information on actual standards of animal care has been requested as the standards in place are not clear from the web links provided.
Neil Yates
07/12/16

Confirmation received - OK to proceed.
NY 13/03/17

Comments by NVS:

This would appear to be satisfactory, although an approximation for the total number of rats to be used per year or over the lifetime of the project should be given. Users should be trained to a level of competency that will ensure humane euthanasia is achieved at all times.

Ewan McNeill 05-09-13

I am happy with the information provided.
E. McNeil 13/3/17

We have contacted the animal house at UPM. The technician confirms that the rats are kept between 18 and 20 C. Reply from Kang Nee Ting 15/2/17

The University of Nottingham

Dear Annemarie

Please find attached the requested information on benefits accrued from this work.

From our record we have used 318 rats between September 2014 until now. Many thanks.
Best wishes
Kang Nee

Update on research output following the approval of UNMC2kn
Publication list

PhD thesis of Bi Juin Loong 2016: Development of a functional bioassay to study the mechanism of action of a novel phenylethylamine alkaloid, schwarzinicine

BJ Loong, KH Lim, Y Mbaki and KN Ting: Calcium mobilisation and relaxant properties of a novel phenyethylamine alkaloid, schwarzinicine A (In preparation)

Mei-Kee Lee, Kuan-Hon Lim, Chon-Seng Tan, Szu-Ting Ng, Sue-Mian Then, Suresh Kumar Mohankumar, Kang-Nee Ting: Bronchodilator effects of *Lignosus rhinocerotis* extract on rat isolated airways is linked to the blockage of calcium entry (Submitted to Journal of Phytomedicine).

Jun-Lee Lim, Kae-Shin Sim, Kien-Thai Yong, Bi-Juin Loong, Kang-Nee Ting, Siew-Huah Lim, Yun-Yee Low, Toh-Seok Kam: Biologically active vallesamine, strychnan, and rhazinilam alkaloids from Alstonia: Pneumatophorine, a nor-secovallesamine with unusual incorporation of a 3-ethylpyridine moiety. *Phytochemistry* 09/2015; 117.

Suet-Pick Wong, Chew-Yan Gan, Kuan-Hon Lim, Kang-Nee Ting, Yun-Yee Low, Toh-Seok Kam: Arboridinine, a Pentacyclic Indole Alkaloid with a New Cage Carbon–Nitrogen Skeleton Derived from a Pericine Precursor. *Organic Letters* 07/2015; 17(14):3628-3631.

B J Loong, J H Tan, K H Lim, Y Mbaki, K N Ting: Contractile function of smooth muscle retained after overnight storage. *Naunyn-Schmiedeberg's Archives of Pharmacology* 06/2015; 388(10):1061-1067.

Veronica Alicia Yap, Bi-Juin Loong, Kang-Nee Ting, Sandy Hwei-San Loh, Kien-Thai Yong, Yun-Yee Low, Toh-Seok Kam, Kuan-Hon Lim: Hispidacine, an unusual 8,4'-oxyneolignan-alkaloid with vasorelaxant activity, and hispiloscine, an antiproliferative phenanthroindolizidine alkaloid, from Ficus hispida Linn. *Phytochemistry* 01/2015; 109:96-102.

Choy-Eng Nge, Chew-Yan Gan, Kuan-Hon Lim, Kang-Nee Ting, Yun-Yee Low, Toh-Seok Kam: ChemInform Abstract: Criofolinine and Vernavosine, New Pentacyclic Indole Alkaloids Incorporating Pyrroloazepine and Pyridopyrimidine Moieties Derived from a Common Yohimbine Precursor. *Organic Letters* 12/2014; 46(21).

Students trained

Bi Juin Loong PhD, graduated 2016
Mei Kee Lee, 3rd year PhD
Kayatri Govindaraju, 2nd year PhD
Fong Kai Lee, 1st year PhD
Undergraduates (final year projects for MPharm and BSc Biomedical Sciences & summer placements) > 10

Justification for extension of the work

At present, we have 3 active PhD students (see the list above) using the post mortem tissues for their organ bath experiments. We have also completed a grant from the Ministry of Higher Education entitled "Mechanism of action of Lignosus rhinocerus (Tiger Milk Mushroom) on airway smooth muscle contractility and mast cells degranulation". We are currently preparing two proposals to be submitted to Newton Senior Fellowship and Wellcome Fellowship for the extension of the Tiger Milk Mushroom work. In addition, we have just submitted two grant

applications to the Ministry of Higher Education to study a series of novel compounds with vasorelaxation effects.
These are our justification for requesting extension of the ethics application for another 4 years from Sept 2017 to August 2021.

Comments by primary reader for the Committee (if applicable):

Comments by Lay Person (If applicable):

Committee decision: Approved

Communicated to applicant (date): 13/3/17

Appendix C Synthesis of PM20

Synthesis of Weinreb amide: 3-(furan-2-yl)-*N*-methoxy-*N*-methylpropanamide (2) (Figure 3.2)

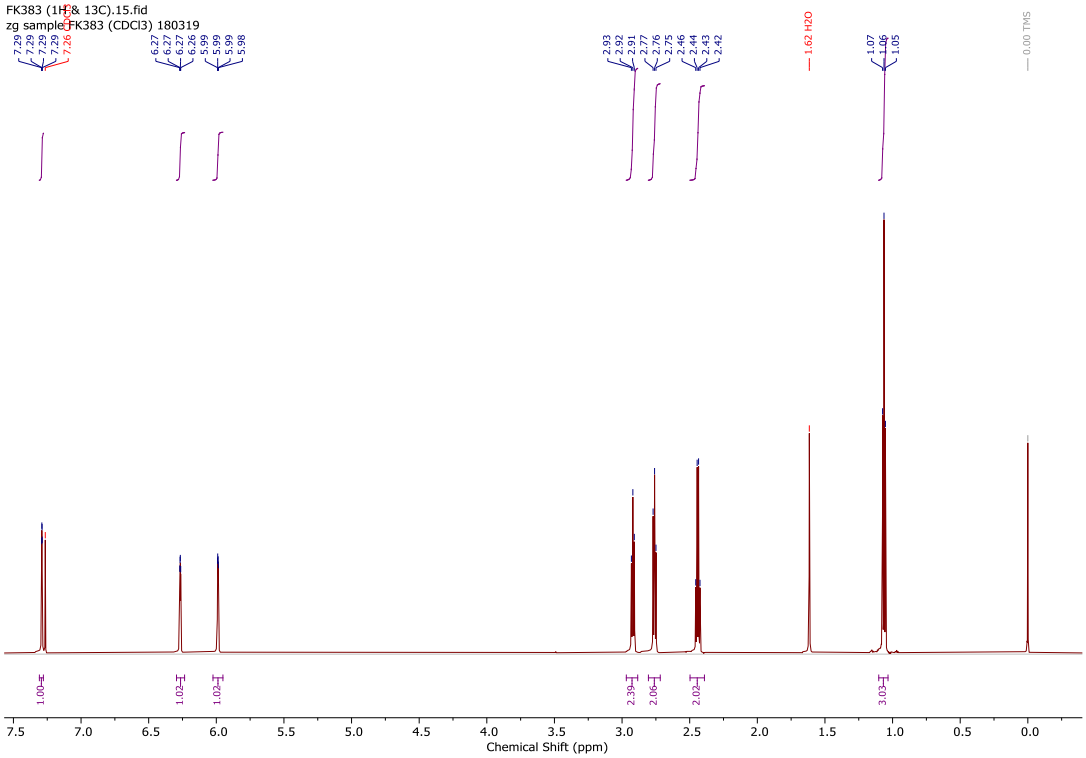
N,O-dimethylhydroxylamine hydrochloride (426.9 mg, 4.38 mM, 1.5 equiv.), 1-ethyl-3-(3-dimethylaminopropyl)carbodiimide (EDC) (823.8 mg, 4.30 mM, 1.5 equiv.) and 4-dimethylaminopyridine (DMAP) (534.0 mg, 4.37 mM, 1.5 equiv.) were added into a stirring solution of 3-(2-furyl)propionic acid **(1)** (402.5 mg, 2.87 mM, 1 equiv.) in CH_2Cl_2 (10 ml). The mixture was stirred at room temperature for 23 hour. Water (8 ml) was added into the mixture and the resulting mixture was extracted with CH_2Cl_2 (3 × 8 ml). The combined organic layer was washed with 5% HCl solution (8 ml) and brine (8 ml). The organic layer was dried over Na_2SO_4 and concentrated *in vacuo*. The crude product was purified by centrifugal radial TLC using an eluent system of Et_2O–hexane (1:1) to yield 3-(furan-2-yl)-*N*-methoxy-*N*-methylpropanamide **(2)** as a light yellow oil (450.3 mg, 2.46 mM, 86%). It was characterised by IR, HRESIMS, ^{1}H NMR and ^{13}C NMR. IR (neat): ν_{max} 2937, 1653, 1423, 1386, 1175 cm^{-1}; ^{1}H NMR ($CDCl_3$, 700 MHz): δ 7.31 (dd, *J* = 1.8, 1.0 Hz, 1H), 6.28 (dd, *J* = 3.2, 1.9 Hz, 1H), 6.04 (dd, *J* = 2.8, 0.9 Hz, 1H), 3.66 (s, 3H), 3.19 (s, 3H), 2.98 (t, *J* = 8.1 Hz, 2H), 2.78 (t, *J* = 7.8 Hz, 2H); ^{13}C NMR ($CDCl_3$, 175 MHz): δ 173.2, 154.9, 141.0, 110.2, 105.2, 61.3, 32.2, 30.4, 23.1. HRESIMS *m/z* 184.0981 $[M + H]^+$ (calculated for $C_9H_{14}NO_3$, 184.0974). The spectroscopic data are in good agreement with those reported in the literature (Rudzinski, Kelly, & Leadbeater, 2012).

Synthesis of ketone: 1-(furan-2-yl)pentan-3-one (3) (Figure 3.2)

A small portion (about 10%) of bromoethane (0.61 ml, 8.2 mM, 1 equiv.) in tetrahydrofuran (THF) (5 ml) was added to magnesium (Mg) turnings (408.1 mg, 16.8 mM, 2 equiv.) in THF (3 ml). The remaining portion of the bromide was added dropwise into the stirring reaction mixture as it was heated up. The resulting mixture was heated and stirred for 5 minutes before left to cool to room temperature to afford ethylmagnesium bromide. The solution of ethylmagnesium bromide prepared earlier was added dropwise into an ice-cold solution of 3-(furan-2-yl)-*N*-methoxy-*N*-methylpropanamide **(2)** (307.1 mg, 1.68 mM, 0.2 equiv.) in THF (10 ml). The reaction mixture was stirred in an ice bath for 2 hours prior to addition of cold 10% hydrochloric acid (HCl) solution (8 ml). After stirring for 5 minutes, the mixture was extracted with

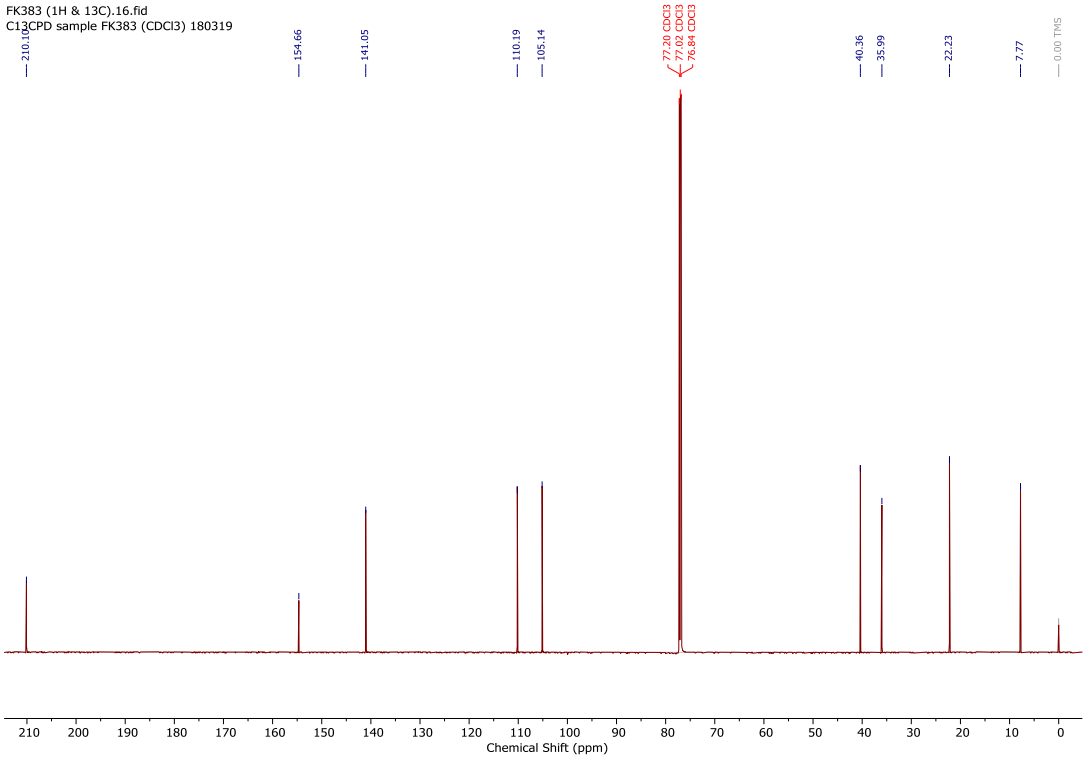
EtOAc (3 × 15 ml). The combined organic layer was washed with brine (10 ml) before drying with $MgSO_4$ and concentrated *in vacuo*. The crude product was purified by centrifugal radial TLC using an eluent system of Et_2O–hexane (1:6) to yield 1-(furan-2-yl)pentan-3-one **(3)** as a yellow oil (182.2 mg, 1.2 mM, 71%). It was characterised by IR, HRESIMS, ^{1}H NMR (**Appendix C.1**) and ^{13}C NMR (**Appendix C.2**). IR (neat): ν_{max} 2925, 2858, 1711, 1369, 1261, 1090, 1020 cm^{-1}; HRESIMS *m/z* 153.0912 [M + H]$^+$ (calculated for $C_9H_{13}O_2$, 153.0916).

^{1}H NMR ($CDCl_3$, 700 MHz): δ 7.29 (dd, *J* = 1.9, 0.8 Hz, 1H), 6.27 (dd, *J* = 3.1, 1.9 Hz, 1H), 5.99 (dd, *J* = 3.2, 1.0 Hz, 1H), 2.92 (t, *J* = 7.5 Hz, 2H), 2.76 (t, *J* = 7.5 Hz, 2H), 2.44 (q, *J* = 7.3 Hz, 2H), 1.06 (t, *J* = 7.3 Hz, 3H)



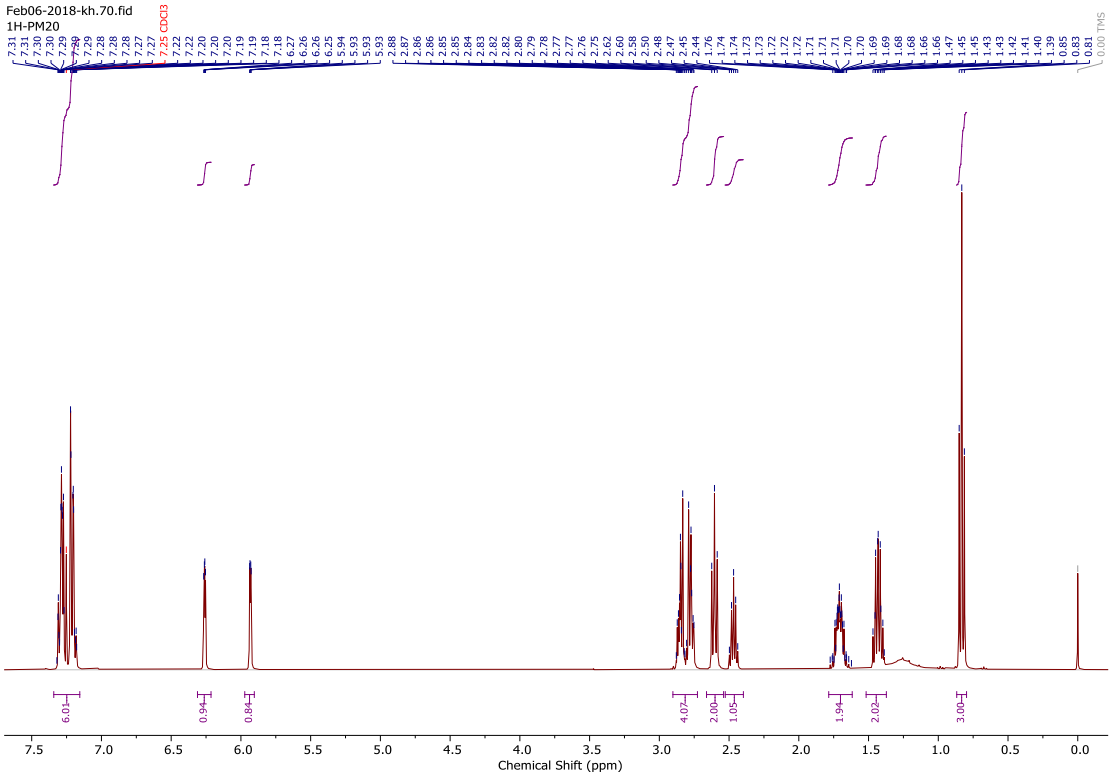
Appendix C.1 ^{1}H NMR spectrum of 1-(furan-2-yl)pentan-3-one (3) ($CDCl_3$, 700 MHz)

^{13}C NMR ($CDCl_3$, 175 MHz): δ 210.1, 154.7, 141.1, 110.2, 105.1, 40.4, 36.0, 22.2, 7.8



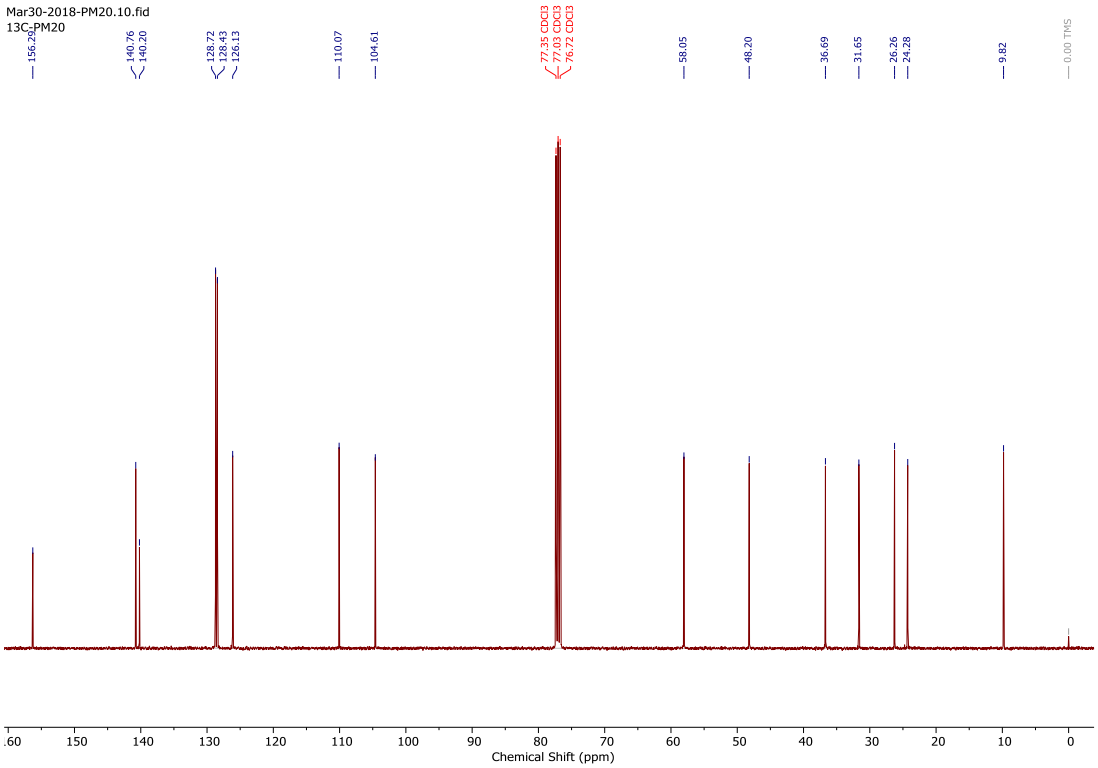
Appendix C.2 ^{13}C NMR spectrum of 1-(furan-2-yl)pentan-3-one (3) ($CDCl_3$, 175 MHz)

^{1}H NMR ($CDCl_3$, 400 MHz): δ 7.34 – 7.16 (m, 6H), 6.26 (dd, *J* = 3.2, 1.9 Hz, 1H), 5.93 (dd, *J* = 3.2, 1.0 Hz, 1H), 2.90 – 2.73 (m, 4H), 2.60 (t, *J* = 7.9 Hz, 2H), 2.47 (p, *J* = 6.0 Hz, 1H), 1.79 – 1.62 (m, 2H), 1.43 (qd, *J* = 7.5, 5.9 Hz, 2H), 0.83 (t, *J* = 7.4 Hz, 3H)



Appendix C.3 ^{1}H NMR spectrum of 1-(furan-2-yl)-N-phenethylpentan-3-amine (PM20) (4) ($CDCl_3$, 400 MHz)

^{13}C NMR ($CDCl_3$, 150 MHz): δ 156.3, 140.8, 140.2, 128.7, 128.4, 126.1, 110.1, 104.6, 58.1, 48.2, 36.7, 31.7, 26.3, 24.3, 9.8



Appendix C.4 ^{13}C NMR spectrum of 1-(furan-2-yl)-N-phenethylpentan-3-amine (PM20) (4) ($CDCl_3$, 100 MHz)

Appendix D Ethics approval – SHR

The University of Nottingham

Animal Welfare and Ethical Review Body

Cover Form applicable to the use of animals in non-regulated procedures

Title of Study: **Investigation on Schwarzinicine A (Sch A), a novel pheylethylamine alkaloid, and its derivatives on their effects in isolated tissues obtained from spontaneous hypertensive rats (SHR)**

Name of Applicant: **Kang Nee TING**

School: **Life Sciences (Malaysia Campus)**

AWERB REF: UNMC18

1. Requests to use animals in non-regulated procedures must incorporate the information required below in the format requested for project licence applicants. The completed form should be returned electronically to the bsu@nottingham.ac.uk. When approved a protocol reference number will be provided to the applicant and must be used when ordering animals for use in the non-regulated study.

Its purpose is to highlight the key points in the proposed programme of work and to provide an executive summary in non-technical language accessible to the lay members of the Animal Welfare and Ethical Review Body.

Your application must be accompanied by this summary written in non-technical terms. You should complete this summary template. We expect that, for all but the most complex of studies, you will be able to provide a satisfactory summary using 500 to 1,000 words.

Study Title (max. 50 characters)	Investigation on Schwarzinicine A (Sch A), a novel pheylethylamine alkaloid, and its derivatives on their effects in isolated tissues obtained from spontaneous hypertensive rats (SHR)		
Key Words (max. 5 words)	Isolated tissues; aorta; bladder; airway		
Expected duration of the study (yrs)	3 years (this forms part of three/four PhD projects and three research proposals awarded in 2017 by the Ministry of Higher Education and Toray Foundation)		
Purpose of the study	Basic research	**Yes**	
	Translational and applied research		No
	Regulatory use and routine production		No
	Protection of the natural environment in the interests of the health or welfare of humans or animals		No
	Preservation of species		No
	Higher education or training	**Yes**	
	Forensic enquiries		No

The University of Nottingham

	Maintenance of colonies of genetically altered animals[1]		No
Describe the objectives of the study (e.g. the scientific unknowns or scientific/clinical needs being addressed)	The objectives of the study are: 1. To compare the effectiveness and the potency of a series of newly synthesised compounds based on the phamacophore of Sch A in the isolated aorta of SHRs. We have some data from previous work to show that these compounds are more efficacious in SHR when compared to normotensive rats (see Appendix 1). 2. To further understand the mechanism of action of Sch A (and derivatives) in SHR. We have data to support the role of calcium entry and and interference of Gq-coupled activation of receptor are affected by Sch A (see Appendix 2). 3. To study the selectivity of Sch A (and derivatives) on other smooth muscle tissues such as bladder and trachea. All the experiments will be carried out in organ bath experiments set up.		
What are the potential benefits likely to derive from this study (how science could be advanced or humans or animals could benefit from the project)?	1. Students will gain a better understanding of the pharmacology of the smooth muscles in different rat species where technical skills will be gained as part of their PhD training. 2. These experiments will provide new information on the effect of these active compounds on isolated smooth muscles from the airways, bladder and aorta in SHR. 3. In Malaysia, the skills on isolated organ bath are limited and this forms part of an important technique for drug discovery. 4. We are able to understand the mechanism of action of Sch A (and derivatives) potentially file a patent of their applications for treatment of hypertension. We have some data to support the action via TRPC channels. This would be a novel target for treatment of hypertension.		
What species and approximate numbers of	Adult rats will be utilised for these experiments. With the current set up, it is estimated about 4		

2

animals do you expect to use over what period of time?	animals will be used for a period of 5 to 6 weeks in a year. An estimate of not more than 80 SHRs to be used for the next 3 years.
What procedures will be conducted?	All animals will be sacrificed by an experienced animal technician according to the methods described in Schedule 1 of the UK Animals (Scientific Procedures) Act 1986.
In the context of what you propose to do to the animals, what are the expected adverse effects and the likely/expected level of severity? What will happen to the animals at the end?	No treatments will be carried out on living animals. After humane killing at the University of Monash (Malaysia campus) animal facility, the tissues will be removed for isolated organ bath experiments.
Application of the 3Rs	
1. Replacement State why you need to use animals and why you cannot use non-animal alternatives	The study of some of the pharmacology can only be meaningful when carried out in complex integrated tissues from animals. We have tried carrying out some experiments on primary smooth muscle cell lines and to date this has not been successful. Cell lines only provide limited information on the effects of the compounds and extracts that we have been working with. Answering a direct question, for example whether a compound would dilate the airway is only possible from investigations on the isolated smooth muscle rings. We have a series of data on the functional responses in normotensive rats and we would like to investigate if the SHRs will be more sensitive to our compounds with smooth muscle relaxant activities.
2. Reduction Explain how you will assure the use of minimum numbers of animals	The maximum number of different organs from each animal will be utilised. For example, the aorta airways (bronchus and trachea) will be used from each rat for two different projects. The extra tissues will be frozen for staining and protein expression work subsequently.
3. Refinement Explain the choice of species and why the animal model(s) you will use are the most refined, having regard to the objectives. Explain the general measures you will take to	At present no other sources of animal tissues are available but, for future planning, sourcing animal tissues from sheep obtained from local slaughter houses will be considered to minimise the use of rats in these experiments.

The University of Nottingham

minimise welfare costs (harms) to the animals.	
4. Housing and Care Please confirm that animals will be housed and cared for according to the requirements of the UK Animals (Scientific Procedures) Act 1986 draft Code of Practice for the care and accommodation of animals (February 2013) **or** provide details and justification for alternative housing and care standards.	Animals will be purchased from the animal facilities in a local university (University of Monash Malaysia) This animal facility is governed by its own institutional animal care and use committee (IACUC). They adhere to the guidelines prepared by the Expert Working Group of the Animal Welfare Committee of the National Health and Medical Research Council, Australia (see attached guidelines).
5. Humane Killing Please confirm that animals will be humanely killed using an appropriate method of humane killing detailed in Schedule 1 of the UK Animals (Scientific Procedures) Act 1986 **or** provide details and justification for alternative methods of killing.	Animals will be killed by concussion of the brain and/or exposure to carbon dioxide gas. Death is confirmed by dislocation of the neck.
For Office Use Only	
Will the study be subject to Retrospective Assessment?	Yes | No | Date due:

Committee use only

Comments by Experimental Officer:
A relatively small number of SHR rats have been proposed over the 3 yr period. No *in vivo* work will take place. The rats will be culled by a S1 method and a range of tissues removed. A comparable approach have been used in the past involving normotensive and SHR rats (UNMC 2, UNMC6 and UNMC12).

- **Could you provide a brief experimental plan to explain how you will meet the objectives** (e.g. what data will be required, use of controls. NY 10/04/18).
  Response: See Annex 1

- **Please provide the same assurances are in place as before regarding:**
  a) **checking that the rats are hypertensive before culling takes place**
  b) **the competency of the person carrying out the humane killing of the rats and**
  c) **the ability to transport the tissues in a manner which does not affect the viability of the tissues.**

Response: The rats will be obtained and killed at the animal facility of University of Monash which is about 40km away from the Nottingham Campus. The required tissues will be removed immediately at Monash and transported back to Nottingham in ice cold Krebs. This protocol has been used previously and the results obtained did not show any loss of tissue viability. A trained technician in Monash University will take the blood pressure using the tail cuff method a day before the sacrificing of the rats by humane killing. He will supply adult rats that registered systolic blood pressure of between 170mmHg and 210mmHg.

A.Kelly 13/3/18

Comments by NVS:

This would appear to be a reasonable request and the applicant has stated specific aims for the study. Can you confirm;

- **No normal rats are required as controls for comparison studies?**

  Response: We have done a series of work on normal rats as control (Sprague Dawley rats under the approved applications UNMC2kn and UNMC12). The current work will be to compare our observations in SD and SHR tissues.

- **There will be no more than 80 SHRs used over the 3 year period (I was unsure how this links to '4 animals will be used for a period of 5 to 6 weeks in a year').**
  (If presumed that this is 4 rats over a 5 week period giving 10 periods per year = 40 rats per year for 3 years then approximately 120 rats and not 80 rats in total could be used over the 3 years of this study – clarification required. NY 10/04/18)

  Response: We plan to use 4 rats per week for a short period of 6 weeks or 6 rats per week for 5 weeks. For the first phase of work we will order 30 rats. Phase two or three will be carried out with the remaining rats in the next two years if we have newer compounds to test in SHR or to clarify the mechanism of these compounds in SHR tissues. We do not plan to use more than 80 rats in total for a period of 3 years.

Ewan McNeill 09-04-18

Comments by primary reader for the Committee (if applicable):

Comments by Lay Person (If applicable):

Committee decision:

Approved following Clarification – NY 13/04/18

Appendix E Ethics approval – Wistar rats

UNIVERSITY OF MALAYA

يونيورسيتي مالايا

21st August 2018

Dr. Amira Hajirah Abd Jamil
Department of Pharmacy
Faculty of Medicine

Dear Researcher,

Effect of *Lignosus sp Mushroom* treatment on cardiovascular function of diabetic rats

This is to inform you that the FOM Institutional Animal Care and Use Committee, University of Malaya (FOM IACUC) has approved your Animal Use Protocol application with the above mentioned title for a duration of three (3) years until **August 2021.**

Please be advised that should you require changes to be made to the approved protocol, you are responsible to submit an application for amendments. Failure to do so may result in the Approval of your Animal Use Protocol be withdrawn by FOM IACUC. If required, AUP must be renewed after the expiry date even if no revision is made. At the end of the animal experiment, a closure report of the animal use is to be submitted to the secretariat FOM IACUC to be documented.

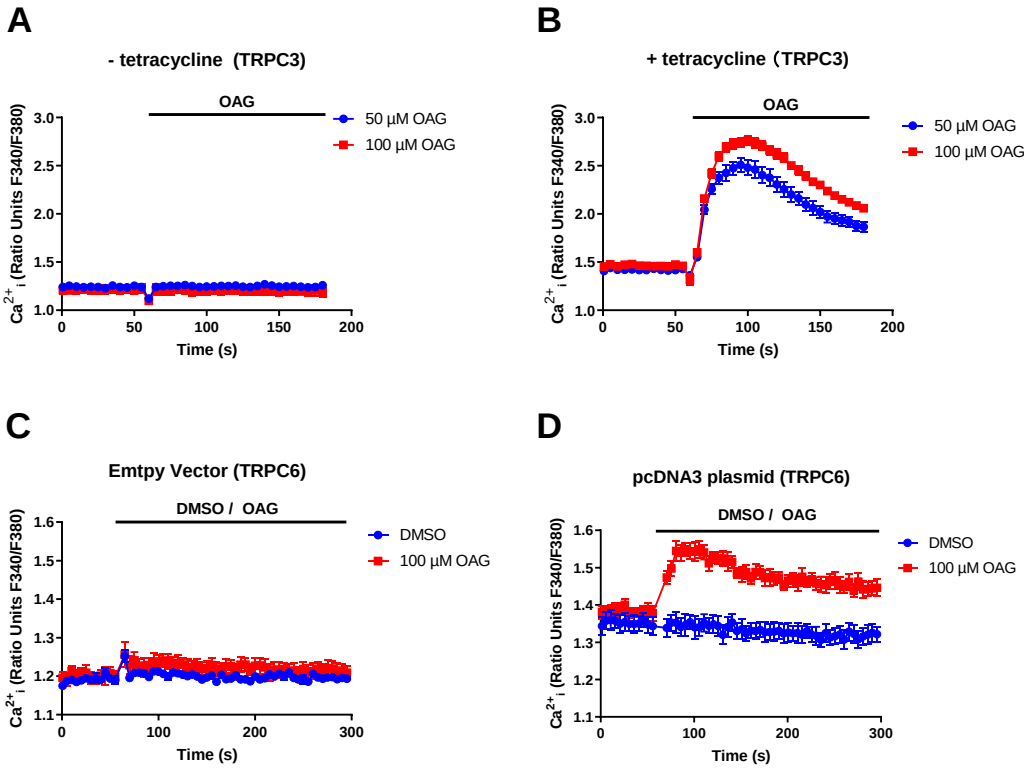
Your Ethics Reference no. : **2018-210807/PHARM/R/AHAJ**

Thank you.

Yours sincerely,

ASSOC. PROFESSOR DR. CHANG LI YEN
Chairman,
Faculty of Medicine Institutional Animal Care and Use Committee (FOM IACUC)

Appendix F Activation of TRPC3 and TRPC6 channels by OAG



Appendix F.1 Preliminary tests showed OAG activates TRPC3 and TRPC6 channels. *HEK T-REx™ cell line expresses the tetracycline repressor protein. Representative Ca^{2+} measurements in HEK T-REx™ cells showing that (A) without tetracycline, there was no Ca^{2+} influx induced by OAG due to no expression of TRPC3 channel. In the presence of tetracycline, tetracycline induced TRPC3 expression, demonstrated by an increase in Ca^{2+} influx upon application of 50 µM and 100 µM OAG. Transfection in WT HEK 293 cells using (C) an empty vector showed no increase in baseline $[Ca^{2+}]_i$ despite the addition of 100 µM OAG. Successful TRPC6-transfection using (D) pcDNA3 plasmid was confirmed by an increase in Ca^{2+} influx upon application of 100 µM OAG.*

References

Abreu, I. C., Marinho, A. S. S., Paes, A. M. A., Freire, S. M. F., Olea, R. S. G., Borges, M. O. R., & Borges, A. C. R. (2003). Hypotensive and vasorelaxant effects of ethanolic extract from Jatropha gossypiifolia L. in rats. *Fitoterapia*, *74*(7–8), 650–657. https://doi.org/10.1016/j.fitote.2003.07.002

Abubakar, I. B., Lim, K.-H., & Loh, H.-S. (2015). Alkaloid extracts of Ficus species and palm oil-derived tocotrienols synergistically inhibit proliferation of human cancer cells. *Natural Product Research*, *29*(22), 2137–2140. https://doi.org/10.1080/14786419.2014.991927

Abubakar, M. G., Ukwuani, A. N., Mande, U. U., & Science, F. (2015). Antihypertensive activity of Hibiscus aqueous calyx extract in Albino rats Sabdariffa. *Sky Journal of Biochemistry Research*, *4*(3), 16–20.

Adebiyi, A., Zhao, G., Narayanan, D., Thomas-Gatewood, C. M., Bannister, J. P., & Jaggar, J. H. (2010). Isoform-selective physical coupling of TRPC3 channels to IP_3 receptors in smooth muscle cells regulates arterial contractility. *Circulation Research*, *106*(10), 1603–1612. https://doi.org/10.1161/CIRCRESAHA.110.216804

Ahmed, M., Hasani, H. J., Kalyaanamoorthy, S., & Barakat, K. (2021). GPCR_LigandClassify.py; a rigorous machine learning classifier for GPCR targeting compounds. *Scientific Reports*, *11*(1), 9510. https://doi.org/10.1038/s41598-021-88939-5

Ahmed, S., & Warren, D. T. (2018). Vascular smooth muscle cell contractile function and mechanotransduction. *Vessel Plus*, *2*(11), 36. https://doi.org/10.20517/2574-1209.2018.51

Aitlhadj, L., & Stürzenbaum, S. R. (2013). The toxicological assessment of two anti-obesity drugs in *C. elegans*. *Toxicology Research*, *2*(2), 145–150. https://doi.org/10.1039/c2tx20096a

Ajay, M., Chai, H. J., Mustafa, A. M., Gilani, A. H., & Mustafa, M. R. (2007). Mechanisms of the anti-hypertensive effect of *Hibiscus sabdariffa* L. calyces. *Journal of Ethnopharmacology*, *109*(3), 388–393. https://doi.org/10.1016/j.jep.2006.08.005

Al-Afifi, N. A., Alabsi, A. M., Bakri, M. M., & Ramanathan, A. (2018). Acute and sub-acute oral toxicity of *Dracaena cinnabari* resin methanol extract in rats. *BMC Complementary and Alternative Medicine*, *18*(1), 1–14. https://doi.org/10.1186/s12906-018-2110-3

Al-Shboul, O. A. (2018). Contraction and relaxation signaling in gastrointestinal smooth Muscle signaling for smooth muscle contraction. *EC Gastroenterology and Digestive System*, *5.5*, 315–321. Retrieved from https://www.ecronicon.com/ecgds/pdf/ECGDS-05-00185.pdf

Alapati, V. R., McKenzie, C., Blair, A., Kenny, D., MacDonald, A., & Shaw, A. M. (2007). Mechanisms of U46619- and 5-HT-induced contraction of bovine pulmonary arteries: Role of chloride ions. *British Journal of Pharmacology*, *151*(8), 1224–1234. https://doi.org/10.1038/sj.bjp.0707338

Albert, A., Saleh, S., & Large, W. (2009). Identification of Canonical Transient Receptor Potential (TRPC) channel proteins in native vascular smooth muscle cells. *Current Medicinal Chemistry*, *16*(9), 1158–1165. https://doi.org/10.2174/092986709787581815

Alex, A., Millan, D. S., Perez, M., Wakenhut, F., & Whitlock, G. A. (2011). Intramolecular hydrogen bonding to improve membrane permeability and absorption in beyond rule of five chemical space. *MedChemComm*, *2*(7), 669. https://doi.org/10.1039/c1md00093d

Alkhani, H., Ase, A. R., Grant, R., O'Donnell, D., Groschner, K., & Séguéla, P. (2014). Contribution of TRPC3 to store-operated calcium entry and inflammatory transductions in primary nociceptors. *Molecular Pain*, *10*(1), 1744-8069-10–43. https://doi.org/10.1186/1744-8069-10-43

Allewelt, A. L., & Day, A. R. (1941). Preparation of some amino ketones and amino alcohols containing the ac-tetrahydro-β-naphthylamine, tetrahydroisoquinoline, or β-phenylethylamine nucleus. *The Journal of Organic Chemistry*, *06*(3), 384–400. https://doi.org/10.1021/jo01203a003

Alonso-Carbajo, L., Kecskes, M., Jacobs, G., Pironet, A., Syam, N., Talavera, K., & Vennekens, R. (2017). Muscling in on TRP channels in vascular smooth muscle cells and cardiomyocytes. *Cell Calcium*, *66*, 48–61. https://doi.org/10.1016/j.ceca.2017.06.004

Alper, S., McElwee, M. K., Apfeld, J., Lackford, B., Freedman, J. H., & Schwartz, D. A. (2010). The *Caenorhabditis elegans* germ line regulates distinct signaling pathways to control lifespan and innate immunity. *Journal of Biological Chemistry*, *285*(3), 1822–1828. https://doi.org/10.1074/jbc.M109.057323

Álvarez-Miguel, I., Cidad, P., Pérez-García, M. T., & López-López, J. R. (2017). Differences in TRPC3 and TRPC6 channels assembly in mesenteric vascular smooth muscle cells in essential hypertension. *The Journal of Physiology*, *595*(5), 1497–1513. https://doi.org/10.1113/JP273327

Alviar, C. L., Devarapally, S., Nadkarni, G. N., Romero, J., Benjo, A. M., Javed, F., Doherty, B., Kang, H., Bangalore, S., & Messerli, F. H. (2013). Efficacy and safety of dual calcium channel blockade for the treatment of hypertension: A meta-analysis. *American Journal of Hypertension*, *26*(2), 287–297. https://doi.org/10.1093/ajh/hps009

Amberg, G. C., & Navedo, M. F. (2013). Calcium dynamics in vascular smooth muscle. *Microcirculation*, *20*(4), 281–289. https://doi.org/10.1111/micc.12046

Ames, M. K., Atkins, C. E., & Pitt, B. (2019). The renin-angiotensin-aldosterone system and its suppression. *Journal of Veterinary Internal Medicine*, *33*(2), 363–382. https://doi.org/10.1111/jvim.15454

Anwar, M. A., Samaha, A. A., Ballan, S., Saleh, A. I., Iratni, R., & Eid, A. H. (2017). *Salvia fruticosa* induces vasorelaxation in rat isolated thoracic aorta: Role of the PI3K/Akt/eNOS/NO/cGMP signaling pathway. *Scientific Reports*, *7*(1), 686. https://doi.org/10.1038/s41598-017-00790-9

Apfeld, J., & Alper, S. (2018). What can we learn about human disease from the nematode C. elegans? *Methods in Molecular Biology*, *1706*, 53–75.

https://doi.org/10.1007/978-1-4939-7471-9_4

Arce, C., Vicente, D., Segura, V., Flacco, N., Montó, F., Almenar, L., Agüero, J., Rueda, J., Jiménez-Altayó, F., Vila, E., Noguera, M. A., D'Ocon, P., & Ivorra, M. D. (2017). Activation of α_{1A}-adrenoceptors desensitizes the rat aorta response to phenylephrine through a neuronal NOS pathway, a mechanism lost with ageing. *British Journal of Pharmacology*, *174*(13), 2015–2030. https://doi.org/10.1111/bph.13800

Armstrong, M., & Moore, R. A. (2019). Physiology, Baroreceptors. In *StatPearls*. Retrieved from http://www.ncbi.nlm.nih.gov/pubmed/30844199

Arsyad, A., & Dobson, G. P. (2016). Adenosine relaxation in isolated rat aortic rings and possible roles of smooth muscle K_V channels, K_{ATP} channels and A_{2a} receptors. *BMC Pharmacology and Toxicology*, *17*(1), 23. https://doi.org/10.1186/s40360-016-0067-8

Ávila-Medina, J., Calderón-Sánchez, E., González-Rodríguez, P., Monje-Quiroga, F., Rosado, J. A., Castellano, A., Ordóñez, A., & Smani, T. (2016). Orai1 and TRPC1 proteins co-localize with $Ca_V1.2$ channels to form a signal complex in vascular smooth muscle cells. *Journal of Biological Chemistry*, *291*(40), 21148–21159. https://doi.org/10.1074/jbc.M116.742171

Avogaro, A., Albiero, M., Menegazzo, L., De Kreutzenberg, S., & Fadini, G. P. (2011). Endothelial dysfunction in diabetes: The role of reparatory mechanisms. *Diabetes Care*, *34*(SUPPL. 2), S285–S290. https://doi.org/10.2337/dc11-s239

Azar, T., Sharp, J., & Lawson, D. (2011). Heart rates of male and female Sprague-Dawley and Spontaneously Hypertensive Rats housed singly or in groups. *Journal of the American Association for Laboratory Animal Science*, *50*(2), 175–184.

Bacsa, B., Tiapko, O., Stockner, T., & Groschner, K. (2020). Mechanisms and significance of Ca^{2+} entry through TRPC channels. *Current Opinion in Physiology*, *17*, 25–33. https://doi.org/10.1016/j.cophys.2020.06.005

Badran, A., Baydoun, E., Samaha, A., Pintus, G., Mesmar, J., Iratni, R., Issa, K., & Eid, A. H. (2019). Marjoram relaxes rat thoracic aorta via a PI3-K/eNOS/cGMP pathway. *Biomolecules*, *9*(6). https://doi.org/10.3390/biom9060227

Bae, Y. M., Kim, A., Lee, Y. J., Lim, W., Noh, Y. H., Kim, E. J., Kim, J., Kim, T. K., Park, S. W., Kim, B., Cho, S. Il, Kim, D. K., & Ho, W. K. (2007). Enhancement of receptor-operated cation current and TRPC6 expression in arterial smooth muscle cells of deoxycorticosterone acetate-salt hypertensive rats. *Journal of Hypertension*, *25*(4), 809–817. https://doi.org/10.1097/HJH.0b013e3280148312

Bai, R. R., Wu, X. M., & Xu, J. Y. (2015). Current natural products with antihypertensive activity. *Chinese Journal of Natural Medicines*, *13*(10), 721–729. https://doi.org/10.1016/S1875-5364(15)30072-8

Bai, Y., Yu, X., Chen, H., Horne, D., White, R., Wu, X., Lee, P., Gu, Y., Ghimire-Rijal, S., Lin, D. C. H., & Huang, X. (2020). Structural basis for pharmacological modulation of the TRPC6 channel. *ELife*, *9*, 1–18. https://doi.org/10.7554/eLife.53311

Baik, J. S., Sohn, J.-T., Ok, S.-H., Kim, J.-G., Sung, H.-J., Park, S.-S., Park, J.-Y.,

Hwang, E. M., & Chung, Y.-K. (2011). Levobupivacaine-induced contraction of isolated rat aorta is calcium dependent. *Canadian Journal of Physiology and Pharmacology*, *89*(7), 467–476. https://doi.org/10.1139/y11-046

Baldassare, J. J., Tarver, A. P., Henderson, P. A., Mackin, W. M., Sahagan, B., & Fisher, G. J. (1993). Reconstitution of thromboxane A_2 receptor-stimulated phosphoinositide hydrolysis in isolated platelet membranes: involvement of phosphoinositide-specific phospholipase C-β and GTP-binding protein G_q. *Biochemical Journal*, *291*(1), 235–240. https://doi.org/10.1042/bj2910235

Barré-Sinoussi, F., & Montagutelli, X. (2015). Animal models are essential to biological research: issues and perspectives. *Future Science OA*, *1*(4), fso.15.63. https://doi.org/10.4155/fso.15.63

Barst, R. J., McGoon, M., Torbicki, A., Sitbon, O., Krowka, M. J., Olschewski, H., & Gaine, S. (2004). Diagnosis and differential assessment of pulmonary arterial hypertension. *Journal of the American College of Cardiology*, *43*(12 SUPPL.), S40–S47. https://doi.org/10.1016/j.jacc.2004.02.032

Bauer, C. C., Boyle, J. P., Porter, K. E., & Peers, C. (2010). Modulation of Ca^{2+} signalling in human vascular endothelial cells by hydrogen sulfide. *Atherosclerosis*, *209*(2), 374–380. https://doi.org/10.1016/j.atherosclerosis.2009.10.004

Bauer, V., & Sotníková, R. (2010). Nitric oxide – the endothelium-derived relaxing factor and its role in endothelial functions. *General Physiology and Biophysics*, *29*, 319–340. https://doi.org/10.4149/gpb_2010_04_319

Beanan, M. J., & Strome, S. (1992). Characterization of a germ-line proliferation mutation in *C. elegans*. *Development*, *116*(3), 755–766.

Beech, D. J., Muraki, K., & Flemming, R. (2004). Non-selective cationic channels of smooth muscle and the mammalian homologues of *Drosophila* TRP. *The Journal of Physiology*, *559*(3), 685–706. https://doi.org/10.1113/jphysiol.2004.068734

Beevers, G., Lip, G. Y. H., & O'brien, E. (2001). The pathophysiology of hypertension. *Bmj*, *322*(7291), 912. https://doi.org/10.1136/bmj.322.7291.912

Benet, L. Z., Hosey, C. M., Ursu, O., & Oprea, T. I. (2016). BDDCS, the Rule of 5 and drugability. *Advanced Drug Delivery Reviews*, *101*(5), 89–98. https://doi.org/10.1016/j.addr.2016.05.007

Berg, C. C., & Corner, E. J. H. (2005). Moraceae: Ficeae. *Flora Malesiana - Series 1, Spermatophyta*, *17*(2), 1–702. Retrieved from http://www.narcis.nl/publication/RecordID/oai%3Anaturalis.nl%3A579346

Bergson, P., Lipkind, G., Lee, S. P., Duban, M. E., & Hanck, D. A. (2011). Verapamil block of T-type calcium channels. *Molecular Pharmacology*, *79*(3), 411–419. https://doi.org/10.1124/mol.110.069492

Berridge, M. J. (2008). Smooth muscle cell calcium activation mechanisms. *The Journal of Physiology*, *586*(21), 5047–5061. https://doi.org/10.1113/jphysiol.2008.160440

Berridge, M. J., Bootman, M. D., & Roderick, H. L. (2003). Calcium signalling: Dynamics, homeostasis and remodelling. *Nature Reviews Molecular Cell Biology*,

4(7), 517–529. https://doi.org/10.1038/nrm1155

Betschinger, J., & Knoblich, J. A. (2004). Dare to be different: Asymmetric cell division in *Drosophila*, *C. elegans* and vertebrates. *Current Biology*, *14*(16), R674–R685. https://doi.org/10.1016/j.cub.2004.08.017

Bhatt, D. L., Kandzari, D. E., O'Neill, W. W., D'Agostino, R., Flack, J. M., Katzen, B. T., Leon, M. B., Liu, M., Mauri, L., Negoita, M., Cohen, S. A., Oparil, S., Rocha-Singh, K., Townsend, R. R., & Bakris, G. L. (2014). A controlled trial of renal denervation for resistant hypertension. *New England Journal of Medicine*, *370*(15), 1393–1401. https://doi.org/10.1056/NEJMoa1402670

Bishara, N. B., Murphy, T. V., & Hill, M. A. (2002). Capacitative Ca^{2+} entry in vascular endothelial cells is mediated via pathways sensitive to 2 aminoethoxydiphenyl borate and xestospongin C. *British Journal of Pharmacology*, *135*(1), 119–128. https://doi.org/10.1038/sj.bjp.0704465

Bolton, T. B., Lang, R. J., & Takewaki, T. (1984). Mechanisms of action of noradrenaline and carbachol on smooth muscle of guinea-pig anterior mesenteric artery. *The Journal of Physiology*, *351*(1), 549–572. https://doi.org/10.1113/jphysiol.1984.sp015262

Bootman, M. D., Collins, T. J., Mackenzie, L., Roderick, H. L., Berridge, M. J., & Peppiatt, C. M. (2002). 2-Aminoethoxydiphenyl borate (2-APB) is a reliable blocker of store-operated Ca^{2+} entry but an inconsistent inhibitor of $InsP_3$-induced Ca^{2+} release. *The FASEB Journal*, *16*(10), 1145–1150. https://doi.org/10.1096/fj.02-0037rev

Boulay, G., Zhu, X., Peyton, M., Jiang, M., Hurst, R., Stefani, E., & Birnbaumer, L. (1997). Cloning and expression of a novel mammalian homolog of Drosophila Transient receptor potential (Trp) involved in calcium entry secondary to activation of receptors coupled by the G_q class of G protein. *Journal of Biological Chemistry*, *272*(47), 29672–29680. https://doi.org/10.1074/jbc.272.47.29672

Bouron, A., Kiselyov, K., & Oberwinkler, J. (2015). Permeation, regulation and control of expression of TRP channels by trace metal ions. *Pflügers Archiv - European Journal of Physiology*, *467*(6), 1143–1164. https://doi.org/10.1007/s00424-014-1590-3

Boyd, W. A., McBride, S. J., Rice, J. R., Snyder, D. W., & Freedman, J. H. (2010). A high-throughput method for assessing chemical toxicity using a *Caenorhabditis elegans* reproduction assay. *Toxicology and Applied Pharmacology*, *245*(2), 153–159. https://doi.org/10.1016/j.taap.2010.02.014

Brayden, J. E. (1996). Potassium channels in vascular smooth muscle. *Clinical and Experimental Pharmacology and Physiology*, *23*, 1069–1076.

Brazer, S. W., Singh, B. B., Liu, X., Swaim, W., & Ambudkar, I. S. (2003). Caveolin-1 contributes to assembly of store-operated Ca^{2+} influx channels by regulating plasma membrane localization of TRPC1. *Journal of Biological Chemistry*, *278*(29), 27208–27215. https://doi.org/10.1074/jbc.M301118200

Bréchard, S., Melchior, C., Plançon, S., Schenten, V., & Tschirhart, E. J. (2008). Store-operated Ca^{2+} channels formed by TRPC1, TRPC6 and Orai1 and non-store-operated channels formed by TRPC3 are involved in the regulation of NADPH

oxidase in HL-60 granulocytes. *Cell Calcium*, *44*(5), 492–506. https://doi.org/10.1016/j.ceca.2008.03.002

Breimann, L., Preusser, F., & Preibisch, S. (2019). Light-microscopy methods in *C. elegans* research. *Current Opinion in Systems Biology*, *13*(Dic), 82–92. https://doi.org/10.1016/j.coisb.2018.11.004

Brenner, S. (1974). The genetics of *Caenorhabditis elegans*. *Genetics*, *77*(1), 71–94.

Bridges, L. E., Williams, C. L., Pointer, M. A., & Awumey, E. M. (2011). Mesenteric artery contraction and relaxation studies using automated wire myography. *Journal of Visualized Experiments*, (55), e3119. https://doi.org/10.3791/3119

Brinks, H. L., & Eckhart, A. D. (2010). Regulation of GPCR signaling in hypertension. *Biochimica et Biophysica Acta (BBA) - Molecular Basis of Disease*, *1802*(12), 1268–1275. https://doi.org/10.1016/j.bbadis.2010.01.005

Broad, L. M., Braun, F.-J., Lievremont, J.-P., Bird, G. S. J., Kurosaki, T., & Putney, J. W. (2001). Role of the phospholipase C-inositol 1,4,5-trisphosphate pathway in calcium release-activated calcium current and capacitative calcium entry. *Journal of Biological Chemistry*, *276*(19), 15945–15952. https://doi.org/10.1074/jbc.M011571200

Brozovich, F. V., Nicholson, C. J., Degen, C. V., Gao, Y. Z., Aggarwal, M., & Morgan, K. G. (2016). Mechanisms of vascular smooth muscle contraction and the basis for pharmacologic treatment of smooth muscle disorders. *Pharmacological Reviews*, *68*(2), 476–532. https://doi.org/10.1124/pr.115.010652

Bulley, S., & Jaggar, J. H. (2014). Cl^- channels in smooth muscle cells. *Pflugers Archiv European Journal of Physiology*, *466*(5), 861–872. https://doi.org/10.1007/s00424-013-1357-2

Bulterijs, S., & Braeckman, B. P. (2020). Phenotypic screening in *C. elegans* as a tool for the discovery of new geroprotective drugs. *Pharmaceuticals*, *13*(8), 1–35. https://doi.org/10.3390/ph13080164

Burn, J., Sheth, H., Elliott, F., Reed, L., Macrae, F., Mecklin, J. P., Möslein, G., McRonald, F. E., Bertario, L., Evans, D. G., Gerdes, A. M., Ho, J. W. C., Lindblom, A., Morrison, P. J., Rashbass, J., Ramesar, R., Seppälä, T., … Side, L. (2020). Cancer prevention with aspirin in hereditary colorectal cancer (Lynch syndrome), 10-year follow-up and registry-based 20-year data in the CAPP2 study: a double-blind, randomised, placebo-controlled trial. *The Lancet*, *395*(10240), 1855–1863. https://doi.org/10.1016/S0140-6736(20)30366-4

Burt, R. P. (2003). Phasic contractions of the rat portal vein depend on intracellular Ca^{2+} release stimulated by depolarization. *American Journal of Physiology - Heart and Circulatory Physiology*, *284*(5 53-5), H1808–H1817. https://doi.org/10.1152/ajpheart.00637.2002

Cai, D., Mulle, J. G., & Yue, D. T. (1997). Inhibition of recombinant Ca^{2+} channels by benzothiazepines and phenylalkylamines: Class-specific pharmacology and underlying molecular determinants. *Molecular Pharmacology*, *51*(5), 872–881. https://doi.org/10.1124/mol.51.5.872

Calhoun, D. A., Jones, D., Textor, S., Goff, D. C., Murphy, T. P., Toto, R. D., White,

A., Cushman, W. C., White, W., Sica, D., Ferdinand, K., Giles, T. D., Falkner, B., & Carey, R. M. (2008). Resistant hypertension: Diagnosis, evaluation, and treatment. *Hypertension*, *51*(6), 1403–1419. https://doi.org/10.1161/HYPERTENSIONAHA.108.189141

Capra, V., Busnelli, M., Perenna, A., Ambrosio, M., Accomazzo, M. R., Galés, C., Chini, B., & Rovati, G. E. (2013). Full and partial agonists of thromboxane prostanoid receptor unveil fine tuning of receptor superactive conformation and G protein activation. *PloS One*, *8*(3), e60475. https://doi.org/10.1371/journal.pone.0060475

Carr, R., Koziol-White, C., Zhang, J., Lam, H., An, S. S., Tall, G. G., Panettieri, R. A., & Benovic, J. L. (2016). Interdicting G_q activation in airway disease by receptor-dependent and receptor-independent mechanisms. *Molecular Pharmacology*. https://doi.org/10.1124/mol.115.100339

Caughey, G. E., Cleland, L. G., Penglis, P. S., Gamble, J. R., & James, M. J. (2001). Roles of cyclooxygenase (COX)-1 and COX-2 in prostanoid production by human endothelial cells: Selective up-regulation of prostacyclin synthesis by COX-2. *The Journal of Immunology*, *167*(5), 2831–2838. https://doi.org/10.4049/jimmunol.167.5.2831

Chamarthy, M. R., Kandathil, A., & Kalva, S. P. (2018). Pulmonary vascular pathophysiology. *Cardiovascular Diagnosis and Therapy*, *8*(3), 208–213. https://doi.org/10.21037/cdt.2018.01.08

Charão, M., Souto, C., Brucker, N., Barth, A., Jornada, D., Fagundes, D., S. de Ávila, D., Eifler-Lima, V., Guterres, S., Pohlmann, A., & Garcia, S. (2015). *Caenorhabditis elegans* as an alternative in vivo model to determine oral uptake, nanotoxicity, and efficacy of melatonin-loaded lipid-core nanocapsules on paraquat damage. *International Journal of Nanomedicine*, *10*, 5093. https://doi.org/10.2147/IJN.S84909

Chaudhary, J., Walia, M., Matharu, J., Escher, E., & Grover, A. K. (2001). Caloxin: A novel plasma membrane Ca^{2+} pump inhibitor. *American Journal of Physiology - Cell Physiology*, *280*(4 49-4), 1027–1030. https://doi.org/10.1152/ajpcell.2001.280.4.c1027

Chaudhry, R., Miao, J. H., & Rehman, A. (2020). Physiology, cardiovascular. In *StatPearls*. Retrieved from https://www.ncbi.nlm.nih.gov/books/NBK493197/

Chen, C. C., Huang, Y. L., Ou, J. C., Su, M. J., Yu, S. M., & Teng, C. M. (1991). Bioactive principles from the roots of *Lindera megaphylla*. *Planta Medica*, *57*(5), 406–408. https://doi.org/10.1055/s-2006-960135

Chen, J., Crossland, R. F., Noorani, M. M. Z., & Marrelli, S. P. (2009). Inhibition of TRPC1/TRPC3 by PKG contributes to NO-mediated vasorelaxation. *American Journal of Physiology - Heart and Circulatory Physiology*, *297*(1), H417–H424. https://doi.org/10.1152/ajpheart.01130.2008

Chen, L., Koh, D. S., & Hille, B. (2003). Dynamics of calcium clearance in mouse pancreatic β-cells. *Diabetes*, *52*(7), 1723–1731. https://doi.org/10.2337/diabetes.52.7.1723

Chen, Xiaoping, Yang, D., Ma, S., He, H., Luo, Z., Feng, X., Cao, T., Ma, L., Yan, Z.,

Liu, D., Tepel, M., & Zhu, Z. (2010). Increased rhythmicity in hypertensive arterial smooth muscle is linked to transient receptor potential canonical channels. *Journal of Cellular and Molecular Medicine*, *14*(10), 2483–2494. https://doi.org/10.1111/j.1582-4934.2009.00890.x

Chen, Xingjuan, Sooch, G., Demaree, I. S., White, F. A., & Obukhov, A. G. (2020). Transient Receptor Potential Canonical (TRPC) Channels: Then and Now. *Cells*, *9*(9), 1983. https://doi.org/10.3390/cells9091983

Cheng, H. S., Ton, S. H., Tan, J. B. L., & Kadir, K. A. (2017). The ameliorative effects of a tocotrienol-rich fraction on the AGE-RAGE axis and hypertension in high-fat-diet-fed rats with metabolic syndrome. *Nutrients*, *9*(9), 1–18. https://doi.org/10.3390/nu9090984

Cheung, B. M. Y., & Li, C. (2012). Diabetes and hypertension: Is there a common metabolic pathway? *Current Atherosclerosis Reports*, *14*(2), 160–166. https://doi.org/10.1007/s11883-012-0227-2

Chevallet, M., Jarvis, L., Harel, A., Luche, S., Degot, S., Chapuis, V., Boulay, G., Rabilloud, T., & Bouron, A. (2014). Functional consequences of the over-expression of TRPC6 channels in HEK cells: Impact on the homeostasis of zinc. *Metallomics*, *6*(7), 1269–1276. https://doi.org/10.1039/c4mt00028e

Chia, Y. C., & Ching, S. M. (2014). Prevalence and predictors of resistant hypertension in a primary care setting: A cross-sectional study. *BMC Family Practice*, *15*(1), 1–7. https://doi.org/10.1186/1471-2296-15-131

Chiou, W. F., Liao, J. F., Shum, A. Y. C., & Chen, C. F. (1996). Mechanisms of vasorelaxant effect of dehydroevodiamine: A bioactive isoquinazolinocarboline alkaloid of plant origin. *Journal of Cardiovascular Pharmacology*, *27*(6), 845–853. https://doi.org/10.1097/00005344-199606000-00012

Cierpial, M. A., & McCarty, R. (1991). Adult blood pressure reduction in spontaneously hypertensive rats reared by normotensive Sprague-Dawley mothers. *Behavioral and Neural Biology*, *56*(3), 262–270. https://doi.org/10.1016/0163-1047(91)90409-J

Clementi, E., & Meldolesi, J. (1996). Pharmacological and functional properties of voltagemi independent Ca^{2+} channels. *Cell Calcium*, *19*(4), 269–279. https://doi.org/10.1016/S0143-4160(96)90068-8

Coca, A., Mazón, P., Aranda, P., Redón, J., Divisón, J. A., Martínez, J., Calvo, C., Galcerán, J. M., Barrios, V., & Coll, A. R.-C. i. (2013). Role of dihydropyridinic calcium channel blockers in the management of hypertension. *Expert Review of Cardiovascular Therapy*, *11*(1), 91–105. https://doi.org/10.1586/erc.12.155

Colabufo, N. A., Pagliarulo, V., Berardi, F., Contino, M., Perrone, R., Niso, M., Albo, G., de Rienzo, G., & Pagliarulo, A. (2007). Human epididymal and prostatic tracts of vas deferens: Different contraction response to noradrenaline stimulation in isolated organ bath assay. *European Journal of Pharmacology*, *577*(1–3), 150–155. https://doi.org/10.1016/j.ejphar.2007.08.038

Condreay, J. P., Witherspoon, S. M., Clay, W. C., & Kost, T. A. (1999). Transient and stable gene expression in mammalian cells transduced with a recombinant baculovirus vector. *Proceedings of the National Academy of Sciences of the United*

States of America, *96*(1), 127–132. https://doi.org/10.1073/pnas.96.1.127

Coppolino, G., Pisano, A., Rivoli, L., & Bolignano, D. (2017). Renal denervation for resistant hypertension. *Cochrane Database of Systematic Reviews*, *2017*(2). https://doi.org/10.1002/14651858.CD011499.pub2

Cox, R. H., & Rusch, N. J. (2002). New expression profiles of voltage-gated ion channels in arteries exposed to high blood pressure. *Microcirculation*, *9*(4), 243–257. https://doi.org/10.1038/sj.mn.7800140

Coyle, P. (1986). Different susceptibilities to cerebral infarction in spontaneously hypertensive (SHR) and normotensive Sprague-Dawley rats. *Stroke*, *17*(3), 520–525. https://doi.org/10.1161/01.STR.17.3.520

Davidson, E. P., Kleinschmidt, T. L., Oltman, C. L., Lund, D. D., & Yorek, M. A. (2007). Treatment of streptozotocin-induced diabetic rats with AVE7688, a vasopeptidase inhibitor: Effect on vascular and neural disease. *Diabetes*, *56*(2), 355–362. https://doi.org/10.2337/db06-1180

Davis, A. J., Shi, J., Pritchard, H. A. T., Chadha, P. S., Leblanc, N., Vasilikostas, G., Yao, Z., Verkman, A. S., Albert, A. P., & Greenwood, I. A. (2013). Potent vasorelaxant activity of the TMEM16A inhibitor T16Ainh-A01. *British Journal of Pharmacology*, *168*(3), 773–784. https://doi.org/10.1111/j.1476-5381.2012.02199.x

de la Peña, E., & Gomis, A. (2019). Characterization of TRPC channels in a heterologous system using calcium imaging and the patch-clamp technique. In *Methods in Molecular Biology* (Vol. 1987, pp. 83–97). https://doi.org/10.1007/978-1-4939-9446-5_6

de la Torre, B. G., & Albericio, F. (2019). The pharmaceutical industry in 2018. An analysis of FDA drug approvals from the perspective of molecules. *Molecules*, *24*(4). https://doi.org/10.3390/molecules24040809

De Mello, W. (2016). Intracellular renin increases the inward calcium current in smooth muscle cells of mesenteric artery of SHR. Implications for hypertension and vascular remodeling. *Peptides*, *84*, 36–43. https://doi.org/10.1016/j.peptides.2016.08.005

De Pittà, M., Ben-Jacob, E., & Berry, H. (2019). G protein-coupled receptor-mediated calcium signaling in astrocytes. In *arXiv* (pp. 115–150). https://doi.org/10.1007/978-3-030-00817-8_5

Deanfield, J. E., Halcox, J. P., & Rabelink, T. J. (2007). Endothelial function and dysfunction: Testing and clinical relevance. *Circulation*, *115*(10), 1285–1295. https://doi.org/10.1161/CIRCULATIONAHA.106.652859

Dettbarn, C., & Palade, P. (1998). Effects of three sarcoplasmic/endoplasmic reticulum Ca^{++} pump inhibitors on release channels of intracellular stores. *Journal of Pharmacology and Experimental Therapeutics*, *285*(2), 739–745.

Didion, S. P. (2016). New insights into mechanisms associated with angiotensin II-induced vascular hypertrophy and remodeling. *Hypertension*, *67*(3), 501–503. https://doi.org/10.1161/HYPERTENSIONAHA.115.06737

Dietrich, A., Mederos y Schnitzler, M., Gollasch, M., Gross, V., Storch, U., Dubrovska,

G., Obst, M., Yildirim, E., Salanova, B., Kalwa, H., Essin, K., Pinkenburg, O., Luft, F. C., Gudermann, T., & Birnbaumer, L. (2005). Increased vascular smooth muscle contractility in TRPC6$^{-/-}$ mice. *Molecular and Cellular Biology*, *25*(16), 6980–6989. https://doi.org/10.1128/MCB.25.16.6980-6989.2005

Dietrich, A., Mederos y Schnitzler, M., Kalwa, H., Storch, U., & Gudermann, T. (2005). Functional characterization and physiological relevance of the TRPC3/6/7 subfamily of cation channels. *Naunyn-Schmiedeberg's Archives of Pharmacology*, *371*(4), 257–265. https://doi.org/10.1007/s00210-005-1052-8

Diochot, S., Richard, S., Baldy-Moulinier, M., Nargeot, J., & Valmier, J. (1995). Dihydropyridines, phenylalkylamines and benzothiazepines block N-, P/Q- and R-type calcium currents. *Pflügers Archiv European Journal of Physiology*, *431*(1), 10–19. https://doi.org/10.1007/BF00374372

Dohi, Y., Kojima, M., & Sato, K. (1996). Endothelial modulation of contractile responses in arteries from hypertensive rats. *Hypertension*, *28*(5), 732–737. https://doi.org/10.1161/01.HYP.28.5.732

Dong, Y. N., Hsu, F.-C., Koziol-White, C. J., Stepanova, V., Jude, J., Gritsiuta, A., Rue, R., Mott, R., Coulter, D. A., Panettieri, R. A., Krymskaya, V. P., Takano, H., Goncharova, E. A., Goncharov, D. A., Cines, D. B., & Lynch, D. R. (2021). Functional NMDA receptors are expressed by human pulmonary artery smooth muscle cells. *Scientific Reports*, *11*(1), 8205. https://doi.org/10.1038/s41598-021-87667-0

Dorn, G. W., Becker, M. W., & Davis, M. G. (1992). Dissociation of the contractile and hypertrophic effects of vasoconstrictor prostanoids in vascular smooth muscle. *Journal of Biological Chemistry*, *267*(34), 24897–24905. https://doi.org/10.1016/s0021-9258(18)35848-4

Dowd, F. J. (2017). Cholinergic agonists and muscarinic receptor antagonists. In *Pharmacology and Therapeutics for Dentistry* (Seventh Ed, pp. 82–97). https://doi.org/10.1016/B978-0-323-39307-2.00006-0

Duan, J., Li, J., Chen, G. L., Ge, Y., Liu, J., Xie, K., Peng, X., Zhou, W., Zhong, J., Zhang, Y., Xu, J., Xue, C., Liang, B., Zhu, L., Liu, W., Zhang, C., Tian, X. L., … Zhang, J. (2019). Cryo-EM structure of TRPC5 at 2.8-Å resolution reveals unique and conserved structural elements essential for channel function. *Science Advances*, *5*(7), eaaw7935. https://doi.org/10.1126/sciadv.aaw7935

Duarte, J. D., Hanson, R. L., & Machado, R. F. (2013). Pharmacologic treatments for pulmonary hypertension: exploring pharmacogenomics. *Future Cardiology*, *9*(3), 335–349. https://doi.org/10.2217/fca.13.6

Durocher, Y., Perret, S., & Kamen, A. (2001). Recombinant protein production by transient transfection of suspension-growing cells. In *Recombinant Protein Production with Prokaryotic and Eukaryotic Cells. A Comparative View on Host Physiology* (pp. 331–337). https://doi.org/10.1007/978-94-015-9749-4_24

Earley, S., & Brayden, J. E. (2015). Transient receptor potential channels in the vasculature. *Physiological Reviews*, *95*(1), 645–690. https://doi.org/10.1152/physrev.00026.2014

Enevoldsen, F. C., Sahana, J., Wehland, M., Grimm, D., Infanger, M., & Krüger, M.

(2020). Endothelin receptor antagonists: Status quo and future perspectives for targeted therapy. *Journal of Clinical Medicine*, *9*(3), 824. https://doi.org/10.3390/jcm9030824

Erac, Y., Selli, C., Kosova, B., Akcali, K. C., & Tosun, M. (2010). Expression levels of TRPC1 and TRPC6 ion channels are reciprocally altered in aging rat aorta: implications for age-related vasospastic disorders. *AGE*, *32*(2), 223–230. https://doi.org/10.1007/s11357-009-9126-z

Erejuwa, O. O., Gan, S. H., Romani, A. M. P., Kamal, M. A., & Nammi, S. (2019). Nonpharmacologic interventions in prevention and treatment of hypertension. *International Journal of Hypertension*, *2019*, 1–2. https://doi.org/10.1155/2019/6709817

Estacion, M., Sinkins, W. G., Jones, S. W., Applegate, M. A. B., & Schilling, W. P. (2006). Human TRPC6 expressed in HEK 293 cells forms non-selective cation channels with limited Ca^{2+} permeability. *Journal of Physiology*, *572*(2), 359–377. https://doi.org/10.1113/jphysiol.2005.103143

Facemire, C. S., Mohler, P. J., & Arendshorst, W. J. (2004). Expression and relative abundance of short transient receptor potential channels in the rat renal microcirculation. *American Journal of Physiology-Renal Physiology*, *286*(3), F546–F551. https://doi.org/10.1152/ajprenal.00338.2003

Falcón, D., Galeano-Otero, I., Martín-Bórnez, M., Fernández-Velasco, M., Gallardo-Castillo, I., Rosado, J. A., Ordóñez, A., & Smani, T. (2020). TRPC channels: Dysregulation and Ca^{2+} mishandling in ischemic heart disease. *Cells*, *9*(1), 173. https://doi.org/10.3390/cells9010173

Falkenburger, B. H., Dickson, E. J., & Hille, B. (2013). Quantitative properties and receptor reserve of the DAG and PKC branch of G_q-coupled receptor signaling. *Journal of General Physiology*, *141*(5), 537–555. https://doi.org/10.1085/jgp.201210887

Fan, M., Zhang, J., Tsai, C.-W., Orlando, B. J., Rodriguez, M., Xu, Y., Liao, M., Tsai, M.-F., & Feng, L. (2020). Structure and mechanism of the mitochondrial Ca^{2+} uniporter holocomplex. *Nature*, *582*(7810), 129–133. https://doi.org/10.1038/s41586-020-2309-6

Feig, P. U., Roy, S., & Cody, R. J. (2010). Antihypertensive drug development: Current challenges and future opportunities. *Journal of the American Society of Hypertension*, *4*(4), 163–173. https://doi.org/10.1016/j.jash.2010.04.003

Félétou, M. (2011). The Endothelium, Part I: Multiple Functions of the Endothelial Cells -- Focus on Endothelium-Derived Vasoactive Mediators. *Colloquium Series on Integrated Systems Physiology: From Molecule to Function*, *3*(4), 1–306. https://doi.org/10.4199/C00031ED1V01Y201105ISP019

Félétou, M., Köhler, R., & Vanhoutte, P. M. (2010). Endothelium-derived vasoactive factors and hypertension: Possible roles in pathogenesis and as treatment targets. *Current Hypertension Reports*, *12*(4), 267–275. https://doi.org/10.1007/s11906-010-0118-2

Félétou, M., Verbeuren, T. J., & Vanhoutte, P. M. (2009). Endothelium-dependent contractions in SHR: A tale of prostanoid TP and IP receptors. *British Journal of*

Pharmacology, Vol. 156, pp. 563–574. https://doi.org/10.1111/j.1476-5381.2008.00060.x

Fellner, S. K., & Arendshorst, W. J. (2002). Store-operated Ca^{2+} entry is exaggerated in fresh preglomerular vascular smooth muscle cells of SHR. *Kidney International*, *61*(6), 2132–2141. https://doi.org/10.1046/j.1523-1755.2002.00383.x

Fellner, S. K., & Arendshorst, W. J. (2007). Voltage-gated Ca^{2+} entry and ryanodine receptor Ca^{2+}-induced Ca^{2+} release in preglomerular arterioles. *American Journal of Physiology - Renal Physiology*, *292*(5), F1568–F1572. https://doi.org/10.1152/ajprenal.00459.2006

Fernández-Tenorio, M., Porras-González, C., Castellano, A., del Valle-Rodríguez, A., López-Barneo, J., & Ureña, J. (2011). Metabotropic regulation of RhoA/Rho-associated kinase by L-type Ca^{2+} channels. *Circulation Research*, *108*(11), 1348–1357. https://doi.org/10.1161/CIRCRESAHA.111.240127

Fester, K. (2010). Plant Alkaloids. In *Encyclopedia of Life Sciences*. https://doi.org/10.1002/9780470015902.a0001914.pub2

Fierro, L., DiPolo, R., & Llano, I. (1998). Intracellular calcium clearance in Purkinje cell somata from rat cerebellar slices. *Journal of Physiology*, *510*(2), 499–512. https://doi.org/10.1111/j.1469-7793.1998.499bk.x

Fitsanakis, V. (2012). *Caenorhabditis elegans*: An emerging model system for pesticide neurotoxicity. *Journal of Environmental & Analytical Toxicology*, *01*(S4). https://doi.org/10.4172/2161-0525.S4-003

Fleichman, M., Schneider, T., Fetscher, C., & Michel, M. C. (2004). Signal transduction underlying carbachol-induced contraction of rat urinary bladder. II. protein kinases. *Journal of Pharmacology and Experimental Therapeutics*, *308*(1), 54–58. https://doi.org/10.1124/jpet.103.058255

Fong, M. C. C., & Shanizza, A. I. A. (2020). Malaysian statistics on medicine 2015-2016. *Pharmaceutical Services Programme Ministry of Health Malaysia*, 1–127.

Fountain, J. H., & Lappin, S. L. (2018). Physiology, renin angiotensin system. In *StatPearls*. Retrieved from http://www.ncbi.nlm.nih.gov/pubmed/29261862

Franco, N. H., Sandøe, P., & Olsson, I. A. S. (2018). Researchers' attitudes to the 3Rs - An upturned hierarchy? *PLoS ONE*, *13*(8), e0200895. https://doi.org/10.1371/journal.pone.0200895

Frankowski, H., Alavez, S., Spilman, P., Mark, K. A., Nelson, J. D., Mollahan, P., Rao, R. V., Chen, S. F., Lithgow, G. J., & Ellerby, H. M. (2013). Dimethyl sulfoxide and dimethyl formamide increase lifespan of *C. elegans* in liquid. *Mechanisms of Ageing and Development*, *134*(3–4), 69–78. https://doi.org/10.1016/j.mad.2012.10.002

Fransen, P., Van Hove, C. E., Leloup, A. J. A., Martinet, W., De Meyer, G. R. Y., Lemmens, K., Bult, H., & Schrijvers, D. M. (2015). Dissecting out the complex Ca^{2+}-mediated phenylephrine-induced contractions of mouse aortic segments. *PLOS ONE*, *10*(3), 1–17. https://doi.org/10.1371/journal.pone.0121634

Freichel, M., Suh, S. H., Pfeifer, A., Schweig, U., Trost, C., Weißgerber, P., Biel, M., Philipp, S., Freise, D., Droogmans, G., Hofmann, F., Flockerzi, V., & Nilius, B.

(2001). Lack of an endothelial store-operated Ca^{2+} current impairs agonist-dependent vasorelaxation in $TRP4^{-/-}$ mice. *Nature Cell Biology*, *3*(2), 121–127. https://doi.org/10.1038/35055019

Fu, S., Ping, P., Wang, F., & Luo, L. (2018). Synthesis, secretion, function, metabolism and application of natriuretic peptides in heart failure. *Journal of Biological Engineering*, *12*(1), 2. https://doi.org/10.1186/s13036-017-0093-0

Fuchs, F. D., & Whelton, P. K. (2020). High blood pressure and cardiovascular disease. *Hypertension*, *75*(2), 285–292. https://doi.org/10.1161/HYPERTENSIONAHA.119.14240

Fukata, Y., Kaibuchi, K., Amano, M., & Kaibuchi, K. (2001). Rho-Rho-kinase pathway in smooth muscle contraction and cytoskeletal reorganization of non-muscle cells. *Trends in Pharmacological Sciences*, *22*(1), 32–39. https://doi.org/10.1016/S0165-6147(00)01596-0

Furchgott, R. F., & Vanhoutte, P. M. (1989). Endothelium-derived relaxing and contracting factors. *The FASEB Journal*, *3*(9), 2007–2018. https://doi.org/10.1096/fasebj.3.9.2545495

Furchgott, R. F., & Zawadzki, J. V. (1980). The obligatory role of endothelial cells in the relaxation of arterial smooth muscle by acetylcholine. *Nature*, *288*(5789), 373–376. https://doi.org/10.1038/288373a0

Galiè, N., Humbert, M., Vachiery, J. L., Gibbs, S., Lang, I., Torbicki, A., Simonneau, G., Peacock, A., Vonk Noordegraaf, A., Beghetti, M., Ghofrani, A., Gomez Sanchez, M. A., Hansmann, G., Klepetko, W., Lancellotti, P., Matucci, M., McDonagh, T., … Sirenko, Y. (2016). 2015 ESC/ERS Guidelines for the diagnosis and treatment of pulmonary hypertension. *European Heart Journal*, *37*(1), 67–119. https://doi.org/10.1093/eurheartj/ehv317

García-Redondo, A. B., Briones, A. M., Martínez-Revelles, S., Palao, T., Vila, L., Alonso, M. J., & Salaices, M. (2015). C-Src, ERK1/2 and Rho kinasemediate hydrogen peroxide-induced vascular contraction in hypertension: Role of TXA2, NAD(P)H oxidase andmitochondria. *Journal of Hypertension*, *33*(1), 77–87. https://doi.org/10.1097/HJH.0000000000000383

Garcia, D. C. G., Pereira, A. C., Gutierrez, S. J. C., Barbosa-Filho, J. M., Lemos, V. S., & Côrtes, S. F. (2016). Structure-related blockage of calcium channels by vasodilator alkamides in mice mesenteric artery. *Vascular Pharmacology*, *82*, 60–65. https://doi.org/10.1016/j.vph.2016.05.001

Gericke, A., Steege, A., Manicam, C., Böhmer, T., Wess, J., & Pfeiffer, N. (2014). Role of the M_3 muscarinic acetylcholine receptor subtype in murine ophthalmic arteries after endothelial removal. *Investigative Ophthalmology and Visual Science*, *55*(1), 625–631. https://doi.org/10.1167/iovs.13-13549

Geron, M., Hazan, A., & Priel, A. (2017). Controllable ion channel expression through inducible transient transfection. *Journal of Visualized Experiments*, *2017*(120), 55370. https://doi.org/10.3791/55370

Ghaemi, R., Tong, J., Gupta, B. P., & Selvaganapathy, P. R. (2020). Microfluidic device for microinjection of *Caenorhabditis elegans*. *Micromachines*. https://doi.org/10.3390/mi11030295

Ghose, A. K., Viswanadhan, V. N., & Wendoloski, J. J. (1998). Prediction of hydrophobic (lipophilic) properties of small organic molecules using fragmental methods: An analysis of ALOGP and CLOGP methods. *Journal of Physical Chemistry A*, *102*(21), 3762–3772. https://doi.org/10.1021/jp980230o

Ghosh, D., Syed, A. U., Prada, M. P., Nystoriak, M. A., Santana, L. F., Nieves-Cintrón, M., & Navedo, M. F. (2017). Calcium channels in vascular smooth muscle. *Advances in Pharmacology*, *78*, 49–87. https://doi.org/10.1016/bs.apha.2016.08.002

Giacomotto, J., & Ségalat, L. (2010). High-throughput screening and small animal models, where are we? *British Journal of Pharmacology*, *160*(2), 204–216. https://doi.org/10.1111/j.1476-5381.2010.00725.x

Gibon, J., Tu, P., Bohic, S., Richaud, P., Arnaud, J., Zhu, M., Boulay, G., & Bouron, A. (2011). The over-expression of TRPC6 channels in HEK-293 cells favours the intracellular accumulation of zinc. *Biochimica et Biophysica Acta - Biomembranes*, *1808*(12), 2807–2818. https://doi.org/10.1016/j.bbamem.2011.08.013

Goel, M., Sinkins, W. G., & Schilling, W. P. (2002). Selective association of TRPC channel subunits in rat brain synaptosomes. *Journal of Biological Chemistry*, *277*(50), 48303–48310. https://doi.org/10.1074/jbc.M207882200

Gohla, A., Schultz, G., & Offermanns, S. (2000). Role for G_{12}/G_{13} in agonist-induced vascular smooth muscle cell contraction. *Circulation Research*, *87*(3), 221–227. https://doi.org/10.1161/01.RES.87.3.221

Goldstein, D. S. (2010). Adrenaline and Noradrenaline. In *eLS*. https://doi.org/10.1002/9780470015902.a0001401.pub2

Golovina, V. A., Platoshyn, O., Bailey, C. L., Wang, J., Limsuwan, A., Sweeney, M., Rubin, L. J., & Yuan, J. X. J. (2001). Upregulated TRP and enhanced capacitative Ca^{2+} entry in human pulmonary artery myocytes during proliferation. *American Journal of Physiology-Heart and Circulatory Physiology*, *280*(2), H746–H755. https://doi.org/10.1152/ajpheart.2001.280.2.H746

Gómez-Orte, E., Cornes, E., Zheleva, A., Sáenz-Narciso, B., de Toro, M., Iñiguez, M., López, R., San-Juan, J.-F., Ezcurra, B., Sacristán, B., Sánchez-Blanco, A., Cerón, J., & Cabello, J. (2018). Effect of the diet type and temperature on the *C. elegans* transcriptome. *Oncotarget*, *9*(11), 9556–9571. https://doi.org/10.18632/oncotarget.23563

González-Cobos, J. C., & Trebak, M. (2011). TRPC channels in smooth muscle cells. *Frontiers in Bioscience*, *15*(518), 1023–1039.

Gordon, S. G., & Kittleson, M. D. (2008). Drugs used in the management of heart disease and cardiac arrhythmias. In *Small Animal Clinical Pharmacology* (2nd ed., pp. 380–457). https://doi.org/10.1016/B978-070202858-8.50019-1

Goto, K., Ohtsubo, T., & Kitazono, T. (2018). Endothelium-dependent hyperpolarization (EDH) in hypertension: The role of endothelial ion channels. *International Journal of Molecular Sciences*, Vol. 19. https://doi.org/10.3390/ijms19010315

Govindarajan, G., Sowers, J. R., & Stump, C. S. (2006). Hypertension and diabetes

mellitus. *European Cardiology Review*, *2*(1), 21. https://doi.org/10.15420/ECR.2006.1.1a

Govindaraju, K. (2019). *Development of in-vitro and in-vivo bioassays to elucidate the mechanism of action of a synthetic novel compound N-phenethyl-1-phenyl-pentan-3-amine (FK70)*. University of Nottingham.

Graham, F. L., Smiley, J., Russell, W. C., & Nairn, R. (1977). Characteristics of a human cell line transformed by DNA from human adenovirus type 5. *Journal of General Virology*, *36*(1), 59–72. https://doi.org/10.1099/0022-1317-36-1-59

Grann, M., Comerma-Steffensen, S., Arcanjo, D. D. R. R., & Simonsen, U. (2016). Mechanisms involved in thromboxane A_2-induced vasoconstriction of rat intracavernous small penile arteries. *Basic & Clinical Pharmacology & Toxicology*, *119*, 86–95. https://doi.org/10.1111/bcpt.12544

Grassi, G., Cattaneo, B. M., Seravalle, G., Lanfranchi, A., & Mancia, G. (1998). Baroreflex control of sympathetic nerve activity in essential and secondary hypertension. *Hypertension*, *31*(1), 68–72. https://doi.org/10.1161/01.HYP.31.1.68

Grassi, G., Robles, N. R., Seravalle, G., & Fici, F. (2017). Lercanidipine in the management of hypertension: An update. *Journal of Pharmacology and Pharmacotherapeutics*, *8*(4), 155–165. https://doi.org/10.4103/jpp.JPP_34_17

Gregory, R. B., Rychkov, G., & Barritt, G. J. (2001). Evidence that 2-aminoethyl diphenylborate is a novel inhibitor of store-operated Ca^{2+} channels in liver cells, and acts through a mechanism which does not involve inositol trisphosphate receptors. *Biochemical Journal*, *354*(2), 285–290. https://doi.org/10.1042/0264-6021:3540285

Grienberger, C., & Konnerth, A. (2012). Imaging calcium in neurons. *Neuron*, *73*(5), 862–885. https://doi.org/10.1016/j.neuron.2012.02.011

Gros, R., Afroze, T., You, X. M., Kabir, G., Van Wert, R., Kalair, W., Hoque, A. E., Mungrue, I. N., & Husain, M. (2003). Plasma membrane calcium ATPase overexpression in arterial smooth muscle increases vasomotor responsiveness and blood pressure. *Circulation Research*, *93*(7), 614–621. https://doi.org/10.1161/01.RES.0000092142.19896.D9

Grynkiewicz, G., Poenie, M., & Tsien, R. Y. (1985). A new generation of Ca^{2+} indicators with greatly improved fluorescence properties. *Journal of Biological Chemistry*, *260*(6), 3440–3450. https://doi.org/10.1016/s0021-9258(19)83641-4

Gudlur, A., Zeraik, A. E., Hirve, N., & Hogan, P. G. (2020). STIM calcium sensing and conformational change. *The Journal of Physiology*, *598*(9), 1695–1705. https://doi.org/10.1113/JP276524

Gürdal, H., Can, A., & Uğur, M. (2005). The role of nitric oxide synthase in reduced vasocontractile responsiveness induced by prolonged α_1-adrenergic receptor stimulation in rat thoracic aorta. *British Journal of Pharmacology*, *145*(2), 203–210. https://doi.org/10.1038/sj.bjp.0706177

Guyenet, P. G. (2006). The sympathetic control of blood pressure. *Nature Reviews Neuroscience*, *7*(5), 335–346. https://doi.org/10.1038/nrn1902

Hadjiisky, P., Peyri, N., & Grosgogeat, Y. (1987). Tunica media changes in the spontaneously hypertensive rat (SHR). *Atherosclerosis*, *65*(1–2), 125–137. https://doi.org/10.1016/0021-9150(87)90014-1

Harada, M., Luo, X., Qi, X. Y., Tadevosyan, A., Maguy, A., Ordog, B., Ledoux, J., Kato, T., Naud, P., Voigt, N., Shi, Y., Kamiya, K., Murohara, T., Kodama, I., Tardif, J.-C., Schotten, U., Van Wagoner, D. R., … Nattel, S. (2012). Transient receptor potential canonical-3 channel–dependent fibroblast regulation in atrial fibrillation. *Circulation*, *126*(17), 2051–2064. https://doi.org/10.1161/CIRCULATIONAHA.112.121830

Harhun, M. I., Sukhanova, K., Gordienko, D., & Dyskina, Y. (2015). Molecular identification of P2X receptors in vascular smooth muscle cells from rat anterior, posterior, and basilar arteries. *Pharmacological Reports*, *67*(6), 1055–1060. https://doi.org/10.1016/j.pharep.2015.03.014

Harteneck, C., Klose, C., & Krautwurst, D. (2011). Synthetic modulators of TRP channel activity. In *Advances in Experimental Medicine and Biology* (Vol. 704, pp. 87–106). https://doi.org/10.1007/978-94-007-0265-3_4

He, C., Preiss, L., Wang, B., Fu, L., Wen, H., Zhang, X., Cui, H., Meier, T., & Yin, D. (2017). Structural simplification of bedaquiline: the Discovery of 3-(4-(N,N-Dimethylaminomethyl)phenyl)quinoline-derived antitubercular lead compounds. *ChemMedChem*, *12*(2), 106–119. https://doi.org/10.1002/cmdc.201600441

He, L. P., Hewavitharana, T., Soboloff, J., Spassova, M. A., & Gill, D. L. (2005). A functional link between store-operated and TRPC channels revealed by the 3,5-bis(trifluoromethyl)pyrazole derivative, BTP2. *Journal of Biological Chemistry*, *280*(12), 10997–11006. https://doi.org/10.1074/jbc.M411797200

Hideharu, H., & Haruo, M. (1994). Fluorescence imaging of intracellular Ca^{2+}. *Journal of Pharmacological and Toxicological Methods*, *31*(1), 1–10. https://doi.org/10.1016/1056-8719(94)90023-X

Hill-Eubanks, D. C., Werner, M. E., Heppner, T. J., & Nelson, M. T. (2011). Calcium signaling in smooth muscle. *Cold Spring Harbor Perspectives in Biology*, *3*(9), 1–20. https://doi.org/10.1101/cshperspect.a004549

Himpens, B., Kitazawa, T., & Somlyo, A. P. (1990). Agonist-dependent modulation of Ca^{2+} sensitivity in rabbit pulmonary artery smooth muscle. *Pflügers Archiv European Journal of Physiology*, *417*(1), 21–28. https://doi.org/10.1007/BF00370764

Hink, U., Li, H., Mollnau, H., Oelze, M., Matheis, E., Hartmann, M., Skatchkov, M., Thaiss, F., Stahl, R. A., Warnholtz, A., Meinertz, T., Griendling, K., Harrison, D. G., Forstermann, U., & Munzel, T. (2001). Mechanisms underlying endothelial dysfunction in diabetes mellitus. *Circulation Research*, *88*(2). https://doi.org/10.1161/01.res.88.2.e14

Hirsch, C., & Schildknecht, S. (2019). In vitro research reproducibility: Keeping up high standards. *Frontiers in Pharmacology*, *10*, 1484. https://doi.org/10.3389/fphar.2019.01484

Hofmann, T., Obukhov, A. G., Schaefer, M., Harteneck, C., Gudermann, T., & Schultz, G. (1999). Direct activation of human TRPC6 and TRPC3 channels by

diacylglycerol. *Nature*, *397*(6716), 259–263. https://doi.org/10.1038/16711

Hofmann, T., Schaefer, M., Schultz, G., & Gudermann, T. (2002). Subunit composition of mammalian transient receptor potential channels in living cells. *Proceedings of the National Academy of Sciences of the United States of America*, *99*(11), 7461–7466. https://doi.org/10.1073/pnas.102596199

Honnen, S. (2017). *Caenorhabditis elegans* as a powerful alternative model organism to promote research in genetic toxicology and biomedicine. *Archives of Toxicology*, *91*(5), 2029–2044. https://doi.org/10.1007/s00204-017-1944-7

Hopkins, A. L., Lamm, M. G., Funk, J. L., & Ritenbaugh, C. (2013). *Hibiscus sabdariffa* L. in the treatment of hypertension and hyperlipidemia: A comprehensive review of animal and human studies. *Fitoterapia*, *85*(1), 84–94. https://doi.org/10.1016/j.fitote.2013.01.003

Hou, T., Li, Y., Zhang, W., & Wang, J. (2009). Recent developments of in silico predictions of intestinal absorption and oral bioavailability. *Combinatorial Chemistry & High Throughput Screening*, *12*(5), 497–506. https://doi.org/10.2174/138620709788489082

Hou, T., & Wang, J. (2008). Structure-ADME relationship: Still a long way to go? *Expert Opinion on Drug Metabolism and Toxicology*, *4*(6), 759–770. https://doi.org/10.1517/17425255.4.6.759

Houde, M., Desbiens, L., & D'Orléans-Juste, P. (2016). Endothelin-1: Biosynthesis, Signaling and Vasoreactivity. *Advances in Pharmacology*, *77*, 143–175. https://doi.org/10.1016/bs.apha.2016.05.002

Hu, C. P., Xiao, L., Deng, H. W., & Li, Y. J. (2002). The cardioprotection of rutaecarpine is mediated by endogenous calcitonin related-gene peptide through activation of vanilloid receptors in guinea-pig hearts. *Planta Medica*, *68*(8), 705–709. https://doi.org/10.1055/s-2002-33794

Hu, Y., Xia, W., Li, Y., Wang, Q., Lin, S., Wang, B., Zhou, C., Cui, Y., Jiang, Y., Pu, X., Wei, X., Wu, H., Zhang, H., Zhu, Z., Liu, D., & Li, Z. (2020). High-salt intake increases TRPC3 expression and enhances TRPC3-mediated calcium influx and systolic blood pressure in hypertensive patients. *Hypertension Research*, *43*(7), 679–687. https://doi.org/10.1038/s41440-020-0409-1

Hunt, P. R. (2017). The *C. elegans* model in toxicity testing. *Journal of Applied Toxicology*, *37*(1), 50–59. https://doi.org/10.1002/jat.3357

Inoue, R., Jensen, L. J., Shi, J., Morita, H., Nishida, M., Honda, A., & Ito, Y. (2006). Transient receptor potential channels in cardiovascular function and disease. *Circulation Research*, *99*(2), 119–131. https://doi.org/10.1161/01.RES.0000233356.10630.8a

Inoue, R., Okada, T., Onoue, H., Hara, Y., Shimizu, S., Naitoh, S., Ito, Y., & Mori, Y. (2001). The transient receptor potential protein homologue TRP6 is the essential component of vascular alpha$_1$-adrenoceptor-activated Ca^{2+}-permeable cation channel. *Circulation Research*, *88*(3), 325–332. https://doi.org/10.1161/01.RES.88.3.325

Inoue, T., Moriya, A., Goto, K., Tanaka, T., & Inazu, M. (1995). What is the difference

of bone growth in SHR and SD Rats? *Clinical and Experimental Pharmacology and Physiology*, *22*(s1), S242–S243. https://doi.org/10.1111/j.1440-1681.1995.tb02900.x

Institute for Public Health. (2020). Non-communicable diseases, healthcare demand, and health literacy—Key findings. *National Health and Morbidity Survey (NHMS) 2019. Ministry of Health Malaysia*. Retrieved from https://www.un-ilibrary.org/content/books/9789210601351c001

Intengan, H. D., & Schiffrin, E. L. (2001). Vascular remodeling in hypertension: roles of apoptosis, inflammation, and fibrosis. *Hypertension*, *38*(3 Pt 2), 581–587. https://doi.org/10.1161/hy09t1.096249

Işık, M., Levorse, D., Mobley, D. L., Rhodes, T., & Chodera, J. D. (2020). Octanol–water partition coefficient measurements for the SAMPL6 blind prediction challenge. *Journal of Computer-Aided Molecular Design*, *34*(4), 405–420. https://doi.org/10.1007/s10822-019-00271-3

Iturriaga-Vásquez, P., Miquel, R., Ivorra, M. D., D'Ocon, M. P., & Cassels, B. K. (2003). Simplified tetrandrine congeners as possible antihypertensive agents with a dual mechanism of action. *Journal of Natural Products*, *66*(7), 954–957. https://doi.org/10.1021/np030022+

IUPHAR database. (2015). Home | IUPHAR/BPS Guide to PHARMACOLOGY. Retrieved July 22, 2021, from http://www.guidetopharmacology.org/

Ivorra, M. D., Cercós, A., Zafra-Polo, M. C., Perez-Prieto, J., Sáez, J., Cortes, D., & D'Ocon, P. (1992). Selective chiral inhibition of Ca^{2+} entry promoted by bisbenzyltetrahydroisoquinolines in rat uterus. *European Journal of Pharmacology*, *219*(2), 303–309. https://doi.org/10.1016/0014-2999(92)90310-Z

Jabeen, Q., Bashir, S., Lyoussi, B., & Gilani, A. H. (2009). Coriander fruit exhibits gut modulatory, blood pressure lowering and diuretic activities. *Journal of Ethnopharmacology*, *122*(1), 123–130. https://doi.org/10.1016/j.jep.2008.12.016

Jackson, W. F. (2000). Ion channels and vascular tone. *Hypertension2*, *35*(2), 173–178.

Jackson, W. F. (2017). Potassium channels in regulation of vascular smooth muscle contraction and growth. In *Advances in Pharmacology* (1st ed., Vol. 78, pp. 89–144). https://doi.org/10.1016/bs.apha.2016.07.001

Jairaman, A., & Prakriya, M. (2013). Molecular pharmacology of store-operated CRAC channels. *Channels*, *7*(5), 402–414. https://doi.org/10.4161/chan.25292

Jakobsen, H., Bojer, M. S., Marinus, M. G., Xu, T., Struve, C., Krogfelt, K. A., & Løbner-Olesen, A. (2013). The alkaloid compound Harmane increases the lifespan of *Caenorhabditis elegans* during bacterial infection, by modulating the nematode's innate immune response. *PLoS ONE*, *8*(3), e60519. https://doi.org/10.1371/journal.pone.0060519

Jalan, M. (2021). What is a Hemocytometer: Definition, Calculation, Counting, & Structure. Retrieved July 28, 2021, from scienceabc.com website: https://www.scienceabc.com/pure-sciences/what-is-a-hemocytometer-calculation-counting-how-to-use.html

Jeon, B. H., Yoo, Y. M., Jung, E. M., & Jeung, E. B. (2020). Dexamethasone treatment

increases the intracellular calcium level through TRPV6 in A549 cells. *International Journal of Molecular Sciences*, *21*(3), 1–15. https://doi.org/10.3390/ijms21031050

Jespersen, B., Tykocki, N. R., Watts, S. W., & Cobbett, P. J. (2015). Measurement of smooth muscle function in the isolated tissue bath-applications to pharmacology research. *Journal of Visualized Experiments*, (95), 1–9. https://doi.org/10.3791/52324

Jia, X. Y., Wu, Y. M., Li, J. Y., Lei, C., & Hou, A. J. (2020). Alkaloid constituents of *Ficus hispida* and their antiinflammatory activity. *Natural Products and Bioprospecting*, *10*(1), 45–49. https://doi.org/10.1007/s13659-020-00233-5

Jiang, H., Xia, Q., Wang, X., Song, J., & Bruce, I. C. (2005). Luteolin induces vasorelaxion in rat thoracic aorta via calcium and potassium channels. *Pharmazie*, *60*(6), 444–447.

Ju, Y. K., Lee, B. H., Trajanovska, S., Hao, G., Allen, D. G., Lei, M., & Cannell, M. B. (2015). The involvement of TRPC3 channels in sinoatrial arrhythmias. *Frontiers in Physiology*, *6*(MAR), 1–12. https://doi.org/10.3389/fphys.2015.00086

Judy, W. V., & Farrell, S. K. (1979). Arterial baroreceptor reflex control of sympathetic nerve activity in the spontaneously hypertensive rat. *Hypertension*, *1*(6), 605–614. https://doi.org/10.1161/01.HYP.1.6.605

Jung, S., Strotmann, R., Schultz, G., & Plant, T. D. (2002). TRCP6 is a candidate channel involved in receptor stimulated cation currents in A7r5 smooth muscle cells. *American Journal of Physiology - Cell Physiology*, *282*(2 51-2), C347–C359. https://doi.org/10.1152/ajpcell.00283.2001

Just, S., Chenard, B. L., Ceci, A., Strassmaier, T., Chong, J. A., Blair, N. T., Gallaschun, R. J., del Camino, D., Cantin, S., D'Amours, M., Eickmeier, C., Fanger, C. M., Hecker, C., Hessler, D. P., Hengerer, B., Kroker, K. S., Malekiani, S., … Moran, M. M. (2018). Treatment with HC-070, a potent inhibitor of TRPC4 and TRPC5, leads to anxiolytic and antidepressant effects in mice. *PLoS ONE*, *13*(1), e0191225. https://doi.org/10.1371/journal.pone.0191225

Kamouchi, M., Philipp, S., Flockerzi, V., Wissenbach, U., Mamin, A., Raeymaekers, L., Eggermont, J., Droogmans, G., & Nilius, B. (1999). Properties of heterologously expressed hTRP3 channels in bovine pulmonary artery endothelial cells. *Journal of Physiology*, *518*(2), 345–358. https://doi.org/10.1111/j.1469-7793.1999.0345p.x

Kaneda, T., Sasaki, N., Urakawa, N., & Shimizu, K. (2016). Endothelium-dependent and -independent vasodilator effects of dimethyl sulfoxide in rat aorta. *Pharmacology*, *97*(3–4), 171–176. https://doi.org/10.1159/000443894

Kellogg, D. L., Zhao, J. L., Coey, U., & Green, J. V. (2005). Acetylcholine-induced vasodilation is mediated by nitric oxide and prostaglandins in human skin. *Journal of Applied Physiology*, *98*(2), 629–632. https://doi.org/10.1152/japplphysiol.00728.2004

Keys, J. R., Greene, E. A., Koch, W. J., & Eckhart, A. D. (2002). G_q-coupled receptor agonists mediate cardiac hypertrophy via the vasculature. *Hypertension*, *40*(5), 660–666. https://doi.org/10.1161/01.HYP.0000035397.73223.CE

Khalil, R. (2011). Modulators of the vascular endothelin receptor in blood pressure regulation and hypertension. *Current Molecular Pharmacology*, *4*(3), 176–186. https://doi.org/10.2174/1874467211104030176

Kho, C., Lee, A., Jeong, D., & Hajjar, R. J. (2010). Refilling intracellular calcium stores. *Drug Discovery Today: Disease Mechanisms*, *7*(2), e145–e150. https://doi.org/10.1016/j.ddmec.2010.08.004

Kiely, D. G., Elliot, C. A., Sabroe, I., & Condliffe, R. (2013). Pulmonary hypertension: diagnosis and management. *BMJ*, *346*(apr16 1), f2028–f2028. https://doi.org/10.1136/bmj.f2028

Kim, B., Jo, C., Choi, H. Y., & Lee, K. (2018). Vasorelaxant and hypotensive effects of Cheonwangbosimdan in SD and SHR rats. *Evidence-Based Complementary and Alternative Medicine*, *2018*, 1–8. https://doi.org/10.1155/2018/6128604

Kiselyov, K., Kim, J. Y., Zeng, W., & Muallem, S. (2005). Protein-protein interaction and function TRPC channels. *Pflügers Archiv - European Journal of Physiology*, *451*(1), 116–124. https://doi.org/10.1007/s00424-005-1442-2

Kiselyov, K., Xu, X., Mozhayeva, G., Kuo, T., Pessah, I., Mignery, G., Zhu, X., Birnbaumer#, L., & Muallem, S. (1998). Functional interaction between $InsP_3$ receptors and store-operated Htrp3 channels. *Nature*, *396*(6710), 478–482. https://doi.org/10.1038/24890

Kiyonaka, S., Kato, K., Nishida, M., Mio, K., Numaga, T., Sawaguchi, Y., Yoshida, T., Wakamori, M., Mori, E., Numata, T., Ishii, M., Takemoto, H., Ojida, A., Watanabe, K., Uemura, A., Kurose, H., Morii, T., … Mori, Y. (2009). Selective and direct inhibition of TRPC3 channels underlies biological activities of a pyrazole compound. *Proceedings of the National Academy of Sciences of the United States of America*, *106*(13), 5400–5405. https://doi.org/10.1073/pnas.0808793106

Klein, S., Mentrup, B., Timmen, M., Sherwood, J., Lindemann, O., Fobker, M., Kronenberg, D., Pap, T., Raschke, M. J., & Stange, R. (2020). Modulation of transient receptor potential channels 3 and 6 regulates osteoclast function with impact on trabecular bone loss. *Calcified Tissue International*, *106*(6), 655–664. https://doi.org/10.1007/s00223-020-00673-8

Kobayashi, S., Kanaide, H., & Nakamura, M. (1985). K^+-depolarization induces a direct release of Ca^{2+} from intracellular storage sites in cultured vascular smooth muscle cells from rat aorta. *Biochemical and Biophysical Research Communications*, *129*(3), 877–884. https://doi.org/10.1016/0006-291X(85)91973-4

Kobayashi, S., Kanaide, H., & Nakamura, M. (1986). Complete overlap of caffeine- and K^+ depolarization-sensitive intracellular calcium storage site in cultured rat arterial smooth muscle cells. *Journal of Biological Chemistry*, *261*(33), 15709–15713. https://doi.org/10.1016/s0021-9258(18)66775-4

Kochukov, M. Y., Balasubramanian, A., Noel, R. C., & Marrelli, S. P. (2012). Role of TRPC1 and TRPC3 channels in contraction and relaxation of mouse thoracic aorta. *Journal of Vascular Research*, *50*(1), 11–20. https://doi.org/10.1159/000342461

Kong, Aziz, A. I., Kakarla, A. B., Kong, I., & Kong, W. (2019). Toxicity evaluation of

graphene and poly(Lactic-acid) using a nematode model. *Solid State Phenomena, 290 SSP*, 101–106. https://doi.org/10.4028/www.scientific.net/SSP.290.101

Kong, X., Qu, X., Li, B., Wang, Z., Chao, Y., Jiang, X., Wu, W., & Chen, S. L. (2017). Modulation of low shear stress-induced eNOS multi-site phosphorylation and nitric oxide production via protein kinase and ERK1/2 signaling. *Molecular Medicine Reports*, *15*(2), 908–914. https://doi.org/10.3892/mmr.2016.6060

Kramer, J. A., Sagartz, J. E., & Morris, D. L. (2007). The application of discovery toxicology and pathology towards the design of safer pharmaceutical lead candidates. *Nature Reviews Drug Discovery*, *6*(8), 636–649. https://doi.org/10.1038/nrd2378

Krishnan, P., Lee, F. K., Yap, V. A., Low, Y. Y., Kam, T. S., Yong, K. T., Ting, K. N., & Lim, K. H. (2020). Schwarzinicines A-G, 1,4-diarylbutanoid-phenethylamine conjugates from the leaves of *Ficus schwarzii*. *Journal of Natural Products*, *83*(1), 152–158. https://doi.org/10.1021/acs.jnatprod.9b01160

Kubo, M., Yatsuzuka, W., Matsushima, S., Harada, K., Inoue, Y., Miyamoto, H., Matsumoto, M., & Fukuyama, Y. (2016). Antimalarial phenanthroindolizine alkaloids from *Ficus septica*. *Chemical and Pharmaceutical Bulletin*, *64*(7), 957–960. https://doi.org/10.1248/cpb.c16-00181

Kullmann, F. A., Daugherty, S. L., de Groat, W. C., & Birder, L. A. (2014). Bladder smooth muscle strip contractility as a method to evaluate lower urinary tract pharmacology. *Journal of Visualized Experiments*, (90), 1–11. https://doi.org/10.3791/51807

Küng, C. F., Moreau, P., Takase, H., & Lüscher, T. F. (1995). L-NAME hypertension alters endothelial and smooth muscle function in rat aorta. *Hypertension*, *26*(5), 744–751. https://doi.org/10.1161/01.HYP.26.5.744

Kuo, I. Y., & Ehrlich, B. E. (2015). Signaling in muscle contraction. *Cold Spring Harbor Perspectives in Biology*, *7*(2), 1–14. https://doi.org/10.1101/cshperspect.a006023

Kuo, I. Y., Wölfle, S. E., & Hill, C. E. (2011). T-type calcium channels and vascular function: The new kid on the block? *Journal of Physiology*, *589*(4), 783–795. https://doi.org/10.1113/jphysiol.2010.199497

Kuwahara, K., Wang, Y., McAnally, J., Richardson, J. A., Bassel-Duby, R., Hill, J. A., & Olson, E. N. (2006). TRPC6 fulfills a calcineurin signaling circuit during pathologic cardiac remodeling. *Journal of Clinical Investigation*, *116*(12), 3114–3126. https://doi.org/10.1172/JCI27702

Kwok, T. C. Y., Ricker, N., Fraser, R., Chan, A. W., Burns, A., Stanley, E. F., McCourt, P., Cutler, S. R., & Roy, P. J. (2006). A small-molecule screen in *C. elegans* yields a new calcium channel antagonist. *Nature*, *441*(7089), 91–95. https://doi.org/10.1038/nature04657

Lainé, V., Frøkjær-Jensen, C., Couchoux, H., & Jospin, M. (2011). The α1 subunit EGL-19, the α2/δ subunit UNC-36, and the β subunit CCB-1 underlie voltage-dependent calcium currents in *Caenorhabditis elegans* striated muscle. *Journal of Biological Chemistry*, *286*(42), 36180–36187. https://doi.org/10.1074/jbc.M111.256149

Lansky, E. P., Paavilainen, H. M., Pawlus, A. D., & Newman, R. A. (2008). *Ficus* spp. (fig): Ethnobotany and potential as anticancer and anti-inflammatory agents. *Journal of Ethnopharmacology*, *119*(2), 195–213. https://doi.org/10.1016/j.jep.2008.06.025

Latayada, F. S., Uy, M. M., Akihara, Y., Ohta, E., Nehira, T., Ômura, H., & Ohta, S. (2017). Ficusnotins A–F: Rare diarylbutanoids from the leaves of *Ficus nota*. *Phytochemistry*, *141*, 98–104. https://doi.org/10.1016/j.phytochem.2017.05.016

Lau, O. C., Shen, B., Wong, C. O., Tjong, Y. W., Lo, C. Y., Wang, H. C., Huang, Y., Yung, W.-H., Chen, Y.-C., Fung, M.-L., Rudd, J. A., & Yao, X. (2016). TRPC5 channels participate in pressure-sensing in aortic baroreceptors. *Nature Communications*, *7*(1), 11947. https://doi.org/10.1038/ncomms11947

Lawson, A. D. G., Maccoss, M., & Heer, J. P. (2018). Importance of rigidity in designing small molecule drugs to tackle protein-protein interactions (PPIs) through stabilization of desired conformers. *Journal of Medicinal Chemistry*, *61*(10), 4383–4389. https://doi.org/10.1021/acs.jmedchem.7b01120

Leblanc, N., Forrest, A. S., Ayon, R. J., Wiwchar, M., Angermann, J. E., Pritchard, H. A. T., Singer, C. A., Valencik, M. L., Britton, F., & Greenwood, I. A. (2015). Molecular and functional significance of Ca^{2+}-activated Cl^- channels in pulmonary arterial smooth muscle. *Pulmonary Circulation*, *5*(2), 244–268. https://doi.org/10.1086/680189

Ledoux, J., Werner, M. E., Brayden, J. E., & Nelson, M. T. (2006). Calcium-activated potassium channels and the regulation of vascular tone. *Physiology*, *21*(1), 69–79. https://doi.org/10.1152/physiol.00040.2005

Lee, C. H., Poburko, D., Sahota, P., Sandhu, J., Ruehlmann, D. O., & van Breemen, C. (2001). The mechanism of phenylephrine-mediated $[Ca^{2+}]_i$ oscillations underlying tonic contraction in the rabbit inferior vena cava. *Journal of Physiology*, *534*(3), 641–650. https://doi.org/10.1111/j.1469-7793.2001.t01-1-00641.x

Lee, F. K. (2020). *Syntheses and structure-activity relationship studies of schwarzinicine alkaloids as vasorelaxant agents*. University of Nottingham.

Lee, F. K., Krishnan, P., Muhamad, A., Low, Y.-Y., Kam, T.-S., Ting, K.-N., & Lim, K.-H. (2021). Concise synthesis of the vasorelaxant alkaloids schwarzinicines A and B. *Natural Product Research*, 1–7. https://doi.org/10.1080/14786419.2021.1903005

Lee, H. J., Noormohammadi, A., Koyuncu, S., Calculli, G., Simic, M. S., Herholz, M., Trifunovic, A., & Vilchez, D. (2019). Prostaglandin signals from adult germline stem cells delay somatic ageing of *Caenorhabditis elegans*. *Nature Metabolism*, *1*(8), 790–810. https://doi.org/10.1038/s42255-019-0097-9

Lee, K. P., Yuan, J. P., Hong, J. H., So, I., Worley, P. F., & Muallem, S. (2010). An endoplasmic reticulum/plasma membrane junction: STIM1/Orai1/TRPCs. *FEBS Letters*, *584*(10), 2022–2027. https://doi.org/10.1016/j.febslet.2009.11.078

Lee, M. K., Lim, K. H., Millns, P., Mohankumar, S. K., Ng, S. T., Tan, C. S., Then, S. M., Mbaki, Y., & Ting, K. N. (2018). Bronchodilator effects of Lignosus rhinocerotis extract on rat isolated airways is linked to the blockage of calcium entry. *Phytomedicine*, *42*(March), 172–179.

https://doi.org/10.1016/j.phymed.2018.03.025

Lee, R. (1985). Vascular changes at the prehypertensive phase in the mesenteric arteries from spontaneously hypertensive rats. *Blood Vessels*, *22*(3), 105–126. https://doi.org/10.1159/000158589

Lee, S. Y., & Kang, K. (2017). Measuring the effect of chemicals on the growth and reproduction of *Caenorhabditis elegans*. *Journal of Visualized Experiments*, *2017*(128), 56437. https://doi.org/10.3791/56437

Leiser, S. F., Jafari, G., Primitivo, M., Sutphin, G. L., Dong, J., Leonard, A., Fletcher, M., & Kaeberlein, M. (2016). Age-associated vulval integrity is an important marker of nematode healthspan. *Age*, *38*(5–6), 419–431. https://doi.org/10.1007/s11357-016-9936-8

Leloup, A. J. A., Van Hove, C. E., De Moudt, S., De Meyer, G. R. Y., De Keulenaer, G. W., & Fransen, P. (2019). Vascular smooth muscle cell contraction and relaxation in the isolated aorta: a critical regulator of large artery compliance. *Physiological Reports*, *7*(4), e13934. https://doi.org/10.14814/phy2.13934

Lemos, V. S., Poburko, D., Liao, C.-H., Cole, W. C., & Breemen, C. van. (2007). Na^+ entry via TRPC6 causes Ca^{2+} entry via NCX reversal in ATP stimulated smooth muscle cells. *Biochemical and Biophysical Research Communications*, *352*(1), 130–134. https://doi.org/10.1016/j.bbrc.2006.10.160

Leuner, K., Kazanski, V., Muller, M., Essin, K., Henke, B., Gollasch, M., Harteneck, C., & Müller, W. E. (2007). Hyperforin—a key constituent of St. John's wort specifically activates TRPC6 channels. *The FASEB Journal*, *21*(14), 4101–4111. https://doi.org/10.1096/fj.07-8110com

Leung, C. K., Wang, Y., Malany, S., Deonarine, A., Nguyen, K., Vasile, S., & Choe, K. P. (2013). An ultra high-throughput, whole-animal screen for small molecule modulators of a specific genetic pathway in *Caenorhabditis elegans*. *PLoS ONE*, *8*(4), e62166. https://doi.org/10.1371/journal.pone.0062166

Leung, F. P., Yung, L. M., Yao, X., Laher, I., & Huang, Y. (2008). Store-operated calcium entry in vascular smooth muscle. *British Journal of Pharmacology*, *153*(5), 846–857. https://doi.org/10.1038/sj.bjp.0707455

Leung, M. C. K., Williams, P. L., Benedetto, A., Au, C., Helmcke, K. J., Aschner, M., & Meyer, J. N. (2008). *Caenorhabditis elegans*: An emerging model in biomedical and environmental toxicology. *Toxicological Sciences*, *106*(1), 5–28. https://doi.org/10.1093/toxsci/kfn121

Li, Z. G. (2019). Measurement of signaling molecules calcium ion, reactive sulfur species, reactive carbonyl species, reactive nitrogen species, and reactive oxygen species in plants. In *Plant Signaling Molecules: Role and Regulation under Stressful Environments*. https://doi.org/10.1016/B978-0-12-816451-8.00005-8

Liao, Y., Erxleben, C., Yildirim, E., Abramowitz, J., Armstrong, D. L., & Birnbaumer, L. (2007). Orai proteins interact with TRPC channels and confer responsiveness to store depletion. *Proceedings of the National Academy of Sciences*, *104*(11), 4682–4687. https://doi.org/10.1073/pnas.0611692104

Lichtenegger, M., Tiapko, O., Svobodova, B., Stockner, T., Glasnov, T. N.,

Schreibmayer, W., Platzer, D., de la Cruz, G. G., Krenn, S., Schober, R., Shrestha, N., Schindl, R., Romanin, C., & Groschner, K. (2018). An optically controlled probe identifies lipid-gating fenestrations within the TRPC3 channel. *Nature Chemical Biology*, *14*(4), 396–404. https://doi.org/10.1038/s41589-018-0015-6

Lievremont, J. P., Bird, G. S., & Putney, J. W. (2005). Mechanism of inhibition of TRPC cation channels by 2- aminoethoxydiphenylborane. *Molecular Pharmacology*, *68*(3), 758–762. https://doi.org/10.1124/mol.105.012856

Lima, L., & Barreiro, E. (2012). Bioisosterism: A useful strategy for molecular modification and drug design. *Current Medicinal Chemistry*, *12*(1), 23–49. https://doi.org/10.2174/0929867053363540

Lin, X.-H., Hong, H.-S., Zou, G.-R., & Chen, L.-L. (2015). Upregulation of TRPC1/6 may be involved in arterial remodeling in rat. *Journal of Surgical Research*, *195*(1), 334–343. https://doi.org/10.1016/j.jss.2014.12.047

Linde, C. I., Karashima, E., Raina, H., Zulian, A., Wier, W. G., Hamlyn, J. M., Ferrari, P., Blaustein, M. P., & Golovina, V. A. (2012). Increased arterial smooth muscle Ca^{2+}-signaling, vasoconstriction, and myogenic reactivity in milan hypertensive rats. *American Journal of Physiology - Heart and Circulatory Physiology*, *302*(3). https://doi.org/10.1152/ajpheart.00950.2011

Lindsey, S. H., & Songu-Mize, E. (2010). Stretch-induced TRPC4 downregulation is accompanied by reduced capacitative Ca^{2+} entry in WKY but not SHR mesenteric smooth muscle cells. *Clinical and Experimental Hypertension*, *32*(5), 288–292. https://doi.org/10.3109/10641960903443525

Lintschinger, B., Balzer-Geldsetzer, M., Baskaran, T., Graier, W. F., Romanin, C., Zhu, M. X., & Groschner, K. (2000). Coassembly of Trp1 and Trp3 proteins generates diacylglycerol- and Ca^{2+}-sensitive cation channels. *Journal of Biological Chemistry*, *275*(36), 27799–27805. https://doi.org/10.1074/jbc.M002705200

Lipinski, C. A., Lombardo, F., Dominy, B. W., & Feeney, P. J. (1997, January 15). Experimental and computational approaches to estimate solubility and permeability in drug discovery and development settings. *Advanced Drug Delivery Reviews*, Vol. 23, pp. 3–25. https://doi.org/10.1016/S0169-409X(96)00423-1

Lipinski, C. A., Lombardo, F., Dominy, B. W., & Feeney, P. J. (2012). Experimental and computational approaches to estimate solubility and permeability in drug discovery and development settings. *Advanced Drug Delivery Reviews*, *64*(SUPPL.), 4–17. https://doi.org/10.1016/j.addr.2012.09.019

Liu, Bandyopadhyay, B. C., Singh, B. B., Groschner, K., & Ambudkar, I. S. (2005). Molecular analysis of a store-operated and 2-acetyl-*sn*-glycerol-sensitive non-selective cation channel: Heteromeric assembly of TRPC1-TRPC3. *Journal of Biological Chemistry*, *280*(22), 21600–21606. https://doi.org/10.1074/jbc.C400492200

Liu, D., Scholze, A., Zhu, Z., Kreutz, R., Wehland-von-Trebra, M., Zidek, W., & Tepel, M. (2005). Increased transient receptor potential channel TRPC3 expression in spontaneously hypertensive rats. *American Journal of Hypertension*, *18*(11), 1503–1507. https://doi.org/10.1016/j.amjhyper.2005.05.033

Liu, D., Scholze, A., Zhu, Z., Krueger, K., Thilo, F., Burkert, A., Streffer, K., Holz, S., Harteneck, C., Zidek, W., & Tepel, M. (2006). Transient receptor potential channels in essential hypertension. *Journal of Hypertension*, *24*(6), 1105–1114. https://doi.org/10.1097/01.hjh.0000226201.73065.14

Liu, D., Yang, D., He, H., Chen, X., Cao, T., Feng, X., Ma, L., Luo, Z., Wang, L., Yan, Z., Zhu, Z., & Tepel, M. (2009). Increased transient receptor potential canonical type 3 channels in vasculature from hypertensive rats. *Hypertension*, *53*(1), 70–76. https://doi.org/10.1161/HYPERTENSIONAHA.108.116947

Lobay, D. (2015). *Rauwolfia* in the treatment of hypertension. *Integrative Medicine*, *14*(3), 40–46. Retrieved from https://www.ncbi.nlm.nih.gov/pmc/articles/PMC4566472/

Lobo, M. D., De Belder, M. A., Cleveland, T., Collier, D., Dasgupta, I., Deanfield, J., Kapil, V., Knight, C., Matson, M., Moss, J., Paton, J. F. R., Poulter, N., Simpson, I., Williams, B., & Caulfield, M. J. (2015). Joint UK societies' 2014 consensus statement on renal denervation for resistant hypertension. *Heart*, *101*(1), 10–16. https://doi.org/10.1136/heartjnl-2014-307029

Lobo, M. D., Sobotka, P. A., & Pathak, A. (2017). Interventional procedures and future drug therapy for hypertension. *European Heart Journal*, *38*(15), 1101–1111. https://doi.org/10.1093/eurheartj/ehw303

Lockwich, T., Singh, B. B., Liu, X., & Ambudkar, I. S. (2001). Stabilization of cortical actin induces internalization of transient receptor potential 3 (Trp3)-associated caveolar Ca^{2+} signaling complex and loss of Ca^{2+} influx without disruption of Trp3-inositol trisphosphate receptor associatio. *Journal of Biological Chemistry*, *276*(45), 42401–42408. https://doi.org/10.1074/jbc.M106956200

Löf, C., Blom, T., & Törnquist, K. (2008). Overexpression of TRPC3 reduces the content of intracellular calcium stores in HEK-293 cells. *Journal of Cellular Physiology*, *216*(1), 245–252. https://doi.org/10.1002/jcp.21396

Loong, B. J. (2016). *Development of a functional bioassay to study the mechanism of action of a novel phenylethylamine alkaloid, schwarzinicine A*. University of Nottingham.

Loong, B. J., Tan, J. H., Lim, K. H., Mbaki, Y., & Ting, K. N. (2015). Contractile function of smooth muscle retained after overnight storage. *Naunyn-Schmiedeberg's Archives of Pharmacology*, *388*(10), 1061–1067. https://doi.org/10.1007/s00210-015-1140-3

Lopez, J. J., Jardin, I., Albarrán, L., Sanchez-Collado, J., Cantonero, C., Salido, G. M., Smani, T., & Rosado, J. A. (2020). Molecular basis and regulation of store-operated calcium entry. In *Advances in Experimental Medicine and Biology* (Vol. 1131, pp. 445–469). https://doi.org/10.1007/978-3-030-12457-1_17

Lopez, J. J., Jardin, I., Sanchez-Collado, J., Salido, G. M., Smani, T., & Rosado, J. A. (2020). TRPC channels in the SOCE scenario. *Cells*, *9*(1), 126. https://doi.org/10.3390/cells9010126

Lopez, J. R., Uryash, A., Faury, G., Estève, E., & Adams, J. A. (2020). Contribution of TRPC channels to intracellular Ca^{2+} dyshomeostasis in smooth muscle from mdx mice. *Frontiers in Physiology*, *11*(February), 1–11.

https://doi.org/10.3389/fphys.2020.00126

Louis, W. J., & Howes, L. G. (1990). Genealogy of the spontaneously hypertensive rat and Wistar-Kyoto rat strains: implications for studies of inherited hypertension. *Journal of Cardiovascular Pharmacology*, *16 Suppl 7*, S1-5. https://doi.org/10.1097/00005344-199006167-00002

Low, A. M., Kwan, C. Y., & Daniel, E. E. (1993). Functional alterations in the aorta of the spontaneously hypertensive rat: Pharmacological assessment with cyclopiazonic acid. *Pharmacology*, *47*(1), 50–60. https://doi.org/10.1159/000139078

Lucanic, M., Garrett, T., Gill, M. S., & Lithgow, G. J. (2018). A simple method for high throughput chemical screening in *Caenorhabditis elegans*. *Journal of Visualized Experiments*, *2018*(133), 1–8. https://doi.org/10.3791/56892

Ludmer, P. L., Selwyn, A. P., Shook, T. L., Wayne, R. R., Mudge, G. H., Alexander, R. W., & Ganz, P. (1986). Paradoxical vasoconstriction induced by acetylcholine in atherosclerotic coronary arteries. *New England Journal of Medicine*, *315*(17), 1046–1051. https://doi.org/10.1056/nejm198610233151702

Lumsden, N. G., Khambata, R. S., & Hobbs, A. J. (2010). C-type natriuretic peptide (CNP): Cardiovascular roles and potential as a therapeutic target. *Current Pharmaceutical Design*, *16*(37), 4080–4088. https://doi.org/10.2174/138161210794519237

Lurie, K. G., Tsujimoto, G., & Hoffman, B. B. (1985). Desensitization of alpha-1 adrenergic receptor-mediated vascular smooth muscle contraction. *Journal of Pharmacology and Experimental Therapeutics*, *234*(1), 147–152. Retrieved from https://jpet.aspetjournals.org/content/234/1/147

Lüscher, T F, & Vanhoutte, P. M. (1986). Endothelium-dependent contractions to acetylcholine in the aorta of the spontaneously hypertensive rat. *Hypertension*, *8*(4), 344–348. https://doi.org/10.1161/01.HYP.8.4.344

Lüscher, Thomas F., & Cosentino, F. (1998). The classification of calcium antagonists and their selection in the treatment of hypertension. A reappraisal. *Drugs*, *55*(4), 509–517. https://doi.org/10.2165/00003495-199855040-00003

Ma, C.-Y., Yang, S.-Y., Zhang, H., Xiang, M.-L., Huang, Q., & Wei, Y.-Q. (2008). Prediction models of human plasma protein binding rate and oral bioavailability derived by using GA–CG–SVM method. *Journal of Pharmaceutical and Biomedical Analysis*, *47*(4–5), 677–682. https://doi.org/10.1016/j.jpba.2008.03.023

Ma, M. M., Gao, M., Guo, K. M., Wang, M., Li, X. Y., Zeng, X. L., Sun, L., Lv, X. F., Du, Y. H., Wang, G. L., Zhou, J. G., & Guan, Y. Y. (2017). TMEM16A contributes to endothelial dysfunction by facilitating Nox2 NADPH oxidase-derived reactive oxygen species generation in hypertension. *Hypertension*, *69*(5), 892–901. https://doi.org/10.1161/HYPERTENSIONAHA.116.08874

Maier, M. E. (2015). Design and synthesis of analogues of natural products. *Organic & Biomolecular Chemistry*, *13*, 5302–5343. https://doi.org/10.1039/c5ob00169b

Maier, T., Follmann, M., Hessler, G., Kleemann, H. W., Hachtel, S., Fuchs, B.,

Weissmann, N., Linz, W., Schmidt, T., Löhn, M., Schroeter, K., Wang, L., Rütten, H., & Strübing, C. (2015). Discovery and pharmacological characterization of a novel potent inhibitor of diacylglycerol-sensitive TRPC cation channels. *British Journal of Pharmacology*, *172*(14), 3650–3660. https://doi.org/10.1111/bph.13151

Majdoub, Y. O. El, Diouri, M., Arena, P., Arigò, A., Cacciola, F., Rigano, F., Dugo, P., & Mondello, L. (2019). Evaluation of the availability of delphinidin and cyanidin-3-O-sambubioside from *Hibiscus sabdariffa* and 6-gingerol from *Zingiber officinale* in colon using liquid chromatography and mass spectrometry detection. *European Food Research and Technology*, *245*(11), 2425–2433. https://doi.org/10.1007/s00217-019-03358-1

Mak, D.-O. D. (2013). A mechanism for different receptors coupled to the same G protein to generate different responses mediated by different second messengers. *Journal of General Physiology*, *141*(5), 513–516. https://doi.org/10.1085/jgp.201311006

Malaysian Society of Hypertension. (2018). Clinical practice guidelines on management of hypertension. In *Ministry of Health Malaysia* (5th ed.). Retrieved from www.msh.org.my

Malczyk, M., Erb, A., Veith, C., Ghofrani, H. A., Schermuly, R. T., Gudermann, T., Dietrich, A., Weissmann, N., & Sydykov, A. (2017). The role of transient receptor potential channel 6 channels in the pulmonary vasculature. *Frontiers in Immunology*, *8*(JUN), 1–11. https://doi.org/10.3389/fimmu.2017.00707

Mancia, G., Ludbrook, J., Ferrari, A., Gregorini, L., & Zanchetti, A. (1978). Baroreceptor reflexes in human hypertension. *Circulation Research*, *43*(2), 170–177. https://doi.org/10.1161/01.RES.43.2.170

Mancia, Giuseppe, & Grassi, G. (2014). The autonomic nervous system and hypertension. *Circulation Research*, *114*(11), 1804–1814. https://doi.org/10.1161/CIRCRESAHA.114.302524

Mann, S. J. (2011). Drug therapy for resistant hypertension: Simplifying the approach. *Journal of Clinical Hypertension*, *13*(2), 120–130. https://doi.org/10.1111/j.1751-7176.2010.00387.x

Mansor, L. S., Gonzalez, E. R., Cole, M. A., Tyler, D. J., Beeson, J. H., Clarke, K., Carr, C. A., & Heather, L. C. (2013). Cardiac metabolism in a new rat model of type 2 diabetes using high-fat diet with low dose streptozotocin. *Cardiovascular Diabetology*, *12*(1), 136. https://doi.org/10.1186/1475-2840-12-136

Marti, C. N., Gheorghiade, M., Kalogeropoulos, A. P., Georgiopoulou, V. V., Quyyumi, A. A., & Butler, J. (2012, October 16). Endothelial dysfunction, arterial stiffness, and heart failure. *Journal of the American College of Cardiology*, Vol. 60, pp. 1455–1469. https://doi.org/10.1016/j.jacc.2011.11.082

Martín-Bórnez, M., Galeano-Otero, I., Del Toro, R., & Smani, T. (2020). TRPC and TRPV channels' role in vascular remodeling and disease. *International Journal of Molecular Sciences*, *21*(17), 1–17. https://doi.org/10.3390/ijms21176125

Maruyama, Kanaji, T., Nakade, S., Kanno, T., & Katsuhiko, M. (1997). 2APB, 2-Aminoethoxydiphenyl borate , a membrane-penetrable modulator of Ins(1,4,5)P_3-

induced Ca^{2+} release. *Journal of Biochemistry*, *122*(3), 498–505.

Maruyama, Nakanishi, Y., Walsh, E. J., Wilson, D. P., Welsh, D. G., & Cole, W. C. (2006). Heteromultimeric TRPC6-TRPC7 channels contribute to arginine vasopressin-induced cation current of A7r5 vascular smooth muscle cells. *Circulation Research*, *98*(12), 1520–1527. https://doi.org/10.1161/01.RES.0000226495.34949.28

Matsukawa, T., Gotoh, E., Hasegawa, O., Shionoiri, H., Tochikubo, O., & Ishii, M. (1991). Reduced baroreflex changes in muscle sympathetic nerve activity during blood pressure elevation in essential hypertension. *Journal of Hypertension*, *9*(6), 537–542. https://doi.org/10.1097/00004872-199106000-00009

Matsuura, H. N., & Fett-Neto, A. G. (2015). Plant alkaloids: Main features, toxicity, and mechanisms of action. In *Plant Toxins* (pp. 1–15). https://doi.org/10.1007/978-94-007-6728-7_2-1

McColl, G., Killilea, D. W., Hubbard, A. E., Vantipalli, M. C., Melov, S., & Lithgow, G. J. (2008). Pharmacogenetic analysis of lithium-induced delayed aging in *Caenorhabditis elegans*. *Journal of Biological Chemistry*, *283*(1), 350–357. https://doi.org/10.1074/jbc.M705028200

McGeown, J. G. (2004). Interactions between inositol 1,4,5-trisphosphate receptors and ryanodine receptors in smooth muscle: one store or two? *Cell Calcium*, *35*(6), 613–619. https://doi.org/10.1016/j.ceca.2004.01.016

McGeown, J. G. (2010). Seeing is believing! Imaging Ca^{2+}-signalling events in living cells. *Experimental Physiology*, *95*(11), 1049–1060. https://doi.org/10.1113/expphysiol.2010.052456

McKenzie, C., MacDonald, A., & Shaw, A. M. (2009). Mechanisms of U46619-induced contraction of rat pulmonary arteries in the presence and absence of the endothelium. *British Journal of Pharmacology*, *157*(4), 581–596. https://doi.org/10.1111/j.1476-5381.2008.00084.x

McKune, C. M., & Watts, S. W. (2001). Characterization of the serotonin receptor mediating contraction in the mouse thoracic aorta and signal pathway coupling. *The Journal of Pharmacology and Experimental Therapeutics*, *297*(1), 88–95. Retrieved from http://www.ncbi.nlm.nih.gov/pubmed/11259531

Meanwell, N. A. (2011). Improving drug candidates by design: A focus on physicochemical properties as a means of improving compound disposition and safety. *Chemical Research in Toxicology*, *24*(9), 1420–1456. https://doi.org/10.1021/tx200211v

Medarov, B. I., & Judson, M. A. (2015). The role of calcium channel blockers for the treatment of pulmonary arterial hypertension: How much do we actually know and how could they be positioned today? *Respiratory Medicine*, *109*(5), 557–564. https://doi.org/10.1016/j.rmed.2015.01.004

Merritt, J. E., Armstrong, W. P., Benham, C. D., Hallam, T. J., Jacob, R., Jaxa-Chamiec, A., Leigh, B. K., McCarthy, S. A., Moores, K. E., & Rink, T. J. (1990). SK&F 96365, a novel inhibitor of receptor-mediated calcium entry. *Biochemical Journal*, *271*(2), 515–522. https://doi.org/10.1042/bj2710515

Michel, M. C., & Vrydag, W. (2006). α_1-, α_1- and β-adrenoceptors in the urinary bladder, urethra and prostate. *British Journal of Pharmacology*, *147*(S2), S88–S119. https://doi.org/10.1038/sj.bjp.0706619

Miller, A. J., & Arnold, A. C. (2019). The renin–angiotensin system in cardiovascular autonomic control: recent developments and clinical implications. *Clinical Autonomic Research*, *29*(2), 231–243. https://doi.org/10.1007/s10286-018-0572-5

Miller, M., Wu, M., Xu, J., Weaver, D., Li, M., & Zhu, M. X. (2016). High-throughput screening of TRPC channel ligands using cell-based assays. In *TRP Channels* (pp. 1–20). https://doi.org/10.1201/b10896-6

Minard, A., Bauer, C. C., Chuntharpursat-Bon, E., Pickles, I. B., Wright, D. J., Ludlow, M. J., Burnham, M. P., Warriner, S. L., Beech, D. J., Muraki, K., & Bon, R. S. (2019). Potent, selective, and subunit-dependent activation of TRPC5 channels by a xanthine derivative. *British Journal of Pharmacology*, *176*(20), 3924–3938. https://doi.org/10.1111/bph.14791

Miner, J., & Hoffhines, A. (2007). The discovery of aspirin's antithrombotic effects. *Texas Heart Institute Journal*, *34*(2), 179–186.

Ministry of Health. (2011). *Clinical practice guidelines: Management of pulmonary arterial hypertension (PAH)* (p. 118). p. 118.

Mita, M., Ito, K., Taira, K., Nakagawa, J., Walsh, M. P., & Shoji, M. (2010). Attenuation of store-operated Ca^{2+} entry and enhanced expression of TRPC channels in caudal artery smooth muscle from Type 2 diabetic Goto-Kakizaki rats. *Clinical and Experimental Pharmacology and Physiology*, *37*(7), 670–678. https://doi.org/10.1111/j.1440-1681.2010.05373.x

Mita, M., Kuramoto, T., Ito, K., Toguchi-Senrui, N., Hishinuma, S., Walsh, M. P., & Shoji, M. (2010). Impairment of α_1-adrenoceptor-mediated contractile activity in caudal arterial smooth muscle from Type 2 diabetic Goto-Kakizaki rats. *Clinical and Experimental Pharmacology and Physiology*, *37*(3), 350–357. https://doi.org/10.1111/j.1440-1681.2009.05308.x

Mohamed. Shabi, M., Rameshkannan, M. P., Haja Nazeer, A., & Avupati, V. R. (2018). *In-vitro* and *in-vivo* contractile effect of *Desmodium Gangeticum* L extract on isolated rat ileum and electrocardiogram recording. *Research Journal of Pharmaceutical Biological and Chemical Sciences*, *9*(1), 189–198.

Mojiminiyi, F. B. O., Dikko, M., Muhammad, B. Y., Ojobor, P. D., Ajagbonna, O. P., Okolo, R. U., Igbokwe, U. V., Mojiminiyi, U. E., Fagbemi, M. A., Bello, S. O., & Anga, T. J. (2007). Antihypertensive effect of an aqueous extract of the calyx of *Hibiscus sabdariffa*. *Fitoterapia*, *78*(4), 292–297. https://doi.org/10.1016/j.fitote.2007.02.011

Molinspiration Cheminformatics. (2002). Calculation of Molecular Properties and Bioactivity score © Molinspiration Cheminformatics. Retrieved July 22, 2021, from http://www.molinspiration.com/cgi-bin/properties

Montell, C., Birnbaumer, L., Flockerzi, V., Bindels, R. J., Bruford, E. A., Caterina, M. J., Clapham, D. E., Harteneck, C., Heller, S., Julius, D., Kojima, I., Mori, Y., Penner, R., Prawitt, D., Scharenberg, A. M., Schultz, G., Shimizu, N., & Zhu, M.

X. (2002). A unified nomenclature for the superfamily of TRP cation channels. *Molecular Cell*, *9*(2), 229–231. https://doi.org/10.1016/S1097-2765(02)00448-3

Montell, C., & Rubin, G. M. (1989). Molecular characterization of the *drosophila* trp locus: A putative integral membrane protein required for phototransduction. *Neuron*, *2*(4), 1313–1323. https://doi.org/10.1016/0896-6273(89)90069-X

Montinari, M. R., Minelli, S., & De Caterina, R. (2019). The first 3500 years of aspirin history from its roots – A concise summary. *Vascular Pharmacology*, *113*, 1–8. https://doi.org/10.1016/j.vph.2018.10.008

Moohammadaree, A., Changtam, C., Wicha, P., Suksamrarn, A., Tocharus, J., & Tocharus, C. (2015). Mechanisms of vasorelaxation induced by hexahydrocurcuminin isolated rat thoracic aorta. *Phytotherapy Research*, *29*(11), 1806–1813. https://doi.org/10.1002/ptr.5448

Morita, A., Ouchi, M., Terada, M., Kon, H., Kishimoto, S., Satoh, K., Otani, N., Hayashi, K., Fujita, T., Inoue, K., & Anzai, N. (2018). Reproducible insulin secretion from isolated rat pancreas preparations using an organ bath. *Experimental Animals*, *67*(1), 15–22. https://doi.org/10.1538/expanim.17-0059

Motoyama, K., Nagata, T., Kobayashi, J., Nakamura, A., Miyoshi, N., Kazui, M., Sakurai, K., & Sakakura, T. (2018). Discovery of a bicyclo[4.3.0]nonane derivative DS88790512 as a potent, selective, and orally bioavailable blocker of transient receptor potential canonical 6 (TRPC6). *Bioorganic & Medicinal Chemistry Letters*, *28*(12), 2222–2227. https://doi.org/10.1016/j.bmcl.2018.03.056

Motulsky, H., & Christopoulos, A. (2003). Fitting models to biological data using linear and nonlinear regression. In *Fitting Models to Biological Data Using Linear and Nonlinear Regression*. GraphPad Software, Inc.

Moy, T. I., Ball, A. R., Anklesaria, Z., Casadei, G., Lewis, K., & Ausubel, F. M. (2006). Identification of novel antimicrobials using a live-animal infection model. *Proceedings of the National Academy of Sciences of the United States of America*, *103*(27), 10414–10419. https://doi.org/10.1073/pnas.0604055103

Nabika, T., Nara, Y., Ikeda, K., Endo, J., & Yamori, Y. (1991). Genetic heterogeneity of the spontaneously hypertensive rat. *Hypertension*, *18*(1), 12–16. https://doi.org/10.1161/01.HYP.18.1.12

Nademi, S., Lu, C., & Dickhout, J. G. (2020). Enhanced myogenic constriction in the SHR preglomerular vessels is mediated by thromboxane A2 synthesis. *Frontiers in Physiology*, *11*, 853. https://doi.org/10.3389/fphys.2020.00853

Nakahata, N. (2008). Thromboxane A_2: Physiology/pathophysiology, cellular signal transduction and pharmacology. *Pharmacology and Therapeutics*, *118*(1), 18–35. https://doi.org/10.1016/j.pharmthera.2008.01.001

Naseem, R., Adam, A. M., Khan, F., Dossal, A., Khan, I., Khan, A., Paul, H., Jawed, H., Aslam, A., Syed, F. M., Niazi, M. A., Nadeem, S., Khan, A., Zia, A., & Arshad, M. H. (2017). Prevalence and characteristics of resistant hypertensive patients in an Asian population. *Indian Heart Journal*, *69*(4), 442–446. https://doi.org/10.1016/j.ihj.2017.01.012

Nass, R., & Hamza, I. (2007). The nematode *C. elegans* as an animal model to explore toxicology *in vivo*: Solid and axenic growth culture conditions and compound exposure parameters. *Current Protocols in Toxicology*, *31*(1), 1.9.1-1.9.18. https://doi.org/10.1002/0471140856.tx0109s31

Nath, P., & Yadav, A. (2015). Acute and sub-acute oral toxicity assessment of the methanolic extract from leaves of *Hibiscus rosa-sinensis* L. in mice. *Journal of Intercultural Ethnopharmacology*, *4*(1), 70. https://doi.org/10.5455/jice.20141028021746

Navedo, M. F., Amberg, G. C., Votaw, V. S., & Santana, L. F. (2005). Constitutively active L-type Ca^{2+} channels. *Proceedings of the National Academy of Sciences*, *102*(31), 11112–11117. https://doi.org/10.1073/pnas.0500360102

Nazer, M. A., & Van Breemen, C. (1998). Functional linkage of Na^{+} -Ca^{2+} exchange and sarcoplasmic reticulum Ca^{2+} release mediates Ca^{2+} cycling in vascular smooth muscle. *Cell Calcium*, *24*(4), 275–283. https://doi.org/10.1016/S0143-4160(98)90051-3

Nguyen, H. B., Lee, S. Y., Park, S. H., Lee, M. Y., Chang, I. H., & Myung, S. C. (2013). Relaxing effect of acetylcholine on phenylephrine-induced contraction of isolated rabbit prostate strips is mediated by neuronal nitric oxide synthase. *Korean Journal of Urology*, *54*(5), 333–338. https://doi.org/10.4111/kju.2013.54.5.333

NICE. (2007). *Final scope for the appraisal of drugs for the treatment of pulmonary arterial hypertension*. 1–5.

NICE. (2019). *Hypertension in adults: diagnosis and management (NG136)*. Retrieved from https://www.nice.org.uk/guidance/ng136/resources/hypertension-in-adults-diagnosis-and-management-pdf-66141722710213

NICE. (2020). *Type 2 diabetes in adults (NG28)*. Retrieved from https://pathways.nice.org.uk/pathways/type-2-diabetes-in-adults%0Ahttps://pathways.nice.org.uk/pathways/type-2-diabetes-in-adults#content=view-node%3Anodes-patient-education-and-lifestyle-advice%0Ahttps://pathways.nice.org.uk/pathways/type-2-diabetes-in-a

Nilius, B., & Flockerzi, V. (2014). Mammalian transient receptor potential (TRP) cation channels. In B. Nilius & V. Flockerzi (Eds.), *Handbook of experimental pharmacology*. https://doi.org/10.1007/978-3-642-54215-2

Nilius, B., Owsianik, G., Voets, T., & Peters, J. A. (2007). Transient receptor potential cation channels in disease. *Physiological Reviews*, Vol. 87, pp. 165–217. https://doi.org/10.1152/physrev.00021.2006

Nimmrich, V., & Gross, G. (2012). P/Q-type calcium channel modulators. *British Journal of Pharmacology*, *167*(4), 741–759. https://doi.org/10.1111/j.1476-5381.2012.02069.x

Nobe, K., & Paul, R. J. (2001). Distinct pathways of Ca^{2+} sensitization in porcine coronary artery: Effects of rho-related kinase and protein kinase C inhibition on force and intracellular Ca^{2+}. *Circulation Research*, *88*(12), 1283–1290. https://doi.org/10.1161/hh1201.092035

Noorani, M. M. Z., Noel, R. C., & Marrelli, S. P. (2011). Upregulated TRPC3 and

downregulated TRPC1 channel expression during hypertension is associated with increased vascular contractility in rat. *Frontiers in Physiology*, *JUL*(July), 1–9. https://doi.org/10.3389/fphys.2011.00042

O'Connell, T. D., Jensen, B. C., Baker, A. J., & Simpson, P. C. (2014). Cardiac alpha$_1$-adrenergic receptors: Novel aspects of expression, signaling mechanisms, physiologic function, and clinical importance. *Pharmacological Reviews*, *66*(1), 308–333. https://doi.org/10.1124/pr.112.007203

Odović, J. V., Trbojević, J. B., Trbojević-Stankovic, J. B., Nešić, D. M., & Jelić, R. M. (2017). Assessment of the relationship between the molecular properties of calcium channel blockers and plasma protein binding data. *Archives of Biological Sciences*, *69*(1), 175–179. https://doi.org/10.2298/ABS160609094O

Oelze, M., Knorr, M., Schuhmacher, S., Heeren, T., Otto, C., Schulz, E., Reifenberg, K., Wenzel, P., Münzel, T., & Daiber, A. (2011). Vascular dysfunction in streptozotocin-induced experimental diabetes strictly depends on insulin deficiency. *Journal of Vascular Research*, *48*(4), 275–284. https://doi.org/10.1159/000320627

Offermanns, S. (2006). Activation of platelet function through G protein-coupled receptors. *Circulation Research*, *99*(12), 1293–1304. https://doi.org/10.1161/01.RES.0000251742.71301.16

Ohya, Y., Tsuchihashi, T., Kagiyama, S., Abe, I., & Fujishima, M. (1998). Single L-type calcium channels in smooth muscle cells from resistance arteries of spontaneously hypertensive rats. *Hypertension*, *31*(5), 1125–1129. https://doi.org/10.1161/01.HYP.31.5.1125

Ok, S.-H., Bae, S. Il, Shim, H. S., & Sohn, J.-T. (2012). Dexmedetomidine-induced contraction of isolated rat aorta is dependent on extracellular calcium concentration. *Korean Journal of Anesthesiology*, *63*(3), 253. https://doi.org/10.4097/kjae.2012.63.3.253

Okada, T., Shimizu, S., Wakamori, M., Maeda, A., Kurosaki, T., Takada, N., Imoto, K., & Mori, Y. (1998). Molecular cloning and functional characterization of a novel receptor- activated TRP Ca^{2+} channel from mouse brain. *Journal of Biological Chemistry*, *273*(17), 10279–10287. https://doi.org/10.1074/jbc.273.17.10279

Okon, E. B., Szado, T., Laher, I., McManus, B., & van Breemen, C. (2003). Augmented contractile response of vascular smooth muscle in a diabetic mouse model. *Journal of Vascular Research*, *40*(6), 520–530. https://doi.org/10.1159/000075238

Ong, H. L., De Souza, L. B., & Ambudkar, I. S. (2016). Role of TRPC channels in store-operated calcium entry. In J. A. Rosado (Ed.), *Advances in Experimental Medicine and Biology* (pp. 87–109). https://doi.org/10.1007/978-3-319-26974-0_5

Oparil, S., Zaman, M. A., & Calhoun, D. A. (2003). Pathogenesis of hypertension. *Annals of Internal Medicine*, *139*(9), 761–776. https://doi.org/10.7326/0003-4819-139-9-200311040-00011

Oron-Herman, M., Kamari, Y., Grossman, E., Yeger, G., Peleg, E., Shabtay, Z., Shamiss, A., & Sharabi, Y. (2008). Metabolic syndrome: Comparison of the two

commonly used animal models. *American Journal of Hypertension*, *21*(9), 1018–1022. https://doi.org/10.1038/ajh.2008.218

Pande, J. (2011). Allosteric inhibitors of plasma membrane Ca^{2+} pumps: Invention and applications of caloxins. *World Journal of Biological Chemistry*, *2*(3), 39. https://doi.org/10.4331/wjbc.v2.i3.39

Pande, J., Mallhi, K. K., Sawh, A., Szewczyk, M. M., Simpson, F., & Grover, A. K. (2006). Aortic smooth muscle and endothelial plasma membrane Ca^{2+} pump isoforms are inhibited differently by the extracellular inhibitor caloxin 1b1. *American Journal of Physiology-Cell Physiology*, *290*(5), C1341–C1349. https://doi.org/10.1152/ajpcell.00573.2005

Pandey, K. N. (2008). Emerging roles of natriuretic peptides and their receptors in pathophysiology of hypertension and cardiovascular regulation. *Journal of the American Society of Hypertension*, *2*(4), 210–226. https://doi.org/10.1016/j.jash.2008.02.001

Pang, H., Guo, Z., Su, W., Xie, Z., Eto, M., & Gong, M. C. (2005). RhoA-Rho kinase pathway mediates thrombin- and U-46619-induced phosphorylation of a myosin phosphatase inhibitor, CPI-17, in vascular smooth muscle cells. *American Journal of Physiology-Cell Physiology*, *289*(2), C352–C360. https://doi.org/10.1152/ajpcell.00111.2005

Panthiya, L., Pantan, R., Tocharus, J., Nakaew, A., Suksamrarn, A., & Tocharus, C. (2019). Endothelium-dependent and endothelium-independent vasorelaxant effects of tiliacorinine 12′-*O*-acetate and mechanisms on isolated rat aorta. *Biomedicine and Pharmacotherapy*, *109*, 2090–2099. https://doi.org/10.1016/j.biopha.2018.11.062

Park, H.-E. H., Jung, Y., & Lee, S.-J. V. (2017). Survival assays using *Caenorhabditis elegans*. *Molecules and Cells*, *40*(2), 90–99. https://doi.org/10.14348/molcells.2017.0017

Park, S. H., Park, S. J., Kim, J. O., Shin, J. H., Kim, E. S., Jo, Y. K., Kim, J. S., Park, S. J., Jin, D. H., Hwang, J. J., Lee, S. J., Jeong, S. Y., Lee, C., Kim, I., & Cho, D. H. (2013). Down-regulation of survivin by nemadipine-A sensitizes cancer cells to TRAIL-induced apoptosis. *Biomolecules and Therapeutics*, *21*(1), 29–34. https://doi.org/10.4062/biomolther.2012.088

Pérez-Vizcaíno, F., Tamargo, J., Hof, R. P., & Ruegg, U. T. (1993). Vascular selectivity of seven prototype calcium antagonists: A study at the single cell level. *Journal of Cardiovascular Pharmacology*, *22*, 768–775.

Persell, S. D. (2011). Prevalence of resistant hypertension in the United States, 2003-2008. *Hypertension*, *57*(6), 1076–1080. https://doi.org/10.1161/HYPERTENSIONAHA.111.170308

Petit, J., Meurice, N., Kaiser, C., & Maggiora, G. (2012). Softening the rule of five - Where to draw the line? *Bioorganic and Medicinal Chemistry*, *20*(18), 5343–5351. https://doi.org/10.1016/j.bmc.2011.11.064

Petrie, J. R., Guzik, T. J., & Touyz, R. M. (2018). Diabetes, hypertension, and cardiovascular disease: Clinical insights and vascular mechanisms. *Canadian Journal of Cardiology*, *34*(5), 575–584.

https://doi.org/10.1016/j.cjca.2017.12.005

Philip Lansky, E., & Maaria Paavilainen, H. (2011). *Figs the genus* Ficus (R. Hardman, Ed.). New York, NY: Taylor and Francis Group, LLC.

Pignier, C., & Potreau, D. (2000). Characterization of nifedipine-resistant calcium current in neonatal rat ventricular cardiomyocytes. *American Journal of Physiology-Heart and Circulatory Physiology*, *279*(5), H2259–H2268. https://doi.org/10.1152/ajpheart.2000.279.5.H2259

Pimenta, E., & Calhoun, D. A. (2016). Drug development for hypertension: Do we need another antihypertensive agent for resistant hypertension? *Current Hypertension Reports*, *18*(4), 25. https://doi.org/10.1007/s11906-016-0634-9

Poburko, D., Lhote, P., Szado, T., Behra, T., Rahimian, R., McManus, B., Van Breemen, C., & Ruegg, U. T. (2004). Basal calcium entry in vascular smooth muscle. *European Journal of Pharmacology*, *505*(1–3), 19–29. https://doi.org/10.1016/j.ejphar.2004.09.060

Polêto, M. D., Rusu, V. H., Grisci, B. I., Dorn, M., Lins, R. D., & Verli, H. (2018). Aromatic rings commonly used in medicinal chemistry: Force fields comparison and interactions with water toward the design of new chemical entities. *Frontiers in Pharmacology*, *9*(APR), 1–20. https://doi.org/10.3389/fphar.2018.00395

Ponce, A., Castillo, A., Hinojosa, L., Martinez-Rendon, J., & Cereijido, M. (2018). The expression of endogenous voltage-gated potassium channels in HEK293 cells is affected by culture conditions. *Physiological Reports*, *6*(8), e13663. https://doi.org/10.14814/phy2.13663

Poulsen, M., Schøler, L., Nielsen, A., Skov, M. N., Kolmos, H. J., Kallipolitis, B. H., Olsen, A., & Klitgaard, J. K. (2014). Combination therapy with thioridazine and dicloxacillin combats meticillin-resistant *Staphylococcus aureus* infection in *Caenorhabditis elegans*. *Journal of Medical Microbiology*, *63*(PART 9), 1174–1180. https://doi.org/10.1099/jmm.0.071837-0

Prakriya, M., Feske, S., Gwack, Y., Srikanth, S., Rao, A., & Hogan, P. G. (2006). Orai1 is an essential pore subunit of the CRAC channel. *Nature*, *443*(7108), 230–233. https://doi.org/10.1038/nature05122

Prakriya, M., & Lewis, R. S. (2015). Store-operated calcium channels. *Physiological Reviews*, *95*(4), 1383–1436. https://doi.org/10.1152/physrev.00020.2014

Prasad, K. (2000). Structure and function of various vascular beds. In *Textbook of Angiology* (pp. 3–10). https://doi.org/10.1007/978-1-4612-1190-7_1

Pratt, P. F., Bonnet, S., Ludwig, L. M., Bonnet, P., & Rusch, N. J. (2002). Upregulation of L-type Ca^{2+} channels in mesenteric and skeletal arteries of SHR. *Hypertension*, *40*(2), 214–219. https://doi.org/10.1161/01.HYP.0000025877.23309.36

Preston, I. R. (2008). PDE5 inhibitors and the cGMP pathway in pulmonary arterial hypertension. In N. S. Hill & H. W. Farber (Eds.), *Pulmonary Hypertension* (pp. 305–319). https://doi.org/10.1007/978-1-60327-075-5_14

Proskocil, B. J., & Fryer, A. D. (2005). β_2-agonist and anticholinergic drugs in the treatment of lung disease. *Proceedings of the American Thoracic Society*. https://doi.org/10.1513/pats.200504-038SR

Putcha, G. V., & Johnson, E. M. (2004). "Men are but worms:" Neuronal cell death in *C. elegans* and vertebrates. *Cell Death and Differentiation*, *11*(1), 38–48. https://doi.org/10.1038/sj.cdd.4401352

Putney, J. W. (2009). Capacitative calcium entry: from concept to molecules. *Immunological Reviews*, *231*(1), 10–22. https://doi.org/10.1111/j.1600-065X.2009.00810.x

Putney, J. W., Broad, L. M., Braun, F. J., Lievremont, J. P., & Bird, G. S. J. (2001). Mechanisms of capacitative calcium entry. *Journal of Cell Science*, *114*(12), 2223–2229.

Qin, X., Hou, X., Zhang, M., Liang, T., Zhi, J., Han, L., & Li, Q. (2014). Relaxation of rat aorta by farrerol correlates with potency to reduce intracellular calcium of VSMCs. *International Journal of Molecular Sciences*, *15*(4), 6641–6656. https://doi.org/10.3390/ijms15046641

Raemsch, K. D., & Sommer, J. (1983). Pharmacokinetics and metabolism of nifedipine. *Hypertension*, *5*(4_pt_2), 18–24. https://doi.org/10.1161/01.HYP.5.4_Pt_2.II18

Rang, H., Dale, M., Flower, R., & Ritter, J. (2012). Rang and Dale's pharmacology. In *Rang and Dale's Pharmacology* (7th Editio). https://doi.org/0443069115

Rashid, S., Heer, J. K., Garle, M. J., Alexander, S. P. H., & Roberts, R. E. (2013). Hydrogen sulphide-induced relaxation of porcine peripheral bronchioles. *British Journal of Pharmacology*, *168*(8), 1902–1910. https://doi.org/10.1111/bph.12084

Ratz, M., Testa, I., Hell, S. W., & Jakobs, S. (2015). CRISPR/Cas9-mediated endogenous protein tagging for RESOLFT super-resolution microscopy of living human cells. *Scientific Reports*, *5*, 1–6. https://doi.org/10.1038/srep09592

Ratz, P. H., & Berg, K. M. (2006). 2-Aminoethoxydiphenyl borate inhibits KCl-induced vascular smooth muscle contraction. *European Journal of Pharmacology*, *541*(3), 177–183. https://doi.org/10.1016/j.ejphar.2006.05.014

Ratz, P. H., Berg, K. M., Urban, N. H., & Miner, A. S. (2005). Regulation of smooth muscle calcium sensitivity: KCl as a calcium-sensitizing stimulus. *American Journal of Physiology-Cell Physiology*, *288*(4), C769–C783. https://doi.org/10.1152/ajpcell.00529.2004

Reading, S. A., Earley, S., Waldron, B. J., Welsh, D. G., & Brayden, J. E. (2005). TRPC3 mediates pyrimidine receptor-induced depolarization of cerebral arteries. *American Journal of Physiology - Heart and Circulatory Physiology*, *288*(5 57-5). https://doi.org/10.1152/ajpheart.00861.2004

Reaven, G. M. (2011). Relationships among insulin resistance, type 2 diabetes, essential hypertension, and cardiovascular disease: Similarities and differences. *The Journal of Clinical Hypertension*, *13*(4), 238–243. https://doi.org/10.1111/j.1751-7176.2011.00439.x

Reilly, J. P., & White, C. J. (2016). Renal denervation for resistant hypertension. *Progress in Cardiovascular Diseases*, *59*, 295–302. https://doi.org/10.1016/j.pcad.2016.10.003

Renwick, A., Robertson, D., Macklin, B., Challenor, V., Waller, D., & George, C. (1988). The pharmacokinetics of oral nifedipine-a population study. *British*

Journal of Clinical Pharmacology, *25*(6), 701–708. https://doi.org/10.1111/j.1365-2125.1988.tb05256.x

Richards, A. M. (2007). Natriuretic peptides. *Hypertension*, *50*(1), 25–30. https://doi.org/10.1161/HYPERTENSIONAHA.106.069153

Rigor, R. R., Shen, Q., Pivetti, C. D., Wu, M. H., & Yuan, S. Y. (2013). Myosin light chain kinase signaling in endothelial barrier dysfunction. *Medicinal Research Reviews*, *33*(5), 911–933. https://doi.org/10.1002/med.21270

Rizzoni, D., Castellano, M., Porteri, E., Bettoni, G., Muiesan, M. L., & Agabiti-Rosei, E. (1994). Vascular structural and functional alterations before and after the development of hypertension in shr. *American Journal of Hypertension*, *7*(2), 193–200. https://doi.org/10.1093/ajh/7.2.193

Rizzoni, D., & Rosei, E. A. (2006). Small artery remodeling in hypertension and diabetes. *Current Hypertension Reports*, *8*(1), 90–95. https://doi.org/10.1007/s11906-006-0046-3

Rodat-Despoix, L., Aires, V., Ducret, T., Marthan, R., Savineau, J. P., Rousseau, E., & Guibert, C. (2009). Signalling pathways involved in the contractile response to 5-HT in the human pulmonary artery. *European Respiratory Journal*, *34*(6), 1338–1347. https://doi.org/10.1183/09031936.00143808

Rosa, A. O., Yamaguchi, N., & Morad, M. (2013). Mechanical regulation of native and the recombinant calcium channel. *Cell Calcium*, *53*(4), 264–274. https://doi.org/10.1016/j.ceca.2012.12.007

Rubaiy, H. N., Ludlow, M. J., Henrot, M., Gaunt, H. J., Miteva, K., Cheung, S. Y., Tanahashi, Y., Hamzah, N., Musialowski, K. E., Blythe, N. M., Appleby, H. L., Bailey, M. A., McKeown, L., Taylor, R., Foster, R., Waldmann, H., Nussbaumer, P., … Beech, D. J. (2017). Picomolar, selective, and subtype-specific small-molecule inhibition of TRPC1/4/5 channels. *Journal of Biological Chemistry*, *292*(20), 8158–8173. https://doi.org/10.1074/jbc.M116.773556

Rudzinski, D. A. M., Kelly, C. B., & Leadbeater, N. E. (2012). A Weinreb amide approach to the synthesis of trifluoromethylketones. *Chemical Communications*, *48*(77), 9610–9612. https://doi.org/10.1039/c2cc35037h

Sabourin, J., Bartoli, F., Antigny, F., Gomez, A. M., & Benitah, J. P. (2016). Transient receptor potential canonical (trpc)/orai1-dependent store-operated Ca^{2+} channels; new targets of aldosterone in cardiomyocytes. *Journal of Biological Chemistry*, *291*(25), 13394–13409. https://doi.org/10.1074/jbc.M115.693911

Saito, Y., & Berk, B. C. (2001). Transactivation: a Novel signaling pathway from angiotensin II to tyrosine kinase receptors. *Journal of Molecular and Cellular Cardiology*, *33*(1), 3–7. https://doi.org/10.1006/jmcc.2000.1272

Sakurada, S., Okamoto, H., Takuwa, N., Sugimoto, N., & Takuwa, Y. (2001). Rho activation in excitatory agonist-stimulated vascular smooth muscle. *American Journal of Physiology - Cell Physiology*, *281*(2 50-2), 571–578. https://doi.org/10.1152/ajpcell.2001.281.2.c571

Saleh, D. O., Bayoumi, A. R., El-Eraky, W. I., & El-Khatib, A. S. (2013). Streptozotocin-induced vascular and biochemical changes in rats: Effects of

rosiglitazone vs. metformin. *Bulletin of Faculty of Pharmacy, Cairo University*, *51*(2), 131–138. https://doi.org/10.1016/j.bfopcu.2013.03.002

Salvetti, A., Brogi, G., Di Legge, V., & Bernini, G. P. (1993). The inter-relationship between insulin resistance and hypertension. *Drugs*, *46*(Supplement 2), 149–159. https://doi.org/10.2165/00003495-199300462-00024

Samanta, K., Bakowski, D., Amin, N., & Parekh, A. B. (2020). The whole-cell Ca^{2+} release-activated Ca^{2+} current, I_{CRAC}, is regulated by the mitochondrial Ca^{2+} uniporter channel and is independent of extracellular and cytosolic Na^{+}. *The Journal of Physiology*, *598*(9), 1753–1773. https://doi.org/10.1113/JP276551

Sandoo, A., Veldhuijzen van Zanten, J. J. C. ., Metsios, G. S., Carroll, D., & Kitas, G. D. (2015). The endothelium and its role in regulating vascular tone. *The Open Cardiovascular Medicine Journal*, *4*(1), 302–312. https://doi.org/10.2174/1874192401004010302

Sandow, S. L., Senadheera, S., Grayson, T. H., Welsh, D. G., & Murphy, T. V. (2012). Calcium and endothelium-mediated vasodilator signaling. *Advances in Experimental Medicine and Biology*, *740*, 811–831. https://doi.org/10.1007/978-94-007-2888-2_36

Sarzani, R., Spannella, F., Giulietti, F., Balietti, P., Cocci, G., & Bordicchia, M. (2017). Cardiac natriuretic peptides, hypertension and cardiovascular risk. *High Blood Pressure & Cardiovascular Prevention*, *24*(2), 115–126. https://doi.org/10.1007/s40292-017-0196-1

Saxena, P. R. (1992). Interaction between the renin-angiotensin-aldosterone and sympathetic nervous systems. *Journal of Cardiovascular Pharmacology*, *19*(SUPPL. 6), S80–S88. https://doi.org/10.1097/00005344-199219006-00013

Schafer, W. (2005). Egg-laying. *WormBook: The Online Review of C. Elegans Biology*, 1–7. https://doi.org/10.1895/wormbook.1.38.1

Schilling, W. P. (2001). TRP proteins: Novel therapeutic targets for regional blood pressure control? *Circulation Research*, *88*(3), 256–259. https://doi.org/10.1161/01.RES.88.3.256

Schlaich, M., Schultz, C., & Shetty, S. (2016). Renal denervation for resistant hypertension: closing in on potential confounders. *Journal of Hypertension*, *34*, 1505–1506. https://doi.org/10.1097/HJH.0000000000001016

Schleifer, H., Doleschal, B., Lichtenegger, M., Oppenrieder, R., Derler, I., Frischauf, I., Glasnov, T., Kappe, C., Romanin, C., & Groschner, K. (2012). Novel pyrazole compounds for pharmacological discrimination between receptor-operated and store-operated Ca^{2+} entry pathways. *British Journal of Pharmacology*, *167*(8), 1712–1722. https://doi.org/10.1111/j.1476-5381.2012.02126.x

Schneider, T., Fetscher, C., Krege, S., & Michel, M. C. (2004). Signal transduction underlying carbachol-induced contraction of human urinary bladder. *Journal of Pharmacology and Experimental Therapeutics*, *309*(3), 1148–1153. https://doi.org/10.1124/jpet.103.063735

Schuh, K., Quaschning, T., Knauer, S., Hu, K., Koçak, S., Roethlein, N., & Neyses, L. (2003). Regulation of vascular tone in animals overexpressing the sarcolemmal

calcium pump. *Journal of Biological Chemistry*, *278*(42), 41246–41252. https://doi.org/10.1074/jbc.M307606200

Seely, E. W., Moore, T. J., Rogacz, S., Gordon, M. S., Gleason, R. E., Hollenberg, N. K., & Williams, G. H. (1989). Angiotensin-mediated renin suppression is altered in non-modulating hypertension. *Hypertension*, *13*(1), 31–37. https://doi.org/10.1161/01.HYP.13.1.31

Séguéla, P., Ase, A. R., Grant, R., O'Donnell, D., & Groschner, K. (2014). Contribution of TRPC3 to store-operated calcium entry and inflammatory transductions in primary nociceptors. *Molecular Pain*, *10*, 43. https://doi.org/10.1186/1744-8069-10-43

Semenov, I., Herlihy, J. T., & Brenner, R. (2012). *In vitro* measurements of tracheal constriction using mice. *Journal of Visualized Experiments*, (64), 1. https://doi.org/10.3791/3703

Sendoel, A., Maida, S., Zheng, X., Teo, Y., Stergiou, L., Rossi, C. A., Subasic, D., Pinto, S. M., Kinchen, J. M., Shi, M., Boettcher, S., Meyer, J. N., Manz, M. G., Bano, D., & Hengartner, M. O. (2014). DEPDC1/LET-99 participates in an evolutionarily conserved pathway for anti-tubulin drug-induced apoptosis. *Nature Cell Biology*, *16*(8), 812–820. https://doi.org/10.1038/ncb3010

Serres, C., Yang, J., & Jouannet, P. (1994). RU486 and calcium fluxes in human spermatozoa. *Biochemical and Biophysical Research Communications*, *204*(3), 1009–1015. https://doi.org/10.1006/bbrc.1994.2563

Sharifi, A. M., Li, J. S., Endemann, D., & Schiffrin, E. L. (1998). Effects of enalapril and amlodipine on small-artery structure and composition, and on endothelial dysfunction in spontaneously hypertensive rats. *Journal of Hypertension*, *16*(4), 457–466. https://doi.org/10.1097/00004872-199816040-00007

Shaye, D. D., & Greenwald, I. (2011). Ortholist: A compendium of *C. elegans* genes with human orthologs. *PLoS ONE*, *6*(5). https://doi.org/10.1371/journal.pone.0020085

Shen, L., Xiao, J., Ye, H., & Wang, D. (2009). Toxicity evaluation in nematode *Caenorhabditis elegans* after chronic metal exposure. *Environmental Toxicology and Pharmacology*, *28*(1), 125–132. https://doi.org/10.1016/j.etap.2009.03.009

Shen, S., Xia, C., & Qiao, L.-Y. (2015). The urinary bladder of spontaneously hypertensive rat demonstrates bladder hypertrophy, inflammation, and fibrosis but not hyperplasia. *Life Sciences*, *121*, 22–27. https://doi.org/10.1016/j.lfs.2014.10.016

Sherman, D., & Harel, D. (2019). Deciphering the underlying mechanisms of the pharyngeal motions in *Caenorhabditis elegans*. *ArXiv Preprint ArXiv:1903.12009*, 1–32.

Shi, J., Ju, M., Large, W. A., & Albert, A. P. (2012). Pharmacological profile of phosphatidylinositol 3-kinases and related phosphatidylinositols mediating endothelinA receptor-operated native TRPC channels in rabbit coronary artery myocytes. *British Journal of Pharmacology*, *166*(7), 2161–2175. https://doi.org/10.1111/j.1476-5381.2012.01937.x

Shi, J., Miralles, F., Birnbaumer, L., Large, W. A., & Albert, A. P. (2017). Store-operated interactions between plasmalemmal STIM1 and TRPC1 proteins stimulate PLCβ1 to induce TRPC1 channel activation in vascular smooth muscle cells. *Journal of Physiology*, *595*(4), 1039–1058. https://doi.org/10.1113/JP273302

Shi, J. S., Yu, J. X., Chen, X. P., & Xu, R. X. (2003). Pharmacological actions of *Uncaria* alkaloids, rhynchophylline and isorhynchophylline. *Acta Pharmacologica Sinica*, *24*(2), 97–101.

Shiga, K., Hirano, K., Nishimura, J., Niiro, N., Naito, S., & Kanaide, H. (2007). Dimethyl sulphoxide relaxes rabbit detrusor muscle by decreasing the Ca^{2+} sensitivity of the contractile apparatus. *British Journal of Pharmacology*, *151*(7), 1014–1024. https://doi.org/10.1038/sj.bjp.0707317

Silva, J. D. P. da, & Ballejo, G. (2019). Pharmacological characterization of the calcium influx pathways involved in nitric oxide production by endothelial cells. *Einstein (Sao Paulo, Brazil)*, *17*(3), eAO4600. https://doi.org/10.31744/einstein_journal/2019AO4600

Singh-Ranger, G. (2018). Aspirin and colorectal cancer chemoprevention. *Mini-Invasive Surgery*, *2*(11), 39. https://doi.org/10.20517/2574-1225.2018.23

Singh, A., Hildebrand, M., Garcia, E., & Snutch, T. (2010). The transient receptor potential channel antagonist SKF96365 is a potent blocker of low-voltage-activated T-type calcium channels. *British Journal of Pharmacology*, *160*(6), 1464–1475. https://doi.org/10.1111/j.1476-5381.2010.00786.x

Sinnott, S. J., Smeeth, L., Williamson, E., & Douglas, I. J. (2017). Trends for prevalence and incidence of resistant hypertension: Population based cohort study in the UK 1995-2015. *BMJ (Online)*, *358*(j3984), 1–8. https://doi.org/10.1136/bmj.j3984

Skomedal, T., Aass, H., & Osnes, J.-B. (1984). Specific binding of [^{3}H]prazosin to myocardial cells isolated from adult rats. *Biochemical Pharmacology*, *33*(12), 1897–1906. https://doi.org/10.1016/0006-2952(84)90545-8

Skovsø, S. (2014). Modeling type 2 diabetes in rats using high fat diet and streptozotocin. *Journal of Diabetes Investigation*, *5*(4), 349–358. https://doi.org/10.1111/jdi.12235

Sobey, C. G. (2001). Potassium channel function in vascular disease. *Arteriosclerosis, Thrombosis, and Vascular Biology*, *21*(1), 28–38. https://doi.org/10.1161/01.ATV.21.1.28

Soboloff, J., Rothberg, B. S., Madesh, M., & Gill, D. L. (2012). STIM proteins: Dynamic calcium signal transducers. *Nature Reviews Molecular Cell Biology*, *13*(9), 549–565. https://doi.org/10.1038/nrm3414

Soboloff, J., Spassova, M., Xu, W., He, L. P., Cuesta, N., & Gill, D. L. (2005). Role of endogenous TRPC6 channels in Ca^{2+} signal generation in A7r5 smooth muscle cells. *Journal of Biological Chemistry*, *280*(48), 39786–39794. https://doi.org/10.1074/jbc.M506064200

Somlyo, A. P., & Somlyo, A. V. (2000). Signal transduction by G-proteins, Rho-kinase

and protein phosphatase to smooth muscle and non-muscle myosin II. *Journal of Physiology*, *522*(2), 177–185. https://doi.org/10.1111/j.1469-7793.2000.t01-2-00177.x

Song, P., Dong, X., & Liu, X. (2016). A microfluidic device for automated, high-speed microinjection of *Caenorhabditis elegans*. *Biomicrofluidics*, *10*(1), 011912. https://doi.org/10.1063/1.4941984

Soualy, A., Deutsch, D., Benallaoua, M., Ait-Omar, A., Mary, F., Helfen, S., Boubaya, M., Levy, V., & Benamouzig, R. (2020). Effect of chemoprevention by low-dose aspirin of new or recurrent colorectal adenomas in patients with Lynch syndrome (AAS-Lynch): study protocol for a multicenter, double-blind, placebo-controlled randomized controlled trial. *Trials*, *21*(1), 764. https://doi.org/10.1186/s13063-020-04674-8

Spassova, M. A., Soboloff, J., He, L. P., Hewavitharana, T., Xu, W., Venkatachalam, K., Van Rossum, D. B., Patterson, R. L., & Gill, D. L. (2004). Calcium entry mediated by SOCs and TRP channels: Variations and enigma. *Biochimica et Biophysica Acta - Molecular Cell Research*, *1742*(1–3), 9–20. https://doi.org/10.1016/j.bbamcr.2004.09.001

Spinelli, A. M., & Trebak, M. (2016). Orai channel-mediated Ca^{2+} signals in vascular and airway smooth muscle. *American Journal of Physiology-Cell Physiology*, *310*(6), C402–C413. https://doi.org/10.1152/ajpcell.00355.2015

Splettstoesser, F., Florea, A.-M., & Büsselberg, D. (2007). IP_3 receptor antagonist, 2-APB, attenuates cisplatin induced Ca^{2+}-influx in HeLa-S3 cells and prevents activation of calpain and induction of apoptosis. *British Journal of Pharmacology*, *151*(8), 1176–1186. https://doi.org/10.1038/sj.bjp.0707335

Sriram, K., Laughlin, J. G., Rangamani, P., & Tartakovsky, D. M. (2016). Shear-induced nitric oxide production by endothelial cells. *Biophysical Journal*, *111*(1), 208–221. https://doi.org/10.1016/j.bpj.2016.05.034

Stamper, R. L., Lieberman, M. F., & Drake, M. V. (2009). Adrenergic antagonists. In *Becker-Shaffer's Diagnosis and Therapy of the Glaucomas* (pp. 392–406). https://doi.org/10.1016/B978-0-323-02394-8.00025-5

Stanfield, C. L. (2005). *Principles of Human Physiology* (5th ed.). San Francisco: Pearson Benjamin Cummings.

Stannov, S. U., Brasen, J. C., Salomonsson, M., Holstein-Rathlou, N. H., & Sorensen, C. M. (2019). Interactions between renal vascular resistance and endothelium-derived hyperpolarization in hypertensive rats in vivo. *Physiological Reports*, *7*(15). https://doi.org/10.14814/phy2.14168

Stead, S., Werstiuk, E. S., & Lee, R. M. K. W. (2000). Nifedipine induces apoptosis in cultured vascular smooth muscle cells from spontaneously hypertensive rats. *Life Sciences*, *67*(8), 895–906. https://doi.org/10.1016/S0024-3205(00)00687-1

Strübing, C., Krapivinsky, G., Krapivinsky, L., & Clapham, D. E. (2003). Formation of novel TRPC channels by complex subunit interactions in embryonic brain. *Journal of Biological Chemistry*, *278*(40), 39014–39019. https://doi.org/10.1074/jbc.M306705200

Sun, X., Gu, X. Q., & Haddad, G. G. (2003). Calcium influx via L- and N-type calcium channels activates a transient large-conductance Ca^{2+} -activated K^{+} current in mouse neocortical pyramidal neurons. *The Journal of Neuroscience*, *23*(9), 3639–3648. https://doi.org/10.1523/JNEUROSCI.23-09-03639.2003

Sutphin, G. L., & Kaeberlein, M. (2009). Measuring *Caenorhabditis elegans* lifespan on solid media. *Journal of Visualized Experiments*, (27), 1–7. https://doi.org/10.3791/1152

Sweeney, M., Yu, Y., Platoshyn, O., Zhang, S., McDaniel, S. S., & Yuan, J. X. J. (2002). Inhibition of endogenous TRP1 decreases capacitative Ca^{2+} entry and attenuates pulmonary artery smooth muscle cell proliferation. *American Journal of Physiology-Lung Cellular and Molecular Physiology*, *283*(1), L144–L155. https://doi.org/10.1152/ajplung.00412.2001

Sweeney, Z. K., Minatti, A., Button, D. C., & Patrick, S. (2009). Small-molecule inhibitors of store-operated calcium entry. *ChemMedChem*, *4*(5), 706–718. https://doi.org/10.1002/cmdc.200800452

Swindle, M. M., Makin, A., Herron, A. J., Clubb, F. J., & Frazier, K. S. (2012). Swine as models in biomedical research and toxicology testing. *Veterinary Pathology*, *49*(2), 344–356. https://doi.org/10.1177/0300985811402846

Takahashi, A., Camacho, P., Lechleiter, J. D., & Herman, B. (1999). Measurement of intracellular calcium. *Physiological Reviews*, *79*(4), 1089–1125. https://doi.org/10.1152/physrev.1999.79.4.1089

Tang, Q., Guo, W., Zheng, L., Wu, J. X., Liu, M., Zhou, X., Zhang, X., & Chen, L. (2018). Structure of the receptor-activated human TRPC6 and TRPC3 ion channels. *Cell Research*, *28*(7), 746–755. https://doi.org/10.1038/s41422-018-0038-2

Tangsucharit, P., Takatori, S., Zamami, Y., Goda, M., Pakdeechote, P., Kawasaki, H., & Takayama, F. (2016). Muscarinic acetylcholine receptor M1 and M3 subtypes mediate acetylcholine-induced endothelium-independent vasodilatation in rat mesenteric arteries. *Journal of Pharmacological Sciences*, *130*(1), 24–32. https://doi.org/10.1016/j.jphs.2015.12.005

Tasaki, K., Hori, M., Ozaki, H., Karaki, H., & Wakabayashi, I. (2003). Difference in signal transduction mechanisms involved in 5-hdroxytryptamine- and U46619-induced vasoconstrictions. *Journal of Smooth Muscle Research*, *39*(5), 107–117. https://doi.org/10.1540/jsmr.39.107

Teh, X. R., Lim, M. T., Tong, S. F., Husin, M., Khamis, N., & Sivasampu, S. (2020). Quality of hypertension management in public primary care clinics in Malaysia: An update. *PLoS ONE*, *15*(8 August), 1–14. https://doi.org/10.1371/journal.pone.0237083

Tenor, J. L., & Aballay, A. (2008). A conserved toll-like receptor is required for *Caenorhabditis elegans* innate immunity. *EMBO Reports*, *9*(1), 103–109. https://doi.org/10.1038/sj.embor.7401104

Tesfai, Y., Brereton, H. M., & Barritt, G. J. (2001). A diacylglycerol-activated Ca^{2+} channel in PC12 cells (an adrenal chromaffin cell line) correlates with expression of the TRP-6 (transient receptor potential) protein. *Biochemical Journal*, *358*(3),

717–726. https://doi.org/10.1042/0264-6021:3580717

Thastrup, O. (1990). Role of Ca^{2+}-ATPases in regulation of cellular Ca^{2+} signalling, as studied with the selective microsomal Ca^{2+}-ATPase inhibitor, thapsigargin. *Agents and Actions*, *29*(1–2), 8–15. https://doi.org/10.1007/BF01964706

The C. elegans Sequencing Consortium. (1998). Genome Sequence of the Nematode *C. elegans*: A Platform for Investigating Biology. *Science*, *282*(5396), 2012–2018. https://doi.org/10.1126/science.282.5396.2012

Thilo, F., Baumunk, D., Krause, H., Schrader, M., Miller, K., Loddenkemper, C., Zakrzewicz, A., Krueger, K., Zidek, W., & Tepel, M. (2009). Transient receptor potential canonical type 3 channels and blood pressure in humans. *Journal of Hypertension*, *27*(6), 1217–1223. https://doi.org/10.1097/HJH.0b013e32832a5a9f

Thilo, F., Loddenkemper, C., Berg, E., Zidek, W., & Tepel, M. (2009). Increased TRPC3 expression in vascular endothelium of patients with malignant hypertension. *Modern Pathology*, *22*(3), 426–430. https://doi.org/10.1038/modpathol.2008.200

Thilo, F., Scholze, A., Liu, D. Y., Zidek, W., & Tepel, M. (2008). Association of transient receptor potential canonical type 3 (TRPC3) channel transcripts with proinflammatory cytokines. *Archives of Biochemistry and Biophysics*, *471*(1), 57–62. https://doi.org/10.1016/j.abb.2007.12.006

Thomas, J. R., & Lee, A. (2016). Measuring Ca^{2+}-dependent modulation of voltage-gated Ca^{2+} channels in HEK-293T cells. *Cold Spring Harbor Protocols*, *2016*(9), 762–767. https://doi.org/10.1101/pdb.prot087213

Thomas, P., & Smart, T. G. (2005). HEK293 cell line: a vehicle for the expression of recombinant proteins. *Journal of Pharmacological and Toxicological Methods*, *51*(3 SPEC. ISS.), 187–200. https://doi.org/10.1016/j.vascn.2004.08.014

Tian, K. ming, Li, J. jie, & Xu, S. wen. (2019). Rutaecarpine: A promising cardiovascular protective alkaloid from *Evodia rutaecarpa* (*Wu Zhu Yu*). *Pharmacological Research*, *141*(January), 541–550. https://doi.org/10.1016/j.phrs.2018.12.019

Tissenbaum, H. A. (2015). Using *C. elegans* for aging research. *Invertebrate Reproduction and Development*, *59*(April), 59–63. https://doi.org/10.1080/07924259.2014.940470

Török, J., & Kristek, F. (2001). Functional and morphological pattern of vascular responses in two models of experimental hypertension. *Experimental and Clinical Cardiology*, *6*(3), 142–148.

Tosun, M., Paul, R. J., & Rapoport, R. M. (1998). Role of extracellular Ca^{++} influx via L-type and non-L-type Ca^{++} channels in thromboxane A_2 receptor-mediated contraction in rat aorta. *Journal of Pharmacology and Experimental Therapeutics*, *284*(3), 921–928. Retrieved from http://www.ncbi.nlm.nih.gov/pubmed/9495850

Touyz, R. M., Alves-Lopes, R., Rios, F. J., Camargo, L. L., Anagnostopoulou, A., Arner, A., & Montezano, A. C. (2018). Vascular smooth muscle contraction in hypertension. *Cardiovascular Research*, *114*(4), 529–539. https://doi.org/10.1093/cvr/cvy023

Trevan, J. W. (1927). The error of determination of toxicity. *Proceedings of the Royal Society of London. Series B, Containing Papers of a Biological Character*, *101*(712), 483–514. https://doi.org/10.1098/rspb.1927.0030

Triggle, C. R., Samuel, S. M., Ravishankar, S., Marei, I., Arunachalam, G., & Ding, H. (2012). The endothelium: influencing vascular smooth muscle in many ways. *Canadian Journal of Physiology and Pharmacology*, *90*(6), 713–738. https://doi.org/10.1139/y2012-073

Tuder, R. M., Marecki, J. C., Richter, A., Fijalkowska, I., & Flores, S. (2007). Pathology of pulmonary hypertension. *Clinics in Chest Medicine*, *28*(1), 23–42. https://doi.org/10.1016/j.ccm.2006.11.010

Uehata, M., Ishizaki, T., Satoh, H., Ono, T., Kawahara, T., Morishita, T., Tamakawa, H., Yamagami, K., Inui, J., Maekawa, M., & Narumiya, S. (1997). Calcium sensitization of smooth muscle mediated by a Rho-associated protein kinase in hypertension [Article]. *Nature*, *389*(6654), 990–994. https://doi.org/10.1038/40187

Unger, T., Borghi, C., Charchar, F., Khan, N. A., Poulter, N. R., Prabhakaran, D., Ramirez, A., Schlaich, M., Stergiou, G. S., Tomaszewski, M., Wainford, R. D., Williams, B., & Schutte, A. E. (2020). 2020 International Society of Hypertension global hypertension practice guidelines. *Hypertension*, *75*(6), 1334–1357. https://doi.org/10.1161/HYPERTENSIONAHA.120.15026

Urena, J., del Valle-Rodriguez, A., & Lopez-Barneo, J. (2007). Metabotropic Ca^{2+} channel-induced calcium release in vascular smooth muscle. *Cell Calcium*, *42*(4–5), 513–520. https://doi.org/10.1016/j.ceca.2007.04.010

Vakil, R. J. (1955). *Rauwolfia serpentina* in the treatment of high blood pressure; a review of the literature. *Circulation*, *12*(2), 220–229. https://doi.org/10.1161/01.CIR.12.2.220

Van Petegem, F. (2012). Ryanodine receptors: structure and function. *Journal of Biological Chemistry*, *287*(38), 31624–31632. https://doi.org/10.1074/jbc.R112.349068

Varghese, A., Hong, Z., & Weir, E. K. (2006). Serotonin-induced inhibition of K_V current: A supporting role in pulmonary vasoconstriction? *Circulation Research*, *98*(7), 860–862. https://doi.org/10.1161/01.RES.0000219683.65556.74

Vasudevan, N. T., Mohan, M. L., Goswami, S. K., & Prasad, S. V. N. (2011). Regulation of β-adrenergic receptor function. *Cell Cycle*, *10*(21), 3684–3691. https://doi.org/10.4161/cc.10.21.18042

Vazquez, G., Wedel, B. J., Aziz, O., Trebak, M., & Putney, J. W. (2004). The mammalian TRPC cation channels. *Biochimica et Biophysica Acta - Molecular Cell Research*, *1742*(1–3), 21–36. https://doi.org/10.1016/j.bbamcr.2004.08.015

Veber, D. F., Johnson, S. R., Cheng, H.-Y., Smith, B. R., Ward, K. W., & Kopple, K. D. (2002). Molecular properties that influence the oral bioavailability of drug candidates. *Journal of Medicinal Chemistry*, *45*(12), 2615–2623. https://doi.org/10.1021/jm020017n

Venkatachalam, K., Zheng, F., & Gill, D. L. (2003). Regulation of canonical transient

receptor potential (TRPC) channel function by diacylglycerol and protein kinase C. *Journal of Biological Chemistry*, *278*(31), 29031–29040. https://doi.org/10.1074/jbc.M302751200

Vergara-Galicia, J., Ortiz-Andrade, R., Castillo-España, P., Ibarra-Barajas, M., Gallardo-Ortiz, I., Villalobos-Molina, R., & Estrada-Soto, S. (2008). Antihypertensive and vasorelaxant activities of *Laelia autumnalis* are mainly through calcium channel blockade. *Vascular Pharmacology*, *49*(1), 26–31. https://doi.org/10.1016/j.vph.2008.04.002

Vergara-Galicia, J., Ortiz-Andrade, R., Rivera-Leyva, J., Castillo-España, P., Villalobos-Molina, R., Ibarra-Barajas, M., Gallardo-Ortiz, I., & Estrada-Soto, S. (2010). Vasorelaxant and antihypertensive effects of methanolic extract from roots of *Laelia anceps* are mediated by calcium-channel antagonism. *Fitoterapia*, *81*(5), 350–357. https://doi.org/10.1016/j.fitote.2009.10.009

Verma, S., Buchanan, M. R., & Anderson, T. J. (2003). Endothelial function testing as a biomarker of vascular disease. *Circulation*, *108*(17), 2054–2059. https://doi.org/10.1161/01.CIR.0000089191.72957.ED

Verma, T., Sinha, M., Bansal, N., Yadav, S. R., Shah, K., & Chauhan, N. S. (2021). Plants used as antihypertensive. *Natural Products and Bioprospecting*, *11*(2), 155–184. https://doi.org/10.1007/s13659-020-00281-x

Vig, M., Beck, A., Billingsley, J. M., Lis, A., Parvez, S., Peinelt, C., Koomoa, D. L., Soboloff, J., Gill, D. L., Fleig, A., Kinet, J. P., & Penner, R. (2006). CRACM1 multimers form the ion-selective pore of the CRAC channel. *Current Biology*, *16*(20), 2073–2079. https://doi.org/10.1016/j.cub.2006.08.085

Villazon, M., Padin, J. F., Cadavid, M. I., Enguix, M. J., Tristán, H., Orallo, F., & Loza, M. I. (2002). Functional characterization of serotonin receptors in rat isolated aorta. *Biological and Pharmaceutical Bulletin*, *25*(5), 584–590. https://doi.org/10.1248/bpb.25.584

Vornanen, M. (1982). Adrenergic responses in different sections of rat airways. *Acta Physiologica Scandinavica*, *114*(4), 587–591. https://doi.org/10.1111/j.1748-1716.1982.tb07028.x

Wallukat, G. (2002). The β-adrenergic receptors. *Herz*, *27*(7), 683–690. https://doi.org/10.1007/s00059-002-2434-z

Wan, C., Chen, C., Li, M., Yang, Y., Chen, M., & Chen, J. (2017). Chemical constituents and antifungal activity of *Ficus hirta* vahl. fruits. *Plants*, *6*(4), 44. https://doi.org/10.3390/plants6040044

Wang, Bin, Xiong, S., Lin, S., Xia, W., Li, Q., Zhao, Z., Wei, X., Lu, Z., Wei, X., Gao, P., Liu, D., & Zhu, Z. (2017). Enhanced mitochondrial transient receptor potential channel, canonical type 3-mediated calcium handling in the vasculature from hypertensive rats. *Journal of the American Heart Association*, *6*(7). https://doi.org/10.1161/JAHA.117.005812

Wang, Bingxiang, Li, C., Huai, R., & Qu, Z. (2015). Overexpression of ANO1/TMEM16A, an arterial Ca^{2+}-activated Cl^- channel, contributes to spontaneous hypertension. *Journal of Molecular and Cellular Cardiology*, *82*, 22–32. https://doi.org/10.1016/j.yjmcc.2015.02.020

Wang, G. J., Wu, X. C., Chen, C. F., Lin, L. C., Huang, Y. T., Shan, J., & Pang, P. K. T. (1999). Vasorelaxing action of rutaecarpine: Effects of rutaecarpine on calcium channel activities in vascular endothelial and smooth muscle cells. *Journal of Pharmacology and Experimental Therapeutics*, *289*(3), 1237–1244.

Wang, H., Cheng, X., Tian, J., Xiao, Y., Tian, T., Xu, F., Hong, X., & Zhu, M. X. (2020). TRPC channels: Structure, function, regulation and recent advances in small molecular probes. *Pharmacology & Therapeutics*, *209*, 107497. https://doi.org/10.1016/j.pharmthera.2020.107497

Wang, I. Y., Bai, Y., Sanderson, M. J., & Sneyd, J. (2010). A mathematical analysis of agonist- and KCl-induced Ca^{2+} oscillations in mouse airway smooth muscle cells. *Biophysical Journal*, *98*(7), 1170–1181. https://doi.org/10.1016/j.bpj.2009.12.4273

Wang, K., Zhou, X.-Y., Wang, Y.-Y., Li, M.-M., Li, Y.-S., Peng, L.-Y., Cheng, X., Li, Y., Wang, Y.-P., & Zhao, Q.-S. (2011). Macrophyllionium and macrophyllines A and B, oxindole alkaloids from *Uncaria macrophylla*. *Journal of Natural Products*, *74*(1), 12–15. https://doi.org/10.1021/np1004938

Wang, M., Tang, Y.-B., Ma, M.-M., Chen, J.-H., Hu, C.-P., Zhao, S.-P., Peng, D.-Q., Zhou, J.-G., Guan, Y.-Y., & Zhang, Z. (2016). TRPC3 channel confers cerebrovascular remodelling during hypertension via transactivation of EGF receptor signalling. *Cardiovascular Research*, *109*(1), 34–43. https://doi.org/10.1093/cvr/cvv246

Wang, R., Wu, Y., Tang, G., Wu, L., & Hanna, S. T. (2000). Altered L-type Ca^{2+} channel currents in vascular smooth muscle cells from experimental diabetic rats. *American Journal of Physiology-Heart and Circulatory Physiology*, *278*(3), H714–H722. https://doi.org/10.1152/ajpheart.2000.278.3.H714

Wang, S. Y., Song, Y., Xu, M., He, Q. H., Han, Q. De, & Zhang, Y. Y. (2007). Internalization and distribution of three α_1-adrenoceptor subtypes in HEK293A cells before and after agonist stimulation. *Acta Pharmacologica Sinica*, *28*(3), 359–366. https://doi.org/10.1111/j.1745-7254.2007.00509.x

Wang, S. Z., Dong, G., & Sheng, C. (2019). Structural simplification: an efficient strategy in lead optimization. *Acta Pharmaceutica Sinica B*, *9*(5), 880–901. https://doi.org/10.1016/j.apsb.2019.05.004

Wassmann, S., Bäumer, A. T., Strehlow, K., Van Eickels, M., Grohé, C., Ahlbory, K., Rösen, R., Böhm, M., & Nickenig, G. (2001). Endothelial dysfunction and oxidative stress during estrogen deficiency in spontaneously hypertensive rats. *Circulation*, *103*(3), 435–441. https://doi.org/10.1161/01.CIR.103.3.435

Watson, N., Magnussen, H., & Rabe, K. F. (1998). The relevance of resting tension to responsiveness and inherent tone of human bronchial smooth muscle. *British Journal of Pharmacology*, *123*(4), 694–700. https://doi.org/10.1038/sj.bjp.0701637

Watts, S. W. (2002). Serotonin-induced contraction in mesenteric resistance arteries: Signaling and changes in deoxycorticosterone acetate-salt hypertension. *Hypertension*, *39*(3), 825–829. https://doi.org/10.1161/hy0302.104668

Wehrwein, E. A., & Joyner, M. J. (2013). Regulation of blood pressure by the arterial

baroreflex and autonomic nervous system. In *Handbook of Clinical Neurology* (Vol. 117, pp. 89–102). https://doi.org/10.1016/B978-0-444-53491-0.00008-0

Weiss, N., & Koschak, A. (2014). Pathologies of calcium channels. In *Pathologies of Calcium Channels*. https://doi.org/10.1007/978-3-642-40282-1

Weissmann, N., Sydykov, A., Kalwa, H., Storch, U., Fuchs, B., Mederos y Schnitzler, M., Brandes, R. P., Grimminger, F., Meissner, M., Freichel, M., Offermanns, S., Veit, F., Pak, O., Krause, K.-H., Schermuly, R. T., Brewer, A. C., Schmidt, H. H. H. W., … Dietrich, A. (2012). Activation of TRPC6 channels is essential for lung ischaemia–reperfusion induced oedema in mice. *Nature Communications*, *3*(1), 649. https://doi.org/10.1038/ncomms1660

Weksler, B. B., Marcus, A. J., & Jaffe, E. A. (1977). Synthesis of prostaglandin I_2 (prostacyclin) by cultured human and bovine endothelial cells. *Proceedings of the National Academy of Sciences of the United States of America*, *74*(9), 3922–3926. https://doi.org/10.1073/pnas.74.9.3922

Welsh, D. G., Morielli, A. D., Nelson, M. T., & Brayden, J. E. (2002). Transient receptor potential channels regulate myogenic tone of resistance arteries. *Circulation Research*, *90*(3), 248–250. https://doi.org/10.1161/hh0302.105662

Wenner, M. M., Wilson, T. E., Davis, S. L., & Stachenfeld, N. S. (2011). Pharmacological curve fitting to analyze cutaneous adrenergic responses. *Journal of Applied Physiology*, *111*(6), 1703–1709. https://doi.org/10.1152/japplphysiol.00780.2011

Wes, P. D., Chevesich, J., Jeromin, A., Rosenberg, C., Stetten, G., & Montell, C. (1995). TRPC1, a human homolog of a *Drosophila* store-operated channel. *Proceedings of the National Academy of Sciences*, *92*(21), 9652–9656. https://doi.org/10.1073/pnas.92.21.9652

Whelton, P. K., Carey, R. M., Aronow, W. S., Casey, D. E., Collins, K. J., Dennison Himmelfarb, C., DePalma, S. M., Gidding, S., Jamerson, K. A., Jones, D. W., MacLaughlin, E. J., Muntner, P., Ovbiagele, B., Smith, S. C., Spencer, C. C., Stafford, R. S., Taler, S. J., … Wright, J. T. (2018). 2017 ACC/AHA/AAPA/ABC/ACPM/AGS/APhA/ASH/ASPC/NMA/PCNA Guideline for the prevention, detection, evaluation, and management of high blood pressure in ddults. *Journal of the American Society of Hypertension*, *12*(8), 579.e1-579.e73. https://doi.org/10.1016/j.jash.2018.06.010

Wicha, P., Tocharus, J., Nakaew, A., Pantan, R., Suksamrarn, A., & Tocharus, C. (2015). Ethyl rosmarinate relaxes rat aorta by an endothelium-independent pathway. *European Journal of Pharmacology*, *766*, 9–15. https://doi.org/10.1016/j.ejphar.2015.09.003

Wierzejska, E., Giernaś, B., Lipiak, A., Karasiewicz, M., Cofta, M., & Staszewski, R. (2020). A global perspective on the costs of hypertension: a systematic review. *Archives of Medical Science*, *16*(5), 1078–1091. https://doi.org/10.5114/aoms.2020.92689

Wilkins, M. R., Redondo, J., & Brown, L. A. (1997). The natriuretic-peptide family. *The Lancet*, *349*(9061), 1307–1310. https://doi.org/10.1016/S0140-6736(96)07424-7

Williams, P. L., & Dusenbery, D. B. (1988). Using the nematode *Caenorhabditis elegans* to predict mammalian acute lethality to metallic salts. *Toxicology and Industrial Health*, *4*(4), 469–478. https://doi.org/10.1177/074823378800400406

Wilson, C., Lee, M. D., & McCarron, J. G. (2016). Acetylcholine released by endothelial cells facilitates flow-mediated dilatation. *The Journal of Physiology*, *594*(24), 7267–7307. https://doi.org/10.1113/JP272927

Wilson, C., Zhang, X., Buckley, C., Heathcote, H. R., Lee, M. D., & McCarron, J. G. (2019). Increased vascular contractility in hypertension results from impaired endothelial calcium signaling. *Hypertension*, *74*(5), 1200–1214. https://doi.org/10.1161/HYPERTENSIONAHA.119.13791

Wittkowski, P., Marx-Stoelting, P., Violet, N., Fetz, V., Schwarz, F., Oelgeschläger, M., Schönfelder, G., & Vogl, S. (2019). *Caenorhabditis elegans* as a promising alternative model for environmental chemical mixture effect assessment - A comparative study. *Environmental Science and Technology*, *53*(21), 12725–12733. https://doi.org/10.1021/acs.est.9b03266

Wong, P. S., Roberts, R. E., & Randall, M. D. (2015). Hyperoxic gassing with Tiron enhances bradykinin-induced endothelium-dependent and EDH-type relaxation through generation of hydrogen peroxide. *Pharmacological Research*, *91*, 29–35. https://doi.org/10.1016/j.phrs.2014.11.001

Wong, R. R., Kong, C., Lee, S. H., & Nathan, S. (2016). Detection of *Burkholderia pseudomallei* toxin-mediated inhibition of protein synthesis using a *Caenorhabditis elegans ugt-29* biosensor. *Scientific Reports*, *6*(May), 1–14. https://doi.org/10.1038/srep27475

Wood, E. J. (2005). An Introduction to Medicinal Chemistry. In *Bioscience Education* (3rd Editio, Vol. 6). https://doi.org/10.3108/beej.2005.06000007

World Health Organization. (2013). *A Global Brief on Hypertension- World Health Day 2013*.

World Health Organization. (2017). Cardiovascular diseases (CVDs). Retrieved from https://www.who.int/news-room/fact-sheets/detail/cardiovascular-diseases-(cvds)

Wu, X., Eder, P., Chang, B., & Molkentin, J. D. (2010). TRPC channels are necessary mediators of pathologic cardiac hypertrophy. *Proceedings of the National Academy of Sciences of the United States of America*, *107*(15), 7000–7005. https://doi.org/10.1073/pnas.1001825107

Wynne, B. M., Chiao, C. W., & Webb, R. C. (2009). Vascular smooth muscle cell signaling mechanisms for contraction to angiotensin II and endothelin-1. *Journal of the American Society of Hypertension*, *3*(2), 84–95. https://doi.org/10.1016/j.jash.2008.09.002

Xavier, F. E., Davel, A. P. C., Rossoni, L. V., & Vassallo, D. V. (2003). Time-dependent hyperreactivity to phenylephrine in aorta from untreated diabetic rats: role of prostanoids and calcium mobilization. *Vascular Pharmacology*, *40*(1), 67–76. https://doi.org/10.1016/S1537-1891(02)00315-4

Xiong, H., Pears, C., & Woollard, A. (2017). An enhanced *C. elegans* based platform for toxicity assessment. *Scientific Reports*, *7*(1), 1–11.

https://doi.org/10.1038/s41598-017-10454-3

Xu, S. Z., Zeng, F., Boulay, G., Grimm, C., Harteneck, C., & Beech, D. J. (2005). Block of TRPC5 channels by 2-aminoethoxydiphenyl borate: A differential, extracellular and voltage-dependent effect. *British Journal of Pharmacology*, *145*(4), 405–414. https://doi.org/10.1038/sj.bjp.0706197

Yan, F., Lu, J., Zhang, Y., Li, X., Chan, W.-H., Zhao, Q., Kwan, H.-Y., Liu, H., & Yao, X. (2020). Resveratrol stimulates the Na^+ -Ca^{2+} exchanger on the plasma membrane to reduce cytosolic Ca^{2+} in rat aortic smooth muscle cells. *Journal of Cardiovascular Pharmacology*, *Publish Ah*(5), 610–616. https://doi.org/10.1097/FJC.0000000000000897

Yan, H., Zhang, M. Z., Wong, G., Liu, L., Kwok, Y. S. (Shelia), Kuang, S. J., Yang, H., Rao, F., Li, X., Mai, L. P., Lin, Q. X., Yang, M., Zhang, Q. H., & Deng, C. Y. (2019). Mechanisms of U46619-induced contraction in mouse intrarenal artery. *Clinical and Experimental Pharmacology and Physiology*, *46*(7), 643–651. https://doi.org/10.1111/1440-1681.13087

Yang, M. Y., Peng, C. H., Chan, K. C., Yang, Y. I. S., Huang, C. N., & Wang, C. J. (2010). The hypolipidemic effect of *Hibiscus sabdariffa* polyphenols via inhibiting lipogenesis and promoting hepatic lipid clearance. *Journal of Agricultural and Food Chemistry*, *58*(2), 850–859. https://doi.org/10.1021/jf903209w

Yaroshevskii, Y. A. (1979). Insulin sensitivity of muscle tissue isolated from rats with manifest alloxan diabetes of varied duration. *Bulletin of Experimental Biology and Medicine*, *88*(4), 1126–1128. https://doi.org/10.1007/BF00838183

Yaxley, J., & Thambar, S. (2015). Resistant hypertension: An approach to management in primary care. *Journal of Family Medicine and Primary Care*, *4*(2), 193. https://doi.org/10.4103/2249-4863.154630

Yip, H., Chan, W. Y., Leung, P. C., Kwan, H. Y., Liu, C., Huang, Y., Michel, V., Yew, D. T. W., & Yao, X. (2004). Expression of TRPC homologs in endothelial cells and smooth muscle layers of human arteries. *Histochemistry and Cell Biology*, *122*(6), 553–561. https://doi.org/10.1007/s00418-004-0720-y

Yonetoku, Y., Kubota, H., Miyazaki, Y., Okamoto, Y., Funatsu, M., Yoshimura-Ishikawa, N., Ishikawa, J., Yoshino, T., Takeuchi, M., & Ohta, M. (2008). Novel potent and selective Ca^{2+} release-activated Ca^{2+} (CRAC) channel inhibitors. Part 3: Synthesis and CRAC channel inhibitory activity of 4′-[(trifluoromethyl)pyrazol-1-yl]carboxanilides. *Bioorganic and Medicinal Chemistry*, *16*(21), 9457–9466. https://doi.org/10.1016/j.bmc.2008.09.047

Yu, S.-M., Hsu, S.-Y., Ko, F.-N., Chen, C.-C., Huang, Y.-L., Huang, T.-F., & Teng, C.-M. (1992). Haemodynamic effects of dicentrine, a novel α_1-adrenoceptor antagonist: comparison with prazosin in spontaneously hypertensive and normotensive Wistar-Kyoto rats. *British Journal of Pharmacology*, *106*(4), 797–801. https://doi.org/10.1111/j.1476-5381.1992.tb14415.x

Yu, S.-M., Kang, Y.-F., Chen, C.-C., & Teng, C.-M. (1993). Effects of dicentrine on haemodynamic, plasma lipid, lipoprotein level and vascular reactivity in hyperlipidaemic rats. *British Journal of Pharmacology*, *108*(4), 1055–1061.

https://doi.org/10.1111/j.1476-5381.1993.tb13505.x

Yu, S. -M, & Kuo, S. -C. (1995). Vasorelaxant effect of isoliquiritigenin, a novel soluble guanylate cyclase activator, in rat aorta. *British Journal of Pharmacology*, *114*(8), 1587–1594. https://doi.org/10.1111/j.1476-5381.1995.tb14943.x

Yu, Y., Fantozzi, I., Remillard, C. V., Landsberg, J. W., Kunichika, N., Platoshyn, O., Tigno, D. D., Thistlethwaite, P. A., Rubin, L. J., & Yuan, J. X. J. (2004). Enhanced expression of transient receptor potential channels in idiopathic pulmonary arterial hypertension. *Proceedings of the National Academy of Sciences of the United States of America*, *101*(38), 13861–13866. https://doi.org/10.1073/pnas.0405908101

Yu, Y., Sweeney, M., Zhang, S., Platoshyn, O., Landsberg, J., Rothman, A., & Yuan, J. X. J. (2003). PDGF stimulates pulmonary vascular smooth muscle cell proliferation by upregulating TRPC6 expression. *American Journal of Physiology-Cell Physiology*, *284*(2), C316–C330. https://doi.org/10.1152/ajpcell.00125.2002

Yuan, J. P., Zeng, W., Huang, G. N., Worley, P. F., & Muallem, S. (2007). STIM1 heteromultimerizes TRPC channels to determine their function as store-operated channels. *Nature Cell Biology*, *9*(6), 636–645. https://doi.org/10.1038/ncb1590

Zafra-Polo, M. C., Tormos, M. J., Cortes, D., & Anselmi, E. (1993). Comparative study of the rat uterine smooth muscle relaxant activity of three bisbenzyltetrahydroisoquinolines with tetrandrine. *Journal of Pharmacy and Pharmacology*, *45*(6), 563–566. https://doi.org/10.1111/j.2042-7158.1993.tb05599.x

Zagranichnaya, T. K., Wu, X., & Villereal, M. L. (2005). Endogenous TRPC1, TRPC3, and TRPC7 proteins combine to form native store-operated channels in HEK-293 cells. *Journal of Biological Chemistry*, *280*(33), 29559–29569. https://doi.org/10.1074/jbc.M505842200

Zerroug, A., Belaidi, S., BenBrahim, I., Sinha, L., & Chtita, S. (2019). Virtual screening in drug-likeness and structure/activity relationship of pyridazine derivatives as Anti-Alzheimer drugs. *Journal of King Saud University - Science*, *31*(4), 595–601. https://doi.org/10.1016/j.jksus.2018.03.024

Zhang-James, Y., Middleton, F. A., & Faraone, S. V. (2013). Genetic architecture of Wistar-Kyoto rat and spontaneously hypertensive rat substrains from different sources. *Physiological Genomics*, *45*(13), 528–538. https://doi.org/10.1152/physiolgenomics.00002.2013

Zhang, B., Liu, B., Roos, C. M., Thompson, M. A., Prakash, Y. S., Miller, J. D., & Guo, R. (2018). TRPC6 and TRPC4 heteromultimerization mediates store depletion-activated NCX1 reversal in proliferative vascular smooth muscle cells. *Channels*, *12*(1), 119–125. https://doi.org/10.1080/19336950.2018.1451696

Zhang, H. J., Tamez, P. A., Aydogmus, Z., Tan, G. T., Saikawa, Y., Hashimoto, K., Nakata, M., Hung, N. Van, Xuan, L. T., Cuong, N. M., Soejarto, D. D., Pezzuto, J. M., & Fong, H. H. S. (2002). Antimalarial agents from plants. III. Trichothecenes from *Ficus fistulosa* and *Rhaphidophora decursiva*. *Planta Medica*, *68*(12), 1088–1091. https://doi.org/10.1055/s-2002-36350

Zhang, L. F., Zalewski, A., Liu, Y., Mazurek, T., Cowan, S., Martin, J. L., Hofmann, S. M., Vlassara, H., & Shi, Y. (2003). Diabetes-induced oxidative stress and low-grade inflammation in porcine coronary arteries. *Circulation*, *108*(4), 472–478. https://doi.org/10.1161/01.CIR.0000080378.96063.23

Zhang, S., Remillard, C. V., Faniozzi, I., & Yuan, J. X. J. (2004). ATP-induced mitogenesis is mediated by cyclic AMP response element-binding protein-enhanced TRPC4 expression and activity in human pulmonary artery smooth muscle cells. *American Journal of Physiology - Cell Physiology*, *287*(5 56-5). https://doi.org/10.1152/ajpcell.00158.2004

Zhang, X., & Trebak, M. (2014). Transient receptor potential canonical 7: A diacylglycerol-activated non-selective cation channel. In *Handbook of Experimental Pharmacology* (Vol. 222, pp. 189–204). https://doi.org/10.1007/978-3-642-54215-2_8

Zhou, Baoping, Wang, Y., Zhang, C., Yang, G., Zhang, F., Yu, B., Chai, C., & Cao, Z. (2018). Ribemansides A and B, TRPC6 inhibitors from *Ribes manshuricum* that suppress TGF-β1-induced fibrogenesis in HK-2 Cells. *Journal of Natural Products*, *81*(4), 913–917. https://doi.org/10.1021/acs.jnatprod.7b01037

Zhou, Bin, Bentham, J., Di Cesare, M., Bixby, H., Danaei, G., Cowan, M. J., Paciorek, C. J., Singh, G., Hajifathalian, K., Bennett, J. E., Taddei, C., Bilano, V., Carrillo-Larco, R. M., Djalalinia, S., Khatibzadeh, S., Lugero, C., Peykari, N., … Zuñiga Cisneros, J. (2017). Worldwide trends in blood pressure from 1975 to 2015: a pooled analysis of 1479 population-based measurement studies with 19.1 million participants. *The Lancet*, *389*(10064), 37–55. https://doi.org/10.1016/S0140-6736(16)31919-5

Zhu, X., Jiang, M., & Birnbaumer, L. (1998). Receptor-activated Ca^{2+} influx via human Trp3 stably expressed in human embryonic kidney (HEK)293 cells: Evidence for a non-capacitative Ca^{2+} entry. *Journal of Biological Chemistry*, *273*(1), 133–142. https://doi.org/10.1074/jbc.273.1.133

Zhu, X., Jiang, M., Peyton, M., Boulay, G., Hurst, R., Stefani, E., & Birnbaumer, L. (1996). *trp*, a novel mammalian gene family essential for agonist-activated capacitative Ca^{2+} entry. *Cell*, *85*(5), 661–671. https://doi.org/10.1016/S0092-8674(00)81233-7

Zullo, J. M., Drake, D., Aron, L., O'Hern, P., Dhamne, S. C., Davidsohn, N., Mao, C. A., Klein, W. H., Rotenberg, A., Bennett, D. A., Church, G. M., Colaiácovo, M. P., & Yankner, B. A. (2019). Regulation of lifespan by neural excitation and REST. *Nature*, *574*(7778), 359–364. https://doi.org/10.1038/s41586-019-1647-8